Nitrogen in the Earth System: planetary budget and cycling during geologic history

by

Benjamin William Johnson
B.Sc., University of Puget Sound, 2006
M.Sc., University of Utah, 2009

A Dissertation Submitted in Partial Fulfillment of the
Requirements for the Degree of

DOCTOR OF PHILOSOPHY

in the School of Earth and Ocean Sciences

Nitrogen in the Earth System: planetary budget and cycling during geologic history

by

Benjamin William Johnson
B.Sc., University of Puget Sound, 2006
M.Sc., University of Utah, 2009

Supervisory Committee

Dr. Colin Goldblatt, Supervisor
(School of Earth and Ocean Sciences)

Dr. Dante Canil, Departmental Member
(School of Earth and Ocean Sciences)

Dr. Michael Whiticar, Departmental Member
(School of Earth and Ocean Sciences)

Dr. Rana El-Sabaawi, Outside Member
(Department of Biology)

ABSTRACT

The distribution and geologic history of nitrogen on Earth is poorly known. Traditionally thought to be an inert gas, with only a small but important biologic cycle, geochemical investigation highlights that it can also be present in rocks and minerals. Even at low concentrations, the great mass of the solid Earth allows for the possibility of substantial N mass and cycling in the geosphere over Earth history. Thus, the assumption that N on the surface of the Earth has remained in steady state over Earth history can be questioned. The research goals of this thesis are to investigate the Earth System N cycle using both large- and small-scale approaches.

I present a comprehensive literature compilation to ascertain the N budget of Earth. Determining the total abundance of N in all reservoirs of the Earth, including the atmosphere, oceans, crust, mantle, and core is crucial to a discussion of its cycling in the past. This budget study suggests that the majority of planetary N is likely in the core, with the Bulk Silicate Earth a more massive reservoir than the atmosphere. I also present experimental data and data from lunar samples as added context.

As quantification of geologic N is difficult, I present research detailing the adaptation of a fluorometric technique common in aquatic geochemistry for use on geologic samples. I compare fluorometry analysis of geochemical standards to several other techniques: colourimetry, elemental analyzer mass spectrometry, and neutron activation analysis. Fluorometry generally behaves well for crystalline samples, and is a relatively quick and easy alternative to more expensive or intensive techniques. As a preliminary application, I have determined a N budget estimate for the continental crust based on analysis of crystalline crustal rocks and glacial tills from North America. This budget is consistent with published work, suggesting about 2×10^{18} kg N, or half a present atmospheric mass of N, is in the continental crust.

I also present a geochemical study measuring N-isotopes and redox sensitive trace elements from a syn-glacial unit deposited during the the Marinoan Snowball Earth. Snowball Earth events were the most extreme glaciations in Earth history. The measurements presented herein are the first to quantify biologic activity via N-isotopes as well as the redox state of the atmosphere and ocean using trace elements from this intriguing time period in Earth history. The data suggests that there was active N-fixing in the biosphere, persistent but limited O_2, nitrification, and nearly quantitative denitrification during the glaciation. After the glacial interval, O_2 levels increased and denitrification levels dropped, indicated by near-modern $\delta^{15}N$ values. The combined

use of N-isotope with redox sensitive trace elements provides a more nuanced and comprehensive view in reconstructing past ocean and biologic conditions.

Lastly, I present an Earth-system N cycle model with nominal results. Previous modelling efforts have agreed with the traditional notion that atmospheric N-levels have remained constant over geologic time. This is in contrast with modern geochemical evidence suggesting net transport of N from the surface into the mantle. The aim, in turn, of this model is to model N cycling over Earth history by explicitly incorporating both biologic and geologic fluxes. The model is driven by a mantle cooling history and calculated plate tectonic speed, as well as a prescribed atmospheric O_2 evolution history. This approach is the first of its kind, to my knowledge, and produces stable model runs over Earth history. While tuning and sensitivity studies may be required for publishable results, nominal runs are compelling. In model output, atmospheric N varies by an factor of $2-3$ over Earth history, and the availability of nutrients (i.e., PO_4) exerts a strong control on biologic activity and movement of N throughout the Earth system.

Such a planetary perspective on N serves as an entry point into discussions of planetary evolution as a whole. With the great increase in the number of discovered exoplanets, the scientific community is charged with developing models of planetary evolution and factors that promote habitability. Comparison of Earth to its solar system neighbours and future data on exoplanets will allow a system of evolution pathways to be explored, with the role of N expected to be prominent in discussions of habitability and planetary evolution.

Contents

List of Tables

List of Figures

ACKNOWLEDGEMENTS

I thank my lovely wife, Lindsey. I thank her for her warmth and understanding and support, and enduring discussion about odd elements and geochemistry. She is a peerless proof-reader and a great friend.

I'd also like to thank both my parents, Peg and Dave, for their encouragement and passing on the gift of intellectual curiosity and exploration. My brother and sister, Tom and Emily, and their partners Emily and Justin, have been supportive and welcoming to me wandering in to their homes when in need of a break.

There are a number of friends in the SEOS department who helped instil sanity. Specifically, Ramses D'Souza, Arlan Dirkson, Bennit Mueller, Jennifer Long, and SEOS alumni JP Desforges, Duncan Mackay, and Brendan Byrne were all wildly good friends and colleagues. Natashia Drage and Nova Hanson helped with fluorometry project development.

I also thank Paul Hoffman for all his help and discussion during my degree. I am grateful to him for taking me to accompany him in the field in Namibia. He has been supportive and willing to discuss science, politics, and baseball, and I thank him for that.

I'd also like to thank a number of the SEOS staff, including Jody Spence for major assistance in the lab, and Kimberly and Allison in the office for great help in keeping me on track.

My committee members have all been extremely helpful during this process. All three have directly participated in research, either through suggestions for areas to explore, feedback on manuscripts, and general guidance and support during my PhD. I would like to acknowledge Dr. Sean Crowe for acting as external member during my defense. His effort in reading the manuscript as well as preparing excellent and engaging questions was most appreciated.

My adviser, Colin Goldblatt, also merits special mention. As I am his first PhD student, and he my first PhD adviser, the completion of this degree required a great deal of learning from both of us. I am a better scientist today, and he a better adviser, and I thank him for his support and welcoming attitude.

The formation of the present earth necessarily involves the destruction of continents in the ancient world; and, by pursuing in our mind the natural operations of a former earth, we clearly see the origin of that land, by the fertility of which, we, and all the animated bodies of the sea, are fed.

-James Hutton

DEDICATION

I would like to dedicate this thesis to my grandparents, Harvey and Shirley Johnson and Dorothy and Jack Robeda. Though I knew them for only a short time, I know they passed on an adventurous spirit, and I hope I have made them proud.

Chapter 1

Introduction

1.1 Background and motivation

Nitrogen was one of the last major biologic elements to be discovered, almost synchronously with oxygen (Weeks, 1933). It was discovered by Daniel Rutherford in 1772 by isolation in a chamber after removing oxygen, water, and carbon dioxide through a series of purification steps (Rutherford, 1772; Dobbin, 1935). It displayed some confusing characteristics and mysterious properties. This isolated gas would extinguish a flame, suffocate a mouse after a time, but otherwise show no reactive properties. In many ways, these mysterious and confounding initial observations carry over to studies of N in the present day.

In the century after its discovery, N was recognized as a key nutrient for life. It was also recognized that nitrogen fixing, breaking the triple bond in N_2 to make bioavailable N, is a process requiring great energy. Splitting of N_2 by lightning was seen as the major, or only, source of fixed N to the biosphere (Breneman, 1889). Additionally, geologic fixed nitrogen was discovered, primarily in deposits of nitrate in Chile and fossilized (or fresh) guano. It was thought, though, that there was no large geologic reservoir with mineral-bound N (Branner, 1897). The recognition of the importance of fixed N for agriculture and industrial processes spurred the invention of efficient artificial fixing (Haber, 1920; Erisman et al., 2008) as well as comprehensive review of all known fixation pathways (Hardy et al., 1977a,b). Despite, or perhaps due to the focus on, its biologic, agricultural, and industrial significance, relatively little work was done on N in geologic settings. Interest in N-fixing and removal of N, via denitrification and anammox, and the interaction of natural and human-

influenced cycles from a variety of environments continues to be an active area of research (Canfield et al., 2010; Crowe et al., 2012)

During the middle of the 20th century, technological advances allowed detection of low (ppm) concentrations of N in rocks and minerals (Hoering, 1955; Scalan, 1955; Mayne, 1957). However, early budget estimates of total planetary N suggested that the majority of N on Earth was in the atmosphere, and the contribution of rocks and minerals was low or uncertain (Baur & Wlotzka, 1969). Measurements of extraterrestrial samples indicated that high concentrations of N exist (Gibson & Moore, 1971; Gibson et al., 1971) in the inner solar system, though exactly how meteoritic material relates to terrestrial bulk composition is still a matter of some debate (Javoy et al., 2010; Marty, 2012; Halliday, 2013; Harries et al., 2015).

Further investigation into the isotopic distribution of geologic N revealed that different sources of N carry distinct isotopic signatures (Peters et al., 1978). Isotopic values matching biologic material were observed not only in sedimentary rocks, but in igneous and metamorphic rocks as well (Itihara & Honma, 1979; Honma & Itihara, 1981; Norris & Schaeffer, 1982). Geologic N, even when found as NH_4^+ in igneous rocks, might be a chemical fossil, a record of life's activity on the planet (Itihara & Suwa, 1985). The N-record in rocks may also hold information on the composition of the ancient atmosphere (Gibson et al., 1986).

Subsequent study revealed that not only does N cycle on the surface of the Earth, it transits into the deeper planet. Correlation between N_2 and ^{40}Ar in mid-ocean ridge basalts, as well as $\delta^{15}N$ values and other noble gasses in ocean island basalts, indicate N has been recycled from the surface into the mantle (Marty, 1995; Marty & Zimmermann, 1999; Goldblatt et al., 2009; Busigny et al., 2011; Barry & Hilton, 2016). The isotopic character of mantle N may record a history of mantle mixing and highlight different mantle domains (Exley et al., 1987; Johnson & Goldblatt, 2015). Similar to C (Holland, 1984), N should be treated as an element that cycles throughout the entire Earth-system. It exists and cycles between all reservoirs of the Bulk Silicate Earth and the surface reservoirs.

It is from this planetary perspective that this dissertation is motivated. A strong knowledge base exists for the behaviour of N in the biosphere, atmosphere, and geosphere as separate entities. The scope of the dissertation herein is to assimilate these various areas into a broader context of Earth System N behaviour. Through the integration of field, laboratory, and numerical modelling studies I will investigate N at a variety of spatial and temporal scales. From its initial discovery, N has proven to

be a mysterious element. I aim to unshroud at least of portion of this mystery.

There are a number of specific questions concerning the planetary N cycle. First, the total amount of N in the planet is a matter of some debate (Marty, 2012; Halliday, 2013). When comparing N with other volatile elements (C, H_2O, noble gases), there is an apparent "missing N" problem. That is, while all volatile elements are depleted in the Earth compared to planetary building blocks (chondritic meteorites), N appears to be an order of magnitude more depleted than other volatiles. Potential solutions to this problem include atmospheric erosion during the early Earth, or sequestration of N into the core (Roskosz et al., 2013). The work in this dissertation suggests that the mantle has ample capacity for N storage, and this reservoir is identified through N-Ar systematics.

The distribution of N in the Earth has direct impacts on planetary habitability. A potential solution to the Faint Young Sun Paradox (FYSP) is the presence of a more massive N_2 atmosphere in the Archean, which increases the greenhouse efficiency of CO_2 through pressure broadening (Goldblatt et al., 2009). An atmosphere with 2 to 3 times as much N_2 as the present atmosphere can, given moderate CO_2 levels, provide warming sufficient for global mean temperatures to be above freezing. This interpretation, however, requires a net drawdown of atmospheric N over time. This is not supported by either traditional planetary budgets (i.e., there is not enough N in the planet for a more massive atmosphere) or some modelling work (e.g., Berner, 2006). In contrast, a number of geochemical studies (Busigny et al., 2011; Barry & Hilton, 2016) are consistent with a net drawdown in atmospheric mass over time. I will assess these options in this dissertation through an Earth system N cycle model.

Lastly, the behaviour of organisms and their role in the Earth system N cycle over time is poorly constrained. The Neoproterozoic Snowball Earth glaciations represent a unique setting in which to investigate this biologic cycle. Originally conceived as a completely ice-covered, "hard Snowball" ocean (Hoffman et al., 1998), recent work is consistent with areas of open water (e.g., Abbot et al., 2011) throughout the duration of the glaciations. If the ocean was isolated from the atmosphere, it would rather quickly become anoxic. If, however, areas of open water allowed for gas exchange, with sustained primary productivity at least part of the ocean would be oxygenated. These opposing states of ocean redox would result in very different biologic metabolisms and nutrient cycling. To investigate this conundrum, I have analyzed the N isotopic and redox-sensitive trace element composition of syn-glacial deposit from Namibia.

1.2 Research goals and dissertation outline

The goals of this dissertation are to investigate the Earth System N cycle over geologic time. I present work that incorporates both whole-Earth, deep time aspects of the N cycle as well as more focused laboratory analyses to answer specific questions.

Due to the new appreciation for the amount of N in geologic reservoirs of the Earth, presenting a thorough compilation and synthesis of existing data was a crucial step to guide further study. Through this compilation, I was able to assess the state of knowledge in the field. Additionally, I was able to make new observations about the distribution of N in the Earth, commenting on possible starting composition during planetary accretion as well as the effects of core formation. The overarching goal was to place N in a planetary context. This work is presented in Chapter 2, and is published in *Earth Science Reviews* (Johnson & Goldblatt, 2015).

To address the significant barrier of analytical difficulty in measuring geologic N, I adapted a fluorometric technique developed for use in biologic and aquatic science for use on geologic materials. As N is present in low concentrations in rocks and minerals, quantifying its concentration is often time consuming. The goal was to both develop a relatively straight-forward technique for measuring N concentration and to compare several techniques (colourimetry, mass spectrometry, neutron activation analysis). Since N can exist in several different species in rocks and minerals (NH_4^+, NO_3^-, organic-N, N_2), and the potential for atmospheric contamination is high, it is non-trivial to determine what species is being measured. This work is presented in Chapter 3, and is currently submitted to *Solid Earth* (Johnson et al., In review).

The operation of the biologic N cycle during times of environmental stress and change is poorly known throughout the geologic record. I collected a series of samples from one such time of stress, the Neoproterozoic Marinoan glaciation, to investigate the state of both N and O_2 during this Snowball Earth glacial interval. This study is based on N-isotopes and redox-sensitive trace element analyses, and are the first from this time period, to my knowledge. This work is presented in Chapter 4, and is currently under review at *Nature Communications* (Johnson & Goldblatt, In review).

The final goal of this dissertation is to integrate the biologic and geologic N cycles together into a numerical model. Through the incorporation of the N cycle in the atmosphere, ocean, sediments, crust, and mantle, I will explore how N has moved throughout the Earth System over geologic time. I also include other species that are either important in the biologic cycle (PO_4 and O_2) or act as inorganic tracers

(K, Ar) of N to give this study the context it requires. I show that N can indeed cycle between the major reservoirs on Earth (atmosphere, mantle, crust) and that cycling is mediated by biologic activity. It is thus imperative to discuss not only N but also other nutrients and oxygen as important features of the Earth system N cycle. This work is presented in Chapter 5, and details include background and previous modelling work, coding strategy, and nominal runs of the model.

Chapter 2

The Nitrogen Budget of Earth

The following chapter is a manuscript published as:

Ben Johnson and Colin Goldblatt, 2015. The nitrogen budget of Earth. *Earth Science Reviews*. **148**. 150 – 173.

It is reproduced verbatim herein. It has been reformatted to fit dissertation guidelines. Minor comments pertaining to the dissertation, but not shown in the publication (with the exception of the footnote describing δ^{15}N), are given as footnotes.

2.1 Abstract

We comprehensively compile and review N content in geologic materials to calculate a new N budget for Earth. Using analyses of rocks and minerals in conjunction with N-Ar geochemistry demonstrates that the Bulk Silicate Earth (BSE) contains $\sim 7 \pm 4$ times present atmospheric N (4×10^{18} kg N, or PAN), with $27 \pm 16 \times 10^{18}$ kg N. Comparison to chondritic composition, after subtracting N sequestered into the core, yields a consistent result, with BSE N between $17 \pm 13 \times 10^{18}$ kg to $31 \pm 24 \times 10^{18}$ kg N. Embedded in the chondritic comparison we calculate a N mass in Earth's core (180 ± 110 to $300 \pm 180 \times 10^{18}$ kg) as well as present discussion of the Moon as a proxy for the early mantle.

Significantly, our study indicates the majority of the planetary budget of N is in the solid Earth. We suggest that the N estimate here precludes the need for a "missing N" reservoir. Nitrogen-Ar systematics in mantle rocks and primary melts

identify the presence of two mantle reservoirs: MORB-source like (MSL) and high-N. High-N mantle is composed of young, N-rich material subducted from the surface and identified in OIB and some xenoliths. In contrast, MSL appears to be made of old material, though a component of subducted material is evident in this reservoir as well.

Taking into account N mass and isotopic character of the atmosphere and BSE, we calculate a δ^{15}N value of $\sim 2‰$. This value should be used when discussing bulk Earth N isotope evolution. Additionally, our work indicates that all surface N could pass through the mantle over Earth history, and in fact the mantle may act as a long-term sink for N. Since N acts as a tracer of exchange between the atmosphere, oceans, and mantle over time, clarifying its distribution in the Earth is critical for evolutionary models concerned with Earth system evolution. We suggest that N be viewed in the same light as carbon: it has a fast, biologically mediated cycle which connects it to a slow, tectonically-controlled geologic cycle.

2.2 Introduction

Nitrogen, the fifth most common element in the solar system, is the main component of the atmosphere, is a key nutrient for life, and has potential to be a tracer of processes linking the surface Earth to different reservoirs in the solid planet. Though N has long been known to exist geologically in fluid inclusions or as NH_4^+ in mineral lattices (Mayne, 1957), it was thought to predominantly reside in the atmosphere and biosphere (Baur & Wlotzka, 1969). It is now clear that N can indeed become incorporated into minerals and rocks in significant amounts and cycles over long time scales through the atmosphere, oceans, crust, and mantle. While the absolute concentration of N in rocks is low (often $\sim$1 ppm, but up to $\sim$100 or 1000 ppm), the great mass of the solid Earth compared to the atmosphere means that it has the potential to sequester large amounts of N. A picture of the behaviour of N in the Bulk Silicate Earth (BSE) has begun to emerge, but necessitates a new review and synthesis of available data (Fig. 2.1).

Similar to C (Holland, 1984), N is cycled in the Earth system in two ways: a fast, biologic cycle; and a slow, geologic cycle. Descriptions of biologic (Kelly, 2000) and geologic (Boyd, 2001; Holloway & Dahlgren, 2002; Kerrich et al., 2006) N cycles exist, but no adequate Earth system-wide picture of the fast and slow N cycles together is currently available. Briefly, the biologic cycle (for the modern Earth) is as follows: N_2

in the atmosphere dissolves in the ocean and is converted to a biologically available form by N-fixing bacteria. This process is termed N-fixation. Nitrogen-fixing bacteria are either consumed by other organisms, or release N in waste, primarily as NH_4^+, which is quickly oxidized to NO_3^- in a bacterially [1] -mediated process called nitrification. The primary return flux of N to the atmosphere is via denitrification, where NO_3^- is used by certain bacteria as the terminal acceptor in the electron transport chain and converted to either N_2 or N_2O. Recently, the importance of an additional reaction, anaerobic ammonium oxidation or anammox has been recognized as a return flux of N to the atmosphere (Thamdrup, 2012). This is another bacterially mediated process whereby NH_4^+ reacts with NO_2^- to produce N_2 and two H_2O molecules.

The slow geologic cycle begins when dead organic matter sinks and settles in oceanic sediment. Organic N breaks down in the sediment via hydrolysis reactions, and converts to NH_4^+ (Hall, 1999). Since NH_4^+ has the same charge and a similar ionic radius as K^+, it substitutes into mineral lattice sites that are normally occupied by K^+. Clay minerals, micas, and K-feldspars are important mineral hosts of N. Once entrained in oceanic sediments and crust, N is carried into subduction zones, where it is either volatilized and removed from the down-going plate or carried into the mantle past the subduction barrier. In general, subduction zones with high geothermal gradients favour volatilization (Elkins et al., 2006), while cooler subduction zones favour N retention (Mitchell et al., 2010). Volatilized N either oxidizes to N_2 and escapes via arc volcanism or is incorporated into intrusive igneous rocks. Nitrogen that is not returned to the surface becomes entrained in mantle circulation. Basalts at both mid-ocean ridges (MORB) (Marty, 1995) and ocean islands (OIB) (Mohapatra et al., 2009) show evidence for this surface-derived N, through either positive δ^{15}N values[2] (OIB) or correlation with radiogenic Ar (Sec. 2.5.1).

While the general outline of the geologic N cycle is known, in order to more fully quantify this cycle and describe changes in it over Earth history, we calculate a thorough inventory of the N on Earth. This is a necessary step to accurately portray the Earth-system nature of the N cycle. To achieve this goal we present

[1] and Archaea

[2] Stable isotope notations are in per mil (‰) notation, where

$$\delta^X\mathrm{E}(‰) = \left(\frac{{}^X\mathrm{E}/{}^x\mathrm{E}_{sample}}{{}^X\mathrm{E}/{}^x\mathrm{E}_{standard}} - 1\right) * 1000 \tag{2.1}$$

E is element of interest, X is heavy isotope, x is light isotope. δ^{13}C standard is V-PDB and the δ^{15}N standard is N_2 in air, which have a δ^{13}C or δ^{15}N value of 0‰ by definition.

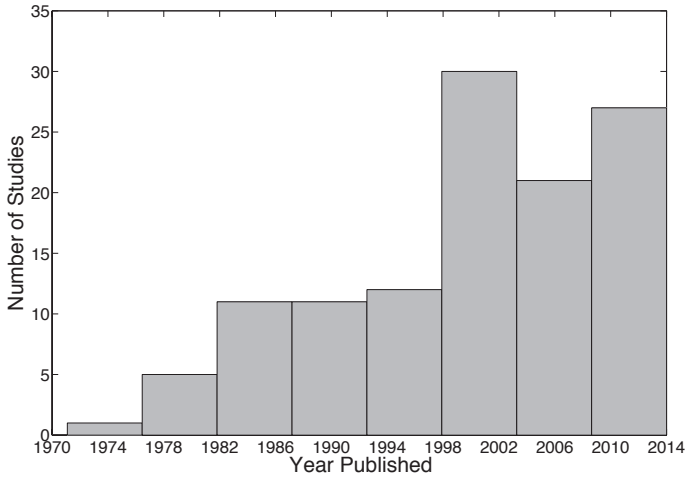

Figure 2.1: Number of studies measuring N in geologic materials since 1975. The number of studies has increased as detection capability improves. Data produced after the mid 1990s have not been incorporated into a broad, Earth system perspective on the N cycle.

two approaches: a "top-down" and "bottom-up" budget estimates. The "top-down" approach uses the composition of planetary building blocks and analogues to bracket total Earth N content. We then subtract the amount of N in the core to estimate BSE N content. For the "bottom-up" approach, we compile analyses of N in terrestrial rocks and minerals. We use these to estimate N concentration in various reservoirs: oceanic and continental sediments, oceanic and continental crust, and the mantle. We also use observed relationships between N and Ar from basalts to estimate the mantle N content. In addition, we briefly discuss the behaviour of N in specific reservoirs. Our approach differs from past attempts by utilizing an extensive literature compilation in conjunction with new experimental results to provide a thorough, comprehensive assessment of the N in all reservoirs of the Earth.

The structure of the paper is to first present description of the speciation and behaviour of N in the solid Earth, then a brief discussion of the data compilation used herein; this is followed by the two budget approaches, and finally a discussion of the implications of results. We present a discussion of N speciation and solubility first to serve as orientation, as N can exist as different species in the Earth depending on physical and chemical conditions. A flurry of recent experiments have elucidated many aspects of N solubility in silicate minerals (Li et al., 2013), metal alloys (Roskosz et al., 2013), and fluids (Li & Keppler, 2014).

Ultimately, we find that both approaches are mutually consistent. Chondritic

Table 2.1: Previous estimates for the N budget of the silicate Earth. There is significant disagreement between estimates, necessitating a more comprehensive approach. All values are 10^{18} kg N

Reservoir	**Amount**	**Reference**
BSE	2.78	Halliday (2013)
Mantle	5	Marty (2012)
	$\geq 8.4 \pm 5.2$	Goldblatt et al. (2009)
Continental Crust	2.1 ± 1.1	Goldblatt et al. (2009)
	1.1	Rudnick & Gao (2003)
		Rudnick & Gao (2014)
	1.3	Wedepohl (1995)
	14	Delwiche (1970)
Continental Sediments	4	Delwiche (1970)

comparison suggests between $17 \pm 13 \times 10^{18}$ kg to $31 \pm 24 \times 10^{18}$ kg N in the BSE; terrestrial compilation suggests $27 \pm 16 \times 10^{18}$ kg N in the BSE. Our work not only suggests a higher N mass in the BSE than previous work (Goldblatt et al., 2009), it arrives at approximately the same value from two independent tactics. A higher N content may have important implications for the geochemical history of N on the Earth. In addition, our budget allows for a reassessment of the overall N-isotopic composition of the planet, which is used to track interaction between various reservoirs on the Earth. These implications are detailed in our discussion (Sec 2.6).

2.3 Nitrogen speciation in geologic materials, experimental results, and budget tools

In this section, we first summarize which N species are found in geologic materials, highlighting silicate rocks and minerals, fluids, and Fe-metal. Secondly, we incorporate recent experimental work to attempt to quantitatively describe N behaviour in geologic materials in response to changes in pressure, temperature, and oxygen fugacity. Thirdly, we describe the database used for subsequent budget calculation. Details pertinent to specific reservoirs will be discussed in the appropriate sections.

2.3.1 Nitrogen speciation in the solid Earth

Nitrogen is present as a number of species in the solid Earth. The primary control on speciation is redox, with temperature, pressure, and even pH playing roles in stability and solubility. Oxygen fugacity (f_{O_2}) is presented relative to some mineralogically controlled buffer (Frost, 1991). Buffers used in this study, in order of decreasing f_{O_2}, are Nickel-Nickel Oxide (NiNiO), Fayalite-Magnetite-Quartz (FMQ), and Iron-Wüstite (IW). Important N species in the solid Earth are, in order of decreasing oxidation state, N_2 (fluid inclusions and degassing magmas) (Marty, 1995), NH_3 (in reduced fluids) (Li & Keppler, 2014), NH_4^+ (stably bound in mineral lattices) (Itihara & Honma, 1979), and nitrides (e.g., FeN) (Adler & Williams, 2005). Small differences in pH (Mikhail & Sverjensky, 2014), especially in the mantle, may also exert some control over N speciation, though this is likely secondary when compared with f_{O_2}.

There are three important reservoirs that contain the various species of N: silicate rocks and minerals, fluids and magmas, and Fe-metal. In general, N in silicate rocks and minerals is found in reduced forms, as either organic material or, more importantly for stable geologic incorporation, as NH_4^+. While there are examples of N-silicates (e.g., buddingtonite ($NH_4AlSi_3O_8$) and tobelite ($(NH_4,K)Al_2(Si_3Al)O_8(OH)_2$)), a much more important path for N incorporation into minerals is the substitution of trace amounts of NH_4^+; this mechanism is the most geologically stable way for N to be found in minerals and rocks. Ammonium has, depending on coordination, an ionic radius that is < 0.2 Ålarger than the ionic radius of K^+ (1.61–1.69 vs. 1.46–1.63), and can readily substitute into K-bearing minerals (Whittaker & Muntus, 1970; Khan & Baur, 1972) or for Na and Ca in plagioclase feldspars (Honma & Itihara, 1981). Indeed, K and N concentrations are correlated in sedimentary (especially metasedimentary) rocks, though this relationship is less clear in other rock types (Busigny et al., 2005b). The source of the NH_4^+ can either be dead organic matter, which breaks down into amino acids and is subsequently hydrolyzed during burial, or some previous inorganic source (Hall, 1999). In general, N concentrations decrease with increasing metamorphic grade (Haendel et al., 1986; Bebout & Fogel, 1992), though the NH_4^+-Si bond can be quite resilient during metamorphism (Pitcairn et al., 2005; Palya et al., 2011). It is also possible for N to be found as N^{3-} (Libourel et al., 2003), which can substitute for O^{2-} in silicate lattices or bond with metals (Roskosz et al., 2013).

In contrast with silicate rocks and minerals, most fluids and magmas originating

from the crust or upper mantle are oxidizing, with an f_{O_2} near the (FMQ) buffer. At fugacity near FMQ, both natural samples (Marty, 1995; Nishizawa et al., 2007) and experimental results (Libourel et al., 2003; Li & Keppler, 2014) show that N_2 is the dominant N species in magmas and fluids. At more reduced (f_{O_2} <FMQ) conditions, NH_3 becomes stable in fluids, and may even dominate in some crustal and upper mantle conditions (Li & Keppler, 2014).

The third important reservoir for N is Fe-metal. Nitrogen is quite soluble in Fe-metal alloys at a variety of depths in the Earth (Kadik et al., 2011; Roskosz et al., 2013). It likely either dissolves as NH_3 or forms Fe-N (nitride) compounds. This has important ramifications for the N distribution in the Earth. Not only could significant N be found in Earth's core, Fe-Ni metal may be present in the mantle transition zone and lower mantle (Frost & McCammon, 2008). There might be $\leq$10 wt.% N in FeNi-metal and $\leq$0.5 wt.% N in silicates in the transition zone and lower mantle (Roskosz et al., 2013). These concentrations indicate that an enormous quantity of N are theoretically plausible in the deeper domains of the mantle. This is discussed in more detail later.

Since N concentrations in geologic materials are usually quite low, analytical techniques present a non-trivial obstacle. A thorough discussion on this subject is provided by both Holloway & Dahlgren (2002) and Bräuer & Hahne (2005). Briefly, N can be measured by dissolution/combustion and analysis on a mass spectrometer, spectral methods, Kjeldahl extraction, or colorimetric methods. These techniques continue to evolve and improve (Yokochi & Marty, 2006; Barry et al., 2012), and the availability of quality N data from rocks will continue to grow.

2.3.2 Experimental results

We have compiled experimental results to augment the discussion in the previous section and to quantitatively describe the N solubility of geologic materials (Figs. 2.2-2.3). Measurements have been made for N in minerals (Li et al., 2013), silicate melt (Libourel et al., 2003; Mysen et al., 2008; Mysen & Fogel, 2010; Mysen et al., 2014), Fe-metal (Kadik et al., 2011; Roskosz et al., 2013), and aqueous fluids (Li & Keppler, 2014; Li et al., 2015). Experimental conditions are variable (e.g., different starting materials, presence of alkalis, etc.), so at times trends are only visible when discussing single studies. Most studies use a basaltic composition for silicate components, with one using a more felsic, haplogranite material (Li et al., 2015). In spite of these

differences, however, general observations can be made from these data. Importantly, results allow for calculation of N capacity and/or contents in poorly or unsampled reservoirs in the Earth, such as the core (Sec. 2.4.2) and parts of the mantle (Sec. 2.5.5.2).

Pressure, temperature, and f_{O_2} all have an effect on N solubility in silicate melts, Fe-metal, and aqueous fluids. A first order observation is that N concentration appears to always be higher in fluids, melts, and Fe-metal than in coexisting silicate minerals (Fig. 2.2). This is especially clear when the distribution coefficients ($D_{metal/fluid} = [N_{metal/fluid}]/[N_{silicate}]$) are calculated (Fig. 2.3). At all measured conditions, N prefers metal or fluid over silicates.

Increasing pressure has noticeable effects on N solubility in silicates and metals, while the effect is less clear in fluids. Silicate N concentration increases with pressure, and, at least in the presence of Fe-metal, saturates at 0.64 wt.% at pressures above about 5 GPa (Roskosz et al., 2013). At lower pressures, solubility appears to follow a Henry's law relationship, given by:

$$[N]_S = k_H p \tag{2.2}$$

where $[N]_S$ is in wt.%, k_H is 0.128 wt.% GPa^{-1}, and p is pressure (GPa). Concentration in Fe-metal also increases with pressure, and appears to be described by a Sievert's law equation:

$$[N]_M = k_s \sqrt{p} \tag{2.3}$$

where $[N]_M$ is in wt.%, k_s is an experimentally determined constant (3.06 wt.% $GPa^{-1/2}$), and p is pressure (GPa). The pressure effect in aqueous fluids appears to be equivalent to silicates and metal, but experiments have been done only at lower pressures (Li et al., 2015).

Increasing temperature results in a decrease in N content in silicate melts (Fig. 2.2). The effect is most clearly seen in data from individual studies (Libourel et al., 2003; Mysen et al., 2008). Higher temperatures favour formation of N_2, which is more easily removed from silicate melts via extraction in fluids. Figure 2.3 shows this well: higher temperature is associated with a higher D_{fluid}. This is partially due to the instability of N-H bonds at high temperature. Experiments done at the highest temperatures have Fe-metal in equilibrium with silicates, and since N-solubility in metal increases with increasing temperature, it is likely that N was lost from the silicates and taken up by the Fe-metal in these experiments (Roskosz et al., 2013).

In contrast, f_{O_2} has a fairly strong effect on N solubility, and especially N partitioning between silicates and fluids (Fig. 2.3). In each experiment shown here, decreasing f_{O_2} results in higher N content in silicates. This effect is less clear in metal, though these experiments were carried out at a narrower f_{O_2} range, and f_{O_2} must be at or below the IW buffer ($= \Delta\text{NNO} - 4$) to even have Fe-metal stable in the experiment. Since oxidizing conditions promote N speciation as more fluid-mobile N_2, as opposed to NH_4^+, D_{fluid} tends to decrease with decreasing f_{O2} as well. While the magnitude of the f_{O_2} effect is different between different studies, the direction is the same throughout: lower f_{O2} results in higher N contents in silicates.

There are also some measurements of N-contents in minerals directly. We utilize equations, described by Li et al. (2013), of N solubility experimental results for olivine, pyroxene, and melt (in the absence of Fe-metal) to guide both estimates of N concentration and distribution coefficients (described below) between minerals and melt in poorly sampled reservoirs:

$$\text{Olivine}: \ \log_{10}[\text{N}] = 2.15 - \frac{6.8 \times 10^3}{\text{T}} + 0.27\text{P} - 0.43\Delta\text{NiNiO}; \ \text{r}^2 = 0.79 \tag{2.4}$$

$$\text{Pyroxene}: \ \log_{10}[\text{N}] = 6.48 - \frac{8.7 \times 10^3}{\text{T}} + 0.086\text{P} - 0.122\Delta\text{NiNiO}; \ \text{r}^2 = 0.64 \tag{2.5}$$

$$\text{Melt}: \ \log_{10}[\text{N}] = 0.92 - \frac{3.50 \times 10^3}{\text{T}} + 0.4\text{P} - 0.083\Delta\text{IW}; \ \text{r}^2 = 0.70 \tag{2.6}$$

The above equations have temperature (T) in K, pressure (P) in GPa, ΔNiNiO or ΔIW is the f_{O_2} relative to the NiNiO or IW buffer, and [N] is in ppm. At appropriate conditions, concentrations of up to 100 ppm may be possible in the lowermost upper mantle (Li et al., 2013), which means the upper mantle may have the capacity to sequester $\sim 80 \times 10^{18} - 200 \times 10^{18}$ kg N, which is $20 - 50$ times PAN.

The last tool based on experiments we utilize is measured or inferred partition coefficients
(K_D $=[\text{Element}]_{\text{mineral}}/[\text{Element}]_{\text{melt}}$); these are often used in conjunction with an equation linking partition coefficients to degree of partial melting (Rollinson, 1993).

$$\frac{[\text{C}_\text{L}]}{[\text{C}_\text{o}]} = \frac{1}{\text{K}_\text{D} + \text{F}(1 - \text{K}_\text{D})} \tag{2.7}$$

$[\text{C}_\text{o}]$ is element concentration in source and $[\text{C}_\text{L}]$ is concentration in melt, and F is degree of partial melting. Note that this equation is for batch (equilibrium) melting,

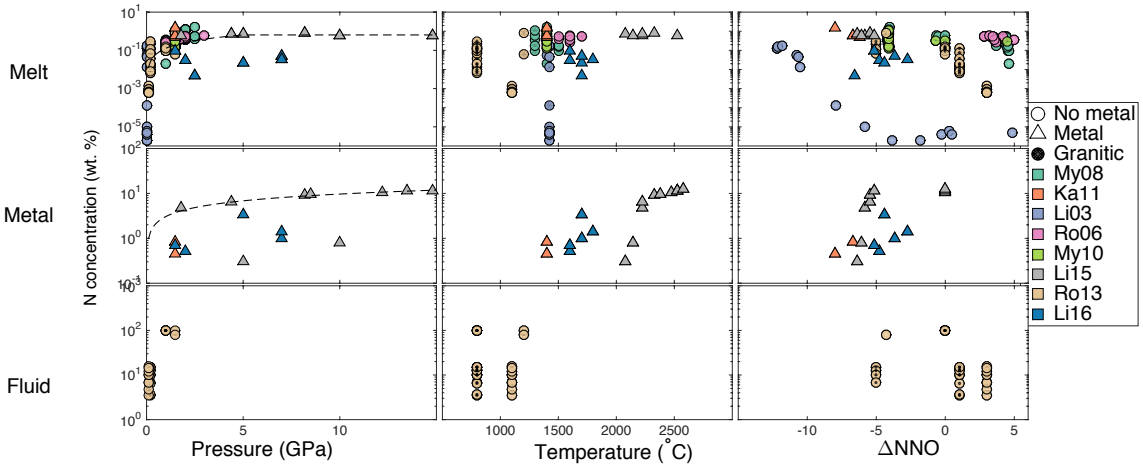

Figure 2.2: Compilation of recent experiments measuring N solubility in silicate melts, Fe-metal, and aqueous fluids. Experiments that have silicate and Fe-metal in equilibrium (Δ) and those with no metal ($\circ$) are shown. Note log scale for N concentration. Different colours refer to specific studies: My08 (Mysen et al., 2008), Ka11 (Kadik et al., 2011), LI03 (Libourel et al., 2003), Ro06 (Roskosz et al., 2006), My10 (Mysen & Fogel, 2010), Li13 (Li et al., 2013), Ro13 (Roskosz et al., 2013), and Li15 (Li et al., 2015). All experimental runs used basaltic composition, aside from the few marked "Granitic". We show concentrations as a function of pressure, temperature, and f_{O_2} (relative to the NiNiO buffer) for all three phases. Dashed lines are empirical fits to data, shown in the text (Eq. 2.2-2.3). Vertical dashed line in ΔNNO plots represent the IW buffer (ΔNNO-4), below which Fe-metal is stable. While f_{O_2} is the primary control on N speciation, pressure appears to be very important in solubility.

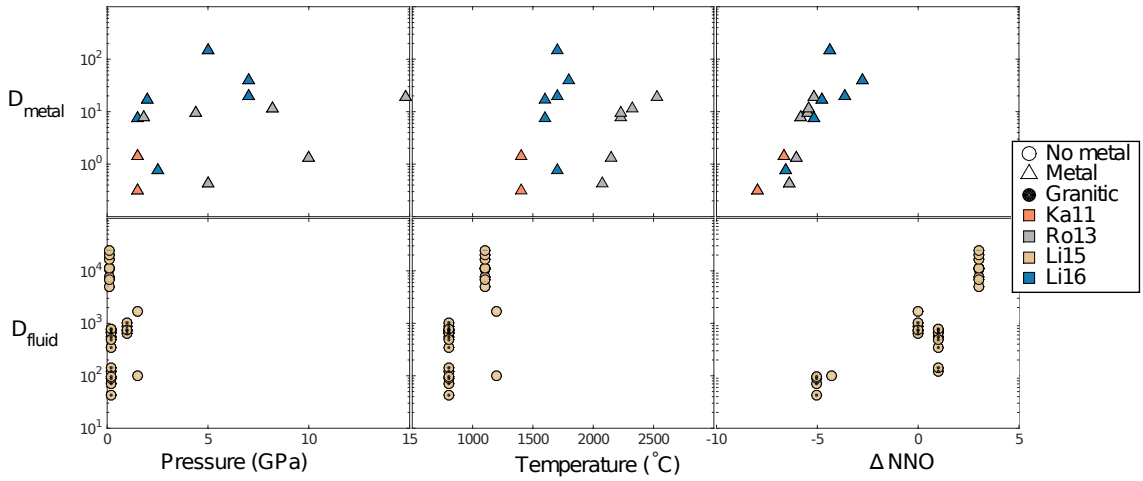

Figure 2.3: Distribution coefficients for metal:silicate melt (top row) and fluid:silicate melt (bottom row) as a function of temperature, pressure, and f_{O_2} (relative to the NiNiO buffer). Increasing pressure and temperature increases D_{metal}. Increasing pressure decreases D_{fluid}, and temperature seems to have a negligible effect. As f_{O_2} increases, N solubility in fluids increases, likely because N is present as N_2. References and symbols are the same as Fig. 2.2.

which means that melt formed equilibrates with residual solids. We assume that any melt must reach a critical threshold ($\sim 1 - 10\%$) before extraction from the source rock, and prior to extraction it would have time to equilibrate fully with residual solids.

2.3.3 Database of geologic N measurements

We have compiled all of the available, published measurements of N concentration and δ^{15}N values of geologic materials. Where they exist, we also include in the database δ^{13}C, age of sample, Ar-isotope ratios and abundance, and concentrations of elements that behave similarly to NH_4^+, including K_2O, Rb, Lu, and Yb. The complete database is available in the supplementary material, which is organized by both rock names, as given in the original publications, and our interpreted geologic settings,

While rock names follow standard naming procedure, we also categorize data based on geologic setting. Unmetamorphosed samples are labeled as oceanic sediments (OS), oceanic lithosphere (OL), continental sediments (CS), and continental lithosphere (CL). Altered reservoirs (i.e., metamorphosed at T < 300 °C) are prefixed with 'A'; those metamorphosed at T > 300 °C are prefixed with 'M'. Data for the mantle are from diamonds (D) and xenoliths (X). We also discuss mid-ocean ridge basalts (MORB) and ocean island basalts (OIB). These reservoirs will be addressed individually in following sections.

Nitrogen concentration from most reservoirs are log-normally distributed. To calculate N mass in a given reservoir, we will generally use the product of the log-normal mean of N concentration and mass of that reservoir. As sample size is often low, we calculate maximum likelihood estimator parameters $\hat{\mu}$ and $\hat{\sigma}^2$, which are the mean and variance of the natural log of concentration, respectively (Limpert et al., 2001).

$$\hat{\mu} = \frac{\sum_i \ln[\mathrm{N}]_i}{n} \tag{2.8}$$

$$\hat{\sigma}^2 = \frac{\sum_i (\ln[\mathrm{N}]_i - \hat{\mu})^2}{n} \tag{2.9}$$

Where n is the number of samples. These parameters are then used to estimate the mean (μ) and standard deviation (σ) of the total population:

$$\mu \simeq \bar{x} = e^{\hat{\mu} + \frac{\hat{\sigma}^2}{2}} \tag{2.10}$$

$$\sigma = \sqrt{(e^{\hat{\sigma}^2} - 1)e^{2\hat{\mu}+\hat{\sigma}^2}} \tag{2.11}$$

Unless otherwise specified, all errors given are standard error of the mean:

$$\mathrm{SE}\bar{x} = \frac{\sigma}{\sqrt{n}} \tag{2.12}$$

2.4 "Top-down" Budget: Accretion through Core formation

In this section, we estimate the N budget of the BSE by comparing the Earth to other inner solar system bodies. The atmosphere of Venus hints that there is more N in the Earth than is found in its atmosphere alone. We bracket mass of N delivered to Earth during accretion by comparison to chondritic compositions. From this, we subtract N sequestered into the core to estimate the remainder in the BSE and atmosphere. While this model is dependent on the N content of accretionary material, we find that it is in reasonable agreement with our terrestrial-based budget, presented in Section 2.5. In addition, the N content of the Moon is calculated, as this may provide some constraints on the composition of the early, but post-core formation, mantle.

2.4.1 Initial N composition and planetary comparison: missing N?

Some motivation for this study comes from comparison of the Earth to extraterrestrial bodies: meteorites and Venus. Undifferentiated meteorites are leftover remnants from the early history of the Solar System, and are often used as proxies for the bulk composition of the protoplanetary disk. Venus is thought to have had a similar initial volatile composition as the Earth (Ringwood & Anderson, 1977; Lécuyer et al., 2000; Chassefière et al., 2012). Comparison to both meteorites and Venus suggest that the Earth should have much more N than is found in the present atmosphere; by extension, we posit that the atmosphere is not the major N reservoir on Earth.

We address Venus first. The Venusian atmosphere contains $3.5 \pm 0.8\%$ N_2, with the remainder composed of predominately (96.5%) CO_2 (von Zahn et al., 1983). We calculate the mass of N (M_{N_2}) in the atmosphere by using the following equation:

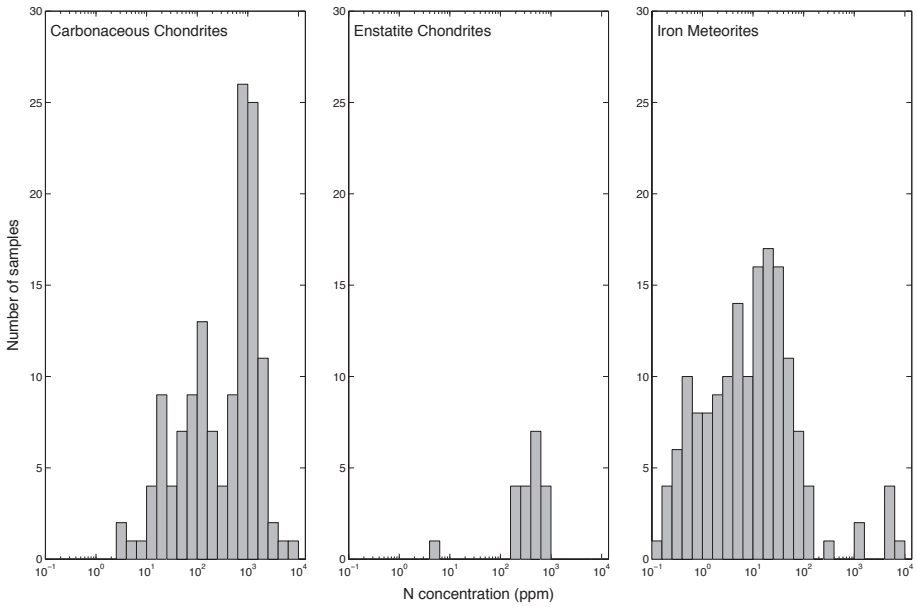

Figure 2.4: Nitrogen concentration in carbonaceous chondrites (CC), enstatite chondrites (EC), and iron meteorites. Nitrogen content of both CC (1235 ± 440 ppm) and EC ($605 \pm 2 - 6$ ppm) are significant, and suggest many atmospheric masses of N were delivered to the Earth during accretion. Iron meteorites are presented as a proxy for N content of the core (140 ± 10 ppm, Sec. 2.4.2 See Appendix A for data table.

$$\mathrm{M_{N_2}} = \frac{\mathrm{m_{N_2}}}{\mathrm{m_a}} \cdot x_{\mathrm{N_2}} \cdot \frac{4\pi \mathrm{r}^2 \mathrm{p}}{\mathrm{g}} \tag{2.13}$$

where $\mathrm{m_{N_2}}$ and $\mathrm{m_a}$ are molar masses of N_2 (0.028 kg mol^{-1}) and Venus' atmosphere (0.04344 kg mol^{-1}); $x_{\mathrm{N_2}}$ is the mixing ratio of N_2 (0.035); r is the radius of Venus (6.052×10^6 m); p is surface pressure (9.2×10^6 Pa); and g is acceleration due to gravity (8.87 m s^{-2}). The resulting N content of Venus' atmosphere is 11×10^{18} kg N. When normalized to planetary mass, Venus' atmosphere has 3.4 times the mass of N in Earth's atmosphere. Given similar initial volatile composition, Earth should have substantial N in non-atmospheric reservoirs. Curiously, the amount of C in the Venusian atmosphere (as CO_2) is nearly identical to the amount of C in carbonate rocks on Earth (Taylor, 1992; Berner, 1998; Lécuyer et al., 2000). If a similar mass balance exists for N, then a substantial amount of N must be in geologic reservoirs on Earth.

Whilst the exact nature and composition of planetary accretionary bodies are a matter of debate, (Marty, 2012; Halliday, 2013), some combination of chondrite-like

material accreted to form the rocky planets, including Earth. The volatile content of these bodies is thought to have decreased with distance from the Sun, though the feeding zones of growing planets may be substantial (Kaid & Cowan, 2015). We bracket terrestrial N content by using volatile-poor enstatite chondrites (EC) and volatile-rich carbonaceous chondrites (CC) as analogs for possible volatile delivery material. Note we are not attempting to find a "perfect fit" meteorite to explain terrestrial volatiles, but simply providing some context for how much N should be present in the planet.

To utilize N contents of chondrite proxies, we follow the approach of Marty (2012) for both CC and EC. Marty compared two chondrites' (Orguiel and Murchison) volatile abundances to a calculated volatile budget for the Bulk Earth (BE). These specific meteorites were chosen as they are primitive in composition and have experienced low grades of metamorphism. We include both a broader suite of CC and EC analyses. Both chondrite types have substantial N content: EC have an average N concentration of 605 ± 206 ppm and CC 1235 ± 440 ppm (Fig. 2.4).

Non-N volatile elements (e.g., C, H_2O, halogens) appear to be depleted in the Earth relative to chondritic concentration (Marty, 2012). These volatiles are expected to have negligible concentrations in the core, which is likely not the case for N, as discussed in the next section. Therefore, we assume that the abundance calculated by Marty for the BSE plus atmosphere accounts for the total abundance, and differences from chondritic values are due to processes during accretion/delivery. Note that we exclude Xe from this comparison, as it is more depleted than other volatiles, and requires explanation beyond the scope of this paper (Pujol et al., 2011).

Overall, we show that the Earth appears to be depleted by about an order of magnitude compared to chondritic values (Table 2.2), which is consistent with (Marty, 2012). Using only Orguiel (CI-chondrite) and Murchison (CM-chondrite) suggests terrestrial volatiles are $2.48 \pm 0.3\%$ as abundant as they are in CI/CM-chondrites. Incorporating analyses of a broader suite of CC gives an indistinguishable volatile abundance pattern, with terrestrial volatiles $2.75 \pm 0.2\%$ as abundant as CC. The latter is adopted here. Enstatite comparison yields less consistent results, though are within an order of magnitude ($9.2 \pm 0.1\%$). This value was calculated without Ne-abundance, as this appears to be distinct from other volatiles (Table 2.2).

If N behaved similarly to other volatiles during accretion/delivery, the abundance values can be used in concert with N concentrations of CC and EC to calculate BE N. Multiplying CC N content (1235 ± 440 ppm) by BE/CC abundance ($2.75 \pm 0.2\%$) gives

BE N mass of $204 \pm 75 \times 10^{18}$ kg N; the same calculation with EC N content (605 ± 206 ppm) and EC/BE abundance of $9.2 \pm 0.1\%$ gives BE N mass of $330 \pm 120 \times 10^{18}$ kg N. These masses are equivalent to a BE N concentration of 34 ± 12 ppm and 55 ± 20 ppm, respectively. For comparison, both N mass estimates are two orders of magnitude greater than the mass of N in the present atmosphere (4×10^{18} kg).

While the preceding approach is appropriate if N had similar behaviour to noble gases, water, and C during accretion, it is possible that N may have existed in reduced forms in the protoplanetary disk. Ammonia in comets is well known (Oró, 1961), and recent identification of NH_3 as inclusions in primitive chondrites indicates that reduced N was also present in the chondrite-forming region of the solar system (Harries et al., 2015). If N was found as NH_4^+ in significant quantities in the Earth-forming region, it may have behaved more like K or Rb than noble gases. We note that NH_3 was likely found mostly in ices, and its behaviour would be quite different than NH_4^+ substituting into silicate lattices or Fe-metal. The following discussion assumes N was found as NH_4^+ in the Earth-forming region[3] .

Estimates of BE N based on K and Rb content of CC and EC are higher than noble gas constraints (Table 2.3). EC have higher K (770 ppm) and Rb (2.5 ppm) concentrations than CC ([K]=400 ppm, [Rb]=1.7 ppm) (Wasson & Kallemeyn, 1988). The Bulk Earth (BE) has 280 ppm K (Arevalo et al., 2009) and 0.6 ppm Rb (Palme & O'Neill, 2014). These abundances suggest the Earth has about 1/3 as much K or Rb as chondrites. If N behaved like K or Rb, it would have a very large mass in the BE of between $870 - 5200 \times 10^{18}$ kg N (Table 2.4). Since N is likely more volatile than K and Rb, this provides a strict upper limit on N abundance in the Earth. For the remainder of the paper we adopt the CC- and EC-volatile based proxy, but do not exclude N behaving somewhere in between more volatile elements and K or Rb during planetary formation.

It should be noted that neither class of chondrite appear to fully satisfy the isotope composition of volatile elements on Earth. Both EC (Grady et al., 1986) and CC (Pearson et al., 2006) have δ^{13}C values similar to the mantle value of -5‰. A significant problem with EC as proxy for volatile delivery is that they have negligible water content, and therefore very low H. In contrast, CC are more water-rich and have δD values are more or less consistent with at least the surface reservoirs of

[3]Recent analysis by Harries et al. (2015) has found the presence of carlsbergite (CrN) in sulfide minerals in primitive chondrites, indicating that ammonia-bearing ices were in the Earth-forming region of the proto-planetary disk.

Earth (Marty, 2012). The δ^{15}N values of the mantle ($-35‰$ to $-5‰$) match more closely with EC, $\sim -35‰$ (Grady et al., 1986), than with CC, which are variable, but consistently positive (Pearson et al., 2006).

Table 2.2: Estimated volatile concentrations for C, H_2O, Ne, Ar, and Kr in chondrites after Marty (2012), used to estimate volatile retention during accretion. Shown are concentrations in CI-CM chondrite (CI/CM), the most primitive carbonaceous chondrites, analyses from all classes of carbonaceous chondrites (CC), enstatite chondrite (EC), and bulk Earth (BE, which is BSE plus atmosphere). We do not include Xe, which is depleted compared to chondrites and other volatiles and requires additional explanation beyond the scope of this paper. Concentrations are in mol g^{-1}, and abundances are shown in percent. References are indicated with superscripts. Errors for concentrations are 1σ. Abundance errors are shown as $SE_{\bar{x}}$, with 1σ values given in parentheses. We calculated $SE_{\bar{x}}$ based on 1σ values and number of analyses for each volatile. $SE_{\bar{x}}$ are used in subsequent calculations.

Species	**CI/CM**[1] **(mol g^{-1})**	**CC**[2–3] **(mol g^{-1})**	**EC**[4–6] **(mol g^{-1})**	**BE**[1] **(mol g^{-1})**	**BSE/CI-CM (%)**	**BSE/CC (%)**	**BSE/EC (%)**
^{12}C	$2.00 \pm 0.2 \times 10^{-3}$	$2.23 \pm 2.2 \times 10^{-3}$	$3.75 \pm 0.4 \times 10^{-4}$	$4.38 \pm 1.7 \times 10^{-5}$	2.19 ± 0.5 (1.4)	1.96 ± 0.2 (2.0)	11.7 ± 2.3 (7.4)
H_2O	$5.50 \pm 0.9 \times 10^{-3}$	$7.50 \pm 1.8 \times 10^{-3}$	–	$1.50 \pm 0.7 \times 10^{-4}$	2.74 ± 0.7 (1.9)	2.00 ± 0.3 (1.4)	–
^{22}Ne	$2.68 \pm 0.2 \times 10^{-12}$	$3.49 \pm 0.5 \times 10^{-12}$	$4.28 \pm 0.2 \times 10^{-12}$	$2.66 \pm 0.02 \times 10^{-14}$	0.99 ± 0.2 (0.5)	0.76 ± 0.1 (0.8)	0.620 ± 0.1 (0.8)
^{36}Ar	$4.51 \pm 0.1 \times 10^{-11}$	$3.36 \pm 0.8 \times 10^{-11}$	$2.22 \pm 0.9 \times 10^{-11}$	$1.01 \pm 0.03 \times 10^{-12}$	2.24 ± 0.7 (1.8)	3.01 ± 0.5 (4.4)	4.55 ± 1.0 (8.0)
^{84}Kr	$4.98 \pm 0.1 \times 10^{-13}$	$1.23 \pm 0.3 \times 10^{-13}$	$1.06 \pm 0.2 \times 10^{-13}$	$2.10 \pm 0.07 \times 10^{-14}$	4.22 ± 1.3 (3.4)	6.03 ± 1.0 (8.3)	19.8 ± 3.1 (24)
Average abundance					2.48 ± 0.3 (1.0)	2.75 ± 0.2 (2.0)	9.2 ± 0.1 (5.3)

[1] (Marty, 2012), [2] (Mazor et al., 1970) [3], (Bogard et al., 1971), [4] (Crabb & Anders, 1981), [5](Patzer & Schultz, 2002), [6](Grady & Wright, 2003)

Table 2.3: Concentrations of K and Rb in carbonaceous chondrites (CC) and enstatite chondrites (EC), compared to their abundance in the BSE (BE). If N were present in the solar nebula as NH_4^+, it may behave more similarly to these alkali elements than to noble gases. It is likely, however, that N would be more volatile than either K or Rb, so these represent upper limit estimates for N abundance in the BSE, compared to chondrites.

Species	**CC (ppm)**	**EC (ppm)**	**BE (ppm)**	**BE/CC (%)**	**BE/EC (%)**
Rb	1.7	2.5	0.6	35	24
K	400	770	280	70	36

Table 2.4: Total Earth, core, and BSE N masses based on abundances (noble gas and K or Rb) calculated above and other proxies. Calculations from volatile and K or Rb proxies use distribution coefficients between silicate and Fe-metal at pressures and temperatures appropriate for core formation (Roskosz et al., 2013). Details are presented in the text. Additional core N estimates are obtained from thermodynamic calculation (Zhang & Yin, 2012) and analysis of iron meteorites (Grady & Wright, 2003). "Atm" is the current atmosphere (4×10^{18} kg N). All values are in 10^{18} kg N. We use the CC- and EC-volatile estimates in the remainder of the text, and these are shown in bold. Errors are $SE_{\bar{x}}$

Proxy	**Bulk Earth N**	**Bulk Earth N (ppm)**	**Core N mass**	**Core N (ppm)**	**BSE+Atm**	**BSE only**	**BSE only (ppm)**
CC-volatile	$\mathbf{204 \pm 75}$	$\mathbf{34 \pm 12}$	$\mathbf{180 \pm 110}$	$\mathbf{102 \pm 63}$	$\mathbf{21 \pm 17}$	$\mathbf{17 \pm 13}$	$\mathbf{4.1 \pm 3.1}$
EC-volatile	$\mathbf{330 \pm 120}$	$\mathbf{55 \pm 20}$	$\mathbf{300 \pm 180}$	$\mathbf{165 \pm 100}$	$\mathbf{35 \pm 28}$	$\mathbf{31 \pm 24}$	$\mathbf{7.3 \pm 5.6}$
K-CC	5200 ± 1850	864 ± 310	4600 ± 3500	2580 ± 2000	530 ± 400	526 ± 396	128 ± 116
Rb-CC	2600 ± 880	430 ± 150	2300 ± 1800	1300 ± 1000	270 ± 250	255 ± 246	64 ± 58
K-EC	1300 ± 500	220 ± 74	1100 ± 900	650 ± 500	140 ± 125	136 ± 121	32 ± 29
Rb-EC	870 ± 300	145 ± 50	780 ± 600	430 ± 330	90 ± 80	86 ± 76	19 ± 0.8
Iron Meteorite			250 ± 20	140 ± 10			
Thermodynamic calculation			1.8 ± 0.2				

2.4.2 Core Formation, N sequestration, and remaining BSE N content

Now that we have established some estimates for initial N content, the next step is to model N behaviour during core formation; some N was likely incorporated into the core. Core formation occurred as gravitational separation of Fe, Ni, and additional elements from silicates during accretion. Nitrogen is siderophile (soluble in metal-Fe) under reducing conditions, allowing large quantities of N to be scavenged during core formation. Because the core is geochemically isolated from the BSE (Halliday, 2004), any scavenged N is effectively removed from the rest of the planet. It is therefore important to constrain how much N is in the core, which will be subtracted from a chondritic starting composition.

There are several types of constraints provided (Table 2.4). The first is N measurements from iron meteorites, which are derived from cores of planetesimals formed early in the solar system's history (Grady & Wright, 2003). While variable, these meteorites have an average N content of 138±12 ppm (Fig. 2.4), mostly contained in the mineral taenite ($Fe_{0.8}Ni_{0.2}$). If iron meteorites are a good proxy for the core, it contains $250 \pm 20 \times 10^{18}$ kg. Secondly, there are calculations, based on thermodynamic properties, indicating the partition coefficient between liquid iron and silicate melt (K_D=$[N]_{metal}/[N]_{silicate}$) of 1.8±0.2. This suggests 0.001 wt% N in the core, for a N content of $1.8 \pm 0.2 \times 10^{18}$ kg (Zhang & Yin, 2012). This estimate matches experimental work done at low pressures (Kadik et al., 2011), but does not agree with experimental work done at higher pressures appropriate for core formation conditions.

The third, and preferred, type of constraint uses our calculated CC- or EC-volatile proxies for BE N content in concert with experimental measurements of K_D under high pressure ($5 - 20$ GPa). Measured K_D is 20 ± 10 (Roskosz et al., 2013). The N concentration of the core can be calculated by using the following two relationships:

$$N_t = N_c + N_b \tag{2.14}$$

$$N_t = [N_c]M_c + [N_b]M_b \tag{2.15}$$

where M is mass, N without brackets is N mass, N in brackets is concentration, and subscripts are t for total Earth, c for core, and b for BSE. Mass of the core is 1.8×10^{24}

kg and mass of the BSE is 4.2×10^{24} kg. Taking $K_D = [N_c]/[N_b]$, we find

$$[N_c] = \frac{N_t}{M_c + \frac{M_b}{K_D}} \tag{2.16}$$

A partition coefficient of 20 ± 10 and bulk Earth N mass that is either CC-like ($204 \pm 75 \times 10^{18}$ kg) or EC-like ($330 \pm 120 \times 10^{18}$ kg) suggests $180 \pm 110 \times 10^{18}$ or $300 \pm 180 \times 10^{18}$ kg N is in the core. These values are very similar to iron meteorites, suggesting they are a good proxy for core composition. Were the volatile concentration based on K-Rb, not noble gases, the N inventory would be $780 - 4600 \times 10^{18}$ kg. Importantly, all proxies indicate that if N were present in the Earth during core formation, the majority of it is sequestered into the core. This may have had an isotopic effect on the N remaining in the BSE, though it may have been minimal due to the high temperature. No measurements of this fractionation have been made, to our knowledge.

We can estimate N remaining in the BSE and atmosphere by subtracting core N mass from the total Earth. This leaves N masses of $21 \pm 17 \times 10^{18}$ kg and $35 \pm 28 \times 10^{18}$ kg remaining in the BSE and atmosphere for CC-like and EC-like models, respectively. Further subtracting the amount in the modern atmosphere (4×10^{18} kg N), suggests between $17 \pm 13 \times 10^{18}$ kg and $31 \pm 24 \times 10^{18}$ kg N (4.1 ± 3.1 to 7.3 ± 5.6 ppm) reside in the BSE. These estimates are higher than previous work for BSE N content, and serve as a useful comparison for the terrestrial-based, literature compilation budget presented in Section 2.5.

2.4.3 A Lunar analogue for the Early Mantle?

The Moon formed after a Mars-size proto-planet (Theia) collided obliquely with a Venus-size proto-Earth (Tellus) at the end of planetary accretion (Hartmann & Davis, 1975), marking the end of the so-called Chaotian Eon and the start of "Earth" history *sensu stricto* (Goldblatt et al., 2010). The density and composition of the Moon indicates that it formed after core-mantle differentiation on Earth. In addition, the identical O-isotope composition (Wiechert et al., 2001) of the Earth-Moon system indicates that the Moon-forming impact was energetic enough to homogenize the Earth and its impactor, Theia. Hence, Lunar rocks may sample the very early Earth mantle.

The N content of Lunar rocks can be used to estimate Lunar mantle, and therefore early Earth mantle, N concentrations. There are a few measurements of N in Lunar

Table 2.5: Estimates of Lunar N content in ppm, shown as a function of f_{O_2}. Hypothetical mineral and melt N concentrations for conditions of basalt melting are calculated using Eq. 2.4, 2.5 2.6. These are used to calculate K_D for a source rock that is 60% olivine and 40% pyroxene. Source concentration based on measurements of glass (3 ppm) are calculated with Eq. 2.7.

	N concentration (ppm)	
Mineral (Modal %)	f_{O_2} =IW-2	f_{O_2} =IW-4
Olivine (60%)	11	82
Pyroxene (40%)	45	77
Melt	31,000	45,000
Bulk K_D	8×10^{-4}	1.8×10^{-3}
	Expected source N (ppm) at bulk K_D = (f_{O_2} as above)	
Percent Partial Melt	$\mathbf{8 \times 10^{-4}}$	$\mathbf{1.8 \times 10^{-3}}$
1%	0.03	0.04
10%	0.3	0.3
Average source rock concentration	0.18 ± 0.15	

rocks, including basaltic glasses (3 ppm), basalts (0.7 ppm), and anorthosites (1.5 ppm) (Mathew & Marti, 2001). We use the concentration from basalt glasses as is done for terrestrial basalts (Section 2.5.5), as these are most quickly quenched and have experienced the least amount of degassing. Lunar glasses appear to be petrogenetically related to Lunar mare basalts (Mathew & Marti, 2001), which have relatively well constrained melting conditions. These basalts are the result of partial melting of 1-10% at a depth of 400 km (2.85 GPa, lower pressure than the equivalent depth on Earth due to the smaller Lunar mass) (Shearer & Papike, 1999) and temperatures of 1125 °C (Marty et al., 2003). Oxygen fugacity is between IW-2 and IW-4 (Marty et al., 2003). By comparison, terrestrial mid-ocean ridge basalts (MORB) formed at much more oxidizing conditions of IW+6 (Frost & McCammon, 2008).

To use these data to calculate N concentration in the Lunar mantle, we calculate a hypothetical K_D based on a basalt-source rock (peridotite) at the given T (1125 °C), P (2.85 GPa), and f_{O_2} (IW-2 to IW-4) conditions (Table 2.5). First, N solubility in olivine, pyroxene, and melt are calculated using Eqs. 2.4, 2.5, and 2.6. Next, bulk K_D is calculated for a source rock is assumed to be 60% olivine and 40% pyroxene. These K_D values, along with percent partial melt, are used in Eq. 2.7 to calculate N concentration in basalt glass source region, given glass concentration of 3 ppm (Table

2.5). Thus we determine the average source N concentration for the Lunar mantle is 0.18 ± 0.15 ppm.

This calculated concentration is lower than what is predicted from the chondritic model, but is similar to analyses of terrestrial xenoliths (0.28 ± 0.25 ppm, Sec. 2.5.5). The lunar value is interpreted as a lower limit for the N concentration of the early Earth mantle, as there may well have been substantial N loss during moon formation. Some N was likely volatilized and lost to space during the moon-forming impact, and later by degassing from a lunar magma-ocean. Although degassing from a magma ocean is possible, we note that under the reducing conditions thought to characterize the lunar mantle, a significant proportion of N present in melts is NH_4^+ (Libourel et al., 2003; Mysen et al., 2008). Ammonium can bond with Si-chains in a melt, and may be retained to a higher degree than N_2, which dissolves in magmas by filling spaces in between Si-chains. This behaviour of "chemical solubility" or "physical solubility" for NH_4^+ and N_2 might promote retention of N in the lunar mantle, and help it resist degassing and loss to space.

2.5 "Bottom-up" approach: terrestrial analyses

In this section, we present our "bottom-up" approach. That is, using analyses of geologic materials to estimate the N budget of the Earth in its present state. We will not make a thorough attempt to describe how N cycling has changed in the past, but will discuss past cycles/characteristics where needed. We organize our budget starting with the best characterized reservoirs (atmosphere, ocean, biomass) then describing those that are less well known (geologic). Bulk reservoir masses (Table 2.7) are used in concert with estimated N concentrations to calculate N mass in poorly characterized reservoirs (Table 2.14). A more complete picture of the current state of N on Earth should provide a more solid springboard from which to leap into interpretations of past processes.

2.5.1 Atmosphere

N_2 is the dominant form of N in the atmosphere; its mass (4×10^{18} kg) is calculated via Equation 2.13: using m_a as molar mass dry air (0.02897 kg mol^{-1}); $x_{N_2} = 0.78$; r = 6.4×10^6 m; p = 1.014×10^5 Pa; and g = 9.8 m s^{-2}.

Other N species in the atmosphere include N_2O, NH_Y (NH_3, NH_4^+), and NO_X

Table 2.6: Well characterized surficial N reservoirs, including the atmosphere, ocean, and biomass.

Reservoir	**Form**	**Size (10^{18} kg N)**
Atmosphere	N_2	4.0
	N_2O	1.5×10^{-6}
	NH_Y	1.7×10^{-9}
	NO_X	7×10^{-10}
Oceans	N_2	2.4×10^{-2}
	NO_3	5.7×10^{-4}
	NH_Y	7×10^{-6}
	N_2O	2×10^{-7}
Biomass	Ocean Living	5×10^{-7}
	Ocean Dead Organic Matter	8×10^{-4}
	Continental Living	1.1×10^{-5}
	Soil organics	1.3×10^{-4}

(NO, NO_2^-, NO_3^-). These are minor species, with abundances of 1.5×10^{12}, 1.7×10^9, and 7×10^8 kg N, respectively (Ussiri & Lal, 2013).

2.5.2 Oceans

The N content of the oceans is small compared to the atmosphere. Dissolved N_2 is the main N species in the ocean, with a mass of about 2.4×10^{16} kg (Ussiri & Lal, 2013). Concentrations of minor species (NO_3^-, NH_4^+, N_2O) can vary over the year, spatially, and with depth. Surface NO_3^- concentration is typically higher in the winter, due to lower productivity, but varies throughout the year at concentrations of 0-30 μM (Garcia et al., 2010). NO_3^- at depth is more constant spatially and is found at higher concentrations, between 10-35 μM. Total NO_3^- in the ocean has a mass of 5.7×10^{14} kg N (Ussiri & Lal, 2013). On average, the NH_4^+ is found at a concentration of 0.4 μM, and N_2O at a concentration of 11 nM. These concentrations yield masses of 7×10^{12} and 2×10^{11} kg N, respectively.

Concentrations of N species also depend on redox conditions. In deep waters of the Black Sea, which are anoxic, NH_4^+ is the dominant N species, with concentrations of up to 40 μM, while NO_3^- concentration is negligible (Fuchsman et al., 2008). A

similar relationship is seen during the winter in Saanich Inlet on Vancouver Island, with deep anoxic waters dominated by NH_4^+ (10 μM) instead of NO_3^- (< 0.2 μM) (Velinsky et al., 1991).

2.5.3 Biomass

The mass of N in living biomass is small compared with dissolved N_2 (above) and inorganic N species. Living biomass in the ocean contains about 5×10^{11} kg N. Marine dead organic matter is a much more substantial reservoir, comparable to inorganic fixed N, with 8×10^{14} kg N (Ussiri & Lal, 2013).

Soil and terrestrial biomass constitute a reservoir of N comparable to oceanic biomass. Soil has a N content of 1.62×10^{14} kg and living biomass has a N mass of 1.1×10^{13} kg (Ussiri & Lal, 2013).

Despite its low mass in biomass[4], we emphasize the importance of biology in fixing N. This process is responsible for transferring N from the atmosphere into other reservoirs in the Earth.

2.5.4 The Crust

2.5.4.1 Oceanic Sediments

Nitrogen concentration in oceanic sediments is ultimately controlled by local biologic activity. In the modern ocean, primary productivity is higher near continental margins. Proximity to continental margins increases the available nutrient pool via river/weathering input and upwelling nutrient-rich deep waters (Gruber & Sarmiento, 1997). Consequently, primary productivity is higher near continental margins. Higher productivity leads to greater organic matter concentration, and the potential for more N to be deposited in sediments. Indeed, concentrations of N in sediments off the Central American margin have >1000 ppm N in some locations, with an average of about 770 ppm (Li & Bebout, 2005). This is notably higher than sediments from the Izu-Bonin-Mariana arc (IBM) in the western Pacific, which is further from continental

[4]Compare with Whitman et al. (1998), which suggests prokaryotes alone may add up to 1.3×10^{14} kg to biomass budgets. Note too that estimates of total dead biomass herein are the same order of magnitude as the Whitman et al. estimate, and still many orders of magnitude lower than the N in the atmosphere and geologic reservoirs.

Table 2.7: Physical characteristics of geologic reservoirs used to calculate N mass. Abbreviations are: OS = oceanic sediments, OL = oceanic lithosphere, CC = continental crust, UM = upper mantle, TZ = transition zone, LM = lower mantle.

Reservoir	**Density (g/cm^3)**	**Thickness (km)**	**Area (km^2)**	**Mass (kg)**
OS[1]	-	-	-	7.4×10^{20}
OL	3	50	3.61×10^{8}	5.4×10^{22}
CC[2, 3]	-	-	-	2.28×10^{22}
MORB-source UM	4	400	3.61×10^{8}	5.8×10^{23}
Off-cratonic UM[4]	4	400	6×10^{7}	9.6×10^{22}
Cratonic UM[4]	4	400	9×10^{7}	1.4×10^{23}
TZ[5]	4.4	240	volume = 1.1×10^{11} km^3	4.8×10^{23}
LM	-	-	-	2.93×10^{24}

References are: [1](Veizer & Mackenzie, 2003), [2](Taylor & McLennan, 1995), [3]Crust 2.0 (http://igppweb.ucsd.edu/ gabi/crust2.html)
[4](Lee et al., 2011), [5](Gu & Dziewonski, 2001)

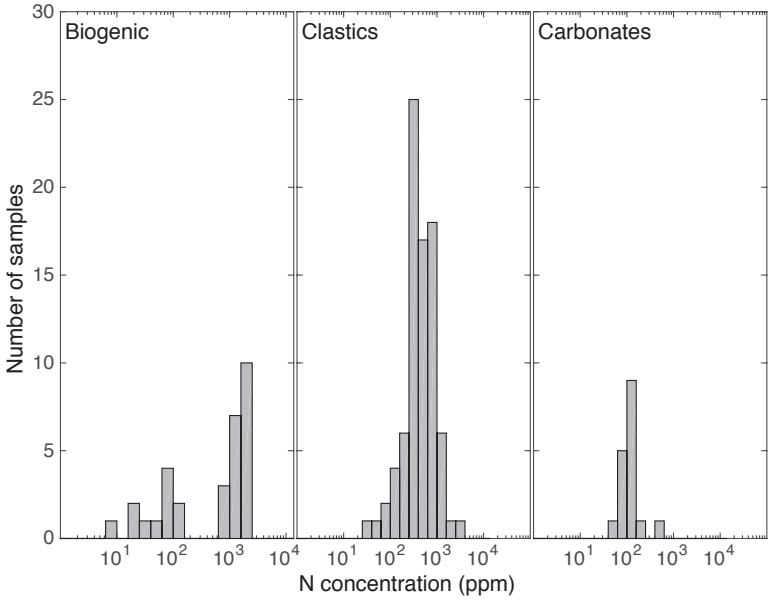

Figure 2.5: Nitrogen concentrations in oceanic crust less than 250 Ma. Sediments are separated into biogenic (organic materials, kerogen, graphite, microbialite, chert), clastic (siltstone, mudstone, clay, shale, sandstone, and pelite), and carbonates (limestone, dolostone). Oceanic lithosphere samples are labeled as OL and AOL.

margins, has lower primary productivity, and an average N content of about 280 ppm (Sadofsky & Bebout, 2004).

Our N abundance estimate in oceanic sediments is based on the proportion of three sediment types covering the sea floor. All samples that are younger than 250 Ma are used, since this is the maximum age of oceanic basins. Current sedimentary cover on the sea floor is composed of carbonate (47.1%), clastic (38.1%), and biogenic (14.8%) sediments (Davies & Gorsline, 1976; Brown et al., 1989). Biogenic sediments include organic materials, kerogen, graphite, microbialite, and chert and have a mean N concentration of 1930±1540 ppm (Fig 2.5, Table 2.8). Clastic sediments include siltstone, mudstone, clay, shale, sandstone, and pelite and have a mean N concentration of 570±56 ppm. Carbonates, limestone and dolostone, have a mean N concentration of 130±17 ppm N. The resulting weighted average is 560±230 ppm, which yields a N content for oceanic sediments of $0.41 \pm 0.2 \times 10^{18}$ kg (Table 2.14).

An important consideration when attempting to estimate N contents in the past is the redox conditions of the overlying water column, as sediments deposited under anoxic water conditions may be more N-rich. A sediment core from the Black Sea shows that sediments deposited under an anoxic water column have twice the N

Table 2.8: Concentration of N in oceanic sediments, crust, and lithospheric mantle. All are shown with standard error of the mean (SE$\bar{x}$). Samples used in budget estimates are 250 Ma or younger, as this is the maximum age of oceanic crust. Oceanic crust and altered includes basalts and gabbros. Metamorphosed oceanic crust comprises basalts, gabbros, blueschists, and eclogites. MORB-source mantle includes peridotite (harzburgite or uncategorized), while altered MORB-source mantle also includes serpentinite. Note that metamorphosed oceanic crust and altered MORB-source mantle samples may be older than 250 Ma.

	Concentration (ppm)		
Rock Type	$\bar{x}$	**SE**$\bar{x}$	**No. samples**
Biogenic	1930	1540	161[1–3]
Clastics	570	56	82[4–6]
Carbonates	130	17	21[6–8]
Sediment Average	560	230	
Oceanic Crust	1.4	1.3	124[9–17]
Altered Oceanic Crust	6.1	0.7	63[16,18,19]
Metamorphosed Oceanic Crust	7.1	1.2	14[17,18,20,21]
Oceanic Lithospheric Mantle	0.14	0.1	10[22]
Altered Oceanic Lithospheric Mantle	3.7	0.5	17[17,18,20,23]

References: [1](Peters et al., 1978), [2](Chicarelli et al., 1993), [3](Quan et al., 2008), [4](Sullivan et al., 1979), [5](Sadofsky & Bebout, 2004), [6](Li & Bebout, 2005), [7](Rau et al., 1987), [8](Sephton et al., 2002), [9](Sakai et al., 1984), [10](Exley et al., 1987), [11](Marty, 1995), [12](Marty & Humbert, 1997), [13](Sano et al., 1998), [14](Marty & Zimmermann, 1999), [15](Nishio et al., 1999), [16](Li et al., 2007), [17](Halama et al., 2012), [18](Busigny et al., 2003), [19](Busigny et al., 2005a), [20](Halama et al., 2010), [21](Busigny et al., 2011), [22] (Yokochi et al., 2009), [23] (Philippot et al., 2007)

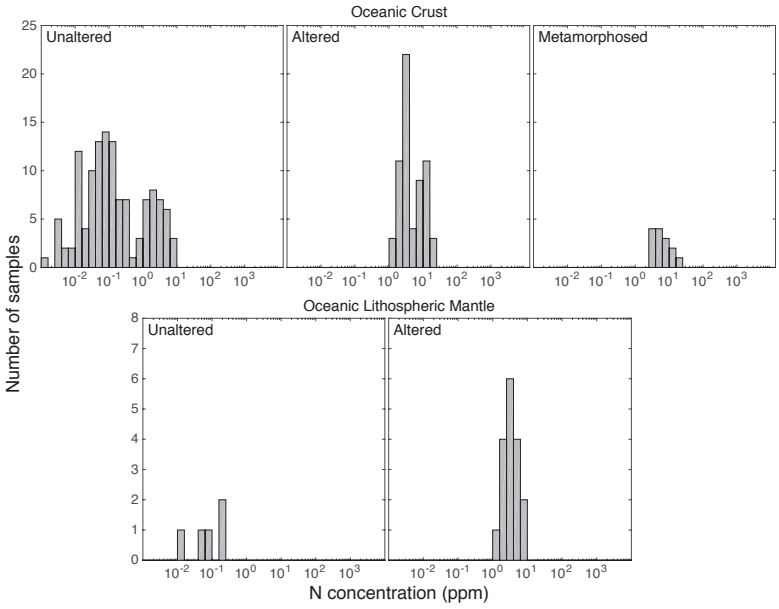

Figure 2.6: Nitrogen concentrations in oceanic crust and lithospheric mantle. Hydrothermal alteration increases the N content of oceanic crust, and it retains high N even during metamorphism. The same increase is seen in the oceanic lithospheric mantle. Samples are as in Table 2.8.

content (1800 ppm) as sediments deposited under an oxic water column (900 ppm) (Quan et al., 2013b). Changes in redox sensitive metal (Fe, Mo) concentrations and lack of significant changes in total organic carbon and δ^{13}C values corroborate redox control over N concentration, as opposed to a purely biological control. The increase of N content with reducing conditions may not be universal, as some shale units do not show N enrichment under anoxic conditions. They do, however, show distinct δ^{15}N values that appear to reflect redox conditions (Quan et al., 2013a).

2.5.4.2 Oceanic Crust and Upper Lithosphere

Fresh gabbros and basalts at mid-ocean ridges inherit N from their mantle source (Marty, 1995). Since these magmas are oxidized, N present in fresh MORB is typically found as N_2 locked in fluid inclusions in glassy rims. Concentrations in fresh crust are low, with an average of 1.4 ± 1.3 ppm. Concentration is unaltered lithospheric mantle (defined here as harzburgite and undifferentiated peridotite) is also low, at 0.24 ± 0.33 ppm (Fig. 2.6, Table 2.8).

Hydrothermal alteration tends to increase the N content of the rocks, to an average of 6.1 ± 0.7 ppm for crustal rocks (altered basalts and gabbros) and 3.7 ± 0.5 ppm for lithospheric mantle (harzburgite and serpentinite). The source of this N is from biologic activity in seawater, identified by positive δ^{15}N values. As seawater enters a hydrothermal system, it carries NH_4^+ from overlying sediments into the crust and mantle (Halama et al., 2010). NH_4^+ substitutes into mineral lattices of hydrothermal minerals, most importantly K-bearing clays. It is possible that some N may be present as N_2 in cordierite (Palya et al., 2011).

Since hydrothermal alteration is the main control on geologically stable N in oceanic crust, estimates of N concentration in these rocks depend on the depth and extent of hydrothermal alteration into the lithosphere. The deepest cores show that alteration occurs at least to a depth of 470 m (Li et al., 2007). Metagabbros and serpentinized mantle rocks in ophiolites show that alteration can reach even deeper, into the upper mantle. Hydrothermal origin of N is confirmed by enriched δ^{15}N values, derived from oceanic biologic processes (Busigny et al., 2011; Halama et al., 2012). Some ophiolites experienced metamorphic pressures of up to 2.5 GPa ($\sim 80 - 90$ km depth), yet still retain N derived from the ocean, indicating the durability of the NH_4^+-silicate bond. Indeed, the concentration of N in metamorphosed oceanic crust (basalt, gabbro, blueschist, eclogite) is identical within error (7.1 ± 1.2 ppm) to altered

crust.

A N budget estimate for the oceanic lithosphere can be calculated assuming shallow or deep alteration. Shallow alteration affecting the entire crust (6.1 ± 0.7 ppm), 0.5 km of mantle (3.7 ± 0.5 ppm), with the remainder of the mantle (9.5 km) at 0.24 ± 0.33 ppm N, yields a N concentration of 2.9 ± 0.3 ppm. This concentration gives N mass of $0.16 \pm 0.02 \times 10^{18}$ kg N. If alteration occurs on a lithospheric scale (8 km crust and 10 km mantle), we calculate an upper estimate of 4.8 ± 0.4 ppm N, which gives total N mass of $0.26 \pm 0.02 \times 10^{18}$ kg N. While these values are orders of magnitude less than the amount of N contained in the atmosphere, N in the oceanic crust is of critical importance as subduction over long time scales has the potential to transport a large amount of N into the mantle.

An average column of oceanic crust, sediments, and lithosphere can subduct substantial N over Earth history. A column with 500 m of sediment (560 ppm N, Table 2.8) and the conservative oceanic crust plus lithosphere concentration of 2.9 ± 0.3 ppm gives an average column concentration of 18 ppm. If we assume that all N gets subducted, which depends on temperature and varies by subduction zone, we can multiply this concentration times the mass of oceanic slab being subduction each year ($\sim 40,000$ km trench length, 18.5 km thick crust, 5 cm/yr convergence rate, and density of 3.5 g/cm^3), and calculate that 2.3×10^9 kg N are subducted every year. Over Earth history (4 Ga, for illustrative purposes), current subduction equates to 9.3×10^{18} kg N, which is twice the current mass of N in the atmosphere. It therefore seems reasonable to suggest that the entire atmosphere may have passed through the mantle at least once, given current subduction efficiency, or more times if subduction of N was more efficient in the past (Sec. 2.6).

2.5.4.3 Continental Crust

The continental crust is composed of two categories of rocks: (meta)sedimentary and (meta)igneous. We base our estimate for the N budget of the continental crust on our literature compilation and the rock abundance estimates of Wedepohl (1995) (Table 2.9). These proportions are based on surface outcrop area for upper crustal rocks and xenolith data for lower crustal rocks.

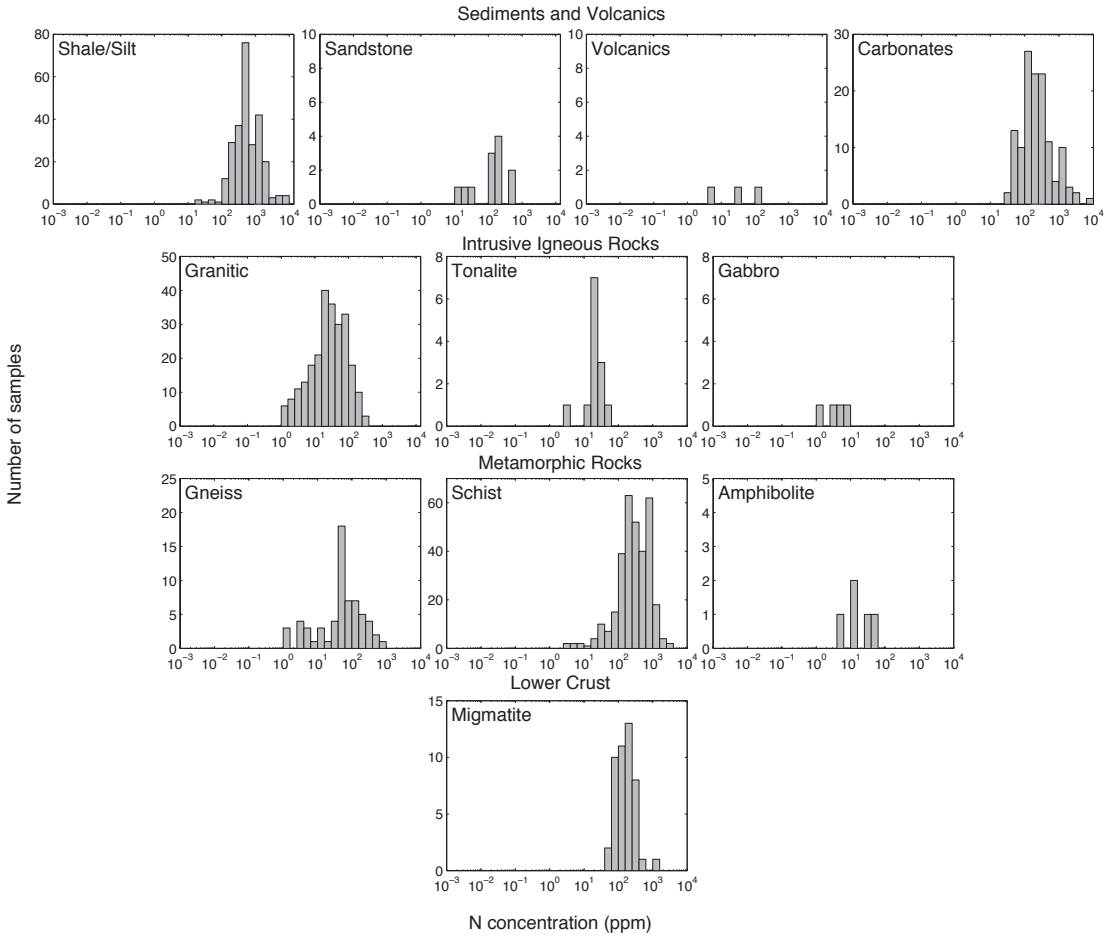

Figure 2.7: Nitrogen concentrations in continental crust. Panels are organized from shallow to deep levels in the crust. See Table 2.9 for average N concentrations.

Table 2.9: Estimates for the amount of N in the continental crust, shown with standard error of the mean (with an arbitrary error of 50% for very poorly known rock types). Rock proportions are based on Wedepohl (1995), who based upper crustal rock abundances on mapped area and lower crustal abundance on xenoliths.

		Concentration (ppm)		
Reservoir (% of crust)	**Rock type (% of reservoir)**	$\bar{x}$	**SE**$\bar{x}$	**No. samples**
Upper Crust (53%)				
Sedimentary/Volcanic Rocks (14%)	Shale/Silt (44%)	860	64	261^{1-11}
	Sandstone (21%)	230	110	12^{12-16}
	Volcanics (20%)	50	60	$3^{2,14}$
	Carbonates (14%)	130	17	$17^{\text{see Table 2.8}}$
	Average	455	38	
Felsic Intrusives (50%)	Granitic (90%)	54	7	$247^{14,17-29}$
	Tonalite (10%)	24	4	$13^{2,18,27-28}$
	Average	52	6	
Mafic Intrusives (6%)	Gabbros (100%)	5	2	$4^{2,28,30-31}$
Metamorphic rocks (30%)	Gneisses (64%)	135	50	$63^{2,17-18,32-37}$
	Mica Schist (16%)	500	44	$323^{2,14,17-18,28,31-33,35-37,38-48}$
	Amphibolites (18%)	22	10	$5^{17,42,49}$
	Marble (3%)	1000	500(?)	1^{50}
	Average	200	36	
Upper Crust Average		150	12	
Lower Crust (47%)				
Felsic/Mafic Granulites (62%)		17	6	$22^{22,27,32,37,47,51-56}$
Mafic Granulites (38%)		17	6	$22^{22,27,32,37,47,51-55,57}$
Lower Crust Average		17	6	
Total crust average		88	9	
Continental Crust N estimate= $2 \pm 0.1 \times 10^{18}$ kg N				

Upper crustal rocks are, unsurprisingly, the most analyzed and well characterized. Clastic sediments (especially shales) are the most sampled, and these include both samples explicitly formed in continental settings and sediments that formed in oceanic settings and are older than 250 Ma. Samples with oceanic provenance older than 250 Ma must now be preserved on continents in order to be sampled, so are included in the continental N budget. Nitrogen in continental sedimentary rocks is incorporated as organic matter, NH_4^+ from the breakdown of organic matter (as described previously), or NH_4^+ in minerals weathered from crystalline rocks.

Crystalline rocks, both igneous and metamorphic, form the majority of the upper continental crust. Nitrogen in both rock types is predominantly NH_4^+, either inherited from source rocks (for igneous) or protoliths (for metamorphic). The presence of biotite exerts a strong control over the distribution of N, as biotite has a strong affinity for NH_4^+ when compared to other K^+-bearing minerals (Honma & Itihara, 1981)[5] . Retention of NH_4^+ in a source region is also promoted by reduced melting conditions. In contrast, more oxidized melt conditions or less biotite-rich sources should preferentially move NH_4^+ into the melt, and therefore into granites, though some NH_4^+ may oxidize to N_2, and either escape the melt or become trapped in fluid inclusions (Hall, 1999).

Hydrothermal alteration, especially if fluids pass through sedimentary country rock, will increase the concentration of N in crystalline rocks. For example, globally, unaltered granitic rocks have an average N concentration of 36 ± 4 ppm; globally, altered granitic rocks average 65 ± 17 ppm N, with concentrations up to 250 ppm (Boyd et al., 1993; Holloway & Dahlgren, 2002).

N analyses from the deeper crust are sparse, but recent measurements suggest that this might be an important long-term reservoir for N (Palya et al., 2011). To calculate the mass of lower crust N, we use two well studied outcrops to represent the average mineralogy of both mafic (Cone Peak, California) (Hansen & Stuk, 1993) and felsic (Gruf Complex, eastern Alps) (Galli et al., 2011) granulites. The majority of N in these rocks should be contained in biotite and potassium feldspar, with some in plagioclase in a ratio of 1:0.38:0.11 (Honma & Itihara, 1981). Mafic granulites have 17% biotite, 59% plagioclase, and negligible potassium feldspar; felsic granulites have 17% biotite, 17% plagioclase, and 10% potassium feldspar. Globally, average N content of biotite in metamorphosed continental igneous and sedimentary rocks

[5]The crystal lattice sizes occupied in biotite are closer in size to the NH_4^+-cation (and Rb^+) than the same sites in feldspar, thus there is more NH_4^+ in biotite than feldspar.

Table 2.10: References for continental crust N budget estimate shown in Table 2.9.

References are: [1](Itihara et al., 1986), [2](Honma, 1996), [3](Watanabe et al., 1997), [4](Yamaguchi, 2002), [5](Krooss et al., 2005), [6](Kerrich et al., 2006), [7](Garvin et al., 2009), [8](Papineau et al., 2009), [9](Busigny et al., 2013), [10](Cremonese et al., 2013),[11](Godfrey et al., 2013) [12](Sullivan et al., 1979), [13](Greenfield, 1988), [14](Greenfield, 1991), [15](Williams et al., 1995), [16](Pontes et al., 2009), [17](Itihara & Honma, 1979), [18](Honma & Itihara, 1981), [19](Hall, 1987), [20](Cooper & Bradley, 1990), [21](Hall et al., 1991) [22](Boyd et al., 1993), [23](Hall et al., 1996), [24](Bebout et al., 1999a), [25](Hall, 1999), [26](Jia & Kerrich, 1999),[27](Jia & Kerrich, 2000), [28] (Ahadnejad et al., 2011), [29](Morford et al., 2011), [30](Halama et al., 2010), [31](Busigny et al., 2005b), [32](Duit et al., 1986), [33](Haendel et al., 1986), [34](Visser, 1993), [35](Mingram & Bräuer, 2001), [36](Jia, 2006), [37](Cruz, 2011), [38](Bebout & Fogel, 1992), [39](Bebout, 1997), [40](Boyd & Philippot, 1998), [41](Bebout et al., 1999b), [42](Holloway et al., 2001), [43](Busigny et al., 2003), [44](Sadofsky & Bebout, 2003), [45](Pitcairn et al., 2005), [46](Yui et al., 2009), [47](Plessen et al., 2010), [48](Palya et al., 2011), [49](Busigny et al., 2011), [50](Dixon et al., 2012), [51](Itihara & Tainosho, 1989), [52](Hall, 1999), [53](Sadofsky & Bebout, 2000), [54](Pinti et al., 2001), [55](Li et al., 2014), For mineral modes: [56](Galli et al., 2011), [57](Hansen & Stuk, 1993)

is 72 ± 22 ppm, which in turn suggests plagioclase (in equilibrium) has 8 ± 2 ppm and potassium feldspar 28 ± 8 ppm. Thus, mafic and felsic granulites have similar N concentrations of 17 ± 6 ppm (Table 2.9).

Our total continental crust estimate, $2 \pm 0.1 \times 10^{18}$ kg N (Table 2.9), suggests a substantial amount of N may be sequestered in the continental crust. This estimate is equivalent to a recent rough estimate (Goldblatt et al., 2009), but higher than another recent study (Rudnick & Gao, 2014) based on older compilations (Wedepohl, 1995) and measurements (Wlotzka, 1972).

2.5.5 The Mantle

The large mass of the mantle, compared to the atmosphere, means that it contains substantial N, even at low concentration. For example, 1 ppm N in the mantle would give N mass of 4×10^{18} kg, which is the same as the atmosphere. Determining the actual abundance of N in the mantle is difficult, as N analyses are rare. Most information concerning volatile elements is from noble gas geochemistry, which is augmented by diamond analyses, xenoliths, and direct mantle melts. We can estimate the N content of the mantle either as a whole or by breaking it into different domains. First we calculate a whole-mantle estimated based on N-Ar geochemistry. Then, we discuss distinct domains (MORB-source, OIB-source, off-cratonic, cratonic) individually, and base N estimates on analyses of xenoliths where available, as well as detail potential N capacity in un-sampled domains (transition zone, lower mantle).

2.5.5.1 Argon geochemistry-based estimate

Nitrogen and Ar behave similarly in basaltic melts under oxidizing conditions (Libourel et al., 2003; Roskosz et al., 2006; Mysen & Fogel, 2010; Li et al., 2014, 2015), so N-Ar systematics may be used to calculate whole-mantle N budgets (Marty, 1995; Marty & Humbert, 1997; Dauphas & Marty, 1999; Marty & Zimmermann, 1999; Goldblatt et al., 2009). This approach is valid for both MORB and OIB, since they are generated from melting of oxidized upper mantle, even though they are geochemically distinct (White, 2010). There are a number of measurements of N_2 and Ar in both basalt types, which can be used to estimate N concentration in their source. Calculating the amount of N in MORB-source and OIB-source mantle depends on establishing three criteria: (a) the amount of Ar in MORB- and OIB-source mantle, (b) the relationship between N and Ar in MORB and OIB, and (c) the proportion of

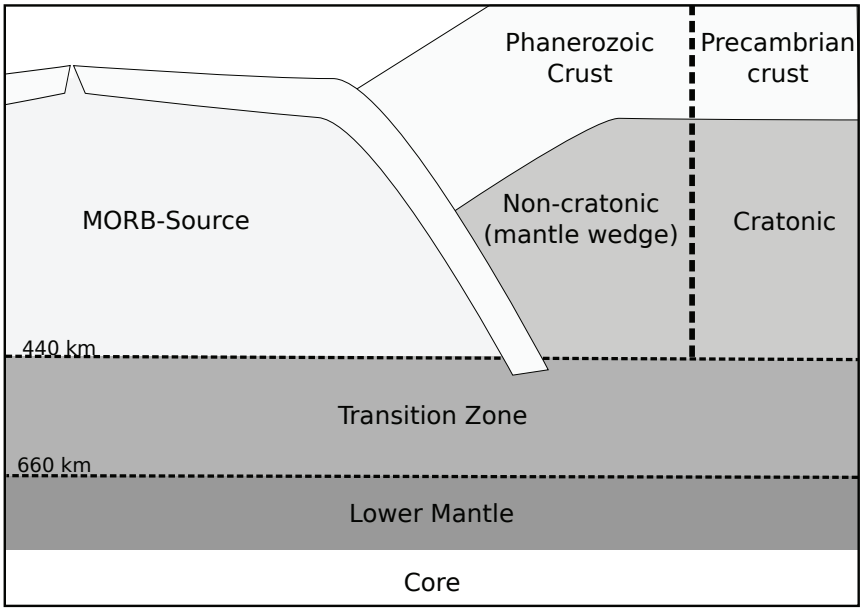

Figure 2.8: Mantle reservoirs as defined for individual domain-based budget (Section 2.5.5.2). The transition zone and lower mantle are defined by mineral phase changes. The mass of non-cratonic and cratonic mantle is estimated by multiplying the area of Phanerozoic-aged crust and pre-Cambrian crust by the depth to the top of the transition zone.

mantle that is MORB- and OIB-source.

Before calculating the N mantle budget, we highlight some aspects of Ar geochemistry, as these are crucial to the following interpretation. Argon has three isotopes, ^{36}Ar, ^{38}Ar, and ^{40}Ar. The first two are primordial (i.e., inherited during planetary formation), while the third is produced by radioactive decay of ^{40}K, and has been increasing over time. Both primordial isotopes are found almost exclusively in the atmosphere, though minor amounts are degassing from the mantle. The radiogenic isotope, ^{40}Ar, is present in both the atmosphere and the BSE, since K is found in the solid Earth. Thus, we chose to compare N to ^{40}Ar, as both elements are found in the atmosphere and BSE; these data are normalized to primordial ^{36}Ar.

The first step needed to estimate N content from ^{40}Ar is to calculate the amount of ^{40}Ar present in the mantle. As mentioned, all ^{40}Ar has been produced from the decay of ^{40}K over time. Based on U/K ratios, the K concentration of the BSE is estimated at 280 ± 120 ppm (Arevalo et al., 2009). Given a known decay rate of ^{40}K ($\lambda = 5.55 \times 10^{-10}$ yr^{-1}), the proportion of this decay which produces ^{40}Ar (10.72%), and the abundance of ^{40}K (0.0117%) (Haynes et al., 2014), we calculate that a total of $4.2 \pm 1.8 \times 10^{18}$ mol ^{40}Ar has been created over Earth history. Subtracting ^{40}Ar in the atmosphere (1.65×10^{18} mol) and continental crust (0.35×10^{18} mol, (Arevalo et al., 2009)) gives the ^{40}Ar content of the mantle to be $2.2 \pm 1.8 \times 10^{18}$ mol.

Next, we observe that the N_2 and ^{40}Ar data fall into two populations (Fig. 2.9): one containing MORB, some OIB, and some xenoliths with $N_2/^{40}$Ar values around 10^2, which we coin as MORB-source like (MSL); and one containing some OIB and xenoliths with $N_2/^{40}$Ar around 10^4, which we coin high-N. Interestingly, the MORB samples fall along a coherent trend with air at one end, as seen in previous work (Marty, 1995). Perhaps this indicates that the atmospheric N and Ar composition is the result of degassing the MORB-source mantle over time. In addition, the correlation between N_2 and ^{40}Ar in the MORB, with weak correlation between N_2 and ^{36}Ar over the same range, indicates that N has been cycled through the mantle; by proxy, it correlates with K^+, which is concentrated in the continental crust, so observing a signal of K-input suggests contribution of continental material (Marty, 1995).

In contrast, OIB and xenolith data appear to describe a three-component mixture between air, a high-MSL end-member, and an end-member composition with high N_2 compared to ^{40}Ar (Fig. 2.9). Although the high-N field has only two OIB samples, we suggest it is a robust feature of the mantle as it is also defined by OIB-associated xenoliths and other xenoliths. OIB-associated xenoliths are thought to represent

OIB-source material on the basis of high $^3He/^4He$ (Mohapatra et al., 2009). High-N xenolith samples are metasomatized, more fertile mantle lithologies (i.e., lherzolite, harzburgite, wehrlite) from locations in Oman and Europe (Yokochi et al., 2009). In addition, MORB samples that fall off the MSL trend are analyses from the East Pacific Rise, which is thought to have a plume-like component (Marty & Zimmermann, 1999), so may represent an intermediate between MSL and high-N mantle types.

To actually estimate N content in mantle source regions, we must determine the $N_2/^{40}Ar$ ratio for MSL and high-N mantle (Fig. 2.9). This is straightforward for MSL, which is described by a well-defined trend, and has a value of 120 ± 11. This value is consistent with previous work ($N_2/Ar = 124 \pm 6$, from (Marty & Zimmermann, 1999)). Determining the high-N ratio is less straightforward, as it defines a more dispersed field. Since OIBs tend to record a somewhat more diverse set of mantle source types (White, 2010), we suggest that taking the average $N_2/^{40}Ar$ ratio from all samples with $N_2/^{40}Ar > 10^3$ is the most appropriate approach to obtain a representative value. This ratio is $9.3 \pm 3.3 \times 10^3$.

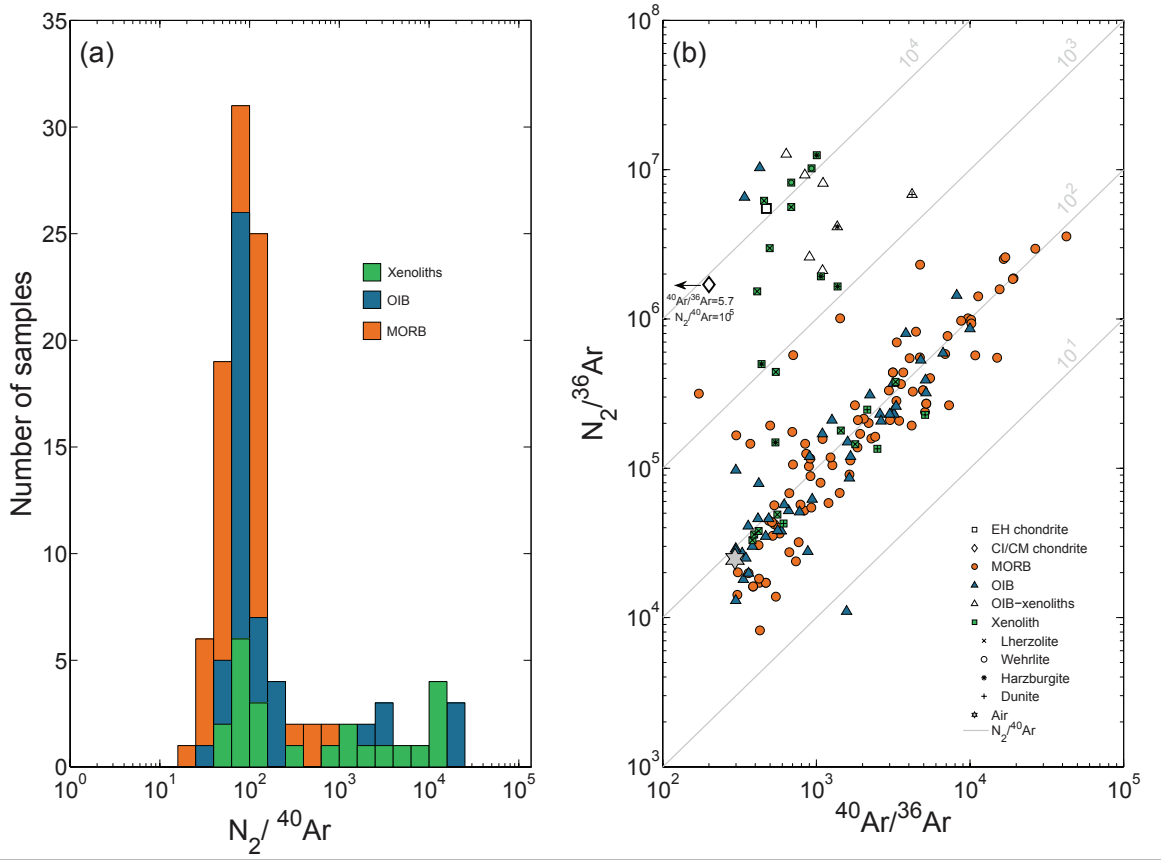

Figure 2.9: (a) N_2 and Ar data showing log-normal distribution of $N_2/^{40}Ar$ MORB (orange), OIB (blue), and xenolith (green) samples and (b) $N_2/^{36}Ar$ as a function of $^{40}Ar/^{36}Ar$ for the same rocks. MORBs are shown in orange circles, OIB basalts in blue triangles, OIB-associated xenoliths in white triangles, and other xenoliths in green squares. Additional symbols indicate known xenolith rock type. MORB samples show clear correlation, confirming previous results (Marty, 1995; Marty & Zimmermann, 1999). OIB samples both overlap with MORB and define a distinct end-member. The existence of this high-$N_2/^{40}Ar$ end member is corroborated by fertile xenolith samples. See text for discussion on the origin of this reservoir.

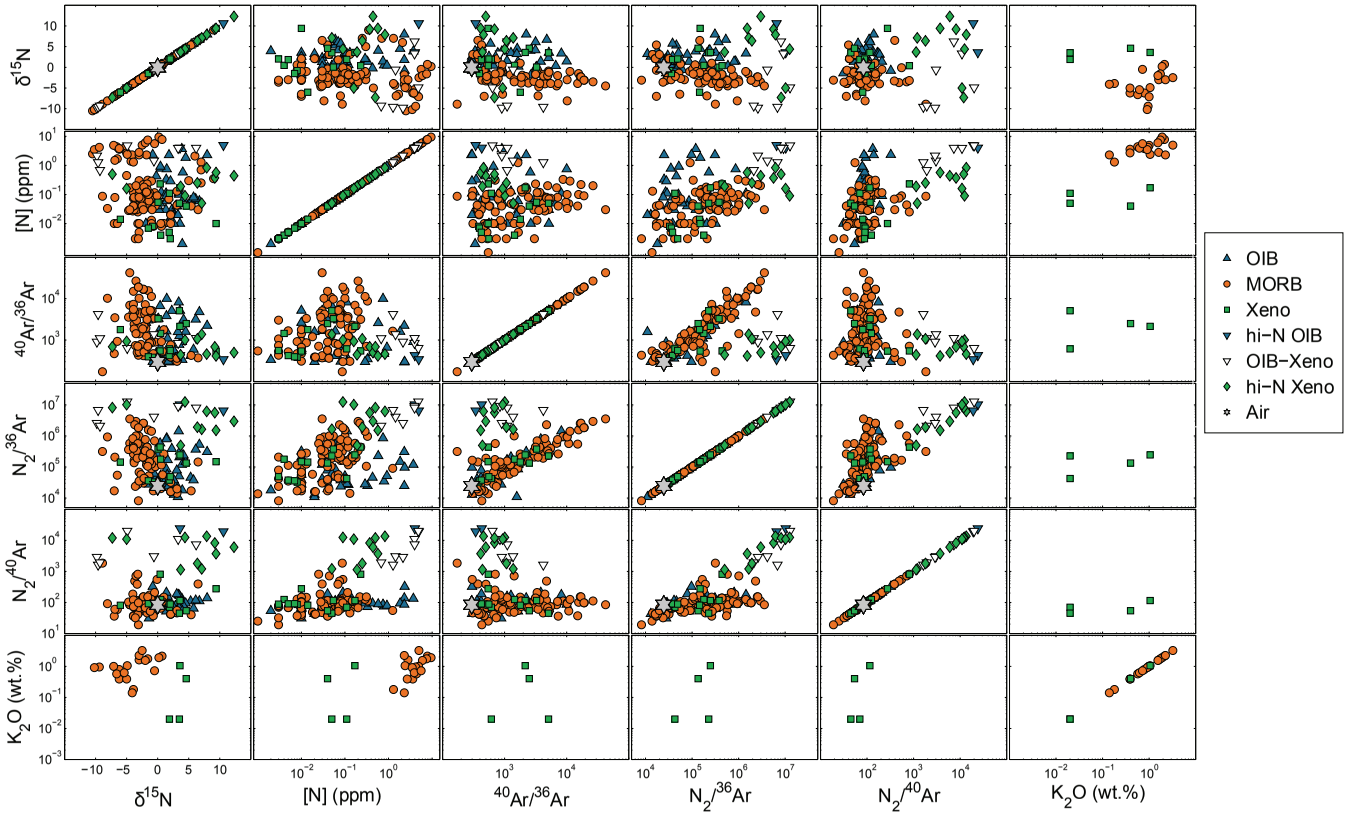

Figure 2.10: All available N concentration, isotope, Ar-isotope, and K concentration data for MORB, OIB, and xenoliths. Two mantle N reservoirs identified in Fig. 2.9: MORB-source like (MSL) and high-N are shown to separate in other plots as well. The high-N mantle tends to have high N concentration, low $N_2/^{40}Ar$, and variable but mostly positive $\delta^{15}N$ values. We interpret these to mean this reservoir is young, N-rich, and derived from subducted surface materials. MSL mantle, by contrast, appears older, as indicated by low $N_2/^{40}Ar$. It is also primarily composed of depleted $\delta^{15}N$, which results from either incorporation of different subducted material (Marty & Dauphas, 2003) or different processing in the mantle

Table 2.11: Nitrogen and Ar isotope data for CC and EC, as shown in Fig. 2.9. CC data are from (Marty, 2012) and EC data from (Hopp et al., 2014). We note that EC values are similar to our high-N mantle end member, while CC are not. This may be a coincidence, as N concentrations and δ^{15}N values of high-N mantle and EC are not equivalent.

Chondrite	$\mathbf{N_2}$ **(mol g^{-1})**	$\mathbf{N_2/^{36}Ar}$	$\mathbf{^{40}Ar/^{36}Ar}$	$\mathbf{N_2/^{40}Ar}$
EC	$2.52 \pm 0.2 \times 10^{-5}$	$5.5 \pm 0.4 \times 10^{6}$	473 ± 10	$1.2 \pm 0.1 \times 10^{4}$
CC	$4.4 \pm 0.1 \times 10^{-5}$	$1.7 \pm 0.1 \times 10^{6}$	5.7 ± 3.5	$3.1 \pm 1.3 \times 10^{5}$

Now armed with ^{40}Ar abundance for the total mantle and $N_2/^{40}$Ar for MSL and high-N reservoirs, the last step required is to estimate the actual proportion of these types of mantle. This is the most difficult of the three criteria. Trace element (e.g., U, Ta) mass balance suggests that the mantle is approximately 80% MORB-source composition and the remaining 20% is OIB-source composition (Workman & Hart, 2005; Arevalo et al., 2009, 2013). Determining what proportion of OIB-source mantle is high-N and what proportion is MSL is difficult, but crucially important to the overall estimate of N in the mantle. As a first attempt, we assume that analyzed OIB represent a statistical sampling of the OIB-source mantle. There are 9 OIB samples with high $N_2/^{40}$Ar ($> 10^3$) out of 61 total OIB samples. This corresponds to high-N being $\sim$ 15% of the OIB-source mantle, or 3% (15% $\times$ 20%) of the total mantle. If we assume uniform distribution of ^{40}Ar in the mantle, MSL (97% of the total) has $2.13 \pm 1.7 \times 10^{18}$ mol ^{40}Ar and the high-N mantle (3% of the total) has $0.066 \pm 0.0054 \times 10^{18}$ mol ^{40}Ar. Given $N_2/^{40}$Ar mentioned above (120 ± 11 for MSL and $9.3 \pm 3.3 \times 10^3$ for high-N), we calculate N mass in the MSL and high-N mantle to be $7.2 \pm 5.9 \times 10^{18}$ and $17 \pm 15 \times 10^{18}$ kg N, respectively. Total mantle N is $24 \pm 16 \times 10^{18}$ kg, which is equivalent to 6 ± 4 ppm N. While there is uncertainty in this estimate, primarily related to the K concentration estimate and distribution in the mantle, we suggest that our calculation represents a lower estimate. A larger proportion of high-N mantle would significantly increase a N mass estimate.

The most interesting and important aspect of our approach is the identification of two distinct mantle N reservoirs. The origin of both MSL and high-N components present a fascinating geochemical quandary. MSL mantle has low $N_2/^{40}$Ar, low N concentration, but its δ^{15}N values describe two sub-populations: depleted δ^{15}N in MORB and enriched δ^{15}N in OIB (Fig. 2.10). Given the low N concentration (< 1 ppm) in most samples, the low $N_2/^{40}$Ar ratio should be caused by a high ^{40}Ar content

resulting from significant time since this material (and by proxy K) was at the surface of the Earth. Subducted material with variable N and K contents would require a long time to acquire enough ^{40}Ar to push all samples towards a common trend. It therefore seems likely that MSL mantle is tapping a reservoir of older material derived from the surface. The δ^{15}N values are interesting, as MORB values of -5‰ are distinct from modern subducted material, which is around +5 to $+7$‰. OIB that fall along the MSL trend, however, show enriched δ^{15}N values, at ~ 5‰. The difference either means that MORB and OIB in the MSL are tapping N reservoirs of subducted material that are different in space (Marty & Dauphas, 2003) but not in time (i.e., both tap old material) or that the way N is processed in the MORB-and OIB-source mantle or eruptions is different. It is difficult to discern between these options at this time, though future modelling and experimental work would aid in this pursuit.

The high-N mantle, in contrast, appears to be tapping relatively recently subducted surface material. This reservoir has high $N_2/^{40}$Ar, high N concentration, and enriched δ^{15}N values in OIB and xenoliths (Fig. 2.10). High N concentration associated with high $N_2/^{40}$Ar implies this material is young, as it has not had sufficient time to accumulate ^{40}Ar through radioactive decay (Marty & Dauphas, 2003). The δ^{15}N values are also very close to modern, oceanic sedimentary values, at 7.1‰. Overall, the high-N mantle appears to be young, N-rich, and received its N from subduction of surficial materials.

In detail, there are differences between high-N OIB, OIB-xenoliths, and xenoliths. While both OIB basalts and OIB-xenoliths have relatively high N content (4.5 and 2.7 ppm), they have distinct δ^{15}N values of 7.1‰ and -3.5‰, respectively. Recall that the OIB-associated xenoliths are thought to represent the source rocks of coexisting OIBs. The difference in N isotopes could mean that N fractionates during partial melting, enriching the melt compared to the source. To our knowledge, there are no studies that quantify isotopic fractionation of N between partial melt and residual material in OIB genesis. If melt preferentially incorporates the heavy isotope, perhaps this could explain the observed relationship between OIB and their source. The remainder of the high-N xenolith population has enriched δ^{15}N values of 4.5 ± 2‰ and low N concentration of 0.35 ± 0.07 ppm.

An alternate approach to explain the high $N_2/^{40}$Ar ratio of the high-N mantle would be some process whereby N is retained preferentially to K during subduction and recycling. Such a process would concentrate N more in the mantle than K, and

therefore this material would have less ^{40}Ar. It is possible that K is more mobile during subduction than N. There are synthesized NH_4^+-bearing micas (phengite), aluminosilicates (K-hollandite) (Watenphul et al., 2009) and clinopyroxenes (Watenphul et al., 2010) that are stable to eclogite-field conditions. As pyroxene is more stable at greater depth in the mantle, it is possible that storage of N as NH_4^+ in pyroxene allows for it to be more effectively retained than K, whose host minerals (feldspars, micas) break down. Further experimental work concerning N and K behaviour during subduction could help address this issue. Discussed in some detail later, other locations that could fractionate N from K are the transition zone and lower mantle. In these reservoirs, metallic Fe is stable and N may be retained in this metal, while K is not. This is highly speculative, but further investigation of this high-N reservoir could help characterize the fate of volatiles in the mantle.

2.5.5.2 Individual Mantle Domain Estimates

An alternate approach to the Ar-based geochemistry is to attempt to break the mantle into different domains, and use measurements of xenoliths from those domains to estimate N mass. This approach may be more limited, due to relative paucity of analyzed samples as well as lack of material from the transition zone and lower mantle. Thus, we suggest the following be viewed as a minimum estimate. We will also only provide quantitative estimates for actual N content in domains that have been sampled, while for domains without direct samples we will discuss the capacity for N storage.

We identify four sampled mantle reservoirs (Table 2.7): MORB-source, OIB-source, off-cratonic, and cratonic mantle. There are two reservoirs, the transition zone and lower mantle, that do not have N analyses from xenoliths (Fig. 2.8). Note this division is not intended to comment on chemical heterogeneity or stratification in the mantle, but merely to utilize different petrologic/geochemical proxies where appropriate to estimate the N content of the total mantle.

2.5.5.2.1 MORB-source Mantle

The amount of N in the MORB mantle is largely a function of the efficiency of degassing during mantle partial melting and MORB genesis. Melting under oxic conditions seems to be efficient at removing N from source rocks into magma (Libourel et al., 2003). Our data compilation of MORB-source mantle rocks (peridotite,

harzburgite) suggests N content of 0.9 ± 0.7 ppm (Fig. 2.11). Using the same MORB-source mass abundance from the previous section (80% of the mantle) yields a N content for the MORB-source mantle of $0.74 \pm 0.1 \times 10^{18}$ kg N. Note that experimental (Li et al., 2013) and theoretical (Mikhail & Sverjensky, 2014) work suggest that in the middle to lowermost upper mantle redox, pressure, and pH conditions may be consistent with the presence of NH_3 or NH_4^+. These molecules may be retained more effectively than N_2, thus this portion of the mantle may be more N rich than indicated by xenoliths alone.

2.5.5.2.2 OIB-source Mantle

For this estimate, we turn to analyses of OIB as well as OIB-associated xenoliths as described in in section 2.5.5.1. These rocks have an average N concentration of 0.7 ± 0.5 and 2.7 ± 0.8 ppm. Note that we include all OIB in this estimate, whereas in section 2.5.5.1 we identified two OIB-source reservoirs. In addition, OIB have likely experienced some degassing upon eruption, so this concentration should be viewed as a minimum. We assume that OIBs represent partial melts that melted under conditions conducive to quantitative N extraction from the source. Therefore, with 10% partial melt (Winter, 2001), source concentration would be 0.07 ± 0.04 ppm N. This is much lower than the OIB-xenolith values, but again should be viewed as a minimum. Given an OIB-source proportion of 20% yields a N mass of $0.06 \pm 0.04 \times 10^{18}$ kg for OIB based N concentration and $2.2 \pm 0.6 \times 10^{18}$ kg for OIB-xenolith based concentration.

Additionally, while degassing during eruption has likely occurred, it is worth noting that the concentration of N in OIBs is of the same order of magnitude as the concentration of N in carbonatites from the Kola peninsula, which are around 0.11 ppm (Dauphas & Marty, 1999). The carbonatites are thought to be sourced from fairly deep, crystallized at depth, and to have experienced minimal degassing during emplacement. Carbonatite magmas, however, are likely sourced from a mantle domain distinct from the OIB-source mantle.

2.5.5.2.3 Off-cratonic Upper Mantle

The sub-continental mantle can be broken into two domains: off-cratonic mantle, which has been influenced by Phanerozoic subduction and cratonic mantle, which is the stable mantle underneath cratons. We discuss the off-cratonic mantle first.

Off-cratonic mantle is roughly equivalent to the mantle wedge associated with

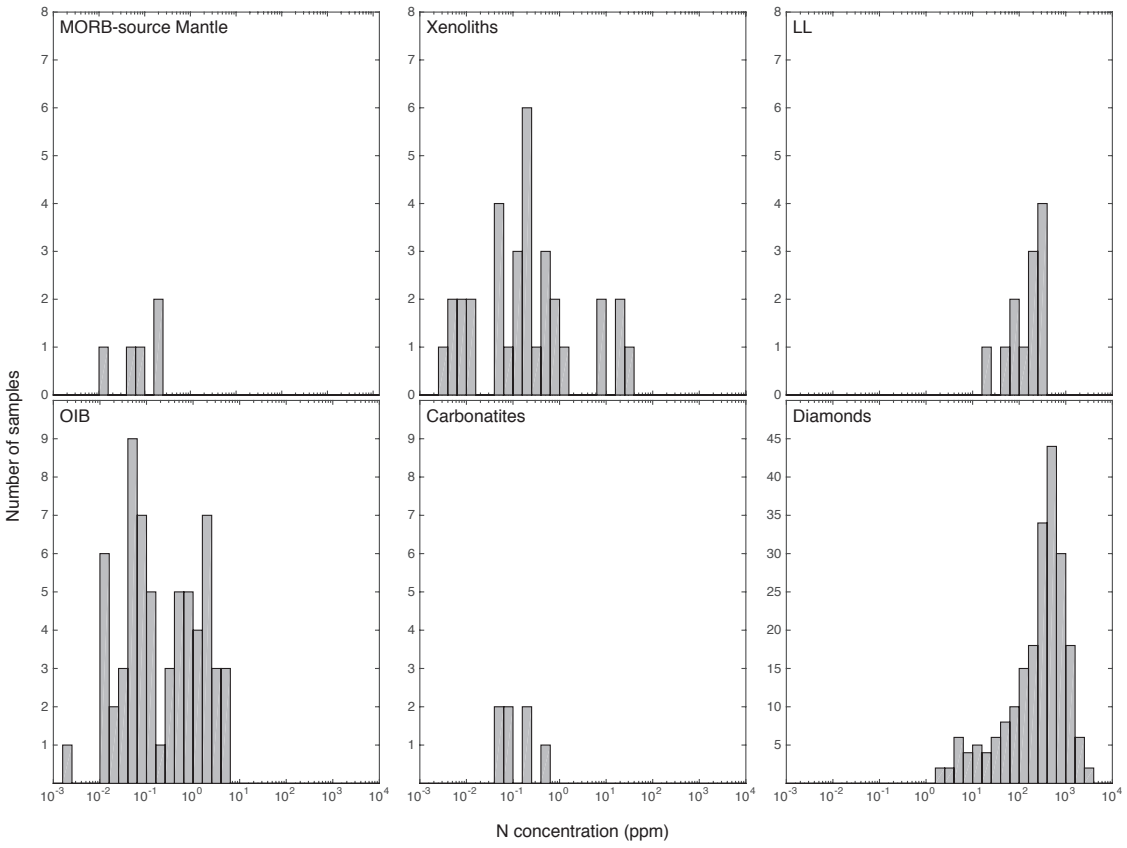

Figure 2.11: Nitrogen concentrations in mantle rocks, melts, and diamonds. While diamonds are well characterized, the number of analyses in other rock types are rare. MORB-source mantle samples include rocks from dredges and from ophiolites, while xenoliths are samples brought to the surface on continents. Lamproite and lamprophyre (LL) are thought to be sourced from hydrated mantle, and their high N concentration suggests effective recycling of N into this region of the mantle (Sec. 2.5.5.2.3). Ocean Island Basalts (OIB) are discussed in detail in Sec. 2.5.5.1, and carbonatites are presented simply as a comparison. See Dauphas & Marty (1999) for a discussion of these samples.

subduction zones. Since mass balance studies suggest the majority of subducted N does not return to the atmosphere via arc magmatism (Mitchell et al., 2010; Busigny et al., 2011), it is possible that some of this N is retained in this reservoir. We invoke analyses of specific alkaline volcanic rocks, lamprophyres and lamproites (LL), as proxy for mantle influenced by subduction. These rocks, though volumetrically small, are geographically widespread (Winter, 2001), which indicates their potential as a useful proxy.

Petrogenetic analysis of LL suggests that they are sourced from hydrated mantle composed of phlogopite (mica)-bearing harzburgite (Tainton & McKenzie, 1994; Mitchell, 1995), though some may be sourced from deeper in the mantle (Murphy et al., 2002). Phlogopite harzburgite may be produced via a two step process: an initial mantle melting event, and the subsequent addition of fluids sourced from subducted continental/marine sediments. Later partial melting ($1-10\%$) of the harzburgite produces LL magmas.

A suite of LL from India have N concentrations that range from 21-394 ppm (Jia et al., 2003), with an average of 210 ± 60 ppm (Fig. 2.11). The corresponding N content of the mantle source of LL depends, then, on the behaviour of NH_4^+ during melting.

The Rare Earth Element (REE) profiles of the Indian LL may both constrain the compatibility of N in the source rock and could perhaps be used as a proxy for N in other samples where N was not measured explicitly. Ytterbium and Lu show a significant correlation with N (when disregarding a sample with high, 400 ppm, N), with r^2 values of 0.70 and 0.79, respectively (Fig. 2.12). This suggests that N, Yb, and Lu behave similarly during LL formation.

The behaviour of Yb and Lu during LL formation is relatively well known, as K_D values have been measured in minerals experimentally (Table 2.12). We use these mineral K_D values to calculate a bulk K_D value, which is a simple weighted average, for a phlogopite-harzburgite source rock with 60% olivine, 30% pyroxene, and 10% phlogopite. Bulk K_D are 0.0505–0.0979 for Yb and 0.0636 for Lu (Fujimaki et al., 1984; Foley & Jenner, 2004).

The K_D of N has not been measured during LL formation, to our knowledge, so as a first approximation we will assume that it is equal to the K_D of Yb or Lu, based on the strong correlation shown in Fig. 2.12. Using Equation 2.7, we calculate a N concentration in LL source of 35 ± 7 ppm based on Yb and 33 ± 9 ppm based on Lu for 10% partial melting. Assuming 1% partial melting gives N concentration of

Table 2.12: Partition coefficients of Yb and Lu in lamproite/lamprophyre (LL). K_D values shown are for a LL source rock that is 60% olivine, 30% pyroxene, and 10% phlogopite.

	$\mathbf{K_D}$		
Mineral	Yb	Lu	Reference
Olivine	0.0091	0.0187	Foley & Jenner (2004)
Pyroxene	0.134–0.292	0.159	Foley & Jenner (2004)
Phlogopite	0.0484	0.0471	Fujimaki et al. (1984)
Bulk rock	0.0505–0.0979	0.0636	

Table 2.13: Nitrogen concentration and total mass estimates in the off-cratonic mantle based on analysis of lamproite/lamprophyre (LL) and K_D values of Yb and Lu (Table 2.12). Nitrogen behaviour is assumed to be similar to Yb and Lu (Fig. 2.12), and bulk K_D values are then used to estimate N mass (10^{18} kg) using Eq. 2.7. We present estimates for 1 and 10% melt.

	N concentration (ppm)		N mass (10^{18} kg)	
Melt	Yb-based	Lu-based	Yb-based	Lu-based
10%	35 ± 7	33 ± 9	3.4 ± 0.7	3.2 ± 0.8
1%	18 ± 4	15 ± 5	1.7 ± 0.5	1.4 ± 0.5

18 ± 4 ppm based on Yb and 15 ± 5 ppm based on Lu. Correspondingly, the mass of N would be between 1.4×10^{18} and 3.4×10^{18} kg.

2.5.5.2.4 Cratonic Mantle

We draw upon three data sources to calculate the N content of the cratonic upper mantle: xenoliths, diamond analyses, and experimental petrology. Xenolith data gives rather different results than the estimate combining diamond and experimental data. We suggest that these approaches provide lower (xenolith) and upper (diamonds plus experiments) limits on the N content of the cratonic mantle.

Xenolith N concentration is 0.28 ± 0.2 ppm. If these are representative of cratonic mantle, this reservoir has very low N mass, of $0.04 \pm 0.03 \times 10^{18}$ kg. There are very few analyses of N in xenoliths, thus it is difficult to say how representative they are.

A second approach is to use the much more plentiful literature database for N analyses in diamonds. The majority of diamonds are formed in the cratonic litho-

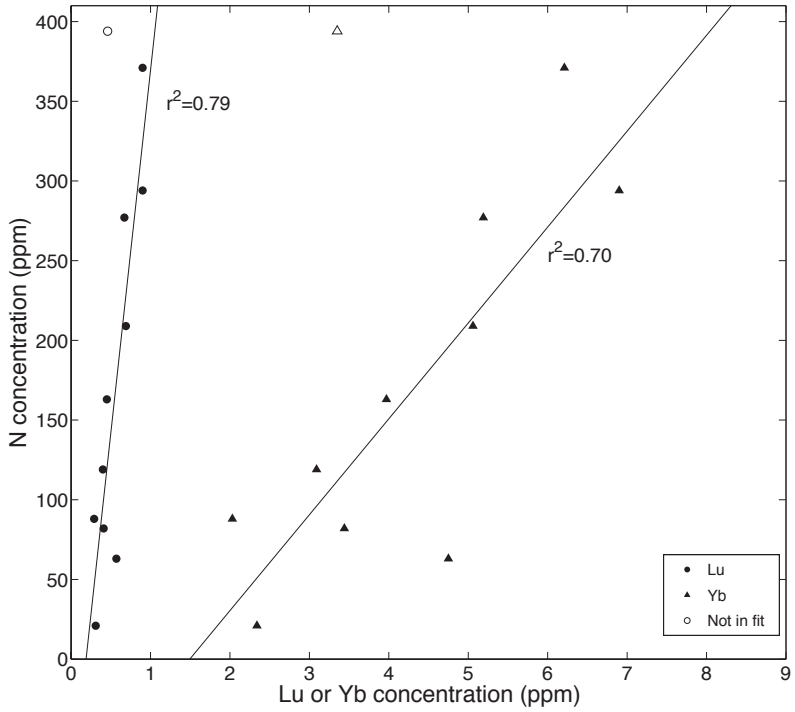

Figure 2.12: Nitrogen and Lu or Yb concentration in lamproites/lamprophyres (LL) from (Jia et al., 2003). Significant correlation suggests these elements behave similarly during melting, and we use this observation as an estimate for the N content of the off-cratonic upper mantle. Empty symbols were not included in regression.

sphere (Cartigny, 2005; Stachel & Harris, 2009), thus they should be able to reveal information about this reservoir. First, we calculate the average N content of diamonds to be 740 ± 176 (Fig. 2.11). Diamonds form via precipitation from a fluid, so the next step is to estimate how much N remains in the fluid after diamond formation, and to assess the ability of the host rocks to absorb this extra N. A K_D between N in diamond and N remaining in the diamond-forming fluid of 4 has been suggested based on study of the Jericho Kimberlite, in the Slave Craton of Canada (Smart et al., 2011). Thus, given a K_D of 4, N concentration in residual diamond-forming fluid is 185 ± 44 ppm.

Next, using experimental results, we calculate the capacity of the sub-cratonic lithosphere to retain N left in diamond-forming fluid after diamond formation (Eqs. 2.4–2.5). P-T-f_{O_2} conditions appropriate to the sub-cratonic lithosphere are: T = 1400° C, P= 6 GPa, and f_{O_2} =FMQ-4 (ΔNiNiO= -2.3) (Frost & McCammon, 2008). Hence, we calculate a N capacity of 120 ppm for pyroxene and 5 ppm for olivine. If we assume a harzburgite-like composition (70% olivine, 30% pyroxene) (Lee et al., 2011), a total N capacity of 40 ppm is calculated. If portions of the mantle are more fertile (i.e., higher pyroxene content) they would have correspondingly a higher N capacity. Analyses of N in natural olivine and pyroxene are much lower (< 1 ppm, (Yokochi et al., 2009)) than this calculated upper limit, implying the actual content may be significantly lower than the capacity.

The capacity of upper mantle minerals is consistent with relatively high ($\sim$ 40 ppm) N contents. We suggest that N remaining in diamond-forming fluid after diamond formation may be effectively sequestered in the sub-cratonic lithosphere. In addition, N concentration in the 10s of ppm is corroborated by estimates of C/N based on diamond analyses (Cartigny et al., 2001). A N concentration of 40 ppm yields a N mass of $\sim 5.6 \times 10^{18}$ kg. This is likely an upper estimate, as it assumes all cratonic mantle was infiltrated by diamond-forming fluids and that all N not included in diamonds was retained in the host rock. Uncertainty in the extent of diamond-forming fluid (if this is the source of N) introduces error to this estimate, though if experimental relationships accurately describe the N solubility in upper mantle minerals there is no issue with storage capacity.

Additional uncertainty may result from disagreement concerning the compatibility of N during diamond growth. An extensive compilation by Cartigny et al. (2001) suggests that the incorporation of N into diamonds from diamond-forming fluids is a kinetic process: slow diamond growth results in low N content. Both measurements

of Slave Craton diamonds (Smart et al., 2011) and synthetic diamonds suggest that N behaves compatibly (Stachel & Harris, 2009). The majority of diamonds with depleted δ^{13}C values that are indicative of a recycled crustal input do not have commensurate enriched δ^{15}N values (Cartigny, 2005), which would be expected if the source of N and C was subducted oceanic material. This either indicates that recycled material that was incorporated into diamond growth had different δ^{15}N values from modern surface reservoirs (Marty & Dauphas, 2003) or that C and N incorporation into diamonds is decoupled/depends only on growth rate (Cartigny et al., 2001).

2.5.5.2.5 Transition Zone

The transition zone (TZ) is the region in the mantle between 410 and 660 km depth, and is defined by mineral phase changes. At 410 km, olivine changes its structure to the more tightly packed spinel-like crystal lattice of wadsleyite then ringwoodite. Below 660 km, another phase change occurs, and the spinel-structure mineral changes to bridgmanite, a high-pressure polymorph. These phase changes control redox chemistry, and the TZ is more reducing than the overlying upper mantle. The f_{O_2} here is around IW-1, and both experiments and calculations suggest the presence of 0.1 wt.% metallic Fe (Frost & McCammon, 2008) in this region.

Therefore, with 0.1-2 wt.% N dissolved (Kadik et al., 2011; Roskosz et al., 2013) in 0.1 wt.% metallic Fe (Frost & McCammon, 2008), N concentration would be 100–2000 ppm. This represents the N capacity of the transition zone, with a strong upper bound between 48×10^{18} to 960×10^{18} kg N. The high N potential of the transition zone, and indeed the lower mantle, was recently suggested based on the observation that the more deeply diamonds form, the less N they contain (Smith et al., 2014). The authors suggest that the low-N diamonds grew in the presence of Fe-metal, which preferentially dissolved N. This is consistent with our literature review.

Sequestering N in the transition zone for significant periods of time may be difficult, however. Whole mantle circulation means that material in the transition zone does not stay there (Nakagawa & Tackley, 2012). Both the upper mantle and lower mantle are more oxidizing that the TZ (Frost & McCammon, 2008). Thus, when material moves out of the TZ, previously metal-bound N may be released into either fluids or minerals. This may preclude long-term N storage in the TZ. Without further evidence (petrologic or experimental), the transition zone remains a hypothetical reservoir for N. It is not considered in our total N estimates for the Earth.

2.5.5.2.6 Lower Mantle

The lower mantle, which is defined by the phase transition at 660 km depth described above, is not represented by xenoliths or inclusions in our N database. We are unaware of any such analyses. As with the transition zone, we may only be able to speak to the storage capacity of this portion of the mantle.

There is speculation that 1 wt.% metallic Fe may exist in the lower mantle (Frost et al., 2004). High pressure/temperature experimental petrology demonstrates that N is quite soluble in metallic Fe at these conditions, with up to 8 wt.% (Roskosz et al., 2013). Given a mantle with these proportions of Fe-metal and N solubility suggests a N capacity of 2.3×10^{23} kg N. This value is orders of magnitude higher than any other reservoir in the planet, perhaps save the core. As with the transition zone, this is highly speculative, and would require further confirmation via geochemical or modelling study.

If there are regions of the lower mantle that remain shielded from mantle convection and mixing, they may represent a location for storage of the Earth's "missing N". That is, the abundance of N compared to other volatiles in the BSE was previously estimated to be about an order of magnitude lower (Marty, 2012). The lower mantle has more than enough capacity to store additional N. If, however, our Ar-based estimate for N abundance in the mantle is correct, there is no need to invoke hidden reservoirs of N, as we calculate mantle N mass in line with other volatile abundances.

Table 2.14: BSE N masses, shown in 10^{18} kg N. When adding oceanic crust into totals, the range (0.16 ± 0.01 to 0.26 ± 0.02) was averaged to 0.21 ± 0.01. The approach column notates which method: literature compilation (LC) or Ar-based geochemistry (AR). The preferred value total is shown in bold. The AR approach for the mantle is preferred, because it more likely "samples" a greater extent of the mantle than xenoliths. Results are presented with comparison to Goldblatt et al. (2009) (CG).

Reservoir	**Location**	**This study**	**Approach**	**CG**
Oceanic Lithosphere	Sediments	0.41 ± 0.2	LC	0.31 ± 0.16
	Crust+Mantle	0.16 ± 0.01 to 0.26 ± 0.02	LC	0.012 ± 0.005
Continental Crust	Igneous			0.55 ± 0.27
	Sedimentary			1.55 ± 0.62
	Total	2 ± 0.1	LC	2.1 ± 1.05
Mantle	MORB-Source	0.9 ± 0.7	LC	
	OIB-source	$> 0.06 \pm 0.04$ to 2.2 ± 0.6	LC	
	Off-cratonic	1.4 to 3.4	LC	
	cratonic	< 5.6	LC	
	transition zone, lower	< 100		
	Total	$> 3.4 \pm 1.3 - 5.8 \pm 1.4$	LC	
Mantle	MORB-source-like Mantle	7.2 ± 5.9	AR	
	high-N	17 ± 15	AR	
	Total	$\mathbf{24.2 \pm 16}$	AR	$\geq 8.4 \pm 5.2$
BSE Total	LC Crusts and LC Mantle	$> 5.7 \pm 1.3 - 8.1 \pm 1.4$		
BSE Total	**LC Crusts and AR Mantle**	**27±16**		10.8 ± 5.3

2.6 Discussion

We find that our two methods for calculating the N budget of the Bulk Silicate Earth (BSE) are consistent. Both comparison to chondrite N abundance ("top-down") and compilation of terrestrial analyses ("bottom-up") of rocks and minerals suggest the BSE contains many atmospheric masses (PAN= 4×10^{18} kg) of N. The chondritic comparison suggests between $17 \pm 13 \times 10^{18}$ and $31 \pm 24 \times 10^{18}$ kg N are in BSE while the terrestrial literature compilation suggests $27 \pm 16 \times 10^{18}$ kg N. Both estimates also have theoretical upper limits that are much higher (Table 2.14), due to increased solubility of N in silicates at depth. This close agreement shows that our budget is internally self-consistent. It may also remove the concept of "missing N" (Marty, 2012; Halliday, 2013), as the mantle appears to have ample capacity for N sequestration.

Importantly, our estimate is higher than previous estimates (Goldblatt et al., 2009). The mantle appears to have a significant portion of the planetary N budget. High N content in the BSE has significant ramifications in relation to Earth and atmospheric geochemistry.

2.6.1 Key uncertainties

Before discussing geochemical implications of the new budget presented herein, we touch briefly on the main uncertainties in our estimate. First, sparsely analyzed reservoirs (specifically the mantle and lower continental crust) inherently limit accuracy in estimates. Further analysis of these important reservoirs should be a focus of future work. Second, though the behaviour and partitioning of N during melting in the mantle is beginning to be tested experimentally (Libourel et al., 2003; Mysen & Fogel, 2010; Li et al., 2013, 2015), the relative lack of studies necessarily introduces uncertainty. We suggest that N behaves similarly to Lu and Yb, though this relationship has not been assessed in all rock types. It is becoming clear that f_{O_2}, temperature, and pressure all exert strong control over N contents in the mantle. More experimental petrology and modelling studies would be valuable in elucidating the behaviour of N at the range of conditions found in the solid Earth.

Thirdly, determining the geochemical character of the high-N mantle reservoir identified in Section 2.5.5.1 more accurately is of crucial importance. This reservoir, despite its small mass, may contain the majority of the N in the mantle. As it appears to be sampled by some OIB and xenoliths, more coupled N-Ar measurements of these

rocks should help define this end member more completely. The stable isotopes are consistent with a recycled component, but the extent, residence time, and other geochemical properties are not fully constrained at this time.

2.6.2 Evolution of the atmosphere-mantle system

The atmosphere is not the main reservoir for N on Earth today. However, the processes responsible for the current distribution are not fully resolved. It remains ambiguous if the distribution between BSE and atmosphere has been the same as the current state, or if it has been different in the past. Nitrogen isotopic evidence and correlation with radiogenic ^{40}Ar indicates that N derived from the surface of the Earth is subducted and cycled into the BSE (Marty, 1995; Marty & Dauphas, 2003; Palya et al., 2011), so exchange has clearly occurred. The setting where this input occurs is subduction zones. At current subduction rates, 9.3×10^{18} kg N could be subducted over 4 Ga of Earth history (Sec. 2.5.4.2). So at modern subduction rates, consistent since at least the Cretaceous (Busigny et al., 2011), the entire atmosphere could be potentially pass through the mantle if $\sim 50\%$ of subducted N is recycled to the mantle (i.e., not returned to the atmosphere). This retention efficiency at modern subduction zones is poorly constrained (Halama et al., 2012), with the Central American margin appearing to return significant sedimentary N (100%) to the atmosphere (Elkins et al., 2006) while the colder Izu-Bonin-Mariana Arc retains most of subducted N ($\sim 85\%$) to mantle depth (Mitchell et al., 2010). As such, there is no reason to rule out different efficiency in the past.

There are two reasons to suggest that N subduction was more efficient in the past. The first is that prior to the Great Oxidation Event, it is likely that the dominant N ion in the oceans was NH_4^+ (Garvin et al., 2009). Since NH_4^+ substitutes into sediments and oceanic lithosphere to enter the geologic cycle, a higher concentration might promote a greater N flux into subducting sediments and lithosphere. Indeed, an increase in N concentration is seen in Black Sea samples in the Quaternary, with sediments deposited under anoxic conditions having about twice as much N as sediments deposited under oxic conditions (Quan et al., 2013b). Additionally, higher mantle temperature in the Archean (Herzberg et al., 2010) has been interpreted to lead to more vigorous mantle convection. Hotter mantle is also thought to produce thicker oceanic crust, due to greater degree of partial melting. Higher heat flow should cause extensive hydrothermal alteration, which could act as a sink for NH_4^+ from the ocean.

A hotter mantle, however, may also be a drier mantle (Korenaga, 2011; Sandu et al., 2011), which would tend to slow convection and subduction. The interplay between these two factors, increased NH_4^+ in the ocean and crust and hotter mantle, and any effects on N subduction are not known.

Progressive N sequestration over time implies a more massive atmosphere in the Archean, which has potentially important effects on greenhouse warming (Goldblatt et al., 2009; Byrne & Goldblatt, 2014). Independent proxies for Archean paleopressure based on fossil raindrops (Som et al., 2012) and hydrothermal inclusions in quartz grains (Marty et al., 2013), however, suggest the Archean atmosphere had the same amount (or less) of N as the modern. The raindrop constraint has subsequently been found to be too low; a more realistic constraint here is up to ten times modern density (Kavanagh & Goldblatt, 2015). The $N_2/^{36}Ar$ ratio from 3.0 Ga hydrothermal inclusions in quartz grains are approximately equal to the modern value (Marty et al., 2013); this is inferred to suggest that the atmosphere may have had the same pressure (and therefore N content) as the modern day Earth. An earlier study on the same grains suggests, however, an upper limit for the $N_2/^{36}Ar$ of 3.3 times the modern value (Nishizawa et al., 2007). A robust empirical constraint on the amount of N_2 in the Archean atmosphere is enigmatic at this time. Our work indicates substantial N is in the mantle, at least some of which has been recycled from the surface, so it is possible that the atmosphere was more massive in the past. Whether this indicates a monotonic drawdown or some more dynamic evolution of the atmosphere-mantle system is unknown at this time.

The fate of subducted N has a direct effect on the $\delta^{15}N$ value of the mantle. In fact, a significant missing piece of the N puzzle is the origin of the depleted $\delta^{15}N$ signature of the MORB-source mantle, which exists in an apparent disequilibrium with isotopically enriched surface reservoirs. As briefly discussed in Sec. 2.5.5.1, there appear to be two classes of solutions to this dilemma: the MORB-source mantle records early subduction of depleted N (Marty & Dauphas, 2003) or that fractionations of N isotopes during deep Earth transport are responsible. A distinct MORB-only source mantle is not supported by our compilation herein, as many OIB have equivalent $N_2/^{40}Ar$ values as MORB. However, MORB and OIB have different $\delta^{15}N$ values at $-5‰$ and $> 0‰$, respectively, so there must be some process to explain this distinction. Possibly they represent pools of different subducted material that has "aged" the same amount to yield equivalent $N_2/^{40}Ar$. Preservation of distinct $\delta^{15}N$ values implies incomplete mantle mixing over time. The existence of the high-N mantle sup-

ports the existence of different mantle domains, though we cannot rule out that the different $N_2/^{40}Ar$ signature of the high-N reservoir could be caused by fractionation of N from during subduction or deeper mantle processing. Redox reactions and possible N sequestration in the transition zone and lower mantle may all affect N geochemical signatures of mantle and mantle melts.

It is becoming apparent experimentally (Li et al., 2013) and theoretically (Mikhail & Sverjensky, 2014) that NH_4^+ is the predominant species of N in much of the mantle. The geochemical behaviour of NH_4^+ in subduction zones and mantle reservoir materials (e.g., silicates, Fe-metal) should be a target for future research, as any isotopic fractionations are unknown to us at this time.

2.6.3 Bulk Earth δ^{15}N and N delivery during accretion

A long-standing conundrum concerns the geochemistry and isotopic signature of N delivered to the planet during accretion. The budget estimate based on CC and EC compositions assumes that significant N was present in the Earth during its early history to ensure its participation in core formation. The implication is that N was not delivered in any late veneer, but instead was delivered during the main phase of accretion. It must have been in a reduced form, either NH_4^+ or as nitride, and contained within either silicate lattices or Fe-metal, as N_2 would be too volatile, and perhaps not present in significant quantity in the inner solar system. Existing isotopic data is inconclusive on identifying a single meteoritic analogue. The presence of very depleted δ^{15}N values from the mantle has been suggested to reflect preservation of primordial EC-like material, though these are analyses from diamonds (Palot et al., 2012), and the behaviour and fractionation of N during diamond growth may not be fully understood. Additionally, CC have δ^{15}N that is generally enriched. Our BSE+atmosphere bulk δ^{15}N, given masses in Table 2.14 and δ^{15}N values for MORB-source mantle (-5‰), high-N mantle ($+5$‰), continental crust (7.3‰), and atmosphere (0‰), is 2.1‰.

This estimate is distinct from either CC ($\sim$ 30‰) or EC (~ -25‰), meaning either the Earth did not acquire its N from a single chondritic source or the process of core formation significantly fractionated N. The Bulk Earth δ^{15}N value could be explained by a $\sim$ 50% contribution of CC-like and a $\sim$ 50% contribution of EC-like material during accretion, given no fractionation during core formation. If there was significant fractionation during core formation, it would have a large effect on residual

N in the BSE. There is suggestion proposed that the dissolution of N into Fe-metal would preferentially fractionate light isotopes into the metal, following a Sievert's law-type reaction of $N_2 \rightleftharpoons 2N$ dissolved (Dauphas & Marty, 1999). This assumption suggests that breaking of the ^{14}N–^{14}N bond is easier, so this isotope goes into the metal, leaving residual silicates enriched in $\delta^{15}N$. Were this the case, it would imply a higher contribution of EC to Earth's N. In principle, the same effect would be seen in NH_4^+, but to our knowledge, there are no experimental studies measuring N isotopes in coexisting metal and silicates.

A possible source of information concerning fractionation during core formation could be measurements of pallasites, which are meteorites thought to represent core-mantle boundaries of planetesimals. Measurements made by Prombo & Clayton (1993) on coexisting silicate and metal in pallasites show that the silicate phase is almost always isotopically enriched compared to the metal phase. The fractionation is up to $\sim 70‰$, which suggests fractionation during core formation could be quite large. Experimental work at pressures appropriate to Earth's core formation could help corroborate or quantify this effect for the Earth.

2.7 Conclusions

We have compiled a nominal, self-consistent, whole-Earth N budget based on two independent approaches. Both a chondritic comparison and literature compilation of terrestrial analyses reveal the BSE contains many present atmospheric masses of N (PAN). Estimates are $17 \pm 13 \times 10^{18}$ kg to $31 \pm 24 \times 10^{18}$ kg N and $27 \pm 16 \times 10^{18}$ kg N, respectively. Both estimates are higher than previous work, and suggest we have found the supposed "missing N". Additionally, several conclusions are apparent from each approach.

The chondritic comparison is consistent with the Earth receiving its N during the main phase of accretion. This indicates significant ($\sim 10^{20}$ kg) N in the core, as N is siderophile under reducing conditions. If there is limited N-isotope fractionation during core formation, $\delta^{15}N$ values for the BSE plus atmosphere suggest a mix of $\sim 50\%$ enstatite-like and $\sim 50\%$ carbonaceous-like chondritic material can explain the N content of Earth.

Our terrestrial literature compilation budget indicates that the continental crust (~ 0.5 PAN) and especially the mantle (~ 6 PAN) contain significant N. Interestingly, N-Ar and $\delta^{15}N$ data from MORB, OIB, and xenoliths identifies the existence of two

distinct N reservoirs: MORB-source like (MSL) and high-N. MSL, which is $\sim$ 98% of the mantle by mass, contains $\sim$ 2 atmospheric masses of N, has depleted δ^{15}N, and its Ar-isotopes suggest material was subducted deep in the geologic past. In contrast, high-N mantle has at least several atmospheric masses of N, enriched δ^{15}N, and appears to have been subducted more recently.

The presence of a large mass of subducted N in the mantle has important implications for the history of atmosphere-mantle communication over time. At present subduction rates, the entire atmospheric mass of N could be mixed into the mantle if only $\sim$ 50% of down-going N is returned to the atmosphere via arc volcanism. Nitrogen-Ar systematics indicate that the atmosphere and MSL are well mixed, and therefore that the mantle may serve to buffer the amount of N in the atmosphere. More reduced geochemical conditions at the surface and hotter mantle temperatures in the Archean may have lead to more efficient N subduction in the past, perhaps indicating a more massive atmosphere early in Earth history that has been progressively sequestered into the mantle.

This is an exciting time for research concerning the geologic N cycle. While the overall cycle is understood, there are areas for future research that are critical for more fully understanding N in the solid Earth. More analyses of N and Ar in OIB and xenoliths would help clarify the nature and extent of the high-N mantle. Experimental work investigating the behaviour of N, specifically as NH_4^+, during subduction and under mantle conditions should help reveal geochemical and isotopic fractionations during mantle transport. Modelling work, anchored to the budget presented herein, can elucidate the interchange of N and other surface materials through the solid Earth over geologic time.

Acknowledgements

The authors would like to acknowledge Dante Canil, Rameses D'Sousza, and Brendan Byrne for constructive feedback and discussion concerning this manuscript. We also thank Ralf Halama and Yuan Li for careful review of the manuscript. Funding was provided by NSERC Discovery grant to CG.

Chapter 3

Measurement of geologic N using mass spectrometry, colourimetry, and a newly adapted fluorometry technique

The following is a manuscript in review as:

Benjamin W. Johnson, Natashia Drage, Jody Spence, Nova Hanson, Rana El-Sabaawi, & Colin Goldblatt. 2016, Measurement of geologic N using mass spectrometry, colourimetry, and a newly adapted fluorometry technique

to *Solid Earth*. A revised submission, including comments from the dissertation committee and two peer-reviews is reproduced here.

3.1 Abstract

Long viewed as a mostly noble, atmospheric species, recent work demonstrates that nitrogen in fact cycles throughout the Earth system, including the atmosphere, biosphere, oceans, and solid Earth. Despite this new-found behaviour, more thorough investigation of N in geologic materials is limited due to its low concentration (1 to 10s ppm) and difficulty in analysis. In addition, N can exist in multiple species (NO_3^-, NH_4^+, N_2, organic-N), and determining which species is actually quantified can be

difficult. In rocks and minerals, NH_4^+ is the most stable form of N over geologic time scales. As such, techniques designed to measure NH_4^+ can be particularly useful.

We measured a number of geochemical rock standards using three different techniques: mass spectrometry, colourimetry, and fluorometry. The fluorometry approach is a novel adaptation of a technique commonly used in biologic science, applied herein to geologic NH_4^+. Briefly, NH_4^+ can be quantified by HF-dissolution, neutralization, addition of a fluorescing reagent, and analysis on a standard fluorometer. We reproduce published values for several rock standards (BCR-2, BHVO-2, and G-2), especially if an additional distillation step is performed. While it is difficult to assess quality of each method, due to lack of international geologic N standards, fluorometry appears better suited to analyzing mineral-bound NH_4^+ than mass spectrometry, and is a simpler, quicker alternative to colourimetry.

To demonstrate a potential application of fluorometry, we calculated a continental crust N budget based on new measurements. We used glacial tills as a proxy for upper crust and analyzed several poorly constrained rock types (volcanics, mid-crustal xenoliths) to determine that the continental crust contains $\sim 2 \times 10^{18}$ kg N. This estimate is consistent with recent budget estimates, and shows that fluorometry is appropriate for large-scale questions where high sample throughput is helpful.

Lastly, we report the first δ^{15}N values of six rock standards: BCR-2 (1.05 ± 0.4‰), BHVO-2 (-0.3 ± 0.2‰), G-2 (1.23 ± 1.32‰), LKSD-4 (3.59 ± 0.1‰), Till-4 (6.33 ± 0.1‰), and SY-4 (2.13 ± 0.5‰). The need for international geologic N standards is crucial for further investigation of the Earth system N cycle, and we suggest that existing rock standards may be suited to this need.

3.2 Introduction

Since its classification as an atmophile element by Goldschmidt (1937), the fate and nature of N in rocks and minerals has received little attention. Many early budgets suggested most of Earth's N was assumed to be in the atmosphere, with only minor amounts in the biosphere, crust, and mantle (e.g., Wlotzka, 1972). And while concentrations are low, typically 1 to 10s of ppm, the great mass of the solid earth compared to the atmosphere allows for a substantial amount of planetary N to be in the Bulk Silicate Earth (BSE). In fact, the BSE and core likely contain the majority of N in the Earth (Johnson & Goldblatt, 2015). In addition, enriched δ^{15}N values from mantle-derived rocks and the correlation of N_2 with ^{40}Ar indicates that N has

cycled between the surface and the deeper planet over geologic time (Marty, 1995; Busigny et al., 2011; Barry & Hilton, 2016).

In spite of the new-found richness of the geologic N cycle, the relative paucity of sample analyses limits robust interpretation or modelling of N cycling over Earth's history. This paucity is due in large part to the difficulty of measuring low concentrations of N in rocks and minerals. Though a variety of analytical techniques are now able to measure N at ppm-level concentrations in rocks and minerals (e.g., Bräuer & Hahne, 2005; Barry et al., 2012; von der Handt & Dalou, 2016), several of these are either analytically expensive or only operational at a handful of labs around the world. The development of techniques that are more easily accessible and able to be performed with standard geochemical equipment would be a great benefit to the community.

In this study, we adapt a fluorometry technique developed by Holmes et al. (1999) that is commonly used in biologic and aquatic chemistry studies, and compare it with two other techniques: colourimetry (Hall, 1993) and elemental analyzer mass spectrometry (e.g., Stüeken, 2013). Through analysis of a number of rock standards, we demonstrate that, while this fluorometry technique has some associated uncertainty, it reproduces published values for standards BCR-2, BHVO-2, and G-2, especially if a distillation step is undertaken. It also performs better than elemental analyzer combustion mass spectrometry or colourimetry methods for quantifying N in crystalline rocks. The fluorometry technique has the advantage over other techniques by being relatively fast, requiring few reagents, and and needed moderate analytical, as well as specifically targeting NH_4^+. There are three main benefits: the potential to increase the number of analyses of N in geologic samples due to relative ease of the method; a screening method that can be used to guide further isotopic investigation; as it only measures NH_4^+, this technique can also be helpful in determining which phase of N is found in geologic samples, which can be difficult using other techniques.

In addition, we also present a preliminary application of the method vis-á-vis a N budget for the continental crust based on glacial tills and crystalline crustal rocks from North America. Along with the atmosphere and mantle, the continental crust is one of the main N reservoirs on the planet (Goldblatt et al., 2009; Johnson & Goldblatt, 2015), thus determining its content is key in the evolution of the N cycle over time.

We also call for the development international geologic N standards (after Ader et al., 2016). Method development for measurement of geologic N suffers without such

Table 3.1: Rock standards from United States Geological Survey (USGS) and Geological Survey of Canada (GSC) analyzed with published values, if any, and N analysis reference.

Standard	Description	N (ppm)	Reference
BCR-1/2	USGS Columbia river basalt	34 ± 12	1, 2, 3
BHVO-2	USGS Hawaiian basalt	22.6 ± 3	1, 3
G-2	USGS Paleozoic granite	34 ± 4	1, 3
Till-4	GSC Till from Scisson's Brook, New Brunswick		
LKSD-4	Big Gull Lake sediment, Ontario		
SY-4	Diorite Gneiss, Ontario		

[1]Govindaraju (1994),[2]Norris & Schaeffer (1982), [3]Murty et al. (1983) ,

standards. We present the first δ^{15}N values of a number of rock standards (BCR-2, BHVO-2, SY-4, LKSD-4, Till-4, G-2), and suggest they may be suited for geologic N standards, given more thorough analysis.

3.3 Methods

3.3.1 Rock standards and samples

We analyzed a number of geochemical rock standards (Table 3.1). Several standards (LKSD-4, Till-4, SY-4) have no previous N concentration measurements, to our knowledge. Remaining standards have published N concentrations (BCR-2, BHVO-2, G-2), with values reported from neutron activation analysis (NAA). This technique works by irradiating samples with neutrons to transform ^{14}N into ^{14}C, where the resulting material can then be purified and assayed radiochemically as a proxy for N concentration (Shukla et al., 1978).

In addition to rock standards, we analyzed a number of other lithologies, including glacial tills, basalts, granites, and carbonates. These samples were chosen as a proof of concept for the adapted fluorometry technique, namely, investigating the N budget of the continental crust. All tills are from British Columbia, Canada, and have eroded a variety of Phanerozoic crustal lithologies. Basalts and welded tuffs are from the Bonanza Arc and Sicker Group on Vancouver Island, British Columbia. Granites

come from a variety of locations in North America. Sample descriptions are given in the supplemental material.

3.3.2 Rock Sample Preparation

Using a rock saw, rock samples were cut into small blocks and the weathered edges were removed. Rock powders were prepared by crushing the blocks in a steel jaw crusher and then powdered using a shatterbox with a tungsten carbide puck. The shatterbox puck and chamber were cleaned in between each crushing step using deionized water and ethanol. Clean quartz sand was run between each sample to prevent cross-contamination.

3.3.3 Method 1: Elemental analyzer mass spectrometry

We analyzed all rock standards at the University of Washington Isolab facilities following Stüeken (2013). First, $\sim$ 1 g of each sample was weighed into a clean (baked at 500 °C overnight) Pyrex test tube. Then, $\sim$ 10 mL 6N HCl was added, stirred with a glass stir rod, sonicated for 30 minutes, and left in an oven set to 60 °C overnight to remove carbonate. Tubes were then centrifuged to settle suspended sediment, acid was decanted, fresh acid was added, and the samples were sonicated and dried a second time as above. This decarbonation was done once more. Subsequently, we rinsed samples 3 times in DI-H_2O, and all were dried for 3 days at 60 °C.

Between 12 to 150 mg of decarbonated sample in 9x5 mm Sn capsules was flash combusted at 1000 °C in a Costech ECS 4010 Elemental Analyzer with an excess of O_2. Combustion products passed over a reduced copper column at 650 °C to convert all N to N_2 and absorb excess O_2 and a magnesium perchlorate trap to absorb water. Sample gas then passed through a 3 m gas chromatography column to separate N_2 from CO_2 before being analyzed on a Finnigan MAT253 continuous flow isotope-ratio mass spectrometer via a ThermoFinnigan Conflo III. All analyses were quantified using IsoDat software. Errors reported are standard deviations from repeated analyses. We used the following isotopic standards: two glutamic acids (GA-1 and GA-2), dried salmon (SA), and an internal rock standard (McRae Shale).

3.3.4 Method 2: Colourimetric

We followed the procedure outlined in Hall (1993) to analyze samples using colourimetry.

3.3.4.1 Reagent list

KOH: A 25% mass:volume solution of KOH was used for HF-neutralizing. We dissolved 250 g KOH in 1 L of water.

Phenol reagent: We weighed out 7.0 g of crystalline phenol and 0.02 g sodium nitroprusside into a 200 mL beaker. To this, we added 20 mL of KOH reagent and 60 mL of deionized water. Solids were stirred to dissolve, and then the solution was topped up to 100 mL total volume with DI-H_2O.

NaOCl: We diluted 20 mL of commercially available NaOCl to 100 mL total volume with DI-H_2O.

3.3.4.2 Stock Solution and working standards

A 1 g NH_4^+/L stock solution was prepared in a 250 mL volumetric flask by dissolving 0.7433 g of NH_4^+Cl salt in 250 mL DI-H_2O. From this, a secondary ammonium standard solution of 0.2 g NH_4^+/L was prepared in a 100 mL volumetric flask using 20 mL of the ammonium stock solution, topped with DI-H_2O. Stock solution was diluted to make working standard solutions of 0.005, 0.01, 0.05, 0.1, and 0.2 g/L, which were used to construct standard curves for sample concentration determination.

3.3.4.3 Sample Digestion

Working standards, blanks (DI$-H_2O$), and rock powder were subjected to HF treatment at room temperature in 25 mL Teflon vials. To these vials, we added 2 mL of working standard, 2 mL of blank, or approximately 0.25 g of rock powder. The samples were digested for seven days in 2 mL of 50% hydrofluoric acid in a fume hood. We swirled vials every two days to facilitate digestion.

After sample digestion period, the solution was neutralized by adding 20 mL of 25% KOH to each vial. Exploratory analysis of different aliquots from the top, middle, and bottom of each vial gave different results, thus the solution was stirred with a glass rod to ensure homogenization. The stir-rod was rinsed with DI-H_2O in between

samples to prevent cross-contamination. Homogenized solutions sat for 15 minutes to allow suspended rock powder to settle.

3.3.4.4 Colourimetric analysis

All liquid, plus undissolved solids, were placed in a 100 mL round bottom flask, which was attached to a standard distillation setup. Samples were boiled for $\sim$ 10 to 15 minutes, and 8 mL of distillate was collected into 8 mL of 0.01 N H_2SO_4. To this, 1 mL of phenol reagent, 1 mL of NaOCl, and 5 mL DI-H_2O were added and stirred. The colour-change reaction was allowed to proceed for 2 hours. Absorbance was measured at 630 nm in a plastic cuvette on an Ocean Optics spectrophotometer and quantified using SpectraSuite software.

Standard solutions were processed the same way as the samples. We made a standard curve of absorbance plotted against starting concentration (0.005, 0.01, 0.05, 0.1, and 0.2 g/L) of standard solutions. This was used to calculate sample concentrations, applying appropriate dilution corrections.

3.3.5 Method 3: Fluorometric

The following is a detailed description of our adaptation of the Holmes et al. (1999) method. Key considerations and suggestions for improvement are discussed in the following section.

3.3.5.1 Reagent list

Working reagent (WR): We made a mixture of sodium sulphite, borate buffer and orthophthaldialdehyde (OPA) solutions. The procedure for preparing the working reagent follows Holmes et al. (1999). To make the sodium sulfite solution, 0.2 g of sodium sulfite was added to 25 mL of DI-H_2O. For the borate buffer, 80 g of sodium tetraborate was added to 2 L of DI-H_2O, which was then stirred for 4 hours with a stir bar. To make the OPA solution, 4 g of OPA was added to 100 mL of 95% ethanol and protected from the light while stirred with a stir bar. The borate buffer, OPA solution and 10mL of the sodium sulfite were mixed in a $>$ 2 L brown polyethylene bottle. The working reagent mixture sat for at least one day prior to use.

3.3.5.2 Stock Solution and working standards

The same stock solution was used for fluorometry as for colourimetry. A range of working standards were made by diluting stock solution (0.2 g NH_4^+/L) into reaction bottles, resulting in concentrations of 0.005, 0.01, 0.05, and 0.1 g NH_4^+/L. This range of working standards was used to construct standard curves.

3.3.5.3 Sample digestion

The same digestion and neutralization procedures were used for fluorometry as for colourimetry.

3.3.5.4 Optional distillation

Some replicates of samples were distilled, as described in section 3.3.4. As this step is the most time-intensive step aside from digestion, we ran most analyses without distilling. As discussed later, this step may be useful for samples with either low N or samples that are difficult to digest completely (e.g., G2).

3.3.5.5 Fluorometric analysis

Brown 50 mL polyethylene bottles were used for the fluorescing reaction. The reaction bottles were first emptied of their storage solution (i.e., clean working reagent) and rinsed with 5 mL DI-H_2O. Using a pipette, 10mL of DI-H_2O was added to each reaction bottle. Subsequently, an aliquot of the neutralized solution was added. About 0.1 mL of sample solution was added to each bottle. Then, 2.5 mL of working reagent was added to each reaction bottle. After adding the working reagent, the reaction bottle was inverted to homogenize.

Immediately after homogenization, an aliquot of solution from the reaction bottle was transferred to a plastic cuvette, and fluorescence was measured in a 1 cm plastic cuvette using a Turner Designs AquaFluor fluorometer. The fluorometer has a 350 nm excitation filter with a 25 nm bandpass, a $\geq$ 420 nm emission filter, and a minimum detection limit of 0.1 μM NH_4^+. After this initial measurement, the aliquot of solution was transferred back into its reaction bottle, the cuvette was rinsed, and the bottle was capped and inverted several times to homogenize. The sample then reacted for three hours. After three hours, fluorescence was measured in three sample aliquots. Sample concentrations were calculated using a standard curve (Fig. 3.1).

After measurement, the remaining solution in the reaction bottle was emptied and a small amount (2 mL each) of working reagent and DI-H_2O was added to the bottles for storage.

3.3.5.6 Calculation of sample NH_4 concentration

Net fluorescence (F_{net}) for working standards and samples were calculated by averaging the three final fluorescence ($\bar{F}$) readings, subtracting initial fluorescence (Fi), then subtracting average fluorescence minus initial from the blank ($\bar{B}$) (Eq. 3.1).

$$F_{\text{net}} = \bar{F} - Fi - \bar{B} \tag{3.1}$$

Then, using standard curves (either corrected to digestion vials or in reaction bottles, slope = s) sample concentration in either digestion vials or reaction bottles was calculated. Importantly, we chose to force standard curves through the origin.

Final NH_4^+ concentrations ($[NH_4^+]$) were calculated by correcting concentration to KOH-neutralized vial, multiplying concentration by total volume in vial (D) to determine a mass of NH_4^+. Then, we divided this NH_4^+ mass by starting sample rock powder mass (m) to get the concentration of NH_4^+ in ppm-mass (Eq. 3.2).

$$[NH_4^+] = \frac{F_{\text{net}}}{s}\frac{D}{m} \tag{3.2}$$

3.4 Results

3.4.1 Method 1: Mass spectrometry

Elemental analyzer mass spectrometry was able to measure N concentration in all rock standards (Table 3.2). Analyses for crystalline standards are lower than published values, likely due to the incomplete liberation of N from silicate lattices during combustion (Bräuer & Hahne, 2005). Values for BCR-1/2 are 62% of published, BHVO-2 59% of published, and G-2 15% of published. Values reported herein for Till-4, SY-4, and LKSD-4 are the first to our knowledge.

In addition, we report $\delta^{15}N$ values for all samples (Table 3.2). While more analyses would need to occur for these to be used as isotopic standards, the fact that there is measurable N in all standards suggests they may be suitable candidates for geologic

Table 3.2: Nitrogen and δ^{15}N data from colourimetric and mass spectrometry analyses. Both techniques appear to underestimate N concentration, perhaps due to incomplete N-extraction during combustion for mass spectrometry or incomplete recovery of NH_4^+ distillation. Concentrations are in ppm.

Standard	**Published**	**Colourimetric**	**Mass spectrometry**	δ^{15}**N**
BCR-1/2	34 ± 12	12.6 ± 8	21	1.05 ± 0.4
BHVO-2	22.6 ± 3	3.5 ± 0.7	13.3 ± 0.6	-0.3 ± 0.2
G-2	34 ± 4	1.6 ± 0.9	5 ± 0.7	1.23 ± 1.32
SY-4		6.9 ± 2.8	14.3 ± 0.6	2.13 ± 0.5
LKSD-4		487 ± 401	16000 ± 8	3.59 ± 0.1
Till-4		82.2 ± 40	440 ± 2	6.33 ± 0.1
Carb		66.1	48.5 ± 1.3	

N-isotopic standards. Samples with high N (presumably some organic N), LKSD-4 and Till-4, could be ideal.

3.4.2 Method 2: Colourimetric

The colourimetric method was able to analyze all rock standards (Table 3.2), with standard curves having r^2 values above 0.99 (Fig 3.1). Measured concentrations are lower than published values, at 37% ,15% and 5% of published values for BCR-2 , BHVO-2, and G-2, respectively (Table 3.2). We suggest that this potential underestimate is due, in part, to difficulty in quantitatively distilling all NH_4^+ from a dissolved sample. The distillation apparatus is imprecise in nature, and controlling the final volume of distillate is difficult.

3.4.3 Method 3: Fluorometric method

3.4.4 Rock standards

Results for rock standard analyses are shown in Table 3.4. Values range from 5.2 to 5200 ppm by mass. Analyses without distillation match published values within error for BCR-2 and BHVO-2, with values of 33 ± 8.3 and 15 ± 5.7 ppm, compared to 34 ± 12 and 22.6 ± 3, respectively. Analyses of G-2 are lower than published, at 11 ± 4.9 from our analyses and 34 ± 4 from literature values. Other standards have

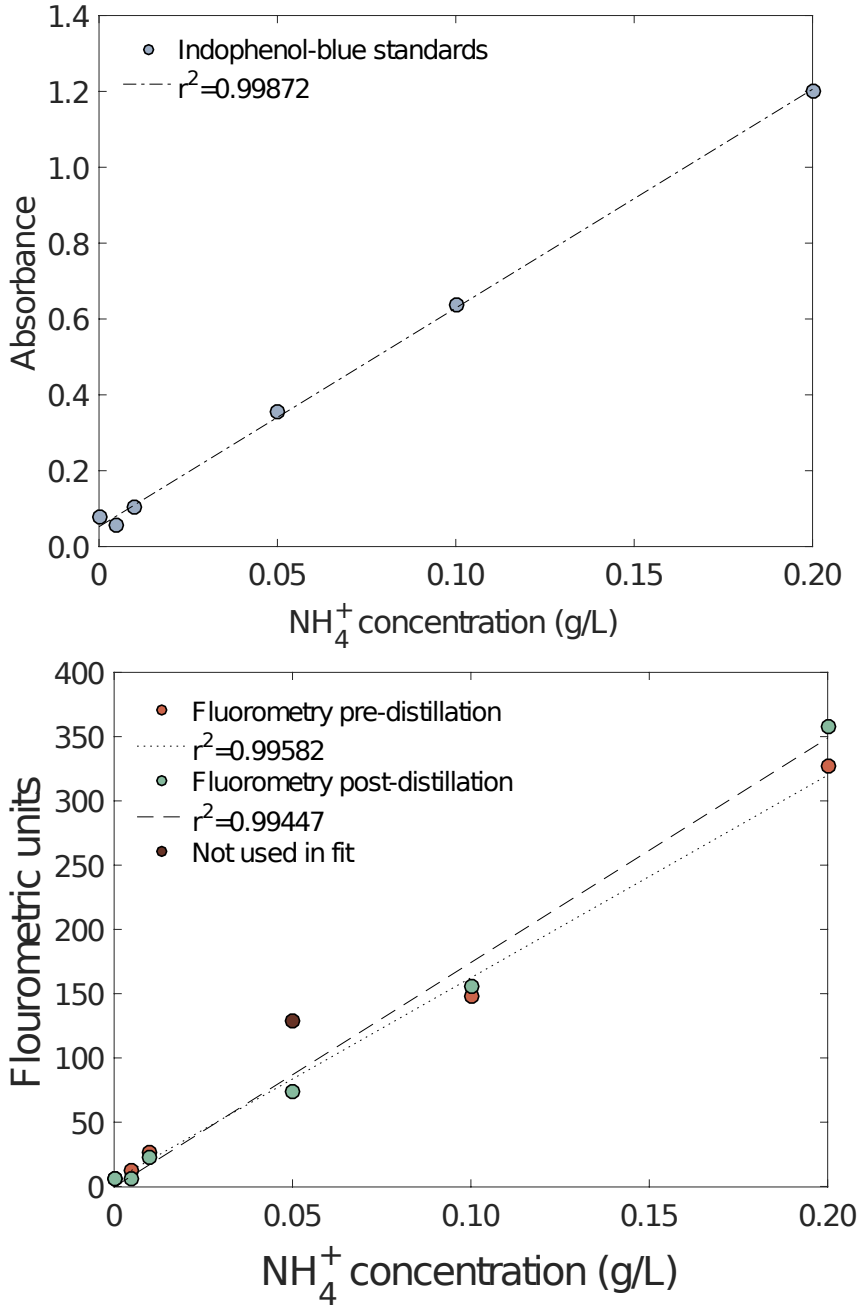

Figure 3.1: Example standard curves for colourimetry and fluorometry analyses. Absorbance is the difference between light that enters the sample cuvette and the light that transmits through the sample cuvette to the detector. Values larger than 1 are due to dilution corrections. These standard curves were used to calculate sample values for those analyses occurring after distillation. In addition, fluorometry curves show that distillation does not greatly affect working standards during distillation, though the same may not be true for actual samples.

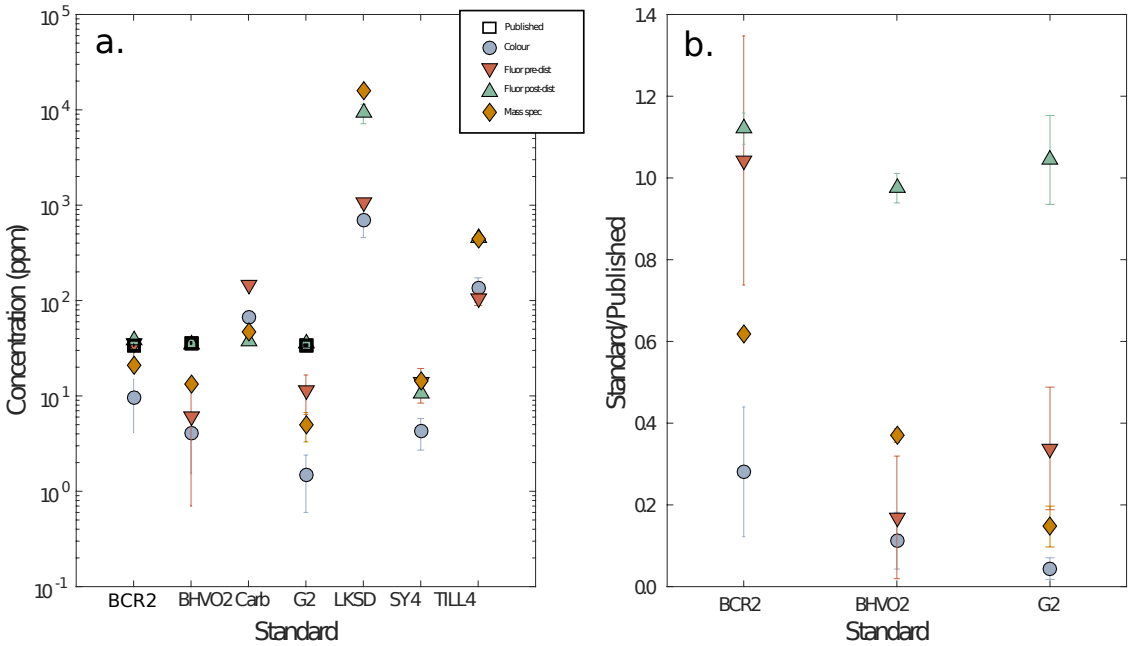

Figure 3.2: a. Comparison of N concentrations in rock standards from three different methods. Colourimetry consistently yields lower values than fluorometry, and values typically lower than EA-mass spectrometry. Fluorometry and EA-mass spectrometry give similar results for sedimentary rocks (LKSD-4, Till-4, 5.1), but tend to differ for crystalline rocks (BCR-2, BHVO-2, SY-4, G-2), with fluorometry giving higher concentrations. b. Though associated errors are larger, fluorometry does reproduce published N concentration values from three standards (BCR-2, BHVO-2, G-2), especially after distillation.

values of 5.2 ± 4.5 (SY-4), 5200 ± 1000 (LKSD-4), and 71 ± 25 ppm. Analyses after distillation are generally higher than those with no distillation step.

3.4.5 Continental Crust

Measured NH_4^+ concentrations from a number of continental crust samples are shown in Table 3.3. We have included analyses of BCR-2 in the "volcanics" category. In general samples of all crystalline rock types have between 10 to 40 ppm, and sedimentary rocks are higher, with values between 100 and 1000 ppm.

Table 3.3: Nitrogen concentration (ppm) in upper crustal rocks using the fluorometry method. Shown are mean ($\bar{x}$), standard deviation (σ), coefficient of variation (c_v), and number of samples (n).

Rock type	$\bar{x} \pm \sigma$	c_v	n
Tills	81.2 ± 36.4	0.45	8
Silt	1060 ± 113	113	1
Volcanics	21.4 ± 12.5	0.11	13
Carbonates	114.2 ± 40.9	0.36	1
Granitic	15.8 ± 14.6	0.92	5
Gabbro	11.3 ± 12.6	1.12	5
Gneiss	29.8 ± 0.8	0.03	1
Xenolith	34.4 ± 16.1	0.47	8

3.5 Discussion

3.5.1 Fluorometry

3.5.1.1 Reproducibility and reproduction of published values

Reproducibility of repeated analysis was between $10 - 50\%$ of mean values for all rock standards (Table 3.4). Overall, error appears to be lowest for samples which are most easily digested: BCR-2 and carbonate. More felsic standards, such as G-2, have higher error but also show lower concentrations than previous work. On runs with distillation, G-2 (36 ± 4 ppm) matched published values (34 ± 4 ppm), BCR-1/2 (38 ± 1 ppm) also matched published values (34 ± 12 ppm), and BHVO-2 (35 ± 1 ppm) had higher than published values (22.6 ± 3 ppm). Runs without distillation gave concentrations below their published values, with 11 ± 4.9 ppm for G-2 and 15 ± 5.7 BHVO-2. Therefore, distillation appears to improve agreement between fluorometry and NAA, though this may be coincidence, as NAA analysis has several unresolved issues with calculation accuracy.

We stress that although NAA is of appropriate sensitivity to measure ppm-level N concentrations (e.g., Kolesov, 1995), there are complicating issues. Neutron bombardment can also create ^{14}C via reaction with ^{17}O, with theoretical apparent N contribution in a sample with 40% O of 18 ppm, though analysis of a synthetic Al_2O_3 doped with 20% ^{17}O suggests the actual effect may only be 6 ppm (Shukla et al., 1978). In addition, 52 analyses of BCR-1 by Murty et al. (1983) yielded a range in concentration from 15 to 62 ppm. The authors suggest this is due to heterogeneous distribution of N in BCR-1. Alternately, such a range in concentration could be due to adsorption of atmospheric N_2. Though sample powders are prepared for irradiation after vacuum pumping (or heating), the possibility of atmospheric N_2 contamination appears unresolved Norris & Schaeffer (1982). Thus, though NAA-analyses of N in rock standards should be able to quantify total N in a sample, several outstanding issues prevent concentrations reported in the literature from being accepted as geochemical standards. A major difficulty in the development of new techniques for measuring geologic N is a lack of international standards.

3.5.1.2 Effects of KOH

The most significant parameter affecting the quality of the standard curves was the concentration of KOH in the reaction bottles. For a given concentration of NH_4^+, varying KOH concentration altered resulting fluorometry readings (Fig. 3.3). Since the fluorescing reaction is pH dependent (operating between pH 8-10 due to borate buffer), addition of excess KOH causes the pH of the solutions to be too high, and the fluorescing reaction to be inhibited. We adjusted sample dilutions and volumes to result in KOH concentrations in reaction bottles to be between 0.05 to 0.2%.

We have verified that small KOH concentrations, as described above, do not affect standard curves (Fig. 3.4). Curves prepared on multiple days with water were identical to those produced with KOH, indicating that the fluorescing reaction had gone to completion. High corrected fluorescence values were due to corrections for dilutions occurring when KOH was added to the initial standard volume, as well as dilutions occurring when preparing reaction bottles. Though there is some variability at concentrations below 0.020 g/L from day to day, similarity of KOH-curves and water only curves implies that the standard curve technique is viable.

3.5.1.3 Digestion length

As sample digestion is only partial, it is possible that length of digestion has an effect on final concentration readings. We conducted a digestion length test for BCR-2 (Fig. 3.5), and found no clear relationship between digestion length and calculated N concentration. It appears as though there are other factors that have a greater effect on N concentration. Determining the length of time needed for the extraction of all NH_4^+ would be an important step, as this could increase sample processing efficiency and sample throughput.

3.5.2 Methods comparison: pros and cons

The main difference between methods discussed in this work is that two (mass spectrometry and NAA) analyze total N while colourimetry and fluorometry specifically target NH_4^+. While assaying total N may be advantageous in samples with mixed N speciation (e.g., sedimentary rocks), total N analysis has a more difficult time accounting for N_2-contamination from the atmosphere. As rock samples are commonly ground to a fine powder before analysis, the possibility of adsorbing some N_2 could

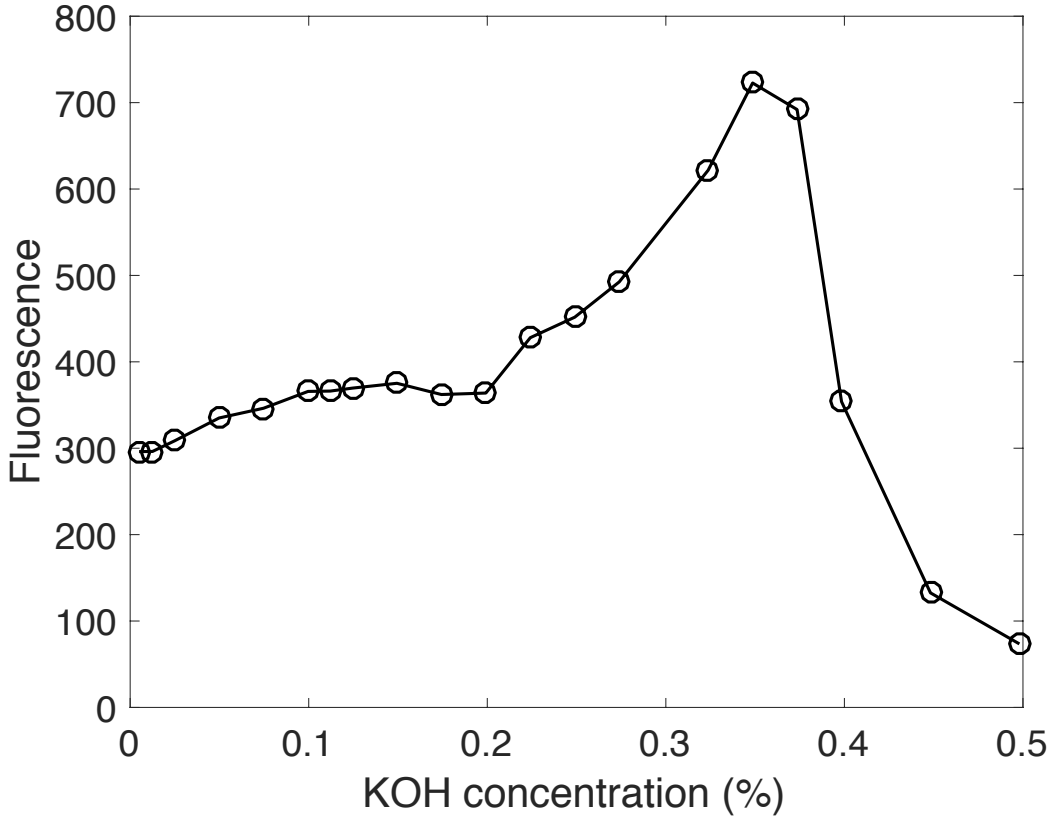

Figure 3.3: Sensitivity test for samples with 0.010 g/L NH_4^+ and varying concentrations of KOH in reaction bottles. KOH clearly has an effect on fluorescence. Fluorescence values are flat between 0 to 0.2% KOH, with a large increase approaching 0.35% KOH, and a steep drop off at higher KOH concentrations. We suggest that high concentrations of KOH overwhelm the buffering capacity of the working reagent and inhibit completion of the fluorescing reaction. All reported runs herein had between 0.05 to 0.2% KOH. Controlling KOH concentration is a key factor in the success of this method.

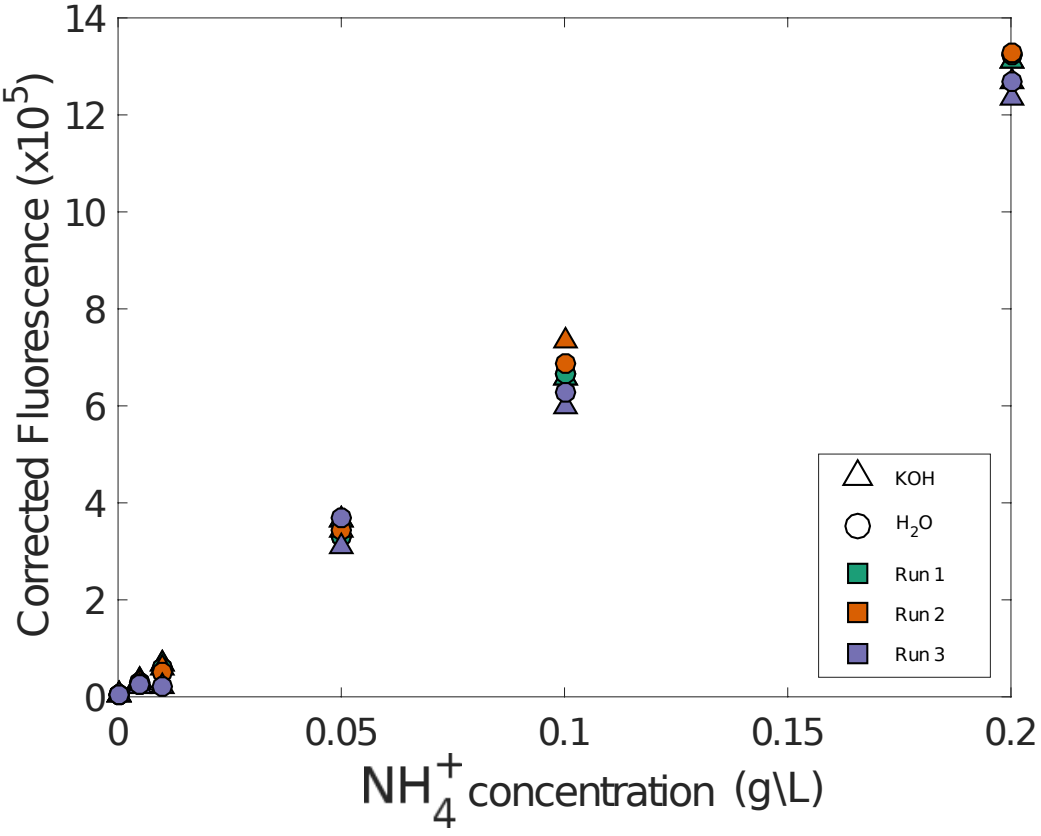

Figure 3.4: Standard curves from three different days comparing preparations made with KOH-solutions to those with only water. Since curves from the same day are indistinguishable with and without KOH, the fluorescing reaction is not affected by the presence of KOH (see text for details). Some variability exists between runs, especially at lower concentrations, but variations are small compared to changes in fluorescence units with changing concentration.

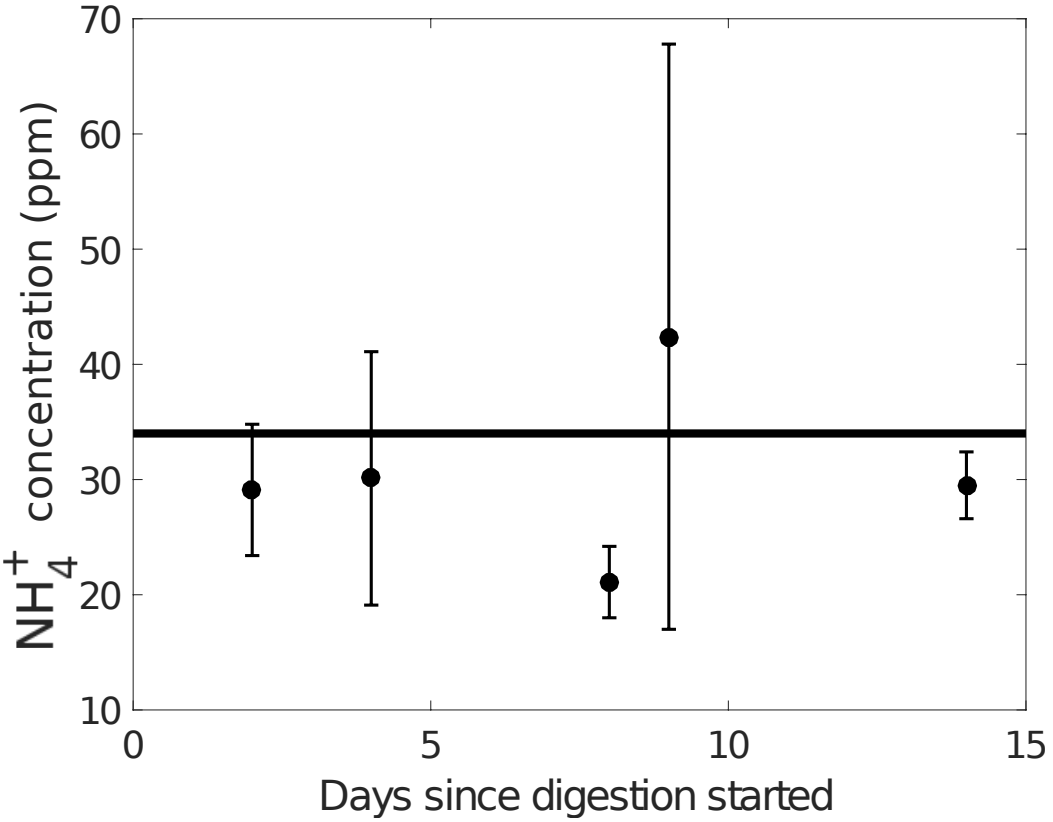

Figure 3.5: Digestion length test for BCR-2 by the fluorometry technique. Samples were digested in 2 mL 50% HF for the number of days indicated. Analyses reproduce published value (34 ppm, black line) within error after only 2 days, and, aside from one analysis 8 days after digestion began, approximate this value afterwards. There is large error in some samples compared to Table 3.4, likely due to increased number of analyses reported in Table 3.4, decreasing standard deviation.

affect the accuracy of total N methods, especially where mineral-bound N concentrations are low. Targeted analysis of NH_4^+ is likely more better suited to crystalline rocks, where NH_4^+ is the primary N-species.

Mass spectrometry has the major advantage over fluorometry or colourimetry by being able to measure N-isotopes in a given sample. Isotopic values are crucial in determining N-cycling, both biologically and in geologic reservoirs. One application of the fluorometry technique is as a "first-pass" analysis to determine N concentration. The concentration of N in a sample dictates what type of mass spectrometric technique (e.g., EA, off-line combustion, etc.) is most appropriate for isotopic analysis.

Given the expense of installing a mass spectrometer, the relative inaccessibility of neutron irradiation sources, and the time required for NAA (weeks to months), fluorometry presents a relatively quick and straight forward alternative. All equipment and reagents are easily obtainable. Fluorometers are much more affordable ($\$3,000$ to $\$10,000$) than mass spectrometers ($\$100,000$s), and do not require any supporting infrastructure, and maintenance is comparatively low. And while the technique in its current state may not fully liberate NH_4^+ in all samples, it performs with similar reproducibility to mass spectrometry and NAA. Fluorometry also performs well without distillation, required for colourimetry. Distillation takes 15-20 minutes per sample, limiting throughput, and makes either fluorometry or colourimetry more on par with mass spectrometry in terms of time needed for analyses. Additionally, it is difficult to consistently distill the same volume for each sample, which limits accuracy and reproducibility.

In regards to fluorometric reagents needed, while HF is extremely dangerous, it is more commonly used in geochemistry than any of the colourimetric reagents (especially phenol and sodium nitroprusside), and with appropriate training and caution can be handled safely. Fluorometric reagents are also less hazardous than colourimetric reagents, and are linked with fewer long-term exposure issues.

The fluorometry technique also has the potential to measure very small quantities of NH_4^+. Its original development was for measuring ppb-level concentrations in natural waters, so if extraction from silicates can be complete, there is no reason to think a similar level of precision could not be developed for geologic samples.

3.5.3 Suggestions for fluorometry improvement

The most difficult to quantify aspect of the fluorometry and colourimetric methods are the efficiency of the extraction of NH_4^+ during HF digestion. since HF digestion is only partial, assessing the amount of NH_4^+ that remains in undigested materials could prove valuable. Undigested materials are likely predominantly organics and/or oxides. Oxides should have low NH_4^+, as there are no crystallographic spaces in mineral lattices to accommodate NH_4^+. Organic content is typically low in crystalline rocks (e.g., granites, gneisses), but would contribute N to bulk rock concentrations. Minimizing the amount of rock sample powder used may increase the efficiency of extraction. Indeed, preliminary tests suggest that measured concentrations are not affected down to the initial rock powder mass of 0.1 g (Fig 3.6), though at very small sample sizes homogeneity issues could become apparent.

Determining the concentration of N in non-dissolved material could be another area for improvement. The OPA reagent is sensitive to amino acids in addition to NH_4^+; the addition of sodium sulphite destroys the sensitivity to amino acids, making OPA react with ammonium alone (Holmes et al., 1999). If residual material left after HF dissolution were dissolved with an acid that dissolves organic matter (e.g., H_2SO_4), one could carry out a fluorometric analysis using a working reagent without sodium sulphite to constrain non-silicate N content.

There are other small areas for fluorometry improvement. One is to filter samples after neutralizing with HF, as sediment may affect fluorescence readings. The second is to attempt a neutralizing agent other than KOH, which may contain trace levels of NH_4^+. KOH was used initially due to its better performance (Hall, 1993) during distillation.

As noted by Ader et al. (2016), acquisition and development of a robust international standard would be extremely helpful in this or any future analytic technique development. Our work demonstrates that existing rock standards may be suited to this charge.

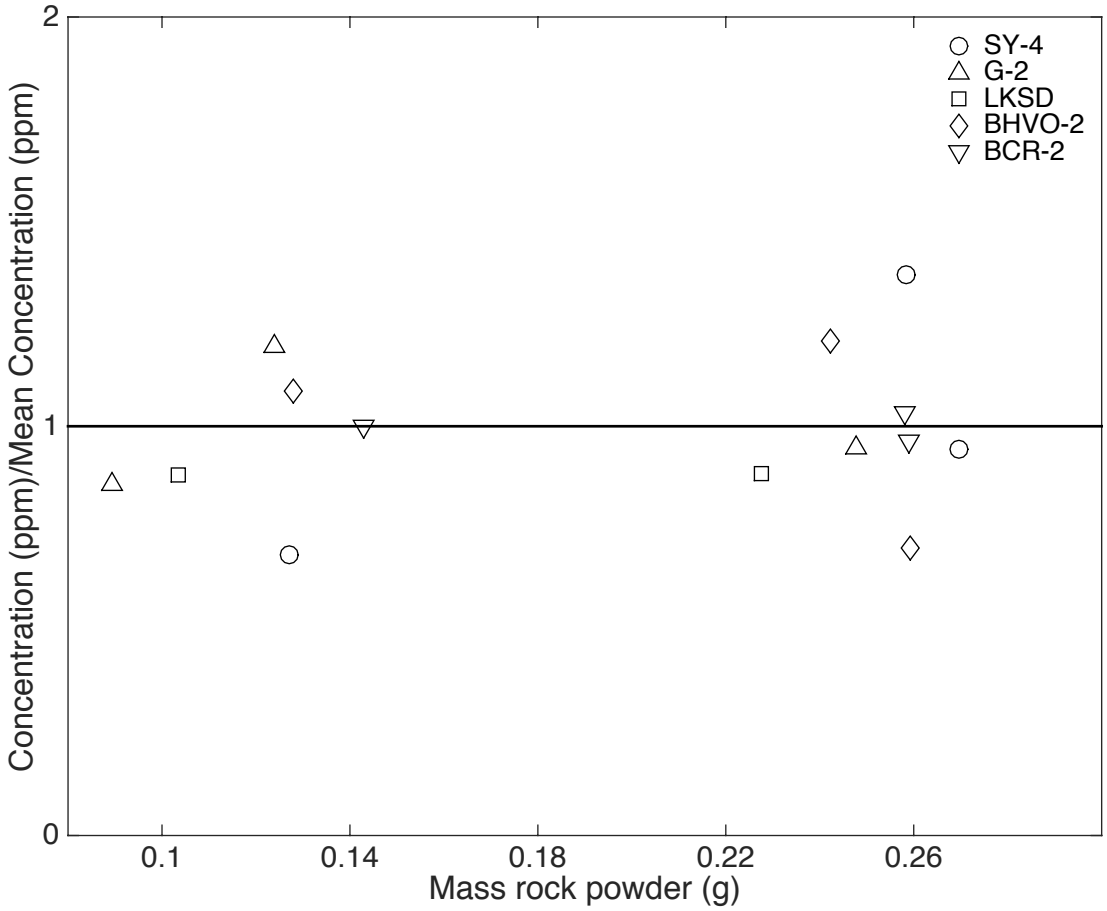

Figure 3.6: Measured concentration for rock standards normalized to mean concentration from analysis day plotted against the mass rock powder. Symbols represent standards, and all analyses shown are fluorometry with and without distillation. Decreasing initial sample mass does not seem to affect concentrations calculated, as measured concentrations show no significant trend away from the mean value given different amounts of rock powder dissolved.

Table 3.4: Nitrogen from all three techniques, mass spectrometry, colourimetry, and fluorometry compared to published values from NAA. Shown are mean with standard deviation and coefficient of variation in parentheses. The values after the commas in the Fluorometry column represent number of separate measurements for non-distilled samples. All concentrations are in ppm.

Standard	**Published**	**Colourimetric**	**Mass spectrometry**	**Post-distillation**	**Fluorometry**
BCR-1/2	34 ± 12 (0.35)	12.6 ± 8 (0.63)	21	38 ± 1 (0.02)	33 ± 8.3 (0.25), 36
BHVO-2	22.6 ± 3 (0.13)	3.5 ± 0.7 (0.2)	13.3 ± 0.6 (0.05)	35 ± 1 (0.03)	15 ± 5.7 (0.38), 9
G-2	34 ± 4 (0.12)	1.6 ± 0.9 (0.56)	5 ± 0.7 (0.14)	36 ± 4 (0.11)	11 ± 4.9 (0.45), 13
SY-4		6.9 ± 2.8 (0.41)	14.3 ± 0.6 (0.04)	11 ± 1 (0.09)	5.2 ± 4.5 (0.87), 9
LKSD-4		487 ± 401 (0.82)	16000 ± 8 (<0.01)	9300 ± 2150(0.23)	5200 ± 1000 (0.19), 9
Till-4		82.2 ± 40 (0.49)	440 ± 2 (<0.01)	455 ± 36 (0.08)	71 ± 25 (0.35), 15
Carb		66.1	48.5 ± 1.3 (0.03)	37	93 ± 18 (0.19), 12

Table 3.5: Comparison of different method requirements and performance. SPAD stands for samples per analysis day, and indicates approximate number of samples that can be run in one day, after all prep work has been completed. Accessibility is a qualitative measure of how common analytical equipment is in the geochemical community. Reproducibility is the average of the coefficient of variation from Table 3.4. Sensitivity indicates minimum concentration able to be potentially measurable.

	Colourimetric	**EA-Mass spectrometry**	**Fluorometry**	**NAA**
Prep time required	1 week digestion	1 week	1 week digestion	weeks to months
SPAD	< 30	18	50, or < 30 with distillation	
Species measured	NH_4^+	easily combusted organic, some NH_4^+	NH_4^+	total
Accessibility of equipment	high	medium	high	low
Reproducibility	0.52	0.05	0.38, 0.09-distilled	0.2
Sensitivity	~ 5 ppm	$\sim$ 10s ppm	ppb	ppm
Reagent toxicity	HF-high	low	HF-high	radioactivity

3.5.4 Preliminary application - continental crust

As a demonstration of the potential of the method, we calculated a N budget of the continental crust using analyses of a variety rock types. Most samples have come from Canada, though several are from other areas of North America. We present only averages here, full analyses are available in the supplemental material.

We calculate the N content of the upper continental crust using two approaches. The first is to use glacial tills as an average of upper crustal rocks (Tables 3.3, 3.6). Again, this should be regarded as a proof of concept approach, as these tills are all from British Columbia, Canada, and primarily erode Phanerozoic rocks. The second method relies on rock abundance data after Wedepohl (1995), measured N in those rocks either from this study (Tables 3.3, 3.6) or as compiled in Johnson & Goldblatt (2015). We stress that while tills are used as a representative of the upper crust, analyses of other rocks are not meant to be representative, and are instead analyzed to fill in gaps in poorly characterized reservoirs (e.g., volcanic, middle crustal xenoliths).

The two upper crust approaches yield results that are distinct from each other (Tables 3.3, 3.7). The rock abundance approach is most similar to Johnson & Goldblatt (2015). A wider range of till samples, which have eroded a greater variety of crustal ages and rock types, could address this discrepancy.

In addition, we use xenolith data to approximate the mafic lower crust and gneisses to approximate the felsic lower crust. These results are quite exploratory, and further analysis of lower crustal samples would assist interpretation greatly. By combining lower crustal our estimate with upper crust estimates, we find total crust N to be $1.1 \pm 0.4 \times 10^{18}$ kg using the till+xenolith approximation and $1.48 \pm 0.1 \times 10^{18}$ kg using rock proportion+xenolith. While these are the same within error, we note that this is primarily due to "diluting" the upper crust estimates with lower crustal values.

As an exercise to assess the impact of uncertainty in fluorometry measurements, we can perform the same budget calculations by using the highest and lowest analyzed values of BCR-2 compared to the mean value to bracket calculation accuracy. Given a maximum measured value of 42 ppm and a minimum measured value of 21 ppm (Supplemental), compared to a mean of 33 ppm for BCR-2, we can assess the effect of multiplying continental budgets by 1.3 and 0.64. This leads to a till-based upper crust range of 0.5×10^{18} to 1.1×10^{18} kg N, rock-abundance based upper crust range of 0.8 to 1.7×10^{18} kg N, and lower crust of 0.2 to 0.4×10^{18} kg N. These differences in continental N budget estimates do not change the broad agreement of our proof of

concept budget with previously published work, that the continental crust contains ~ 0.5 present atmospheric mass of N (PAN $= 4 \times 10^{18}$ kg N). For large scale questions, fluorometry is an appropriate technique. For questions that require finer resolution, such as biologic incorporation of rock-bound N (Morford et al., 2011), more method development is required.

The fluorometry technique has the potential to increase the number of analyses of under-sampled rock types such as volcanics and middle to lower crustal xenoliths. These poorly sampled reservoirs have the potential to sequester large amounts of N, and the continental crust can be both a long-term storage reservoir of N and an important source of biologically available N (Morford et al., 2011). Thus, determining its abundance is of interest to both geology and biology.

3.6 Conclusions

We have measured N concentration in a number of rock standards using three different methods: EA-mass spectrometry, colourimetry, and newly adapted fluorometry, and compared them to previously published values using neutron-activation analysis. Our analysis shows that fluorometry reproduces previously published values for BCR-2, and may also do so for BHVO-2 and G-2 given an additional distillation step. Fluorometry appears more well-suited to measuring geologic NH_4^+ in silicate rocks than either colourimetry or EA-mass spectrometry, while mass spectrometry is more well suited to high-N samples with significant organic N. No one method appears to be a "gold standard" for geologic N analysis, and we call for further development in this area. There are several suggested avenues for improving fluorometry, namely improving HF-digestion efficiency and fine tuning of HF-neutralization. Minimizing the volume of liquid required for digestion (HF) or neutralization would increase the sensitivity of the method, which could work for very low concentrations, down to ppb levels.

To demonstrate a potential application of fluorometry, we calculated a continental N budget. This budget is based on analysis of glacial tills (proxy for upper crust), a number of Phanerozoic volcanics, and a variety of mid-crustal xenoliths to augment existing literature analyses. Our approach estimates that $1.1 \pm 0.4 \times 10^{18}$ kg N (till+xenolith approach) and $1.48 \pm 0.1 \times 10^{18}$ kg N (rock abundance approach) is in the continental crust, consistent with recent estimates (Goldblatt et al., 2009; Johnson & Goldblatt, 2015). The fluorometry technique appears most appropriate

Table 3.6: Nitrogen concentration in upper and lower crustal rocks based on Wedepohl (1995). Proportions are of upper or lower crust mass, N concentration (ppm) are from this study (where error is shown) or from Johnson & Goldblatt (2015). Nitrogen contribution is simply concentration multiplied by proportion of crust. We use gneisses as a proxy for felsic granulites, and xenoliths for mafic granulites. Values from Johnson and Goldblatt, 2015 (JandG) given for comparison, with error shown as standard error of the mean.

Rock type	**Proportion crust (%)**	**N (ppm)**	**N contribution**	**JandG**
		Upper crust		
Shale/silt	6.16	1064 ± 113	65.6 ± 7.0	860 ± 64
Sandstone	2.94	230	6.8	230 ± 110
Volcanics	2.80	$21. \pm 12.54$	0.6 ± 0.3	50 ± 60
Carbonates	1.96	114.2 ± 40.9	2.2 ± 0.8	130 ± 17
Granitic	45	30.8 ± 14.5	13.8 ± 14.0	54 ± 7
Tonalite	5	24	1.2	24 ± 7
Gabbro	6	11.3 ± 12.6	0.7 ± 0.8	5 ± 2
Gneisses	19.20	29.8 ± 0.8	5.7 ± 0.2	135 ± 50
Mica schist	4.80	500	24.0	500 ± 44
Amphibolites	5.40	22	1.2	22 ± 10
Marble	1	1000	9.0	1000 ± 500
Total Average			124 ± 6.7	150 ± 12
		Lower crust		
Felsic granulites	62	29.8 ± 0.8	18.4 ± 0.5	17 ± 6
Mafic granulites	38	27.3 ± 16.6	13.1 ± 6.1	17 ± 6
Total Average			28.9 ± 6.8	17 ± 6

Table 3.7: Total continental crust N based on tills, rock proportions, and xenolith concentrations. Our results are consistent with previous work that suggests there is about 2×10^{18} kg N in the continental crust. All N masses are 10^{18} kg. Abbreviations are T (tills), RA (rock abundance), and LC (lower crust)

Reservoir	**Mass in kg (% of total)**	**N (ppm)**	**N mass**
Upper crust (T)	1.01×10^{22} (53%)	81.2 ± 36.4	0.82 ± 0.4
Upper crust (RA)	1.01×10^{22} (53%)	131 ± 14.1	1.32 ± 0.1
LC	8.9×10^{21} (47%)	28.9 ± 6.8	0.26 ± 0.06
Total crust (T + LC)	1.9×10^{22}	58 ± 21	1.1 ± 0.4
Total crust (RA + LC)	1.9×10^{22}	78 ± 7	1.48 ± 0.1

for these large scale questions, where exact precision is not required. An additional application could be as an initial analysis to determine approximate concentration, which is a key step in further isotopic investigations.

All methods assessed herein have strengths and weaknesses, which are amplified due to the ability of N to exist as multiple species in the same sample. We call here again for the development of internationally accepted geologic N standards. New method development is difficult without such standards, and care should be taken to classify what species of N (NO_3, NH_4^+, organic N, N_2) is being measured. We also report the first $\delta^{15}N$ values for a series of rock standards, as isotope values should be part of any international standard development.

3.7 Author Contributions

Benjamin W Johnson, Rana El-Sabaawi, and Colin Goldblatt designed the experiments and overall structure of the research. Samples were collected/procured by Benjamin W Johnson and Natashia Drage. Analysis was done by Benjamin W Johnson, Natashia Drage, and Nova Hanson. Laboratory support and technical input were given by Jody Spence. All authors contributed to the study.

3.8 Acknowledgements

The authors would like to thank NSERC Discovery grant to CG for funding CG and BWJ, a University of Victoria NSERC Undergraduate Student Research Award to ND, and NSERC awards to RES for funding support. Nitrogen isotope measurements were done at the University of Washington, and funded by the Virtual Planetary Laboratory.

Chapter 4

Marine primary productivity and oxygen production during Snowball Earth

The following is a manuscript that, at time of thesis submission, is under review as:

Ben Johnson and Colin Goldblatt. 2016. Marine primary productivity and oxygen production during Snowball Earth

at *Nature Communications*. Reviews were received on October 29th, 2016. The chapter presented herein is the manuscript version accounting for the reviews and has been resubmitted.

4.1 Abstract

The Neoproterozoic Earth experienced two Snowball Earth glaciations with ice at equatorial latitudes. Models permit either a "hard Snowball" with total sea ice cover or regions of open water, but complete sea ice is hard to reconcile with the absence of evidence for extinction of marine organisms. However, there is no direct data on the state of the ocean, or marine biological productivity, during the glacials. Here we present the first nitrogen isotope and trace element data from during a Neoproterozoic glacial episode. Synglacial sedimentary nitrogen is isotopically heavier

than the modern atmosphere, requiring an active biological nitrogen cycle with nitrogen fixation, nitrification and denitrification. Sedimentary barium enrichment may indicate active biological productivity. Uranium, vanadium and molybdenum concentrations suggest that surface waters had been in contact with the oxygenated atmosphere, and heterogeneous ocean chemistry including pools of oxic, anoxic and euxinic waters. These results require that there were biogeochemically significant regions of open water, allowing the hard Snowball model to be rejected, and show that there was active marine productivity throughout the harshest glaciations in Earth history.

4.2 Snowball Earth biogeochemistry

The late Neoproterozoic was a time of remarkable climatic and biological dynamism on Earth. After more than a billion years of stable climate through much of the Proterozoic, the Cryogenian period was punctuated by two long-lived Snowball Earth global glaciations (Hoffman et al., 1998). The appearance of multicellular organisms is thought to have occurred near this time period (Narbonne, 2005), as well as a rise in atmospheric oxygen in the Ediacaran (Och & Shields-Zhou, 2012). Thus, some of the greatest climatic fluctuation and evolutionary innovations (e.g., multicellularity) occurred during this crucial interval.

It was initially postulated that sea ice hundreds of metres thick covered the ocean during low-latitude glaciation, the so-called "hard Snowball Earth" (Hoffman et al., 1998; Kirschvink, 1992). This would have isolated the ocean from sunlight and atmospheric oxygen, presenting a formidable barrier to survival of oceanic species. However, no obvious mass extinction event seen in the fossil record (Corsetti et al., 2006), though this is difficult to determine given lack of body fossils. Solutions to survivability typically include invoking various "refugia" for organisms, ranging from global, low-latitude open-water belts (Abbot et al., 2011) to smaller features such as sea-ice cracks (Hoffman & Schrag, 2002) and ice shadows (Campbell et al., 2011). Geochemical calculations show that small areas of open water would permit sufficient air sea-gas exchange for the atmosphere and surface ocean to equilibrate (Le Hir et al., 2008). However, there are to-date no proxy data for the chemical state of the Snowball Earth ocean, and no direct evidence for biological productivity. An additional issue is that the long duration (10s Myr) of the glaciations would allow for oxic weathering

and reaction with metamorphic gases to deplete atmospheric oxygen completely if photosynthesis was low or absent.

We have recovered and analysed two sections of synglacial sedimentary rocks and one section of deglacial rocks representing the Marionan glacial (the second Neoproterozoic Snowball) from the Namibian Ghaub Formation. Using nitrogen isotope and redox-sensitive trace element (TE) geochemical data, we show that there was an active N-cycle, primary productivity, oxygen production, and an oxygenated atmosphere with at least pockets of oxygenated ocean water, despite extreme environmental stress.

4.3 Geologic nitrogen isotopes and redox-sensitive trace elements

Nitrogen isotopes in sedimentary rocks can record past biologic activity in the ocean (Ader et al., 2016); redox-sensitive TE concentrations in marine rocks are controlled by the redox state of both fluids delivering these elements to the ocean and the ocean itself. Post-depositional fluid alteration could also affect values. Combining N-isotopes with TE analyses is a powerful technique for interpreting past oceanic and biologic conditions in the ocean.

The modern N-cycle begins when atmospheric N_2 dissolved in the ocean is fixed (i.e., the triple bond is broken) into a biologically available form by a variety of single-celled organisms. This process is associated with a minimal isotopic [1] fractionation of ~ -2 to $+2$‰ (Hoering & Ford, 1960; Zerkle et al., 2008). Nitrogen fixing organisms then die, release waste, or are consumed by other organisms, and N is released into the water column as NH_4^+. In oxygenated water, NH_4^+ is quickly converted to NO_3^- via bacterial nitrification, which leaves residual NH_4^+ isotopically heavier by 16‰ (Pinti & Hashizume, 2011). However, if conversion from NH_4^+ to NO_3^- is complete, as in the modern ocean, this fractionation is not preserved. Nitrate can be converted back to N_2 or N_2O either in the water column or in sediments via denitrification ($NO_3 \longrightarrow N_2$) or anammox ($NO_2 + NH_4 \longrightarrow N_2$); both occur most rapidly in

[1] Stable isotope notations are in per mil (‰) notation, where

$$\delta^X \mathrm{E}(‰) = \left(\frac{{}^X\mathrm{E}/{}^x\mathrm{E}_{sample}}{{}^X\mathrm{E}/{}^x\mathrm{E}_{standard}} - 1 \right) * 1000 \tag{4.1}$$

E is element of interest, X is heavy isotope, x is light isotope. The standard used for δ^{15}N values is N_2 in air, which has a δ^{15}N value of 0‰ by definition.

low-O_2 waters/sediment pore space (Gruber & Sarmiento, 1997), and leave residual NO_3^- isotopically heavier by $> 25‰$. Alternatively, dissimilatory nitrate reduction to ammonium can transform NO_3^- to NH_4^+, again with no preserved isotopic effect if this goes to a completion (Godfrey et al., 2011). We use "denitrification" throughout the manuscript to include all pathways of NO_3^- removal.

A small amount of biologically processed N sinks to the sediment, and its isotopic composition reflects the overall N-cycle in the overlying water column (Tesdal et al., 2013). In the absence of biologic cycling, there would be very little N transferred to sediments and fixed N would likely have negative $\delta^{15}N$ values (Sigman et al., 2009). Organic N breaks down in sediment, releasing NH_4^+, which is absorbed by, or substitutes for K^+, in clay minerals. This process has little isotopic fractionation, especially in anoxic sediments (Freudenthal et al., 2001), thus sedimentary N faithfully records the isotopic signature of the water column from which it was deposited (Ader et al., 2016). Since $\delta^{15}N$ values depend on the balance of inputs (N fixation, minimal isotopic fractionation) and outputs (denitrification and anammox, large positive isotopic fractionation), sedimentary $\delta^{15}N$ indicates the state of the past N-cycle. Additionally, as the balance of outputs depend on O_2 concentrations, sedimentary $\delta^{15}N$ is a proxy for the redox state of the water.

Though sedimentary $\delta^{15}N$ reflects water column N-cycling, different balances of inputs and outputs can result in identical $\delta^{15}N$ values. For example, low, but positive, $\delta^{15}N$ can potentially result from either quantitative or minimal water column denitrification. Given that the amount of water column denitrification is directly related to the volume of anoxic water in the global ocean (Gruber & Sarmiento, 1997), a redox proxy is required to break this degeneracy.

A complication could arise if there is a fully anoxic ocean with ample NH_4^+. Since there is a fractionation associated with NH_4^+-assimilation, one would expect biomass in a N-replete ocean to be negative (Thomazo et al., 2009). Modern sediments generally reflect biologic cycling in the overlying water column (Tesdal et al., 2013), thus negative $\delta^{15}N$ values could record such an anoxic, but N-replete environment. If there is a deficit in dissolved NH_4^+, however, the fractionation from assimilation would not be preserved, as all available N would likely be assimilated into biomass. Complete assimilation of NH_4^+ in an anoxic ocean should result in biomass that is isotopically equal to fixed N. Again, we recognize the need for a redox proxy to assist in interpretation of N-isotopic data.

Redox-sensitive trace element data can be used to interpret confounding N-isotopic

data by determining water-column redox (Tribovillard et al., 2006). Uranium, V, and Mo are all more soluble in oxygenated water than in reduced water. These elements are delivered via oxic weathering (i.e., atmospheric oxygen is required), and their residence times are long ($> 10^4$ yr) in oxic waters. In anoxic waters, all precipitate rapidly and are deposited to sediments. In euxinic conditions, Mo is scavenged faster than U or V. Thus, given a supply of TE to the ocean via oxic weathering, sediments which record no enrichment in these elements were likely formed under an oxic water column, those with moderate enrichments under low-O_2 to anoxic conditions, and those with more Mo than U or V under euxinic conditions.

4.4 Geologic Setting and Sample Description

Neoproterozoic strata of Namibia (Hoffman, 2011) are characterised marginal continental deposits: carbonate platform with occasional subaerial exposure, slope deposits, and deeper water units. Interspersed are two distinctive glacial units, the Sturtian Chuos Formation and the Marinoan Ghaub Formations. Each glacial unit is overlain by a cap carbonate, the Rasthoff Formation and Keilberg Member, respectively. We have sampled and analysed samples from three sections of the Ghaub (Fig. 4.1). Importantly, all sampled intervals occur within the glacial interval, as evidenced by stratigraphic position below the uppermost diamictite (deposited synglacially) and cap carbonate, which indicates the end of Snowball glaciation (Hoffman et al., 2007).

The first sampled section is a synglacial siliciclastic (SGS) sequence from the Bethanis area. The Ghaub Fm. in this area grades upward from a laminated quartz siltstone, with authigenic pyrite, into bedded laminations (sampled) with frequent ice-rafted debris (IRD), and finally into a massive carbonate diamictite. It is interpreted to represent an ice advance, though the timing of this advance during the glaciation is unknown. There is no evidence of wave action, so it is likely a deep water setting. This unit is synglacial, evidenced by minor IRD at the bottom of the section.

Other sampled sections are from Fransfontein ridge, 80 km to the east. There are four facies at this location: massive carbonate diamictite, thinly laminated detrital carbonate with minor clay with and without IRD, and turbidites. Glacier activity in this region primarily eroded underlying carbonate platform units. The non-diamictite units at this section were likely deposited beneath a grounded ice sheet. Detrital carbonate was delivered, possibly by subglacial flow, into open water beneath floating ice. We sampled the thinly laminated beds without IRD, as this facies, synglacial with

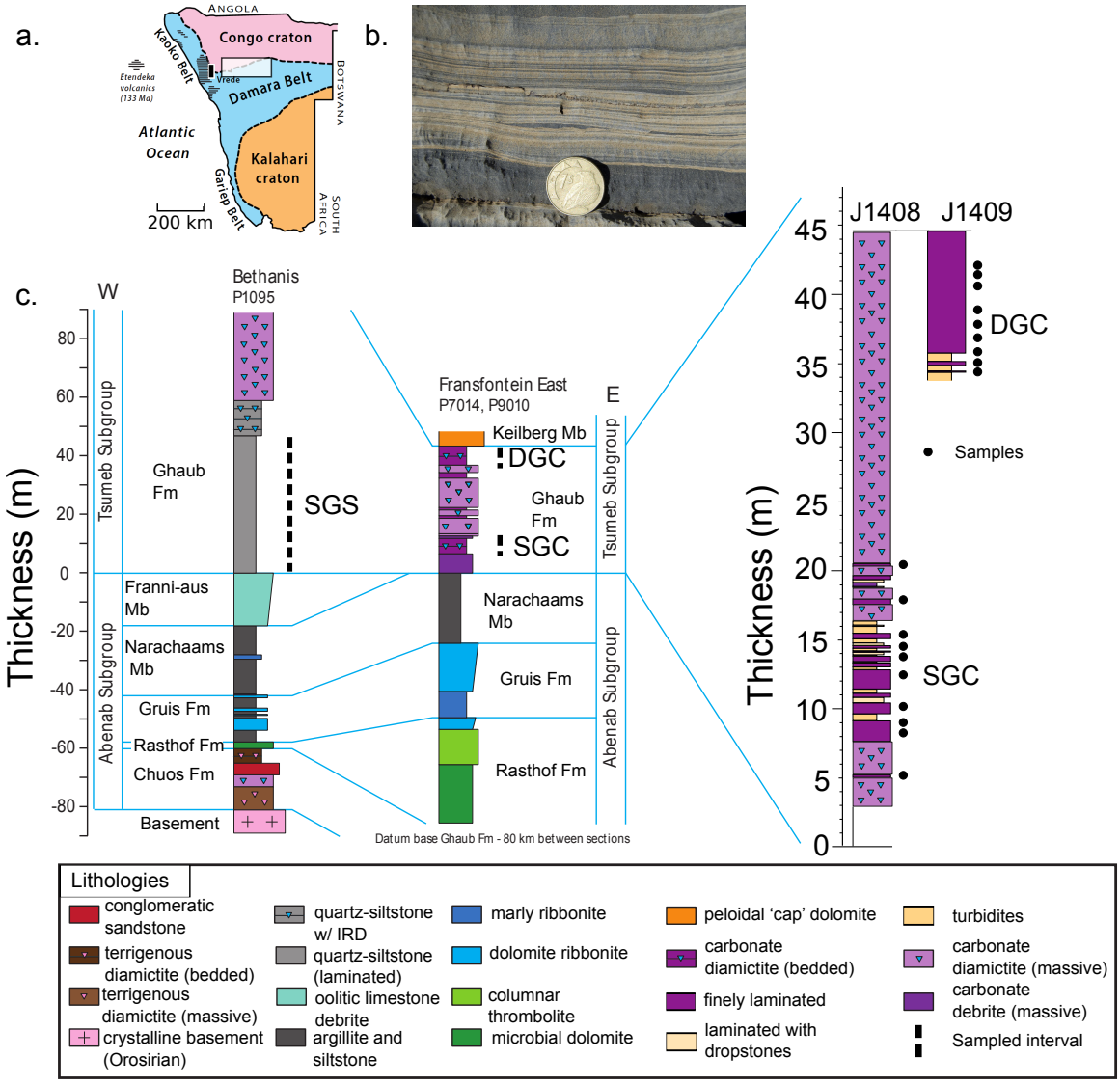

Figure 4.1: a.) Location map (Hoffman et al., 2014), b.) typical sample photo from section J1408, and c.) stratigraphy of studied sections. Fransfontein section is from Hoffman (2011), and Bethanis section is from Hoffman & Halverson (2008). Detailed section at Fransfontein highlights samples taken from only finely laminated beds without ice rafted debris or turbidites. Samples at Bethanis were taken at about 10 m spacing throughout the marked section. Sample section abbreviations are SGS (synglacial siliciclastic), SGC (synglacial with carbonate) and DGC (deglacial with carbonate).

carbonate (SGC), should best represent ambient water conditions. The laminated facies are overlain by 30 m of diamictite. We stress that analyses that follow focus on the clay fraction in these units, and not detrital carbonate.

Above the last glacial diamictite of SGC is the Bethanis member. This unit represents the terminal deglaciation. It is a dark coloured, bedded, detrital Fe-rich dolostone with minor clay. It is conformably overlain by the Keilberg cap carbonate (Hoffman, 2011). Again, we have sampled well-bedded intervals in an effort to analyze ambient water conditions during the deglacial (DGC).

In all units, there is the potential that any measured biogeochemical data samples reworked, detrital material. Any such material could mask information about the water column during deposition. However, modern N in most marine settings mostly comes from sinking organic material sourced from primary production. In addition, previous work suggests the source of the majority of Ghuab sediments was the Ombaatijie Fm., representing a near-shore carbonate platform (Hoffman, 2011), The Ombaatjie Fm. is relatively organic-poor (Halverson et al., 2005); thus, we suggest that detrital organic input is minimal in the sampled sections.

4.5 Geochemical data supporting periodic oxygenation

4.5.1 Nitrogen isotopes record primary values

Both synglacial sections have δ^{15}N (< 3‰) values distinct from modern marine average sediments (~ 5 to 7‰) (Fig. 4.2). Synglacial δ^{15}N values are all below 3‰ in SGS and SGC, with a small but significant decrease seen upsection in SGS and an increase followed by a decrease in SGC. In DGC, δ^{15}N increases overall upsection, to values approaching that of modern seawater NO_3^- δ^{15}N, but with more variability than either SGC or SGS.

Post-depositional conditions and geochemical indicators suggest that δ^{15}N values are primary. Under anoxic depositional conditions, there is little to no isotopic fractionation as organic matter breaks down and N substitutes into clays (Scholten, 1991; Williams et al., 1995; Thomazo et al., 2009). It is possible that under oxic conditions, a small ($1 - 3$‰) positive shift occurs. On a larger scale, regional metamorphism occurred at $\sim$ 250 to 300 °C (Clauer & Kröner, 1979), and local mineralogy and

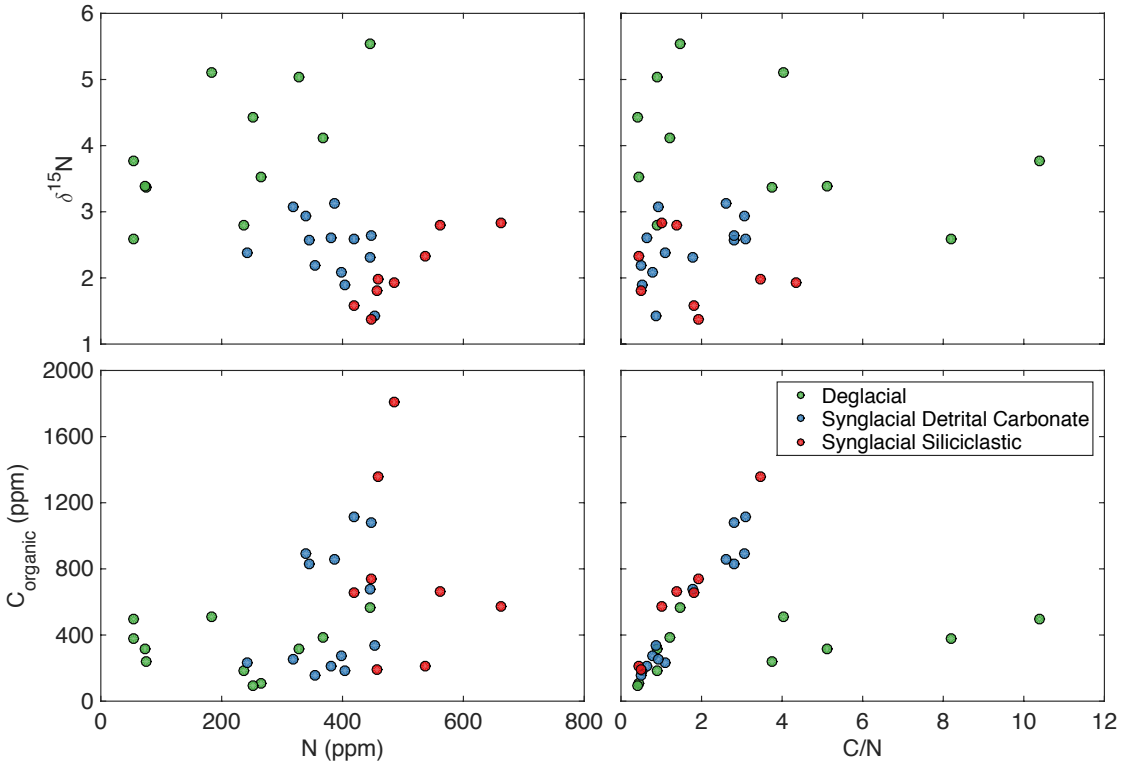

Figure 4.2: Nitrogen isotopes, C and N concentrations, and C/N ratio from decarbonated powders. Lack of correlation between δ^{15}N and N concentration, as well as δ^{15}N and C/N, indicate the δ^{15}N values have not been altered during metamorphism. Carbon, however, seems to be altered, as strong correlation between C concentration and C/N indicates C loss. Additionally, there is no correlation seen between C and N concentrations, suggesting these two elements are decoupled in their preservation in measured sections.

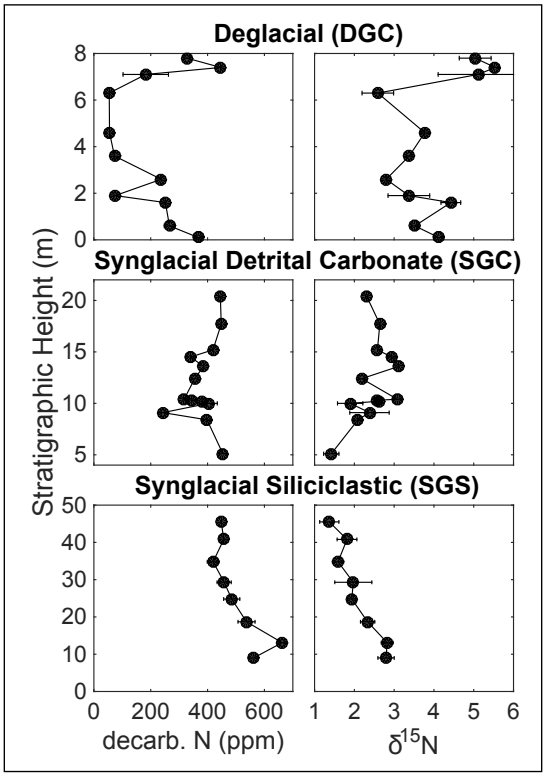

Figure 4.3: Nitrogen concentration (in decarbonated samples) and δ^{15}N for synglacial siliciclastic (SGS), synglacial detrital carbonate (SGD), and deglacial carbonate (DGC). SGS and SGC have δ^{15}N values between $1 - 3‰$, lower than the modern average NO_3^- is $5 - 7‰$. DGC values approach modern NO_3^- near the top of the section.

structure indicate no major metamorphism in sample locations. While no studies have specifically quantified metamorphic temperatures at sample locations, close spatial association with quartz dislocation creep in basement rocks suggests temperatures of $\sim$ 325 °C, and previous work has suggested temperatures experienced by nearby basement are similar to conditions experienced by cover rocks (Hoffman et al., 1988). In addition, linear correlation between Zr (incompatible, fluid-immobile) and Cs (incompatible, fluid-mobile) in all sections suggests post-depositional fluid alteration was minimal (Supplemental Fig. 4.11).

Nitrogen retention in sedimentary rocks is resilient to greenschist facies metamorphism, with primary values unaffected at temperatures up to 350 °C (Bebout & Fogel, 1992; Palya et al., 2011). If N were volatilized and lost with progressive metamorphism, concentration and δ^{15}N would be negatively correlated, which is not observed (Fig. 4.2). As N is likely found primarily as NH_4^+ in clays in these units, it should be strongly bonded into clay mineral lattices rather than weaker bonds in organic matter (Ader et al., 2016).

Since N fixation has a very small fractionation, δ^{15}N values approaching atmospheric values (assumed to be 0‰) suggest denitrification is either complete in the water column, occurs exclusively in sediments, or there is no denitrification at all. In either case with denitrification, large fractionation associated with denitrification, which leaves residual water column NO_3^- isotopically heavier, will not be preserved if all NO_3^- is consumed during denitrification. Similarly, sedimentary denitrification has no effect on bulk ocean δ^{15}N values, as it tends to go to completion. Thus, the choices to explain low δ^{15}N values in both SGS and SGC are either: fully oxygenated water column with denitrification in the sediments only, or extensive water-column anoxia causing complete denitrification.

In contrast, DGC δ^{15}N values are more enriched, and even approach modern values (which are the result of the balance between N fixation and partial denitrification in the water column) near the top of the section. This would indicate that water column denitrification is only partial at this time. That is, some NO_3^- must remain in the water column to preserve the large fractionation associated with denitrification.

4.5.2 Trace element concentrations controlled by redox variations

TE data (Fig. 4.6) constrain the oxidation state of the ocean, with two key implications. First, contemporaneous oxic weathering supported by a biological oxygen source is required. Second, ocean oxidation state must have varied between oxic, allowing TE to accumulate in the water column, and anoxic and in some cases euxinic, when TE were scavenged to the sediments.

We suggest that variations in redox sensitive TE could are not due to changes in detrital influence alone. By normalizing TE to non-redox sensitive elements with similar geochemistry (i.e., Sc, Zr) and comparing with a detrital proxy (Al), we show that variations in detrital input, as indicated by Al, cannot fully explain these data (Fig. 4.5). These plots are corrected for non-carbonate fraction. In addition, laser ablation analyses indicate that the clay-fraction, and not the detrital carbonate, is the host for the TE of interest (Fig. 4.4). Laser analytical spots with moderate CaO and MgO and high K_2O content compared with total major oxides in general have a higher concentration of V and U. While fine grain size and standardless data normalization (Liu et al., 2008) do not allow for quantitative conclusions based on laser ablation data alone, the analyses do indicate that the clay fraction, and not detrital carbonate, is the host of TE.

Trace element whole rock (WR) concentrations, corrected for non-carbonate fraction, show evidence for oxygenated water with limited euxinia in synglacial sections, with more euxinia in DGC where Mo contents are higher than U. TE are transported to the sediment primarily associated with organic matter (Tribovillard et al., 2006). As C contents of samples analyzed herein have likely been altered (Fig. 4.2), we present data normalised to Zn, which exhibits nutrient-like behaviour and correlates with organic matter produced by algae (Peel et al., 2009). Since Zn-normalied concentrations have a very similar pattern as WR data (Fig. 4.6), we suggest that, though C has been altered, TE were originally associated with sinking organic matter. Thus, we also present data as enrichment factors (EF) to estimate water-column O_2-conditions. EFs are calculated by first normalizing each analysis to Al to correct for detrital influence (Tribovillard et al., 2006). Then, we divide by the same element to Al ratio in Post-Archean Average Australian Shale (PAAS) (Taylor & McLennan, 1985), and finally divide each by the fraction residue (i.e., non-carbonate). While local, reservoir effects cannot be conclusively ruled out, studies of TEs in shales indicate that these

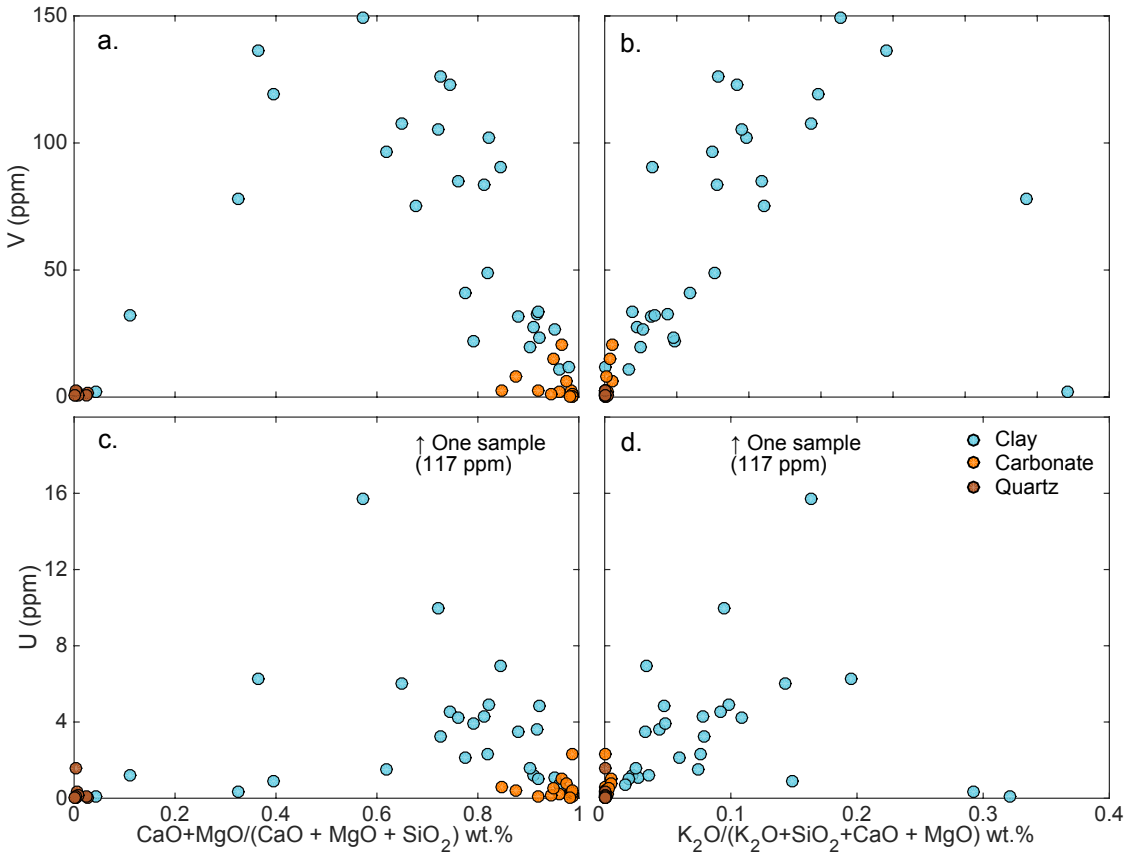

Figure 4.4: Laser ablation ICP-MS analyses of carbonate-, clay-, and quartz-rich locations from all sampled sections. Clay-rich fractions contain the majority of trace elements, shown clearly for V (a., b.), both when plotted against proportion carbonate ($CaO+MgO/(CaO+MgO+SiO_2)$) or against proportion K_2O, which will be highest in clays. Although the relationship is less clear for U (c., d.), it is still found predominately in clay. Since clay minerals contain most of the TEs, we suggest the TE signal directly reflects ocean water oxygen concentrations, and not a detrital overprint.

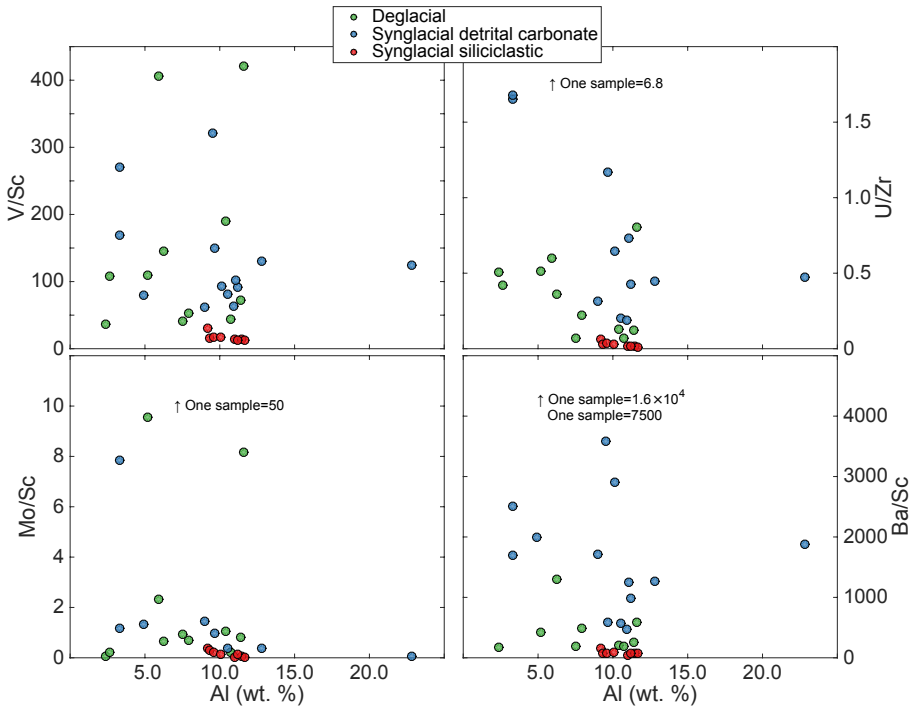

Figure 4.5: Whole-rock analyses of redox-sensitive trace elements of interest, and Ba, normalized to geochemically similar but redox-insensitive elements and plotted against Al. If all variation seen in redox-sensitive trace elements were due to changes in detrital input alone, they would correlate to Al. Since this correlation is not seen, we suggest that variation in redox-sensitive trace elements is due to changes in water column chemistry.

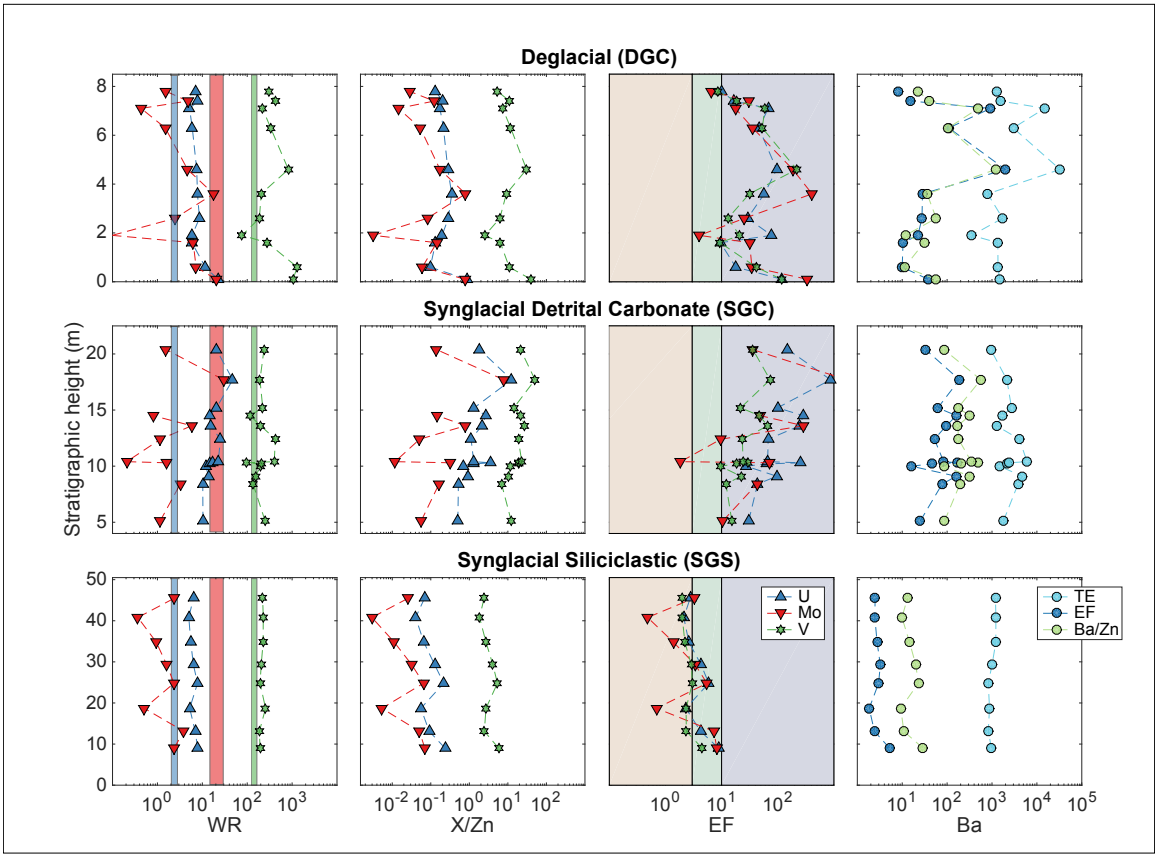

Figure 4.6: Uranium, Mo, V, and Ba concentration data. All data are shown corrected for non-carbonate fraction. Whole rock (WR) values are shown in column a., with boxes representing average Mesoproterozoic U (blue) (Partin et al., 2013) and Mo (red) (Scott et al., 2008) concentrations, and Post-Archean Average Shale (PAAS) V composition (green). b. Trace elements normalised to Zn, c. Enrichment factors (EF), see text for details. Tan boxes represent low enrichment (EF<3), green boxes moderate enrichment (EF $3-10$), and purple boxes high enrichment (EF>10).

elements can record a global signal (Algeo & Tribovillard, 2009).

In SGS, all three redox sensitive elements vary between low (EF$<$ 3) and moderate (3$<$EF$<$10) enrichment. Low enrichment factors could be explained either by lack of oxic weathering input or by sediment deposition under oxygenated water, which would keep TE in solution and out of the sediments. Moderate EF requires both supply of TE, requiring input from oxic weathering, and sub-oxic waters. Since SGS are deep water facies, our preferred explanation for the TE data is a redox-cline at some depth with oxygenated water above and anoxic water below; variations in height of this redox-cline would change local water oxygen content. Following this, low δ^{15}N would be explained by fixation, nitrification in oxic waters and near complete denitrification in anoxic waters below the redox-cline.

SGC shows high EFs for all TE, requiring local anoxia. Uranium is generally more enriched than Mo, so the water is not euxinic, given a similar dissolved U/Mo ratio to the modern ocean. Barium is highly enriched, which may suggest high productivity, which would mean high oxygen demand. We note again that these are nearshore, and clearly glacially derived. A likely explanation, then, for these geochemical signals is high nutrient input from glacial runoff, supporting high productivity and oxygen use. Sea ice cover is possible, restricting oxygen delivery but still allowing primary productivity.

EFs in the DGC section vary between moderate and high, indicating variation between low oxygen and anoxic water. During anoxic phases, Mo appears more enriched that U, indicating euxinia, again given modern-like U/Mo. Barium is again enriched, perhaps indicating high productivity. This unit is the uppermost section of the glacial Ghaub, directly underlies the cap carbonate, and likely represents the terminal deglaciation, suggesting abundant inputs of TE and nutrients. δ^{15}N is highest, similar to Quaternary deglacial values, when the water appears low in oxygen. We suggest, then, that both the higher δ^{15}N values and EFs indicate a water column that varies between oxic to sub-oxic, allowing partial water column denitrification, and anoxic to euxinic, when TEs are scavenged from the water column and into the sediment.

Measurable TE concentrations, and enrichments particularly, require contemporaneous oxic weathering of the continents, as the residence times of these elements in the ocean (modern ocean times are 400 kyr for U, 50 kyr for V and 800 kyr for Mo (Algeo & Tribovillard, 2009), these times would be shorter given lower O_2) are much less than the duration of the Marinoan glaciation (4 to 20 Myr, (Prave et al., 2016)). The

delivery fluid must have been in contact with atmospheric oxygen. The present day lifetime of atmospheric oxygen with respect to oxic weathering is $\sim 2\,\mathrm{Myr}$ (Catling & Claire, 2005), and would have been similar or shorter in the Neoproterozoic, when atmospheric oxygen was lower, due to the rate dependence of oxic weathering on oxygen concentration to a power of 0.5 to 1 (Canfield, 2005; Kanzaki & Murakami, 2013).

Even if oxic continental weathering were to shut off completely, a modern amount (3.5×10^{19} mol) of O_2 would be completely exhausted in $\sim$ 10 Myr given a volcanic/metamorphic reducing gas flux of 3 Tmol yr^{-1} (Berner, 1991). If atmospheric O_2 goes down, and reducing input stays constant, the time needed to deplete atmospheric O_2 time will go down. Given that the residence time of atmospheric oxygen is shorter than the glaciation, a contemporaneous source of oxygen from primary productivity followed by burial of organic matter is required to maintain O_2 levels sufficient for oxidative weathering, as required by TE concentrations. It is possible that a "hard" Snowball ocean may have existed for a time, but its duration would have to be much shorter than the timescale of oxic weathering ($\sim$ 2 Myr) in order to satisfy TE constraints.

Barium is a productivity proxy in the modern ocean (Dymond et al., 1992). Barium released during organic matter degradation bonds with sulphate to form barite, which is preserved in oxic sediments (Griffith & Paytan, 2012). High Ba EFs (Fig. 4.6) in all sections may indicate active biologic ecosystems during Snowball ocean was productive. This proxy, however, is sensitive to oxygen concentrations, as barite tends to dissolve in anoxic waters, since SO_4^{2-} is undersaturated. While the Ba-proxy is also sensitive to changes in detrital influence (Klump et al., 2000), we suggest that Ba concentrations are not controlled by detrital influence alone (Fig. 4.5), as Ba/Sc ratios do not correlate with Al content when corrected for non-carbonate fraction. It is thus possible, though speculative, that there is some biologic control over Ba abundances. The rough correlation between Ba EF and $\delta^{15}N$ in SGC suggests that in SGC the N-cycle and productivity are linked.

4.6 Palaeoenvironmental implications and context

Our data from the Marinoan glaciation present a very different picture of the palaeoenvironment during low-latitude glaciation than the canonical "hard Snowball Earth" model. There is evidence of an active biosphere with oxygen production and gas ex-

change between atmosphere and ocean and contemporaneous nutrient input from the continents. There was an active nitrogen cycle, including nitrogen fixation, nitrification and denitrification. The oxidation state of the ocean, while generally sub-oxic or anoxic and sometimes euxinic, was variable with periods or regions of oxic water (Fig. 4.7). The hard Snowball Earth model restricted ocean-atmosphere exchange and marine productivity entirely and posited an anoxic ocean throughout; our data call for that model to be rejected.

Low δ^{15}N values indicate a nitrogen cycle with nitrogen fixation, nitrification and denitrification. The balance between these is distinct from the modern balance. Nitrification occurs efficiently at O_2 concentrations < 10 μM (Rysgaard et al., 1994) or even nM levels (Bristow et al., 2016), though denitrification would have been sufficient to process all NO_3^- at such oxygens levels. Extensive, but not quantitative, denitrification is suggested, which is consistent with low oxygen levels. If removal of NO_3^- produced N_2 or N_2O, N could have been limiting, though on long time scales biologic N-fixation rates are likely sufficient to mitigate limitation.

Even if there were a lower oceanic N reservoir, our dataset provides evidence for O_2 production and primary productivity. Evidence for N fixation itself indicates some primary production with additional productivity occurring from already fixed N. The TE data require oxidative weathering to occur throughout the glacial, which is unlikely if O_2 production is shut off or greatly decreased. Reaction with reducing volcanic and metamorphic gases and weathering of reduced carbon in the continental crust would exhaust atmospheric O_2 before the end of the glacial period without O_2 produced by primary production.

The robustness and flexibility of the N-cycle is also apparent when viewed in the context of the rest of the Neoproterozoic (Fig. 4.8), the modern ocean, and the last glacial maximum and associated deglaciation. After the Marinoan, multiple proxies indicate an increase in atmospheric O_2 (Och & Shields-Zhou, 2012). Correspondingly, δ^{15}N values increase. This trend suggests an increase in partial water-column denitrification, consistent with our interpretation of Snowball deglaciation. N-isotopic values decreased throughout the Ediacaran, perhaps in response to more quantitative denitrification, before varying widely immediately after the start of the Cambrian. Major changes to the biosphere occurred at this time, perhaps associated with changes in surface O_2 (Cremonese et al., 2013). Similarly, during the last glacial maximum, ocean waters were more pervasively oxygenated than the Holocene, and low δ^{15}N values indicate water-column denitrification was less prevalent (Ganeshram et al., 2000).

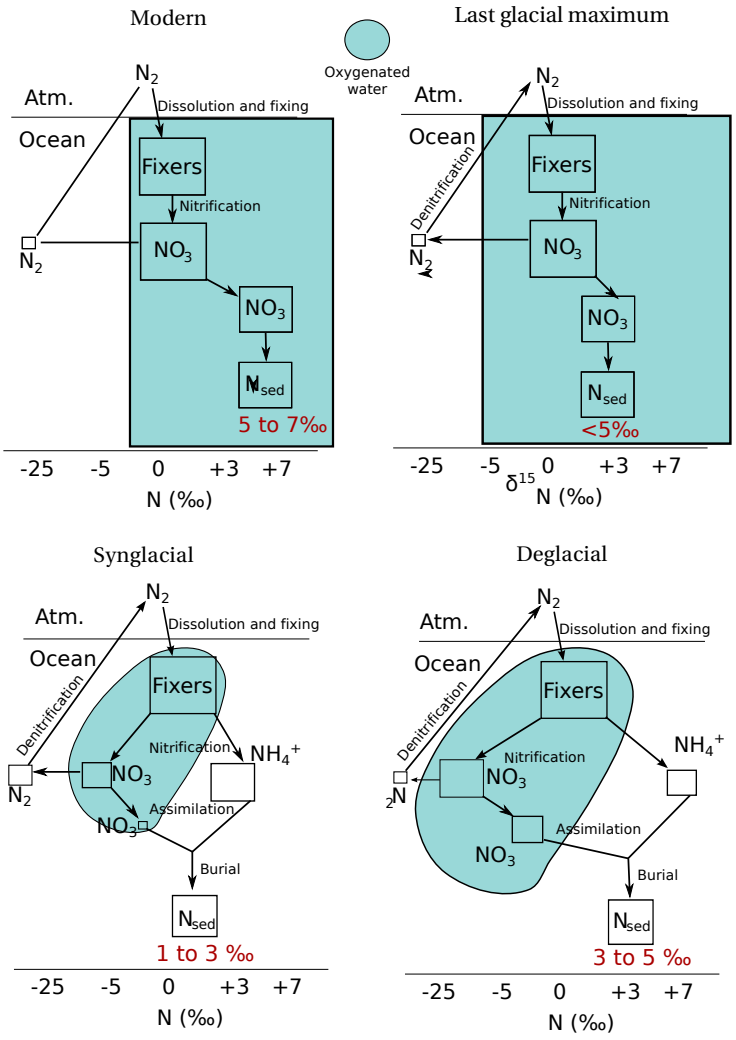

Figure 4.7: Schematic of N-cycle in modern, last glacial maximum (LGM), and proposed syn- and deglacial in Marinoan glaciation. Boxes indicate size of reservoir, and position of boxes corresponds to δ^{15}N values. The modern N-cycle is characterized by partial water-column denitrification, preserving large fractionation in residual NO_3^-. During the LGM, extensive oxygenation limited water column denitrification, lowering δ^{15}N values globally. The Marinoan synglacial ocean had oxygenated shallow water and an extensive chemocline. Most NO_3^- was denitrified, thus isotopic fractionation was not preserved. During deglaciation, higher O_2 allowed for larger pool of NO_3^-, partial water-column denitrification, and an increase in δ^{15}N values approaching modern.

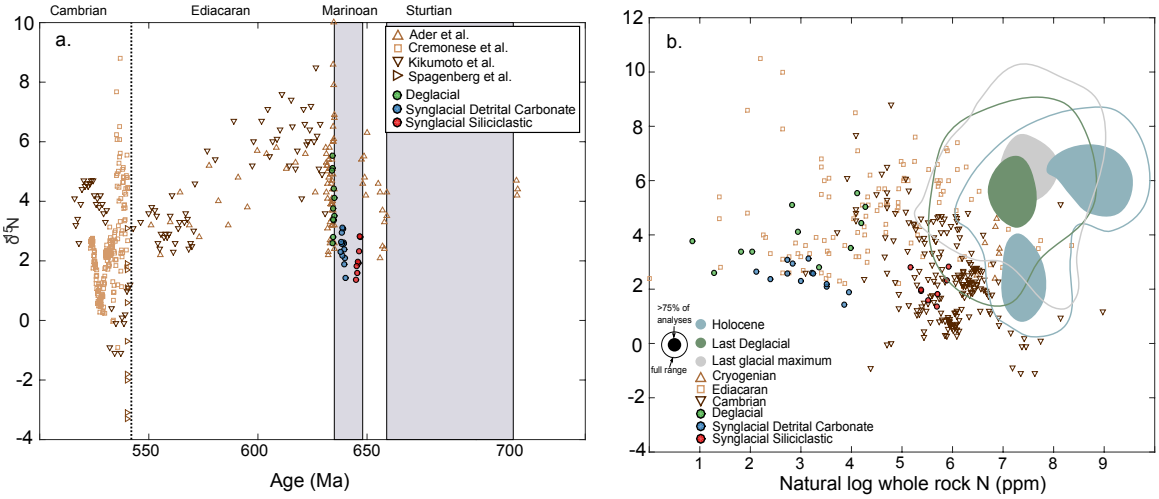

Figure 4.8: Nitrogen isotopic and whole-rock concentration comparison to late Neoproterozoic, Cambrian (a.) and recent marine samples (b.). synglacial samples from this study are very similar to those from the Cambrian. Deglacial samples are isotopically similar to Ediacaran data as well as some modern deglacial samples. We suggest the similarity of deglacial units is due to a similar effect: increase in the amount of *partial* water column denitrification. The N-cycle responds dynamically to changing environmental conditions.

During the subsequent deglaciation and continuing into the Holocene, N-isotopic values increase, and cover a greater range. This increasing trend reflects an increase in partial water-column denitrification and the greater range a heterogenous ocean.

The N-cycle and the history of O_2 are intertwined, especially during times of great environmental change or stress. During the Neoproterozoic Marinoan glaciation, all modern N-cycle processes were present as indicated by enriched $\delta^{15}N$ values in synglacial sediments, though their relative activity was markedly different than modern (Fig. 4.7). The resilience and flexibility of the N and O_2 cycles, as revealed by TE values, have implications for not only the survival of life on Earth but also for life on other cosmic bodies. The presence of an active biosphere on a nearly frozen planet is indicative of life's propensity to endure.

4.7 Acknowledgments

We would like to thank Paul Hoffman for assistance in field work and selecting sampling locations and Eric Bellefroid for sampling assistance. The manuscript benefitted from comments by Rameses D'Souza and Michael Whiticar and from three anony-

mous reviewers.

Funding for geochemical analysis was provided via an NSERC discovery grant to CG and from the NASA Astrobiology Virtual Planetary Laboratory at the University of Washington.

4.8 Methods

4.8.1 Rock powder preparation

All samples were cut and trimmed as to remove weathered exteriors. Sample chips ($\sim 1-4$ cm) were then crushed into smaller pieces using a jaw crusher. Small chips were then powdered in a tungsten-carbide shatter box. Clean quartz sand was crushed in between each sample to ensure no contamination between samples occurred. The shatterbox puck and container were cleaned with deionized water and ethanol between samples.

4.8.2 Nitrogen and carbon

All N and C isotope and concentration analyses were undertaken at the University of Washington's IsoLab. Each sample was decarbonated prior to analyses. Approximately 1 g of sample powder was weighed into glass test tubes that had been cleaned and sterilized (baked at 500 °C overnight). Depending on the sample, between one and three 100 g tubes were prepared. To each tube, 30 mL of 6N HCl was added. Samples were then sonicated for 30 minutes. All tubes were then placed in a 60 °C oven overnight. The next day, samples were centrifuged to settle all undissolved material. Acid was poured off, fresh acid was added as before, and samples sat in the oven overnight. This acid refresh was repeated once more. To clean samples, all were rinsed three times with DI H_2O, centrifuging between each rinse. Sample powders then dried at 60 °C for two days; all vials containing multiples of the same sample powder were combined and homogenized after drying.

Samples were then analysed on a Thermo-Finnigan MAT 253 coupled to a Costech Elemental Analyzer. Between $50-100$ mg sample powder was weighed into a Sn capsule, as well as standards: two glutamic acids (GA-1 and GA-2), dried salmon (SA), and an internal rock standard (McRae Shale). All samples were flash-combusted with an excess of O_2 at 1000 °C in a combustion column packed with cobaltous

oxide (combustion aid) and silvered cobaltous oxide (sulphur scrubber). Combustion products passed over a reduced copper column at 650 °C to reduce all N to N_2 and absorb excess O_2. Lastly, sample gas passed through a magnesium perchlorate trap to absorb water and a 3 m gas chromatography column to separate N_2 from CO_2. All analyses were quantified using IsoDat software. Errors reported are standard deviations from repeated analyses.

4.8.3 Trace elements

Trace elements were measured at the University of Victoria in two ways: whole rock solutions and laser ablation. For the first, approximately 100 mg of samples/standards were weighed into 5 mL Teflon vials. To this, 5 mL 50% HF was added, vials were capped, and samples sat on a 170 °C hotplate for two days. Then, caps were removed, and HF was allowed to evaporate until nearly dry. Five mL of 8N nitric acid was added, vials were capped, and again samples sat on a hotplate for two days. Evaporation procedure was repeated, 5 mL of 4N nitric acid along with 0.5 mL oxalic acid was added, and samples sat on a hotplate for one day. Finally, samples were diluted to 100 mL with DI H_2O in clean 100 mL bottles. Sample solutions were analysed on a Thermo X-Series II (X7) quadrupole ICP-MS. Errors were estimated from duplicate samples and standard reproducibility. We used the following standards: JLS-1, BCR-2, SY-4, SY-4, DR-N, BIR-1a, IF-G, LKSD-2, and IAEA-405.

Laser ablation was undertaken using the same mass spectrometer with a UP-213 (213 nm) solid state Nd-YAG UV laser. Beam size was set to 30 μm, and all analyses were either spots or raster lines $\sim$ 100 μm in length. Samples are normalized to the sum of all major element oxides (Na_2O, MgO, Al_2O_3, SiO_2, P_2O_5, K_2O, CaO, MnO, FeO) instead of an internal standard element of known concentration (Liu et al., 2008). External standards were BCR-2g and BIR-1g. Analyses that summed to less than 90% total oxides were excluded from further discussion. In addition we tested accuracy by calculating composition of NIST 611 glass assuming it was an unknown, and based on calibration from BCR-2g and BIR-1g. Calculated trace element concentrations were within 5% of their accepted values, with most other elements within $10 - 15$% of their accepted values (Table 4.1).

TE analyses indicate the presence of oxygen in the atmosphere and shallow ocean. Samples have a major component of detrital carbonate, however, which might dilute or obfuscate TEs contained in clay minerals. We rely primarily on whole-rock (WR)

analyses via solution ICP-MS for redox interpretation, as sample petrology varies at finer than laser ablation resolution. We are confident, though, that the clay mineral fraction in all samples retains the majority of TE concentration for several reasons. TE are incompatible in carbonate lattices, and should be in low concentrations. Decarbonated powders, used for N isotopic analyses, are more enriched in TE than non decarbonated WR powders. Analysis of clay-rich and clay-poor spots by laser ablation show enrichment in TE in clay-rich domains compared to carbonate grains (Fig. 4.4).

All TE abundances are reported as enrichment factors (EF) (Algeo & Tribovillard, 2009), which are WR concentrations compared to Post-Archean Average Australian Shale (PAAS) (Taylor & McLennan, 1985) and corrected for detrital influence and clay fraction. This approach is used in many redox estimates in ancient shales (Lyons et al., 2009), and although rocks analysed here are not shales, the redox signal is contained in clay, a primary mineral component of shale. The complete TE dataset is available in supplemental materials. EFs less than 3 are classified as low enrichment, those between 3 and 10 are moderate enrichment, and those greater than 10 high enrichment.

4.9 Supplementary Information

Table 4.1: Calculated element concentration from laser ablation analysis of standard NIST glass using BCR-2g and BIR-1a calibration based on Liu et al. (2008). Values for redox sensitive trace elements are within 5% of their accepted values with most others within 10%. Values for Na, Mg, Al, Si, K, Ti, Mn, and Fe are in weight % oxide, all others are in ppm.

Element	**Calculated**	**Accepted**
Na	14.6	12.87
Mg	0.08	0.07
Al	1.88	2.22
Si	70.5	69.6
P	0.11	0.12
K	0.054	0.06
Ca	12.1	11.71
Sc	507	455
Ti	0.075	0.08
V	441	450
Cr	529	408
Mn	0.003	0.05
Fe	0.07	0.035
Rb	405	417
Sr	530	492
Zr	520	437
Mo	416	417
Ba	432	430
La	462	426
Ce	452	447
Eu	496	444
Ho	545	440
Lu	533	430
U	448	452
Total Oxides	99.5	

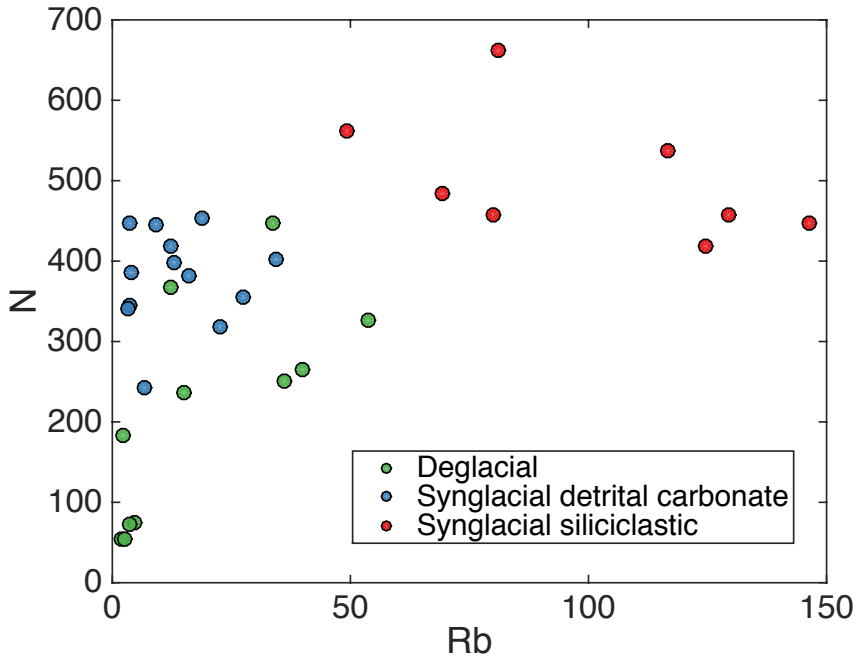

Figure 4.9: Nitrogen concentration plotted against Rb. These species are similar in ionic size and charge when N is found as NH_4^+. The rough, positive correlation seen is consistent with N being contained primarily in clay minerals, where the majority of Rb is as well.

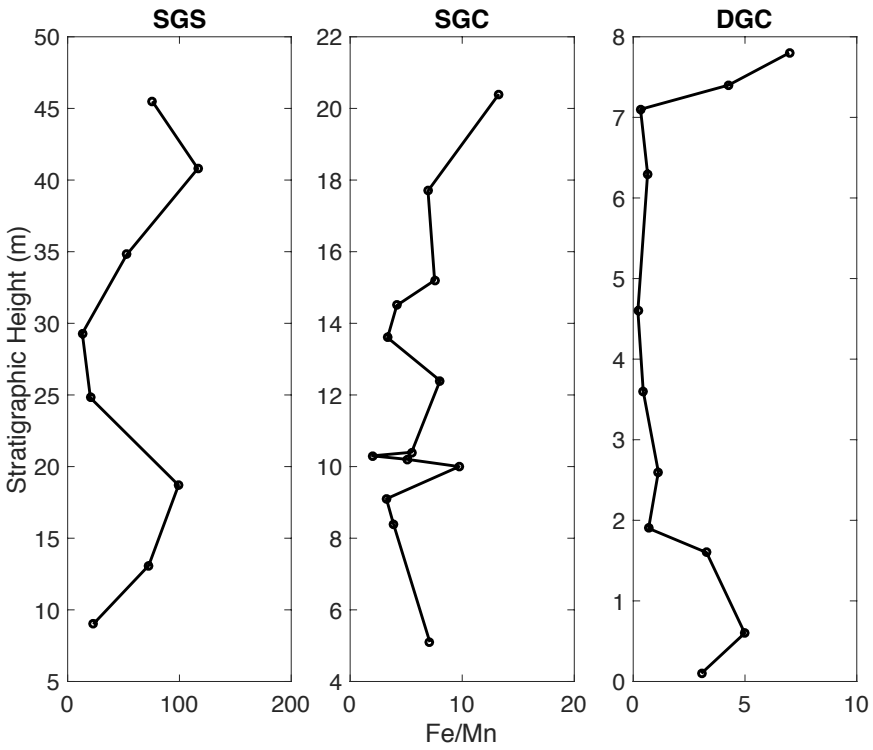

Figure 4.10: Iron:Mn ratio for three measured sections. If there was prominent hydrothermal input into the system, high Fe/Mn ratios would be expected. While values are high in SGS, an anoxic deep ocean would tend to restrict the influence of hydrothermal input of Mo, V, and U as they would precipitate near a hydrothermal vent. We thus suggest that hydrothermal influence, at least in SGC and DGC are minimal.

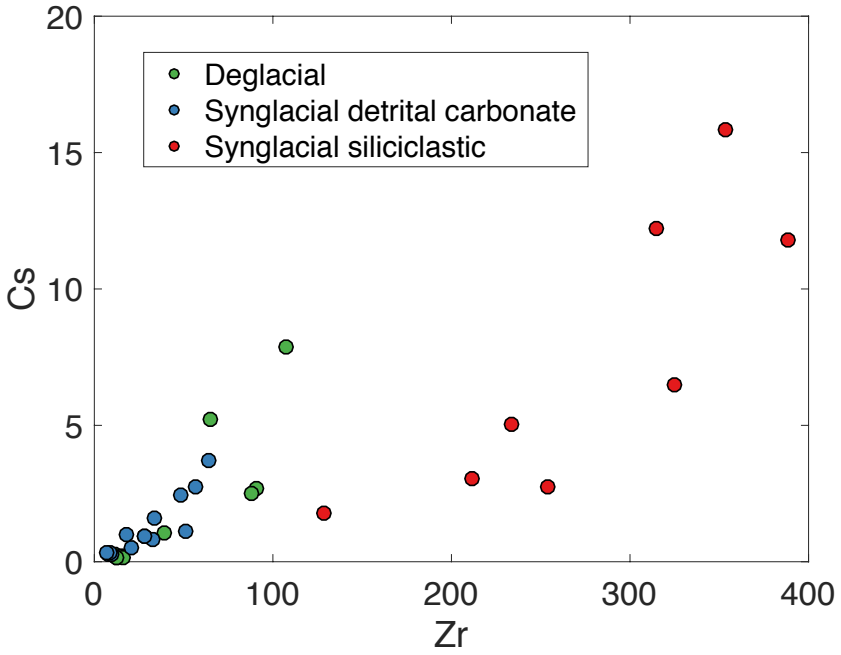

Figure 4.11: Caesium plotted against Zr whole rock analyses for all sections. As Cs is fluid-mobile and Zr is not, if substantial fluid alteration had occurred in these units one would not expect a linear correlation between the two elements, since Cs would be preferentially removed. We suggest that these data are consistent with low fluid-alteration, and consistent with our interpretations of primary water-column chemistry and biologic productivity.

Chapter 5

Earth system nitrogen cycle model

5.1 Motivation and background

The fate of N in the Earth System over time is poorly constrained. While the major biologic and geologic fluxes are known, their behaviour and the distribution of N is not constrained. For example, atmospheric N_2 is assumed to be constant over geologic time. While some recent studies are consistent with this notion (Marty et al., 2013)., others suggest a lower atmospheric mass (Som et al., 2012, 2016), and still others are permissive of a greater atmospheric mass in the past (Nishizawa et al., 2007; Goldblatt et al., 2009; Johnson & Goldblatt, 2015; Barry & Hilton, 2016). The assumption that atmospheric mass should be constant over Earth history is not an inherent property of the planet.

Preliminary modelling efforts considered sedimentary rocks as the main geologic storage and recycling vector for N (Zhang & Zindler, 1993; Berner, 2006) and compared N geochemically to the noble gases (Tolstikhin & Marty, 1998). These studies found that there was little change ($< 1\%$) in atmospheric N_2 over at least the Phanerozoic (Berner, 2006) and possibly the majority of Earth history (Zhang & Zindler, 1993). Additionally, while comparison to noble gases is valid for outgassing of oxidized magmas (Libourel et al., 2003), this comparison is not valid at subduction boundaries, as N is mostly found as NH_4^+ in subducted sediments (Bebout & Fogel, 1992) and oceanic crust (Busigny et al., 2011).

The Berner model, specifically, only considered sedimentary rocks as a geologic sink for N. It also based flux estimates strictly on N/C ratios, and N and C may behave quite differently in rocks and minerals, as N is likely found primarily as NH_4^+ and C as

organic C or CO_3^{2-}. More recent work has also shown that hydrothermal alteration of oceanic crust can incorporate N. The positive correlation between increased N concentration and δ^{15}N (Fig. 5.1) in oceanic lithosphere indicates that biologic N is being added to oceanic crust, which originally has a mantle-like N signature ($\bar{x} = -1.8$‰). Increased N content source from oceanic biology (δ^{15}N = 5 to 7‰) causes the δ^{15}N values of oceanic lithosphere to increase up to 5.6‰ on average.

The whole-Earth model of Tolstikhin & Marty (1998) maintains a stable upper mantle, in terms of N-isotopes and concentration, by recycling of sedimentary and seawater-sourced N from the surface and N from the lower mantle entrained in plumes. This approach is incomplete, as, again, surface N is subducted to the mantle as NH_4 and it is likely that the mantle as a whole is not layered. Therefore, a mechanism of "re-filling" the upper mantle from the lower mantle slowly over time appears untenable.

In addition, studies of several subduction zones suggest that there is overall net transport of N into the solid Earth, either the mantle or the arc-generated crust. Importantly, the N that survives the subduction barrier seems to mostly reside in the oceanic crust (Li et al., 2007; Mitchell et al., 2010). As discussed in Chapter 2, there are many possible mineral hosts for such N, including NH_4^+-bearing feldspars, pyroxenes, beryls, and phlogopite in the mantle. This is counter to sedimentary bound N, which is almost all returned to the atmosphere at subduction zones (Fischer et al., 2002; Elkins et al., 2006).

As such, we are presented with a conundrum. Modelling efforts suggest that the atmosphere and solid Earth have remained in equilibrium in terms of N-content over time. Contrastingly, geochemical evidence suggests there may be net transport of N from the surface to the mantle over time. It is from this conundrum that the construction of an Earth-system N cycle model presented herein is motivated.

Previous models implicitly have biologic processing, but none so far actually explicitly model the behaviour of organisms. This is a key oversight, as biologic productivity and activity is the gate-keeper between the atmosphere and the solid Earth. Nitrogen can cycle throughout the atmosphere, biosphere, sedimentary rocks, and crystalline Earth, thus constructing a model that integrates both biologic and geologic fluxes is critical for investigating the N-cycle over Earth history.

The scope of this chapter is to describe the model, demonstrate its fitness, present investigation of model output of nominal runs, and discuss areas for further development. The model description makes up the bulk of this chapter. Fitness of the model

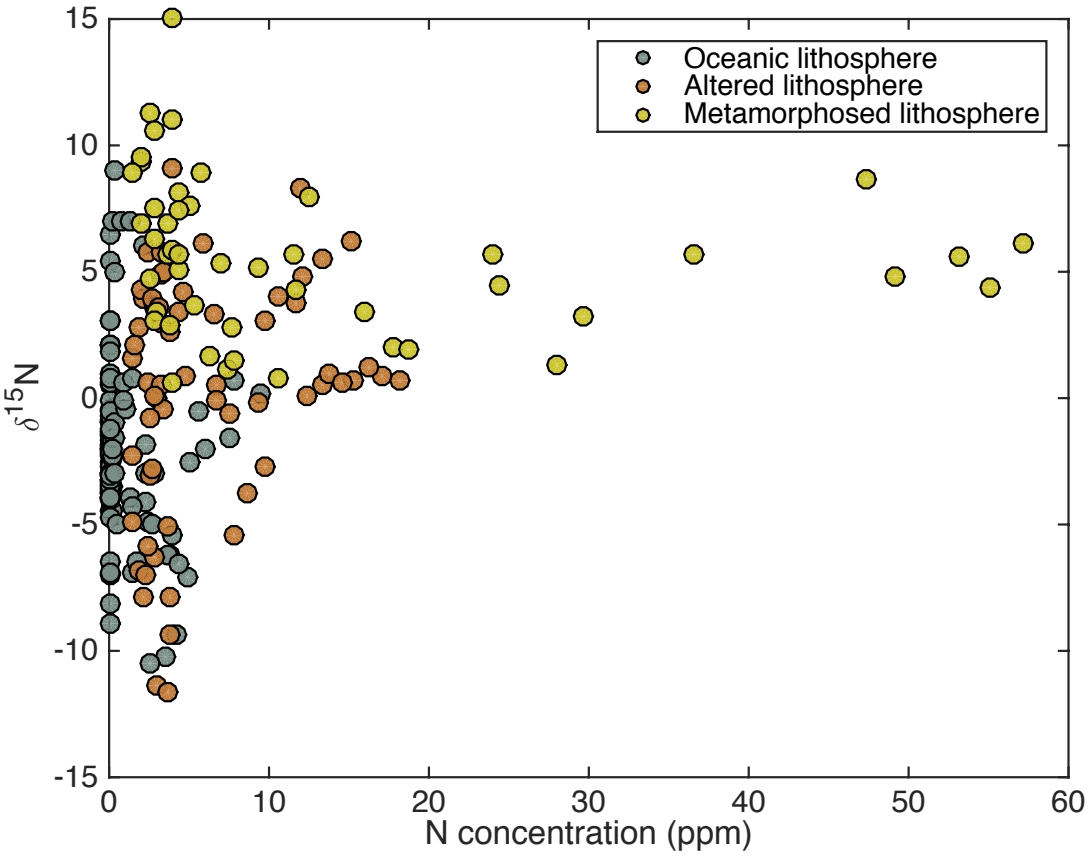

Figure 5.1: δ^{15}N plotted against N concentration (ppm) for oceanic lithosphere. Data are from Johnson & Goldblatt (2015). Shown are values from fresh lithosphere, altered lithosphere, and metamorphosed. Altered lithosphere has experienced temperatures of < 300 °C and metamorphosed samples have experienced temperatures > 300 °C. As oceanic lithosphere experiences alteration, N concentration increases, and initially depleted δ^{15}N values ($\bar{x} = -1.8‰$) are enriched, indicating additional N is sourced from biologic material, which has δ^{15}N of 5‰. Altered lithosphere rocks include MORBs while metamorphosed lithosphere rocks include blueschists, eclogites, and metagabbros.

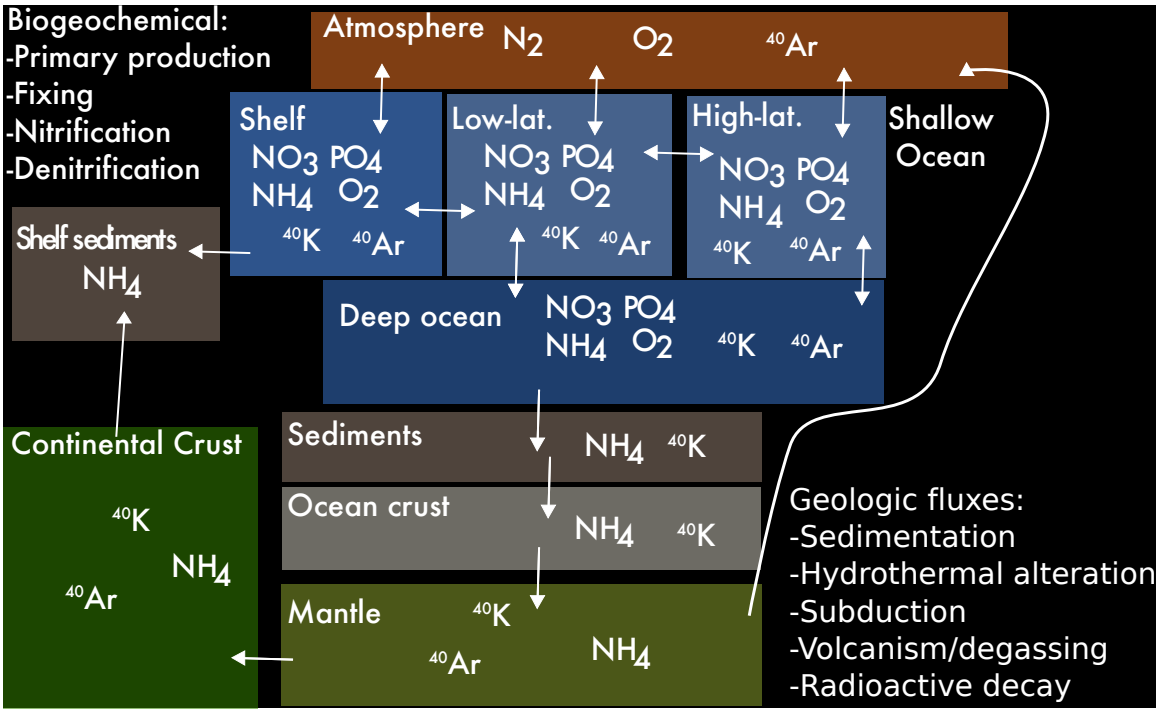

Figure 5.2: Earth system nitrogen cycle model schematic

is shown through stable model behaviour over Earth history and mass conservation. Nominal runs show that N can cycle between the atmosphere, crust, and mantle over long time scales, and these fluxes are directly influenced by biologic activity. In order to produce publishable results, model tuning and incorporation of a dynamic O_2 and C cycle are needed. Tuning is non-trivial, and improvements and adjustments to several key biologic fluxes, specifically nitrification and denitrification, may prove crucial in future development.

5.2 Model setup

The model is arranged as a budget/box model (Fig. 5.2), with species able to move between various boxes in a number of ways. There are four of species of N:

- N_2
- NO_3^-
- NH_4^+
- geologic N.

I also include other biologically relevant species: PO_4 and O_2, as well as inorganic tracers: K, ^{40}K, ^{40}Ar, and ^{36}Ar. Phosphate directly affects biologic productivity and O_2 affects both productivity and which pathways of the biologic N cycle are in operation. Nitrogen is geochemically similar to K when found as NH_4^+ and geochemically similar to Ar when found as N_2. As K and Ar are not biologically important elements, they serve as both a calibration and validation of the purely physical aspects of the model.

The model boxes are:

- atmosphere
- low-latitude shallow ocean
- high-latitude shallow ocean
- shelf ocean
- deep ocean
- shelf sediments
- deep sediments
- oceanic crust
- continental crust
- mantle

The model begins at 4.5 Ga ($t = 0$), after a spin up period of 50 Myr to equilibrate atmosphere, ocean, and sediment boxes.

In general, biogeochemical fluxes are from Fennel et al. (2005), updated where needed. Most geologic fluxes are driven by mantle cooling history after Korenaga (2010), which produces estimates of mantle temperature, crust production, and spreading rate through time (Fig. 5.3).

The following is first a brief description of element cycles, then a detailed description of the model setup. I will discuss each model box, the species contained within said box, and the fluxes that affect the amount of each species in the box. I use R_j^i to represent reservoir in moles size of species j in box i, C_j^i to represent concentration, and F_k^i to represent fluxes of type k in box i (Table 5.1). There are a number of fluxes that are sensitive to reactant concentration (e.g., Michaelis-Menten behaviour), and are shown as v_l where l is specific to each sensitivity v.

5.2.1 Brief element cycle descriptions

The Earth-system N cycle is as follows (for a more complete N cycle description, see Section 2.2). Atmospheric N_2 dissolves in the ocean, where it can be fixed (i.e., breaking the N≡N bond) by bacteria. Fixed N then cycles biologically, and is released as waste or when organisms die. In oxygenated water, this reduced biologic N is quickly nitrified ($NH_4^+ \longrightarrow NO_3^-$) by bacteria; in anoxic water it remains as NH_4^+. Some organic material sinks into the deep ocean, where most gets remineralized into either NH_4^+ or NO_3^- depending on O_2 levels, and a small portion sinks to the sediments. In the sediments, organic matter breaks down and bonds as NH_4^+ into clays and other K-bearing minerals. Some N also gets incorporated into oceanic crust during hydrothermal alteration. Sediments and oceanic crust get subducted, with a portion of N going into the mantle, a portion outgassed to the atmosphere, and a portion incorporated into arc-generated crust. Mantle N can be outgassed at mid-ocean ridges or at hot-spots. Continental crust N, organic or inorganic, can be weathered and added back to the ocean.

The PO_4 cycle is simpler. Phosphate enters the ocean due to continental weathering and from mid-ocean ridge outgassing. In the shallow ocean, it is consumed during primary production, both that based on already fixed N and that based on fixing new N. It is then exported to the deep or lower shelf ocean, where it is either remineralized or buried in sediments. Sedimentary PO_4, along with that added to ocean crust during hydrothermal alteration, can be subducted. A portion goes into the mantle, and a portion into the continental crust.

The cycles for K and Ar are only affected by physical, non-biologic processing. All isotopes of both elements mix between ocean boxes, and ^{40}K decays to ^{40}Ar in every box where it is found. Continental weathering releases K to the shelf ocean, and Ar to the atmosphere. Air sea gas exchange moves Ar from the surface ocean boxes to the atmosphere. Both species can get incorporated into oceanic crust during hydrothermal alteration, and K can be incorporated into sediments. Again, during subduction, some K and Ar is transported to the mantle, and the remainder either goes to the continental crust (K) or the atmosphere (Ar). Both are added to the deep ocean during mid-ocean ridge outgassing.

Table 5.1: Full list of fluxes used in model. Shown are flux symbol, brief description, and which model species are affected by each flux. In ocean boxes (low, high, shelf, deep), all species includes NO_3^- and NH_4^+, while in geologic boxes, all species just includes moles of N.

Flux	**Description**	**Species affected**
F_{rd}	radioactive decay	^{40}Ar, ^{40}K
F_{as}	air-sea gas exchange	^{40}Ar, ^{36}Ar, N_2
F_{mix}	water-mixing	all species
F_{nit}	nitrification	NO_3^-, NH_4^+
F_{denit}	denitrification	NO_3^-, N_2
F_{oldN}	production from fixed N	NO_3^-, NH_4^+, PO_4
F_{newN}	production from newly fixed N	N_2, PO_4
F_{out}	export from shallow ocean boxes	NO_3^-, NH_4^+, N_2, PO_4
F_{remin}	remineralization in shelf and deep	NO_3^-, NH_4^+, PO_4
F_{bur}	burial in sediments	N, PO_4
F_{seddif}	diffusion into sediments, out of water	NH_4^+
F_{sub}	subduction of crust and sediments	all species
F_{subT}	total subduction	all species
F_{subnet}	net subduction	all species
F_{hydro}	hydrothermal alteration	all species
F_{w}	weathering	all species
F_{cg}	continental growth	all species
F_{scg}	continental growth from shelf sediments	all species
F_{ogarc}	outgassing-arcs	all species
F_{ogmor}	outgassing-mid ocean ridge	all species

5.2.2 ^{40}K-decay

Radioactive decay of ^{40}K produces ^{40}Ar in all boxes where ^{40}K is present:

$$F^i_{\text{rd}} = \lambda X_{40\text{K}} R^i_{40\text{K}} \tag{5.1}$$

for i ={all boxes} where $X_{40\text{K}}$ is the proportion of decays that form ^{40}Ar and λ is the decay constant of ^{40}K.

5.2.3 Atmosphere

The atmosphere contains N_2, O_2, and both isotopes of Ar. N_2, ^{40}Ar, and ^{36}Ar exchange with the ocean following stagnant-lid gas exchange (Liss & Slater, 1974), with fluxes positive in the direction of sea to air:

$$F^i_{\text{as}} = \nu_{\text{l},j} A^i \left(C^i_j - H_j P_j \right) \tag{5.2}$$

for boxes i = {low, high, shelf} oceans and species $j = \{N_2, {}^{40}\text{Ar}, {}^{36}\text{Ar}\}$. $\nu_{\text{l},j}$ is piston velocity in m yr^{-1} calculated by dividing the diffusion constant (D_i) by thickness of stagnant boundary (z_{film} m); A^i is ocean box surface area (m^2); C^j_i is concentration of species j in box i; H^j is Henry's law constant for species j (mol L^{-1} atm^{-1}); and P^j is partial pressure of gas j, calculated as:

$$P_j = \frac{R^{\text{atm}}_j}{n_{\text{a}}} \tag{5.3}$$

where n_{a} is the number of moles corresponding to one atmosphere pressure (Table 5.2).

Gasses are also added to the atmosphere via outgassing at arcs and both isotopes of Ar are added from continental crust weathering (Sec. 5.2.5).

Oxygen levels are prescribed. Levels start at 10^{-6} present atmospheric level (PAL $= 2 \times 10^{19}$ mol) for the first 2.1 Gyr of model runs. Atmospheric O_2 increases to 0.01 PAL over 100 Myr from 2.1 to 2.2 Gyr, then to 0.8 PAL from 3.865 to 3.965 Gyr (beginning of the Ediacaran). Oxygen rises to modern levels from 4.08 to 4.18 Gyr (Devonian). Ocean O_2 concentrations are calculated assuming a Henry's law equilibrium.

Table 5.2: Model constants used for atmospheric and ocean physical cycling with references. Ocean boxes are low- and high-latitude shallow, shelf, and deep. References are H14 (Haynes et al., 2014), S99 (Sander, 1999), F05 (Fennel et al., 2005), and LS74 (Liss & Slater, 1974)

Parameter	**Definition**	**Value**	**Reference**
$D_{\mathrm{N_2}}$	Diffusion constants	1.88×10^{-5}	H14
D_{Ar}	in $\mathrm{cm}^2\ \mathrm{s}^{-1}$	1.88×10^{-5}	H14
$D_{\mathrm{O_2}}$		2.5×10^{-5}	H14
$H_{\mathrm{N_2}}$	Henry's law constants	1.3×10^{-3}	S99
H_{Ar}	in mol L^{-1} atm $^{-1}$	6.1×10^{-4}	S99
$H_{\mathrm{O_2}}$		6.1×10^{-4}	S99
n_a	moles equal to one atm pressure	1.72×10^{20}	this study
d	ocean depth (m)	4500	F05
z_{film}	stagnant lid thickness (m)	1.5×10^{-5}	LS74
A^{high}	ocean box surface area (m^2)	2.3×10^{12}	F05
A^{low}		2.3×10^{12}	F05
A^{shelf}		5.1×10^{11}	F05
V^{high}	ocean box volumes (L)	9×10^{18}	F05
V^{low}		9×10^{18}	F05
V^{shelf}		1.5×10^{18}	F05
V^{deep}	volume of the deep ocean	8.1×10^{20}	F05
$\Delta^{\mathrm{low\text{-}high}}$	mixing between ocean boxes	9.46×10^{15}	F05
$\Delta^{\mathrm{low\text{-}shelf}}$	in L^{-1}	1.58×10^{15}	F05
$\Delta^{\mathrm{low\text{-}deep}}$		9.46×10^{15}	F05
$\Delta^{\mathrm{high\text{-}shelf}}$		1.58×10^{15}	F05
$\Delta^{\mathrm{high\text{-}deep}}$		1.58×10^{16}	F05
$\Delta^{\mathrm{shelf\text{-}deep}}$		1.58×10^{15}	F05

5.2.4 Ocean

The ocean is divided into four boxes: high- and low-latitude shallow ocean, shelf ocean, and deep ocean. All species in the model exist in the ocean. There are a number of fluxes, both physical and biogeochemical that occur. Some can occur in all boxes, and some only in specific boxes. Broadly, primary production occurs in shallow ocean boxes, remineralization and burial occur in deep and shelf boxes, and nitrification and denitrification occur in all boxes.

5.2.4.1 All boxes

There is physical water mixing between all ocean boxes. Mixing out of an ocean box is simply the product of concentration of species j in box i and the sum of the water fluxes (Δ^{i-i*}, in L yr^{-1}) between box i and all other boxes ($i*$). Mixing in to box i is the sum of the product of concentration of species j in each other box ($i*$) and the water flux between box i and each other box (Δ^{i-i*}):

$$F^i_{\mathrm{mix},j} = -C^i_j \sum_{i*} \Delta^{i-i*} + \sum_{i*} C^{i*}_j \Delta^{i-i*} \tag{5.4}$$

If, for example, i ={low}, then $i*$ ={high, shelf, deep}, and Δ^{i-i*} is mixing between low and high, low and shelf, and low and deep boxes.

Nitrification occurs in all boxes. The rate of nitrification is dependent on O_2 and NO_3^- concentrations:

$$v^i_{\mathrm{Onit}} = \frac{C^i_{\mathrm{O2}}}{C^i_{\mathrm{O2}} + K_{\mathrm{Oni}}} \tag{5.5}$$

$$v^i_{\mathrm{NOnit}} = \frac{C^i_{\mathrm{NO3}}}{C^i_{\mathrm{NO3}} + K_{\mathrm{Nni}}} \tag{5.6}$$

and can occur up to a maximum, $n_{\max}$, empirically determined rate based from a bacterial culture experiment (Rysgaard et al., 1994). Thus, the full equation can be parameterized as:

$$F^i_{\mathrm{nit}} = v^i_{\mathrm{Onit}} v^i_{\mathrm{NOnit}} n_{\max} V^i \tag{5.7}$$

for box i ={low, high, shelf, deep}, and where K_{Oni} is the half-saturation uptake concentration of O_2 used in nitrification (20 μM), K_{Nni} is half-saturation uptake

concentration of O_2 used in nitrification (100 μM), $n_{\max}$ is a maximum nitrification rate (0.25 μmol hr^{-1} L^{-1}), and V^i is the volume (L) of individual ocean boxes.

Denitrification can also occur in every ocean box (i ={low, high, shelf, deep}). Its rate is based on a study of denitrification in permeable sediments (Evrard et al., 2013). The reaction rate follows Michaelis-Menten kinetics in relation to NO_3^- concentration, where K_{d} is the average constant from six sediment cores:

$$v^i_{\mathrm{NOde}} = \frac{C^i_{\mathrm{NO3}}}{C^i_{\mathrm{NO3}} + K_{\mathrm{d}}} \tag{5.8}$$

In contrast to nitrification, denitrification only occurs at low O_2 levels (Crowe et al., 2012), herein parameterized as a hyperbolic tangent function, tuned cause denitrification to increase greatly at O_2 levels below 20 μM:

$$v^i_{\mathrm{Ode}} = 0.5\left(1.01 - 0.99\tanh\left(C^i_{\mathrm{O2}} \times 10^6 - 10\right)\right) \tag{5.9}$$

Combining both dependencies (O_2, NO_3^-), I parameterize denitrification as:

$$F^i_{\mathrm{den}} = v^i_{\mathrm{Ode}} v^i_{\mathrm{NOde}} d_{\max} V^i \tag{5.10}$$

where there is an empirically determined maximum rate ($d_{\max}$ nmol mL^{-1} hr^{-1}), again set to the average of six sediment cores from (Evrard et al., 2013).

5.2.4.2 Shallow ocean

The shallow ocean, both high- and low-latitude, is where primary production occurs. I keep track of production in terms of moles of PO_4. There are two types of productivity (Fennel et al., 2005):

- Productivity based on fixed N (F_{oldN})
- Productivity based on newly-fixed N_2 (F_{newN})

which when summed equal total export production (F^i_{ExT}).

F_{oldN} can be PO_4 or N-limited:

$$L^i_{\mathrm{N}} = \frac{N^i_{\mathrm{all}}}{N^i_{\mathrm{all}} + K_{\mathrm{N}}} \tag{5.11}$$

$$L^i_{\mathrm{P}} = \frac{C^i_{\mathrm{PO4}}}{C^i_{\mathrm{PO4}} + K_{\mathrm{P}}} \tag{5.12}$$

where K_{N} and K_{P} are the half saturation uptake values for N and PO_4. N^i_{all} is the sum of C^i_{NH4} and C^i_{NO3} in box i. Thus, F^i_{oldN} is:

$$F^i_{\mathrm{oldN}} = \mu_1 \; R^i_{\mathrm{PO4}} \; \min(L^i_{\mathrm{P}}, L^i_{\mathrm{N}}) \tag{5.13}$$

for boxes i ={low, high, shelf} and where μ_1 is an efficiency term, set to 1.

Production based off of N_2 fixing is PO_4-limited, but also depends on N-concentrations and partial pressure of N_2. There is a Michaelis-Menten relationship to partial pressure (Klingler et al., 1989):

$$v_{fix} = \frac{R^{\mathrm{atm}}_{\mathrm{N2}}}{R^{\mathrm{atm}}_{\mathrm{N2}} + K_{\mathrm{f}}}; \tag{5.14}$$

where K_{f} is 9.87×10^{18} moles, or about the equivalent of 50 mbar pressure. Nitrogen fixing typically only occurs when N is limiting, thus I parameterize dependence on N concentration as:

$$v^i_{\mathrm{Nfi}} = \tanh\left(\frac{2 \times 10^{-6}}{N^i_{\mathrm{all}}}\right) \tag{5.15}$$

where, as before, N^i_{all} is the sum of C^i_{NH4} and C^i_{NO3} in box i.

Thus, total production based on newly-fixed N_2 is:

$$F^i_{\mathrm{newN}} = L^i_{\mathrm{P}} v_{\mathrm{fix}} v^i_{\mathrm{Nfi}} f_{\mathrm{max}} V^i \tag{5.16}$$

for boxes i ={low, high, shelf} and where f_{max} is a maximum fixing rate (nmol PO_4 L^{-1} hr^{-1}) based on a culture-study (McInnes et al., 2014).

Total export production (F^i_{ExT}) from boxes i ={low, high, shelf} is the sum of F^i_{oldN} and F^i_{newN}. Export production in both the low- and high-latitude boxes go to the deep ocean, and shelf export stays in the shelf box. Phosphate loss ($F^i_{\mathrm{out},PO4}$) from shallow boxes is equal to F^i_{ExT}. Fixed NO_3^- and NH_4^+ losses are equal to:

$$F^i_{\mathrm{out},j} = 16 F^i_{oldN} \frac{C^i_j}{N^i_{\mathrm{all}}} \tag{5.17}$$

for j ={NO_3^-, NH_4^+} and N_2 loss is:

$$F^i_{\mathrm{out,N2}} = 8 F^i_{\mathrm{newN}} \tag{5.18}$$

5.2.4.3 Shelf and Deep ocean

PO_4 and N can be remineralized or buried, and K can be buried in sediments. Remineralization of PO_4 is:

$$F^i_{\text{remin,PO4}} = F^i_{\text{ExT}}(1 - f^i_{\text{bur}}) \tag{5.19}$$

where f^i_{bur} is fraction buried, held constant. 0.1889 for shelf burial and 0.01 for deep.

Nitrogen remineralization and burial is assumed to be in Redfield ratio (i.e.,16:1) PO_4 burial. Nitrogen can be remineralized either as NO_3^- or NH_4^+, depending on the fraction of anoxic water, which is calculated as:

$$f^i_{\text{anox}} = \exp\left(-\frac{C^i_{\text{O2}}}{k_{\text{anox}}}\right). \tag{5.20}$$

Thus,

$$F^i_{\text{remin,NO3}} = 16F^i_{\text{remin,PO4}}\ (1 - f^i_{\text{anox}}) \tag{5.21}$$

and

$$F^i_{\text{remin,NH4}} = 16F^i_{\text{remin,PO4}}\ f^i_{\text{anox}} \tag{5.22}$$

Table 5.3: Model constants used in biogeochemical cycling with reference. References are F05 (Fennel et al., 2005), R94 (Rysgaard et al., 1994), E13 (Evrard et al., 2013), M14 (McInnes et al., 2014), and K89 (Klingler et al., 1989).

Parameter	**Definition**	**Value**	**Reference**
K_{Oni}	half-saturation uptake of O_2 in nitrification	20 μM	F05
K_{Nni}	half-saturation uptake of NH_4^+ in nitrification	100 μM	F05
$n_{\max}$	maximim nitrification rate	0.25 μM hr^{-1} L^{-1}	R94
K_{d}	half-saturation uptake of NO_3^- in denitrification	8.47 μM	E13
$d_{\max}$	maximum denitrification rate	4.62 nmol hr^{-1} mL^{-1}	E13
K_{N}	half-saturation uptake of total N	1.6 μM	F05
K_{P}	half-saturation uptake of PO_4	0.1 μM	F05
μ_1	productivity efficiency term	1	F05
$f_{\max}$	maximum productivity based on new fixing	0.5 nmol PO_4 hr^{-1} L^{-1}	M14
K_{f}	half-saturation uptake of N_2 during fixing	9.87×10^{18} mol	K89
k_{anox}	anoxic water extent factor	10 μM	F05
$f_{\mathrm{bur}}^{\mathrm{deep}}$	fraction of export production buried -deep ocean	0.01	F05
$f_{\mathrm{bur}}^{\mathrm{shelf}}$	fraction of export production buried -shelf ocean	0.1889	F05

5.2.5 Geologic model

The model is driven by a mantle cooling history from (Korenaga, 2010) and (Padhi et al., 2012). This model suggests that mantle temperatures (T_m) increased through the early Archean, reached their peak in the middle Archean, and have been decreasing to the modern day (Table 5.4, Fig. 5.3). Heat flux (Q) followed a distinct evolution, reaching its maximum later than the mantle temperature apex (Table 5.6). Temperature and heat flux are used to parameterize a plate velocity (u_c):

$$u_c = u_{co} \frac{Q}{Qo} \left(\frac{T_o}{T_m} \right)^2 \tag{5.23}$$

where u_{co}, Q_o, and T_o are modern plate velocity (0.05 m yr^{-1}), heat flux (39 TW), and average mantle temperature (1350 °C).

The model then calculates crust production at mid-ocean ridges by combining spreading rate with ridge length (L_r, m) and crust thickness (h_c, m):

$$O_p = u_c h_c L_r \rho_c \tag{5.24}$$

where ρ_c is crust density (kg m^{-3}), and h_c decreases linearly through time (Sleep & Windley, 1982) from 16 km at the beginning of the model to 8 km at $t = 4.5$ Gyr. I assume that the amount of crust subducted (O_s) is equal to O_p.

5.2.6 Sediments

A constant fraction of export production gets buried (F^i_{bur}) in sediments:

$$F^i_{\text{bur}} = F^i_{\text{ExT}} f^i_{\text{bur}} \tag{5.25}$$

where PO_4 burial is equal to F^i_{bur} and N buried is $16F^i_{\text{bur}}$.

Ammonium can also diffuse into or out of sediments, representing equilibrium with clay minerals. There are empirical measurements of equilibrium concentrations

Table 5.4: Mantle temperature (T_m) history, heat flux (Q), and spreading rat (u_c) evolution from Korenaga (2010); Padhi et al. (2012).

Age (Ga)	T_m **°C**	Q **(TW)**	u_c **(cm yr^{-1})**
0	1350	39	5.00
0.5	1425	43	5.55
1.0	1490	41	4.68
1.5	1540	40	4.22
2.0	1600	39	3.75
2.5	1680	38	3.28
3.0	1700	37	3.05
3.5	1700	37	3.05
4.0	1670	37.5	3.23
4.5	1650	38	3.38

Table 5.5: Constants used in plate tectonic and mantle temperature equations from Korenaga (2010).

Parameter	**Definition**	**Value**
u_{co}	Modern spreading rate	0.05 m yr^{-1}
T_o	Modern mantle potential temperature	1350 °C
L_r	Mid-ocean ridge length	8×10^7 m
h_c	Ocean crust thickness[1]	1600 to 8000 m
ρ_c	Ocean crust density	3000 kg m^{-3}

[1] crust thickness decreases linearly throughout model run

Table 5.6: Constants used in geologic model equations. References are H14 (Haynes et al., 2014), SK16 (Sieczka & Koda, 2016), JG15 (Johnson & Goldblatt, 2015), J03 (Jarrard, 2003), K10 (Korenaga, 2010), and W10 (Winter, 2001) .

Parameter	**Definition**	**Value**	**Reference**
λ	decay constant of ^{40}K (yr $^{-1}$)	5.543×10^{-10}	H14
X_{40}	fraction of decay producing ^{40}Ar	0.1072	H14
f_{sed}	fraction sediments that diffusively exchange	5×10^{-5}	SK16
M_{desed}	mass of deep sediments (g)	7.3×10^{23}	JG15
M_{occrust}	mass of ocean crust (g)	5.4×10^{24}	JG15
M_{mantle}	mass of mantle (g)	4×10^{27}	JG15
τ_{shcg}	rate constant of shelf sediments to cont. crust (yr $^{-1}$)	5×10^{9}	this study
$\tau_{\text{h,K}}$	rate constant of hydrothermal alteration (yr $^{-1}$)	5×10^{9}	J03
τ_{W}	rate constant of weathering (yr $^{-1}$)	2×10^{9}	
P_m	percent partial melt during MORB-genesis	10%	W01
K_{dist}	percent of species extracted during MORB-genesis	0.90	
S	spreading rate (m yr^{-1})	varies	K10
h_{sed}	sediment thickness (m)	500	this study
L_s	length of subduction zones (m)	4×10^{7}	this study
f_{shsed}	fraction shelf sediments subducted	1×10^{-7}	this study
f_{Ncgarc}	fraction N added to continental crust	0.5	this study

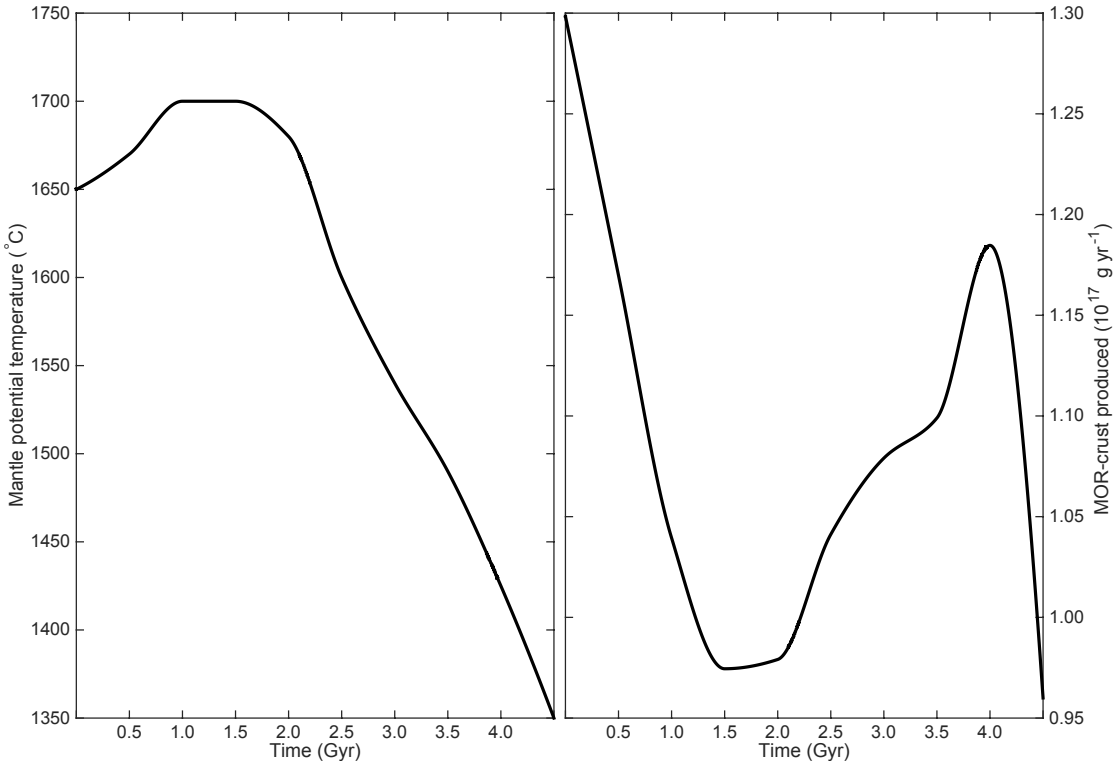

Figure 5.3: Average mantle temperature in °C and mass of crust produced at mid-ocean ridges over the course of a model run (Korenaga, 2010). Time zero is equivalent to 4.5 Ga.

of NH_4^+ in clay at a given NH_4^+-concentration in overlying water (Sieczka & Koda, 2016):

$$C^i_{\mathrm{se}} = \frac{q_m b\ (C^i_{\mathrm{NH4}})^{1/n}}{1 + b\ (C^i_{\mathrm{NH4}})^{1/n}} \tag{5.26}$$

where q_m, b, and n are maximum absorbance capacity (mg g^{-1}), Redlich-Peterson isotherm constant (L mg^{-1}), and the Sips isotherm model exponent. C_{se} is in mg g^{-1}. To calculate a NH_4^+ flux into the sediments, I first calculate C_{se}, multiply by fraction of the sediments (f_{sed}) which can exchange (5×10^{-5}, equivalent to 5 mm thickness) to determine the total mass of NH_4^+ that would exist in equilibrium (C_{seT}).

$$C^i_{\mathrm{seT}} = C^i_{\mathrm{se}} f_{\mathrm{sed}} \tag{5.27}$$

If the concentration in sediments is below equilibrium, NH_4^+ is added to sediments from the water column. If sediments have more NH_4^+ than the equilibrium value, NH_4^+ is added to the water column from the sediments:

$$F^i_{\mathrm{seddif}} = \left(\frac{C^i_{\mathrm{seT}} - C^i_{\mathrm{se}}}{1.8 \times 10^4} \right) \tag{5.28}$$

where F_{sd} is flux to sediments, and the denominator converts from mg NH_4^+ to moles N. For equations 5.25 to 5.28, boxes $i = \{$shelf sediments, deep sediments$\}$.

Species are subducted from both deep and shelf sediments. A constant fraction of shelf sediment species gets subducted,:

$$F^{\mathrm{shsed}}_{\mathrm{sub,j}} = f_{\mathrm{shsed}} R^{\mathrm{shsed}}_j \tag{5.29}$$

where f_{shsed} is the fraction of shelf sediments that subduct (1×10^{-7}). Deep sediments subducted are equal to:

$$F^{\mathrm{dsed}}_{\mathrm{sub,j}} = \frac{m^{\mathrm{dsed}}_{\mathrm{sub}} R^{\mathrm{dsed}}_j}{M^{\mathrm{dsed}}} \tag{5.30}$$

where m^{desed} is the mass of deep sediments subducted and M^{dsed} is the mass of deep sediments (7.4×10^{23} g). Mass of sediments subducted is:

$$m^{\mathrm{dsed}}_{\mathrm{sub}} = L_{\mathrm{s}} S h_{\mathrm{sed}} \rho_{\mathrm{sed}} \tag{5.31}$$

where L_s is subduction zone length (m), S is spreading rate (m yr^{-1}) calculated from

Korenaga model, h_{sed} is thickness of sediments (500 m), and ρ_{sed} is sediment density (2.5 g cm^{-3}).

In addition, shelf sediments have a residence time of 200 Myr, or a rate constant of $\tau_{\rm scg} = 5 \times 10^{-9}$. Shelf sediments are added to the continental crust, representing a proxy for continental growth by collision and accretion:

$$F_{\rm scg,j} = \tau_{\rm scg} R_j^{\rm shsed} \tag{5.32}$$

for j ={all species }.

5.2.7 Crust

5.2.7.1 Oceanic

Species can enter the oceanic crust through hydrothermal alteration, and the leave the oceanic crust during subduction. The amount of hydrothermal alteration is related to both speciation and to the temperature of the mantle.

Hydrothermal alteration is a net source of dissolved species to the oceanic crust. this is supported by the increase seen in δ^{15}N values with age of oceanic crust (Fig. 5.1), as well as mass balance considerations from K. In the modern ocean, the residence time of K is 12 Myr, or a rate constant of $\tau_{\rm h,K} = 8.33 \times 10^{-8}$ yr^{-1} (Jarrard, 2003). Thus, the hydrothermal addition of K to oceanic crust is described as:

$$F_{\rm hydro,\ K} = \tau_{\rm h,K} R_{\rm K}^{\rm deep} \tag{5.33}$$

Due to their geochemical similarity, the residence time of NH_4^+ is assumed to be equal to K. The residence times of NO_3^- is assumed to be ten times longer than NH_4^+, as there would need to be additional energy input to reduce NO_3^- to incorporate it hydrothermally into minerals. Phosphate flux into the ocean crust during alteration is estimated to be 2.8×10^{10} moles per year (Wheat et al., 2003), which is about 10 times less than the 1.5×10^{11} mole per year flux for K (Jarrard, 2003). Thus, I assume the residence time of PO_4 is also 10 times longer than that of K. The residence time of Ar is set to 1000 times more than K, since it will not bond in mineral structures, but could be found in spaces in crystal lattices. Thus, hydrothermal flux is:

$$F_{{\rm hydro},j} = \tau_{{\rm h},j} R_j^{\rm deep} \tag{5.34}$$

for species j ={NH_4^+, PO_4, ^{36}Ar, ^{40}Ar}.

The subduction flux is calculated by multiplying the mass of crust subducted per year (Fig. 5.3) by each species concentration in the crust:

$$F_{\mathrm{sub},j}^{\mathrm{oc}} = \frac{R_j^{\mathrm{ocrust}} O_p}{M_{\mathrm{oc}}} \tag{5.35}$$

where O_p is ocean crust produced and M_{oc} is the total mass of crust (g).

Thus, the total amount of each species subducted (F_{subt}) is

$$F_{\mathrm{subT},j} = F_{\mathrm{sub},j}^{\mathrm{oc}} + F_{\mathrm{sub},j}^{\mathrm{dsed}} + F_{\mathrm{sub},j}^{\mathrm{shsed}} \tag{5.36}$$

Subducted species will either be driven off the slab and sediments or carried beyond the subduction barrier and into the mantle. The proportion that is driven off the slab is determined by mantle temperature: higher temperature means less material goes into the mantle, and lower temperature means more material goes into the mantle. Subducted fraction is calculated from an average geothermal gradient, which in turn is calculated from an average mantle temperature (T_m):

$$G_{\mathrm{sub}} = \frac{12.2(T_m - 273)}{2900} \tag{5.37}$$

where T_m is in kelvin, 2900 is mantle depth in km, and 12.2 is a conversion factor to adjust average mantle temperature, consistent with the modern average mantle geothermal gradient. Subducted fraction is a hyperbolic tangent fit to the data from modern geothermal gradients and subducted fluxes at three modern subduction zones (Elkins et al., 2006; Mitchell et al., 2010; Zelenski et al., 2012), and can vary between 0.1 and 1:

$$f_{\mathrm{sub}} = 0.5\left(1.1 - 0.9\tanh\left(\frac{G_{\mathrm{sub}} - 6}{0.6}\right)\right) \tag{5.38}$$

Thus, the flux of species subducted to the mantle is the product of subducted fraction, concentration in sediments or crust, and mass of sediments/crust subducted per year:

$$F_{\mathrm{subnet,j}} = f_{\mathrm{sub}} F_{\mathrm{subT,j}}. \tag{5.39}$$

for j ={all species}.

5.2.7.2 Continental

That which is not subducted will either be outgassed at arcs (F_{ogarc}) or be incorporated into the continental crust (F_{cg}). All Ar is outgassed, all K and PO_4 goes into the continental crust, and f_{Ncgarc} of N that does not get subducted goes into the continental crust and $1 - f_{\mathrm{Ncgarc}}$ to the atmosphere. Thus, I write:

$$F_{\mathrm{cg},j} = (1 - f_{\mathrm{sub}})F_{\mathrm{subT,j}} \tag{5.40}$$

for j ={K, ^{40}K, ^{40}Ar, ^{36}Ar} and

$$F_{\mathrm{cg,N}} = f_{\mathrm{Ncgarc}}(1 - f_{\mathrm{sub}})F_{\mathrm{subT,N}} \tag{5.41}$$

for N. All subducted PO_4 is added to the continental crust.

Species in the continental crust have a residence time of 500 Myr, or time constant (τ_w) of 2×10^{-9} yr^{-1}. Removal occurs by weathering. Weathered ^{36}Ar and ^{40}Ar are released to the atmosphere, while all other species (N, PO_4, K) are added to the shelf ocean. As there is no crustal organic material in the model, all continental N is weathered as NH_4^+, which is the mineralogically most stable form of N. Weathering (F_{w}) is parameterized as:

$$F_{\mathrm{w},j} = \tau_{\mathrm{w},j} R_j^{\mathrm{contcrust}} \tag{5.42}$$

5.2.8 Mantle

Species are added to the mantle at subduction zones (F_{subnet}). It is assumed that they instantly homogenize into the mantle (i.e., there are no separate mantle domains). Species leave the mantle through degassing at mid-ocean ridges. Degassing is the product of the concentration (C_j^{man}) of the species in the mantle and the mass of mantle involved in crust genesis (M_{melt}). M_{melt} is set to 10 times the mass of oceanic crust produced (O_p), from the Korenaga mantle evolution model, and represents generation of crust by 10% partial melt. I assume 90% of all species are partitioned to the melt during partial melting (K_D), with 10% remaining in the residual. Thus, mid-ocean ridge outgassing is:

$$F_{\mathrm{ogmor},j} = C_j^{\mathrm{man}} M_{\mathrm{melt}} O_p K_D \tag{5.43}$$

with M_{mantle} as the mantle mass (g).

5.2.9 Differential equations

Based on the above discussion, I write a series of differential equations to solve for model species in boxes.

Atmosphere

$$\frac{dR_j^{\rm atm}}{dt} = \sum_{i*} F_{\rm as,j}^{atm-i*} + F_{\rm ogarc,j} \tag{5.44}$$

for j ={N_2, ^{40}Ar, ^{36}Ar} and $i*$ includes air-sea flux from all shallow ocean boxes ({low, high, shelf}).

Low- and high-latitude shallow ocean

$$\frac{dR_{\rm 40Ar}^i}{dt} = F_{\rm mix,40Ar}^i + F_{\rm rd}^i - F_{\rm as,40Ar}^{atm-i} \tag{5.45}$$
$$\frac{dR_{\rm 36Ar}^i}{dt} = F_{\rm mix,36Ar}^i + F_{\rm rd}^i - F_{\rm as,36Ar}^{atm-i} \tag{5.46}$$
$$\frac{dR_{\rm 40K}^i}{dt} = F_{\rm mix,40K}^i - F_{\rm rd}^i \tag{5.47}$$
$$\frac{dR_{\rm K}^i}{dt} = F_{\rm mix,K}^i \tag{5.48}$$
$$\frac{dR_{\rm PO4}^i}{dt} = F_{\rm mix,PO4}^i - F_{\rm ExT}^i \tag{5.49}$$
$$\frac{dR_{\rm NO3}^i}{dt} = F_{\rm mix,NO3}^i - F_{\rm out,NO3}^i + F_{\rm nit}^i - F_{\rm den}^i \tag{5.50}$$
$$\frac{dR_{\rm NH4}^i}{dt} = F_{\rm mix,NH4}^i - F_{\rm out,NH4}^i - F_{\rm nit}^i \tag{5.51}$$
$$\frac{dR_{\rm N2}^i}{dt} = F_{\rm mix,N2}^i - F_{\rm out,N2}^i + 0.5F_{\rm den}^i \tag{5.52}$$

for i ={low, high}.

Shelf ocean

$$\frac{dR^i_{40\mathrm{Ar}}}{dt} = F^i_{\mathrm{mix},40\mathrm{Ar}} + F^i_{\mathrm{rd}} - F^{atm-i}_{\mathrm{as},40\mathrm{Ar}} \quad (5.53)$$

$$\frac{dR^i_{36\mathrm{Ar}}}{dt} = F^i_{\mathrm{mix},36\mathrm{Ar}} + F^i_{\mathrm{rd}} - F^{atm-i}_{\mathrm{as},36\mathrm{Ar}} \quad (5.54)$$

$$\frac{dR^i_{40\mathrm{K}}}{dt} = F^i_{\mathrm{mix},40\mathrm{K}} - F^i_{\mathrm{rd}} + F_{\mathrm{w},40\mathrm{K}} \quad (5.55)$$

$$\frac{dR^i_{\mathrm{K}}}{dt} = F^i_{\mathrm{mix,K}} + F_{\mathrm{w,K}} \quad (5.56)$$

$$\frac{dR^i_{\mathrm{PO4}}}{dt} = F^i_{\mathrm{mix,PO4}} - F^i_{\mathrm{ExT}} + F^i_{\mathrm{remin,PO4}} + F_{\mathrm{w,PO4}} \quad (5.57)$$

$$\frac{dR^i_{\mathrm{NO3}}}{dt} = F^i_{\mathrm{mix,NO3}} - F^i_{\mathrm{out,NO3}} + F^i_{\mathrm{nit}} - F^i_{\mathrm{den}} + F^i_{\mathrm{remin,NO3}} \quad (5.58)$$

$$\frac{dR^i_{\mathrm{NH4}}}{dt} = F^i_{\mathrm{mix,NH4}} - F^i_{\mathrm{out,NH4}} - F^i_{\mathrm{nit}} + F^i_{\mathrm{remin,NH4}} + F_{\mathrm{w,NH4}} - F^i_{\mathrm{seddif}} \quad (5.59)$$

$$\frac{dR^i_{\mathrm{N2}}}{dt} = F^i_{\mathrm{mix,N2}} - F^i_{\mathrm{out,N2}} + 0.5F^i_{\mathrm{den}} \quad (5.60)$$

$$(5.61)$$

for $i = \{\mathrm{shelf}\}$.

Deep ocean

$$\frac{dR^i_{40\mathrm{Ar}}}{dt} = F^i_{\mathrm{mix},40\mathrm{Ar}} + F^i_{\mathrm{rd}} - F^i_{\mathrm{hydro},40\mathrm{Ar}} + F_{\mathrm{ogmor},40\mathrm{Ar}} \quad (5.62)$$

$$\frac{dR^i_{36\mathrm{Ar}}}{dt} = F^i_{\mathrm{mix},36\mathrm{Ar}} + F^i_{\mathrm{rd}} - F^i_{\mathrm{hydro},36\mathrm{Ar}} + F_{\mathrm{ogmor},36\mathrm{Ar}} \quad (5.63)$$

$$\frac{dR^i_{40\mathrm{K}}}{dt} = F^i_{\mathrm{mix},40\mathrm{K}} - F^i_{\mathrm{rd}} - F_{\mathrm{hydro},40\mathrm{K}} + F_{\mathrm{ogmor},40\mathrm{K}} \quad (5.64)$$

$$\frac{dR^i_{\mathrm{K}}}{dt} = F^i_{\mathrm{mix,K}} - F_{\mathrm{hydro,K}} + F_{\mathrm{ogmor,K}} \quad (5.65)$$

$$\frac{dR^i_{\mathrm{PO4}}}{dt} = F^i_{\mathrm{mix,PO4}} + F^i_{\mathrm{remin,PO4}} - F_{\mathrm{hydro,PO4}} + F_{\mathrm{ogmor,PO4}} \quad (5.66)$$

$$\frac{dR^i_{\mathrm{NO3}}}{dt} = F^i_{\mathrm{mix,NO3}} + F^i_{\mathrm{remin,NO3}} + F^i_{\mathrm{nit}} - F^i_{\mathrm{den}} - F^i_{\mathrm{hydro,NO3}} \quad (5.67)$$

$$\frac{dR^i_{\mathrm{NH4}}}{dt} = F^i_{\mathrm{mix,NH4}} - F^i_{\mathrm{out,NH4}} - F^i_{\mathrm{nit}} + F^i_{\mathrm{remin,NH4}} + F_{\mathrm{w,NH4}} - F^i_{\mathrm{seddif}} \quad (5.68)$$

$$\frac{dR^i_{\mathrm{N2}}}{dt} = F^i_{\mathrm{mix,N2}} + 0.5F^i_{\mathrm{den}} + 0.5F_{\mathrm{ogmor,N}} \quad (5.69)$$

$$(5.70)$$

for $i = \{\mathrm{deep}\}$.

Sediments

$$\frac{dR^i_{\rm N}}{dt} = F^i_{\rm bur,N} + F^i_{\rm seddif} - F^i_{\rm sub,N} \quad (5.71)$$
$$\frac{dR^i_{\rm PO4}}{dt} = F^i_{\rm bur,PO4} - F^i_{\rm sub,PO4} \quad (5.72)$$
$$(5.73)$$

for $i =$\{shelf sediments, deep sediments\}.

Ocean crust

$$\frac{dR^i_{\rm 40Ar}}{dt} = F_{\rm rd} - F^i_{\rm sub,40Ar} \quad (5.74)$$
$$\frac{dR^i_{\rm 40K}}{dt} = -F_{\rm rd} - F^i_{\rm sub,40K} \quad (5.75)$$
$$\frac{dR^i_{\rm K}}{dt} = F_{\rm hydro,K} - F^i_{\rm sub,K} \quad (5.76)$$
$$\frac{dR^i_{\rm N}}{dt} = F_{\rm hydro,N} - F^i_{\rm sub,N} \quad (5.77)$$
$$\frac{dR^i_{\rm PO4}}{dt} = F_{\rm hydro,PO4} - F^i_{\rm sub,PO4} \quad (5.78)$$
$$(5.79)$$

for $i =$\{ocean crust\}.

Continental crust

$$\frac{dR^i_{\rm 40Ar}}{dt} = F^i_{\rm rd} - F_{\rm w,40Ar} \quad (5.80)$$
$$\frac{dR^i_{\rm 40K}}{dt} = -F^i_{\rm rd} - F_{\rm w,40K} \quad (5.81)$$
$$\frac{dR^i_{\rm K}}{dt} = -F^i_{\rm rd} - F_{\rm w,K} \quad (5.82)$$
$$\frac{dR^i_{\rm N}}{dt} = F_{\rm cg,N} - F_{\rm w,N} \quad (5.83)$$
$$\frac{dR^i_{\rm PO4}}{dt} = F_{\rm cg,PO4} - F_{\rm w,PO4} \quad (5.84)$$
$$(5.85)$$

for $i =$\{continental crust\}.

Mantle

$$\frac{dR^i_{40\mathrm{Ar}}}{dt} = F^i_{\mathrm{rd}} - F_{\mathrm{ogm,40Ar}} + F_{\mathrm{subN,40Ar}} \quad (5.86)$$

$$\frac{dR^i_{40\mathrm{K}}}{dt} = -F^i_{\mathrm{rd}} - F_{\mathrm{ogm,40K}} + F_{\mathrm{subN,40K}} \quad (5.87)$$

$$\frac{dR^i_j}{dt} = -F_{\mathrm{ogm},j} + F_{\mathrm{subN},j} \quad (5.88)$$

$$(5.89)$$

for $i =$\{mantle\} and $j =$\{^{36}Ar, N, PO_4, and K\}.

5.3 Details on code structure

The model code was constructed to prioritize flexibility. Due to the high number of unknowns in the system, giving flexibility was important. I set up the reservoir bookkeeping as a structure array in Matlab. This allows for dynamic field names to be used, which assists in ease of code reading. I also constructed it so that initial conditions are read in through a separate text file. This allows easy changes, but it is also flexible as not every species has to be in every box. It also calculates ^{40}K from K initial conditions, reducing input time and error.

The differential equation file is arranged so that it is straightforward to turn various fluxes off and on. The purpose for this design is that this model, or one like it, could be used for not only Earth history, but could be applied to planetary evolution in general. Different planetary evolution pathways may or may not involve subduction, different atmospheric compositions, or differing biologic pathways and metabolisms. Testing the response of the system to such differences, perturbations, and the presence of absence of one or more fluxes could be of great value in studying planetary evolution.

In detail, I used Matlab's ode15s solver. This is a variable-step, variable-order solver that uses numerical differentiation formulas of orders 1 to 5. I set the relative error tolerance to 1×10^{-7} and a maximum step size of 10^6 years.

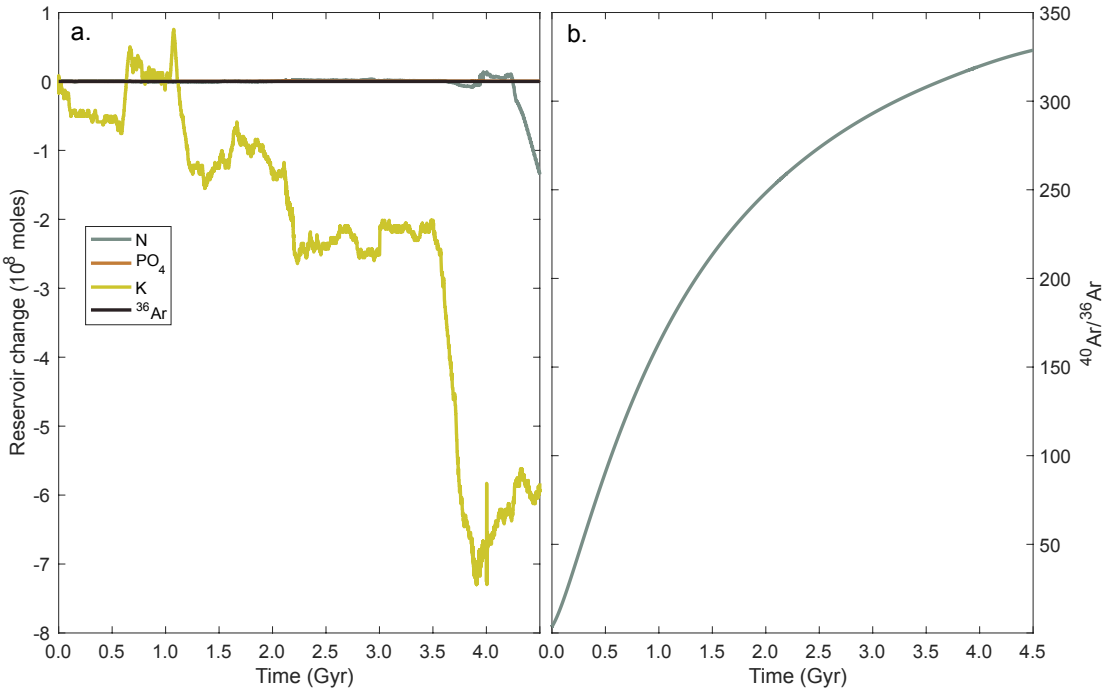

Figure 5.4: Shown are model conservative species in a. and atmospheric ^{40}Ar/^{36}Ar in b. Reservoir change is the total amount of species j at time t minus the initial amount. There is some numerical drift, especially evident in K, but it is many orders of magnitude smaller than the total amount of K in the model (10^{22} moles). Atmospheric ^{40}Ar/^{36}Ar ratio evolves and nearly exactly reproduces the observed modern value (295). Time zero is equivalent to 4.5 Ga.

5.4 Nominal runs

5.4.1 Model performance check

As the model contains a high number of fluxes, and masses of species can vary by many orders of magnitude, it is important to ensure that mass is conserved. While some model numerical drift is evident, it is many orders of magnitude smaller than the total amount of each model species (Fig. 5.4). For example, K changes by 10^8 moles over the course of the model run, but the total amount of K is on the order of 10^{22} moles. The loss caused by numerical drift is negligible.

In addition, the model very nearly matches the modern atmospheric ratio of ^{40}Ar/^{36}Ar, which is 295 in the modern atmosphere and 330 in the model (Fig. 5.4). This suggests that the outgassing and subduction fluxes are reasonable.

Table 5.7: Initial conditions for nominal model runs. Three test cases are shown: high-atmospheric N (high-N), low-atmospheric N (low-N), and low-PO_4 (low-P). Geologic reservoirs and atmosphere (note atmosphere given as moles N_2) are given in 10^{20} moles, while ocean reservoirs are given in μM.

Reservoir	**high-N**	**low-N**	**low-P**
Atmosphere-N_2	4	0.5	4
Continental crust -N	1×10^{-8}	1×10^{-8}	1×10^{-8}
Continental crust -PO_4	0.27	0.27	0.27×10^{-4}
Oceanic crust -N	1×10^{-8}	1×10^{-8}	1×10^{-8}
Oceanic crust -PO_4	1×10^{-8}	1×10^{-8}	1×10^{-8}
Deep sediments -N	0.001	0.001	0.001
Deep sediments -PO_4	1×10^{-7}	1×10^{-7}	1×10^{-7}
Shelf sediments -N	0.001	0.001	0.001
Shelf sediments -PO_4	1×10^{-7}	1×10^{-7}	1×10^{-7}
Mantle -N	1	8	1
Mantle -PO_4	0.001	0.001	1×10^{-4}
Ocean boxes -NH_4^+	100	100	100
Ocean boxes -NO_3^-	100	100	100
Ocean boxes -PO_4	100	100	100

As the model seems to be performing ably, I performed three initial model experiments. The first starts with a high-N atmosphere, the second with a high-N mantle, and the third is a sensitivity test with very low PO_4 abundance (Table 5.7). Again, I stress that these are only exploratory model runs to demonstrate the fitness of the model. From such an exploration, I can draw initial conclusions and identify areas for further model development. Model tuning and sensitivity studies may well be required for robust and publishable output.

5.4.2 High initial atmosphere N_2

Nitrogen is seen to move dynamically through the Earth system on 100 Myr timescales (Fig. 5.5). Atmospheric N is drawn down from $t = 0$ until the Great Oxidation event (GOE) at $t = 2.1$ Gyr. Nitrogen is sequestered in the continental crust and mantle, with relatively high rates of total subduction outpacing mantle outgassing. Such sequestration is aided by the higher potential of NH_4^+ to be incorporated hydrothermally into the oceanic crust. Even with high mantle temperatures, which leads to more effective return of subducted N to the surface, atmospheric drawdown

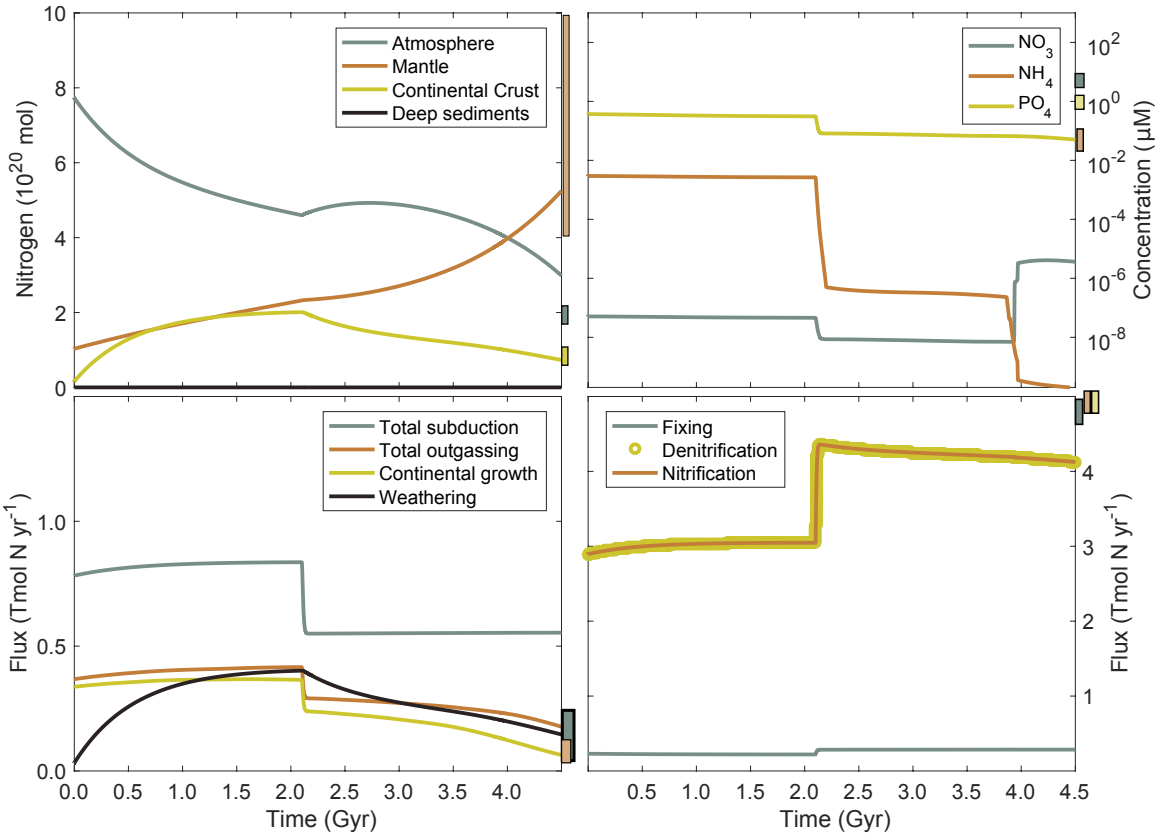

Figure 5.5: Nitrogen distribution in the atmosphere, mantle, continental crust, deep sediments, and oceanic nutrient values over time. Geologic fluxes and major biologic fluxes are shown. Major cycling changes occur at the Great Oxidation Event, with an increase in nitrification-denitrification leading to an increase in atmospheric N. After the Neoproterozoic Oxygenation Event, NO_3^- becomes the main species in the ocean. Cooling mantle temperatures lead to more efficient sequestration during subduction, causing drawdown of atmospheric N_2 over the Phanerozoic. Modern values are shown as coloured bars on the right-hand margin of subplots. Time zero is equivalent to 4.5 Ga.

is seen in model output.

At the GOE, a large drop in oceanic NH_4^+ is seen, with a corresponding increase in rates of both nitrification and denitrification. Correspondingly, the amount of total N in the oceans decreases, and this denitrified N is released to the atmosphere. As mantle temperatures continue to cool, recycling of N into the mantle at subduction zones is favoured, thus atmospheric drawdown continues even with substantial denitrification removing N from the oceans. During the Proterozoic, both NO_3^- and NH_4^+ exist in the ocean, with concentrations that are more similar than during the Archean or Phanerozoic.

With the rise of O_2 to 80% then 100% PAL in the late Proterozoic and early Phanerozoic, NO_3^- becomes the dominant species of N in the oceans. There is no discernible difference in geologic fluxes at this time.

The main interpretations of this run are that, again, N can cycle throughout the Earth system and the dominant N reservoir on the Earth could change over time. At the end of the model run, the mantle appears to be the main repository for N, consistent with previous budget estimates (Goldblatt et al., 2009; Johnson & Goldblatt, 2015). This run is consistent with a more massive atmosphere in the past, and is not consistent with paleobarometry data suggesting modern pressure at 3.0 Ga (Marty et al., 2013) or lower pressures during the Archean (Som et al., 2012, 2016). Methodology problems indicate such low pressure estimates may not be robust (Niemi et al., 2005; Kavanagh & Goldblatt, 2015), and the model run initialized with high-atmospheric N herein is not congruent with low pressures in the past.

5.4.3 Low initial atmosphere N_2

The general shape of the atmospheric N-curve is similar during this low initial atmospheric-N run as in the previous section. There is a modest drawdown initially, with an inflection at the GOE, a rise in atmospheric O, then a decrease from $t = 3.5$ Gyr till the end of the model run. The mantle remains the dominant N-reservoir throughout the entire run. Again, the increase in nitrification-denitrification at the GOE is an important event, as an increase in atmospheric N is seen after this time.

As in the previous run, the continental crust N reservoir grows until the GOE, then slowly decreases through time. Since the input of N into the continental crust is controlled by subduction and mantle temperatures, while weathering is constant through time, as mantle temperatures decrease, more N at subduction zones is carried

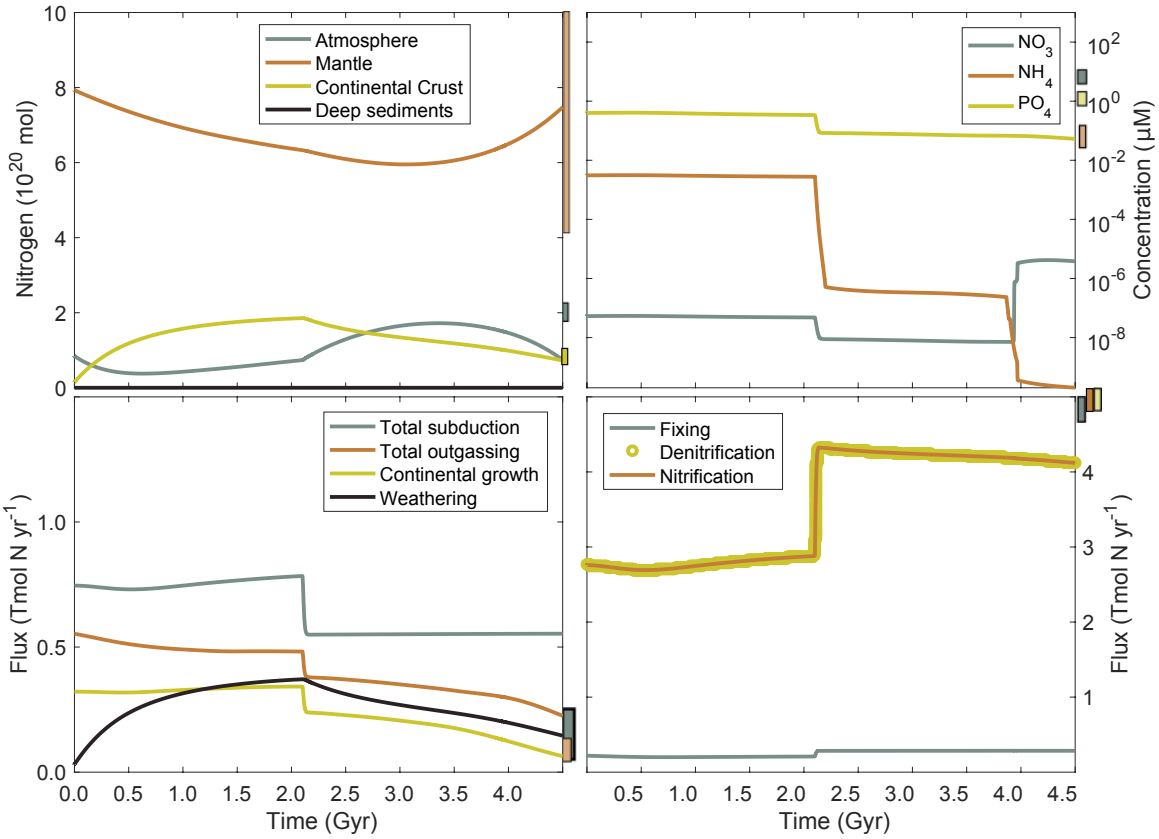

Figure 5.6: Panels are the same as in Fig. 5.5. Initial drawdown of the atmosphere sequesters N into the mantle and continental crust as in runs with higher initial atmospheric N_2. The solid Earth tends to retain N throughout the Archean, with atmospheric mass increasing at the Great oxygenation event. Modern values are shown as coloured bars on the right-hand margin of subplots. Time zero is equivalent to 4.5 Ga.

into the mantle, meaning the supply of N to the continental crust decreases over time. At $t = 4.5$ Gyr, there is 1×10^{20} moles of N in the continental crust, which is approximately half of PAN, a value consistent with the budget estimate presented in Chapter 2.

5.4.4 High initial atmosphere N_2, low PO_4

The amount and availability of PO_4 is an important controlling parameter on the distribution of N. Given total PO_4 of only 3×10^{16} mol, with $\frac{2}{3}$ in the continental crust and the remainder in the mantle, very little change is observed in N distribution with time (Fig. 5.7). As biologic activity is PO_4-limited, and biologic processing is

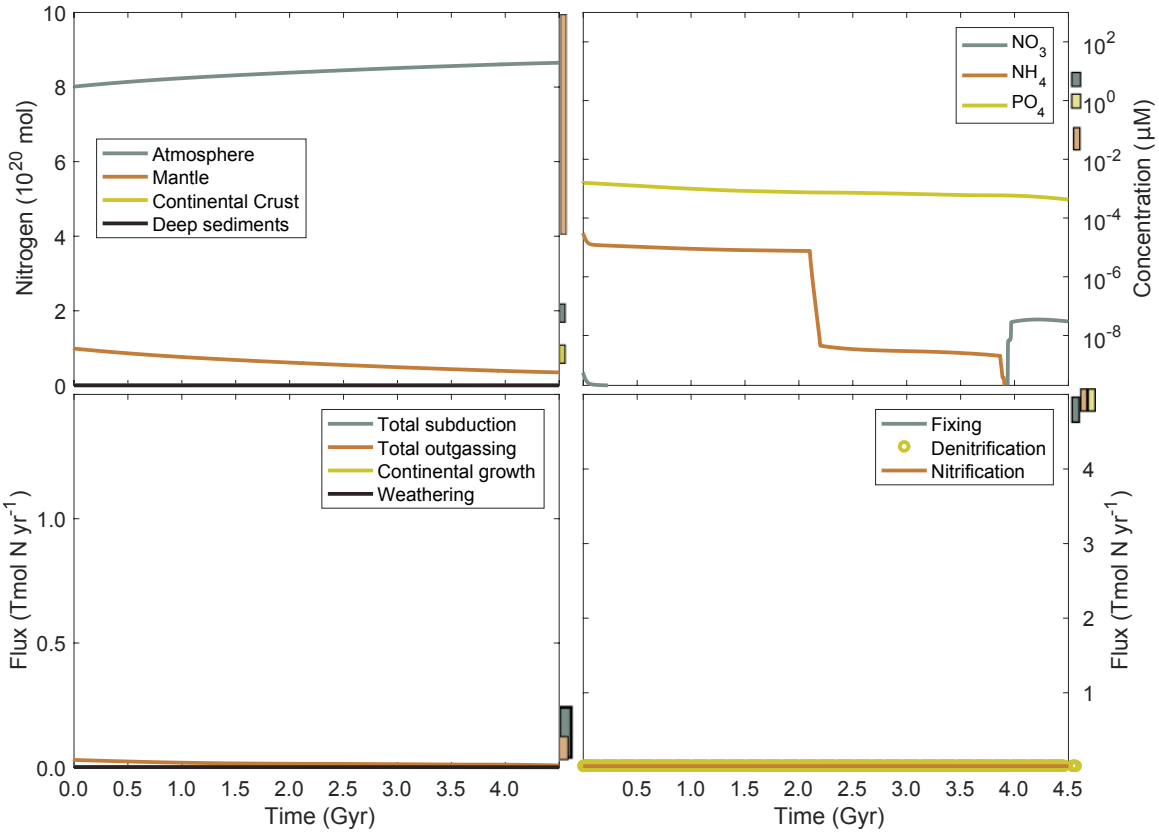

Figure 5.7: Lack of nutrients results in low biologic activity, and stasis of N in the Earth system. Modern values are shown as coloured bars on the right-hand margin of subplots. Time zero is equivalent to 4.5 Ga.

the key mechanism of transferring N from the atmosphere to the geosphere, low PO_4 will necessarily lead to slower processing and more reservoir stability over time.

5.4.5 Initial conclusions

There are several key preliminary conclusions. The first is that contrary to canonical assumptions, the mass of N and the distribution of this element in the Earth system could be dynamic over Earth history. Given differing oxygen levels, and the availability of key nutrients (i.e., PO_4), biology can be efficient at removing N from the atmosphere, and geologic fluxes have the potential to sequester and cycle N over hundred-million year time scales.

There are a number of inputs to this model that affect model output. The first is the overall amount of PO_4 in the Earth system. Ample continental PO_4 provides the nutrient capacity for N-fixing and atmospheric drawdown. Initial N distribution

also has a significant effect on atmospheric and BSE N abundances over time. More initial atmospheric N_2 leads to a more dynamic cycle, while more geologic N leads to a more stable system.

Lastly, the rise in oxygen during both the GOE and Neoproterozoic Oxygenation event have pronounced influences on the N-cycle. The effect is mostly due to changes in the denitrification flux. Free O_2 is required for nitrification to occur and produce NO_3^-, which can subsequently denitrify to N_2 given sufficient low-O_2 waters. In this model, such denitrification is the primary means of returning N to the atmosphere, though other studies suggest there reaction of NH_4^+ with Fe^{2+} might be an inorganic pathway in anoxic water that could remove fixed N from the ocean (Stüeken et al., 2016).

5.5 Future development

5.5.1 O_2 cycle

The O_2 in this model is prescribed. In reality, there are feedbacks between the O_2 and N-cycles. For example, nitrification uses O_2 to oxidize NH_4^+. In addition, O_2 acts as an inhibitor to N-fixation, though many organisms have evolved enzyme protection strategies to minimize this effect. Low O_2 conditions are a requisite for denitrification, or anammox, thus high O_2 should limit the return flux of fixed N to the atmosphere. The levels of O_2 in the atmosphere directly affect weathering of both organic and inorganic materials on the continents. This dependency is not incorporated in the model, as weathering is parameterized as a only a residence time.

5.5.2 Low nutrient levels

In all model runs, NO_3^- and NH_4^+ are well below their average value in all ocean boxes at $t = 4.5$ Gyr. The modern ocean deep has a NO_3^- concentration of $10 - 30$ μM (Garcia et al., 2010), while the model output deep ocean NO_3^- concentration is 3.6×10^{-6} μM. This is extremely low. As nitrification and denitrification are equal in all model runs (Fig. 5.5 - 5.7), all newly formed NO_3^- is immediately denitrified. In addition, the denitrification flux is larger than the NO_3^--remineralization flux. Addressing how denitrification is parametrized appears to be critical in the robustness of this model.

5.5.3 Nutrient excursions

The history of Earth is punctuated by large basaltic eruptions. Such eruptions bring an enormous amount of weatherable material to the surface. Since basalt has a high concentration of PO_4, this has the potential to cause a 10^5 to 10^6 year pulse of nutrients into the ocean. This input would serve to depress the N:P Redfield ratio, which could cause N-fixing bacteria to increase in activity, drawing down N from the atmosphere. If this increased productivity is not completely remineralized and denitrified, it could sequester N into sedimentary rocks and entrain it more effectively into the geologic cycle.

5.5.4 Isotopic fractionations

Adding in isotopic fractionations to model fluxes could provide a valuable mechanism to vet model predictions in the geologic record. Specifically, the balance of N-fixing to denitrification in the global ocean changes the N-isotopic character of the ocean, and this oceanic character is recorded in sediments (Ader et al., 2016). While incomplete, there are some constraints on N-isotopic fractionation during subduction (Bebout & Fogel, 1992; Busigny et al., 2011), suggesting N in sediments increases in δ^{15}N values as metamorphism proceeds and N is driven off.

It is conceivable that the model herein could broadly predict changes in the geologic N-isotopic record. This predicted record could be compared to the rock record, where there exists some data, especially in the sedimentary record. The model could also predict, then, the isotopic values of the atmosphere and mantle through time, which are much more difficult to ascertain in the rock record.

5.6 Summary

To address the conundrum that modelling efforts suggest little change in N-distribution over time, while geochemistry indicates change may be substantial, I have constructed an Earth-system N cycle model incorporating physical, geologic, and biologic fluxes. This model contains all the major N-fluxes, and is unique among Earth system N-models in that it explicitly solves for biologic and geologic fluxes over long time-scales.

Preliminary conclusions suggest that N in the Earth system may not be in steady-

state at present. In both nominal runs, high- and low-atmospheric N, atmospheric drawdown is apparent throughout the Phanerozoic. This output is consistent with sparse estimates at modern subduction zones. Such drawdown occurs even with relatively high denitrification. The inflection in the N-evolution curves of the atmosphere, continental crust, and mantle seen at the GOE are consistent with a geochemical reorganization occurring at this time, not only in terms of O_2 and C but in the N-cycle as well.

Broadly, this model can also be applied to planetary evolution in general. The built-in flexibility allows for all fluxes to be switched on and off, or to vary in magnitude in time. The effects of different O_2 histories, varying abundance of nutrients, or tectonic style could all be investigated in this model. Viewing the Earth as a system, affected by changes in geology and biology both, will prove a valuable vantage.

Chapter 6

Conclusions

Since its discovery, nitrogen and its behaviour have been shrouded in uncertainty. A mysterious gas was isolated from the air, and though its importance as a nutrient for organisms was clear by the late 1800s, it was thought to be chiefly an atmospheric gas into the early 20th century (Goldschmidt, 1937). As such, it was thought to remain noble and inert in the atmosphere, even when appreciation of the great age of the Earth became apparent in the mid-20th century (Patterson, 1956).

The primary goal of this dissertation was to build on the idea that substantial N might actually be contained in the Bulk Silicate Earth (BSE) (Goldblatt et al., 2009), and that this element can indeed cycle throughout the Earth system (Marty, 1995; Busigny et al., 2011). I used a novel and extensive literature compilation, conducted a laboratory investigation (method development and isotopic study), and constructed an Earth-system model to achieve this research goal.

The N budget of Earth research, as shown in Chapter 2, indicates that the Bulk Silicate Earth (BSE) contains substantial N, some 7 ± 4 present atmospheric masses (PAN= 4×10^{18} kg). In addition, the core may contain 45 to 75 PAN, sequestered from the BSE and surface Earth during planetary formation. Theoretical (Marty & Zimmermann, 1999), iron meteorite (Prombo & Clayton, 1993; Johnson & Goldblatt, 2015), and recent experimental evidence (Li et al., 2016) suggest that the core is also isotopically lighter than the BSE, indicating that core segregation directly affected the δ^{15}N evolution and character of the Earth. This is an important observation, as δ^{15}N values have been used to argue for or against certain chondrites as planetary building blocks. In addition, N abundances have been used to suggest that the Earth is "missing" N. My work may negate the need to seek out mysterious, missing N.

The N budget work also highlighted the need for more scrutiny and development

of analytical methods appropriate for geologic N. Nitrogen is often found as NH_4^+, and at low quantities in rocks and minerals, thus it is useful to adapt a fluorometric technique developed to measure low quantities of NH_4^+ in water (Holmes et al., 1999). Additionally, since N can exist as several species, knowing exactly what species is analyzed is very useful. The fluorometry technique also provides a relatively quick alternative to more intensive mass spectrometric techniques for assessing N concentration. Despite the promise of techniques as detailed in Chapter 3, the need for more methodology to be developed is apparent. Crucially, the adoption of international geologic N concentration and isotopic standards is paramount.

Where lithologies are amenable to analysis and N-contents are relatively high, a record of oceanic N-cycling can be gleaned from sedimentary rocks. Analysis of units from the Neoproterozoic Ghaub formation of Namibia indicate an active N-cycle during the Marinoan Snowball Earth (Chapter 4). Measured $\delta^{15}N$ values are lower than, and distinct from, modern average ocean values. Redox-sensitive trace elements (U, V, Mo) indicate that there was oxidative weathering on the continents, consistent with small volumes of oxic water in the ocean and oxygenic photosynthesis during the Snowball glaciation. As such, nitrification occurred in the oxic waters, with denitrification nearly quantitative in the remaining ocean, lowering $\delta^{15}N$ values recorded in analyzed units. As the glacial period ended, O_2-levels rose, and the N-cycle responded by decreasing denitrification. These data are the first N and trace element analyses from the Snowball Earth glaciation, to my knowledge, and they add important nuance and detail to this distinct period of Earth history. In addition, the dovetailing between O_2 and N is a key observation and conclusion of this study.

This interplay between O_2 and N-cycling is evident over much longer time scales as well (Chapter 5). Indeed, the short-time scale adjustments of the biologic cycle caused, for example, by the Great Oxidation Event, propagate into the geologic cycle. Increased O_2 leads to increased nitrification, with resulting NO_3^- denitrified and returned to the atmosphere, keeping atmospheric mass relatively high. The cooling of the interior of the planet eventually favours sequestration of N at subduction zones, congruent with geochemical evidence of net transport of N into the mantle at several modern subduction zones. The amount of N that transfers into the mantle is ultimately controlled by geologic forcing, plate speed, and mantle temperature, but it is only allowed into the sediments and crust if biologic cycling acts as intermediary between the atmosphere and geologic units. Given the current state of knowledge, the planet appears to not be in steady-state in terms of its N distribution and whole-Earth

cycle.

Thus, I have been able to answer the series questions proposed in the introduction to this dissertation. There appears to be ample N in the solid Earth to both negate the need to invoke "missing N" and is consistent with a larger atmospheric mass in the early Earth that has been drawn down into the mantle over time. There remain, though, a number of outstanding questions concerning N in the solid Earth.

An important and under-explored process in the Earth system N cycle is the hydrothermal alteration-mediated addition of N to the oceanic lithosphere. This process may be the most important mechanism in transferring N from the atmosphere-biosphere into the lithosphere, where it can be subducted in the mantle. Nitrogen found in altered oceanic crust appears to be more strongly bonded in mineral lattices, and much more likely to be subducted, than N in sedimentary rocks. The hydrothermal flux may have been even more important during the Archean, when higher mantle temperatures and thicker oceanic crust likely promoted enhanced hydrothermal circulation. In addition, N was most likely found as NH_4^+, which is more easily incorporated into mineral lattices than other N species.

While the work presented in this dissertation is consistent with many atmospheric masses of N in the mantle, the exact amount, distribution, and when/how that N was emplaced in the mantle are all unconstrained. Mantle N mass could be better constrained by additional analyses of basalts, xenoliths, and diamonds in conjunction with Ar and K studies. Comparing N with geochemically similar elements is a powerful way to increase the robustness of any interpretations or proclamations concerning N in the solid Earth. Comparisons with C may be important, though N and C may behave very differently in the mantle. Nitrogen appears to be predominantly found as NH_4^+ in the upper mantle, while C can exist as diamond or carbonate. In the transition zone and lower mantle, however, redox conditions suggest that in fact nitrides may be the predominant form of N in the mantle. In addition, modelling studies should strive to treat the mantle as more than just a single box, and instead incorporate strategies of mantle circulation used in geophysical models. This approach would allow for treatment of mantle chemical evolution over time, which would have a significant effect on N speciation in the mantle, and specifically its retention during subduction (Mikhail & Sverjensky, 2014) and behaviour during diamond growth (Mikhail & Howell, 2016).

The uncertainty in the amount and behaviour of N in the mantle leads directly to uncertainties concerning the δ^{15}N value of the Earth. Typically, the mantle is thought

to have a δ^{15}N value of -5‰ or less, based on analyses of MORBs (Marty, 1995) and diamonds (Cartigny et al., 2001). This depleted N-isotopic character has been assumed to be a remnant of accretion of enstatite-chondrite like material, and presents a confusing comparison with the atmosphere. Given equilibrium isotopic effects during mantle degassing, one would expect the atmosphere to be *depleted* compared to the mantle, which is in fact the opposite of what is observed. There are several possible solutions to this conundrum, including subduction of isotopically depleted biologic matter in the Archean (Marty & Dauphas, 2003) and mixing between an isotopically depleted enstatite chondrite-like mantle with an isotopically enriched carbonaceous chondrite-like atmosphere (Jia & Kerrich, 2004). There are a number of issues with these solutions, including determining the overall isotopic character of the mantle at present, and how it may have evolved in the past. An additional possibility is that there is some isotopic fractionation during mantle melting. There is some evidence for fractionation during melting from OIBs and associated xenoliths (Chap. 2) as well as fractionation during metal-silicate equilibrium (Li et al., 2016). In spite of the high temperatures associated with these processes, there is evidence for isotopic fractionations that have not been incorporated in isotopic evolution models.

The isotopic composition of the mantle is important to constrain not only N cycling in the Earth over time but also determining the source of N during planetary accretion. The source of volatile elements to the Earth, including N, has been the subject of much inquiry (Javoy, 1998; Marty, 2012; Halliday, 2013). Most models implicate some sort of chondritic starting composition and addition of N during a late veneer phase after the bulk of planetary accretion has occurred. An alternative view is emerging, however, suggesting that no such late veneer is required. Instead, the presence of stably bound, reduced N in the inner solar system (Harries et al., 2015) and the accretion of already differentiated planetesimals could be sufficient delivery vehicles for N to the Earth and other terrestrial planets. This would help explain why no one chondritic compositional comparison is satisfactory for the Earth: the Earth is a mix of different kinds of chondrites (enstatitic plus minor carbonaceous), or the Earth formed from a feeding zone in the accretionary disk that was distinct from all extant chondrites, though it itself was "chondritic". This would suggest, then, that the Earth acquired its volatiles from the both the solar nebula and already differentiated planetesimals early during its accretionary history. Nitrogen isotopic differentiation of enstatitic material during core formation could account for the isotopic character of the mantle (Dauphas & Marty, 1999). Both measurements of

pallasites (Prombo & Clayton, 1993) and experimental results (Li et al., 2016) suggest that metal is isotopically depleted in N compared to coexisting silicates. This could cause initially enstatitic material, with δ^{15}N of -25‰ to fractionate light isotopes to the core and drive the Bulk Silicate Earth towards more enriched values, either the -5‰ as typically suggested or 2.1‰ as suggested in this thesis (Chap. 2).

The distribution of N in a planet has direct impacts on its habitability. The mass of N in the atmosphere can have a direct effect on the efficacy of greenhouse warming (Goldblatt et al., 2009). Its importance in biologic compounds is well-known, and the presence of a large nutrient reservoir, the atmosphere, provides a kind of long-term storage space, though one which few organisms can access. There must be input of new nutrients into the biosphere in order for organisms to survive. On long-time scales, this must either come from the atmosphere or be released from the solid Earth.

Thus, it appears to be insufficient to view the mantle and the atmosphere-ocean system as separate reservoirs over the course of Earth history. There are several key biologic elements (N, C, H_2O) that are cycled between the two reservoirs, and on the scales of planetary evolution the mantle and atmosphere may even be well-mixed. This is in stark contrast to planets such as Venus and Mars, where the lack of plate tectonics, or mixing between the atmosphere and mantle, isolates the two reservoirs to a high degree. In a way, this stirring of Earth may help to buffer nutrients and solutes at amiable levels on the surface of the planet. Such planetary recycling is important for long-term habitability.

Appendix A

Nitrogen budget of Earth supplemental data

Presented in this appendix are the literature compilation datasets used as the basis for the research presented in Chapter 2. All data are available as an electronic file in the supplemental material in the publication (Johnson & Goldblatt, 2015). The following provides a reference and sample ID. Note that some samples have entries in multiple tables, which was necessary to fit the format requirements of this document.

I first present a table of data on N and C analyses in rocks and minerals from terrestrial samples (Table A.1). I include reference and sample name as given in original reference. Geologic Setting abbreviations, assigned by me, are: O = Oceanic, C = Continental, S = Sediment, L = Lithosphere, A = altered ($<$ 300 °C), M = metamorphosed ($>$ 300 ° C), M = primary mantle volcanics, X = xenoliths, OIB = Ocean Island Basalt, and VV= Volcanic volatiles. Rock names are also assigned by me, and abbreviations are: BIF = banded iron formation, MORB = mid-ocean ridge basalt, OIB = ocean island basalt, F = fluid, and G = gas.

I present sample age (Ga), δ^{15}N and error, N concentration (ppm), δ^{13}C, K_2O (wt. %) and Rb (ppm) concentrations (Table A.2), Ar-isotopic data where available (Table A.3), and Yb Lu and Rb concentration (ppm) (Table A.4), .

Table A.5 presents literature compilation of experimental results for silicate melts, with or without Fe-metal. Some mineral data is shown as well. One experimental study measured N-isotopic exchange between crystals and melt, and is shown in Table A.6.

Compilation of meteorite N and C data, both concentration and isotopes, is shown in Table A.7.

Table A.1: Terrestrial N and C geochemical literature compilation. See first page of Appendix A for full description.

Reference	Sample	Setting	Rock	Age	δ^{15}N	[N]	δ^{13}C
Hoering-1955	Granite	CL	Granite		-0.2		
	Granite	CL	Granite		-0.9		
	Pitchblende	ACS	Kerogen		-2.3		
Power et al.1974	1	AOS	Shale	0.03		25	
Peters et al.1978	17	OS	Organic	0	6.9		-21.0
East Bering Sea	24	OS	Organic	0	8.7		-21.7
	35	OS	Organic	0	8.9		-21.1
	35	OS	Kerogen	0	8.1		-22.9
	65	OS	Organic	0	7.6		-21.5
Gulf of Alaska	1	OS	Organic	0	6.2		-24.0
	41	OS	Organic	0	6.6		-23.9
	50	OS	Organic	0	4.1		-24.1
	50	OS	Kerogen	0	3.4		-25.6
	52	OS	Organic	0	5.3		-24.4
	105	OS	Organic	0	6.6		-22.0
	107b	OS	Organic	0	6.0		-22.3
	102	OS	Organic	0	6.3		-22.6
	119	OS	Organic	0	7.0		-22.0
	119	OS	Kerogen	0	5.3		-23.0
	123	OS	Organic	0	6.3		-21.7
	137	OS	Kerogen	0	5.6		-24.3
	13	OS	Kerogen	0	5.2		-24.8
Santa Catalina	26	OS	Organic	0	6.9		-21.4
Basin	85	OS	Organic	0	7.7		-23.7
	285	OS	Organic	0	7.7		-21.6
	326	OS	Organic	0	4.2		-22.7
	335	OS	Organic	0	5.7		-23.4
	376	OS	Organic	0	6.3		-22.8
	385	OS	Organic	0	6.4		-23.6
Santa Barbara	81	OS	Organic	0	7.6		-22.0
Basin	91a	OS	Organic	0	7.4		-21.6
	331	OS	Organic	0	9.4		-20.6
	381	OS	Organic	0	8.2		-21.8
	530	OS	Organic	0	8.5		-21.7
	Water	OS	Organic	0	4.2		-21.7
	770	OS	Organic	0	5.5		-23.4
	965	OS	Organic	0	5.7		-22.8
	1	OS	Kerogen	0	7.1		-22.3
	SB-K	OS	Kerogen	0	6.1		-22.1
Tanner	0	OS	Organic	0	7.8		-21.4
Basin	Catcher	OS	Organic	0	8.4		-21.0
	0	OS	Organic	0	8.1		-21.4
	50	OS	Organic	0	5.5		-21.7
	80	OS	Organic	0	8.3		-21.2
	IIIA	OS	Kerogen	0	9.9		-21.4
	Basin	OS	Kerogen	0	5.7		-21.9
	2	OS	Kerogen	0	6.0		-22.3
San Pedro	Outfall	OS	Organic	0	3.2		-24.5
Shelf	3b	OS	Organic	0	5.9		-22.0
	91a	OS	Organic	0	5.9		-22.0
	5D2	OS	Kerogen	0	3.8		-23.4
	1D2	OS	Kerogen	0	6.8		-22.2
Bandaras Bay	1	OS	Kerogen	0	4.0		-24.6
Mexico	A2	OS	Kerogen	0	2.8		-24.2
	B2	OS	Kerogen	0	3.4		-24.2
	A3	OS	Kerogen	0	4.2		-24.4
	B3	OS	Kerogen	0	3.3		-24.3
	B2	OS	Kerogen	0	2.4		-24.8
	d	OS	Kerogen	0	2.4		-25.2

Continued on next page

Table A.1 – continued from previous page

Reference	Sample	Setting	Rock	Age	δ^{15}N	[N]	δ^{13}C
Black Sea	1	OS	Anoxic	0	4.6		-24.7
	2	OS	Anoxic	0	4.1		-25.2
	Trance	OS	Anoxic	0	2.8		-21.0
	Walvis Bay	OS	Anoxic	0	9.2		-20.0
Peters et	Eel	CS	Organic	0	2.9		-25.7
al.1978	Kern	CS	Organic	0	5.3		-25.6
Rivers	Kern	CS	Kerogen	0	2.9		-24.4
	Klamath	CS	Organic	0	6.9		-24.9
	Klamath	CS	Kerogen	0	0.6		-24.4
	Redwood	CS	Organic	0	5.4		-24.9
	Redwood	CS	Kerogen	0	0.3		-24.0
	San Joaquin	CS	Organic	0	6.4		-25.7
	San Joaquin	CS	Organic	0	5.6		-26.9
	Staten muck	CS	Organic	0	2.5		-26.6
Lake	Duck Lake	CS	Organic	0	4.1		-23.5
	Duck Lake	CS	Kerogen	0	4.9		-24.1
	Laguna Mormona	CS	Kerogen	0	3.0		-15.0
Sullivan et	32A	CS	Gravel	0.0001		73	
al.1979	32 B	CS	Mudstone	0.001		4832	
Sedimentary	34 A	CS	S and stone	0.002		178	
rocks from	34 B	CS	Mudstone	0.003		113	
San Joaquin	81	CS	Mudstone	0.004		1402	
Valley	17A	OS	S and stone	0.005		119	
	17B	OS	S and stone	0.006		250	
	17C	OS	S and stone	0.007		124	
	17D	OS	S and stone	0.008		172	
	18A	OS	Siltstone	0.009		48	
	19A	OS	S and stone	0.01		33	
	20A	OS	Shale	0.011		3315	
	20B	OS	S and stone	0.012		1573	
	21	OS	Conglomerate	0.013		332	
	80A	OS	Shale	0.014		565	
	80B	OS	Shale	0.015		897	
	23	OS	Shale	0.016		446	
	25	OS	Shale	0.017		2210	
	26A	OS	Shale	0.018		811	
	26B	OS	Shale	0.019		899	
	77B	OS	Shale	0.02		647	
	1A	OS	Siltstone	0.021		1266	
	32 B	OS	S and stone	0.022		261	
	5A	OS	S and stone	0.023		336	
	5B	OS	Shale	0.024		330	
	5C	OS	Wacke	0.025		199	
	7A	OS	S and stone	0.026		268	
	9B	OS	Shale	0.027		1275	
	9C	OS	S and stone	0.028		998	
	16	OS	Shale	0.029		541	
	75A	OS	Shale	0.03		594	
	75C	OS	Shale	0.031		605	
	76A	OS	Shale	0.032		664	
	76B	OS	Shale	0.033		647	
	12A	OS	Shale	0.034		495	
	12B	OS	S and stone	0.035		311	
	12C	OS	Shale	0.036		1462	
	13	OS	Shale	0.037		394	
	15	OS	Shale	0.038		312	
	72A	OS	Mudstone	0.039		1147	
	72B	OS	Shale	0.04		476	
	72C	OS	Shale	0.041		558	
	48	OS	Marl	0.042		140	
	50	OS	Marl	0.043		86	
	71	OS	S and stone	0.044		56	
	39	OS	S and stone	0.045		208	
	41	OS	S and stone	0.046		1974	
	43	OS	S and stone	0.047		158	
	44A	OS	Shale	0.048		178	
	44B	OS	S and stone	0.049		259	
	46A	OS	S and stone	0.05		259	

Continued on next page

Table A.1 – continued from previous page

Reference	Sample	Setting	Rock	Age	δ^{15}N	[N]	δ^{13}C
	46B	OS	Shale	0.051		778	
	46C	OS	Shale	0.052		229	
	47	OS	S and stone	0.053		221	
	51	OS	S and stone	0.054		122	
	54	OS	S and stone	0.055		245	
	56	OS	Conglomerate	0.056		191	
	60	OS	Shale	0.057		222	
	63	OS	Shale	0.058		284	
	66A	OS	S and stone	0.059		339	
	66B	OS	Shale	0.06		956	
Itihara and	1	MOS	Schist	0.095		269	
Honma-1979	2	MOS	Gneiss	0.095		192	
	3	MOS	Gneiss	0.095		268	
NH4,	4	MOS	Gneiss	0.095		122	
Metaseds.	5	MOS	Gneiss	0.095		232	
granites in	6	MOS	Amphibolite	0.095		53	
Japan	7	MOS	Migmatite	0.095		304	
	8	MOS	Migmatite	0.095		388	
	9	MOS	Migmatite	0.095		415	
	10	CL	Granite	0.095		18	
	11	CL	Granite	0.095		116	
	12	CL	Granodiorite	0.095		37	
	13	CL	Granodiorite	0.095		60	
	14	CL	Granodiorite	0.095		66	
	15	CL	Granodiorite	0.095		64	
	16	CL	Granodiorite	0.095		19	
	17	CL	Granodiorite	0.095		41	
	18	CL	Granite	0.095		74	
	19	CL	Granodiorite	0.095		23	
	20	CL	Granite	0.095		12	
	21	CL	Granite	0.095		16	
	22	CL	Granite	0.095		52	
	23	CL	Granite	0.095		41	
	24	CL	Granite	0.095		19	
	25	CL	Granodiorite	0.095		18	
	26	CL	Granite	0.095		23	
	27	CL	Granite	0.095		8	
	28	CL	Granite	0.095		16	
	29	CL	Granite	0.095		20	
	30	CL	Granite	0.095		41	
	31	CL	Granodiorite	0.095		30	
	32	CL	Granite	0.095		4	
	33	CL	Granite	0.095		4	
	34	CL	Granodiorite	0.095		7	
Stiehl and	1	ACS	Organic		6.3	9200	
Lehmann-	2	ACS	Organic		5.0	13500	
1980							
	3	ACS	Organic		5.3	10000	
	4	ACS	Organic		5.1	12200	
	5	ACS	Organic		3.7	14400	
	6	ACS	Organic		3.5	14200	
	7	ACS	Organic		4.2	11600	
	8	ACS	Organic		4.6	80000	
	9	ACS	Organic		6.0	8000	
	10	ACS	Organic		4.8	15100	
	11	ACS	Organic		5.0	14400	
	12	ACS	Organic		7.0	5800	
	13	ACS	Organic		4.2	2200	
	14	ACS	Organic		5.3	8000	
	15	ACS	Organic		4.9	4000	
	16	ACS	Organic		5.5	500	
	17	ACS	Organic		6.9	1300	
	18	ACS	Organic		10.7	1000	
Hayes et	BURRA	AOS	Kerogen	0.8	5.1		
al.1983	GROUP						
Avg. of	Bitter	AOS	Kerogen	0.9	7.4		
	Springs Fm						
Precambrian	Roper group	AOS	Kerogen	1.4	3.4		

Continued on next page

Table A.1 – continued from previous page

Reference	Sample	Setting	Rock	Age	δ^{15}N	[N]	δ^{13}C
sedimentary rocks	Bungle Bungle Dolomite	AOS	Kerogen	1.6	7.8		
	Earaheedy Gp.	AOS	Kerogen	1.8	6.2		
	Wyloo Gp.	AOS	Kerogen	2	3.6		
	Gunflint Fm	AOS	Kerogen	2	7.2		
	Belcher Gp.	AOS	Kerogen	2.1	4.4		
	Hamersly Gp.	AOS	Kerogen	2.5	3.3		
	Gorge Creek Gp.	AOS	Kerogen	3.4	2.3		
	Swaziland Sequence	AOS	Kerogen	3.5	3.1		
Sakai et al.1984	Cayman	OL	Basalt	0.01	0.6	0.9	
	FAMOUS	OL	Basalt	0.01	0.8	1.4	
	Galapagos	OL	Basalt	0.01		0.3	
	Galapagos	OL	Basalt	0.01		2.8	
	Kilauea	OL	Basalt	0.01	-0.4	1.1	
	Juan de Fuca	OL	Basalt	0.01		2.3	
	Juan de Fuca	OL	Basalt	0.01	-0.1	0.9	
Itihara and Suwa-1985	1-1	CL	Granite	1.85		6	
	1-2	CL	Granite	1.85		2	
Granites and	1-4	CL	Granite	1.85		8	
	5-1	CL	Granite	1.85		4	
meta. rocks,	5-3A	CL	Tonalite	1.85		13	
Finland.	6-6	CL	Granite	1.85		6	
Biotites measured,	6-7	CL	Granite	1.85		5	
but I present	6-8	CL	Gabbro	1.85		1	
whole rock values based on	6-9	CL	Granite	1.85		5	
NH4 ratios	6-10	CL	Granodiorite	1.85		2	
from Itihara	7-3B	CL	Granodiorite	1.85		28	
and Honma 1981	7-7	CL	Schist	2		3	
	3-2	MOS	Schist	2		257	
	3-3	MOS	Schist	2		169	
	3-4	MOS	Gneiss	2		536	
	4-4	MOS	Schist	2		248	
	4-5	MOS	Gneiss	2		204	
	4-6	MOS	Gneiss	2		48	
	4-7	MOS	Gneiss	2		63	
	4-8	MOS	Gneiss	2		12	
	5-3B	MOS	Gneiss	2		3	
	7-1	MOS	Schist	2		155	
	7-3A	MOS	Schist	2		87	
	7-4	MOS	Gneiss	2		61	
	7-5	MOS	Schist	2		582	
	9-6	MOS	Gneiss	2		12	
	2-1a	MOS	Schist	2		3	
	2-1b	MOS	Schist	2		6	
	4-1	MOS	Gneiss	2		4	
Gibson et al.1986	Isua	MOS	Chert	3.8	1.8		-11.0
Cherts measured	Warrawoona	MOS	Chert	3.5	-0.5		-10.0
by step heating	Barberton	MOS	Chert	3.2	1.0		
between	Manjeri	MOS	Chert	2.6	2.0		-11.0
700-900 deg C.	Hamersley	MOS	Chert	2.5			-9.0
data read f	Beck Spring	MOS	Chert	1.3	0.5		
rom graph	Rhynie	MOS	Chert	0.4	0.5		
	Magadi	MOS	Chert	0.2			
Rigby and	Loy Yang	ACS	Coal	0.02	0.5	5000	

Continued on next page

Table A.1 – continued from previous page

Reference	Sample	Setting	Rock	Age	δ^{15}N	[N]	δ^{13}C
Batts-1986	Morwell	ACS	Coal	0.02	0.8	5700	
Coals and	Yallourn	ACS	Coal	0.01	1.9	4000	
oil shales,	Leigh Creek	ACS	Coal	0.185	0.5	8000	
Australia	Lake Phillipson	ACS	Coal	0.26	3.7	15500	
	Millmerran	ACS	Coal	0.316	1.6	10000	
	Wonthaggi	ACS	Coal	0.12	1.8	13200	
	Bluff	ACS	Coal	0.19	2.3	10000	
	Lagoon	ACS	Coal	0.19	3.1	10000	
	Styx	ACS	Coal	0.1	1.0	12000	
	Liddell	ACS	Coal	0.26	2.5	18600	
	Portl and	ACS	Coal	0.1	1.2	15000	
	Nymboida	ACS	Coal	0.19	0.3	9000	
	Collinsville	ACS	Coal	0.24	1.7	11000	
	Wongawilli	ACS	Coal	0.24	1.6	17800	
	Excel	ACS	Coal	0.24	1.0	20300	
	Stockton	ACS	Coal	0.05	1.3	11400	
	Beaver Lake	ACS	Coal	0.24	3.0	17000	
	Tasmanite	ACS	Oil Shale	0.27	12.7	5800	
	Mount Marangaroo	ACS	Oil Shale	0.27	5.4	3800	
	Glen Davis	ACS	Oil Shale	0.27	4.2	5600	
	Rundle	ACS	Oil Shale	0.01	3.0	2100	
	Julia Creek	ACS	Oil Shale	0.1	-0.7	4700	
	Bedourie-1	ACS	Oil Shale	0.1	-0.5	2200	
	Tambo-31	ACS	Oil Shale	0.1	1.7	4300	
	Springvale-9	ACS	Oil Shale	0.1	-2.3	5200	
	Mayneside-1	ACS	Oil Shale	0.1	-2.5	3800	
	Nagoorin	ACS	Oil Shale	0.01	2.7	13800	
	Condor	ACS	Oil Shale	0.01	2.2	18900	
	Condor	ACS	Oil Shale	0.01	-0.5	14900	
Duit et al.1986	Zone 1	MOS	Schist	0.3		800	
Mica data, Europe	Zone 2	MOS	Schist	0.3		300	
also some calculated	Zone 3	MOS	Gneiss	0.3		100	
whole rock data.	Zone 4	MOS	Gneiss	0.3		100	
	Zone 5	MOS	Gneiss	0.3		100	
	23	MOS	Biotite	0.3		1060	
	25	MOS	Muscovite	0.3		580	
	32	MOS	Biotite	0.3		300	
	46A	MOS	Biotite	0.3		745	
	71	MOS	Biotite	0.3		130	
	106	MOS	Biotite	0.3		320	
	107	MOS	Biotite	0.3		60	
	118	MOS	Biotite	0.3		380	
	118	MOS	Muscovite	0.3		170	
	119	MOS	Biotite	0.3		255	
	119	MOS	Muscovite	0.3		150	
	121	MOS	Biotite	0.3		280	
	121	MOS	Muscovite	0.3		120	
	123	MOS	Biotite	0.3		470	
	126A	MOS	Biotite	0.3		635	
	126A	MOS	Muscovite	0.3		30	
	126B	MOS	Biotite	0.3		680	
	127	MOS	Biotite	0.3		1490	
	129B	MOS	Biotite	0.3		510	
	129B	MOS	Muscovite	0.3		190	
	136	MOS	Biotite	0.3		1330	
	136	MOS	Muscovite	0.3		410	
	146	MOS	Biotite	0.3		1540	
	149	MOS	Biotite	0.3		250	
	149	MOS	Muscovite	0.3		80	
	153	MOS	Biotite	0.3		340	
	153	MOS	Muscovite	0.3		115	
	154	MOS	Biotite	0.3		240	
	156	MOS	Biotite	0.3		300	

Continued on next page

Table A.1 – continued from previous page

Reference	Sample	Setting	Rock	Age	δ^{15}N	[N]	δ^{13}C
	160	MOS	Biotite	0.3		680	
	161	MOS	Biotite	0.3		280	
	161	MOS	Muscovite	0.3		75	
	162	MOS	Biotite	0.3		860	
	162	MOS	Muscovite	0.3		80	
	164	MOS	Biotite	0.3		100	
	164	MOS	Muscovite	0.3		110	
	165	MOS	Biotite	0.3		215	
	165	MOS	Muscovite	0.3		530	
	169A	MOS	Biotite	0.3		1880	
	169B	MOS	Biotite	0.3		1360	
	169B	MOS	Muscovite	0.3		530	
	170A	MOS	Biotite	0.3		1280	
	170A	MOS	Muscovite	0.3		320	
	170B	MOS	Biotite	0.3		250	
	172	MOS	Biotite	0.3		250	
	177B	MOS	Biotite	0.3		840	
	177B	MOS	Muscovite	0.3		270	
	177C	MOS	Muscovite	0.3		260	
	177D	MOS	Muscovite	0.3		360	
	178B	MOS	Biotite	0.3		430	
	178B	MOS	Muscovite	0.3		390	
	178C	MOS	Muscovite	0.3		80	
	179	MOS	Biotite	0.3		715	
	180	MOS	Biotite	0.3		240	
	181A	MOS	Biotite	0.3		1060	
	181A	MOS	Muscovite	0.3		370	
	181B	MOS	Biotite	0.3		1100	
	181B	MOS	Muscovite	0.3		400	
	182A	MOS	Muscovite	0.3		570	
	182B	MOS	Biotite	0.3		1370	
	182B	MOS	Muscovite	0.3		470	
	183A	MOS	Muscovite	0.3		370	
	183B	MOS	Biotite	0.3		1330	
	183B	MOS	Muscovite	0.3		310	
	186	MOS	Biotite	0.3		180	
	188A	MOS	Biotite	0.3		720	
	188B	MOS	Muscovite	0.3		1140	
	190	MOS	Biotite	0.3		340	
	191	MOS	Biotite	0.3		150	
	192	MOS	Biotite	0.3		500	
	193	MOS	Biotite	0.3		260	
	194	MOS	Muscovite	0.3		330	
	196	MOS	Biotite	0.3		1450	
	196B	MOS	Biotite	0.3		1145	
	197	MOS	Biotite	0.3		620	
	197	MOS	Muscovite	0.3		150	
	198	MOS	Biotite	0.3		300	
	198	MOS	Muscovite	0.3		130	
	200	MOS	Biotite	0.3		540	
	200	MOS	Muscovite	0.3		200	
	201	MOS	Biotite	0.3		90	
	201	MOS	Muscovite	0.3		30	
	202	MOS	Biotite	0.3		160	
	202	MOS	Muscovite	0.3		50	
	205	MOS	Biotite	0.3		410	
	205	MOS	Muscovite	0.3		130	
	206	MOS	Biotite	0.3		450	
Itihara et al.1986	1	MOS	Shale	2.6		61	
	2	MOS	Shale	2.6		54	
	3	MOS	Shale	2.6		25	
Haendel et al.1986	1	MOS	Phyllite	0.23	5.4	439	
Ezbergite metaseds.	2	MOS	Phyllite	0.23	5.9	397	
	3	MOS	Phyllite	0.23	6.8	245	
Avg. of	17	MOS	Phyllite	0.23	5.1	620	
metamorphic	18a	MOS	Phyllite	0.23	7.8	550	

Continued on next page

Table A.1 – continued from previous page

Reference	Sample	Setting	Rock	Age	δ^{15}N	[N]	δ^{13}C
grades	19	MOS	Phyllite	0.23	3.3	650	
	20	MOS	Phyllite	0.23	3.8	550	
	74	MOS	Phyllite	0.23	5.6	571	
	75	MOS	Phyllite	0.23	6.6	464	
	75b	MOS	Phyllite	0.23	6.5	223	
	75c	MOS	Phyllite	0.23	4.4	513	
	a75	MOS	Phyllite	0.23	3.6	640	
	a78	MOS	Phyllite	0.23	3.2	550	
	91a	MOS	Phyllite	0.23	5.4	250	
	11	MOS	Schist	0.23	7.1	304	
	33	MOS	Schist	0.23	3.4	261	
	34	MOS	Schist	0.23	9.6	190	
	35	MOS	Schist	0.23	6.3	502	
	36	MOS	Schist	0.23	9.8	214	
	a64	MOS	Schist	0.23	5.3	188	
	99	MOS	Schist	0.23	10.8	234	
	101	MOS	Schist	0.23	8.7	221	
	107b	MOS	Schist	0.23	7.7	187	
	2203	MOS	Schist	0.23	9.2	115	
	121	MOS	Schist	0.23	15.0	95	
	107b	MOS	Gneiss	0.23	15.1	35	
	2	MOS	Gneiss	0.23	7.7	59	
	3b	MOS	Gneiss	0.23	6.7	180	
	8	MOS	Gneiss	0.23	6.9	62	
	91a	MOS	Gneiss	0.23	7.6	63	
	82	MOS	Gneiss	0.23	17.0	40	
	83	MOS	Gneiss	0.23	6.8	40	
	84	MOS	Gneiss	0.23	7.9	42	
	85	MOS	Gneiss	0.23	2.5	339	
	86	MOS	Gneiss	0.23	11.8	82	
	87	MOS	Gneiss	0.23	6.2	14	
	88	MOS	Gneiss	0.23	5.1	40	
	89	MOS	Gneiss	0.23	4.1	104	
	90	MOS	Gneiss	0.23	5.6	48	
	97	MOS	Gneiss	0.23	7.6	78	
	98	MOS	Gneiss	0.23	9.0	52	
	106	MOS	Gneiss	0.23	9.9	100	
	122	MOS	Gneiss	0.23	12.7	25	
Rau et al.1987	Marlstone	AOS	Marlstone	0.1	-2.7	1000	-27.3
Marine sediments	Marlstone	AOS	Marlstone	0.1	2.3	1000	-27.4
Atlantic Ocean	Limestone	AOS	Limestone	0.1	1.5	100	-26.9
	Limestone	AOS	Limestone	0.1	5.6	100	-26.9
Exley et al.1987	Atlantic/Pacific	OL	MORB	0.01	5.0	0.3	
Basalt glasses	Atlantic/Pacific	OL	MORB	0.01	7.0	0.3	
	Atlantic/Pacific	OL	MORB	0.01	9.0	0.4	
	Atlantic/Pacific	OL	MORB	0.01	7.0	0.7	
	Atlantic/Pacific	OL	MORB	0.01	7.0	1.3	
	Atlantic/Pacific	OL	MORB	0.01	6.0	2.1	
	Indian Ocean	OL	MORB	0.01	-5.0	0.5	
	Indian Ocean	OL	MORB	0.01	-3.0	0.3	
	Lohi Seamount	OIB	Basalt	0.01	15.0	0.2	
	Lohi Seamount	OIB	Basalt	0.01	12.0	0.5	
	Lohi Seamount	OIB	Basalt	0.01	13.0	1.1	
	Kilauea	OIB	Basalt	0.01	9.0	1.3	
	Lau/Fiji	OIB	Basalt	0.01	5.0	0.5	
	Lau/Fiji	OIB	Basalt	0.01	11.0	0.5	
	Lau/Fiji	OIB	Basalt	0.01	14.0	0.3	
Hall-1987	1	CL	Granite	0.4		19	
	2	CL	Granite	0.4		2	

Continued on next page

Table A.1 – continued from previous page

Reference	Sample	Setting	Rock	Age	δ^{15}N	[N]	δ^{13}C
	3	CL	Granite	0.4		6	
	4	CL	Granite	0.4		21	
	5	CL	Granite	0.4		27	
	6	CL	Granite	0.4		6	
	7	CL	Granite	0.4		3	
	8	CL	Granite	0.4		130	
	9	CL	Granite	0.4			
	10	CL	Granite	0.4		16	
	11	CL	Granite	0.4		8	
	12	CL	Granite	0.4		25	
	13	CL	Granite	0.4		6	
	14	CL	Granite	0.4		12	
	15	CL	Granite	0.4		121	
	16	CL	Granite	0.4		113	
	17	CL	Granite	0.4		9	
	18	CL	Granite	0.4		11	
	19	CL	Granite	0.4		46	
	20	CL	Granite	0.4		2	
	21	CL	Granite	0.4		37	
	22	CL	Granite	0.4		71	
	23	CL	Granite	0.4		2	
	24	CL	Granite	0.4		4	
	25	CL	Granite	0.4		3	
	26	CL	Granite	0.4		30	
	27	CL	Granite	0.4		16	
	28	CL	Granite	0.4		6	
	29	CL	Granite	0.4		3	
	30	CL	Granite	0.4		12	
	31	CL	Granite	0.4		7	
	32	CL	Granite	0.4		4	
	33	CL	Granite	0.4		7	
	34	CL	Granite	0.4		7	
	35	CL	Granite	0.4		100	
Greenfield-1988	Control	CS	S and stone			13	
Hall-1988	C7	CL	Granite			139	
	C7	CL	Orthoclase			351	
	C7	CL	Muscovite			271	
	C7	CL	Biotite			494	
	C203	ACL	Granite			264	
	C203	ACL	Orthoclase			700	
	C203	ACL	Muscovite			496	
	C221	ACL	Orthoclase			223	
	C221	ACL	Muscovite			537	
Itihara and Tainosho-1989	1	CL	Biotite	1.5		19	103.0
	2	CL	Biotite	1.5		36	108.0
	3	CL	Biotite	1.5		16	117.0
	4	CL	Biotite	1.5		30	
	5	MOS	Biotite	1.5		80	
	6	MOS	Biotite	2		84	
	7	MOS	Biotite	2		91	
	8	MOS	Biotite	2		16	
	9	MOS	Biotite	2.6		10	
	10	MOS	Biotite	2.6		6	
	11	MOS	Biotite	2.6		26	
	12	MOS	Biotite	2.6		12	
	13	MOS	Biotite	2.6		18	
	14	MOS	Biotite	2.6		12	
Sano and Pillinger-1990	Onverwacht	AOS	Chert	3.2	1.51 ± 0.5	13	
	Marra Mamba	AOS	Chert	2.5	-0.07 ± 1	0.65	
Chert, average of step heating analysis	Frere Formation	AOS	Chert	1.8	1.29 ± 0.4	4	
	Beck Spring	AOS	Chert	1.4	0.83 ± 0.5	5	
	Rhynie	AOS	Chert	0.5	5.55 ± 0.5	16	
	Magadi	AOS	Chert	0.01	9.93 ± 0.5	7	
Cooper and Bradley-1990	Eskdale	CL	Granite	0.429		16	
	Eskdale	CL	Granodiorite	0.427		23	

Continued on next page

Table A.1 – continued from previous page

Reference	Sample	Setting	Rock	Age	δ^{15}N	[N]	δ^{13}C
	Ennerdale	CL	Granite	0.42		21	
	Shap	CL	Granite	0.394		9	
	Skiddaw	CL	Granite	0.392		23	
	Threkeld	CL	Granite	0.438		29	
Greenfield-1991	1	CS	Soil			281	
Rocks from	2	CS	Soil			477	
Antarctica	3	MOS	Schist			122	
	4	CS	Soil			706	
	5	MOS	Schist			266	
	6	CS	S and stone			17	
	7	CS	S and stone			101	
	8	MCS	Quartzite			77	
	9	CS	Siltstone			1424	
	10	CS	Soil			55	
	11	MCS	Quartzite			57	
	12	MCS	Quartzite			23	
	13	CL	Granodiorite			85	
	14	CL	Granite			126	
	15	CL	Basalt			27	
	16	CS	S and stone			36	
	17	CL	Granodiorite			51	
	18	CL	Basalt			102	
	19	CL	Scoria			56	
	20	CS	Soil			441	
	21	CS	Soil			2310	
	22	CS	Soil			2100	
	23	CL	Granite			36	
Williams and	1	AOS	Shale	0.07		2000	
Ferrell-1991	2	AOS	Shale	0.07		2500	
Pierre shale	3	AOS	Shale	0.07		2600	
Colorado	4	AOS	Shale	0.07		3000	
values read	5	AOS	Shale	0.07		3100	
from graph	6	AOS	Shale	0.07		3200	
	7	AOS	Shale	0.07		3300	
	8	AOS	Shale	0.07		4000	
	9	AOS	Shale	0.07		500	
	10	AOS	Shale	0.07		3500	
	11	AOS	Shale	0.07		3100	
	12	AOS	Shale	0.07		3400	
	13	AOS	Shale	0.07		3400	
	14	AOS	Shale	0.07		3500	
	15	AOS	Shale	0.07		3400	
	16	AOS	Shale	0.07		3000	
	17	AOS	Shale	0.07		3000	
Hall et al.1991	EC2	CL	Granite			24	
	EC3	CL	Granite			21	
	EP6	CL	Granite			11	
	EP7	CL	Granite			14	
	ES2	CL	Granite			3	
	ES3	CL	Granite			13	
	ES4	CL	Granite			12	
	ES5	CL	Granite			15	
	ES8a	CL	Granite			9	
	ES14a	CL	Granite			12	
	ESP3	CL	Granite				
	ESP4	CL	Granite			8	
	ESP6	CL	Granite			2	
	ESP10a	CL	Granite			2	
	PO22	CL	Granite			27	
	PO2	CL	Granite			9	
	PO36i	CL	Granite			13	
	E12LP	CL	Granite			2	
	E12LA	CL	Granite			2	
	E12SP	CL	Granite			8	
	E12SA	CL	Granite			7	
	ES8b	CL	Granite			14	
	ES14b	CL	Granite			16	

Continued on next page

Table A.1 – continued from previous page

Reference	Sample	Setting	Rock	Age	δ^{15}N	[N]	δ^{13}C
	PO48	CL	Granite			16	
	PO57	CL	Granite			16	
	PO66	CL	Granite			19	
	PO74	CL	Granite			39	
	PO304	CL	Granite			13	
	PO52	CL	Granite			31	
	PO65	CL	Granite			24	
	PO53	CL	Granite			25	
	PO301	CL	Granite			35	
	PO63	CL	Granite			14	
	PO408	CL	Granite			13	
	PO412	CL	Granite			7	
	PO404	CL	Granite			7	
	MV7	CL	Granite			17	
	GAV3	CL	Granite			32	
	GAV2	ACL	Granite			66	
	GAV24	ACL	Granite			47	
	GAV40	ACL	Granite			40	
	GAV100	ACL	Granite			50	
	GAV103	ACL	Granite			100	
	GAV106	ACL	Granite			37	
	S2-700	ACL	Granite			112	
	S2-711	ACL	Granite			100	
	S2-744	ACL	Granite			61	
	S2-761	ACL	Granite			138	
	S2-779	ACL	Granite			59	
	S2-790	ACL	Granite			85	
	D2-807	ACL	Granite			35	
	S2-811	ACL	Granite			44	
	S2-836	ACL	Granite			42	
	S2-838	ACL	Granite			36	
	S2-844	ACL	Granite			44	
	S2-861	ACL	Granite			123	
	D2-896	ACL	Granite			35	
	S2-913	ACL	Granite			30	
	S3-883	ACL	Granite			33	
	S3-833.5	ACL	Granite			121	
	S2-892	ACL	Granite			44	
	S2-901	ACL	Granite			61	
	S3-912	ACL	Granite			34	
	MS1-440	ACL	Granite			282	
	MS1-445	ACL	Granite			25	
	MS1-465	ACL	Granite			28	
	MS1-484	ACL	Granite			38	
	MS1-513	ACL	Granite			51	
Bebout and Fogel-1992	LA	MOS	Schist	0.1	2 ± 0.1	735	
Catalina Schist complex	LA	MOS	Schist	0.1	1.9 ± 0.1		
	LA	MOS	Schist	0.1	1.3	695	
LA = Lawsonite-albite	LA	MOS	Schist	0.1	1.1 ± 0.2	465	
BS=Bluschist	LA	MOS	Schist	0.1	1.0	410	
GG= Gluacophane - Greenshc.	LA	MOS	Schist	0.1	2 ± 0.1	540	
	LA	MOS	Schist	0.1	2.0	790	
	LA	MOS	Schist	0.1	1.3 ± 0.1	805	
EA = Epidote -amphibolite	LA	MOS	Schist	0.1	2.1 ± 0.1	900	
	LA	MOS	Schist	0.1	2.7	810	
A = amphibolite	LA	MOS	Schist	0.1	2.4	710	
	LA	MOS	Schist	0.1	2.3 ± 0.1	360	
	LA	MOS	Schist	0.1	2.7 ± 0.1	640	
	LA	MOS	Schist	0.1	1.2	360	
	BS	MOS	Schist	0.1	3.1 ± 0.1	130	
	BS	MOS	Schist	0.1	3 ± 0.1	120	

Continued on next page

Table A.1 – continued from previous page

Reference	Sample	Setting	Rock	Age	δ^{15}N	[N]	δ^{13}C
	BS	MOS	Schist	0.1	2.4	200	
	BS	MOS	Schist	0.1	2.1 ± 0.1	660	
	BS	MOS	Schist	0.1	2.4 ± 0.3	315	
	BS	MOS	Schist	0.1	2.5 ± 0.1	710	
	BS	MOS	Schist	0.1	2.3 ± 0.2	150	
	BS	MOS	Schist	0.1	2.1 ± 0.2	780	
	BS	MOS	Schist	0.1	2.2 ± 0.1	1075	
	BS	MOS	Schist	0.1	2 ± 0.1	335	
	BS	MOS	Schist	0.1	2.3 ± 0.1	540	
	BS	MOS	Schist	0.1	2.7 ± 0.1	200	
	BS	MOS	Schist	0.1	2.7	100	
	BS	MOS	Schist	0.1	2.4 ± 0.2	720	
	GG	MOS	Schist	0.1	3.3	65	
	GG	MOS	Schist	0.1	2.6 ± 0.2	110	
	GG	MOS	Schist	0.1	3.7 ± 0.1	170	
	GG	MOS	Schist	0.1	4 ± 0.1	810	
	GG	MOS	Schist	0.1	1.1 ± 0.1	180	
	EA	MOS	Schist	0.1	5.3	165	
	EA	MOS	Schist	0.1	4 ± 0.1	740	
	EA	MOS	Schist	0.1	4.6	90	
	EA	MOS	Schist	0.1	4.4 ± 0.1	265	
	EA	MOS	Schist	0.1	3.8 ± 0.1	180	
	EA	MOS	Schist	0.1	3.9 ± 0.1	230	
	EA	MOS	Schist	0.1	4.4	30	
	A	MOS	Schist	0.1	3.6 ± 0.3	65	
	A	MOS	Schist	0.1	3.6 ± 0.5		
	A	MOS	Schist	0.1	3.6 ± 0.2	110	
	A	MOS	Schist	0.1	4.5 ± 0.1	150	
	A	MOS	Schist	0.1	4.2 ± 0.2		
	A	MOS	Schist	0.1	3.6	1585	
	A	MOS	Schist	0.1	4.7 ± 0.1	160	
	A	MOS	Schist	0.1	5.9 ± 0.4	35	
	A	MOS	Schist	0.1	4.3	260	
Imbus et al.1992		ACS	Kerogen	1	3.5	480	-34.1
Mid-Proterozoic lacustrine shale and kerogen		ACS	Kerogen	1	8.5	1240	-34.6
		ACS	Kerogen	1	5.4	440	-34.7
		ACS	Kerogen	1	4.4	420	-34.0
		ACS	Kerogen	1	3.5	400	-34.0
		ACS	Kerogen	1	4.2	260	-33.3
		ACS	Kerogen	1	4.4	460	-33.6
		ACS	Kerogen	1	3.2	440	-33.9
		ACS	Kerogen	1	5.0	520	-33.4
		ACS	Kerogen	1	3.1	480	-32.7
		ACS	Kerogen	1	3.2	280	-33.8
		ACS	Kerogen	1	3.8	540	-34.1
		ACS	Kerogen	1	3.9	1000	-33.6
		ACS	Kerogen	1	4.8	910	-33.4
		ACS	Kerogen	1	2.9	420	-33.3
		ACS	Kerogen	1	3.4		-33.9
		ACS	Kerogen	1	3.3	320	-33.8
		ACS	Kerogen	1	2.7	380	-33.2
		ACS	Kerogen	1	3.2	440	-33.5
		ACS	Kerogen	1	3.8	340	-33.9
		ACS	Kerogen	1	3.2	360	-33.6
		ACS	Kerogen	1	3.3	340	-33.0
		ACS	Kerogen	1	3.7	400	-33.1
		ACS	Kerogen	1	3.3	540	-34.1
		ACS	Kerogen	1	3.8	440	-33.7
		ACS	Kerogen	1	3.1	520	-33.9
Williams et al.1992	Wilcox 1	AOS	Mudstone	0.04		1600	
Organic rich mudstones, oil-producing area, Louisiana	Wilcox 1	AOS	S and stone	0.04		1900	
	Wilcox 2	AOS	Mudstone	0.04		1600	
	Wilcox 2	AOS	S and stone	0.04		2300	

Continued on next page

Table A.1 – continued from previous page

Reference	Sample	Setting	Rock	Age	δ^{15}N	[N]	δ^{13}C
	Wilcox 4	AOS	S and stone	0.04		3600	
	Midway 1	AOS	Mudstone	0.04		1800	
	Midway 2	AOS	S and stone	0.04		2300	
Boyd et al. 1993	C7-WR	CL	Granite	0.3	9.85 ± 0.4	180	
Granites from	P477	CL	Granite	0.3	7 ± 0.2	8	
S.W. England	G11	CL	Granite	0.3	10.2 ± 0.3	82	
	P452	CL	Granite	0.3	9.4 ± 0.3	75	
	P453	CL	Granite	0.3	9.8 ± 0.3	77	
	P450	CL	Granite	0.3	5.1 ± 0.3	15	
	P114	CL	Granite	0.3	8.4 ± 0.2	93	
	P517	CL	Granite	0.3	9.1 ± 0.3	109	
	P402	CL	Granite	0.3	8.5 ± 0.3	35	
	P404	CL	Granite	0.3	9 ± 0.3	16	
	C203-O	CL	Orthoclase	0.3	10.55 ± 0.6	1047	
	C221-M	CL	Muscovite	0.3	12.2 ± 0.45	625	
	C7-M	CL	Muscovite	0.3	12.18 ± 1.1	370	
	C7-O	CL	Orthoclase	0.3	9.23 ± 0.6	521	
	R20-Bi	CL	Biotite	0.3	15.37 ± 1.2	128	
	R20-Mic	CL	Microcline	0.3	9.2 ± 0.4	9	
	R21-Bi	CL	Biotite	0.3	1.85 ± 0.8	21	
Visser-1993	DV 122	MOS	Gneiss	1		250	
	MA 780	MOS	Gneiss	1		458	
Chicarelli et al.1993	Kerogen	OS	Kerogen	0.239	-0.9		
	Organic Extract	OS	Organic	0.239	-4.0		
	1	OS	Organic	0.239	-3.3		
	2	OS	Organic	0.239	-3.3		
	3	OS	Organic	0.239	-3.1		
	4	OS	Organic	0.239	-3.0		
	5	OS	Organic	0.239	-3.4		
	6	OS	Organic	0.239	-3.4		
	7	OS	Organic	0.239	-3.2		
Marty-1995	ERP 21 981R26	OL	N-MORB	0		0.013	
MORB Glasses	EPR 13 CY82 09 03	OL	N-MORB	0		0.003	
EPR=East Pac Rise	EPR 13 CY82 31 02	OL	N-MORB	0		0.003	
MAR = Mid Atlantic	EPR 13 CL DR01 5V	OL	N-MORB	0		0.091	
N=Normal	EPR 13 CY82 30-b	OL	E-MORB	0		0.005	
E = Enriched	MAR 36 CH31 DR09	OL	T-MORB	0		0.018	
T= Transitional	MAR 36 CH31 DR11	OL	E-MORB	0		0.048	
	MAR 36 CH31 DR10	OL	E-MORB	0		0.003	
	MAR 30 CH98 DR11	OL	N-MORB	0		0.048	
	MAR 30 CH98 DR12	OL	N-MORB	0		0.054	
	MAR 30 CH98 DR15	OL	N-MORB	0		0.330	
	MAR 30 CH98 DR17	OL	N-MORB	0		0.15	
	MAR 14 2PiD43	OL	E-MORB	0		1.25	
Williams et al.1995	Sparta B	ACS	S and stone	0.04	-1.2 ± 0.8	150	
N from Kerogen bitumen	Sparta B	ACS	S and stone	0.04	-1.4 ± 1.1	150	

Continued on next page

Table A.1 – continued from previous page

Reference	Sample	Setting	Rock	Age	δ^{15}N	[N]	δ^{13}C
mudstone and sandstone from oil-producing basin in Louisiana	Sparta B	ACS	Oil	0.04	11.1 ± 0.3		
	Sparta B	ACS	Bitumen	0.04	3.5 ± 0.2		
	Sparta B	ACS	Kerogen	0.04	3.4 ± 0.1		
Averages read from graph	Sparta B	ACS	Mudstone	0.04	2.6 ± 1.9	400	
	Wilcox	ACS	S and stone	0.04	0.2 ± 2.4	200	
	Wilcox	ACS	S and stone	0.04	3 ± 1.2	200	
	Wilcox	ACS	Oil	0.04	5.2 ± 0.4		
	Wilcox	ACS	Bitumen	0.04	4.4 ± 0.1		
	Wilcox	ACS	Kerogen	0.04	3.2 ± 0.1		
	Wilcox	ACS	Mudstone	0.04	3.2 ± 1.2	389	
Hall et al.1996	B-136	CL	Ganodiorite	0.3		21	
	B-137	CL	Ganodiorite	0.3		35	
	B-170	CL	Ganodiorite	0.3		210	
	B-176	CL	Ganodiorite	0.3		162	
	B-178	CL	Ganodiorite	0.3		39	
	B-165	CL	Ganodiorite	0.3		243	
	B-2	CL	Granite	0.3		83	
	B-511	CL	Granite	0.3		74	
	B-B12	CL	Granite	0.3		88	
	B-511	CL	Granite	0.3		69	
	B-116	CL	Granodiorite	0.3		51	
	B-182	CL	Granite	0.3		13	
	B-97	CL	Granite	0.3		18	
	SIO-10331	CL	Granodiorite	0.3		14	
	SIO-10371	CL	Granite	0.3		1	
	JAL-4	CL	Granite	0.3		222	
Honma-1996	1	MOS	Schist	3.8		67	
Isua first (1-9)	2	MOS	Schist	3.8		53	
	3	MOS	Schist	3.8		37	
	4	MOS	Schist	3.8		21	
	5	MOS	Schist	3.8		19	
	6	MOS	Schist	3.8		13	
	7	MOS	Schist	3.8		5	
	8	MOS	Schist	3.8		27	
	9	MOS	Gneiss	3.8		7	
Abitibi	1	MOS	Shale	2.7		101	
	2	MOS	Shale	2.7		33	
	3	MOS	Shale	2.7		21	
	4	CL	Tholeiite	2.7			
	5	CL	Tholeiite	2.7		0.78	
	6	CL	Basalt	2.7		4.7	
Wagiboon greenstone belt	7	CL	Granite	2.7		6.2	
English River Dryden	8	MOS	Schist	2.7		38	
	9	MOS	Schist	2.7		40	
	10	MOS	Schist	2.7		42	
	11	MOS	Schist	2.7		7.8	
	13	CL	Tonalite	2.7		21	
English River Kenora	14	MOS	Schist	2.7		23	
	15	MCL	Basalt	2.7		11	
	16	MOS	Schist	2.7		7.8	
	17	MOS	Amphibolite	2.7		4.7	
	18	MOS	Amphibolite	2.7		11	
	19	MCL	Gneiss	2.7		4.7	
	20	MCL	Gneiss	2.7		3.1	
	21	MCL	Gneiss	2.7		3.1	
	22	MCL	Tonalite	2.7		3.1	

Continued on next page

Table A.1 – continued from previous page

Reference	Sample	Setting	Rock	Age	δ^{15}N	[N]	δ^{13}C
	23	MCL	Gneiss	2.7		3.1	
	24	MCL	Gneiss	2.7		1.6	
	25	MCL	Gneiss	2.7		1.6	
	26	MCL	Gneiss	2.7		1.6	
	27	MCL	Gneiss	2.7		4.7	
Hall et al.1996	GREB-600	CL	Migmatite			118	
	GREB-601	CL	Migmatite			271	
	GREB-602	CL	Migmatite			131	
	GREB-603	CL	Migmatite			278	
	GREB-604	CL	Migmatite			136	
	GREB-605	CL	Migmatite			217	
	GREB-606	CL	Migmatite			122	
	GREB-607	CL	Migmatite			215	
	GREB-608	CL	Migmatite			124	
	GREB-609	CL	Migmatite			236	
	B-509	CL	Granite			67	
	B-508	CL	Granite			58	
	B-507	CL	Granite			57	
	B-510	CL	Granite			72	
	B-506	CL	Granite			71	
	B-505	CL	Granite			75	
	B-504	CL	Granite			87	
	B-503	CL	Granite			99	
	B-502	CL	Granite			89	
	B-501	CL	Granite			88	
	B-500	CL	Granite			88	
	Alijo-Sanfins	CL	Granite			159	
Watanabe et al.1997	Silverton	AOS	Shale	2.22		300	-30.7
Archean Proterozoic	Strubenkop	AOS	Shale	2.22		300	-25.3
Kaapvaal Craton	Timeball Hill	AOS	Shale	2.22		400	-27.2
Peak meta. conditions:	Black Reef	AOS	Shale	2.56		100	-31.6
Top:110-170degC	Selati	AOS	Shale	2.56		100	-22.4
and 1 kb	Bothaville	AOS	Shale	2.63			-30.3
bottom: 350deg C	K-8	AOS	Shale	2.72		100	-29.9
and 1-2kb	Booysens	AOS	Shale	2.72		100	-28.8
	Roodepoort	AOS	Shale	2.91		100	-29.0
	Orange	AOS	Shale	2.91		100	-31.3
Cartigny et al.1997	CHL 1	D	Peridotitic	0.46	-11.7	416	-3.2
Diamonds	CHL 1-2	D	Peridotitic	0.46	-10.4	381	-3.3
continental	CHL 2-1	D	Peridotitic	0.46	-3.1	789	0.4
lithosphere P =	CHL 2-2	D	Peridotitic	0.46	-4.4	810	-0.1
peridotitic	CHL 2-3	D	Peridotitic	0.46	-3.2	897	0.4
	CHL 3	D	Peridotitic	0.46	-9.8	628	-4.5
	CHL 4	D	Peridotitic	0.46	-5.4	673	-6.1
	CHL 5	D	Peridotitic	0.46	-12.5	752	-3.3
	CHL 6-1	D	Peridotitic	0.46	-6.9	179	-3.2
	CHL 6-2	D	Peridotitic	0.46	-5.0	91	-3.1
	CHL 7-1	D	Peridotitic	0.46	-4.7	809	-3.3
	CHL 7-2	D	Peridotitic	0.46	-3.9	666	-3.3
	CHL 8	D	Peridotitic	0.46	-2.8	1036	-1.6
	CHL 9-1	D	Peridotitic	0.46	-7.4	123	-3.6
	CHL 9-2	D	Peridotitic	0.46	-4.2	235	-4.0
	CHL 10	D	Peridotitic	0.46	-8.2	988	-4.5
	CHL 11	D	Peridotitic	0.46	-2.2	95	-2.6
	CHL 12	D	Peridotitic	0.46	-24.2	339	-4.4
	CHL 13	D	Peridotitic	0.46	-11.4	315	-3.2
	CHL13-2	D	Peridotitic	0.46	-10.9	270	0.0
	CHL 14	D	Peridotitic	0.46	-8.0	330	-4.7
	CHL 14-2	D	Peridotitic	0.46	-9.2	336	-4.9

Continued on next page

Table A.1 – continued from previous page

Reference	Sample	Setting	Rock	Age	δ^{15}N	[N]	δ^{13}C
	CHL 15-1	D	Peridotitic	0.46	-11.4	658	-4.8
	CHL 15-2	D	Peridotitic	0.46	-11.0	565	-4.8
	CHL 15-3	D	Peridotitic	0.46	-14.1	684	-4.8
	CHL 15-4	D	Peridotitic	0.46	-11.5	685	-4.8
	CHL 16	D	Peridotitic	0.46	-9.3	1471	-3.2
	CHL 17-1	D	Peridotitic	0.46	-1.8	969	-3.4
	CHL 17-2	D	Peridotitic	0.46	-1.1	831	-3.3
	CHL 18	D	Peridotitic	0.46	7.5	391	-3.5
	CHL 18-2	D	Peridotitic	0.46	6.9	337	-3.5
	CHL 19	D	Peridotitic	0.46	-6.9	252	-3.5
	CHL 22-1	D	Peridotitic	0.46	-11.5	332	-3.3
	CHL 22-2	D	Peridotitic	0.46	-16.7	464	-4.3
	CHL 22-3	D	Peridotitic	0.46	-11.7	544	-4.0
	CHL 23-2	D	Peridotitic	0.46	-6.2	790	-4.5
	CHL 24	D	Peridotitic	0.46	-15.9	496	-4.2
	CHL 25-1	D	Peridotitic	0.46	-7.9	476	-3.9
	CHL 25-2	D	Peridotitic	0.46	-7.7	392	-4.0
	CHL 25-3	D	Peridotitic	0.46	-7.9	489	-4.1
	CHL 29	D	Peridotitic	0.46	-11.7	150	-3.2
	CHL 30-1	D	Peridotitic	0.46	-5.5	215	-3.8
	CHL 30-2	D	Peridotitic	0.46	-5.5	276	-4.1
	CHL 30-3	D	Peridotitic	0.46	-7.4	277	-4.4
	CHL 31	D	Peridotitic	0.46	-18.0	164	-3.9
	CHL 31-2	D	Peridotitic	0.46	-18.6	148	-3.5
	CHL 32	D	Peridotitic	0.46	-13.6	230	-3.7
	CHL 33	D	Peridotitic	0.46	-15.3	437	-3.7
	CHL 35	D	Peridotitic	0.46	-4.8	415	-5.8
	CHL 36	D	Peridotitic	0.46	-6.1	231	-3.6
	CHL 37	D	Peridotitic	0.46	-13.1	172	-3.6
	CHL 38	D	Peridotitic	0.46	-10.1	414	-4.4
	CHL 38-2	D	Peridotitic	0.46	-8.3	397	-4.9
	CHL 38-5	D	Peridotitic	0.46	-7.3	445	-4.3
	CHL 39-4	D	Peridotitic	0.46	-1.7	100	-4.0
	CHL 41-2	D	Peridotitic	0.46	-3.9	141	-2.9
	CHL 44	D	Peridotitic	0.46	-21.0	385	-2.8
	CHL 45	D	Peridotitic	0.46	-6.4	659	-5.7
	CHL 48	D	Peridotitic	0.46	-6.4	588	-4.0
	CHL 48-2	D	Peridotitic	0.46	-8.5	487	-3.8
	CHL 49	D	Peridotitic	0.46	-0.9	901	-1.6
	CHL 50	D	Peridotitic	0.46	-0.3	325	-0.7
	CHL 51	D	Peridotitic	0.46	-6.5	614	-4.5
	CHL 52	D	Peridotitic	0.46	-6.1	1387	-6.0
	CHL 53	D	Peridotitic	0.46	-5.6	162	-0.1
	CHL 56	D	Peridotitic	0.46	-6.9	155	-3.3
	CHL56-2	D	Peridotitic	0.46	-2.7		-3.3
Marty and Humbert-1997	CH98DR11	OL	N-MORB	0	-1.8 ± 1.2	0.12	
	CH98DR11	OL	N-MORB	0	-1.9 ± 1.3	0.12	
MAR=Mid Atlantic Ridge	CH98DR11	OL	N-MORB	0	-2.2 ± 0.2	0.18	
	CH98DR11	OL	N-MORB	0	-3 ± 1.6	0.08	
	CH98DR11	OL	N-MORB	0	-3.5 ± 0.6	0.20	
	CH98DR11	OL	N-MORB	0	-4.5 ± 0.7	0.03	
	CH98DR11	OL	N-MORB	0	-4.5 ± 0.7	0.17	
	CH98DR12	OL	N-MORB	0	-3 ± 0.4	0.15	
	CH98DR12	OL	N-MORB	0	-3 ± 0.4	0.10	
	CH98DR15	OL	N-MORB	0	-1.5 ± 0.6	0.10	
	CH98DR15	OL	N-MORB	0	-1.7 ± 0.8	0.15	
	CH98DR17	OL	N-MORB	0	-3.8 ± 0.6	0.08	
	CH31DR01r10	OL	E-MORB	0	6.5 ± 0.6	0.03	
	CH31DR01r100	OL	E-MORB	0	2.1 ± 1	0.01	
	Total	OL	E-MORB	0	5.4 ± 0.7	0.04	
	CH31 DR02	OL	E-MORB	0	-0.9 ± 0.5	0.03	
	CH31DR01r10	OL	E-MORB	0	-3 ± 1	0.01	
	CH31DR01r100	OL	E-MORB	0	-2.3 ± 0.8	0.03	
	Total	OL	E-MORB	0	-2.5 ± 0.8	0.04	
	CH31DR11	OL	E-MORB	0	-1.4 ± 0.5	0.06	

Continued on next page

Table A.1 – continued from previous page

Reference	Sample	Setting	Rock	Age	δ^{15}N	[N]	δ^{13}C
	CH31DR11	OL	E-MORB	0	-1.7 ± 0.7	0.05	
	CH31DR11	OL	E-MORB	0	-2.8 ± 0.7		
	CH31DR11	OL	E-MORB	0	-3.9 ± 0.6	0.04	
	CH31DR11	OL	E-MORB	0		0.001	
	Total	OL	E-MORB	0	-3.9 ± 0.6	0.04	
EPR=East Pacific Rise	CY84	OL	T-MORB	0	-1 ± 1	0.01	
	CLDRO1	OL	N-MORB	0	-2 ± 0.6	0.04	
	CLDRO1	OL	N-MORB	0	-3.8 ± 0.5	0.03	
	Total	OL	N-MORB	0	-2.7 ± 0.5	0.07	
	CY82	OL	E-MORB	0	-6.5 ± 1.8	0.01	
	CY82	OL	N-MORB	0	-3.4 ± 0.9	0.03	
	CY82	OL	T-MORB	0	-2 ± 0.4	0.08	
Red Sea	KS	OL	E-MORB	0	-7 ± 1	0.01	
	KS	OL	E-MORB	0	3.1 ± 0.4	0.13	
	KS	OL	E-MORB	0	2.1 ± 0.6	0.02	
	MR80	OIB	Basalt	0	3.1 ± 0.3	0.04	
Galapagos	PL2	OL	E-MORB	0	-3.2 ± 1.6	0.01	
	PL2	OL	E-MORB	0	0.5 ± 1.5	0.01	
	PL2	OIB	Basalt	0	2.6 ± 1.6	0.01	
	PL2	OL	N-MORB	0	-0.4 ± 0.8	0.04	
	PL2-24-32	OIB	Basalt	0	-1.4 ± 2	0.01	
	PL2-RC-O1	OIB	Basalt	0	-1.9 ± 1.3	0.01	
McDonald Seamount	TH30-3	OIB	Basalt	0	-0.8 ± 0.5	2.35	
Manus Basin	AQ39C-108	OL	E-MORB	0	-0.1 ± 1	0.09	
Drits et al.1997	x1	OS	Shale			200	
from core in North Sea and Danish Sea	112	OS	Shale			600	
	82	OS	Shale			100	
	x3	OS	Shale			900	
	x17	OS	Shale			900	
	87	OS	Shale			1400	
	89	OS	Shale			1700	
	86	OS	Shale			1900	
	x18	OS	Shale			1900	
	x12	OS	Shale			2000	
	x13	OS	Shale			2100	
	99	OS	Shale			500	
	95	OS	Shale			500	
Bebout-1997	2-1-23	MOS	Schist	0.1	1.6 ± 0.6	860	
	2-1-24	MOS	Schist	0.1	2.0	1190	
	2-1-25	MOS	Schist	0.1	1.7	880	
	2-1-28	MOS	Schist	0.1	1.9	870	
	WE-1	MOS	Muscovite	0.1	1.8	2140	
	WE-2	MOS	Muscovite	0.1	2.0	2100	
	SL-1	MOS	Muscovite	0.1	2.3	1990	
	SL-4	MOS	Muscovite	0.1	1.9	1850	
	2-1-4	MOS	Schist	0.1	2.4	78	
	2-1-5	MOS	Schist	0.1	2.1	80	
	2-1-8	MOS	Schist	0.1	2.2	1370	
	2-1-9	MOS	Schist	0.1	2.2	600	
	2-1-11	MOS	Schist	0.1	2.0	110	
	2-1-36	MOS	Schist	0.1	2.5	790	
	12-1-37	MOS	Schist	0.1	2.7	400	
	2-1-37	MOS	Schist	0.1	2.4	60	
	2-1-38	MOS	Schist	0.1	2.6	1230	
	2-1-38	MOS	Schist	0.1	2.5	66	
	2-1-40	MOS	Schist	0.1	2.0	880	
	2-1-40	MOS	Schist	0.1	2.5	16	
	3-1-37a	MOS	Schist	0.1	2.4	1200	
	3-1-41	MOS	Schist	0.1	2.1	1480	
	MBW-1	MOS	Muscovite	0.1	2.5	1770	
	LCC-1	MOS	Muscovite	0.1	2.6	1680	
	0-1-3V	MOS	Vein	0.1	1.9	300	
	0-1-4V	MOS	Vein	0.1	2.0	95	
	0-1-5V	MOS	Vein	0.1	2.1	110	

Continued on next page

Table A.1 – continued from previous page

Reference	Sample	Setting	Rock	Age	δ^{15}N	[N]	δ^{13}C
	6-5-72V	MOS	Vein	0.1	2.1	270	
	6-2-46V	MOS	Vein	0.1	2.0	50	
	32-1-39V	MOS	Vein	0.1	2.1	190	
	8-3-90	MOS	Conglomerate	0.1	2.2	690	
	9-1-50a	MOS	Conglomerate	0.1	2.0	570	
	9-1-50b	MOS	Conglomerate	0.1	2.0	750	
	9-1-50c	MOS	Conglomerate	0.1	2.2	730	
	9-1-50d	MOS	Conglomerate	0.1	2.2	730	
	SC4-56	MOS	Conglomerate	0.1	2.2	680	
	SC4-82	MOS	Conglomerate	0.1	2.1	640	
	SC4-96	MOS	Conglomerate	0.1	2.1	400	
	SC4-26	MOS	Conglomerate	0.1	2.0	290	
	SC3-2	MOS	Conglomerate	0.1	2.2	680	
	SC4-58	MOS	Conglomerate	0.1	2.2	660	
	LCC-218	MOS	Conglomerate	0.1	2.6	420	
	LCC-214	MOS	Conglomerate	0.1	2.3	400	
	LH3-42	MOS	Conglomerate	0.1	2.5	720	
	LHCNGL66	MOS	Conglomerate	0.1	2.7	45	
Schroeder and McLain-1998	1005	AOS	Shale	0.01			
Illite/smectite clays	1880	AOS	Shale	0.01		640	
Sample names	2036	AOS	Shale	0.01		540	
are core depths	2719	AOS	Shale	0.01		540	
	2796	AOS	Shale	0.01		670	
	3328	AOS	Shale	0.01		710	
	3404	AOS	Shale	0.01		750	
	3841	AOS	Shale	0.01		630	
	3903	AOS	Shale	0.01		790	
	4049	AOS	Shale	0.01		640	
Boyd and Philippot-1998	MS-2	MOS	Schist	1.2	16.6	341	
Whole Rock data	MS-3	MOS	Schist	1.2	12.4	422	
Moine metasedi-	MS-4	MOS	Schist	1.2	14.4	380	
ments, Scotland	MS-5	MOS	Schist	1.2	14.8	232	
	MS-7	MOS	Schist	1.2	15.0	336	
	MS-14	MOS	Schist	1.2	14.3	140	
	MS-15	MOS	Schist	1.2	8.4	206	
Sano et al.1998	KH93-3-DR3	OL	MORB	0	-1.7		
MORB Glasses	KH93-3-DR6	OL	MORB	0	-2.0		
	KH93-3-DR25	OL	MORB	0	-2.3		
	CH31-DR11	OL	MORB	0	-1.2		
	CH98-DR11	OL	MORB	0	-3.1		
BABB	KT84-1-24-1	OL	BABB	0	-1.9		
	KT84-1-24-2	OL	BABB	0	1.9		
	KT84-1-24-3	OL	BABB	0	-2.7		
	ST4-DV17-3	OL	BABB	0	-1.1		
	ST4-DV19-1	OL	BABB	0	0.4		
	ST4-DV21-5	OL	BABB	0	1.8		
Minerals	Atsukawa	OL	Quartz	0	-0.5		
	Houei	OL	Fluorite	0	5.0		
	Unzen	OL	Plagioclase	0	4.1		
	Miyake-jima	OL	Plagioclase	0	0.0		
	Hachijo-jima	OL	Plagioclase	0	1.4		
Beaumont and Robert-1999	PPRG 193	AOS	Kerogen	3.5	5.9	22	-35.2

Continued on next page

Table A.1 – continued from previous page

Reference	Sample	Setting	Rock	Age	δ^{15}N	[N]	δ^{13}C
Cherts mostly marine some terrestrial	PPRG 182	AOS	Kerogen	3.5	-3.0	7	-31.7
	Boudou 7025val	AOS	Kerogen	3.5	1.4	16	-25.3
	Boudou 396A	AOS	Kerogen	3.5	2.0	45	-27.8
Average of multiple analyses of the same sample.	2	AOS	Kerogen	3.5	-1.6	39	-29.9
	4	AOS	Kerogen	3.5	-0.3	81	-28.4
	4	AOS	Kerogen	3.5	-2.6	17	-35.7
	1	AOS	Kerogen	3.5	-4.3	41	-32.4
	PPRG 0113	AOS	Kerogen	3.5	3.3	52	-35.2
	PPRG 006	AOS	Kerogen	3.5	-4.4	22	-32.7
	PPRG 002	AOS	Kerogen	3.5	4.9	2	-33.7
	PPRG 023	AOS	Kerogen	3.4	-4.7	106	-28.3
	PPRG 331	AOS	Kerogen	2.7	30.0	61	-17.0
	PPRG 330	AOS	Kerogen	2.7	3.0	32	-25.2
	PPRG 325	AOS	Kerogen	2.7	5.0	6	-31.3
	3	AOS	Kerogen	2.7	8.8	5	-47.4
	6	AOS	Kerogen	2.7	5.1	3	-46.5
	SBO 297	AOS	Kerogen	2.7	2.4	11	-29.3
	SBO 283	AOS	Kerogen	2.8	9.4	7	-38.1
	PPRG 278	AOS	Kerogen	2.8	-2.5	6	-37.7
	36	AOS	Kerogen	2.8	3.7	7	-40.8
	66	AOS	Kerogen	2.1	2.1	4	-40.6
	5	AOS	Kerogen	2.1	2.8	6	-28.9
	4	AOS	Kerogen	2.1	3.1	33	-35.1
	3	AOS	Kerogen	2	7.7	16	-34.5
	lc	AOS	Kerogen	2	4.8	4	-31.3
	la	AOS	Kerogen	2	4.3	30	-32.0
	l	AOS	Kerogen	2	2.5	13	-33.6
	5	AOS	Kerogen	0.8	3.4	3	-27.0
	4	AOS	Kerogen	0.7	2.1	4	-30.2
Bebout et al.1999b	LA	MOS	Schist	0.1		640	
Catalina Schist complex terreginous metaseds.	LA	MOS	Schist	0.1		695	
LA = Lawsonite-albite	LA	MOS	Schist	0.1		410	
LB = Lawsonite-blueschist	LA	MOS	Schist	0.1		200	
EB = Epidote-blueschist	LA	MOS	Schist	0.1		900	
EA = Epidote-amphibolite	LA	MOS	Schist	0.1		810	
A = amphibolite	LA	MOS	Schist	0.1		540	
	LA	MOS	Schist	0.1		790	
	LB	MOS	Schist	0.1		710	
	LB	MOS	Schist	0.1		735	
	LB	MOS	Schist	0.1		315	
	LB	MOS	Schist	0.1		710	
	EB	MOS	Schist	0.1		1075	
	EB	MOS	Schist	0.1		810	
	EB	MOS	Schist	0.1		110	
	EB	MOS	Schist	0.1		65	
	EB	MOS	Schist	0.1		180	
	EB	MOS	Schist	0.1		170	
	EB	MOS	Schist	0.1		313	
	EB	MOS	Schist	0.1		194	
	EB	MOS	Schist	0.1		592	

Continued on next page

Table A.1 – continued from previous page

Reference	Sample	Setting	Rock	Age	δ^{15}N	[N]	δ^{13}C
	EA	MOS	Schist	0.1		740	
	EA	MOS	Schist	0.1		90	
	EA	MOS	Schist	0.1		230	
	EA	MOS	Schist	0.1		180	
	EA	MOS	Schist	0.1		30	
	EA	MOS	Schist	0.1		265	
	A	MOS	Schist	0.1		65	
	A	MOS	Schist	0.1		150	
	A	MOS	Schist	0.1		160	
	A	MOS	Schist	0.1		260	
	A	MOS	Schist	0.1		35	
	A	MOS	Schist	0.1		60	
	A	MOS	Schist	0.1		110	
	A	MOS	Schist	0.1		165	
	A	MOS	Schist	0.1		205	
	A	MOS	Schist	0.1		323	
Hall-1999	Jabal Ras	CL	Granite	0.05		3	
Granites	Jabal Ras	CL	Granite	0.05		2	
	Dubas	CL	Granite	0.05		4	
	Jabal Kabba	CL	Granite	0.05		1	
	Jabal Ash Sharqi	CL	Granite	0.3		5	
	Jabal Sabir	CL	Granite	0.05		3	
	Jabal Sabir	CL	Granite	0.42		1	
	Jabal Ash Sharqi	CL	Granite	0.42		2	
	Jabal Bura	CL	Granite	0.275		3	
	Donegal	CL	Granite	0.295		9	
	Cornwall	CL	Granite	0.32		116	
	B5	CL	Granite			69	
	B176	CL	Granodiorite			162	
	B170	CL	Granodiorite			210	
	JAL4	CL	Granite			222	
	D5	CL	Granite			156	
	B178	CL	Granodiorite			39	
	P450	CL	Granite			15	
	B2	CL	Granite			83	
	B511	CL	Aplite			74	
	ESTR11	CL	Granite			32	
	ESTR9	CL	Granite			59	
	P452	CL	Granite			111	
	B165	CL	Granodiorite			243	
	D3	CL	Granite			129	
	ALIJO	CL	Granite			165	
	D1	CL	Granite			91	
	ESTR10	CL	Granite			42	
Alteration zones:	S Piero	CL	Granite			4	
Greisenization	Fresh	CL	Granite			87	
	Altered	ACL	Granite			212	
Potassic alteration	Fresh	CL	Granite			73	
	Altered	ACL	Granite			259	
Kaolinization	Fresh	CL	Granite			69	
	Altered	ACL	Granite			104	
Bebout et al.1999a	1718	ACL	Granite	0.4	1.0	225	
Altered granite	SAG 278.6	ACL	Granite	0.4	4.7	46	
	SAG 196.73	ACL	Granite	0.4	3.3	17	
	1717	ACL	Granite	0.4	1.6	58	
	SAG 178.7	ACL	Granite	0.4	4.8	73	
	SAG 96.25	ACL	Granite	0.4	3.1	24	
	SAG 96.8	ACL	Granite	0.4	4.0	36	
	1715	ACL	Granite	0.4	2.8	95	
Jia and Kerrich-1999	B4	ACL	Mica	2.7	16.8	186	
Hydrothermal micas	B4-1	ACL	Mica	2.7	17.2	191	

Continued on next page

Table A.1 – continued from previous page

Reference	Sample	Setting	Rock	Age	δ^{15}N	[N]	δ^{13}C
and granites from	B5	ACL	Mica	2.7	16.7	170	
Superior province/	D-1	ACL	Mica	2.7	15.6	160	
Australia	HGI-A	ACL	Mica	2.7	15.1	80	
	HGI-B	ACL	Mica	2.7	14.6	100	
	HGI-C	ACL	Mica	2.7	17.8	120	
	HGI-D	ACL	Mica	2.7	15.6	111	
	HGI-E	ACL	Mica	2.7	16.0	113	
	HGI-F	ACL	Mica	2.7	17.4	128	
	HGII-1	ACL	Mica	2.7	14.7	30	
	HGII-2	ACL	Mica	2.7	17.1	40	
	HGII-3	ACL	Mica	2.7	20.9	38	
	HGII-4	ACL	Mica	2.7	21.0	42	
	HGII-5	ACL	Mica	2.7	17.0	42	
	GHIA	ACL	Mica	2.7	18.1	150	
	GHIB	ACL	Mica	2.7	19.8	170	
	GHIC	ACL	Mica	2.7	16.9	140	
	NMT170	ACL	Mica	2.7	11.8	110	
	NMT230	ACL	Mica	2.7	13.5	114	
	WL170	ACL	Mica	2.7	12.8	19	
	WL230	ACL	Mica	2.7	14.8	19	
	WL100	ACL	Mica	2.7	20.7	19	
	WL230	ACL	Mica	2.7	16.6	20	
	DVB100	ACL	Mica	2.7	10.1	40	
	DVB170	ACL	Mica	2.7	11.4	35	
	DVB230	ACL	Mica	2.7	11.1	35	
	HD-1	ACL	Mica	2.7	13.6	23	
	HD-2	ACL	Mica	2.7	10.4	19	
	MCT	ACL	Mica	2.7	7.0	57	
	MCT-1	ACL	Mica	2.7	14.0	53	
	PL	ACL	Mica	2.7	14.3	28	
	PL-1	ACL	Mica	2.7	13.9	30	
	CHR-A	ACL	Mica	2.7	12.9	30	
	CHR-B	ACL	Mica	2.7	14.6	31	
	PL1	CL	Granite	2.7	5.3	20	
	PL1a	CL	Granite	2.7	5.0	20	
	PL1b	CL	Granite	2.7	2.6	20	
	PL2	CL	Granite	2.7	-1.6	50	
	PL2-1	CL	Granite	2.7	-3.0	20	
	MRAI-1	ACL	Mica	2.6	13.0	20	
	MRAI-2	ACL	Mica	2.6	19.0	20	
	MRAII-1	ACL	Mica	2.6	14.0	20	
	NNM-1	ACL	Mica	2.6	10.9	30	
	NNM-2	ACL	Mica	2.6	16.4	30	
	NNM-a	ACL	Mica	2.6	20.6	50	
	NNM-b	ACL	Mica	2.6	16.1	40	
	NR10-1	ACL	Mica	2.6	8.7	20	
	NR7-1	ACL	Mica	2.6	22.6	70	
	RT-1	ACL	Mica	2.6	15.9	20	
	RT-2	ACL	Mica	2.6	23.7	20	
	VHW-1	ACL	Mica	2.6	12.6	10	
Dauphas and Marty-1999		X	Dunite	0.37	1.9 ± 1.1	0.11	
Carbonitite magmas		X	Dunite	0.37	3.5 ± 1.4	0.05	
with some xenoliths		M	Turjaite	0.37	3.5 ± 1.1	0.17	
D = Dunite		X	Dunite	0.37	4.6 ± 1.3	0.04	
T = Turjaite		M	Phoscorite	0.37	6 ± 1.3	0.04	
Ph = Phoscorite		M	Pyroxenite	0.37	2.7 ± 2.2	0.01	
Py = Pyroxenite		M	Pyroxenite	0.37	2.6 ± 1.2	0.10	
Cc = Calcite Carbonatite		M	Pyroxenite	0.37	-0.2 ± 2.5	0.02	
Dc = Dolomite Carbonatite	Cc	M	Carbonatite	0.37	5.3 ± 1.1	0.22	

Continued on next page

Table A.1 – continued from previous page

Reference	Sample	Setting	Rock	Age	δ^{15}N	[N]	δ^{13}C
I = Ijolite	Cc	M	Carbonatite	0.37	1.7 ± 1.2	0.57	
O =Ore	D	X	Dunite	0.37	3.6 ± 1.4	0.17	
Cpx = Clinopyroxenite	Dc	M	Carbonatite	0.37	6.5 ± 1.5	0.07	
	I	M	Ijolite	0.37	4.3 ± 1.5	0.05	
	O	M	Ore	0.37	2.6 ± 1.2	0.04	
	O	M	Ore	0.37	1.1 ± 1.2	0.19	
	Cpx	M	Pyroxenite	0.37	0.7 ± 1.1	0.10	
	Dc	M	Carbonatite	0.37	5.1 ± 1.2	0.08	
Marty and Zimmerman-1999	CLDR01	OL	MORB	0	-8.1 ± 0.6	0.033	-3.8
	CLDR04	OL	MORB	0	-3.7 ± 0.5	0.075	-3.4
	CY82 31 01	OL	MORB	0	-3.1 ± 2.8	0.003	
	SR1DR04	OL	MORB	0	-3.6 ± 1.2	0.003	-6.3
	ND 11-2 #1	OL	MORB	0	-3.3 ± 0.7	0.069	
	ND 11-2 #2	OL	MORB	0	-3.5 ± 0.5	0.044	
	ND 11-2 #3	OL	MORB	0	-8.9 ± 0.5	0.087	
	ND 12-2	OL	MORB	0	0.6 ± 0.9	0.008	
	ND 15-4	OL	MORB	0	-1 ± 0.9	0.013	
	ND 18-1	OL	MORB	0			
	ND 19-8	OL	MORB	0	1 ± 0.9	0.010	
	ND 21-3	OL	MORB	0			
	ND21-4	OL	MORB	0	-4 ± 0.4	0.027	-3.7
	SR2DR02	OL	MORB	0	-3 ± 0.6	0.005	
	SR2DR03	OL	MORB	0	-3.2 ± 0.7	0.025	
	KS 11 A	OL	MORB	0	-0.7 ± 1.0	0.008	-6.3
	KS 12 A	OL	MORB	0			
	KS 04 A	OL	MORB	0	2.1 ± 0.6	0.021	
	MR80 59 4	OL	MORB	0	3.1 ± 0.7	0.043	-5.9
	HY09-07H	OL	MORB	0	-1.3 ± 1	0.111	-6.4
	JC 217 D1 (3)	OL	MORB	0	-2.1 ± 0.6	0.034	-2.5
	JC 0300703D1	OL	MORB	0	1.8 ± 0.3	0.070	-5.3
	MD23-4	OL	MORB	0	-6.9 ± 0.6	0.079	-3.2
	MD57 D4-4	OL	MORB	0	-4.7 ± 0.3	0.028	
	MD23-2	OL	MORB	0	-3.9 ± 0.4	0.118	-4.0
	MD370301	OL	MORB	0	-3.9 ± 0.3	0.074	
	SWIR DR2-3	OL	MORB	0	-2.4 ± 0.4	0.147	-6.1
	MD23-1	OL	MORB	0			
	ST2-17-6	OL	MORB	0	0.8 ± 0.5	0.010	
	ST2-17-7	OL	MORB	0	-0.5 ± 0.4	0.115	-4.3
	ST-17-10	OL	MORB	0		0.01	-3.3
Nishio et al.1999	KH93-3-DR3-A1	OL	MORB	0	-1.7	0.23	-2.6
	KH93-3-DR1-f1	OL	MORB	0	-2.2	0.10	-3.0
	KH93-3-DR9-G1	OL	MORB	0	-1.0	0.29	-5.6
	KH93-3-DR25-A1	OL	MORB	0	-2.3	0.22	-3.1
	KH93-3-DR25-A2	OL	MORB	0	-1.6	0.31	-2.1
	KH93-3-DR6-A1	OL	MORB	0	-2.0	0.20	-4.0
	CH31-DR11	OL	MORB	0	-1.2	0.07	-5.7
	CH98-DR11	OL	MORB	0	-3.1	0.09	-3.1
Bebout et al.1999a	KDC-50	MOS	Schist	0.4	3.7	803	
Altered sedimentary rocks from the Skiddaw aureole	KDC-45	MOS	Schist	0.4	3.7	908	
	KDC-30	MOS	Schist	0.4	3.1	848	
	KDC-26	MOS	Schist	0.4	3.9	837	
	KDC-23	MOS	Schist	0.4	3.6	893	

Continued on next page

Table A.1 – continued from previous page

Reference	Sample	Setting	Rock	Age	δ^{15}N	[N]	δ^{13}C
	KDC-19	MOS	Schist	0.4	4.1	863	
	KDC-13	MOS	Schist	0.4	3.7	667	
	KDC-12	MOS	Schist	0.4	3.3	859	
	KDC-8	MOS	Schist	0.4	4.2	740	
	KDC-7	MOS	Schist	0.4	3.9	831	
	KDC-50	MOS	Schist	0.4	5.0	1039	
	KDC-61	MOS	Schist	0.4	7.3	466	
	KDC-62	MOS	Schist	0.4	6.8	462	
	KDC-65	MOS	Schist	0.4	4.7	425	
	KDC-66	MOS	Schist	0.4	4.2	493	
	KDC-70	MOS	Schist	0.4	7.3	528	
	KDC-72	MOS	Schist	0.4	7.2	147	
	JKDC-73	MOS	Schist	0.4	6.5	150	
	KDC-75	MOS	Schist	0.4	4.1	409	
	KDC-76	MOS	Schist	0.4	6.6	141	
	KDC-77	MOS	Schist	0.4	8.7	206	
	KDC-80	MOS	Schist	0.4	4.9	113	
	KDC-81	MOS	Schist	0.4	4.6	85	
	KDC-82	MOS	Schist	0.4	5.3	237	
Sadofsky and Bebout-2000	3	MOS	Biotite	0.41	9.6	19	
Biotite analyses from	5	MOS	Biotite	0.41	8.5	14	
Vermont and Maine	7a	MOS	Biotite	0.41	4.5	915	
Siluro-devonian in age	7b	MOS	Biotite	0.41	4.4	1134	
	7c	MOS	Biotite	0.41	4.4	1270	
	7d	MOS	Biotite	0.41	4.5	1122	
	15a	MOS	Biotite	0.41	3.6	688	
	15b	MOS	Biotite	0.41	3.9	655	
	16a	MOS	Biotite	0.41	3.9	767	
	16b	MOS	Biotite	0.41	4.7	668	
	20a	MOS	Biotite	0.41	3.5	578	
	20b	MOS	Biotite	0.41	3.9	541	
	21	MOS	Biotite	0.41	5.3	623	
	23	MOS	Biotite	0.41	6.3	497	
	23v	MOS	Biotite	0.41	6.4	302	
	27	MOS	Biotite	0.41	8.6	709	
	26a	MOS	Biotite	0.41	9.2	817	
	26b	MOS	Biotite	0.41	10.2	451	
	26d	MOS	Biotite	0.41	11.0	542	
	26c	MOS	Biotite	0.41	10.7	262	
	37.5	MOS	Biotite	0.41	10.8	223	
	42	MOS	Biotite	0.41	7.3	801	
	45	MOS	Biotite	0.41	6.7	608	
	18	MOS	Biotite	0.41	7.4	994	
	50	MOS	Biotite	0.41	8.6	217	
	6b	MOS	Biotite	0.41	11.9	57	
	6a	MOS	Biotite	0.41	6.8	32	
	24	MOS	Biotite	0.41	3.3	66	
	20a	MOS	Biotite	0.41	4.1	13	
Maine	7a	MOS	Biotite	0.41	6.0	996	
	8a	MOS	Biotite	0.41	6.5	510	
	10	MOS	Biotite	0.41	4.4	1412	
	12	MOS	Biotite	0.41	6.2	1351	
	5b	MOS	Biotite	0.41	6.6	1820	
	13	MOS	Biotite	0.41	7.2	1144	
	16	MOS	Biotite	0.41	8.9	1181	
White micas	3	MOS	Muscovite	0.41	9.6	13	
	7a	MOS	Muscovite	0.41	4.4	258	
	7b	MOS	Muscovite	0.41	3.8	196	
	7c	MOS	Muscovite	0.41	4.5	153	
	7d	MOS	Muscovite	0.41	4.2	299	
	15a	MOS	Muscovite	0.41	4.5	234	
	16a	MOS	Muscovite	0.41	4.0	242	
	16b	MOS	Muscovite	0.41	4.3	276	

Continued on next page

Table A.1 – continued from previous page

Reference	Sample	Setting	Rock	Age	δ^{15}N	[N]	δ^{13}C
	20b	MOS	Muscovite	0.41	3.8	391	
	23	MOS	Muscovite	0.41	6.4	65	
	27	MOS	Muscovite	0.41	8.3	300	
	26a	MOS	Muscovite	0.41	8.8	220	
	26b	MOS	Muscovite	0.41	9.2	237	
	26d	MOS	Muscovite	0.41	9.1	224	
	26c	MOS	Muscovite	0.41	9.4	155	
	37.5	MOS	Muscovite	0.41	8.8	53	
	45	MOS	Muscovite	0.41	6.8	401	
	18	MOS	Muscovite	0.41	7.5	258	
	50	MOS	Muscovite	0.41	8.5	62	
	53	MOS	Muscovite	0.41	8.3	35	
	25c	MOS	Muscovite	0.41	8.9	30	
	6b	MOS	Muscovite	0.41	9.1	56	
	6c	MOS	Muscovite	0.41	10.3	54	
	24	MOS	Muscovite	0.41	3.9	23	
	22	MOS	Muscovite	0.41	6.5	9	
Maine	982	MOS	Muscovite	0.41	4.1	773	
	987	MOS	Muscovite	0.41	5.4	483	
	988a	MOS	Muscovite	0.41	6.6	496	
	9810	MOS	Muscovite	0.41	4.6	286	
	9812	MOS	Muscovite	0.41	6.4	397	
	985b	MOS	Muscovite	0.41	6.4	233	
	9813	MOS	Muscovite	0.41	6.6	333	
Kao and Liu-2000	Rock	AOS	Slate	0.01	3.9 ± 0.1	800	-25.0
Jia and Kerrich-2000	Abitibi-K	CL	Granite	2.7	5.3	20	
Minerals from	Abitibi-K	CL	Granite	2.7	5.0	20	
Archean granites	Abitibi-K	CL	Granite	2.7	2.3	20	
K = K-spar	Abitibi-L	CL	Granite	2.7	1.3	20	
B = Biotite	Abitibi-M	CL	Granite	2.7	1.6	20	
L = lepidolite	Uchi-B	CL	Tonalite	2.7	-1.6	50	
M = Muscovite	Uchi-B	CL	Tonalite	2.7	-3.0	20	
	Uchi-B	CL	Tonalite	2.7	0.3	30	
Abitibi = peralumi-nous	Uchi-B	CL	Tonalite	2.7	-1.2	30	
granites	Uchi-B	CL	Tonalite	2.7	-5.3	20	
Uchi = tonalites	Uchi-B	CL	Tonalite	2.7	-3.8	20	
	Uchi-B	CL	Tonalite	2.7	2.3	20	
	Uchi-B	CL	Tonalite	2.7	5.1	20	
	Uchi-B	CL	Tonalite	2.7	-0.9	20	
Jia and Kerrich-2000	KA II-1	ACL	Muscovite	2.7	19.4	195	
	KA II-2	ACL	Muscovite	2.7	18.9	203	
	KA II-3	ACL	Muscovite	2.7	19.2	198	
	KA I-1	ACL	Muscovite	2.7	20.3	202	
	KA I-2	ACL	Muscovite	2.7	19.4	205	
	KA I-3	ACL	Muscovite	2.7	18.2	194	
	KA I-4	ACL	Muscovite	2.7	19.9	193	
	B4	MCL	Muscovite	2.7	16.8	186	
	B4-1	MCL	Muscovite	2.7	17.2	191	
	B5	MCL	Muscovite	2.7	16.7	170	
	D-1	MCL	Muscovite	2.7	15.6	160	
	GH IA	MCL	Muscovite	2.7	18.2	150	
	GH IB	MCL	Muscovite	2.7	19.8	170	
	GH IC	MCL	Muscovite	2.7	16.9	140	
	GH I-B	MCL	Muscovite	2.7	15.1	100	
	GH I-C	MCL	Muscovite	2.7	14.6	120	
	GH I-D	MCL	Muscovite	2.7	17.8	111	
	GH I-E	MCL	Muscovite	2.7	15.6	113	
	GH I-F	MCL	Muscovite	2.7	16.0	128	
	GH II-1	MCL	Muscovite	2.7	14.7	30	

Continued on next page

Table A.1 – continued from previous page

Reference	Sample	Setting	Rock	Age	δ^{15}N	[N]	δ^{13}C
	GH II-2	MCL	Muscovite	2.7	17.1	40	
	GH II-3	MCL	Muscovite	2.7	20.9	38	
	GH II-4	MCL	Muscovite	2.7	21.0	42	
	GH II-5	MCL	Muscovite	2.7	17.0	42	
	MAC	MCL	Muscovite	2.7	17.0	57	
	MAC-1	MCL	Muscovite	2.7	14.0	53	
	HD-1	MCL	Muscovite	2.7	13.6	23	
	HD-2	MCL	Muscovite	2.7	10.4	19	
	WL170	MCL	Muscovite	2.7	12.8	19	
	WL230	MCL	Muscovite	2.7	14.8	19	
	WL100	MCL	Muscovite	2.7	20.7	19	
	WL230	MCL	Muscovite	2.7	16.6	20	
	NR7-1	MCL	Biotite	2.7	22.6	70	
	NR10	MCL	Biotite	2.7	8.7	20	
	MRAI-1	MCL	Biotite	2.7	13.0	20	
	MRA 1-2	MCL	Biotite	2.7	19.0	20	
	MRA II-1	MCL	Biotite	2.7	14.0	20	
	VHW-1	MCL	Biotite	2.7	12.6	10	
	NNM-1	MCL	Biotite	2.7	10.9	30	
	NNM-2	MCL	Biotite	2.7	20.6	30	
	NNM-a	MCL	Biotite	2.7	16.1	50	
	NNM-b	MCL	Biotite	2.7	16.4	40	
	RT-1	MCL	Biotite	2.7	15.9	20	
	RT-2	MCL	Biotite	2.7	23.7	20	
Pinti et al.-2001	SJM43	MOS	Metapelite	3.8	7.1 ± 0.9	26.31	
Metasediments.	SJM43a	MOS	Biotite	3.8	10.7 ± 1.3	72.00	
Pilbara Australia	SJM43	MOS	Biotite	3.8	9.4 ± 0.6	74.27	
Greenl and	1021	MOS	BIF	3.8	8.2 ± 0.4	3.60	
WR = Whole Rock	136	MOS	BIF	3.8	0.8 ± 0.7	2.62	
B = biotite	611	MOS	Metachert	3.8	9.2 ± 0.6	0.73	
I = Iron sep.	702	MOS	Metachert	3.8	12.2 ± 1.1	0.41	
C = Chert	Pano D-136	AOS	Chert	3	-3.8 ± 0.7		
	Pano C-85	AOS	Chert	3	5.2 ± 0.5	0.36	
	Chert-Barite	AOS	Chert	3	6.9 ± 0.5	0.27	
	458	AOS	Chert	3	6.1 ± 0.9	0.93	
	LBR-31	AOS	BIF	3	7.2 ± 1.2	4.13	
	HR-28-544	AOS	Chert	3	11.5 ± 0.5	1.94	
Mingram and Brauer-2001	LG	AOS	Slate	0.45	3.0	572	-27.9
Passive margin metaseds	LG	AOS	Slate	0.45	2.0	603	-28.3
undergone	LG	AOS	Slate	0.45	3.2	499	-25.0
HP-UHP metamorphism, Bavaria/Alps	LG	AOS	Slate	0.45	1.2	482	-26.6
LG = Low-grade	P	MOS	Phyllite	0.45	2.2	498	-26.1
P= Phyllite	P	MOS	Phyllite	0.45	2.3	483	-23.7
GP = Garnet Phyllite	P	MOS	Phyllite	0.45	0.0	369	-28.3
MS = Mica schist	P	MOS	Phyllite	0.45	2.6	420	-27.1
GE = Gneiss/Eclogite	P	MOS	Phyllite	0.45	1.7	358	-27.8
T = Transition zone	P	MOS	Phyllite	0.45	1.8	681	-27.4
G = gneiss	GP	MOS	Phyllite	0.45	3.1	397	-24.7
	GP	MOS	Phyllite	0.45	3.6	697	-24.5
	GP	MOS	Phyllite	0.45	4.2	373	-27.9
	GP	MOS	Phyllite	0.45	5.5	334	-28.7
	GP	MOS	Phyllite	0.45	3.3	292	-25.6
	GP	MOS	Phyllite	0.45	2.3	630	-29.2

Continued on next page

Table A.1 – continued from previous page

Reference	Sample	Setting	Rock	Age	δ^{15}N	[N]	δ^{13}C
	GP	MOS	Phyllite	0.45	3.3	483	-27.2
	GP	MOS	Phyllite	0.45	2.9	657	-29.6
	MS	MOS	Schist	0.48	2.8	389	-26.3
	MS	MOS	Schist	0.48	4.2	217	-23.9
	MS	MOS	Schist	0.48	4.3	397	-29.2
	MS	MOS	Schist	0.48	3.4	323	-28.2
	MS	MOS	Schist	0.48	4.0	419	-26.0
	MS	MOS	Schist	0.48	3.8	232	-26.2
	MS	MOS	Schist	0.48	4.6	303	-29.9
	MS	MOS	Schist	0.48	2.5	334	-27.8
	MS	MOS	Schist	0.48	5.2	143	-26.7
	MS	MOS	Schist	0.48	10.3	117	-28.1
	GE	MOS	Gneiss	0.48	10.5	88	-23.8
	GE	MOS	Gneiss	0.48	7.0	101	-27.8
	GE	MOS	Gneiss	0.48	5.7	59	-23.4
	T	MOS	Gneiss	0.48	3.8	264	-26.8
	T	MOS	Gneiss	0.48	3.6	62	-28.0
	T	MOS	Gneiss	0.48	1.3	78	-28.2
	T	MOS	Gneiss	0.48	1.2	43	-30.3
	T	MOS	Gneiss	0.48	2.0	43	-29.0
	T	MOS	Gneiss	0.48	1.8	288	-27.7
	T	MOS	Gneiss	0.48	7.5	31	-29.0
	G	MOS	Gneiss	0.55	2.9	93	-28.9
	G	MOS	Gneiss	0.55	2.5	66	-28.7
	G	MOS	Gneiss	0.55	3.6	34	-30.1
	G	MOS	Gneiss	0.55	3.2	27	-28.6
Jenkyns et al.-2001	Bore hole from engl and	AOS	Shale	0.185	-0.8		
read from graph		AOS	Shale	0.185	0.0		
		AOS	Shale	0.185	0.2		
		AOS	Shale	0.185	-0.6		
		AOS	Shale	0.185	-1.2		
		AOS	Shale	0.185	-1.2		
		AOS	Shale	0.185	-2.0		
		AOS	Shale	0.185	-1.8		
		AOS	Shale	0.185	-1.4		
		AOS	Shale	0.185	-1.4		
		AOS	Shale	0.185	-1.0		
		AOS	Shale	0.185	-1.2		
		AOS	Shale	0.185	-1.4		
		AOS	Shale	0.185	-1.6		
		AOS	Shale	0.185	-2.0		
		AOS	Shale	0.185	-0.8		
		AOS	Shale	0.185	-3.0		
		AOS	Shale	0.185	-0.1		
		AOS	Shale	0.185	1.8		
Cartigny et al.-2001	Sn 10	D	Eclogitic	0.37		1272	-7.0
Diamonds	Gm 97-2	D	Eclogitic	0		622	-16.5
E = eclogitic	Gm 97-8	D	Eclogitic	0		261	-18.0
F =Fibrous	D5	D	Eclogitic	0.07		1808	-7.0
P = peridotitic	Dm 101 K	D	Eclogitic	0.07		1929	-8.2
	Dm 101 A	D	Eclogitic	0.07		3350	-6.4
	JW 67	D	Peridotitic	0.235		1148	-13.2
	F 71	D	Peridotitic	0.118		1194	-7.3
	F 5	D	Peridotitic	0.118		1108	-6.9
	OR 36-1	D	Peridotitic	0.093		36	-19.9
	OR 36-2	D	Peridotitic	0.093		21	-19.1
	OR 35	D	Peridotitic	0.093		189	-18.1
	CHL 52	D	Peridotitic	0.46		1189	-6.0
	JW 25	D	Eclogitic	0.0856			-24.4
	J222	D	Eclogitic	0.0856		42	-23.8
	E 9012	D	Eclogitic	0.026		23	-21.7
	J 11	D	Eclogitic	0.0856		88	-21.1
	OR 32	D	Eclogitic	0.093		100	-19.8
	JW 42	D	Eclogitic	0.235		145	-19.2

Continued on next page

Table A.1 – continued from previous page

Reference	Sample	Setting	Rock	Age	δ^{15}N	[N]	δ^{13}C
	J 23	D	Eclogitic	0.0856		65	-18.9
	OR 7	D	Eclogitic	0.093		414	-18.0
	J 36	D	Eclogitic	0.0856		172	-17.9
	OR 54	D	Eclogitic	0.093		389	-17.2
	OR 2	D	Eclogitic	0.093		359	-17.1
	J 17	D	Eclogitic	0.0856		175	-16.8
	OR 51	D	Eclogitic	0.093		494	-16.6
	JW 13	D	Eclogitic	0.235		267	-16.3
	JW 36	D	Eclogitic	0.235		340	-16.3
	OR 1	D	Eclogitic	0.093		489	-16.0
	JW 20	D	Eclogitic	0.235		318	-15.5
	OR 28	D	Eclogitic	0.093		334	-14.9
	OR 4	D	Eclogitic	0.093		539	-14.1
	OR 24	D	Eclogitic	0.093		514	-14.1
	OR 20	D	Eclogitic	0.093		575	-14.1
	OR 8	D	Eclogitic	0.093		448	-13.9
	OR 10	D	Eclogitic	0.093		693	-13.4
	OR 3	D	Eclogitic	0.093		443	-13.3
	E 9004	D	Eclogitic	0.026		1211	-10.2
	OR 6	D	Eclogitic	0.093		804	-9.8
	ER 9001	D	Eclogitic	0.026		1109	-8.5
	K 54	D	Eclogitic	0.094		1130	-7.8
	JW 33	D	Eclogitic	0.235		1222	-6.3
	JW 1	D	Eclogitic	0.235		72	-21.1
	OR 7-2	D	Eclogitic	0.093		265	-18.3
	OR 7-1	D	Eclogitic	0.093		173	-17.6
	DP 354-1	D	Eclogitic	0.1		478	-16.1
	OR 1-2	D	Eclogitic	0.093		417	-15.9
	DP 354-2	D	Eclogitic	0.1		428	-15.9
	OR 1-1	D	Eclogitic	0.093		421	-15.8
	OR 10	D	Eclogitic	0.093		723	-14.3
	OR 3-2	D	Eclogitic	0.093		393	-13.8
	JW 36	D	Eclogitic	0.235		459	-12.1
	W 43	D	Eclogitic	0.026		2473	-5.9
	B14	D	Eclogitic	0.026		1800	-7.5
Sano et al.-2001	OIB	VV	Glass	0	-0.4		
Island arc gas/fluid	OIB	VV	Glass	0	0.4		
back arc basin glass (BABB)	OIB	VV	Glass	0	0.4		
OIB glass	BABB	VV	Glass	0	-1.9		
	BABB	VV	Glass	0	1.9		
	BABB	VV	Glass	0	-2.7		
	BABB	VV	Glass	0	-1.1		
	BABB	VV	Glass	0	0.4		
	BABB	VV	Glass	0	1.8		
	BABB	VV	Glass	0	1.6		
	BABB	VV	Glass	0	-0.6		
	BABB	VV	Glass	0	0.0		
	IA	VV	Gas/Fluid	0	2.8		
	IA	VV	Gas/Fluid	0	3.7		
	IA	VV	Gas/Fluid	0	0.1		
	IA	VV	Gas/Fluid	0	1.5		
	IA	VV	Gas/Fluid	0	4.0		
	IA	VV	Gas/Fluid	0	1.1		
	IA	VV	Gas/Fluid	0	0.9		
	IA	VV	Gas/Fluid	0	0.1		
	IA	VV	Gas/Fluid	0	3.2		
	IA	VV	Gas/Fluid	0	3.3		
	IA	VV	Gas/Fluid	0	4.6		
Holloway et al. 2001	Exchequer	AOS	Slate			1370	
	Auburn	MCL	Schist			480	
Sephton et al.-2002	1	AOS	Shale	0.199	3.4		-32.0
Triassic AOS values read	2	AOS	Limestone	0.199	2.0		-31.8

Continued on next page

Table A.1 – continued from previous page

Reference	Sample	Setting	Rock	Age	δ^{15}N	[N]	δ^{13}C
from graph	3	AOS	Limestone	0.199	2.1		-31.2
	4	AOS	Shale	0.199	1.3		-31.9
	5	AOS	Limestone	0.199	0.3		-30.4
	6	AOS	Shale	0.199	0.1		-30.4
	7	AOS	Shale	0.199	1.5		-28.7
	8	AOS	Shale	0.2	-0.6		-29.7
	9	AOS	Shale	0.21	1.9		-29.0
	10	AOS	Shale	0.22	4.7		-30.3
	11	AOS	Shale	0.22	5.0		-30.7
	12	AOS	Shale	0.22	3.2		-29.7
	13	AOS	Shale	0.22	2.3		-30.0
	14	AOS	Mudstone	0.22	2.5		-30.9
	15	AOS	Shale	0.22	3.5		-30.8
	16	AOS	Limestone	0.22	3.1		-30.7
	17	AOS	Shale	0.22	2.7		-30.9
Yamaguchi-2002	Timeball Hill	AOS	Shale	2.22	5.9 ± 0.5	400	
PhD dissertation. Measurements of a number of Archean shales	Oak Tree	AOS	Shale	2.56	2.1 ± 0.7	100	
	Wittenoom	AOS	Dolostone	2.6	5.8 ± 0.3	200	
We report the average of multiple analyses from each formation	Carawine	AOS	Dolostone	2.6	0.2 ± 0.3	600	
	Marra Mamba	AOS	Shale	2.6	2.2 ± 2	100	
	Lewin Shale	AOS	Shale	2.69	3.4 ± 3.1	700	
	Sheba Fm	AOS	Kerogen	3.25	0.9 ± 1.3	100	
	Sheba Fm	AOS	Shale	3.25	3.4 ± 0.7	400	
Matsumoto et al.-2002	VIC51	X	Lherzolite	0.01	0.06 ± 1.2	0.054	
	VIC51A	X	Lherzolite	0.01	0.48 ± 1.8	0.004	
Anhydrous lherzolites	GAMVL3	X	Lherzolite	0.01	-6.01 ± 1.2	0.014	
Mantle xenoliths from Australia	VIC53C	X	Lherzolite	0.01	-0.8 ± 1.2	0.008	
	VIC53C	X	Lherzolite	0.01	-1.5 ± 1.3	0.007	
	VIC54F	X	Lherzolite	0.01	1.86 ± 1.4	0.005	
	SHD6	X	Lherzolite	0.01	2.02 ± 1.7	0.003	
Fischer et al.-2002	Zunil	VV	Gas	0	6.1	68	
Central American volcanic gases and fluids	San Marcos	VV	Gas	0	6.0	180	
	Volcan Fuego	VV	Gas	0	6.3	3190	
N=vol N2	Amatitlan	VV	Gas	0	0.0	4648	
	Amatitlan	VV	Gas	0	6.0	2	
	Amatitlan	VV	Fluid	0	3.1	2	
	Amatitlan	VV	Fluid	0	5.5	650	
	Tecuamburro	VV	Gas	0	6.9	936	
	Tecuamburro	VV	Gas	0	6.9	2030	
	Tecuamburro	VV	Gas	0	0.0	1038	
	Moyuta	VV	Fluid	0	6.7		
	Moyuta	VV	Fluid	0	6.2	40	
	Poas	VV	Gas	0	-1.9	46	
	Poas	VV	Gas	0	-4.8	74	
	Poas	VV	Gas	0	-4.9	42	
	Poas	VV	Gas	0	-3.0	204	
	Turrialba	VV	Gas	0	0.8	136	
	Turrialba	VV	Gas	0	-4.8	1074	
	Irazu	VV	Gas	0	4.2		
	B835.Cp	X	Clinopyroxene		-0.1	1	

Continued on next page

Table A.1 – continued from previous page

Reference	Sample	Setting	Rock	Age	δ^{15}N	[N]	δ^{13}C
Busigny et al.-2003 ophiolite shaly-marly -limestone protolith	00Li10	AOS	Pelite	0.1	3.8	441	
	00Li8S	AOS	Pelite	0.1	4.1	762	
	00Li9	AOS	Marlstone	0.1	3.1	226	
	00Li7	AOS	Pelite	0.1	4.7	234	
	C18	MOS	Schist	0.1	2.9	169	
	98SE3	MOS	Schist	0.1	3.0	313	
	SL98-2P	MOS	Schist	0.1	3.7	560	
	98SE5	MOS	Schist	0.1	2.8	1721	
	98SE6	MOS	Schist	0.1	3.2	1069	
	SL98-3C	MOS	Schist	0.1	3.2	232	
	SL98-3P	MOS	Schist	0.1	3.7	1637	
	98SE7	MOS	Schist	0.1	2.6	228	
	98SE8	MOS	Schist	0.1	3.7	621	
	98SE9	MOS	Schist	0.1	4.4	523	
	90-25B	MOS	Schist	0.1	4.8	195	
	90-25A	MOS	Schist	0.1	3.6	446	
Sadofsky and Bebout-2003 Metasediments from Franciscan complex and the Baja Terrane	VD 2a	MOS	Schist	0.1	3.0	891	-25.2
	VD 5c	MOS	Schist	0.1	2.4	503	-25.3
	VD 9b	MOS	Schist	0.1	2.4	256	-25.3
	Mendo 8	MOS	Schist	0.1	2.8	748	-25.4
	KW98-14a	MOS	Schist	0.1	3.4	689	-24.9
	KW98-21b	MOS	Schist	0.1	1.4	106	-25.2
	KW98-93	MOS	Schist	0.1	2.9	677	-25.8
	Eel4 Shale	MOS	Schist	0.1	1.5	380	-24.2
	JC c4a	MOS	Schist	0.1	1.3	675	-24.7
	JC 5	MOS	Schist	0.1	1.5	214	-24.6
	JC 6	MOS	Schist	0.1	1.7	599	-25.0
	AP c5b	MOS	Schist	0.1	1.7	108	-24.8
	Apc5a	MOS	Schist	0.1	1.6	219	-28.2
	AP 8	MOS	Schist	0.1	1.2	195	-25.6
	CR 2b	MOS	Schist	0.1	1.0	777	-23.8
	CR 1a2 mafic	MOS	Schist	0.1	0.3	30	-25.9
	Alder 1c	MOS	Schist	0.1	1.4	604	-25.7
	Alder 2	MOS	Schist	0.1	1.8	385	-26.9
	WGE-Q34	MOS	Schist	0.1	2.2	166	-24.5
	WGE-Q26f	MOS	Schist	0.1	0.7	36	-26.0
	WGE-Q20	MOS	Schist	0.1	1.5	170	-24.7
	WGE-Q38	MOS	Schist	0.1	2.1	166	-24.2
	WGE-Q26g	MOS	Schist	0.1	1.1	58	-26.8
	6-4-8-1	MOS	Schist	0.1	0.6	801	
	6-4-1-1	MOS	Schist	0.1	0.2	463	
	SS3-1	MOS	Schist	0.1	2.2	866	
	SS3-2	MOS	Schist	0.1	1.9	559	
Baja	RLS-585-1	MOS	Schist	0.1	1.9	226	-28.8
	RLS-585-14	MOS	Schist	0.1	0.1	305	-25.3
	RLS-486-105	MOS	Schist	0.1	2.5	692	-25.5
	RLS-585-71	MOS	Schist	0.1	1.9	425	-24.2
	RLS-486-130	MOS	Schist	0.1	2.8	300	-23.3
Marty and Dauphas-2003 Recent OIBs Averages shown	SO47-5D2	OIB	Basalt	0	3.89 ± 1.6	3.7	
	2SO47-9D2	OIB	Basalt	0	0.58 ± 1.6	0.1	
	TH09-02	OIB	Basalt	0	1.38 ± 1.6	0.3	
Teahitia	TH09-05	OIB	Basalt	0	1.35 ± 1.6	0.1	
	TH12-06	OIB	Basalt	0	0.51 ± 1.6	0.8	
	TH14-02	OIB	Basalt	0	-0.23 ± 1.6	0.4	
	TH14-03-4	OIB	Basalt	0	1.46 ± 1.6	0.8	
	TH14-03-5	OIB	Basalt	0	7.97 ± 1.3	2.3	
	TH14-05	OIB	Basalt	0	4.05 ± 1.3	0.6	
Mehetia	TH10-04	OIB	Basalt	0	0.45 ± 1.6	0.9	

Continued on next page

Table A.1 – continued from previous page

Reference	Sample	Setting	Rock	Age	δ^{15}N	[N]	δ^{13}C
Cyana	SO47-81DS	OIB	Basalt	0	5.31 ± 1.6	0.06	
	TH25-03-4	OIB	Basalt	0	3.58 ± 1.3	0.01	
Rocard	SO47-34DS	OIB	Basalt	0	4.51 ± 1.3	1.8	
	TH21	OIB	Basalt	0	2.85 ± 1.6	0.04	
Seamount1	DTH02-01-1	OIB	Basalt	0	6.71 ± 1.6	0.06	
	DTH02-01-2	OIB	Basalt	0	6.13 ± 1.8	0.07	
	DTH02-01-3	OIB	Basalt	0	0.4 ± 1.8	0.05	
	DTH02-01-4	OIB	Basalt	0	3.51 ± 1.6	0.13	
	DTH02-01-5	OIB	Basalt	0	2.28 ± 1.3	0.03	
	DTH02-02-1	OIB	Basalt	0	3.38 ± 1.6	0.11	
	DTH02-02-2	OIB	Basalt	0	4.18 ± 1.2	0.07	
Seamount2	DTH03-02	OIB	Basalt	0	1.33 ± 1.3	0.03	
Seamount3	DTH04-01-1	OIB	Basalt	0	5.77 ± 1.6	0.08	
	DTH04-01-2	OIB	Basalt	0	3.46 ± 1.7	0.10	
	DTH04-01-3	OIB	Basalt	0	1.39 ± 1.7	0.06	
Seamount4	DTH05-02	OIB	Basalt	0	3.96 ± 1.3	0.002	
Cook-Austral	TH28-07	OIB	Basalt	0	2.63 ± 1.7	0.02	
MacDonald	TH30-03	OIB	Basalt	0	1.82 ± 1.6	2.30	
Hawaii	T4D3#3	OIB	Basalt	0	2.07 ± 1.3	0.29	
Loihi	T4D3#7	OIB	Basalt	0	1.72 ± 1.3	0.08	
East pacific rise	G324G	OIB	Basalt	0	3.08 ± 1.3	0.04	
	G296G	OIB	Basalt	0	1.6 ± 1.3	0.01	
	G136D	OIB	Basalt	0	1.4 ± 1.3	0.09	
	G178D	OIB	Basalt	0	1.55 ± 1.3	0.01	
Iceland	DICE10-10	OIB	Basalt	0	0.23 ± 1.8	0.03	
	DICE10-10	OIB	Basalt	0	0.02 ± 1.8	0.04	
	DICE10-10	OIB	Basalt	0	0.12 ± 1.9	0.07	
	DICE11-10#	OIB	Basalt	0	-0.6 ± 1.9	0.05	
	DICE11-10#	OIB	Basalt	0	-1.5 ± 1.8	0.07	
	DICE11-10#	OIB	Basalt	0	3.26 ± 1.8	0.02	
Jia et al.-2003	CP60/93	M	Lamproite	0.1	4.4	163	
Lamprolite = L	B-4	M	Lamproite	0.1	3.9	88	
Lamprophyre = LP	SD-1	M	Lamproite	0.1	4.3	209	
	SD-2	M	Lamproite	0.1	6.2	63	
	SD-3	M	Lamproite	0.1	1.5	232	
	P-1	M	Lamproite	0.1	1.6	277	
	P-2	M	Lamproite	0.1	2.2	294	
	M2/1	M	Lamproite	0.1	4.1	119	
	M-2/2	M	Lamproite	0.1	5.5	394	
	KH-1	M	Lamprophyre	0.1	1.6	82	
	KH-2	M	Lamprophyre	0.1	3.3	371	
	R839A	M	Lamproite	0.1	8.7	21	
Glasmacher et al.-2003	C-M-t	MOS	Slate	0.485		500	
	C-M-m	MOS	Slate	0.485		600	
	C-M-b	MOS	Slate	0.485		700	
	M-I-M	MOS	Slate	0.485		200	
	T-M	MOS	Slate	0.485		400	
Sadofsky and Bebout 2004	1	OS	Clay	0.01	8.2	330	
N from Izu-Bonin-Mariana Arc	3	OS	Clay	0.01	6.1	371	
Oceanic Drilling Project	6	OS	Clay	0.01	6.7	350	
Sites 1149 (35) 800 (6) 801(8) 802(2)	26	OS	Clay	0.01	6.1	462	

Continued on next page

Table A.1 – continued from previous page

Reference	Sample	Setting	Rock	Age	δ^{15}N	[N]	δ^{13}C
Sample names are core depths (m)	27	OS	Clay	0.01	6.2	448	
	28	OS	Clay	0.01	6.1	508	
	39	OS	Clay	0.01	5.8	395	
	40	OS	Clay	0.01	5.7	366	
	45	OS	Clay	0.01	6.3	383	
	56	OS	Clay	0.01	5.7	355	
	58	OS	Clay	0.01	5.5	103	
	66	OS	Clay	0.01	5.5	416	
	75	OS	Clay	0.01	5.3	383	
	85	OS	Clay	0.01	5.3	295	
	93	OS	Clay	0.01	4.8	365	
	104	OS	Clay	0.01	5.0	400	
	113	OS	Clay	0.01	4.7	281	
	121	OS	Clay	0.01	4.7	240	
	135	OS	Clay	0.01	3.9	281	
	142	OS	Clay	0.01	3.7	214	
	1515	OS	Clay	0.01	4.6	329	
	160	OS	Clay	0.01	4.7	340	
	161	OS	Clay	0.01	4.9	335	
	165	OS	Clay	0.01	4.5	285	
	171	OS	Clay	0.01	4.9	259	
	180	OS	Clay	0.01	4.6	97	
	196	OS	Clay	0.01	4.6	236	
	237	OS	Chert	0.01	2.5	26	
	341	OS	Chert	0.01	3.0	18	
	388	OS	Chert	0.01	4.0	23	
	248	OS	Siltstone	0.01	-0.9	661	
	465	OS	Clay	0.01	-0.2	37	
	444	OS	S and stone	0.01	3.9	78	
	342	OS	Clay	0.01	4.5	127	
	422	OS	Clay	0.01	4.2	116	
Ueno et al.-2004	T005	AOS	Kerogen	3.5	-4.1 ± 0.2		-34.8
Kerogens from Australia	T013B	AOS	Kerogen	3.5	1.78 ± 1.5		-34.6
North Pole	T070B	AOS	Kerogen	3.5	3.98 ± 1.6		-35.9
	96NP452	AOS	Kerogen	3.5	0.98 ± 1.2		-37.2
	Panp E296a	AOS	Kerogen	3.5	-3.37 ± 0.1		-33.1
	Pano E299aB	AOS	Kerogen	3.5	-2.78 ± 1.3		-34.2
Brauer et al.-2004	Bublak	VV	Gas	0	-3.7 ± 0.7	0	-2.0
Gas from mineral springs	Brambach	VV	Gas	0	-0.57 ± 0.3	0	-4.3
on the Czech German border	Elster	VV	Gas	0	-0.88 ± 0.2	19	-4.2
	Schonbrunn	VV	Gas	0	-1.16 ± 0.2	97	-16.4
Papineau et al.-2005	MS-2	MOS	Mica	1.2	16.04 ± 2.2	1139	
Biotites from metasedi- ments	MS-4	MOS	Mica	1.2	10.22 ± 1.6	1300	
MS= Moine, Scotland	FIK-97-7	MOS	Mica	1.9	4.94 ± 2	525	
FIK/FISIJ=Finland	FIK-97-11	MOS	Mica	1.9	7.78 ± 1.5	497	
GR = Isua	FISIJ-2-15415	MOS	Mica	1.9	19.72 ± 1	189	
	GR97im45	MOS	Mica	3.8	10.7 ± 1.6	232	
	GR97im46	MOS	Mica	3.8	12.69 ± 1.5	181	
	GR97im47	MOS	Mica	3.8	12.7 ± 1.5	224	
	GR9817	MOS	Mica	3.8	-1.85 ± 1.3	333	
van-Zuilen et al.-2005	6.4D2 P	MOS	Graphite	3.76	1.79 ± 0.8	9	

Continued on next page

Table A.1 – continued from previous page

Reference	Sample	Setting	Rock	Age	δ^{15}N	[N]	δ^{13}C
Isua metasedi-ments.	6.4D2 C	MOS	Graphite	3.76	1.58 ± 0.7	2	
Mostly graphite	AL43-3 P	MOS	Graphite	3.76	1.04 ± 0.5	4	
	AL43-3 C	MOS	Graphite	3.76	1.91 ± 0.8	0.77	
	6.4D1 P	MOS	Graphite	3.76	2.58 ± 3.5	0.60	
	6.4D1 C	MOS	Graphite	3.76	-3.66 ± 1.3	8.2	
	6.3A2 P	MOS	Graphite	3.76	6.4 ± 1.8	2.7	
	6.3A2 C	MOS	Graphite	3.76	-2.79 ± 1.2	6.0	
	23	OS	Clay	0.01	5.0	289	
Pitcairn et al.-2005	B14	MOS	Schist	0.14	5.1	279	
Mica and Whole Rock	B30	MOS	Schist	0.14	1.3	128	
New Zealand	B14	MOS	Muscovite	0.14	4.1	163	
I show analyses	B30	MOS	Muscovite	0.14	3.6	206	
where there are	C90	MOS	Schist	0.14	4.2 ± 0.5	428	
both mica and	C90	MOS	Muscovite	0.14	4.9 ± 1.1	1061	
whole rock	B82	AOS	Schist	0.14	4.5	138	
	B82	AOS	Mica	0.14	7.0	245	
	B92	MOS	Schist	0.14	0.9	249	
	B92	MOS	Mica	0.14	2.0	278	
	C50	MOS	Schist	0.14	2.9	119	
	C50	MOS	Mica	0.14	4.3	459	
	C66	MOS	Schist	0.14	2.0	459	
	C66	MOS	Mica	0.14	1.3	421	
Busigny et al.-2005	MS#5	MOS	Schist	1.2	14.9	245	
Methods that	SL98-3P	MOS	Schist	0.14	3.7	1637	
also measure some schists	98SE9	MOS	Schist	0.14	4.4	523	
and oceanic lithosphere	90-25B	MOS	Schist	0.14	4.8	195	
Li and Bebout-2005	0.21	OS	S and stone	0.005	7.0	1296	2.5
ODP leg 170 Central American	1.42	OS	S and stone	0.005	6.3	1283	
Margin.	3.73	OS	S and stone	0.005	7.4	2382	
Sample names are core depths	6.66	OS	Chert	0.005	6.7	2081	
	8.38	OS	Chert	0.005	6.9	2262	
Chert=diatomaceous ooze	10.15	OS	Chert	0.005	7.6	2270	
	14.37	OS	Chert	0.005	5.7	1680	
	18.66	OS	Chert	0.005	6.2	1979	
Site 1039—¿	21.86	OS	Chert	0.005	5.2	2221	
	25.55	OS	Chert	0.005	7.7	1210	
	28.93	OS	Chert	0.005	6.9	1673	
	32.77	OS	Chert	0.005	5.7	1763	
	36.38	OS	Chert	0.005	5.3	1610	
	40.5	OS	Chert	0.005	7.0	1395	
	45.83	OS	Chert	0.005	6.2	1157	
	50.7	OS	Chert	0.005	4.4	1107	
	55.39	OS	Chert	0.005	6.3	1191	
	60	OS	Chert	0.005	5.0	1121	
	64.87	OS	Chert	0.005	6.0	790	
	69.99	OS	Chert	0.005	5.1	1619	
	174.41	OS	Chert	0.005	5.6	951	
	80	OS	Chert	0.005	5.4	1168	
	83.91	OS	Chert	0.005	6.4	717	
	89.99	OS	Siltstone	0.005	5.9	780	2.6
	94.88	OS	Siltstone	0.005	5.3	1075	

Continued on next page

Table A.1 – continued from previous page

Reference	Sample	Setting	Rock	Age	δ^{15}N	[N]	δ^{13}C
	100.2	OS	Siltstone	0.005	5.6	1042	
	106.91	OS	Siltstone	0.005	6.1	909	3.2
	112.33	OS	Siltstone	0.005	4.7	981	
	117.43	OS	Siltstone	0.005	6.2	749	
	120.37	OS	Siltstone	0.005	6.2	792	
	126.76	OS	Siltstone	0.005	6.9	699	
	131.55	OS	Siltstone	0.005	6.8	633	
	136.54	OS	Clay	0.005	6.0	866	
	146.08	OS	Clay	0.005	7.9	361	0.1
	147.64	OS	Clay	0.005	8.2	499	1.0
	152.67	OS	Clay	0.005	5.6	804	
	157.22	OS	Clay	0.005	6.1	406	0.3
	162.09	OS	Clay	0.005	8.5	403	1.3
	168.44	OS	Clay	0.005	6.1	358	1.3
	173.46	OS	Clay	0.005	7.6	519	1.3
	177.93	OS	Clay	0.005	7.2	344	1.2
	187.52	OS	Clay	0.005	4.2	110	2.2
	197.12	OS	Clay	0.005	5.0	99	1.5
	206.83	OS	Chert	0.005	5.4	62	1.5
	216.41	OS	Chert	0.005	3.4	76	1.6
	223.01	OS	Chert	0.005	3.4	105	2.0
	234.23	OS	Chert	0.005	3.1	79	1.9
	252.02	OS	Chert	0.005	2.9	78	1.9
	261.72	OS	Chert	0.005	3.5	66	2.9
	269.93	OS	Chert	0.005	3.2	106	2.3
	279.48	OS	Limestone	0.005	3.3	143	2.2
	289.17	OS	Limestone	0.005	3.8	100	2.2
	309.89	OS	Limestone	0.005	3.1	72	2.5
	319.47	OS	Limestone	0.005	4.5	62	2.3
	2332.08	OS	Limestone	0.005	3.9	85	1.9
	348.26	OS	Limestone	0.005	2.4	196	2.4
	360.87	OS	Limestone	0.005	5.0	96	2.2
	371.97	OS	Limestone	0.005	3.6	141	2.0
	374.06	OS	Limestone	0.005	8.0	576	2.3
	365.65	OS	Limestone	0.005	5.1	85	1.9
	384.94	OS	Limestone	0.005	4.3	144	2.2
	393.19	OS	Limestone	0.005	4.0	119	2.1
	401.57	OS	Limestone	0.005	4.0	130	2.0
	416.95	OS	Limestone	0.005	3.5	148	1.4
	421.62	OS	Limestone	0.005	4.2	67	1.0
Busigny et al.-2005a	09-02WR	MOL	Gabbro	0.14	7.4	4.40	
	ETF7	MOL	peridotite	0.14	9.4	2.00	
	16R-1	AOL	Basalt	0.01	3.6	2.80	
Tappert et al.-2005	P	D	Peridotitic	0.0856		500	-5.0
Diamonds	E	D	Eclogitic	0.0856		700	-15.0
P=peridotitic E=eclogitic S=sublithospheric	S	D	S	0.0856		60	-20.0
Krooss et al.-2005	Parchim	OS	Shale	0.31		600	
Carboniferous Shales from Germany	Parchim	OS	Shale	0.31		1140	
	Parchim	OS	Shale	0.31		1030	
	Parchim	OS	Shale	0.31		760	
	Parchim	OS	Shale	0.31		1160	
	Eldena	OS	Shale	0.31		4090	
	Prottlin	OS	Shale	0.31		1180	
	Prottlin	OS	Shale	0.31		2660	
	Prottlin	OS	Shale	0.31		3090	
	Prottlin	OS	Shale	0.31		1050	
	Prottlin	OS	Shale	0.31		1260	
	Prottlin	OS	Shale	0.31		1270	
	Prottlin	OS	Shale	0.31		1470	
	Prottlin	OS	Shale	0.31		1200	
	Prottlin	OS	Shale	0.31		1410	
	Prottlin	OS	Shale	0.31		2550	

Continued on next page

Table A.1 – continued from previous page

Reference	Sample	Setting	Rock	Age	δ^{15}N	[N]	δ^{13}C
	Prottlin	OS	Shale	0.31		2080	
	Loissin	OS	Shale	0.31		570	
	Loissin	OS	Shale	0.31		1350	
	Loissin	OS	Shale	0.31		1280	
	Loissin	OS	Shale	0.31		1130	
	Loissin	OS	Shale	0.31		1100	
	Grimmen	OS	Shale	0.31		640	
	Grimmen	OS	Shale	0.31		6940	
	Hundisburg	OS	Shale	0.31		520	
	Dranske	OS	Shale	0.31		8220	
	Schwalmtal	OS	Shale	0.31		710	
	Schwalmtal	OS	Shale	0.31		1050	
	Schwalmtal	OS	Shale	0.31		970	
	Schwalmtal	OS	Shale	0.31		2350	
	Liaohe China	OS	Buddingtonite	0.31		17130	
	Ruhr Germ.	OS	Shale	0.31		1810	
	Ruhr Germ.	OS	Shale	0.31		530	
Busigny et al.-2005b	4R-1	AOL	MORB	0.02	3.1	9.8	
Listed as core section	8R-1	AOL	MORB	0.02	5.8	2.4	
	9R-4	AOL	MORB	0.02	5.8	3.2	
	12R-8	AOL	MORB	0.02	3.9	2.1	
	16R-1	AOL	MORB	0.02	3.7	2.8	
	22R-2	AOL	MORB	0.02	4.3	2.0	
	24R-1	AOL	MORB	0.02	3.6	3.0	
	26R-6	AOL	MORB	0.02	9.1	3.9	
	27R-1	AOL	MORB	0.02	3.0	3.2	
	32R-1	AOL	MORB	0.02	4.9	3.2	
	37R-1	AOL	MORB	0.02	2.8	1.8	
	41R-2	AOL	MORB	0.02	3.9	2.7	
	47R-2	AOL	MORB	0.02	3.6	3.1	
	52R-1	AOL	MORB	0.02	5.0	3.4	
	57R-2	AOL	MORB	0.02	-2.7	9.7	
	57R-3	AOL	MORB	0.02	-3.8	8.6	
	57R-4	AOL	MORB	0.02	3.4	4.3	
	67R-1	AOL	MORB	0.02	6.1	5.9	
	69R-1	AOL	MORB	0.02	2.6	3.8	
	74R-2	AOL	MORB	0.02	1.6	1.4	
	BAS-206	AOL	MORB	0.02	2.1	1.6	
Kerrich et al.-2006	Mangambeta	AOS	Shale	1.8	6 ± 0.6	442	
	Marcapur	MCS	Shale	1.8	3.9 ± 0.5	347	
India. Avgs. of	Bhimangundi	MCS	Shale	2.7	3.5 ± 0.9	841	
several locations	Vibutigudda	MCS	Shale	2.7	13.1 ± 1.3	73	
Kerrich et al.-2006	Kidd Creek	MCL	Mica	2.7	17.5	14	
	Ansil	MCL	Mica	2.7	14.4	21	
	Matagami	MCL	Mica	2.7	17.1	26	
	Jerome	MCL	Mica	1.8	12.7	37	
	Kolar	MCL	Gold	2	18.0	32	
	Mangambeta	ACL	Kerogen	1	6 ± 0.6	442	-30.5
	Marcapur	ACL	Kerogen	1	3.9 ± 0.5	347	-28.3
	Bhimangundi	ACL	Kerogen	2	3.5 ± 0.9	841	-32.0
	Vibutigudda	ACL	Kerogen	2	13.1 ± 1.3	73	-27.3
Elkins et al.-2006	Mombacho	VV	Gas/Fluid	0	0.5 ± 0.8		
Central American volcanics	Mombacho	VV	Gas/Fluid	0	-2.2 ± 0.8		
	Masaya	VV	Gas/Fluid	0	1.2 ± 0.1		
	Masaya	VV	Gas/Fluid	0	3 ± 0.1		
	Masaya	VV	Gas/Fluid	0	4.9 ± 0.6		
	Momotombo	VV	Gas/Fluid	0	2.1 ± 0.1		
	Momotombo	VV	Gas/Fluid	0	5.3 ± 0.1		
	Momotombo	VV	Gas/Fluid	0	4.9 ± 0.5		
	Momotombo	VV	Gas/Fluid	0	6.9 ± 0.5		
	Momotombo	VV	Gas/Fluid	0	-2.3 ± 0.2		

Continued on next page

Table A.1 – continued from previous page

Reference	Sample	Setting	Rock	Age	δ^{15}N	[N]	δ^{13}C
	Cerro Negro	VV	Gas/Fluid	0	-0.6 ± 0.2		
	Cerro Negro	VV	Gas/Fluid	0	0.4 ± 0.2		
	Cerro Negro	VV	Gas/Fluid	0	4.9 ± 0.1		
	Telica	VV	Gas/Fluid	0	3.2 ± 0.1		
	Telica	VV	Gas/Fluid	0	2.3 ± 0.1		
	San Cristobal	VV	Gas/Fluid	0	-0.5 ± 0.1		
	San Cristobal	VV	Gas/Fluid	0	0.1 ± 0.2		
	Cosegunia	VV	Gas/Fluid	0	-1.7 ± 0.2		
Jia-2006	Low grade	AOS	Slate	0.44	2 ± 0.7	120	
	Chlorite	MOS	Schist	0.44	2.9 ± 0.6	110	
	Biotite	MOS	Schist	0.44	3.1 ± 0.5	86	
	and alusite	MOS	Gneiss	0.44	3.8 ± 1.2	81	
	Sillimanite	MOS	Gneiss	0.44	10.4 ± 1.5	43	
	Migmatite	MOS	Gneiss	0.44	10.6 ± 1.5	41	
Westerlund et al.-2006	PD2	D	Peridotitic	3.55		537	
	PD3	D	Peridotitic	3.55		506	
	PD4	D	Peridotitic	3.55		516	
	PD5	D	Peridotitic	3.55		477	
	PD6	D	Peridotitic	3.55		419	
	PD7	D	Peridotitic	3.55		273	
	PD9	D	Peridotitic	3.55		384	
	PD10	D	Peridotitic	3.55		292	
Li et al.-2007	41R1 26-30	OL	MORB	0.17	0.7	7.8	
ODP Legs 129 and 185	43R1 22-27	OL	MORB	0.17	0.2	9.5	
Site 801 NW Pacific	43R1 132-135	OL	MORB	0.17	-3.0	2.8	
	1R1 109-141	OL	MORB	0.17	-1.6	7.5	
	1R5 80-82	OL	MORB	0.17	-4.9	2.4	
	4R1 72-77	AOL	MORB	0.17	0.0	3.0	
	5R2 12-17	AOL	MORB	0.17	0.5	13	
	5R2 123-130	AOL	MORB	0.17	0.9	17	
	5R3 99-104	AOL	MORB	0.17	1.2	16	
	5R3 125-131	AOL	MORB	0.17	0.7	15	
	7R3 0-5	AOL	MORB	0.17	0.1	12	
	8R1 18-21	AOL	MORB	0.17	0.7	18	
	8R1 65-67	AOL	MORB	0.17	-0.2	9.3	
	10R6 67-70	AOL	MORB	0.17	0.5	6.7	
	11R2 131-136	AOL	MORB	0.17	-0.1	6.7	
	12R1 101-104	AOL	MORB	0.17	1.0	14	
	12R3 57-62	AOL	MORB	0.17	0.9	4.8	
	15R1 57-61	AOL	MORB	0.17	-2.3	1.5	
	15R7 31-34	AOL	MORB	0.17	-0.4	3.4	
	17R4 15-18	AOL	MORB	0.17	-11.4	3.0	
	19R2 24-27	AOL	MORB	0.17	-6.8	1.8	
	21R2 69-71	AOL	MORB	0.17	-6.3	2.8	
	25R1 10-13	AOL	MORB	0.17	-7.0	2.3	
	34R1 93-96	OL	MORB	0.17	-3.9	1.3	
	37R5 112-114	AOL	MORB	0.17	-3.1	2.5	
	40R1 24-27	AOL	MORB	0.17	-11.6	3.6	
	43R1 13-15	AOL	MORB	0.17	-9.4	3.8	
	43R3 50-55	OL	MORB	0.17	-3.0	2.3	
	44R3 23-26	AOL	MORB	0.17	-5.9	2.4	
	TAB FLO	AOL	MORB	0.17	-7.9	3.8	
	TAB VCL	OL	MORB	0.17	-2.0	6.0	
	TAB MIX	OL	MORB	0.17	-2.5	5.0	
	MORB 0-110 FLO	OL	MORB	0.17	-6.2	3.8	
	MORB 0-110 MIX	OL	MORB	0.17	-7.1	4.9	
	MORB 110-220 FLO	OL	MORB	0.17	-4.1	2.3	

Continued on next page

Table A.1 – continued from previous page

Reference	Sample	Setting	Rock	Age	δ^{15}N	[N]	δ^{13}C
	MORB 110-220 VCL	OL	MORB	0.17	-9.4	4.2	
	MORB 110-220 MIX	OL	MORB	0.17	-6.2	3.6	
	MORB 220-420 FLO	OL	MORB	0.17	-5.0	2.7	
	MORB 220-420 VCL	OL	MORB	0.17	-10.2	3.5	
	MORB 220-420 MIX	OL	MORB	0.17	-6.6	4.4	
	SUPER	OL	MORB	0.17	-5.4	3.9	
	SED	OL	MORB	0.17	-0.5	5.6	
	30R1 61-66	AOL	MORB	0.17	-4.9	1.4	
	30R2 56-62	OL	MORB	0.17	-1.8	2.3	
	10R2 47-51	AOL	MORB	0.17	-2.8	2.7	
	7R1 37-42	AOL	MORB	0.17	-0.8	2.5	
	9R3 30-32	AOL	MORB	0.17	-7.9	2.1	
	11R2 86-92	OL	MORB	0.17	-6.9	1.5	
	16R3 2-8	OL	MORB	0.17	-6.5	1.7	
	17R1 92-98	OL	MORB	0.17	-4.3	1.4	
	19R1 85-89	OL	MORB	0.17	-10.5	2.5	
Other oceans	13R2 0-2	AOL	MORB	0.05	0.5	3.3	
	13R2 16-120	AOL	MORB	0.05	4.2	4.7	
	3R4 50-53	AOL	MORB	0.01	0.1	2.8	
	33R2 77-80	AOL	MORB	0.005	-5.4	7.8	
	15R3 83-89	AOL	MORB	0.005	4.8	12.1	
	38R8 ALT	AOL	MORB	0.1	0.6	14.6	
	44R4 ALT	AOL	MORB	0.1	8.3	11.9	
	33R5 ALT	AOL	MORB	0.1	4.0	10.6	
	41R1 2-7	AOL	MORB	0.05	3.3	6.5	
	61	AOL	MORB	0.05	3.8	11.7	
	33R2 74-77	AOL	MORB	0.15	5.5	13.4	
	66R1 100-102	AOL	MORB	0.15	6.2	15.2	
	22R2 120-124	AOL	MORB	0.17	-0.6	7.6	
	35R1 10-15	AOL	MORB	0.02	-5.1	3.6	
Philippot et al.-2007	DR23-2	MOL	Peridotite	0.04	6.3	2.9	
	DR23-2-8	MOL	Peridotite	0.04	7.5	2.9	
	DR23-3-5	MOL	Peridotite	0.04	6.9	2.0	
	ETF1	MOL	Peridotite	0.04	8.9	5.8	
	ETF2	MOL	Peridotite	0.04	15.0	4.0	
	ETF3	MOL	Peridotite	0.04	11.0	3.9	
	ETF4	MOL	Serpentinite	0.04	11.3	2.6	
	ETF6	MOL	Serpentinite	0.04	10.6	2.8	
	ETF6	MOL	Serpentinite	0.04	9.5	2.0	
	ET09032R	MOL	Serpentinite	0.04	8.9	1.4	
	ET0903V	MOL	Serpentinite	0.04	3.7	5.3	
Quan et al.-2008 organic N from Tr-J boundary core of Mingolsheim Fm.	208.2	AOS	Kerogen	0.201	1.8		-28.0
	208	AOS	Kerogen	0.201	1.8		-27.5
	207.5	AOS	Kerogen	0.201	-0.1		-25.5
	207.3	AOS	Kerogen	0.201	0.4		-26.7
	206.8	AOS	Kerogen	0.201	0.7		-26.3
	206.6	AOS	Kerogen	0.201	0.3		-27.6
	206.4	AOS	Kerogen	0.201	1.8		-27.7
Sample names are core depths	206.2	AOS	Kerogen	0.201	2.1		-27.6
	206	AOS	Kerogen	0.201	0.6		-26.7
	205.45	AOS	Kerogen	0.201	0.6		-26.1
	205.23	AOS	Kerogen	0.201	0.7		-26.1
	205	AOS	Kerogen	0.201	-0.3		-26.1
	204.65	AOS	Kerogen	0.201	0.4		-26.3
	204.3	AOS	Kerogen	0.201	0.2		-26.7

Continued on next page

Table A.1 – continued from previous page

Reference	Sample	Setting	Rock	Age	δ^{15}N	[N]	δ^{13}C
	203.72	AOS	Kerogen	0.201	0.5		-26.5
	202.95	AOS	Kerogen	0.201	1.2		-25.4
	202.75	AOS	Kerogen	0.201	0.5		-25.2
	202.25	AOS	Kerogen	0.201	0.9		-25.1
	202	AOS	Kerogen	0.201	1.0		-25.2
	201.8	AOS	Kerogen	0.201	0.9		-25.5
	201.54	AOS	Kerogen	0.201	1.0		-25.3
	201.3	AOS	Kerogen	0.201	1.1		-25.7
	201.1	AOS	Kerogen	0.201	1.1		-25.4
	200.9	AOS	Kerogen	0.201	0.9		-25.4
	200.7	AOS	Kerogen	0.201	1.0		-25.3
	200.18	AOS	Kerogen	0.201	0.8		-25.6
	200	AOS	Kerogen	0.201	1.5		-29.6
	199.6	AOS	Kerogen	0.201	0.8		-25.7
	199.05	AOS	Kerogen	0.201	0.9		-25.5
	98.56	AOS	Kerogen	0.201	0.7		-26.1
	198.1	AOS	Kerogen	0.201	0.6		-26.2
	198.1	AOS	Kerogen	0.201	0.9		-25.6
	197.3	AOS	Kerogen	0.201	1.5		-27.7
	197.1	AOS	Kerogen	0.201	1.4		-27.7
	196.9	AOS	Kerogen	0.201	1.4		-28.3
	196.5	AOS	Kerogen	0.201	1.3		-27.7
	196.2	AOS	Kerogen	0.201	1.5		-27.6
	195.9	AOS	Kerogen	0.201	1.1		-28.6
	195.7	AOS	Kerogen	0.201	1.1		-27.7
	195.14	AOS	Kerogen	0.201	1.5		-28.1
	194.85	AOS	Kerogen	0.201	1.7		-28.7
	193.75	AOS	Kerogen	0.201	1.8		-27.8
	192.75	AOS	Kerogen	0.201	1.1		-28.2
	191.75	AOS	Kerogen	0.201	1.8		-28.6
	191.25	AOS	Kerogen	0.201	1.7		-29.3
	190.75	AOS	Kerogen	0.201	1.9		-29.9
	190.25	AOS	Kerogen	0.201	2.1		-29.9
	189.25	AOS	Kerogen	0.201	2.2		-29.5
	187.75	AOS	Kerogen	0.201	2.0		-28.9
	186.2	AOS	Kerogen	0.201	1.9		-28.8
Svensen et al.-2008	61.85	AOS	Shale	0.17	5.0	473	
Bulk shales from a	67.85	AOS	Shale	0.17	14.2	1421	
contact aureole,	87.15	AOS	Shale	0.17	14.2	528	
Karoo basin	92.6	AOS	Shale	0.17	4.7	627	
Sample name	94.7	AOS	Shale	0.17	5.3	639	
is core depth	103.6	AOS	Shale	0.17	4.5	783	
	126.75	AOS	Shale	0.17	4.4	802	
	238.3	AOS	Shale	0.17	6.5	1718	
	273.22	AOS	Shale	0.17	12.5	4591	
	322.5	AOS	Shale	0.17	8.2	2626	
	372	AOS	Shale	0.17	11.8	5245	
	393.26	AOS	Shale	0.17	11.1	2013	
	402.11	AOS	Shale	0.17	11.8	2306	
	415.7	AOS	Shale	0.17	12.7	946	
	534.4	AOS	Shale	0.17	14.2	1344	
Schulze et al.-2008	4	D	Eclogitic			400	-9.7
Diamonds from	5	D	Eclogitic			300	-6.8
Yavapai craton	10	D	Peridotitic			920	-6.2
Garvin et al.-2009	109	AOS	Shale	2.5	2.9	400	-35.0
Sample names	110.7	AOS	Shale	2.5	3.6	600	-33.3
are core depths	111	AOS	Shale	2.5	3.6	400	-32.7
McRae Shale	112.52	AOS	Shale	2.5	2.9	500	-34.2
Pilbara Australia	113.46	AOS	Shale	2.5	2.6	900	-35.7

Continued on next page

Table A.1 – continued from previous page

Reference	Sample	Setting	Rock	Age	δ^{15}N	[N]	δ^{13}C
	114.5	AOS	Shale	2.5	4.2	500	-35.5
	116.49	AOS	Shale	2.5	2.6	500	-34.0
	117.31	AOS	Shale	2.5	3.4	300	-33.4
	119.24	AOS	Shale	2.5	4.3	400	-33.9
	120.24	AOS	Shale	2.5	4.5	300	-33.1
	121.2	AOS	Shale	2.5	3.9	400	-34.6
	121.39	AOS	Shale	2.5	3.6	300	-34.1
	122.32	AOS	Shale	2.5	3.7	600	-35.2
	123.32	AOS	Shale	2.5	4.9	300	-35.6
	124.22	AOS	Shale	2.5	5.7	700	-35.3
	126.15	AOS	Shale	2.5	5.0	700	-36.8
	127.25	AOS	Shale	2.5	5.6	800	-36.4
	128.17	AOS	Shale	2.5	5.0	900	-36.8
	129.01	AOS	Shale	2.5	6.2	900	-37.6
	129.55	AOS	Shale	2.5	5.3	1000	-36.7
	132.13	AOS	Shale	2.5	5.2	1100	-38.6
	133.97	AOS	Shale	2.5	6.2	1300	-41.4
	135.58	AOS	Shale	2.5	6.6	900	-41.3
	136.15	AOS	Shale	2.5	5.9	1300	-41.5
	136.67	AOS	Shale	2.5	5.4	1300	-40.7
	137.96	AOS	Shale	2.5	6.1	1400	-39.5
	138.38	AOS	Shale	2.5	6.1	1400	-39.8
	139.01	AOS	Shale	2.5	6.0	1300	-40.2
	139.65	AOS	Shale	2.5	6.7	1400	-40.5
	139.71	AOS	Shale	2.5	7.5		-39.8
	139.97	AOS	Shale	2.5	6.3	1600	-40.5
	140.25	AOS	Shale	2.5	6.5	1600	-40.5
	140.5	AOS	Shale	2.5	6.9	1400	-39.9
	140.95	AOS	Shale	2.5	5.6	1700	-40.1
	141.17	AOS	Shale	2.5	6.6	1600	-40.3
	141.47	AOS	Shale	2.5	5.8	1300	-40.2
	142.08	AOS	Shale	2.5	6.4	1500	-40.3
	143.45	AOS	Shale	2.5	4.7	1100	-38.3
	144.36	AOS	Shale	2.5	5.0	1000	-38.2
	145.61	AOS	Shale	2.5	3.2	1500	-36.7
	146.45	AOS	Shale	2.5	2.7	1400	-36.7
	147.3	AOS	Shale	2.5	4.2	1600	-36.8
	148.27	AOS	Shale	2.5	4.4	1400	-36.8
	149.3	AOS	Shale	2.5	3.9	1500	-36.9
	150.24	AOS	Shale	2.5	3.9	900	-37.0
	152.65	AOS	Shale	2.5	3.9	700	-38.3
	153.08	AOS	Shale	2.5	3.0	600	-39.9
	154.43	AOS	Shale	2.5	4.0	700	-38.4
	156.05	AOS	Shale	2.5	2.8	700	-38.6
	157.8	AOS	Shale	2.5	2.7	500	-39.7
	158.91	AOS	Shale	2.5	1.8	600	-39.0
	161.32	AOS	Shale	2.5	1.3	500	-39.0
	162.8	AOS	Shale	2.5	1.5	400	-38.7
	163.95	AOS	Shale	2.5	1.0	400	-39.3
	165.56	AOS	Shale	2.5	1.7	200	-38.5
	167.76	AOS	Shale	2.5	3.0	100	-37.5
	168.36	AOS	Shale	2.5	2.6	200	-37.8
	168.9	AOS	Shale	2.5	2.1	100	-37.6
	169.28	AOS	Shale	2.5	2.6	300	-38.5
	169.47	AOS	Shale	2.5	3.2	200	-38.6
	169.68	AOS	Shale	2.5	3.8	200	-38.2
	169.94	AOS	Shale	2.5	3.4	200	-38.2
	170.17	AOS	Shale	2.5	3.4	200	-38.1
	170.39	AOS	Shale	2.5	1.5	200	-40.1
	170.55	AOS	Shale	2.5	2.2	200	-38.2
	170.86	AOS	Shale	2.5	2.4	200	-38.5
	170.94	AOS	Shale	2.5	2.8	200	-38.8
	171.22	AOS	Shale	2.5	3.2	200	-38.6
	173.09	AOS	Shale	2.5	2.7	200	-38.5
	173.5	AOS	Shale	2.5	2.8	200	-37.7
	173.73	AOS	Shale	2.5	2.3	200	-38.0
	180.33	AOS	Shale	2.5	2.2		
	181.2	AOS	Shale	2.5	2.5		
	182.5	AOS	Shale	2.5	1.3	400	-38.4

Continued on next page

Table A.1 – continued from previous page

Reference	Sample	Setting	Rock	Age	δ^{15}N	[N]	δ^{13}C
	183.65	AOS	Shale	2.5	2.0	300	
	185.43	AOS	Shale	2.5	2.9	200	-39.4
	188.01	AOS	Shale	2.5	3.2		
	196.36	AOS	Shale	2.5	1.5	300	
	197	AOS	Shale	2.5	1.5	200	
	198.83	AOS	Shale	2.5	3.5		-37.1
	199.26	AOS	Shale	2.5	1.3	400	
	199.93	AOS	Shale	2.5	2.7		-37.0
Godfrey and Falkowski-2009	197.93	AOS	Chert	2.46	10.1	1450	
Sample names are core depths	244.69	AOS	Chert	2.521	4.4	480	
	267.18	AOS	Chert	2.521	10.1	450	
Transvaal area, South Africa 1st group=bulk rock 2nd=kerogen.	279.39	AOS	Chert	2.521	7.6	390	
	292.2	AOS	Dolostone	2.521	4.6	220	
	310.57	AOS	Mudstone	2.521	5.3	520	
	312.83	AOS	Mudstone	2.521	4.6	530	
	322.12	AOS	Mudstone	2.552	4.3	380	
	360.7	AOS	Mudstone	2.552	4.5	530	
	413.63	AOS	Dolostone	2.552	6.7	270	
	482.69	AOS	Dolostone	2.552	3.6	200	
	491.15	AOS	Dolostone	2.552	3.5	160	
	494.2	AOS	Dolostone	2.552	4.2	150	
	499.32	AOS	Dolostone	2.552	7.1	50	
	515.95	AOS	Dolostone	2.552	4.4	230	
	574.76	AOS	Dolostone	2.552	8.5	40	
	606.5	AOS	Dolostone	2.552	5.7	150	
	614.55	AOS	Dolostone	2.552	4.1	260	
	626	AOS	Dolostone	2.552	8.0	80	
	637	AOS	Dolostone	2.552	2.4	270	
	637.7	AOS	Dolostone	2.552	3.4	340	
	640.3	AOS	Dolostone	2.552	2.5	300	
	682.52	AOS	Dolostone	2.568	5.5	190	
	689.1	AOS	Dolostone	2.568			
	721.63	AOS	Dolostone	2.568	2.1	210	
	733.4	AOS	Dolostone	2.568	1.8	700	
	738.95	AOS	Dolostone	2.568	2.4	110	
	743.1	AOS	Dolostone	2.568	3.9	130	
	798.46	AOS	Dolostone	2.568	5.8	250	
	798.5	AOS	Dolostone	2.568	3.7	180	
	871.83	AOS	Microbialite	2.568	3.3	40	
	890.6	AOS	Microbialite	2.568	4.7	130	
	891.25	AOS	Dolostone	2.568	4.0	120	
	892.4	AOS	Dolostone	2.568	8.5	40	
	965.1	AOS	Dolostone	2.568	5.9	200	
	970.75	AOS	Dolostone	2.568	2.9	260	
	974.05	AOS	Dolostone	2.568	4.1	240	
	980.04	AOS	Dolostone	2.568	5.8	230	
	1008	AOS	Dolostone	2.568	3.3	390	
	1012.1	AOS	Dolostone	2.568	4.7	50	
	1019.9	AOS	Dolostone	2.568	2.0	350	
	1029.1	AOS	Dolostone	2.568	3.3	390	
	1035.7	AOS	Dolostone	2.568	2.4	410	
	1036.8	AOS	Dolostone	2.568	3.1	110	
	1047.7	AOS	Dolostone	2.568	3.4	280	
	1077	AOS	Dolostone	2.568	3.8	40	
	1079.9	AOS	Dolostone	2.65	3.3	40	
	1087.8	AOS	Dolostone	2.669	2.6	30	
	1150.9	AOS	Limestone	2.669	3.3	30	
	1155.15	AOS	Limestone	2.669	3.9	70	
	1163	AOS	Limestone	2.669	4.5	60	
	1200.95	AOS	Mudstone	2.669	4.4	40	
	1272.1	AOS	Mudstone	2.669	5.5	40	
	197.93	AOS	Kerogen	2.46	3.1		-33.5

Continued on next page

Table A.1 – continued from previous page

Reference	Sample	Setting	Rock	Age	δ^{15}N	[N]	δ^{13}C
	244.69	AOS	Kerogen	2.521	4.0		
	267.18	AOS	Kerogen	2.521	5.0		-32.8
	279.39	AOS	Kerogen	2.521	2.8		-33.8
	292.2	AOS	Kerogen	2.521	4.5		-34.6
	310.57	AOS	Kerogen	2.521	2.2		-38.7
	312.83	AOS	Kerogen	2.521	3.2		
	322.12	AOS	Kerogen	2.552	2.7		-36.1
	360.7	AOS	Kerogen	2.552	6.0		-32.6
	413.63	AOS	Kerogen	2.552	7.3		-30.2
	482.69	AOS	Kerogen	2.552	2.8		-33.3
	515.95	AOS	Kerogen	2.552	3.9		-28.7
	574.76	AOS	Kerogen	2.552	0.6		-31.5
	637	AOS	Kerogen	2.552	2.2		-38.2
	689.1	AOS	Kerogen	2.568	3.0		
	721.63	AOS	Kerogen	2.568	2.6		-33.8
	798.46	AOS	Kerogen	2.568	3.3		-30.5
	871.83	AOS	Kerogen	2.568	3.2		-37.5
	890.6	AOS	Kerogen	2.568	3.0		-35.2
	965.1	AOS	Kerogen	2.568	4.0		-25.0
	970.75	AOS	Kerogen	2.568	4.2		-35.2
	1008	AOS	Kerogen	2.568	0.9		-36.5
	1019.9	AOS	Kerogen	2.568	2.3		-37.2
	1029.01	AOS	Kerogen	2.568	0.5		-36.9
	1047.7	AOS	Kerogen	2.568	2.3		-35.1
	1077	AOS	Kerogen	2.568	2.5		-35.3
	1200.95	AOS	Kerogen	2.669	3.5		-42.4
Papineau et al.-2009	AB-1	MOS	Shale	1.9	19.1	600	-29.3
Paleoproterozoic	AB-2	MOS	Shale	1.9	17.9	900	-29.2
sediments	AB-3	MOS	Shale	1.9	16.1	1400	-29.4
from India							
Amberi	AB-4	MOS	Shale	1.9	6.6	6400	-29.0
	AB-5	MOS	Shale	1.9	16.9	1900	-29.3
	UV0606	MOS	Shale	1.9	5.6	600	-28.5
	UV0608	MOS	Shale	1.9	-4.7	300	-28.4
	UV0609	MOS	Shale	1.9	2.4	300	-28.9
	UV0610	MOS	Shale	1.9	5.0	300	-29.2
	UV0611	MOS	Shale	1.9	2.3	200	-29.4
	AM0701	MOS	Shale	1.9	6.5	600	-29.2
	AM0702	MOS	Shale	1.9	4.3	500	-29.6
	AM0703	MOS	Shale	1.9	6.0	700	-29.1
	AM0703	MOS	Shale	1.9	6.1	500	-29.4
	AM0705	MOS	Shale	1.9	6.2	400	-29.3
	AM0706	MOS	Shale	1.9	5.7	500	-29.1
	AM0707	MOS	Shale	1.9	1.2	300	-28.8
Lakarwas	BKP-1	MOS	Shale	1.9	28.4	500	-26.3
	KDR-1	MOS	Shale	1.9	8.0	1800	-24.5
	KDR-3	MOS	Shale	1.9	24.6	600	-25.5
	KDR-4	MOS	Shale	1.9	17.3	900	-23.6
	LW-2	MOS	Shale	1.9	5.0	2300	-27.4
Dhamdhar Block	DD-1	MOS	Shale	1.9	21.9	500	-24.1
	DD-3	MOS	Shale	1.9	16.0	300	-23.1
Oda Block	OD-1	MOS	Shale	1.9	12.7	1500	-23.3
Berawas Block	BW-1	MOS	Shale	1.9	12.0	1000	-26.2
	BW-2	MOS	Shale	1.9	12.6	900	-25.0
Umra	UM-1	MOS	Shale	1.9	11.2	1900	-15.1
	UM-2	MOS	Shale	1.9	9.3	2000	-14.1
	UM-3	MOS	Shale	1.9	10.0	1100	-17.0
	UM-4	MOS	Shale	1.9	10.6	1000	-16.5
	UM-5	MOS	Shale	1.9	9.8	1000	-18.6
	UM-6	MOS	Shale	1.9	12.4	1000	-17.8
Ghasiar	GH-1	MOS	Shale	1.9	8.7	1700	-25.5
	GH-2	MOS	Shale	1.9	6.7	2000	-25.3
	GH-4	MOS	Shale	1.9	6.5	2100	-25.6
	GH-5	MOS	Shale	1.9	10.0	1600	-25.4
	GH-7	MOS	Shale	1.9	11.1	700	-21.1
	GH-8	MOS	Shale	1.9	7.6	1700	-21.8

Continued on next page

Table A.1 – continued from previous page

Reference	Sample	Setting	Rock	Age	δ^{15}N	[N]	δ^{13}C
	GH-9	MOS	Shale	1.9	6.2	1200	-15.7
	GH-10	MOS	Shale	1.9	11.6	500	-22.5
	GH-11	MOS	Shale	1.9	6.0	2000	-28.3
	GH-12	MOS	Shale	1.9	8.5	600	-28.5
	GH-13	MOS	Shale	1.9	12.8	800	-28.1
	GH-14	MOS	Shale	1.9	8.0	1300	-28.4
	GH-15	MOS	Shale	1.9	10.5	400	-28.1
Rama	RM-1	MOS	Shale	1.9	6.7	5100	-16.1
	RM-2	MOS	Shale	1.9	6.2	9000	-16.4
	RM-3	MOS	Shale	1.9	6.5	5100	-16.0
	RM-4	MOS	Shale	1.9	9.3	6100	
	RM-5	MOS	Shale	1.9	10.0	2100	-17.0
Mohapatra et al.-2009	FVB03	OIB	Olivine	0	7.1 ± 1.2	2.2	
Ocean Island Basalts	LP01	OIB	Olivine	0	4.1 ± 0.8	0.8	
	Dice 2	OIB	Basalt	0	3.6 ± 1.2	4.0	
	Dice 12	OIB	Basalt	0	10.6 ± 3.1	5.0	
	Chisny	OIB	Harzburgite	0	-0.6 ± 1	1.5	
	DRE	OIB	Xenolith	0	-9.8 ± 2.7	2.2	
	ILR	OIB	Dunite	0	-9.6 ± 3.4	1.3	
	REF2	OIB	Xenolith	0	-4.9 ± 2.2	4.8	
	REF3-1	OIB	Xenolith	0	-9.3 ± 1.5	0.7	
	REF3-2	OIB	Xenolith	0	3.3 ± 1.1	4.0	
	REF3-3	OIB	Xenolith	0	6.2 ± 2.4	4.0	
	Samoa	OIB	Olivine	0	-10.7 ± 0.4	2.2	
Yokochi et al.-2009	JK7B	X	Lherzolite		9.2 ± 0.5	0.37	
Total N2 released above 900 deg. C	JK7U	X	Lherzolite		12.3 ± 0.5	0.44	
	JK8B	X	Lherzolite		9.4 ± 0.6	0.57	
	BA8U	X	Lherzolite		7.9 ± 0.5	0.83	
	MM2B	X	Harzburgite		9.4 ± 0.2	0.01	
	MM2U	X	Harzburgite		4.4 ± 0.8	0.09	
	MM13C	X	Clinopyroxene		9.1 ± 1	0.24	
	MM13-W	X	Lherzolite		0.4 ± 0.9	0.23	
	MM13-M	X	Amphibole		6.8 ± 0.5	0.64	
	DU25	X	Harzburgite		7.1 ± 0.8	0.05	
	DU25U	X	Harzburgite		3.7 ± 0.8	0.19	
	DU24P	X	Phlogopite		-20.1 ± 1.7	7.6	
	DU24H	X	Phlogopite		-17.3 ± 0.6	17	
	DU24O	X	Olivine		8.1 ± 0.6	0.10	
	DU24C	X	Clinopyroxene		2.9 ± 0.7	0.12	
	DU24B	X	Wehrlite		-7.3 ± 0.8	0.50	
	DU26B	X	Wehrlite		-5 ± 0.5	0.16	
	DU26P	X	Phlogopite		-2.8 ± 0.6	26	
	F100P	X	Phlogopite		3.6 ± 0.7	17	
	F100B	X	Harzburgite		6.4 ± 0.1	0.25	
	F100A	X	Amphibole		5 ± 0.6	6.96	
Yui et al.-2009	C-63	AOS	Slate	0.05	3.2	996	
	C-60	AOS	Schist	0.05	5.3	535	
	C-59	MOS	Schist	0.05	5.0	667	
	C-55	MOS	Schist	0.05	5.1	1143	
	C-49	MOS	Schist	0.05	5.6	584	
	C-46	MOS	Schist	0.05	3.1	998	
	C-43	AOS	Slate	0.05	3.3	1026	
	C-41	AOS	Slate	0.05	2.3	630	
	C-38	AOS	Slate	0.05	3.1	1025	
	C-35	MOS	Schist	0.05	3.4	1142	
	C-33	MOS	Schist	0.05	3.4	1136	
	C-31	MOS	Schist	0.05	3.2	880	
	C-27	MOS	Schist	0.05	2.9	784	
	C-25	MOS	Schist	0.05	1.4	400	
	C-23	MOS	Schist	0.05	1.0	400	
	C-20	MOS	Schist	0.05	2.6	332	
	C-14	MOS	Schist	0.05	1.8	327	
	S-1	AOS	Shale	0.05	3.3	585	

Continued on next page

Table A.1 – continued from previous page

Reference	Sample	Setting	Rock	Age	δ^{15}N	[N]	δ^{13}C
	S-5	AOS	Shale	0.05	3.8	725	
	S-6	AOS	Shale	0.05	3.9	953	
	S-8	AOS	Shale	0.05	4.0	593	
	S-15	AOS	Shale	0.05	4.0	776	
	S-17	AOS	Shale	0.05	3.8	1192	
	S-28	AOS	Shale	0.05	4.3	784	
	s-34	AOS	Shale	0.05	3.9	972	
	s-43	AOS	Shale	0.05	3.9	779	
	s-49	AOS	Shale	0.05	4.1	774	
	s-65	AOS	Shale	0.05	3.6	745	
	s-72	MOS	Slate	0.05	4.5	618	
	s-78	MOS	Slate	0.05	3.4	889	
	s-81	MOS	Slate	0.05	4.5	636	
	s-87	MOS	Slate	0.05	3.9	736	
	S-120	MOS	Schist	0.05	4.0	890	
	S-137	MOS	Schist	0.05	3.6	758	
	S-152	MOS	Schist	0.05	3.5	797	
	S-184	MOS	Schist	0.05	2.8	1109	
	S-188	MOS	Schist	0.05	4.6	1014	
	S9190	MOS	Schist	0.05	5.5	728	
	S-194	MOS	Schist	0.05	4.1	379	
	S-196	MOS	Schist	0.05	1.4	105	
	S-200	MOS	Schist	0.05	3.7	227	
	S-201	MOS	Schist	0.05	3.7	225	
	S-203	MOS	Schist	0.05	3.9	166	
	S-204	MOS	Schist	0.05	3.8	1028	
	S-205	MOS	Schist	0.05	4.4	764	
Burgess et al.-2009	1	D	Fibrous	3.55	-3.1 ± 0.6	1136	-6.9
	2	D	Fibrous	3.55	-8.8 ± 0.5	1352	-5.3
	4	D	Fibrous	3.55	-2.3 ± 0.5	1899	-5.1
	5	D	Fibrous	3.55	-2.3 ± 0.7	775	-5.2
	9	D	Fibrous	3.55	-4.1 ± 0.7	418	-5.5
	10	D	Fibrous	3.55	-1.2 ± 0.5	1872	-6.2
	11	D	Fibrous	3.55	-1.7 ± 0.6	1222	-4.5
Pontes et al.-2009	S and stone 1	CS	S and stone			624	
	S and stone 2	CS	S and stone			181	
	S and stone 3	CS	S and stone			553	
Halama et al.-2010	Blueschist	MOL	Blueschist	0.15	5.7	24.0	
High pressure ophiolites	Eclogite	MOL	Eclogite	0.15	5.3	6.9	
Raspas Complex Ecuador	Zoisite eclogite	MOL	Eclogite	0.15	7.9	12.5	
Lago di Cignana Italy	Serpezd perid.	MOL	peridotite	0.15	5.2	9.3	
Zambezi Belt Zambia	Eclogite	MOL	Eclogite	0.041	1.5	7.9	
Cabo Ortegal Spain	Gabbro	MOL	Gabbro	0.6	6.9	3.7	
	Eclogite	MOL	Eclogite	0.6	2.9	3.8	
Averages shown	Eclogite	MOL	Eclogite	0.39	5.1	4.4	
	Serpezd perid.	MOL	peridotite	0.39	5.7	4.3	
Plessen et al.-2010	1	MOS	Schist	0.4	5.5	760	
Shown are measure-ments of	2	MOS	Schist	0.4	4.6	346	

Continued on next page

Table A.1 – continued from previous page

Reference	Sample	Setting	Rock	Age	δ^{15}N	[N]	δ^{13}C
total N. Most is NH4 but there are small amounts of organic	3	MOS	Schist	0.4	6.3	339	
	4	MOS	Schist	0.4	5.7	393	
	5	MOS	Schist	0.4	4.6	323	
	6	MOS	Schist	0.4	4.0	299	
	7	MOS	Schist	0.4	5.9	307	
	8	MOS	Schist	0.4	8.4	279	
	1	MOS	Biotite	0.4	6.1	2750	
	2	MOS	Biotite	0.4	6.7	2027	
	3	MOS	Biotite	0.4	5.7	1644	
	4	MOS	Biotite	0.4	4.7	1437	
	5	MOS	Biotite	0.4	4.1	1484	
	6	MOS	Biotite	0.4	4.6	1472	
	7	MOS	Biotite	0.4	5.2	1398	
	7'	MOS	Biotite	0.4	6.4	1391	
	8	MOS	Biotite	0.4	7.7	749	
	8'	MOS	Biotite	0.4	6.8	670	
	9	MOS	Biotite	0.4	6.9	218	
Thomazo et al.-2011	S	AOS	Stromatolite	2.72	23 ± 1.6	0.80	-29.2
Stromatolite = S	MS	AOS	Mudstone	2.72	25.8 ± 2.1	9.20	-50.4
Mudstone = M	MS	AOS	Mudstone	2.72	36.8 ± 1.5	4.90	-55.9
Siltstone = SS	MS	AOS	Mudstone	2.72	14 ± 1.1	3.90	-39.9
	S	AOS	Stromatolite	2.72	35.4 ± 3	1.90	-45.4
	SS	AOS	Siltstone	2.72	30.4 ± 1.6	6.00	-44.9
	S	AOS	Stromatolite	2.72	15.5 ± 1	4.70	-35.2
	SS	AOS	Siltstone	2.72	33.8 ± 2.1	3.10	-29.2
	MS	AOS	Mudstone	2.72	34.6 ± 2.1	8.00	-44.5
	SS	AOS	Siltstone	2.72	34 ± 1.8	4.10	-34.4
	SS	AOS	Siltstone	2.72	8.6 ± 0.9	1.90	-29.1
	S	AOS	Stromatolite	2.72	24.6 ± 2.1	2.70	-30.6
	MS	AOS	Mudstone	2.72	30.4 ± 1.9	10.80	-45.3
	S	AOS	Stromatolite	2.72	15.1 ± 1.1	2.90	-34.9
	SS	AOS	Siltstone	2.72	28.5 ± 3.2	1.60	-32.8
	SS	AOS	Siltstone	2.72	19.4 ± 1.7	3.30	-31.6
	S	AOS	Stromatolite	2.72	29.9 ± 2.6	0.50	-35.6
	S	AOS	Stromatolite	2.72	28.6 ± 2	7.30	-39.6
	S	AOS	Stromatolite	2.72	26 ± 1.7	2.50	-42.4
	SS	AOS	Siltstone	2.72	32.5 ± 1	4.50	-43.1
	MS	AOS	Mudstone	2.72	50.4 ± 1.8	13.50	-42.5
	SS	AOS	Siltstone	2.72	22.1 ± 2	3	-23.8
	MS	AOS	Mudstone	2.72	38.4 ± 2.5	7	-45.7
	MS	AOS	Mudstone	2.72	46.5 ± 4.4	6	-48.2
	MS	AOS	Mudstone	2.72	24.6 ± 1.2	5	-31.5
	MS	AOS	Mudstone	2.72	47.4 ± 3.1	4	-44.3
	MS	AOS	Mudstone	2.72	43 ± 2.8	5	-52.7
	SS	AOS	Siltstone	2.72	37.1 ± 1.4	4	-53.3
	SS	AOS	Siltstone	2.72	26.3 ± 1.9	7	-43.0
	SS	AOS	Siltstone	2.72	23.6 ± 3.2	1	-24.7
Busigny et al.-2011	CH-129	MOL	Amphibolite	0.06	4.3	12	
Ophiolites, Alps	CH-80-02	MOL	Amphibolite	0.06	1.3	28	
most analyses are meta-gabbros	G6004A	MOL	Blueschist	0.06	5.7	12	
	G6004b	MOL	Blueschist	0.06	4.7	2.6	
	G6004c	MOL	Blueschist	0.06	5.7	3.7	
	09-02WR	MOL	Blueschist	0.06	8.1	4.4	
	VS-1	MOL	Eclogite	0.06	7.6	5.1	
	Vi-52	MOL	Eclogite	0.06	2.8	7.7	
	Vi-262M	MOL	Mylonite	0.06	1.7	6.3	
	Vi-389M	MOL	Mylonite	0.06	0.8	11	

Continued on next page

Table A.1 – continued from previous page

Reference	Sample	Setting	Rock	Age	δ^{15}N	[N]	δ^{13}C
	Vi-385M	MOL	Mylonite	0.06	2.0	18	
	Vi-385V	MOL	Vein	0.06	1.9	19	
	Vi387V	MOL	Vein	0.06	5.9	3.9	
	Vi-79V	MOL	Vein	0.06	3.4	16	
	VS-14V	MOL	Vein	0.06	4.4	55	
Morford et al.-2011	BWDC	CL	Granodiorite	0.15	18.4 ± 1.6	55	
	SFM	MCS	Schist	0.1	3.3 ± 0.2	682	
Palya et al.-2011	Zone 1	MCS	Schist	1.8	4.4	333	-23.4
high T Metasedi-ments	1	MCS	Schist	1.8	2.4	317	-27.5
Australia	1	MCS	Schist	1.8	2.8	212	-27.0
Zone 1-4=low to high	1	MCS	Schist	1.8	2.4	346	-23.5
T metamor-phism,	1	MCS	Schist	1.8	2.3	107	-24.2
some migmatism	1	MCS	Schist	1.8	6.2	232	-25.0
	1	MCS	Schist	1.8	4.6	232	-24.8
	2A	MCS	Schist	1.8	5.2	218	-22.5
	2A	MCS	Schist	1.8	5.9	211	-22.3
	2A	MCS	Schist	1.8	5.0	100	
	2A	MCS	Schist	1.8	11.7	153	-21.0
	2A	MCS	Schist	1.8	2.3	341	-21.6
	2A	MCS	Schist	1.8	4.6	116	
	2A	MCS	Schist	1.8	3.9	114	
	2A	MCS	Schist	1.8	5.1	247	-23.2
	2B	MCS	Schist	1.8	2.1	291	-21.8
	2B	MCS	Schist	1.8	4.5	140	-24.6
	2B	MCS	Schist	1.8	4.0	36	
	2B	MCS	Schist	1.8	3.7	226	-22.6
	2B	MCS	Schist	1.8	4.4	145	
	2B	MCS	Schist	1.8	4.7	51	
	2B	MCS	Schist	1.8	2.9	80	
	2B	MCS	Schist	1.8	3.6	157	
	2B	MCS	Schist	1.8	2.5	193	-22.5
	2B	MCS	Schist	1.8	3.8	226	-15.5
	2B	MCS	Schist	1.8	4.4	214	
	2B	MCS	Schist	1.8	2.2	116	
	2B	MCS	Schist	1.8	2.7	181	-24.0
	2C	MCS	Schist	1.8	10.8	365	
	2C	MCS	Schist	1.8	3.9	112	
	Zone 3	MCS	Migmatite	1.8	3.6	79	-21.4
		MCS	Migmatite	1.8	4.1	120	-28.3
		MCS	Migmatite	1.8	4.4	75	-21.1
		MCS	Migmatite	1.8	3.7	1333	
		MCS	Migmatite	1.8	5.9	112	-21.8
		MCS	Migmatite	1.8	2.3	56	-18.1
		MCS	Migmatite	1.8	1.7	68	-25.5
	Zone 4	MCS	Migmatite	1.8	5.2	209	-19.6
		MCS	Migmatite	1.8	4.0	242	
		MCS	Migmatite	1.8	7.9	139	
		MCS	Migmatite	1.8	5.2	213	
		MCS	Migmatite	1.8	5.4	185	
		MCS	Migmatite	1.8	4.7	239	
		MCS	Migmatite	1.8	4.1	96	-17.7
		MCS	Migmatite	1.8	2.1	74	-21.9
		MCS	Migmatite	1.8	4.7	98	
		MCS	Migmatite	1.8	7.4	156	
		MCS	Migmatite	1.8	6.3	217	
		MCS	Migmatite		8.5	43	
		MCS	Migmatite	1.8	4.7	361	
		MCS	Migmatite	1.8	5.6	194	-22.3
		MCS	Migmatite	1.8	2.8	235	-21.7
		MCS	Migmatite	1.8	2.5	261	-24.8
		MCS	Migmatite	1.8	7.9	257	-23.1

Continued on next page

Table A.1 – continued from previous page

Reference	Sample	Setting	Rock	Age	δ^{15}N	[N]	δ^{13}C
		MCS	Migmatite	1.8	3.9	205	
		MCS	Migmatite	1.8	7.6	158	
		MCS	Migmatite	1.8	3.0	99	
		MCS	Migmatite	1.8	3.0	253	
		MCS	Migmatite	1.8	6.4	154	
		MCS	Migmatite	1.8	5.9	83	
		MCS	Migmatite	1.8	7.8	94	
		MCS	Migmatite	1.8	5.5	87	
		MCS	Migmatite	1.8	2.4	201	-26.8
Ahadnejad et al.-2011	38	CL	Granite	0.15		30	
	44	CL	Granodiorite	0.15		30	
Read from graph,	54	CL	Granite	0.15		30	
NH4	56	CL	Granodiorite	0.15		30	
measurements	61	CL	Granite	0.15		36	
from Iran	68	CL	Granite	0.15		30	
made using	77	CL	Granite	0.15		16	
colorimetric	80	CL	Granite	0.15		30	
method							
	87	CL	Tonalite	0.15		26	
	91	CL	Granite	0.15		38	
	149	CL	Granite	0.15		30	
	150	CL	Diorite	0.15		13	
	186	CL	Granite	0.15		27	
	192	CL	Gabbro	0.15		8	
	106	ACL	Granite	0.15		51	
	116	ACL	Granite	0.15		45	
	161	ACL	Granodiorite	0.15		47	
	200	MCS	Slate	0.15		454	
	201	MCS	Slate	0.15		449	
	209	MCS	Phyllite	0.15		403	
	211	MCS	Phyllite	0.15		397	
	232	MCS	Phyllite	0.15		400	
	237	MCS	Phyllite	0.15		404	
	241	MCS	Schist	0.15		201	
	250	MCS	Schist	0.15		180	
	256	MCS	Schist	0.15		186	
Cruz-2011	MP-2	MOS	Biotite	0.065		430	
	MP-3	MOS	Muscovite	0.065		560	
	MP-4	MOS	Muscovite	0.065		540	
	MP-6	MOS	Gneiss	0.065		650	
	MP-8	MOS	Biotite	0.065		890	
	MP-22	MOS	Biotite	0.065		520	
	MP-21	MOS	Schist	0.065		290	
	MP-23	MOS	Schist	0.065		280	
	MP-24	MOS	Schist	0.065		210	
	MP-25	MOS	Muscovite	0.065		360	
	MP-26	MOS	Muscovite	0.065		670	
	MP-26	MOS	Biotite	0.065		2450	
	RMP-26-3	MOS	Biotite	0.065		1770	
Halama et al.-2012	N-MORB	OL	N-MORB	0	-2.3 ± 2.3		
Compilation paper	E-MORB	OL	E-MORB	0	-0.4 ± 2.6		
	Low-grade serpentinites	AOL	Serpentinite	0.165	0.6 ± 3.4	2.4	
	High-P peridotites	MOL	peridotite	0.165	3.4 ± 1.3	3.0	
	High-P ultramafic veins	MOL	Vein	0.165	0.6 ± 1.4	3.9	
	Chlorite harzburgite	MOL	Harzburgite	0.165	1.1 ± 2.3	7.4	
	High-P ultramafic veins	MOL	Vein	0.165	3.1 ± 1.5	2.9	
Roulleau et al.-2012	Mt Royal	CL	Amphibole	0.124	-2.4 ± 1.1	0.01	

Continued on next page

Table A.1 – continued from previous page

Reference	Sample	Setting	Rock	Age	δ^{15}N	[N]	δ^{13}C
Mafic Intrusions mineral separates Monteregian Hills Quebec	St Bruno	CL	Clinopyroxene	0.124	-3.6 ± 0.6	0.22	
	St Hilaire	CL	Clinopyroxene	0.124	-5.8 ± 1.7	0.01	
	St Gregoire	CL	Clinopyroxene	0.124	-1 ± 0.4	0.02	
	Rougemont	CL	Clinopyroxene	0.124	10.5 ± 1.9	0.002	
	Rougemont	CL	Clinopyroxene	0.124	-7.6 ± 0.5	0.05	
	Yamaska	CL	Clinopyroxene	0.124	-7.4 ± 1.4	0.01	
	Shefford	CL	Amphibole	0.124	7 ± 0.8	0.01	
	Brome	CL	Amphibole	0.124	8.1 ± 1.2	0.01	
Dixon et al.-2012 Metasediments from Sweden	Black Schist	MCS	Schist	0.455		3348	
	Marble	MCS	Marble	0.455		1031	
	Garnet Schist	MCS	Schist	0.455		3530	
	Hard Schist	MCS	Schist	0.455		1283	
Smelov et al.-2012 Russian diamonds Mesoarchean age	1	D	Eclogitic	3		133	
	2	D	Eclogitic	3		3766	
	3	D	Eclogitic	3		150	
	4	D	Eclogitic	3		131	
	7	D	Eclogitic	3		241	
	8	D	Eclogitic	3		288	
	9	D	Eclogitic	3		912	
	10	D	Eclogitic	3		426	
	11	D	Eclogitic	3		266	
	13	D	Eclogitic	3		847	
	14	D	Eclogitic	3		435	
Palot et al.-2012 Diamonds from South America	1-102/LP	D	Peridotitic	0.093	-4.6 ± 1	14	-4.4
	1-35/LP	D	Peridotitic	0.093	-3.4 ± 0.5	48	-5.5
	BZ-213/LP	D	Peridotitic	0.093	-3.3 ± 0.5	30	-3.4
	BZ-124/AB	D	Basaltic	0.093	1 ± 2	510	-12.3
Lithospheric = LP Asthenospheric P= AP Lower Man./Transition zone= LMT Lower Mantle = LM Lithospheric Eclogitic = LE Top samples are from Juina	BZ-127/AB	D	Basaltic	0.093	0.2 ± 0.5	77	-8.4
	BZ-129/AB	D	Basaltic	0.093	1.2 ± 0.5	66	-6.3
	BZ-209/AB	D	Basaltic	0.093	3.8 ± 0.5	750	-12.1
	BZ-215/AB	D	Basaltic	0.093	1.3 ± 0.5	166	-8.8
	BZ-217/AB	D	Basaltic	0.093	1.2 ± 0.5	62	-8.6
	1 - 1/LMT	D	Peridotitic	0.093	-2.1 ± 0.5	331	-4.7
	1 - 5/LMT	D	Peridotitic	0.093	-5.8 ± 0.5	61	-4.3
	1 - 8LMT	D	Peridotitic	0.093	-8.8 ± 0.5	125	-4.2
	1 - 30 -4/LMT	D	Peridotitic	0.093	-1.5 ± 0.5	34	-10.3
	5 - 107/LMT	D	Peridotitic	0.093	-4.4 ± 0.5	42	-4.3
	BZ-237/LMT	D	Basaltic	0.093	-5.6 ± 0.5	166	-5.1
	1 - 4 -3 LM	D	Peridotitic	0.093	-4 ± 0.7	26	-4.0
	1 - 4 - 4/LM	D	Peridotitic	0.093	-0.8 ± 0.5	477	-5.3
	1 - 31/LM	D	Peridotitic	0.093	-3.2 ± 0.5	74	-4.7
	1 - 36/LM	D	Peridotitic	0.093	-1 ± 0.5	20	-5.4
	3 - 1/LM	D	Peridotitic	0.093	-3.7 ± 0.5	806	-4.9
	5 - 17/LM	D	Peridotitic	0.093	-2.5 ± 0.5	63	-4.9
	5 - 103/LM	D	Peridotitic	0.093	-2.8 ± 2.6	13	-5.1
	BZ-88-2/LM	D	Basaltic	0.093	-1.5 ± 0.5	13	-9.6
	BZ-201/LM	D	Basaltic	0.093	-8.2 ± 1.5	8	-4.8
	BZ-207/LM	D	Basaltic	0.093	-3.1 ± 0.5	36	-4.5
KK= samples from Kakan	KK-47	D	?	0.1	-2.9 ± 0.5	987	-4.1
	KK-3/LE	D	Eclogitic	0.1	-4.7 ± 0.5	873	-4.8

Continued on next page

Table A.1 – continued from previous page

Reference	Sample	Setting	Rock	Age	δ^{15}N	[N]	δ^{13}C
	KK-4/LE	D	Eclogitic	0.1	8.5 ± 0.5	279	-0.8
	KK-40/LE	D	Eclogitic	0.1	-0.3 ± 0.5	481	-5.1
	KK-67/LE	D	Eclogitic	0.1	7.8 ± 0.5	1193	-9.2
	KK-68/LE	D	Eclogitic	0.1	-4.1 ± 0.5	1292	-10.4
	KK-75/LE	D	Eclogitic	0.1	-11.2 ± 0.5	499	-4.8
	KK-77/LE	D	Eclogitic	0.1	-0.3 ± 0.5	134	-2.0
	KK-80/LE	D	Eclogitic	0.1	-7 ± 0.5	907	-4.7
	KK-86/LE	D	Eclogitic	0.1	-4.3 ± 0.5	1151	-4.8
	KK-21LP	D	Peridotitic	0.1	$-39. \pm 0.54$	196	-3.4
	KK-26/LP	D	Peridotitic	0.1	4.9 ± 0.5	81	-4.1
	KK-28/LP	D	Peridotitic	0.1	-0.2 ± 0.5	107	-4.8
	KK-49/LP	D	Peridotitic	0.1	-4.9 ± 0.5	426	-4.8
	KK-65/LP	D	Peridotitic	0.1	9.6 ± 0.5	163	-2.4
	KK-70/LP	D	Peridotitic	0.1	-5.1 ± 1.5	10	-3.8
	KK-73/LP	D	Peridotitic	0.1	5.8 ± 0.5	21	-2.9
	KK-78/LP	D	Peridotitic	0.1	1 ± 0.5	80	-2.8
	KK-79/LP	D	Peridotitic	0.1	2.4 ± 0.5	38	-4.8
	KK-90/LP	D	Peridotitic	0.1	4.5 ± 0.5	295	-4.6
	KK?92-2/LP	D	Peridotitic	0.1	-30.4 ± 0.5	251	-3.2
	KK-93/LP	D	Peridotitic	0.1	-1.2 ± 0.5	794	-4.4
	KK-7/LP	D	Peridotitic	0.1	-4.8 ± 0.5	47	-3.7
	KK-11/LM	D	Peridotitic	0.1	-24.9 ± 0.5	115	-3.5
	KK-31/LM	D	Peridotitic	0.1	-1.3 ± 1	8	-3.9
	KK-36/LM	D	Peridotitic	0.1	-1 ± 0.7		-4.0
	KK-37/LM	D	Peridotitic	0.1	-6.5 ± 1.6	7	-3.5
	KK-39-5/LM	D	Peridotitic	0.1	-2.7 ± 2.3	2	-1.1
	KK-39-1/LM	D	Peridotitic	0.1	4.6 ± 3	2	-1.4
	KK-43/LM	D	Peridotitic	0.1	-0.2 ± 1	4	-3.7
	KK-54/LM	D	Peridotitic	0.1	-1.3 ± 0.9	3	-3.3
	KK-57/LM	D	Peridotitic	0.1	0.8 ± 1	4	-4.0
	KK-63/LM	D	Peridotitic	0.1	0.8 ± 1.2	3	-3.2
	KK-71/LM	D	Peridotitic	0.1	-3.4 ± 1	4	-3.4
	KK-74/LM	D	Peridotitic	0.1	-0.1 ± 1.5	8	-4.4
	KK-83/LM	D	Peridotitic	0.1	-2.8 ± 1	4	-3.4
	KK-87/LM	D	Peridotitic	0.1	-8.2 ± 2	6	-4.6
	KK-89/LM	D	Peridotitic	0.1	2.6 ± 0.6	6	-3.5
	KK-103/LM	D	Peridotitic	0.1	-3.9 ± 0.7	10	-4.0
Ekpo et al.-2012	NK-1	AOS	Shale	0.115		1100	
Cretaceous seds.	NK-2a	AOS	Shale	0.115		1300	
from Nigeria	NK-2B	AOS	Shale	0.115		700	
	NK2C	AOS	Shale	0.115		4600	
	NK-2D	AOS	Shale	0.115		4400	
	NK-2E	AOS	Shale	0.115		4400	
	NK-2F	AOS	Shale	0.115		4800	
	NK-2G	AOS	Shale	0.115		4000	
	NK-2H	AOS	Shale	0.115		4400	
	NK-3A	AOS	Shale	0.115		4700	
	NK-3B	AOS	Shale	0.115		1000	
	NK-3C	AOS	Shale	0.115		1000	
	NK-3D	AOS	Shale	0.115		1100	
	NK-3E	AOS	Shale	0.115		1100	
	NK-3F	AOS	Shale	0.115		1100	
	NK-4	AOS	Shale	0.115		1000	
	NK-5	AOS	Shale	0.115		600	
	NN-1	AOS	Shale	0.115		200	
	NN-2	AOS	Shale	0.115		200	
	NN-3A	AOS	Shale	0.115		300	
	NN-3B	AOS	Shale	0.115		400	
	NN-3C	AOS	Shale	0.115		400	
	NN-3D	AOS	Shale	0.115		400	
	NN-3E	AOS	Shale	0.115		200	
	EK-1	AOS	Shale	0.115		400	
	EK-2	AOS	Shale	0.115		600	
	EK-3	AOS	Shale	0.115		800	
	EK-4	AOS	Shale	0.115		700	
	EK-5	AOS	Shale	0.115		1000	
	MF-1	AOS	Shale	0.115		200	

Continued on next page

Table A.1 – continued from previous page

Reference	Sample	Setting	Rock	Age	δ^{15}N	[N]	δ^{13}C
	MF-2	AOS	Shale	0.115		200	
	MF-3	AOS	Shale	0.115		200	
	MF-4	AOS	Shale	0.115		600	
	MF-5	AOS	Shale	0.115		200	
	MF-6	AOS	Shale	0.115		100	
	AW-1A	AOS	Shale	0.115		1300	
	AW-1B	AOS	Shale	0.115		500	
	AW-1C	AOS	Shale	0.115		600	
	AW-1D	AOS	Shale	0.115		1800	
	AW-1E	AOS	Shale	0.115		1600	
	AW-2A	AOS	Shale	0.115		100	
	AW-2B	AOS	Shale	0.115		100	
Cremonese et al.-2013 pre-Camb-Camb Yuanshan, China	XTY 61	AOS	Siltstone	0.51	2.4	420	-25.1
	XTY 60	AOS	Siltstone	0.510203	2.7	600	-31.9
	XTY 59	AOS	Siltstone	0.510406	2.5	500	-27.8
	XTY 58	AOS	Siltstone	0.510609	2.7	620	-27.0
	XTY 57	AOS	Siltstone	0.510812	2.7	630	-27.9
	XTY 56	AOS	Siltstone	0.511015	2.6	500	-26.4
	XTY 55	AOS	Siltstone	0.511218	2.7	620	-26.8
	XTY 54	AOS	Siltstone	0.511421	2.7	680	-27.3
	XTY 53	AOS	Siltstone	0.511624	2.5	290	-26.0
	XTY 52	AOS	Siltstone	0.511827	2.8	640	-28.9
	XTY 51	AOS	Siltstone	0.51203	2.8	640	-29.1
	XTY 50	AOS	Siltstone	0.512233	2.5	190	-26.2
	XTY 49	AOS	Siltstone	0.512436	2.7	700	-27.6
	XTY 48	AOS	Siltstone	0.512639	1.8	570	-28.6
	XTY 47	AOS	Siltstone	0.512842	2.0	620	
	XTY 44	AOS	Siltstone	0.513045	2.2	650	-28.4
	XTY 43	AOS	Siltstone	0.513248	2.3	630	-28.5
	XTY 42	AOS	Siltstone	0.513451	2.3	760	-28.2
	XTY 41	AOS	Siltstone	0.513654	2.2	650	-27.6
	XTY 40	AOS	Siltstone	0.513857	1.9	500	-28.0
	XTY 39	AOS	Siltstone	0.51406	1.9	780	-27.2
	XTY 38	AOS	Siltstone	0.514263	2.0	750	-27.3
	XTY 37	AOS	Siltstone	0.514466	1.9	790	-27.4
	XTY 36	AOS	Siltstone	0.514669	1.8	820	-27.8
	XTY 35	AOS	Siltstone	0.514872	1.8	880	-27.6
Shiyantou Formation	XTY 34	AOS	Shale	0.515075	1.2	200	-28.8
	XTY 33	AOS	Shale	0.515278	1.5	250	-29.5
	XTY 32	AOS	Shale	0.515481	1.4	220	-30.4
	XTY 31	AOS	Shale	0.515684	1.1	210	-30.5
	XTY 30	AOS	Shale	0.515887	1.5	280	-29.7
	XTY 29	AOS	Shale	0.51609	1.7	320	-30.0
	XTY 28	AOS	Shale	0.516293	0.6	400	-29.9
	XTY 27	AOS	Shale	0.516496	0.9	380	-30.4
	XTY 26	AOS	Shale	0.516699	0.9	460	-29.8
	XTY 25	AOS	Shale	0.516902	0.6	420	-29.4
	XTY 24	AOS	Shale	0.517105	1.0	370	-29.6
	XTY 23	AOS	Shale	0.517308	1.0	440	-29.8
	XTY 22	AOS	Shale	0.517511	1.2	440	-30.1
	XTY 21	AOS	Shale	0.517714	0.5	440	-30.2
	XTY 20	AOS	Shale	0.517917	1.1	430	-30.3
	XTY 19	AOS	Shale	0.51812	1.1	420	-30.1
	XTY 18	AOS	Shale	0.518323	0.7	380	-30.0
	XTY 17	AOS	Shale	0.518526	0.3	360	-29.7
	XTY 16	AOS	Shale	0.518729	0.5	410	-30.5
	XTY 15	AOS	Shale	0.518932	0.7	380	-30.2
	XTY 14	AOS	Shale	0.519135	0.7	390	-30.1
	XTY 13	AOS	Shale	0.519338	0.7	440	-30.7
	XTY 12	AOS	Shale	0.519541	0.5	460	-31.1
	XTY 11	AOS	Shale	0.519744	0.7	430	-31.4
	XTY 10	AOS	Shale	0.519947	0.5	370	-31.6
	XTY 09	AOS	Shale	0.52015	1.3	480	-31.7
	XTY 08	AOS	Shale	0.520353	0.9	330	-30.5
	XTY 07	AOS	Shale	0.520556	0.8	260	-31.1
	XTY 06	AOS	Shale	0.520759	0.8	350	-31.2

Continued on next page

Table A.1 – continued from previous page

Reference	Sample	Setting	Rock	Age	δ^{15}N	[N]	δ^{13}C
	XTY 05	AOS	Shale	0.520962	0.8	380	-32.0
	XTY 04	AOS	Shale	0.521165	0.9	370	-31.3
	XTY 03	AOS	Shale	0.521368	0.8	310	-29.3
	XTY 02	AOS	Shale	0.521571	0.3	350	-28.8
	XTY 01	AOS	Shale	0.521774	0.3	440	-30.0
	CX-XTMS 14	AOS	Shale	0.521977	1.1	200	-28.8
	CX-XTMS 13	AOS	Shale	0.52218	1.4	170	-27.0
	CX-XTMS 12	AOS	Shale	0.522383	0.4	230	-28.0
	CX-XTMS 11	AOS	Shale	0.522586	1.3	220	-29.9
	CX-XTMS 10	AOS	Shale	0.522789	1.2	240	-28.8
	CX-XTMS 9	AOS	Shale	0.522992	0.2	230	-30.6
	CX-XTMS 8	AOS	Shale	0.523195	1.5	230	-31.1
	CX-XTMS 7	AOS	Shale	0.523398	1.7	260	-29.6
	CX-XTMS 6	AOS	Shale	0.523601	1.8	270	-29.5
	CX-XTMS 5	AOS	Shale	0.523804	2.3	350	-29.7
	CX-XTMS 4	AOS	Shale	0.524007	2.3	280	-29.0
	CX-XTMS 3	AOS	Shale	0.52421	2.2	300	-30.0
	CX-XTMS 2	AOS	Shale	0.524413	2.2	200	-29.6
	CX-XTMS 1	AOS	Shale	0.524616	2.1	500	-29.9
	XT 29	AOS	Shale	0.524819	2.4	470	-29.7
	XT 28	AOS	Shale	0.525022	2.5	450	-29.3
	XT 27	AOS	Shale	0.525225	2.3	560	
	XT 26	AOS	Shale	0.525428	2.2	600	-35.8
	XT 25	AOS	Shale	0.525631	2.2	540	-31.7
	XT 24	AOS	Shale	0.525834	2.0	570	-31.7
	XT 23	AOS	Shale	0.526037	2.3	550	-31.5
	XT 22	AOS	Shale	0.52624	1.7	510	-31.3
	XT 21	AOS	Shale	0.526443	2.3	590	-34.3
	XT 20	AOS	Shale	0.526646	1.9	600	-34.5
	XT 19	AOS	Shale	0.526849	2.1	520	-34.4
	XT 18	AOS	Shale	0.527052	1.9	580	-34.2
	XT 17	AOS	Shale	0.527255	1.8	490	-33.9
	XT 16	AOS	Shale	0.527458	2.4	690	-33.8
	XT 15	AOS	Shale	0.527661	2.7	730	-33.9
	XT14	AOS	Shale	0.527864	3.1	490	-33.4
	XT13	AOS	Shale	0.528067	2.2	490	-33.9
	XT12	AOS	Shale	0.52827	2.2	570	-33.9
	XT11	AOS	Shale	0.528473	2.8	650	-33.9
	XT10	AOS	Shale	0.528676	2.6	590	-33.7
	XT9	AOS	Shale	0.528879	2.1	620	-32.9
	XT 8	AOS	Shale	0.529082	2.2	500	-28.7
	XT 7	AOS	Shale	0.529285	2.5	550	-31.8
	XT 6	AOS	Shale	0.529488	2.4	330	-30.0
	XT5	AOS	Shale	0.529691	2.2	430	-27.9
	XT 4	AOS	Shale	0.529894	2.4	460	-27.8
	XT 3	AOS	Shale	0.530097	2.5	470	-28.5
	XT2	AOS	Shale	0.5303	2.7	640	-28.6
	XT1	AOS	Shale	0.530503	2.6	110	-26.4
Dahai	XT103	AOS	Limestone	0.530706	1.3	140	-27.6
Formation	XT105	AOS	Limestone	0.530909	0.0	110	-29.5
	XT107	AOS	Limestone	0.531112	0.0	120	-30.3
	XT 109	AOS	Limestone	0.531315	0.7	1010	-29.8
	XT 111	AOS	Limestone	0.531518	0.9	3410	-24.3
	XT 113	AOS	Limestone	0.531721	0.9	1000	-21.7
	XT 115	AOS	Limestone	0.531924	1.2	7900	-21.5
	XT 117	AOS	Limestone	0.532127	2.3	1270	-24.0
	XT 119	AOS	Limestone	0.53233	2.3	1000	-23.7
	XT 121	AOS	Limestone	0.532533	2.8	1200	-23.7
	XT 123	AOS	Limestone	0.532736	3.0	900	-22.9
	XT 125	AOS	Limestone	0.532939	2.7	500	-22.3
	XT 127	AOS	Limestone	0.533142	3.0	1210	-23.7
	XT 129	AOS	Limestone	0.533345	1.9	1310	-22.2
	XT 131	AOS	Limestone	0.533548	2.1	1640	-22.3
	XT 133	AOS	Limestone	0.533751	2.0	500	

Continued on next page

Table A.1 – continued from previous page

Reference	Sample	Setting	Rock	Age	δ^{15}N	[N]	δ^{13}C
	XT 135	AOS	Limestone	0.533954	4.9	1220	-21.5
	XT 137	AOS	Limestone	0.534157	6.3	100	-21.5
	XT 139	AOS	Limestone	0.53436	7.7	60	-22.2
	XT 145	AOS	Limestone	0.534563	6.1	50	-22.6
	XT 151	AOS	Limestone	0.534766	4.9	60	-22.8
	XT 153	AOS	Limestone	0.534969	4.5	60	-24.7
	XT 155	AOS	Limestone	0.535172	2.7	330	-25.5
	XT 156	AOS	Limestone	0.535375	-0.9	80	-24.4
Zhongyicun	XT 159	AOS	Limestone	0.535578	1.2	830	-26.2
formation	XT 161	AOS	Limestone	0.535781	3.2	310	-24.4
	XT 163	AOS	Limestone	0.535984	5.0	110	-30.3
	XT 164	AOS	Limestone	0.536187	5.3	110	-30.0
	XT 165	AOS	Limestone	0.53639	4.5	250	-26.4
	XT 166	AOS	Limestone	0.536593	4.0	740	-29.3
	XT 168	AOS	Limestone	0.536796	6.1	160	-28.3
	XT 170	AOS	Limestone	0.536999	5.5	90	
	XT 172	AOS	Limestone	0.537202	6.5	110	-30.4
	XT 174	AOS	Limestone	0.537405	8.8	120	-30.5
	XT 175	AOS	Limestone	0.537608	5.6	170	-28.2
	XT 176	AOS	Limestone	0.537811	3.3	590	-32.0
	XT 182	AOS	Limestone	0.538014	2.3	130	-32.9
	XT 183	AOS	Limestone	0.538217	1.7	310	-31.9
	XT 186	AOS	Limestone	0.53842	4.1	360	-30.9
	XT 190	AOS	Limestone	0.538623	2.4	250	-33.8
	XT 192	AOS	Limestone	0.538826	1.1	320	-33.9
	XT 193	AOS	Limestone	0.539029	2.9	580	-33.9
	XT 196	AOS	Limestone	0.539232	3.0	560	-33.5
	XT 198	AOS	Limestone	0.539435	2.1	1230	-34.2
	XT 199	AOS	Limestone	0.539638	2.3	1820	-33.4
	XT 201	AOS	Limestone	0.539841	5.1	1800	-33.7
	XT 204	AOS	Limestone	0.540044	4.6	440	-33.2
	XT 206	AOS	Limestone	0.540247	4.8	1540	-30.5
	XT 207	AOS	Limestone	0.54045	4.6	300	-32.3
	XT 208	AOS	Limestone	0.540653	5.1	3420	-27.3
	XT 210	AOS	Limestone	0.540856	3.9	210	-32.3
	XT 212	AOS	Limestone	0.541059	4.8	550	-32.1
	XT 214	AOS	Limestone	0.541262	3.8	290	-32.7
	XT 216	AOS	Limestone	0.541465	4.3	390	-32.0
	XT 218	AOS	Limestone	0.541668	3.3	270	-29.2
	XT 219	AOS	Limestone	0.541871	3.9	230	-33.6
	XT 221	AOS	Limestone	0.542074	3.8	290	-33.1
	XT 223	AOS	Limestone	0.542277	3.4	320	-32.6
	XT 226	AOS	Limestone	0.54248	2.9	270	-30.5
	XT 228	AOS	Limestone	0.542683	4.2	460	-31.7
	XT 229	AOS	Limestone	0.542886	4.4	330	-30.5
	XT 236	AOS	Limestone	0.543089	4.9	160	-32.3
Daibu	XT 240	AOS	Limestone	0.543292	1.8	140	-31.1
formation	XT 242	AOS	Limestone	0.543495	2.4	70	-32.3
	XT 260	AOS	Limestone	0.543698	5.6	110	-34.9
	XT 262	AOS	Limestone	0.543901	4.8	60	-30.4
Dengying	XT 264	AOS	Limestone	0.544104	4.8	130	-29.5
formation	XT 266	AOS	Limestone	0.544307	4.4	190	-23.3
	XT 268	AOS	Limestone	0.54451	4.5	170	-25.4
	XT 270	AOS	Limestone	0.544713	2.7	210	-23.8
Busigny et	J1-124-1	AOS	Mudstone	2.5	9.5	87	-28.3
al.-2013							
	J1-138-1	AOS	Mudstone	2.5	8.1	17	-28.7
Carbon	J1-148-3	AOS	Mudstone	2.5	9.5	47	-28.6
isotopes							
from	J1-148-2	AOS	Mudstone	2.5	8.6	40	-28.2
organics							
	J1-162-1	AOS	Mudstone	2.5	7.4	121	-28.7
	WS188	AOS	Mudstone	2.5	5.1	9	-29.0
	WS196	AOS	Mudstone	2.5	6.0	173	-27.6
	DGM236	AOS	Mudstone	2.5	9.0	54	-28.3
	DGM243	AOS	Mudstone	2.5	9.2	100	-29.0
	DGM258-1	AOS	Mudstone	2.5	13.4	63	-28.5
	DGM258-2	AOS	Mudstone	2.5	11.6	63	-28.6
	DGM268	AOS	Mudstone	2.5	4.2	114	-29.2

Continued on next page

Table A.1 – continued from previous page

Reference	Sample	Setting	Rock	Age	δ^{15}N	[N]	δ^{13}C
	DGM271-2	AOS	Mudstone	2.5	7.6	31	-28.6
	DGM287	AOS	Mudstone	2.5	4.8	186	-31.3
	DGM288-1	AOS	Mudstone	2.5	0.4	41	-30.0
	DGM288-2	AOS	BIF	2.5	5.8	6	-28.9
	DGM302	AOS	Chert	2.5	6.3	6	-28.7
	DGM307-4	AOS	Mudstone	2.5	8.0	6	-28.3
	DGM307-6	AOS	Mudstone	2.5	7.9	1	-26.4
	DGM325	AOS	Mudstone	2.5	8.8	24	-28.8
	DGM337	AOS	Mudstone	2.5	9.9	11	-28.4
	DGM350	AOS	Mudstone	2.5	11.1	8	-29.2
	CC364	AOS	BIF	2.5	6.7	84	-28.2
	CC367	AOS	Mudstone	2.5	3.2	39	-28.5
	CC373	AOS	Mudstone	2.5	7.0	30	-28.9
	CC376	AOS	Mudstone	2.5	6.9	62	-28.6
	MR379	AOS	Marl	2.5	5.4	385	-28.8
	MR381	AOS	Marl	2.5	5.7	386	-28.6
	MR382	AOS	Shale	2.5	4.4	786	-29.4
	MR383	AOS	Marl	2.5	4.4	498	-29.2
	MR387	AOS	Marl	2.5	4.6	420	-30.5
Bebout et al.-2013	SL99-21B	MOS	Schist	0.05	3.6	596	
	SL99-21D	MOS	Schist	0.05	3.4	448	
	SL99-36B	MOS	Schist	0.05	2.9	1494	
	SL99-36A	MOS	Schist	0.05	4.1	758	
	ALB-957	MOS	Schist	0.05	4.2	337	
	MIU-955	MOS	Schist	0.05	2.7	1185	
	PEL-942	MOS	Schist	0.05	4.1	621	
	02-LDCS-11	MOS	Schist	0.05	4.5	855	
	LC99-4A	MOS	Schist	0.05	5.0	157	
	02-LDCS-01	MOS	Schist	0.05	4.8	331	
Godfrey et al.-2013	398.6	AOS	Shale	1.85	4.7		
Bulk rock and kerogen analyses Drill cores samples shown as height above basement	362.2	AOS	Shale	1.85	4.3		
	360.6	AOS	Shale	1.85	4.5		
	352.5	AOS	Shale	1.85	6.4		
	352.5	AOS	Shale	1.85	6.4		
	350.6	AOS	Shale	1.85	4.6		
	342.5	AOS	Shale	1.85	5.5		
	342.5	AOS	Shale	1.85	5.5		
	338.6	AOS	Shale	1.85	4.6		
	326	AOS	Shale	1.85	6.5		
	326	AOS	Shale	1.85	6.5		
	325.6	AOS	Shale	1.85	4.9		
	325.6	AOS	Shale	1.85	7.5		
	325	AOS	Shale	1.85	7.5		
	315	AOS	Shale	1.85	7.0		
	315	AOS	Shale	1.85	7.0		
	313.6	AOS	Shale	1.85	4.8		
	308.6	AOS	Shale	1.85	5.0		
	301.6	AOS	Shale	1.85	6.1		
	296.6	AOS	Shale	1.85	6.4		
	292.6	AOS	Shale	1.85	6.9		
	276.146	AOS	Shale	1.85	4.6		
	276.146	AOS	Shale	1.85	4.6		
	276.078	AOS	Shale	1.85	6.1		
	276.078	AOS	Shale	1.85	6.1		
	260.6	AOS	Shale	1.85	6.4		
	248.6	AOS	Shale	1.85	4.7		
	243.5	AOS	Shale	1.85	5.7		
	240.5	AOS	Shale	1.85	5.8		
		AOS	Shale	1.85	4.6		
		AOS	Shale	1.85	6.1		
		AOS	Shale	1.85	6.3		
		AOS	Shale	1.85	6.3		
		AOS	Shale	1.85	5.9		
		AOS	Shale	1.85	4.7		

Continued on next page

Table A.1 – continued from previous page

Reference	Sample	Setting	Rock	Age	δ^{15}N	[N]	δ^{13}C
		AOS	Shale	1.85	7.0		
		AOS	Shale	1.85	4.7		
		AOS	Shale	1.85	4.5		
		AOS	Shale	1.85	6.2		
		AOS	Shale	1.85	4.7		
		AOS	Shale	1.85	4.5		
		AOS	Shale	1.85	5.8		
		AOS	Shale	1.85	5.2		
		AOS	Shale	1.85	5.4		
		AOS	Shale	1.85	5.0		
		AOS	Shale	1.85	3.7		
		AOS	Shale	1.85	4.7		
		AOS	Shale	1.85	6.0		
		AOS	Shale	1.85	4.6		
		AOS	BIF	1.85	4.6		
		AOS	BIF	1.85	5.5		
		AOS	BIF	1.85	5.8		
		AOS	BIF	1.85	4.0		
		AOS	BIF	1.85	4.2		
		AOS	BIF	1.85	4.2		
		AOS	BIF	1.85	5.1		
		AOS	BIF	1.85	5.0		
		AOS	BIF	1.85	5.6		
		AOS	BIF	1.85	4.8		
		AOS	BIF	1.85	5.9		
		AOS	BIF	1.85	5.6		
		AOS	BIF	1.85	4.9		
		AOS	BIF	1.85	6.2		
		AOS	BIF	1.85	5.1		
		AOS	BIF	1.85	5.8		
		AOS	BIF	1.85	6.4		
		AOS	BIF	1.85	5.7		
		AOS	Shale	1.85	5.8		
		AOS	Shale	1.85	4.1		
		AOS	Shale	1.85	5.7		
		AOS	Shale	1.85	4.4		
		AOS	Shale	1.85	5.4		
		AOS	Shale	1.85	4.3		
		AOS	Shale	1.85	4.6		
		AOS	Shale	1.85	5.1		
		AOS	Shale	1.85	4.8		
		AOS	Shale	1.85	5.1		
		AOS	Shale	1.85	4.8		
		AOS	Shale	1.85	4.9		
		AOS	Shale	1.85	6.9		
		AOS	Shale	1.85	5.9		
		AOS	Shale	1.85	5.5		
		AOS	Shale	1.85	7.5		
		AOS	Shale	1.85	5.6		
		AOS	Shale	1.85	4.6		
		AOS	Shale	1.85	8.2		
		AOS	Shale	1.85	11.3		
		AOS	Shale	1.85	3.0		
		AOS	Shale	1.85	10.1		
		AOS	Shale	1.85	8.3		
		AOS	Shale	1.85	9.5		
		AOS	Shale	1.85	9.2		
		AOS	Shale	1.85	9.9		
		AOS	Shale	1.85	8.1		
		AOS	Shale	1.85	9.0		
		AOS	Shale	1.85	9.8		
		AOS	Shale	1.85	9.6		
		AOS	Shale	1.85	5.1		
		AOS	Shale	1.85	5.2		
		AOS	Shale	1.85	5.7		
		AOS	Shale	1.85	4.8		
		AOS	Shale	1.85	5.5		
		AOS	Shale	1.85	6.0		
		AOS	Shale	1.85	5.2		

Continued on next page

Table A.1 – continued from previous page

Reference	Sample	Setting	Rock	Age	δ^{15}N	[N]	δ^{13}C
		AOS	Shale	1.85	5.3		
		AOS	Shale	1.85	5.9		
		AOS	Shale	1.85	6.1		
		AOS	Shale	1.85	5.9		
		AOS	Shale	1.85	4.0		
		AOS	Shale	1.85	4.2		
		AOS	Shale	1.85	6.0		
		AOS	Shale	1.85	6.0		
		AOS	Shale	1.85	5.4		
		AOS	Shale	1.85	4.0		
		AOS	Shale	1.85	4.3		
		AOS	Shale	1.85	5.4		
		AOS	Shale	1.85	5.4		
		AOS	Shale	1.85	5.3		
		AOS	Shale	1.85	5.5		
		AOS	Shale	1.85	4.5		
		AOS	Shale	1.85	6.3		
		AOS	Shale	1.85	5.3		
		AOS	Shale	1.85	4.4		
		AOS	Shale	1.85	5.2		
		AOS	Shale	1.85	4.3		
		AOS	Shale	1.85	5.5		
		AOS	Shale	1.85	4.9		
		AOS	Shale	1.85	4.7		
		AOS	Shale	1.85	4.9		
		AOS	Shale	1.85	4.1		
		AOS	Shale	1.85	4.5		
		AOS	Shale	1.85	6.0		
		AOS	Shale	1.85	3.5		
		AOS	BIF	1.85	5.2		
		AOS	BIF	1.85	8.2		
		AOS	BIF	1.85	4.5		
		AOS	BIF	1.85	5.8		
		AOS	BIF	1.85	6.0		
		AOS	Shale	1.85	2.5		
		AOS	Shale	1.85	3.5		
		AOS	Shale	1.85	4.6		
		AOS	Shale	1.85	3.2		
		AOS	Shale	1.85	3.7		
		AOS	Shale	1.85	4.2		
		AOS	Shale	1.85	1.9		
		AOS	Shale	1.85	4.1		
		AOS	Shale	1.85	3.9		
		AOS	Shale	1.85	4.3		
		AOS	Shale	1.85	3.7		
		AOS	Shale	1.85	3.8		
		AOS	Shale	1.85	3.6		
		AOS	Shale	1.85	4.0		
		AOS	Shale	1.85	3.2		
		AOS	Shale	1.85	4.0		
		AOS	Shale	1.85	3.5		
		AOS	Shale	1.85	3.9		
		AOS	Shale	1.85	4.5		
		AOS	Shale	1.85	3.8		
		AOS	Shale	1.85	2.4		
		AOS	Shale	1.85	4.3		
		AOS	Shale	1.85	3.7		
		AOS	Shale	1.85	3.5		
		AOS	Shale	1.85	3.8		
		AOS	Shale	1.85	4.3		
		AOS	Shale	1.85	3.9		
		AOS	Shale	1.85	4.5		
		AOS	BIF	1.85	4.4		
		AOS	BIF	1.85	4.6		
		AOS	BIF	1.85	5.4		
		AOS	BIF	1.85	4.0		
		AOS	BIF	1.85	3.8		
		AOS	BIF	1.85	6.2		
		AOS	BIF	1.85	5.3		

Continued on next page

Table A.1 – continued from previous page

Reference	Sample	Setting	Rock	Age	δ^{15}N	[N]	δ^{13}C
		AOS	BIF	1.85	4.3		
		AOS	BIF	1.85	6.5		
		AOS	Shale	1.85	5.6		
		AOS	Shale	1.85	5.0		
		AOS	Shale	1.85	5.0		
		AOS	Shale	1.85	4.6		
		AOS	Shale	1.85	4.1		
		AOS	Shale	1.85	5.0		
		AOS	Shale	1.85	4.4		
		AOS	Shale	1.85	3.9		
		AOS	Shale	1.85	4.7		
		AOS	Shale	1.85	4.0		
		AOS	Shale	1.85	2.3		
		AOS	Shale	1.85	4.4		
		AOS	Shale	1.85	4.4		
		AOS	Shale	1.85	3.2		
		AOS	Shale	1.85	3.9		
		AOS	Shale	1.85	3.9		
		AOS	Shale	1.85	4.7		
		AOS	Shale	1.85	4.6		
		AOS	Shale	1.85	3.6		
		AOS	Shale	1.85	3.9		
		AOS	Shale	1.85	4.3		
		AOS	Shale	1.85	4.5		
		AOS	Shale	1.85	4.3		
		AOS	Shale	1.85	4.4		
		AOS	Shale	1.85	4.8		
		AOS	Shale	1.85	4.8		
		AOS	Shale	1.85	4.4		
		AOS	Shale	1.85	3.9		
		AOS	Shale	1.85	4.0		
		AOS	Shale	1.85	3.9		
		AOS	Shale	1.85	3.9		
		AOS	Shale	1.85	3.8		
		AOS	Shale	1.85	2.8		
		AOS	Shale	1.85	4.1		
		AOS	Shale	1.85	4.1		
		AOS	Shale	1.85	4.6		
		AOS	Shale	1.85	4.0		
		AOS	Shale	1.85	4.5		
		AOS	BIF	1.85	3.8		
		AOS	BIF	1.85	4.0		
		AOS	BIF	1.85	3.3		
		AOS	BIF	1.85	3.3		
		AOS	BIF	1.85	3.2		
		AOS	BIF	1.85	3.6		
		AOS	BIF	1.85	3.3		
		AOS	BIF	1.85	2.9		
		AOS	BIF	1.85	3.6		
		AOS	BIF	1.85	3.8		
		AOS	BIF	1.85	3.7		
		AOS	BIF	1.85	3.9		
		AOS	BIF	1.85	3.8		
		AOS	BIF	1.85	4.0		
		AOS	BIF	1.85	4.8		
		AOS	BIF	1.85	3.9		
		AOS	BIF	1.85	5.0		
		AOS	BIF	1.85	5.4		
deMoor et al.-2013	Songwe2	VV	F	0	-5.9 ± 0.5	13	
N concentration in mmol/mol N2. F=fluid G=gas	Songwe3	VV	G	0	-2.7 ± 0.2	4	
	Songwe1	VV	G	0	-0.1 ± 0.2	5	
	Kafwira	VV	F	0	-0.6 ± 0.2	25	
	Ikama	VV	G	0	2 ± 0.1	28	
	Kibila	VV	G	0	-3.4 ± 0.2	6	
	Kiejo	VV	G	0	-4.1 ± 0.2	7	

Continued on next page

Table A.1 – continued from previous page

Reference	Sample	Setting	Rock	Age	δ^{15}N	[N]	δ^{13}C
	Kiejo	VV	G	0	-5.2 ± 0.4	3	
	Kilambo	VV	F	0		11	
	Kilambo	VV	G	0	-5 ± 0.2	8	
	Mampulo	VV	G	0	-0.9 ± 0.2	7	
	Mampulo	VV	G	0	-2.9 ± 0.3	8	
	Mampulo	VV	F	0		6	
	Kasimilo	VV	F	0	-0.8 ± 0.5	8	
	Kasimulo	VV	F	0	-0.6 ± 0.4	12	
Li et al.-2014	97M11	MOL	Phlogopite	0.76	4.5	24	
	97M15	MOL	Phlogopite	0.76	3.2	30	
	95HN24-1	MOL	Phlogopite	0.76	5.7	37	
	95NH24-2	MOL	Phlogopite	0.76	4.8	49	
	95NH68	MOL	Phlogopite	0.76	5.6	53	
	95HN61	MOL	Phlogopite	0.76	6.1	57	
	95HN07	MOL	Muscovite	0.76	8.7	47	
	99MB06	MCL	Phlogopite	0.76	3.5	33	
	99QL12	MCL	Phlogopite	0.76	-5.1 ± 0.1	35	
	00QL30	MCL	Phlogopite	0.76	-2.2	37	
	00HT01	MCL	Phlogopite	0.76	-2.3	50	
	00HT09	MCL	Phlogopite	0.76	4.9	18	
	99HS03	MCL	Muscovite	0.76	3.1	46	
	00BH10	MCL	Biotite	0.76	-7.4 ± 0.4	116	
	00BH17a	MCL	Biotite	0.76	-4.8 ± 0.3	207	
	00BH21	MCL	Biotite	0.76	-15.8	450	

Table A.2: Terrestrial K and Rb. See first page of Appendix A for full description. Potassium is given in wt. % K_2O and Rb in ppm. See table A.1 for sample notes.

Reference	Sample	K_2O	Rb	Reference	Sample	K_2O	Rb
Sakai et	Cayman	0.28		Busigny et al., 2003	00Li10	2.44	117
al., 1984	FAMOUS	0.07			00Li8S	4.75	229
	Galapagos	0.08			00Li9	1.20	62
	Galapagos	0.08			00Li7	2.22	96
	Kilauea	0.16			C18	0.93	51
	Juan de Fuca	0.29			98SE3	1.36	72
	Juan de Fuca	0.19			SL98-2P	2.48	126
Duit et	23		360		98SE5	7.07	341
al., 1986	71		455		98SE6	5.23	272
	118		310		SL98-3C	0.88	45
	118		285		SL98-3P	7.96	347
	121		550		98SE7	0.61	39
	126B		430		98SE8	3.52	151
	127		625		98SE9	2.94	127
	129B		970		90-25B	1.59	75
	129B		390		90-25A	2.23	109
	153		220	Sadofsky	VD 2a	4.16	166
	160		560	and Bebout 2003			
	161		390		KW98-21b	1.92	72
	161		380		Eel4 Shale	2.33	101
	162		520		JC c4a	1.90	90
	162		250		JC 5	1.41	54
	164		250		Apc5a	1.02	39
	169B		480		AP 8	2.14	74
	177B		320		CR 2b	1.31	44
	183B		315		Alder 2	1.14	48
	190		690		RLS-585-1	1.10	35
	191		380		RLS-585-14	1.52	65
	192		450		RLS-486-105	3.24	106
	196B		700		RLS-585-71	0.85	36
	197		1130		RLS-486-130	0.93	35
	198		400	Jia et al., 2003	CP60/93	2.89	85.5
	201		810		B-4	5.32	133
	201		390		SD-1	7.09	54.3
	202		555		SD-2		81.8
	202		380		SD-3	7.14	
	205		390		P-1	7.31	83.2
	205		420		P-2	7.56	91.5

Continued on next page

Table A.2 – continued from previous page

Reference	Sample	K_2O	Rb	Reference	Sample	K_2O	Rb
	206				M2/1	3.42	57
Greenfield 1988	Control				M-2/2	4.69	85.2
Hall 1988	C7	4.66			KH-1	4.91	67.5
	C7	13.51			KH-2	4.96	20.4
	C7	9.92			R839A	2.41	137
	C7	9.46		Glasmacher et	C-M-t	4.01	0.169
	C203	5.22		al., 2003	C-M-m	3.99	0.16
	C203	15.39			C-M-b	4.42	0.173
	C203	10.40			M-I-M	3.07	0.115
	C221	4.39			T-M	4.92	0.209
	C221	10.47		Pitcairn et	B14	4.21	162.4
Hall et	EC2	4.19		al., 2005	B30	3.05	110.6
al., 1991	EC3	4.31			C90	3.60	123.5
	EP6	4.36			B82	2.56	92.8
	EP7	4.50			B92	3.29	112.4
	ES2	4.46			C50	4.47	168.5
	ES3	4.34			C66	5.95	220.8
	ES4	4.30		Jia 2006	Low grade	5.61	
	ES5	4.15			Chlorite	5.14	
	ES8a	3.66			Biotite	4.49	
	ES14a	3.06			and alusite	4.29	
	ESP3	4.10			Sillimanite	2.88	
	ESP4	3.92			Migmatite	2.77	
	ESP6	4.39		Li et	41R1 26-30	2.14	
	ESP10a	4.87		al., 2007	43R1 22-27	1.90	
	PO22	4.14			43R1 132-135	1.61	
	PO2	2.34			1R1 109-141	1.75	
	PO36i	3.92			1R5 80-82	1.05	
	E12LP	6.31			4R1 72-77	0.01	
	E12LA	4.91			5R2 12-17	4.39	
	E12SP	5.55			5R2 123-130	1.88	
	E12SA	4.63			5R3 99-104	1.73	
	ES8b	5.98			5R3 125-131	1.28	
	ES14b	5.12			7R3 0-5	0.44	
	PO48	4.79			8R1 18-21	0.27	
	PO57	4.27			8R1 65-67	0.84	
	PO66	4.71			10R6 67-70	0.07	
	PO74	4.53			11R2 131-136	0.10	
	PO304	4.71			12R1 101-104	0.26	
	PO52	5.49			12R3 57-62	0.08	
	PO65	6.28			15R1 57-61	0.06	
	PO53	4.04			15R7 31-34	0.53	
	PO301	4.09			17R4 15-18	4.15	
	PO63	4.26			19R2 24-27	0.84	
	PO408	4.71			21R2 69-71	0.09	
	PO412	4.77			25R1 10-13	0.05	
	PO404	6.68			34R1 93-96	0.18	
	MV7	5.00			37R5 112-114	0.43	
	GAV3	4.76			40R1 24-27	0.58	
	GAV2	5.41			43R1 13-15	0.07	
	GAV24	5.64			43R3 50-55	2.24	
	GAV40	4.98			44R3 23-26	0.37	
	GAV100	6.30			TAB FLO	3.66	
	GAV103	5.85			TAB VCL	1.55	
	GAV106	6.60			TAB MIX	3.24	
	S2-700	10.89			MORB 0-110 FLO	0.79	
	S2-711	6.90			MORB 0-110 MIX	1.00	
	S2-744	6.69			MORB 110-220 FLO	0.14	
	S2-761	7.14			MORB 110-220 VCL	0.95	
	S2-779	5.46			MORB 110-220 MIX	0.39	
	S2-790	6.77			MORB 220-420 FLO	0.39	
	D2-807	5.83			MORB 220-420 VCL	0.91	
	S2-811	5.46			MORB 220-420 MIX	0.57	
	S2-836	5.69			SUPER	0.62	
	S2-838	4.99			SED	0.72	
	S2-844	4.89		Yokochi et	DU25		34.5
	S2-861	5.41		al., 2009	DU24H		340.1
	D2-896	4.47		Yui et	C-63		
	S2-913	5.00		al., 2009	C-60	4.93	

Continued on next page

Table A.2 – continued from previous page

Reference	Sample	K_2O	Rb	Reference	Sample	K_2O	Rb
	S3-883	5.34			C-59	4.44	
	S3-833.5	6.86			C-55	3.53	
	S2-892	5.31			C-49	4.02	
	S2-901	6.27			C-43	4.16	
	S3-912	5.01			C-41	3.86	
	MS1-440	10.33			C-35	3.77	
	MS1-445	4.88			C-27	4.54	
	MS1-465	7.65			S-6	4.34	
	MS1-484	5.50			S-15	3.68	
	MS1-513	7.83			s-34	2.13	
Marty 1995	ERP 21 981R26				s-49	3.72	
	EPR 13 CY82 09 03				s-78	2.78	
	EPR 13 CY82 31 02				s-87	4.01	
	EPR 13 CL DR01 5V				S-137	4.10	
	EPR 13 CY82 30-b				S-152	4.15	
	MAR 36 CH31 DR09			Busigny et	CH-129		
	MAR 36 CH31 DR11			al., 2011	CH-80-02	0.05	
	MAR 36 CH31 DR10				G6004A		4.2
	MAR 30 CH98 DR11				G6004b		0.8
	MAR 30 CH98 DR12				G6004c		
	MAR 30 CH98 DR15				09-02WR		0.6
	MAR 30 CH98 DR17				VS-1	0.02	2.9
	MAR 14 2PiD43				Vi-52		
Hall et	B-136	2.40			Vi-262M	0.03	
al., 1996	B-137	2.82			Vi-389M		0.7
	B-170	3.60			Vi-385M	0.20	6.7
	B-176	4.14			Vi-385V	0.30	7.1
	B-178	3.73			Vi387V		
	B-165	3.98			Vi-79V	0.04	1.1
	B-2	5.15			VS-14V		2.3
	B-511	3.49		Palya et	Zone 1	5.56	243
	B-B12	4.00		al., 2011	1	7.25	311
	B-511	4.37			1	6.91	285
	B-116	3.60			1	6.54	295
	B-182	4.21			1	5.86	260
	B-97	4.41			1	6.34	265
	SIO-10331	3.92			1	6.04	256
	SIO-10371	3.80			2A	6.40	668
	JAL-4	4.61			2A	6.38	664
Hall et	GREB-600	3.30			2A	2.33	325
al., 1996	GREB-601	3.55			2A	7.07	330
	GREB-602	3.30			2A	5.21	184
	GREB-603	4.76			2A	2.48	159
	GREB-604	5.43			2A	6.64	344
	GREB-605	3.87			2A	6.65	300
	GREB-606	5.60			2B	6.16	284
	GREB-607	4.17			2B	5.49	294
	GREB-608	5.07			2B	6.00	
	GREB-609	3.47			2B	5.71	265
	B-509		584		2B	4.65	201
	B-508		535		2B	3.37	144
	B-507		563		2B	2.00	1423
	B-510		386		2B	4.97	216
	B-506		318		2B	6.64	296
	B-505		363		2B	4.99	252
	B-504		318		2B	4.41	220
	B-503		310		2B	3.30	127
	B-502		297		2B	5.16	234
	B-501		286		2C	6.14	272
	B-500		274		2C	6.88	
	Alijo-Sanfins				Zone 3	6.43	430
Bebout 1997	8-3-90	3.64				5.56	222
	9-1-50a	2.72				4.93	201
	9-1-50b	4.16				5.11	230
	9-1-50c	4.04				6.09	226
	9-1-50d	4.00				4.00	496
	SC4-56	3.44				3.98	487
	SC4-82	3.20			Zone 4	1.60	176
	SC4-96	2.98				6.47	246

Continued on next page

Table A.2 – continued from previous page

Reference	Sample	K_2O	Rb	Reference	Sample	K_2O	Rb
	SC4-26	1.96				2.47	103
	SC3-2	3.88				5.07	272
	SC4-58	3.62				4.97	174
	LCC-218	2.62				5.83	212
	LCC-214	2.52				5.74	222
	LH3-42	3.82				4.89	211
	LHCNGL66	0.60				1.31	105
Bebout et	LA	1.96	70			5.94	241
al., 1999b	LA	2.72	120			5.61	205
	LA	2.35	110			5.16	159
	LA	1.26	52			1.19	79
	LA	4.40	160			6.17	205
	LA	4.40	162			5.36	170
	LA	1.54	79			6.08	166
	LA	3.67	125			3.83	136
	LA	3.02	114			4.39	185
	LB	2.96	92			5.90	184
	LB	1.63	41			6.23	27
	LB	4.19	145			5.84	261
	LB	1.59	61			2.88	123
	EB	2.34	73			3.02	151
	EB	0.78	24			4.70	204
	EB	0.40	33			5.43	279
	EB	0.74	27			3.37	123
	EB	1.50	32	Ahadnejad et	38	3.83	
	EB	2.08	59	al., 2011	44	3.21	
	EB	3.20	72		54	3.77	
	EB	1.82	46		56	4.37	
	EA	5.47	167		61	3.66	
	EA	0.74	20		68	3.91	
	EA	2.17	67		77	3.25	
	EA	2.12	64		80	3.40	
	EA	0.07	10		87	2.63	
	EA	2.70	80		91	3.88	
	A	1.50	54		149	3.14	
	A	2.68	124		150	2.47	
	A	2.84	112		186	3.88	
	A	0.78	75		192	1.06	
	A	1.98	27		106	2.64	
	A	1.58	45		116	6.80	
	A	3.20	44		161	10.60	
	A	2.20	63		200	4.12	
	A	2.87	85		201	4.35	
	A	3.21	114		209	3.15	
	Fresh	5.23			211	4.21	
	Altered	4.17			232	3.77	
	Fresh	5.50			237	3.94	
	Altered	7.56			241	3.31	
	Fresh	4.95			250	2.95	
	Altered	4.58			256	3.11	
Bebout et	1718	4.62		Cruz 2011	MP-2	9.62	
al., 1999a	1717	4.47			MP-8	7.70	
	1715	6.17			MP-22	9.87	
	KDC-50	3.07	151		MP-26	8.95	
	KDC-45	2.89	147		RMP-26-3	8.23	
	KDC-30	3.50	160	Dixon et	Black Schist	1.76	
	KDC-26	3.11	146	al., 2012	Marble	0.25	
	KDC-23	3.31	157		Garnet Schist	0.40	
	KDC-19	3.34	155		Hard Schist	0.27	
	KDC-13	3.07	150	Busigny	J1-124-1	11.36	
	KDC-12	3.04	151	et al., 2013	J1-138-1	1.47	
	KDC-8	3.25	155		J1-148-3	2.48	
	KDC-7	3.35	165		J1-148-2	1.54	
	KDC-50	4.43	201		J1-162-1	3.90	
	KDC-61	2.74	146		WS188	4.26	
	KDC-62	3.25	150		WS196	5.90	
	KDC-65	3.27	158		DGM236	4.06	
	KDC-66	3.26	161		DGM243	10.48	
	KDC-70	2.90	159		DGM258-1	2.33	

Continued on next page

Table A.2 – continued from previous page

Reference	Sample	K_2O	Rb	Reference	Sample	K_2O	Rb
	KDC-72	3.36	192		DGM258-2	2.00	
	JKDC-73	3.76	218		DGM268	2.91	
	KDC-75	3.65	155		DGM271-2	0.51	
	KDC-76	3.39	186		DGM287	5.60	
	KDC-77	3.18	170		DGM288-1	0.62	
	KDC-80	4.46	158		DGM288-2	0.37	
	KDC-81	4.64	196		DGM302	0.97	
	KDC-82	3.60	149		DGM307-4	0.56	
Jia and	KA II-1	11.28			DGM307-6	0.05	
Kerrich 2000	KA I-1	11.30			DGM325	1.67	
	B4	11.20			DGM337	1.09	
	B4-1	11.25			DGM350	1.29	
	B5	11.14			CC364	0.12	
	D-1	11.05			CC367	1.07	
	GH IA	10.87			CC373	1.38	
	GH IB	11.04			CC376	1.37	
	GH IC	10.79			MR379	4.98	
	GH I-B	11.14			MR381	4.51	
	GH I-C	11.28			MR382	9.34	
	GH I-F	11.29			MR383	6.03	
	GH II-1	10.59			MR387	3.91	
	GH II-2	10.66		Bebout et	SL99-21B	2.69	126
	GH II-3	9.77		al., 2013	SL99-21D	3.86	183
	MAC	9.39			SL99-36B	6.12	314
	MAC-1	9.80			SL99-36A	2.98	142
	HD-1	9.69			ALB-957	1.73	71
	HD-2	9.50			MIU-955	3.91	191
	WL170	9.81			PEL-942	4.62	173
	NR7-1	9.87			02-LDCS-11	4.21	185
	NR10	9.43			LC99-4A	3.05	129
	MRAI-1	9.60			02-LDCS-01	3.15	102
	MRA 1-2	9.83					
	MRA II-1	9.88					
	VHW-1	9.40					
	NNM-1	9.26					
	NNM-2	9.44					
	NNM-a	9.68					
	NNM-b	9.60					
	RT-1	9.78					
Dauphas and		0.02					
Marty 1999		0.02					
		0.25					
		0.40					
		0.02					
		0.48					
		1.20					
		0.95					
	Cc	1.38					
	Cc	0.03					
	D	1.05					
	Dc	0.12					
	I	2.81					
	O	0.80					
	O	2.06					
	Cpx	0.22					
	Dc	0.02					
Mingram and	LG	3.60					
Brauer 2001	LG	2.97					
	LG	4.24					
	LG	4.06					
	P	4.00					
	P	3.41					
	P	3.22					
	P	3.87					
	P	3.48					
	P	5.04					
	GP	4.55					
	GP	6.18					
	GP	4.79					

Continued on next page

Table A.2 – continued from previous page

Reference	Sample	K_2O	Rb	Reference	Sample	K_2O	Rb
	GP	4.17					
	GP	2.75					
	GP	5.01					
	GP	4.48					
	GP	7.24					
	MS	4.70					
	MS	3.60					
	MS	5.82					
	MS	4.68					
	MS	6.08					
	MS	4.43					
	MS	5.48					
	MS	4.81					
	MS	3.00					
	MS	5.86					
	GE	4.84					
	GE	4.50					
	GE	6.12					
	T	3.93					
	T	2.53					
	T	2.63					
	T	3.61					
	T	4.84					
	T	5.85					
	T	4.94					
	G	3.38					
	G	3.38					
	G	4.23					

Table A.3: Terrestrial Ar isotopic and N_2 data. See first page of Appendix A for full description, and Table A.1 for sample notes. Total Ar (Ar-tot) and 36Ar are shown in mol/g, with all others as molar ratios.

Reference	Sample	40Ar/36Ar	36Ar	Ar-tot	N2/36Ar	N2/40Ar
Sano and	Onverwacht			6.79E-03		
Pillinger 1990	Marra Mamba			8.88E-04		
	Frere Formation			5.36E-03		
	Beck Spring			9.55E-04		
	Rhynie			4.25E-03		
	Magadi			2.33E-03		
Marty 1995	ERP 21 981R26	3321	1.71E-15	5.68E-12	2.82E+05	85
	EPR 13 CY82 09 03	3020	4.47E-16	1.35E-12	2.10E+05	70
	EPR 13 CY82 31 02	1065	1.36E-15	1.45E-12	8.01E+04	75
	EPR 13 CL DR01 5V	4043	5.94E-15	2.40E-11	5.46E+05	135
	EPR 13 CY82 30-b	1668	1.43E-15	2.38E-12	1.13E+05	68
	MAR 36 CH31 DR09	1200	1.07E-14	1.28E-11	5.86E+04	49
	MAR 36 CH31 DR11	10828	2.98E-15	3.23E-11	5.70E+05	53
	MAR 36 CH31 DR10	532	2.27E-15	1.21E-12	4.22E+04	79
	MAR 30 CH98 DR11	1273	1.63E-14	2.07E-11	1.05E+05	82
	MAR 30 CH98 DR12	9717	1.91E-15	1.86E-11	1.01E+06	104
	MAR 30 CH98 DR15	8756	1.21E-14	1.06E-10	9.75E+05	111
	MAR 30 CH98 DR17	2279	3.38E-14	7.70E-11	1.58E+05	69
	MAR 14 2PiD43	1641	4.89E-13	8.03E-10	9.09E+04	55
Marty and	CH98DR11	1237	3.59E-14	4.44E-11	1.18E+05	95
Humbert 1997	CH98DR11	1929	2.60E-14	5.01E-11	1.70E+05	88
	CH98DR11	2190	3.27E-14	7.16E-11	2.01E+05	92
	CH98DR11	4723	5.23E-15	2.47E-11	5.53E+05	117
	CH98DR11	26621	2.43E-15	6.46E-11	2.95E+06	111
	CH98DR11	42366	2.60E-16	1.10E-11	3.57E+06	84
	CH98DR11	6907	1.01E-14	6.99E-11	5.83E+05	84
	CH98DR12	2035	2.48E-14	5.04E-11	2.15E+05	106
	CH98DR12	10180	3.76E-15	3.83E-11	9.86E+05	97
	CH98DR15	15587	2.29E-15	3.57E-11	1.58E+06	101
	CH98DR15			4.73E-11		
	CH98DR17	2417	1.73E-14	4.19E-11	1.63E+05	68
	CH31DR01r10	371.8	7.53E-15	2.80E-12	1.46E+05	393

Continued on next page

Table A.3 – continued from previous page

Reference	Sample	40Ar/36Ar	36Ar	Ar-tot	N2/36Ar	N2/40Ar
	CH31DR01r100	766.4	1.19E-14	9.10E-12	3.20E+04	42
	Total	425.9	8.66E-14	3.69E-11	1.71E+04	40
	CH31 DR02	5094	4.67E-15	2.38E-11	2.38E+05	47
	CH31DR01r10	1420	6.24E-15	8.86E-12	6.83E+04	48
	CH31DR01r100	419.9	3.24E-14	1.36E-11	3.05E+04	73
	Total	577.9	3.89E-14	2.25E-11	3.65E+04	63
	CH31DR11	831.2	4.27E-14	3.55E-11	5.22E+04	63
	CH31DR11	4172	9.11E-15	3.80E-11	1.93E+05	46
	CH31DR11	4307	5.06E-15	2.18E-11		
	CH31DR11	15029	2.40E-15	3.61E-11	5.50E+05	37
	CH31DR11	546.1	2.75E-15	1.50E-12	1.38E+04	25
	Total	7302	5.15E-15	3.76E-11	2.64E+05	36
	CY84	915	3.04E-15	2.78E-12	8.85E+04	97
	CLDRO1	565.6	3.52E-14	1.99E-11	4.01E+04	71
	CLDRO1	1850	7.41E-15	1.37E-11	1.38E+05	74
	Total	789	4.26E-14	3.36E-11	5.71E+04	72
	CY82	928	4.42E-15	4.10E-12	5.45E+04	59
	CY82	2964	3.41E-15	1.01E-11	3.32E+05	112
	CY82	7145	3.50E-15	2.50E-11	7.69E+05	108
	KS	469.5	1.58E-14	7.40E-12	1.71E+04	36
	KS	306.5	3.37E-13	1.03E-10	1.42E+04	46
	KS	387.9	4.69E-14	1.82E-11	1.61E+04	42
	MR80	362.3	7.78E-14	2.82E-11	1.98E+04	55
	PL2	667.9	7.44E-15	4.97E-12	2.74E+04	41
	PL2	308.6	2.04E-14	6.29E-12	2.01E+04	65
	PL2	560.3	7.12E-15	3.99E-12	3.83E+04	68
	PL2	895.1	1.36E-14	1.22E-11	1.03E+05	115
	PL2-24-32	880.7	8.15E-15	7.18E-12	2.77E+04	31
	PL2-RC-O1	2635	2.16E-15	5.69E-12	2.07E+05	78
	TH30-3	299.4	8.66E-12	2.59E-09	9.71E+04	324
	AQ39C-108	300.6	1.91E-13	5.73E-11	1.66E+05	551
Sano et	KH93-3-DR3	3150			4.39E+05	139
al., 1998	KH93-3-DR6	4940			3.32E+05	67
	KH93-3-DR25	16600			2.52E+06	152
	CH31-DR11	5190			2.71E+05	52
	CH98-DR11	19200			1.87E+06	97
	KT84-1-24-1	1780			2.09E+05	117
	KT84-1-24-2	391			3.67E+04	94
	KT84-1-24-3	619			6.63E+04	107
	ST4-DV17-3	352			6.78E+04	193
	ST4-DV19-1	2020			7.15E+05	354
	ST4-DV21-5	362			2.99E+04	83
	Atsukawa	303			2.89E+04	95
	Houei	300			4.58E+05	1527
	Unzen	377			5.91E+04	157
	Miyake-jima	293			2.28E+04	78
	Hachijo-jima	311			3.03E+04	97
Dauphas and		612	9.28E-14	5.69E-11	4.27E+04	70
Marty 1999		5103	7.62E-15	3.89E-11	2.28E+05	45
		4281	3.04E-14	1.30E-10	1.01E+05	24
		2497	1.05E-14	2.63E-11	1.35E+05	54
		2376	1.08E-14	2.57E-11	1.20E+05	51
		2062	2.04E-15	4.20E-12	1.33E+05	64
		2102	1.87E-14	3.93E-11	1.82E+05	87
		1485	4.24E-15	6.30E-12	1.34E+05	90
	Cc	532	1.32E-13	7.01E-11	6.05E+04	114
	Cc	691	3.94E-13	2.73E-10	5.13E+04	74
	D	2144	2.46E-14	5.27E-11	2.47E+05	115
	Dc	745	4.54E-14	3.38E-11	5.51E+04	74
	I	3720	1.26E-14	4.68E-11	1.39E+05	37
	O	1415	1.48E-14	2.10E-11	1.00E+05	71
	O	1456	6.34E-14	9.24E-11	1.09E+05	75
	Cpx	926	5.51E-14	5.11E-11	6.39E+04	69
	Dc	716	4.65E-14	3.33E-11	6.08E+04	85
Marty and	CLDR01	10215	1.25E-15	1.28E-11	9.34E+05	91
Zimmerman 1999	CLDR04	4734	1.16E-15	5.50E-12	2.31E+06	487
	CY82 31 01	429.7	1.46E-14	6.30E-12	8.20E+03	19
	SR1DR04	735.8	4.21E-15	3.10E-12	2.38E+04	32
	ND 11-2 #1	500.9	1.28E-14	6.40E-12	1.93E+05	385

Continued on next page

Table A.3 – continued from previous page

Reference	Sample	40Ar/36Ar	36Ar	Ar-tot	N2/36Ar	N2/40Ar
	ND 11-2 #2	1427	1.54E-15	2.20E-12	1.01E+06	710
	ND 11-2 #3	171.8	9.84E-15	1.70E-12	3.16E+05	1840
	ND 12-2	913.8	2.40E-15	2.20E-12	1.16E+05	127
	ND 15-4	859.7	3.83E-15	3.30E-12	1.25E+05	146
	ND 18-1	1098	1.36E-16	1.50E-13	1.57E+05	143
	ND 19-8	1782	1.40E-15	2.50E-12	2.64E+05	148
	ND 21-3	697.8	1.72E-16	1.20E-13	1.75E+05	250
	ND21-4	4456	1.17E-15	5.20E-12	8.23E+05	185
	SR2DR02	519.7	5.38E-15	2.80E-12	3.53E+04	68
	SR2DR03	706.5	1.55E-15	1.10E-12	5.72E+05	810
	KS 11 A	469.5	1.57E-14	7.41E-12	1.71E+04	37
	KS 12 A	423	2.19E-15	9.30E-13	1.82E+04	43
	KS 04 A	387.9	4.68E-14	1.82E-11	1.62E+04	42
	MR80 59 4	362.3	7.76E-14	2.82E-11	1.98E+04	55
	HY09-07H	845.6	2.72E-14	2.30E-11	1.46E+05	173
	JC 217 D1 (3)	4249	3.74E-15	1.59E-11	3.26E+05	77
	JC 0300703D1	491.9	5.64E-14	2.78E-11	4.45E+04	90
	MD23-4	3463	1.35E-14	4.69E-11	2.08E+05	60
	MD57 D4-4	3555	2.76E-15	9.80E-12	3.66E+05	103
	MD23-2	3676	9.63E-15	3.54E-11	4.39E+05	120
	MD370301	5509	6.62E-15	3.65E-11	4.02E+05	73
	SWIR DR2-3	1862	2.50E-14	4.65E-11	2.10E+05	113
	MD23-1	1886	3.50E-15	6.60E-12		
	ST2-17-6	531.9	6.19E-15	3.30E-12	5.65E+04	106
	ST2-17-7	3339	5.90E-15	1.97E-11	6.97E+05	209
	ST-17-10	666.7	5.24E-15	3.50E-12	6.81E+04	102
Nishio et	KH93-3-DR3-A1	3150	1.87E-14	5.90E-11	4.38E+05	139
al., 1999	KH93-3-DR1-f1	515	7.96E-14	4.11E-11	4.36E+04	85
	KH93-3-DR9-G1	11300	7.17E-15	8.10E-11	1.42E+06	125
	KH93-3-DR25-A1	17000	3.06E-15	5.20E-11	2.59E+06	152
	KH93-3-DR25-A2	704	1.04E-13	7.31E-11	1.06E+05	151
	KH93-3-DR6-A1	4950	2.10E-14	1.04E-10	3.33E+05	67
	CH31-DR11	5190	9.25E-15	4.80E-11	2.71E+05	52
	CH98-DR11	19000	1.74E-15	3.30E-11	1.85E+06	97
Pinti et	SJM43	189352	7.04E-14	1.33E-08	1.33E+07	70
al., 2001	SJM43a	143898	3.10E-13	4.47E-08	8.29E+06	58
	SJM43	168108	3.15E-13	5.29E-08	8.43E+06	50
	1021	2817	2.39E-14	6.74E-11	5.37E+06	1907
	136	2848	1.80E-14	5.14E-11	5.19E+06	1822
	611	11641	1.54E-14	1.79E-10	1.70E+06	146
	702	17126	6.03E-15	1.03E-10	2.43E+06	142
	Pano D-136	29792	3.87E-14	1.15E-09		
	Pano C-85	4950	1.87E-14	9.24E-11	6.89E+05	139
	Chert-Barite	786	2.00E-14	1.57E-11	4.83E+05	615
	458	3755	3.32E-14	1.25E-10	1.00E+06	266
	LBR-31	395	1.99E-14	7.88E-12	7.41E+06	18755
	HR-28-544	14715	8.17E-15	1.20E-10	8.48E+06	576
Matsumoto et	VIC51	3277	5.11E-15	3.75E-07	3.79E+05	116
al., 2002	VIC51A	1444	7.23E-16	2.34E-08	1.79E+05	124
	GAMVL3	1790	3.45E-15	1.38E-07	1.45E+05	81
	VIC53C	384	9.06E-15	7.82E-08	3.30E+04	86
	VIC53C	394	6.45E-15	5.71E-08	3.60E+04	91
	VIC54F	421	4.70E-15	4.44E-08	3.80E+04	90
	SHD6	558	2.19E-15	2.74E-08	4.90E+04	88
Marty and	SO47-5D2	905	1.14E-12	1.04E-09	1.20E+05	133
Dauphas 2003	2SO47-9D2	329	1.56E-13	5.16E-11	2.70E+04	82
	TH09-02	348	4.70E-13	1.64E-10	2.50E+04	72
	TH09-05	299	1.33E-13	4.00E-11	2.90E+04	97
	TH12-06	468	7.95E-13	3.73E-10	3.50E+04	75
	TH14-02	490	3.28E-13	1.61E-10	4.60E+04	94
	TH14-03-4	9995	3.12E-14	3.12E-10	8.60E+05	86
	TH14-03-5	2231	2.64E-13	5.90E-10	3.10E+05	139
	TH14-05	2597	8.97E-14	2.33E-10	2.30E+05	89
	TH10-04	660	6.35E-13	4.20E-10	5.20E+04	79
	SO47-81DS	417	4.78E-14	2.00E-11	4.60E+04	110
	TH25-03-4	5175	1.40E-15	7.26E-12	3.20E+05	62
	SO47-34DS	1598	4.46E-13	7.13E-10	1.50E+05	94
	TH21	384	4.47E-14	1.72E-11	3.00E+04	78
	DTH02-01-1	4786	4.03E-15	1.93E-11	5.30E+05	111

Continued on next page

Table A.3 – continued from previous page

Reference	Sample	40Ar/36Ar	36Ar	Ar-tot	N2/36Ar	N2/40Ar
	DTH02-01-2	3156	6.81E-15	2.15E-11	3.70E+05	117
	DTH02-01-3	6681	3.29E-15	2.20E-11	5.90E+05	88
	DTH02-01-4	1264	2.30E-14	2.91E-11	2.10E+05	166
	DTH02-01-5	5134	3.00E-15	1.54E-11	3.90E+05	76
	DTH02-02-1	8202	2.49E-15	2.04E-11	1.44E+06	176
	DTH02-02-2	3130	1.10E-14	3.44E-11	2.40E+05	77
	DTH03-02	360	2.77E-14	1.00E-11	4.10E+04	114
	DTH04-01-1	592	7.39E-14	4.38E-11	3.80E+04	64
	DTH04-01-2	777	7.28E-14	5.66E-11	5.10E+04	66
	DTH04-01-3	1641	2.28E-14	3.74E-11	8.60E+04	52
	DTH05-02	335	4.20E-15	1.41E-12	1.80E+04	54
	TH28-07	299	5.87E-14	1.76E-11	1.30E+04	43
	TH30-03	291	3.25E-12	9.49E-10	2.50E+04	86
	T4D3#3	298	3.75E-13	1.12E-10	2.80E+04	94
	T4D3#7	305	1.27E-13	3.89E-11	2.40E+04	79
	G324G	422	1.70E-14	7.21E-12	7.90E+04	187
	G296G	1095	2.18E-15	2.39E-12	1.70E+05	155
	G136D	3825	3.92E-15	1.50E-11	8.00E+05	209
	G178D	618	4.88E-15	3.02E-12	5.70E+04	92
	DICE10-10	1669	1.01E-14	1.69E-11	1.20E+05	72
	DICE10-10	3203	5.90E-15	1.89E-11	2.30E+05	72
	DICE10-10	3302	1.03E-14	3.41E-11	2.60E+05	79
	DICE11-10#	940	2.91E-14	2.74E-11	6.20E+04	66
	DICE11-10#	3004	1.10E-14	3.30E-11	2.30E+05	77
	DICE11-10#	1574	5.49E-15	8.64E-12	1.10E+04	7
van Zuilen et	6.4D2 P	13400	1.32E-12	1.76E-08	2.39E+05	18
al., 2005	6.4D2 C	12000	6.99E-13	8.39E-09	1.24E+05	10
	AL43-3 P	10900	2.54E-12	2.76E-08	6.00E+04	6
	AL43-3 C	4500	2.58E-13	1.16E-09	1.06E+05	24
	6.4D1 P	8900	1.31E-12	1.17E-08	1.62E+04	2
	6.4D1 C	9975	5.91E-13	5.89E-09	4.94E+05	49
	6.3A2 P	15400	6.15E-13	9.46E-09	1.58E+05	10
	6.3A2 C	7900	2.26E-13	1.79E-09	9.45E+05	120
Mohapatra et	FVB03	1051	1.25E-14		6.18E+06	5878
al., 2009	LP01	576	1.60E-14		1.87E+06	3250
	Dice 2	428	1.40E-14		1.03E+07	24006
	Dice 12	341	2.71E-14		6.53E+06	19139
	Chisny	1368	1.25E-14		4.14E+06	3028
	DRE	902	2.95E-14		2.60E+06	2885
	ILR	4198	6.65E-15		6.82E+06	1624
	REF2	637	1.36E-14		1.27E+07	19954
	REF3-1	1098	1.15E-14		2.11E+06	1920
	REF3-2	842	1.53E-14		9.21E+06	10942
	REF3-3	1106	1.75E-14		8.10E+06	7326
	Samoa	330	3.63E-13		2.12E+05	641
Yokochi et	JK7B	686	2.33E-15	1.60E-12	5.62E+06	8188
al., 2009	JK7U	497.3	5.23E-15	2.61E-12	2.98E+06	6000
	JK8B	412.4	1.33E-14	5.51E-12	1.53E+06	3709
	BA8U	456.9	4.82E-15	2.20E-12	6.19E+06	13545
	MM2B	541.5	2.22E-15	1.20E-12	1.49E+05	275
	MM2U	1006.1	2.48E-16	2.50E-13	1.25E+07	12400
	MM13C	371.5	4.60E-14	1.71E-11	1.89E+05	509
	MM13 W	544.9	1.85E-14	1.01E-11	4.42E+05	812
	MM13 M	477.9	2.03E-14	9.72E-12	1.13E+06	2361
	DU25	1374.6	1.09E-15	1.50E-12	1.65E+06	1200
	DU25U	440	1.36E-14	6.01E-12	4.99E+05	1133
	DU24P	415.5	1.78E-13	7.41E-11	1.52E+06	3667
	DU24H	443.8	1.46E-13	6.49E-11	4.15E+06	9344
	DU24O	1181.6	2.03E-16	2.40E-13	1.67E+07	14167
	DU24C	1046.8	1.41E-14	1.48E-11	3.04E+05	291
	DU24B	686.4	2.19E-15	1.50E-12	8.19E+06	11933
	DU26B	930.8	5.69E-16	5.31E-13	1.02E+07	10943
	DU26P	582	5.62E-14	3.28E-11	1.63E+07	28018
	F100P	421.8	7.80E-13	3.30E-10	7.85E+05	1862
	F100B	1070.1	4.67E-15	5.00E-12	1.93E+06	1800
	F100A	470.5	4.14E-13	1.95E-10	6.00E+05	1274
Roulleau et	Mt Royal	531.4	1.03E-14	5.48E-12	2.63E+06	4951
al., 2012	St Bruno	448.3	4.23E-14	1.90E-11	1.89E+07	42235
	St Hilaire	609.8	2.65E-14	1.62E-11	9.21E+05	1510

Continued on next page

Table A.3 – continued from previous page

Reference	Sample	40Ar/36Ar	36Ar	Ar-tot	N2/36Ar	N2/40Ar
	St Gregoire	336.6	2.14E-14	7.22E-12	3.43E+06	10190
	Rougemont	413.9	2.39E-14	9.92E-12	7.69E+06	18580
	Yamaska	682.2	3.30E-15	2.25E-12	6.64E+06	9728
	Shefford	570.5	1.37E-14	7.83E-12	2.75E+06	4824
	Brome	605.4	4.90E-15	2.97E-12	6.14E+06	10147

Table A.4: Ytterbium and Lu data from rocks which also have N measurements. These elements displayed correlation in lamproites and lamprophyres, and may in other rocks. See table A.1 for sample notes.

Reference	Sample	Yb	Lu
Sadofsky and Bebout 2003	VD 2a	3.27	0.48
Metaseds. Franciscan cmpx.	VD 9b	2.22	0.32
and the Baja Terrane	KW98-21b	2.52	0.37
	Eel4 Shale	2.03	0.38
	JC c4a	2.5	0.28
	JC 5	2.02	0.2
	Apc5a	2.82	0.27
	AP 8	1.72	0.4
	CR 2b	2.08	0.24
	Alder 2	2.09	0.27
Baja	RLS-585-1	2.67	0.27
	RLS-585-14	1.59	0.38
	RLS-486-105	1.37	0.32
	RLS-585-71	1.84	0.2
	RLS-486-130	1.83	
Jia et al., 2003	CP60/93	3.97	0.45
Lamprolite = L	B-4	2.03	0.29
Lamprophyre = LP	SD-1	5.06	0.69
	SD-2	4.75	0.57
	SD-3		
	P-1	5.19	0.67
	P-2	6.9	0.9
	M2/1	3.09	0.4
	M-2/2	3.35	0.46
	KH-1	3.44	0.41
	KH-2	6.21	0.9
	R839A	2.34	0.31
Busigny et al., 2011	CH-129	9.7	1.3
Ophiolites from the Alps	CH-80-02	9.5	1.3
most analyses are meta-gabbros	G6004A	1.4	0.2
	G6004b	5.4	0.8
	G6004c	2.1	0.3
	09-02WR	1	0.2
	VS-1	2.2	0.4
	Vi-52	0	
	Vi-262M	8.1	1.2
	Vi-389M	8.1	1.2
	Vi-385M	4.6	0.7
	Vi-385V	5.6	0.8
	Vi387V	0.6	0.1
	Vi-79V	1.1	0.2
	VS-14V	0.5	0.1
Halama et al., 2012	N-MORB	8.1	
Compilation paper	E-MORB	8.1	
	Low-grade serpentinites	4.6	
	High-P peridotites	5.6	
	High-P ultramafic veins	0.6	
	Chlorite harzburgite	1.1	
	High-P ultramafic veins	0.5	

Table A.5: Compilation of experimental data. Shown are reference, and type of analysis is silicate melt (Melt), silicate melt in equilibrium with metal (MeltM), Fe-metal (Metal), ratio of melt to metal, or mineral names. Mineral abbreviations are Fo (forsterite), Py (pyrope), Di, (diopside), and En (enstatite). RunID, time (minutes), pressure (P, GPa), and temperature (T, °C), and redox buffer are all taken from original reference. I then calculate the oxygen fugacity, in log units, at given P-T conditions, and what that f_{O2} would be at the NNO buffer ($\log f_{O2\text{-NNO}}$) using constants from Frost (1991). Then, I show f_{O2} difference from the NNO buffer (Δ_{NNO}) and measured N concentration (ppm) with error.

Reference	Type	RunID	Time	P	T	Buffer	$f_{O2\text{-o}}$	$f_{O2\text{-NNO}}$	Δ_{NNO}	N	error
Mysen et	Melt	NS4	60	1	1300	MH	-1.66	-6.2	4.54	900	300
al., 2008	Melt	NS4	30	1	1400	MH	-0.69	-5.27	4.58	200	200
	Melt	NS4	30	1	1500	MH	0.17	-4.44	4.61	900	200
	Melt	NS4	60	1	1300	IW	-10.42	-6.2	-4.23	3600	1100
	Melt	NS4	30	1	1400	IW	-9.4	-5.27	-4.13	3100	700
	Melt	NS4	30	1	1500	IW	-8.49	-4.44	-4.05	1600	200
	Melt	NS4	30	1	1400	MM	-1.57	-5.27	3.7	1700	200
	Melt	NS4	30	1	1400	NNO	-5.27	-5.27	0	2400	200
	Melt	NS4	30	1	1400	IW	-9.4	-5.27	-4.13	2200	500
	Melt	NS4	60	1.5	1300	MH	-1.6	-6.05	4.45	1800	1800
	Melt	NS4	30	1.5	1400	MH	-0.63	-5.13	4.5	1400	1400
	Melt	NS4	30	1.5	1500	MH	0.22	-4.31	4.53	1800	900
	Melt	NS4	60	1.5	1300	IW	-10.25	-6.05	-4.2	5800	900
	Melt	NS4	30	1.5	1400	IW	-9.24	-5.13	-4.11	6800	1100
	Melt	NS4	30	1.5	1400	MM	-1.51	-5.13	3.62	3000	700
	Melt	NS4	30	1.5	1400	NNO	-5.13	-5.13	0	2300	1000
	Melt	NS4	30	1.5	1400	MW	-5.85	-5.13	-0.72	3100	200
	Melt	NS4	60	2	1300	IW	-10.07	-5.9	-4.17	11400	700
	Melt	NS4	30	2	1400	IW	-9.07	-4.99	-4.08	12300	600
	Melt	NS4	15	2	1400	IW	-9.07	-4.99	-4.08	10100	800
	Melt	NS4	60	2	1400	IW	-9.07	-4.99	-4.08	12200	400
	Melt	NS4	180	2	1400	IW	-9.07	-4.99	-4.08	12400	500
	Melt	NS4	30	2	1400	MH	-0.58	-4.99	4.41	5100	800
	Melt	NS4	30	2	1400	MM	-1.45	-4.99	3.54	4600	900
	Melt	NS4	30	2	1400	NNO	-4.99	-4.99	0	3500	600
	Melt	NS4	30	2	1400	MW	-5.61	-4.99	-0.61	5900	600
	Melt	NS4	30	2.5	1400	MH	-0.52	-4.85	4.33	5100	800
	Melt	NS4	30	2.5	1400	NNO	-4.85	-4.85	0	3800	1300
	Melt	NS4	30	2.5	1400	MW	-5.36	-4.85	-0.5	5600	900
	Melt	NS4	30	2.5	1400	IW	-8.91	-4.85	-4.05	16400	2100
	Melt	NS2	30	2	1400	MH	-0.58	-4.99	4.41	4600	900
	Melt	NS2	30	2	1400	NNO	-4.99	-4.99	0	5900	900
	Melt	NS2	30	2	1400	IW	-9.07	-4.99	-4.08	11700	1000
Kadik et	MeltM	3S		1.5	1400	IW-1.9	-11.3	-5.13	-6.17	4700	1300
al., 2011	MeltM	6S		1.5	1400	IW-2.4	-11.8	-5.13	-6.67	6200	1900
	MeltM	7S		1.5	1400	IW-2.4	-11.8	-5.13	-6.67	6000	1900
	MeltM	8S		1.5	1400	IW-3.7	-13.1	-5.13	-7.97	14700	2400
	Metal	7S		1.5	1400	IW-2.4	-11.8	-5.13	-6.67	8400	1600
	Metal	8S		1.5	1400	IW-3.7	-13.1	-5.13	-7.97	4500	2100
	Dmetal	7S		1.5	1400	IW-2.4	-11.8	-5.13	-6.67	1.4	
	Dmetal	8S		1.5	1400	IW-3.7	-13.1	-5.13	-7.97	0.31	
Libourel et	Melt	CM-1#4A	2880	1atm	1400	IW-8.3	-17.7	-5.54	-12.16	1335	118
al., 2003	Melt	CM-1#4B	4320	1atm	1400	IW-8.3	-17.7	-5.54	-12.16	1249	127
	Melt	CM-1#5	2880	1atm	1425	IW-8.3	-17.46	-5.32	-12.14	1517	80
	Melt	CM-1#6	4320	1atm	1425	IW-8	-17.16	-5.32	-11.84	1735	29
	Melt	CM-1#7	4320	1atm	1400	IW-6.9	-16.3	-5.54	-10.76	570	64
	Melt	CM-1#8	5760	1atm	1425	IW-6.8	-15.96	-5.32	-10.64	447	27
	Melt	CM-1#9	2880	1atm	1425	IW-6.7	-15.86	-5.32	-10.54	136	7
	Melt	CM-1#10	2160	1atm	1425	IW-4.1	-13.26	-5.32	-7.94	1.37	0.46
	Melt	CM-1#11	2880	1atm	1425	IW-2	-11.16	-5.32	-5.84	0.1	0.09
	Melt	CM-1#12	2880	1atm	1425	IW	-9.16	-5.32	-3.84	0.02	0.02
	Melt	CM-1#13	2880	1atm	1425	IW+2	-7.16	-5.32	-1.84	0.02	0.03
	Melt	CM-1#14	2880	1atm	1425	IW+3.6	-5.56	-5.32	-0.24	0.04	0.06
	Melt	CM-1#15	2880	1atm	1425	IW+4.1	-5.06	-5.32	0.26	0.06	0.05
	Melt	CM-1#16	2940	1atm	1425	IW+4.3	-4.86	-5.32	0.46	0.04	0.03
	Melt	CM-1#17	2880	1atm	1425	IW+8.7	-0.46	-5.32	4.86	0.05	0.03
Roskosz et	Melt	NS2	60	2	1400			-4.99	4.99	3500	600
al., 2006	Melt	NS2	60	2	1500			-4.18	4.18	4100	600

Continued on next page

Table A.5 – continued from previous page

Reference	Type	RunID	Time	P	T	Buffer	$f_{O2\text{-}o}$	$f_{O2\text{-}NNO}$	Δ_{NNO}	N	error
	Melt	NS2	60	2	1600			-3.46	3.46	4500	600
Read	Melt	NS2	60	2	1700			-2.81	2.81	5300	600
from	Melt	NS4	60	2	1500			-4.18	4.18	5100	600
graph	Melt	NS4	60	2	1600			-3.46	3.46	5200	600
	Melt	NS4	60	2	1700			-2.81	2.81	5500	600
	Melt	NS2	60	1	1600			-3.7	3.7	3000	600
	Melt	NS2	60	2	1600			-3.46	3.46	4300	600
	Melt	NS2	60	3	1600			-3.21	3.21	5800	600
	Melt	NS4	60	1	1600			-3.7	3.7	2600	600
	Melt	NS4	60	1.7	1600			-3.53	3.53	3600	600
	Melt	NS4	60	2	1600			-3.46	3.46	5100	600
Mysen and	Melt	NS1.7	30	1.5	1400	IW	-9.24	-5.13	-4.11	2100	100
Fogel 2010	Melt	NS1.7	60	1.5	1400	IW	-9.24	-5.13	-4.11	2800	100
	Melt	NS2	30	1.5	1400	IW	-9.24	-5.13	-4.11	1300	100
	Melt	NS2	60	1.5	1400	IW	-9.24	-5.13	-4.11	1600	100
	Melt	NS2.5	30	1.5	1400	IW	-9.24	-5.13	-4.11	5500	100
	Melt	NS2.5	60	1.5	1400	IW	-9.24	-5.13	-4.11	4100	100
	Melt	NS4	5	1.5	1400	IW	-9.24	-5.13	-4.11	7500	100
	Melt	NS4	15	1.5	1400	IW	-9.24	-5.13	-4.11	9100	100
	Melt	NS4	30	1.5	1400	IW	-9.24	-5.13	-4.11	8200	100
	Melt	NS4	60	1.5	1400	IW	-9.24	-5.13	-4.11	7500	100
	Melt	NS5	30	1.5	1400	IW	-9.24	-5.13	-4.11	9800	100
	Melt	NS5	60	1.5	1400	IW	-9.24	-5.13	-4.11	10600	100
	Melt	NS2.5	30	1.5	1400	MW	-5.85	-5.13	-0.72	3300	100
	Melt	NS2.5	30	1.5	1400	NNO	-5.13	-5.13	0	3100	100
	Melt	NS2.5	30	1.5	1400	MH	-0.63	-5.13	4.5	2900	100
Li et	Fo	LY16	4320	2.5	1200	IW	-11.03	-6.78	-4.24	2.43	0.3
al., 2013	Fo	LY17	4320	3.5	1200	IW	-10.65	-6.47	-4.18	0.55	0.2
	Fo	LY28	5760	1.5	1100	NNO	-8.29	-8.29	0		
	Fo	LY29	5760	1.5	1100	CoCO	-9.86	-8.29	-1.56	0.64	1
	Fo	LY15	4320	1.5	1200	IW	-11.4	-7.1	-4.3	0.69	1
	Fo	LY33	5760	3.5	1150	NNO	-7.03	-7.03	0		
	Fo	PS8	7200	1.5	1100	IW	-12.72	-8.29	-4.42		
	Fo	PS3	7200	3	1100	IW	-12.12	-7.79	-4.33		
	Fo	LY39	7200	1.5	1100	IW	-12.72	-8.29	-4.42		
	Fo	LY40	1440	1.5	1300	IW	-10.25	-6.05	-4.2	0.48	0.2
	Fo	LY24	450	3.5	1300	IW	-9.55	-5.47	-4.08	7	2
	Py	LY32	10080	3.5	1000	NNO	-8.96	-8.96	0	6.2	8
	Py	LY33	5760	3.5	1150	NNO	-7.03	-7.03	0	20	0
	Py	PS11	4320	1.5	1100	IW	-12.72	-8.29	-4.42	14.78	10
	Di	PS05	7200	2.3	1100	IW	-12.4	-8.03	-4.37	28.33	12
	Di	PS06	7200	2.3	1100	IW	-12.4	-8.03	-4.37	3.63	5
	Di	LY31	2880	1.5	1100	NNO	-8.29	-8.29	0		
	Di	LY18	6840	1.5	1100	IW	-12.72	-8.29	-4.42	4.3	1
	Di	LY34	6912	2.5	1100	NNO	-7.96	-7.96	0		
	Di	LY30	5760	1.5	1100	CoCO	-9.86	-8.29	-1.56	1.1	2
	Di	LY35	6912	3.5	1100	NNO	-7.62	-7.62	0	5.85	6
	En	LY23	7200	1.5	1300	IW	-10.25	-6.05	-4.2	83.5	11
	En	LY22	6480	1.5	1100	IW	-12.72	-8.29	-4.42	12.67	1
	En	LY41	7200	2.5	1100	NNO	-7.96	-7.96	0	1.63	1
	En	PS7	7200	1.5	1100	IW	-12.72	-8.29	-4.42	25.77	35
	En	LY21	5040	1.5	1200	IW	-11.4	-7.1	-4.3	3.02	3
	En	LY36	7200	1.5	1100	NNO	-8.29	-8.29	0		
	En	LY42	5760	3.5	1100	NNO	-7.62	-7.62	0	15.23	25
	En	PS11	4320	1.5	1100	IW	-12.72	-8.29	-4.42	75.5	36
	En	PS10	7200	1.5	1100	IW	-12.72	-8.29	-4.42	71	1
Li et	Melt	HP-02	20160	0.2	800	NNO+1	-12.79	-13.79	1	1250	220
al., 2015	Melt	HP-03	20160	0.2	800	NNO+1	-12.79	-13.79	1	730	10
	Melt	HP-04	20160	0.2	800	NNO+1	-12.79	-13.79	1	370	10
HP=	Melt	HP-15	5760	0.2	800	IW	-18.81	-13.79	-5.03	2090	90
Haplogranite	Melt	HP-16	5760	0.2	800	IW	-18.81	-13.79	-5.03	2930	90
Ba=Basalt	Melt	HP-17	5760	0.2	800	IW	-18.81	-13.79	-5.03	1140	90
	Melt	HP-18	5760	0.2	800	IW	-18.81	-13.79	-5.03	710	90
	Melt	HP-PC-01	7200	1	800	NNO	-13.45	-13.45	0	1420	260
	Melt	HP-PC-02	7200	1	800	NNO	-13.45	-13.45	0	1140	260
	Melt	HP-PC-03	5760	1	800	NNO	-13.45	-13.45	0	970	260
	Melt	HP-PC-04	4320	1	800	NNO	-13.45	-13.45	0	1590	260
	Melt	HP-PC-05	7200	1	800	NNO	-13.45	-13.45	0	1330	260
	Melt	HPR-08	20160	0.2	800	NNO+1	-12.79	-13.79	1	65	2

Continued on next page

Table A.5 – continued from previous page

Reference	Type	RunID	Time	P	T	Buffer	$f_{O2\text{-}o}$	$f_{O2\text{-}NNO}$	Δ_{NNO}	N	error
	Melt	HPR-09	20160	0.2	800	NNO+1	-12.79	-13.79	1	96	1
	Melt	HPR-10	20160	0.2	800	NNO+1	-12.79	-13.79	1	132	3
	Melt	HPR-11	20160	0.2	800	NNO+1	-12.79	-13.79	1	185	34
	Melt	HPR-12	20160	0.2	800	NNO+1	-12.79	-13.79	1	193	2
	Melt	HPR-13	20160	0.2	800	NNO+1	-12.79	-13.79	1	76	2
	Melt	Ba-01	8640	0.1	1100	NNO+3	-5.76	-8.76	3	14	2
	Melt	Ba-02	8640	0.1	1100	NNO+3	-5.76	-8.76	3	9	3
	Melt	Ba-03	8640	0.1	1100	NNO+3	-5.76	-8.76	3	9	2
	Melt	Ba-05	8640	0.1	1100	NNO+3	-5.76	-8.76	3	7	1
	Melt	Ba-06	8640	0.1	1100	NNO+3	-5.76	-8.76	3	7	1
	Melt	Ba-07	8640	0.1	1100	NNO+3	-5.76	-8.76	3	6	0
	Melt	Ba-08	8640	0.1	1100	NNO+3	-5.76	-8.76	3	6	1
	Melt	Ba-09	5760	0.1	1100	NNO+3	-5.76	-8.76	3	6	1
	Melt	Ba-10	5760	0.1	1100	NNO+3	-5.76	-8.76	3	6	0
	Melt	Albite-1	1440	1.5	1200	NNO	-7.1	-7.1	0	590	10
	Melt	Albite-2	1440	1.5	1200	IW	-11.4	-7.1	-4.3	8080	10
	Fluid	HP-02	20160	0.2	800	NNO+1	-12.79	-13.79	1	150000	38121
	Fluid	HP-03	20160	0.2	800	NNO+1	-12.79	-13.79	1	102200	2023
	Fluid	HP-04	20160	0.2	800	NNO+1	-12.79	-13.79	1	129500	5093
	Fluid	HP-15	5760	0.2	800	IW	-18.81	-13.79	-5.03	148390	8952
	Fluid	HP-16	5760	0.2	800	IW	-18.81	-13.79	-5.03	123060	4783
	Fluid	HP-17	5760	0.2	800	IW	-18.81	-13.79	-5.03	100320	11243
	Fluid	HP-18	5760	0.2	800	IW	-18.81	-13.79	-5.03	67450	12070
	Fluid	HP-PC-01	7200	1	800	NNO	-13.45	-13.45	0	1008200	261064
	Fluid	HP-PC-02	7200	1	800	NNO	-13.45	-13.45	0	1003200	323007
	Fluid	HP-PC-03	5760	1	800	NNO	-13.45	-13.45	0	999100	381423
	Fluid	HP-PC-04	4320	1	800	NNO	-13.45	-13.45	0	1001700	228279
	Fluid	HP-PC-05	7200	1	800	NNO	-13.45	-13.45	0	997500	278972
	Fluid	HPR-08	20160	0.2	800	NNO+1	-12.79	-13.79	1	35100	1690
	Fluid	HPR-09	20160	0.2	800	NNO+1	-12.79	-13.79	1	65088	1175
	Fluid	HPR-10	20160	0.2	800	NNO+1	-12.79	-13.79	1	100320	3488
	Fluid	HPR-11	20160	0.2	800	NNO+1	-12.79	-13.79	1	123950	31808
	Fluid	HPR-12	20160	0.2	800	NNO+1	-12.79	-13.79	1	150540	2482
	Fluid	HPR-13	20160	0.2	800	NNO+1	-12.79	-13.79	1	36480	1798
	Fluid	Ba-01	8640	0.1	1100	NNO+3	-5.76	-8.76	3	154000	31397
	Fluid	Ba-02	8640	0.1	1100	NNO+3	-5.76	-8.76	3	101700	48154
	Fluid	Ba-03	8640	0.1	1100	NNO+3	-5.76	-8.76	3	68400	21567
	Fluid	Ba-05	8640	0.1	1100	NNO+3	-5.76	-8.76	3	34860	7036
	Fluid	Ba-06	8640	0.1	1100	NNO+3	-5.76	-8.76	3	48300	10871
	Fluid	Ba-07	8640	0.1	1100	NNO+3	-5.76	-8.76	3	67200	2700
	Fluid	Ba-08	8640	0.1	1100	NNO+3	-5.76	-8.76	3	99000	20055
	Fluid	Ba-09	5760	0.1	1100	NNO+3	-5.76	-8.76	3	120000	29000
	Fluid	Ba-10	5760	0.1	1100	NNO+3	-5.76	-8.76	3	144000	10200
	Fluid	Albite-1	1440	1.5	1200	NNO	-7.1	-7.1	0	997100	24472
	Fluid	Albite-2	1440	1.5	1200	IW	-11.4	-7.1	-4.3	808000	80806
	Dfluid	HP-02	20160	0.2	800	NNO+1	-12.79	-13.79	1	120	
	Dfluid	HP-03	20160	0.2	800	NNO+1	-12.79	-13.79	1	140	
	Dfluid	HP-04	20160	0.2	800	NNO+1	-12.79	-13.79	1	350	
	Dfluid	HP-15	5760	0.2	800	IW	-18.81	-13.79	-5.03	71	
	Dfluid	HP-16	5760	0.2	800	IW	-18.81	-13.79	-5.03	42	
	Dfluid	HP-17	5760	0.2	800	IW	-18.81	-13.79	-5.03	88	
	Dfluid	HP-18	5760	0.2	800	IW	-18.81	-13.79	-5.03	95	
	Dfluid	HP-PC-01	7200	1	800	NNO	-13.45	-13.45	0	710	
	Dfluid	HP-PC-02	7200	1	800	NNO	-13.45	-13.45	0	880	
	Dfluid	HP-PC-03	5760	1	800	NNO	-13.45	-13.45	0	1030	
	Dfluid	HP-PC-04	4320	1	800	NNO	-13.45	-13.45	0	630	
	Dfluid	HP-PC-05	7200	1	800	NNO	-13.45	-13.45	0	750	
	Dfluid	HPR-08	20160	0.2	800	NNO+1	-12.79	-13.79	1	540	
	Dfluid	HPR-09	20160	0.2	800	NNO+1	-12.79	-13.79	1	678	
	Dfluid	HPR-10	20160	0.2	800	NNO+1	-12.79	-13.79	1	760	
	Dfluid	HPR-11	20160	0.2	800	NNO+1	-12.79	-13.79	1	670	
	Dfluid	HPR-12	20160	0.2	800	NNO+1	-12.79	-13.79	1	780	
	Dfluid	HPR-13	20160	0.2	800	NNO+1	-12.79	-13.79	1	480	
	Dfluid	Ba-01	8640	0.1	1100	NNO+3	-5.76	-8.76	3	11000	
	Dfluid	Ba-02	8640	0.1	1100	NNO+3	-5.76	-8.76	3	11300	
	Dfluid	Ba-03	8640	0.1	1100	NNO+3	-5.76	-8.76	3	7600	
	Dfluid	Ba-05	8640	0.1	1100	NNO+3	-5.76	-8.76	3	4980	
	Dfluid	Ba-06	8640	0.1	1100	NNO+3	-5.76	-8.76	3	6900	
	Dfluid	Ba-07	8640	0.1	1100	NNO+3	-5.76	-8.76	3	11200	

Continued on next page

Table A.5 – continued from previous page

Reference	Type	RunID	Time	P	T	Buffer	$f_{O2\text{-}o}$	$f_{O2\text{-}NNO}$	Δ_{NNO}	N	error
	Dfluid	Ba-08	8640	0.1	1100	NNO+3	-5.76	-8.76	3	16500	
	Dfluid	Ba-09	5760	0.1	1100	NNO+3	-5.76	-8.76	3	20000	
	Dfluid	Ba-10	5760	0.1	1100	NNO+3	-5.76	-8.76	3	24000	
	Dfluid	Albite-1	1440	1.5	1200	NNO	-7.1	-7.1	0	1690	
	Dfluid	Albite-2	1440	1.5	1200	IW	-11.4	-7.1	-4.3	100	
Roskosz et	MeltM	LHDAC-1		1.8	2227	IW	-6.12	-0.28	-5.84	6000	3000
al., 2013	MeltM	LHDAC-2		4.4	2227	IW	-5.27	0.2	-5.46	7000	2000
	MeltM	LHDAC-3		8.2	2327	IW	-4.22	1.22	-5.44	8000	2000
	MeltM	LHDAC-7		14.8	2527	IW	-2.27	2.89	-5.16	6000	3000
	MeltM	MA-1		5	2077	IW	-6.66	-0.27	-6.39	7000	2000
	MeltM	MA-2		10	2147	IW	-5.1	0.96	-6.06	6000	2000
	Metal	LHDAC-1		1.8	2227	IW	-6.12	-0.28	-5.84	47000	3000
	Metal	LHDAC-2		4.4	2227	IW	-5.27	0.2	-5.46	66000	3000
	Metal	LHDAC-3		8.2	2327	IW	-4.22	1.22	-5.44	91000	3000
	Metal	LHDAC-4		8.5	2377					97000	6000
	Metal	LHDAC-5		12.2	2477				0	103000	4000
	Metal	LHDAC-6		13.5	2527				0	117000	6000
	Metal	LHDAC-7		14.8	2527	IW	-2.27	2.89	-5.16	114000	5000
	Metal	LHDAC-8		17.7	2577				0	124000	7000
	Metal	MA-1		5	2077	IW	-6.66	-0.27	-6.39	3000	1000
	Metal	MA-2		10	2147	IW	-5.1	0.96	-6.06	8000	5000
	Dmetal	LHDAC-1		1.8	2227	IW	-6.12	-0.28	-5.84	7.83	
	Dmetal	LHDAC-2		4.4	2227	IW	-5.27	0.2	-5.46	9.43	
	Dmetal	LHDAC-3		8.2	2327	IW	-4.22	1.22	-5.44	11.38	
	Dmetal	LHDAC-7		14.8	2527	IW	-2.27	2.89	-5.16	19	
	Dmetal	MA-1		5	2077	IW	-6.66	-0.27	-6.39	0.43	
	Dmetal	MA-2		10	2147	IW	-5.1	0.96	-6.06	1.33	
Li et	MeltM	Y-1	120	2	1600	IW-0.84	-8.23	-3.46	-4.77	308	11
al., 2016	MeltM	A-659	90	1.5	1600	IW-1.2	-8.73	-3.58	-5.15	910	32
	MeltM	A-666	30	2.5	1700		-9.25	-2.69	-6.56	47.6	2
	MeltM	YS-5	90	5	1700	IW-0.66	-6.5	-2.11	-4.39	224	8
	MeltM	YS-1	30	7	1700		-5.28	-1.64	-3.64	504	18
	MeltM	YS-2	30	7	1800	IW-0.83	-3.87	-1.11	-2.76	350	10
	Metal	Y-1	120	2	1600	IW-0.84	-8.23	-3.46	-4.77	5180	182
	Metal	A-659	90	1.5	1600	IW-1.2	-8.73	-3.58	-5.15	6860	252
	Metal	A-666	30	2.5	1700		-9.25	-2.69	-6.56	36.4	1
	Metal	YS-5	90	5	1700	IW-0.66	-6.5	-2.11	-4.39	33600	1218
	Metal	YS-1	30	7	1700		-5.28	-1.64	-3.64	10080	364
	Metal	YS-2	30	7	1800	IW-0.83	-3.87	-1.11	-2.76	14000	532

Table A.7: Data used in all chondrite calculations. Source and notes are given in the first column along with individual meteorite names where provided. Sample classifications are given both as class (Column 3) and specific type (Column 2) Meteorite classes are: E= enstatite, C=carbonaceous, O = ordinary, I = Iron, MA = martian, MO= moon, and A = achondrite. Both N and C concentrations are in ppm.

Reference	Type	Class	$\delta^{15}N$	±	N	$\delta^{13}C$	C
Gibson et al., 1971	CI	C			3185		34800
	CM	C			1240		19200
	CM	C			1300		18000
	CM	C			1700		21700
	CM	C			1299		25700
	CM	C			1550		20300
	CM	C			1905		21900
	CO	C			86		6400
	CO	C			97		6100
	CO	C			86		5200
	CO	C			137		2750
	CO	C			92		8000
	CO	C			184		6900
	CO	C			172		6000
	CO	C			108		8000
	CO	C			128		11500
	CK	C			62		2500
	CK	C			51		2000
	CK	C			58		1000

Continued on next page

Table A.7 – continued from previous page

Reference	Type	Class	δ^{15}N	±	N	δ^{13}C	C
Gibson and Moore 1971	I	I			35		
	IIA	I			15		
	IIB	I			18		
	IIC	I			14		
	IID	I			38		
	IIIA	I			25		
	IIIB	I			46		
	IVA	I			4		
	IVB	I			2		
Kung and Clayton 1978	CM	C	26.8		693		
Murchison	CM	C	43.9		828		
Cold Bokkeveld	CR	C	2.7		545		
Renazzo	CV	C	173.0		514		
Allende	CV	C	-43.0		18		
Leoville	CO	C	-24.3		88		
Ornans	CV	C	-13.4		12		
Grosnaja	C4	C	-25.4		54		
Coolidge	CK	C	0.7		15		
Karoonda	EH	E	2.3		5		
Abee	EH	E	-28.5		277		
Indarch	EL	E	-26.1		544		
Hvittis	EL	E	-43.0		544		
Pillistfer	EL	E	-36.2		310		
Daniel's Kuil	EL	E	-24.2		167		
Parnallee	LL	O	-3.5		10		
Hamlet	LL	O	8.0		11		
Soko-Banja	LL	O	6.6		74		
Olivenza	H	O	19.6		5		
Tysnes Island	H	O	21.8		11		
Weston	H	O	14.0		7		
Richardton	H	O	14.2		6		
Bjurbole	LL	O	7.3		13		
Pasamonte	EU	A	5.4		8		
Norton County	AU	A	4.4		10		
Goalpara	UR	A	11.8		18		
Mason 1979	CI	C			3185		
C2	CM	C			1500		
C3	CV	C			105		
H	H	O			48		
L	L	O			43		
LL	LL	O			70		
E	E	E			260		
Roberts and Epstein 1981	CM	C	39.0		1520	6.3	7520
Murray	CM	C	37.0		1500	8.2	10170
Orgueil	CI	C	39.0		2260	-15.6	27070
Renazzo	CV	C	190.0		1600		
Halbout et al., 1986	CI	C	31.8		1143		
	CM	C	25.3		690		
	CM2	C	6.3		979		
	CM	C	22.3		728		
	CR	C	43.5		1311		
Grady and Pillinger 1986	EH	E	-12.7		973		
Abee 2	EH	E	-7.0		481		
Abee 3	EH	E	-15.7		220		
Indarch	EL	E	-30.5		896		
Indarch	EL	E	-24.1		428		
Kota-Kota	EH	E	-26.1		533		
South Oman	EH	E	0.6		786		
St Mark's	EH	E	-12.2		195		
Atlanta	EL	E	-10.6		325		
Daniel's Kuil	EL	E	-31.0		474		
Khairpur	EL	E	-47.4		948		
NW Forrest	EL	E	-44.6		490		
Yilmia	EL	E	-24.2		214		
Pepin and Becker 1982	IIID	I	-55.5	1.5	15		
	IIIA	I	-32.3	1.5	20.6		
	IAB	I	-27.2	2.0	5.7		
	IVB	I	7.5	1.5	0.8		
	IVB	I	12.7	0.9	2.1		

Continued on next page

Table A.7 – continued from previous page

Reference	Type	Class	δ^{15}N	±	N	δ^{13}C	C
	I	I	11.0	1.0	3.2		
	I	I	15.8	1.0	6.6		
Franchi et al., 1993	IAB	I	-53.9	1.6	2.9		
	IAB	I	-51.6	1.6	4.1		
	IAB	I	-54.6	1.6	3.8		
	IAB	I	-60.2	1.6	21		
	IAB	I	-42.9	0.1	36.6		
	IAB	I	-42.8	0.1	34		
	IAB	I	-54.5	0.6	44.9		
	IAB	I	-55.4	0.6	117.6		
	IAB	I	-60.1	0.6	85.5		
	IAB	I	-64.4	0.6	40.3		
	IAB	I	-63.3	0.6	13		
	IAB	I	-59.7	0.6	62.7		
	IC	I	-87.5	0.6	67.5		
	IIAB	I	-95.8	0.6	13.9		
	IIC	I	155.6	0.6	16.9		
	IID	I	12.5	0.6	16.3		
	IIE	I	20.7	0.6	2.7		
	IIF	I	14.4	0.6	23.7		
	IIIAB	I	-80.0	0.6	20.7		
	IIIAB	I	-86.2	0.6	16.9		
	IIIAB	I	-85.5	0.5	32.5		
	IIIAB	I	-74.2	0.5	32.8		
	IIIAB	I	-38.1	0.5	2.1		
	IIIAB	I	-74.5	0.5	13.8		
	IIIAB	I	-78.7	0.5	43.9		
	IIIAB	I	-79.1	0.5	15.6		
	IIICD	I	-62.3	0.5	38.7		
	IIIE	I	-33.3	0.5	5.8		
	IIIF	I	-16.3	0.5	5.1		
	IVA	I	18.0	0.5	0.4		
	IVB	I	10.0	0.5	1.3		
Prombo and Clayton 1993	IAB	I	-61.8		38		
Part of analytical setup used	IAB	I	-73.2		21.6		
a Mo support, which is now	IAB	I	-63.7		77.8		
known to react with N, treat	IAB	I	-57.0		52.9		
with caution	IAB	I	-60.2		7.7		
	IC	I	-84.9		15.1		
	IIAB	I	-89.2		8.7		
	IIAB	I	-80.5		11.1		
	IIAB	I	-82.7		3.5		
	IIAB	I	-82.2		13.2		
	IIC	I	125.3		4.1		
	IIC	I	144.6		4.4		
	IIC	I	153.2		10.5		
	IIC	I	127.4		8.1		
	IID	I	7.5		27.9		
	IIE	I	14.6		0.9		
	IIE	I	46.7		2.7		
	IIE	I	116.7		4.8		
	IIF	I	7.1		15.7		
	IIIAB	I	-82.3		16.1		
	IIIAB	I	-84.6		36.7		
	IIIAB	I	-84.6		23.8		
	IIIAB	I	-83.2		28		
	IIIAB	I	79.7		4.6		
	IIIAB	I	-75.6		20.5		
	IIICD	I	-60.2		32.4		
	IIICD	I	-66.1		69		
	IIIE	I	-73.5		12.1		
	IIIF	I	8.6		1.4		
	IVA	I	-3.4		4.8		
	IVA	I	3.3		0.4		
	IVB	I	11.2		0.6		
	I	I	-32.8		1.9		
	I	I	20.6		0.3		
	I	I	33.6		2.5		
	I	I	0.9		1.2		

Continued on next page

Table A.7 – continued from previous page

Reference	Type	Class	δ^{15}N	±	N	δ^{13}C	C
	I	I	-87.1		3.8		
	I	I	4.8		16		
	I	I	2.5		0.8		
	I	I	19.3		0.4		
	I	I	49.1		0.2		
	I	I	-25.1		8.2		
	I	I	-0.5		0.4		
	I	I	-18.4		7.4		
	I	I	37.3		0.6		
	I	I	10.5		0.2		
	I	I	-4.3		0.2		
	I	I	8.2		0.3		
	P	I			13.1		
	P	I	-54.3		1.2		
	P	I	29.7		21		
	P	I	-66.2		0.1		
	P	I	8.0		4.6		
	P	I	-59.1		6.6		
	P	I	-51.0		9.7		
	P	I	19.1		1.7		
	P	I	-27.9		2.5		
	P	I	12.7		5.4		
	P	I	12.2		0.4		
	P	I	12.7		1.6		
	P	I	-54.8		3.8		
	P	I	-7.6		14.1		
Kerridge 1985	CI	C	31.0		1250	-10.3	44600
	CI	C				-7.5	40300
	CI	C				-6.6	33000
	CI	C	52.0		1855	-9.4	37000
	CI	C	46.0		1476	-11.6	37500
	CI	C				-11.4	28000
	CI	C	39.0		1360	-15.6	27100
	CM	C	43.0		784	-4.8	19600
	CM	C					
	CM	C	47.0		685	-22	24900
	CM	C	335.0		744	-4.3	24200
	CM	C	16.0		520	-7.7	18100
	CM	C	35.0		670	-10.6	20300
	CM	C	22.0		560	-7.2	23500
	CM	C				-7.3	1600
	CM	C	35.0		850	-13.7	2000
	CM	C	20.0		1078	-20.4	84600
	CM	C	23.0		1030	-19.6	58300
	CM	C				-7.6	23000
	CM	C	43.0		700	-9.3	18500
	CM	C			1340	-0.4	35800
	CM	C				-3.7	16000
	CM	C	26.0		810	-10.3	28500
	CM	C	27.0		690	-9.9	26000
	CM	C	39.0		760	-4.5	17000
	CM	C	43.0		845	-0.5	21500
	CM	C	44.0		830	-7.2	25000
	CM	C	36.0		367	-10.6	15600
	CM	C	43.0		345		
	CM	C	39.0		990	0	21000
	CM	C				-3.9	19000
	CM	C	46.0		1020	-5.6	
	CM	C				-10	22400
	CM	C				-21.8	19000
	CM	C	13.0		550	-7.5	52100
	CM	C	39.0		1150	-14.7	19600
	CM	C				-4.3	32200
	CM	C			850	-5.1	22000
	CO	C				-16.4	19800
	CO	C	-22.0		29	-14.2	4700
	CO	C	-30.0		33	-18.6	6400
	CO	C				-15.7	3900
	CO	C	13.0		37	-17	3400

Continued on next page

Table A.7 – continued from previous page

Reference	Type	Class	δ^{15}N	±	N	δ^{13}C	C
	CO	C			14	-16	4600
	CO	C	-13.0		12		1200
	CO	C	8.0		25	-19.3	
	CV	C	-43.0		18	-16.4	2500
	CV	C	6.0		19	-17.3	2700
	CV	C	-26.0		21		3000
	CV	C	-34.0		20		
	CV	C	-36.0		17		
	CV	C	20.0		18		
	CV	C	24.0		30	-21.2	3300
	CV	C	-10.0		50	-21.6	7500
	CV	C			97	-18.6	6400
	CV	C	-25.0		54	-23.7	11000
	CV	C	-22.0		173		
	CV	C	-24.0		102	-17.3	10700
	CV	C	-24.0		88	-12.8	7700
	CV	C					
	CV	C				-18.3	7400
	CV	C				-18.1	7500
	CV	C	-45.0		66	-17.5	7000
	CV	C	-11.0		73	-18.7	10000
	C	C	2.0		130	-7.5	830
	C	C	140.0		850	-11.8	23800
	C	C					
	C	C	165.0		1890	-9.3	33400
	C	C	6.0		18	-23.6	200
	C	C	2.0		5	-25.2	1000
	C	C	190.0		800	-10.2	15000
	C	C	175.0		500	-9.9	17000
	C	C	170.0		510		
Sugiura and Zashu 1995	CK	C	-28.5		40.67		
	CK	C	3.7		3.17		
	CK	C	4.5		9.5		
	CK	C	-33.8		3.62		
Hashizume and Sugiura 1995	H	O	-1.0	12.0	0.63		
Trapped N component	H	O	16.8	1.0	5.23		
i.e. Not cosmogenic	H	O	-15.0	3.9	0.79		
	H	O	-2.9	1.5	8.25		
	H	O	10.4	7.7	3.07		
	H	O	17.0	1.6	1.86		
	H	O	-8.3	3.4	0.8		
	H	O	45.1	2.7	0.89		
	H	O	74.0	1.6	0.37		
	H	O	32.9	1.4	1.72		
	H	O	6.6	4.0	3.45		
	H	O	-14.6	1.8	1.14		
	H	O	4.4	1.4	1.18		
	H	O	12.5	1.8	1.23		
	L	O	8.3	1.2	25.2		
	L	O	-10.8	111.0	0.9		
	L	O	24.1	0.9	12.18		
	L	O	21.5	8.9	0.67		
	L	O	0.0	7.6	1.66		
	L	O	8.0	18.1	0.8		
	LL	O	3.9	1.4	5.1		
	LL	O	-2.8	8.1	0.62		
Sugiura et al., 1998	O	O	-7.5				
	O	O	-7.5		11.8		
	O	O	-16.1		2.25		
	O	O	-7.8		4.22		
	O	O	-50.2		4.86		
	O	O	-226.4		3.49		
	O	O	-62.0		5.08		
	O	O	-69.4		5.29		
	O	O	-101.5		4.21		
	O	O	-37.4		12.9		
	O	O	-33.7		3.13		
	O	O	-30.6		10.8		
	O	O	-26.0		12.9		

Continued on next page

Table A.7 – continued from previous page

Reference	Type	Class	δ^{15}N	±	N	δ^{13}C	C
	O	O	229.0		7.59		
	O	O	759.0		3.45		
	O	O	157.5		2.2		
	O	O	113.0		1.19		
	O	O	61.9		11.7		
	O	O	91.5		5.38		
	O	O			7.42		
	O	O			0.77		
	O	O			0.85		
	O	O			1.4		
	O	O			1.58		
	O	O			0.55		
Sugiura 1998	Taenite	I			380		8
	Taenite	I			1100		12
	Taenite	I	163.5	4.7	98	-28.2	62.0
	Taenite	I	-85.2	6.8	1200	-85.2	260.0
	Taenite	I	-79.1	5.2	4500	-16.6	16.0
	Taenite	I	-76.5	4.3	5100	-14.9	50.0
	Taenite	I	-90.5	5.7	5400	-17.5	460.0
	Taenite	I	-67.9	7.3	7000	22	320.0
	Taenite	I	-65.3	4.3	29000	-11.3	140.0
	Taenite	I	-52.8	4.2	12000	-19.3	300
	Taenite	I	-52.1	6.0	5200	-28.2	84
Mathew et al., 2000	IVA	I	-8.6		1.836		
	IVA	I	-11.5		0.304		
	IVA	I	-3.4		0.601		
	IVA	I	0.1		0.718		
	IVA	I	27.3		1.545		
	IVA	I	-0.1		0.4		
	IVA	I	-0.5		0.199		
	IVA	I	15.9		3.092		
	IVA	I	-16.8		92		
	IVA	I	-14.1		62.48		
	IVA	I	-4.0		0.693		
	IVB	I	7.4		0.564		
	IVB	I	-10.5		0.314		
	IIE	I	7.0		0.956		
	IIE	I	6.7		1.01		
	IIE	I	19.2		1.317		
	IIE	I	3.0		0.983		
	IIE	I	-4.4		5.601		
	IIE	I	31.9		0.953		
	IIE	I	8.1		0.386		
	IIE	I	38.3		1.272		
	IIE	I	-3.3		0.322		
	IIE	I	-42.9		3.84		
	IIE	I	-44.5		4.847		
Mathew and Marti 2001	Anorthosite	MO	13.0	1.2	1.4		
	Glass	MO	13.0	1.2	3.1		
	Basalt	MO	13.0	1.2	0.7		
Grady and Wright 2003	CI2	C	67.0		1218		
	CI1	C	32.0		2000		
	CM1	C	41.0		967		
	CM2	C	17.0		285		
Mathew et al., 2003	MA	MA	34.6	1.7	7.69		
	MA	MA	21.5	1.7	3.03		
	MA	MA	10.4	1.7	6.51		
	MA	MA	14.7	1.1	9.24		
	MA	MA	3.3	1.2	4.1		
Mohapatra and Murty 2003	MA	MA	46.0	5.0	0.75		
	MA	MA	21.0	5.0	0.87		
	MA	MA	-23.2	1.2	4.58		
	MA	MA	8.8	1.0	3.24		
	MA	MA	85.0	11.0	0.25		
	MA	MA	175.0	8.0	0.264		
	MA	MA	7.2	3.8	0.62		
	MA	MA	4.6	8.6	0.4		
Sephton et al., 2003	C	C	32.2		2070	-16	45000
Whole rock or HF/HCl analyses	C	C	40.6		968	-2.7	22000

Continued on next page

Table A.7 – continued from previous page

Reference	Type	Class	δ^{15}N	±	N	δ^{13}C	C
	C	C	-7.3		9300	-7	178800
	C	C	-7.5		1200	-10.6	308000
	C	C	26.5		1100	-5.6	179200
Pearson et al., 2006	CI1	C	44.6	8.0	5300	-17.5	48800
	CI1	C	52.0	1.1	2000	-4.6	54000
	CI2	C	61.5	5.2	1900	12.73	42500
	CM2	C	27.0	2.6	800	-8.1	21600
	CM2	C	21.1	0.4	1100	-8.1	24000
	CM2	C	28.3	3.7	1300	-11.4	40500
	CM2	C	48.0	3.7	1000	-2.62	22500
	CM2	C	52.7	0.3	1400	-1.61	27000
	CM2	C	15.7	2.0	1200	-13.9	26000
	CR2	C	103.0	24.7	1900	-11.7	27400
	CR2	C	157.0	9.2	900	-5.29	12500
	CO3	C	-11.1	10.1	400	-21	7900
	CO3	C	-8.8	2.3	900	-23.9	8300
	CO3	C	-10.5	3.6	100	-19	2400
	CO3	C	-7.4	1.5	300	-21.7	6500
	CO3	C	-6.8	3.3	200	-24.1	4400
	CV3	C	-9.2	1.9	700	-15.7	13600
	CV3	C	-15.9	3.0	200	-17	15000
	CV3	C	-18.0	0.9	200	-22.1	7100
	CV3	C	-18.6	2.0	100	-18.6	27700
	CK4	C	-28.4	1.6	100	-31.5	700
	CM2	C	19.9	2.7	100	-13.8	26200
	CO3	C	14.8	9.5	100	-15.2	12900
	CV3	C	-17.1	2.9	400	-13.6	11400
	CK4	C	17.0	1.8	200	-24	2800
	C4	C	0.0	18.3	100	-17.4	100
Ponganis and Marti 2007	IAB	I	-53.9		28		
Step combustion	IAB	I	-25.9		75		
total N listed	IAB	I	-31.4		48		
	IAB	I	-50.8		38		
	IIICD	I	-58.5		25		
	IAB	I	-68.4		39		
	IAB	I	-72.9		103		
	IIICD	I	-58.6		17		
	IAB	I	-58.5		54		
	IIICD	I	-42.6		9		
	IIICD	I	-65.9		61		
	IAB	I	-64.1		110		
	IAB	I	-65.3		117		
	IAB	I	-12.8		8		
	IAB	I	-57.3		50		
	IIICD	I	-62.8		29		
	IIICD	I	-10.0		11		
Ivanova et al., 2008	CH	C	1124.0		106		

Full literature compilation reference list: Hoering (1955); Peters et al. (1978); Power et al. (1974); Sullivan et al. (1979); Itihara & Honma (1979); Stiehl & Lehmann (1980); Hayes et al. (1983); Sakai et al. (1984); Itihara & Suwa (1985); Gibson et al. (1986); Rigby & Batts (1986); Duit et al. (1986); Itihara et al. (1986); Rau et al. (1987); Haendel et al. (1986); Exley et al. (1987); Hall (1987); Greenfield (1988); Hall (1988); Itihara & Tainosho (1989); Sano & Pillinger (1990); Cooper & Bradley (1990); Greenfield (1991); Williams & Ferrell Jr (1991); Hall et al. (1991); Bebout & Fogel (1992); Imbus et al. (1992); Williams et al. (1992); Boyd et al. (1993); Visser (1993); Chicarelli et al. (1993); Marty (1995); Williams et al. (1995); Hall et al. (1996); Honma (1996); Bebout et al. (1999a); Hall et al. (1996); Watanabe et al. (1997); Cartigny et al. (1997); Marty & Humbert (1997); Drits et al. (1997); Bebout (1997); Schroeder & McLain (1998); Boyd & Philippot (1998); Sano et al. (1998); Beaumont & Robert (1999); Bebout et al. (1999b); Hall (1999); Bebout et al. (1999a); Jia & Kerrich (1999); Dauphas & Marty (1999); Marty & Zimmermann (1999); Nishio et al. (1999); Sadofsky & Bebout (2000); Kao & Liu (2000); Jia & Kerrich (2000); Pinti et al. (2001); Mingram & Bräuer (2001); Jenkyns et al. (2001); Cartigny et al. (2001); Sano et al. (2001); Holloway et al. (2001); Sephton et al. (2002); Yamaguchi (2002); Matsumoto et al. (2002); Fischer et al. (2002); Busigny et al. (2003); Sadofsky & Bebout (2003); Marty & Dauphas (2003); Jia et al. (2003); Glasmacher et al. (2003); Sadofsky & Bebout (2004); Ueno et al. (2004); Papineau et al. (2005); van Zuilen et al. (2005); Pitcairn et al. (2005); Busigny et al. (2005a); Li & Bebout (2005); Tappert et al. (2005); Busigny et al. (2005b); Bräuer et al. (2004); Kerrich et al. (2006); Elkins et al. (2006); Jia (2006); Westerlund et al. (2006); Li et al. (2007); Philippot et al. (2007); Quan et al. (2008); Svensen et al. (2008); Schulze et al. (2008); Garvin et al. (2009); Godfrey & Falkowski (2009); Papineau et al. (2009); Mohapatra et al. (2009); Yokochi et al. (2009); Yui et al. (2009); Burgess et al. (2009); Halama et al. (2010); Plessen et al. (2010); Thomazo et al. (2011); Busigny et al. (2011); Morford et al. (2011); Palya et al. (2011); Ahadnejad et al. (2011); Cruz (2011); Pontes et al. (2009); Halama et al. (2012); Roulleau et al. (2012); Dixon et al. (2012); Smelov et al. (2012); Palot et al. (2012); Ekpo et al. (2012); Cremonese et al. (2013); Busigny et al. (2013); Bebout et al. (2013); Godfrey et al. (2013); De Moor et al. (2013); Li et al. (2014); Gibson et al. (1971); Gibson & Moore (1971); Kung & Clayton (1978); Mason (1979); Robert & Epstein (1982); Halbout et al. (1986); Grady & Pillinger (1986); Pepin & Becker (1982); Franchi et al. (1993); Prombo & Clayton (1993); Kerridge (1985); Sugiura & Zashu (1995); Hashizume & Sugiura (1995); Sugiura et al.

Table A.6: Nitrogen isotope data from Mysen & Fogel (2010), with δ^{15}N shown from the end of the run and Δ^{15}N the difference from starting material. Starting δ^{15}N = 2.6‰. See table A.5 for sample notes.

Reference	**Type**	**RunID**	δ^{15}**N**	Δ^{15}**N**
Mysen and	Melt	NS1.7	2.9	0.3
Fogel 2010	Melt	NS1.7	2.23	-0.37
	Melt	NS2	3.6	1
	Melt	NS2	2.65	0.05
	Melt	NS2.5	2.2	-0.4
	Melt	NS2.5	1.86	-0.74
	Melt	NS4	3.1	0.5
	Melt	NS4	2	-0.6
	Melt	NS4	4.2	1.6
	Melt	NS4	0.95	-1.65
	Melt	NS5	2	-0.6
	Melt	NS5	1.21	-1.39
	Melt	NS2.5	4.3	1.7
	Melt	NS2.5	3	0.4
	Melt	NS2.5	2.7	0.1

(1998); Sugiura (1998); Mathew et al. (2000); Mathew & Marti (2001); Grady & Wright (2003); Mathew et al. (2003); Mohapatra & Murty (2003); Sephton et al. (2003); Pearson et al. (2006); Ponganis & Marti (2007); Ivanova et al. (2008); Mysen et al. (2008); Kadik et al. (2011); Libourel et al. (2003); Roskosz et al. (2006); Mysen & Fogel (2010); Li et al. (2013, 2015); Roskosz et al. (2013)

Appendix B

Measurement of geologic N supplemental data

The following presents raw data for fluorometric and colourimetric analyses described in Chapter 3. All data shown herein are available as electronic supplemental files to the publication (Johnson et al., In review)). Raw fluorometry data used for construction of standard calibration curves and calculation of sample concentrations are split over two tables (Tables B.1-B.2). Table B.3 presents a summary of N concentration measurements form rocks used in continental crust estimate, as well as standards. Table B.4 presents colourimetry readings and resulting N concentrations. Table B.5 gives brief sample description and location information for samples used in the continental crust budget estimate from the same chapter.

Table B.1: Raw fluorometry data used in method development and continental crust budget. Standards and sample data are shown. Standard curves were constructed by averaging three fluorescence readings (R-1, R-2, R-3), subtracting initial fluorescence (Initial), and subtracting blank values. Shown are volume of standard/sample initially digested (Sample VP or mass rock), total volume of HF and KOH used for digestion and neutralization, amount of neutralized sample drawn from neutralized solution (Sample V, mL), and amount of H_2O added to sample aliquot for fluorometry. Corrected fluorometry (Corrfluor) is net fluorescence corrected for dilutions either in fluorescence reaction bottle or digestion vial. A slope is calculated, forcing this slope through zero, along with an r^2 value. This slope is used to calculate sample concentration, which is then corrected for dilutions.

Sample	KOH+HF	Sample VP	H_2O	Sample V	Initial	R-1	R-2	R-3
Blank	22	2	9.94	0.06	-0.289	15.77	15.85	15.80
10ppm	17	2	9.7	0.3	-0.292	100.80	101.20	101.20
50ppm	22	2	9.94	0.06	-0.248	154.40	156.20	156.10
BCR-2(1)	17	0.5	9.94	0.06	-0.273	26.55	27.12	27.05
BCR-2(2)	17	0.5	9.94	0.06	-0.277	30.25	31.47	30.75
BCR-2(3)	17	0.5	9.94	0.06	-0.324	31.66	32.58	32.53
Blank	22	2	9.905	0.095	1.844	9.13	9.13	9.02
10ppm	22	2	9.53	0.47	0.623	168.20	168.20	171.20
50ppm	22	2	9.905	0.095	0.019	200.50	204.00	204.00
BCR-2(1)	21	0.5	9.92	0.08	0.81	28.06	28.00	28.02
BCR-2(2)	21	0.5	9.92	0.08	0.065	18.90	19.12	19.12
BCR-2(3)	21	0.5	9.92	0.08	0.419	17.98	18.04	18.43
BlankB	22	2	9.955	0.045	-0.001	6.09	5.99	5.95
5ppm	22	2	9.1	0.9	-0.118	138.50	141.30	141.20
10ppm	22	2	9.55	0.45	-0.229	139.70	141.20	140.80
50ppm	22	2	9.91	0.09	0.061	170.50	174.00	173.90
100ppm	22	2	9.955	0.045	-0.301	208.20	211.00	211.00
BJ1604(1)	17	0.5	9.91	0.09	0.045	250.50	251.70	251.00
BJ1604(2)	17	0.5	9.91	0.09	-0.11	151.30	152.00	151.60
BJ1604(3)	17	0.5	9.91	0.09	0.028	184.10	188.40	188.20
Llang Gabbro(1)	17	0.5	9.91	0.09	0.584	20.71	20.52	20.41

Continued on next page

Table B.1 – continued from previous page

Sample	KOH+HF	Sample VP	H_2O	Sample V	Initial	R-1	R-2	R-3
Llang Gabbro(2)	17	0.5	9.91	0.09	-0.042	8.09	7.39	7.33
Llang Gabbro(3)	17	0.5	9.91	0.09	0.468	7.91	7.99	7.85
BJ1602(1)	17	0.5	9.91	0.09	0.882	19.50	19.41	19.35
BJ1602(2)	17	0.5	9.91	0.09	-0.098	22.69	22.95	22.41
BJ1602(3)	17	0.5	9.91	0.09	-0.053	20.39	20.51	20.48
BCR-2(1)	17	0.5	9.91	0.09	-0.088	22.81	22.86	22.85
BCR-2(2)	17	0.5	9.91	0.09	1.113	21.25	21.58	21.52
BCR-2(3)	17	0.5	9.91	0.09	0.046	18.29	18.53	18.22
ACG(1)	17	0.5	9.91	0.09	0.116	11.31	11.36	11.18
ACG(2)	17	0.5	9.91	0.09	0.105	10.41	10.59	10.50
ACG(3)	17	0.5	9.91	0.09	-0.034	9.42	9.31	9.26
Ruby Xenolith(1)	17	0.5	9.91	0.09	-0.019	12.37	12.55	12.49
Ruby Xenolith(2)	17	0.5	9.91	0.09	-0.082	9.99	9.73	9.70
Ruby Xenolith(3)	17	0.5	9.91	0.09	-0.007	8.60	8.71	9.40
BJ1603(1)	17	0.5	9.91	0.09	0.436	15.01	154.84	14.89
BJ1603(2)	17	0.5	9.91	0.09	1.004	11.32	12.14	12.14
BJ1603(3)	17	0.5	9.91	0.09	0.472	10.29	9.99	10.00
J1408-5.1(1)	17	0.5	9.91	0.09	0.722	57.45	58.19	58.47
J1408-5.1(2)	17	0.5	9.91	0.09	-0.089	63.43	64.21	63.91
J1408-5.1(3)	17	0.5	9.91	0.09	-0.268	62.18	62.26	62.26
Ruby mtn Basalt(1)	17	0.5	9.91	0.09	0.033	44.14	44.37	44.23
Ruby mtn Basalt(2)	17	0.5	9.91	0.09	0.001	7.38	7.31	7.26
Ruby mtn Basalt(3)	17	0.5	9.91	0.09	-0.078	5.92	5.85	5.74
Llang 955LML1(1)	17	0.5	9.91	0.09	-0.046	51.01	52.80	53.04
Llang 955LML1(2)	17	0.5	9.91	0.09	-0.193	26.97	27.69	27.67
Llang 955LML1(3)	17	0.5	9.91	0.09	-0.026	17.30	17.06	17.39
BJ1601(1)	17	0.5	9.91	0.09	0.119	15.67	16.19	16.13
BJ1601(2)	17	0.5	9.91	0.09	0.053	8.16	8.33	8.20
BJ1601(3)	17	0.5	9.91	0.09	0.643	11.01	10.00	9.86
OMNG(1)	17	0.5	9.91	0.09	0.544	27.75	26.58	26.53
OMNG(2)	17	0.5	9.91	0.09	0.152	25.64	26.78	26.63
OMNG(3)	17	0.5	9.91	0.09	-0.145	26.58	27.36	27.34
Blank	22	2	9.905	0.095	-0.021	26.97	27.69	27.67
10ppm	22	2	9.53	0.47	5.64	339.50	345.60	345.90
50 ppm	22	2	9.905	0.095	2.13	365.00	384.40	384.80
BCR-2(1)	18.5	0.5	9.73	0.27	-0.122	251.90	253.90	254.20
BCR-2(2)	18.5	0.5	9.73	0.27	-0.236	246.70	251.30	251.30
BCR-2(3)	18.5	0.5	9.73	0.27	-0.166	127.10	128.40	127.40
BCR-2(1.2)	18.5	0.5	9.55	0.45	-0.241	293.70	305.60	305.80
BCR-2(2.2)	18.5	0.5	9.55	0.45	-0.249	135.70	135.60	135.40
BCR-2(3.2)	18.5	0.5	9.55	0.45	-0.245	84.11	85.11	85.10
Blank A	22	2	9.975	0.025	0.043	7.73	6.70	6.57
Blank B	22	2	9.975	0.025	-0.165	8.00	7.96	7.81
5ppm	22	2	9.05	0.95	-0.083	376.20	384.20	384.40
10ppm	22	2	9.5	0.5	-0.23	368.80	378.40	380.20
50ppm	22	2	9.905	0.095	-0.28	424.00	435.40	436.80
200ppm	22	2	9.975	0.025	-0.157	246.80	249.20	249.20
BJ1605(1)	23.5	0.5	9.905	0.095	0.567	18.24	18.02	18.13
BJ1605(2)	23.5	0.5	9.905	0.095	2.006	19.76	19.08	19.07
BJ1605(3)	23.5	0.5	9.905	0.095	0.442	17.11	17.33	17.34
BJ1606(1)	23.5	0.5	9.905	0.095	1.705	45.98	42.42	45.53
BJ1606(2)	23.5	0.5	9.905	0.095	1.428	36.11	37.46	36.13
BJ1606(3)	23.5	0.5	9.905	0.095	1.216	42.72	41.05	40.73
96CR4(1)	23.5	0.5	9.905	0.095	0.955	40.06	40.16	40.00
96CR4(2)	23.5	0.5	9.905	0.095	0.576	17.61	17.42	17.16
96CR4(3)	23.5	0.5	9.905	0.095	0.592	16.96	16.03	15.88
S. Lake(1)	23.5	0.5	9.905	0.095	0.235	9.74	9.84	9.81
S. Lake(2)	23.5	0.5	9.905	0.095	0.177	11.32	11.41	11.36
S. Lake(3)	23.5	0.5	9.905	0.095	-0.075	12.18	12.13	
CR56 Xenolith(1)	23.5	0.5	9.905	0.095	0.328	23.15	23.22	23.20
CR56 Xenolith(2)	23.5	0.5	9.905	0.095	0.328	20.70	20.29	20.08
CR56 Xenolith(3)	23.5	0.5	9.905	0.095	0.145	23.26	23.88	23.67
Till 1253(1)	23.5	0.5	9.905	0.095	1.12	36.12	37.45	37.46
Till 1253(2)	23.5	0.5	9.905	0.095	0.006	29.45	29.59	29.51
Till 1253(3)	23.5	0.5	9.905	0.095	0	27.57	28.21	28.16
BCR-2(1)	23.5	0.5	9.905	0.095	-0.163	29.34	29.75	29.67
BCR-2(2)	23.5	0.5	9.905	0.095	0.283	32.13	31.76	31.64
BCR-2(3)	23.5	0.5	9.905	0.095	0.073	30.34	30.07	29.88

Continued on next page

Table B.1 – continued from previous page

Sample	KOH+HF	Sample VP	H_2O	Sample V	Initial	R-1	R-2	R-3
CM Basalt(1)	23.5	0.5	9.905	0.095	0.388	41.88	42.74	42.61
CM Basalt(2)	23.5	0.5	9.905	0.095	0.11	18.43	17.65	17.53
CM Basalt(3)	23.5	0.5	9.905	0.095	-0.082	17.53	18.89	18.70
CM 25(1)	23.5	0.5	9.905	0.095	0.322	63.29	64.42	64.92
CM 25(2)	23.5	0.5	9.905	0.095	0.266	16.54	16.66	17.24
CM 25(3)	23.5	0.5	9.905	0.095	0.278	25.80	25.92	25.91
Till 1236(1)	23.5	0.5	9.905	0.095	0.126	75.49	75.93	75.68
Till 1236(2)	23.5	0.5	9.905	0.095	0.088	80.39	80.44	80.08
Till 1236(3)	23.5	0.5	9.905	0.095	-0.005	119.70	121.90	122.40
CR15(1)	23.5	0.5	9.905	0.095	0.344	12.44	12.56	12.31
CR15(2)	23.5	0.5	9.905	0.095	0.324	13.25	13.47	13.44
CR15(3)	23.5	0.5	9.905	0.095	0.976	67.86	68.86	68.74
CR56 Basalt(1)	23.5	0.5	9.905	0.095	1.393	23.31	20.57	20.53
CR56 Basalt(2)	23.5	0.5	9.905	0.095	1.526	22.83	23.17	23.17
CR56 Basalt(3)	23.5	0.5	9.905	0.095	0.245	25.93	26.40	26.46
S. Tuya(1)	23.5	0.5	9.905	0.095	0.174	29.56	29.45	29.46
S. Tuya(2)	23.5	0.5	9.905	0.095	2.451	16.58	16.98	17.08
S. Tuya(3)	23.5	0.5	9.905	0.095	0.358	11.31	11.10	11.01
CM Xenolith(1)	23.5	0.5	9.905	0.095	0.147	28.58	28.63	28.42
CM Xenolith(2)	23.5	0.5	9.905	0.095	0.355	28.34	28.58	48.46
CM Xenolith(3)	23.5	0.5	9.905	0.095	0.421	29.11	29.40	
Till 4(1)	23.5	0.5	9.905	0.095	1.371	51.14	52.21	52.58
Till 4(2)	23.5	0.5	9.905	0.095	1.456	66.00	67.14	67.19
Till 4(3)	23.5	0.5	9.905	0.095	1.695	71.03	70.40	70.33
Volc Creek(1)	23.5	0.5	9.905	0.095	0.793	19.97	19.85	19.75
Volc Creek(2)	23.5	0.5	9.905	0.095	0.052	21.82	21.88	21.84
Volc Creek(3)	23.5	0.5	9.905	0.095	0.067	18.98	18.88	18.84
Till 1234(1)	23.5	0.5	9.905	0.095	3.618	72.89	73.93	73.95
Till 1234(2)	23.5	0.5	9.905	0.095	0.432	70.31	70.24	69.87
Till 1234(3)	23.5	0.5	9.905	0.095	-0.055	88.78	90.05	90.30
J1408-5.1(1)	23.5	0.5	9.905	0.095	0.313	99.85	95.65	97.68
J1408-5.1(2)	23.5	0.5	9.905	0.095	0.19	73.07	73.07	72.30
J1408-5.1(3)	23.5	0.5	9.905	0.095	1.876	90.01	91.68	91.45
94BRE330 Xenolith(1)	23.5	0.5	9.905	0.095	0.728	36.56	36.77	36.55
94BRE330 Xenolith(2)	23.5	0.5	9.905	0.095	0.02	36.55	20.40	20.29
94BRE330 Xenolith(3)	23.5	0.5	9.905	0.095	0.102	29.69	30.08	29.99
S. Tuya Basalt(1)	23.5	0.5	9.905	0.095	0.006	15.79	16.03	16.25
S. Tuya Basalt(2)	23.5	0.5	9.905	0.095	-0.151	15.72	15.52	15.48
S. Tuya Basalt(3)	23.5	0.5	9.905	0.095	-0.129	18.49	18.67	18.56
Blank B	22	2	9.975	0.025	-0.067	6.74	7.22	6.75
5ppm	22	2	9.05	0.95	0.239	301.10	304.10	304.20
10ppm	22	2	9.5	0.5	0.228	335.70	340.30	340.30
50ppm	22	2	9.905	0.095	0.04	288.20	295.40	295.00
100ppm	22	2	9.95	0.05	0.044	310.30	310.30	310.40
200ppm	22	2	9.975	0.025	0.736	282.80	286.50	286.20
Till 3072(1)	17	0.5	9.905	0.095	0.03	80.14	81.36	81.28
Till 3072(2)	17	0.5	9.905	0.095	0.261	104.00	104.20	104.20
Till 3072(3)	17	0.5	9.905	0.095	1.921	86.18	84.96	84.36
Till-4(1)	17	0.5	9.905	0.095	1.674	124.10	126.30	126.80
Till-4(2)	17	0.5	9.905	0.095	1.744	109.50	108.40	108.00
Till-4(3)	17	0.5	9.905	0.095	0.498	87.85	86.96	87.00
J1408-5.1(1)	17	0.5	9.905	0.095	0.267	82.18	83.15	83.01
J1408-5.1(2)	17	0.5	9.905	0.095	0.221	69.42	68.81	69.31
J1408-5.1(3)	17	0.5	9.905	0.095	0.907	104.90	106.30	106.50
Till 3292(1)	17	0.5	9.905	0.095	1.075	89.64	90.97	90.99
Till 3292(2)	17	0.5	9.905	0.095	0.441	50.10	50.74	50.61
Till 3292(3)	17	0.5	9.905	0.095	0.439	68.30	69.45	69.35
Till 3095(1)	17	0.5	9.905	0.095	2.209	56.47	57.42	57.42
Till 3095(2)	17	0.5	9.905	0.095	0.605	57.39	57.06	57.13
Till 3095(3)	17	0.5	9.905	0.095	0.378	56.66	56.39	56.32
Till 3079(1)	17	0.5	9.905	0.095	0.074	48.46	49.04	48.95
Till 3079(2)	17	0.5	9.905	0.095	-0.074	44.02	44.78	44.78
Till 3079(3)	17	0.5	9.905	0.095	-0.08	59.98	61.46	61.27
BCR-2(1)	17	0.5	9.905	0.095	0.125	33.34	32.72	32.51
BCR-2(2)	17	0.5	9.905	0.095	0.565	38.12	38.86	38.81
BCR-2(3)	17	0.5	9.905	0.095	0.433	34.45	35.14	34.71
BJ1601(1)	17	0.5	9.905	0.095	0.599	24.53	25.17	25.77
BJ1601(2)	17	0.5	9.905	0.095	0.407	14.39	14.12	14.08
BJ1601(3)	17	0.5	9.905	0.095	0.483	21.06	21.32	21.31

Continued on next page

Table B.1 – continued from previous page

Sample	KOH+HF	Sample VP	H_2O	Sample V	Initial	R-1	R-2	R-3
BJ1602(1)	17	0.5	9.905	0.095	0.699	31.94	32.56	32.36
BJ1602(2)	17	0.5	9.905	0.095	0.401	22.39	22.85	22.86
BJ1602(3)	17	0.5	9.905	0.095	2.965	29.82	29.81	29.85
BJ1603(1)	17	0.5	9.905	0.095	0.466	19.72	19.98	19.69
BJ1603(2)	17	0.5	9.905	0.095	0.53	16.47	16.55	16.49
BJ1603(3)	17	0.5	9.905	0.095	0.16	20.76	20.81	20.75
BJ1604(1)	17	0.5	9.905	0.095	0.97	195.50	201.10	200.60
BJ1604(2)	17	0.5	9.905	0.095	0.964	261.60	261.60	260.40
BJ1604(3)	17	0.5	9.905	0.095	0.961	200.30	201.10	201.40
Blank B	22	2	9.975	0.025	0.01	7.02	6.93	6.58
5ppm	22	2	9.975	0.025	0.012	11.92	11.64	11.51
10ppm	22	2	9.975	0.025	-0.244	21.96	22.22	22.16
50ppm	22	2	9.975	0.025	-0.349	72.03	73.05	72.85
100ppm	22	2	9.975	0.025	-0.134	146.10	148.90	148.70
200ppm	22	2	9.975	0.025	1.014	252.90	256.40	255.80
BCR-2.1(1)	17		9.905	0.095	-0.053	28.30	28.78	28.63
BCR-2.1(2)	17		9.905	0.095	0.11	20.98	20.52	20.58
BCR-2.1(3)	17		9.905	0.095	-0.106	23.22	23.15	23.36
BCR-2.2(1)	17		9.905	0.095	0.218	34.55	34.34	34.08
BCR-2.2(2)	17		9.905	0.095	-0.02	32.66	32.47	32.54
BCR-2.2(3)	17		9.905	0.095	0.639	31.59	32.27	31.80
BCR-2.3(1)	17		9.905	0.095	0.023	32.08	32.38	32.35
BCR-2.3(2)	17		9.905	0.095	-0.208	27.57	27.81	27.56
BCR-2.3(3)	17		9.905	0.095	0.248	22.04	21.70	21.64
Till-4.1(1)	17		9.905	0.095	2.066	104.50	107.10	111.90
Till-4.1(2)	17		9.905	0.095	2.453	112.20	112.00	113.60
Till-4.1(3)	17		9.905	0.095	2.61	113.30	113.40	113.10
Till-4.2(1)	17		9.905	0.095	1.412	89.06	89.85	89.89
Till-4.2(2)	17		9.905	0.095	1.6	93.79	94.76	94.58
Till-4.2(3)	17		9.905	0.095	1.905	91.79	93.57	93.32
Till-4.3(1)	17		9.905	0.095	1.428	104.50	106.00	106.20
Till-4.3(2)	17		9.905	0.095	1.485	100.30	100.10	99.76
Till-4.3(3)	17		9.905	0.095	1.667	114.90	115.20	114.80
LKSD-4.1(1)	17		9.905	0.095	5.863	846.40	819.60	820.40
LKSD-4.1(2)	17		9.905	0.095	6.734	752.40	803.60	804.80
LKSD-4.1(3)	17		9.905	0.095	8.738	825.20	842.40	842.80
LKSD-4.2(1)	17		9.905	0.095	6.202	724.40	740.00	742.80
LKSD-4.2(2)	17		9.905	0.095	7.462	840.80	846.80	847.20
LKSD-4.2(3)	17		9.905	0.095	8.026	890.40	910.00	910.40
LKSD-4.3(1)	17		9.905	0.095	6.055	734.80	742.40	743.60
LKSD-4.3(2)	17		9.905	0.095	7.86	966.80	972.40	972.00
LKSD-4.3(3)	17		9.905	0.095	8.53	963.60	987.60	989.20
G-2.1(1)	17		9.905	0.095	-0.165	13.03	12.99	12.85
G-2.1(2)	17		9.905	0.095	-0.199	11.20	11.32	11.27
G-2.1(3)	17		9.905	0.095	0.133	15.63	15.57	15.56
G-2.2(1)	17		9.905	0.095	-0.173	8.29	8.09	7.99
G-2.2(2)	17		9.905	0.095	-0.103	7.48	7.15	7.19
G-2.2(3)	17		9.905	0.095	-0.076	14.54	14.70	14.44
G-2.3(1)	17		9.905	0.095	-0.052	8.28	8.42	8.40
G-2.3(2)	17		9.905	0.095	0.568	6.85	6.74	6.78
G-2.3(3)	17		9.905	0.095	0.108	12.40	12.50	12.45
SY-4.1(1)	17		9.905	0.095	0.552	7.19	7.23	7.29
SY-4.1(2)	17		9.905	0.095	0.142	8.11	7.21	7.68
SY-4.1(3)	17		9.905	0.095	0.462	8.00	7.88	7.79
SY-4.2(1)	17		9.905	0.095	-0.173	10.58	10.66	10.52
SY-4.2(2)	17		9.905	0.095	-0.103	10.59	10.20	10.40
SY-4.2(3)	17		9.905	0.095	-0.076	11.90	11.89	12.00
SY-4.3(1)	17		9.905	0.095	-0.062	18.55	18.72	18.63
SY-4.3(2)	17		9.905	0.095	0.033	20.75	20.77	20.82
SY-4.3(3)	17		9.905	0.095	-0.223	23.57	23.68	23.65
BHVO-2.1(1)	17		9.905	0.095	1.267	23.33	23.59	23.60
BHVO-2.1(2)	17		9.905	0.095	0.144	13.48	13.18	13.14
BHVO-2.1(3)	17		9.905	0.095	0.564	12.47	12.51	12.60
BHVO-2.2(1)	17		9.905	0.095	-0.372	9.64	9.71	9.65
BHVO-2.2(2)	17		9.905	0.095	0.302	10.73	10.11	10.10
BHVO-2.2(3)	17		9.905	0.095	0.302	8.01	7.71	7.67
BHVO-2.3(1)	17		9.905	0.095	0.133	9.24	9.24	9.30
BHVO-2.3(2)	17		9.905	0.095	0.382	11.53	11.58	11.41
BHVO-2.3(3)	17		9.905	0.095	0.133	10.68	10.29	10.21

Continued on next page

Table B.1 – continued from previous page

Sample	KOH+HF	Sample VP	H_2O	Sample V	Initial	R-1	R-2	R-3
Blank A	22		2	10	0.025	1112.00	6.14	6.11
Blank B	22		2	10	0.025	1114.00	6.97	6.99
5ppm	22		2	10	0.025	1124.00	7.64	7.70
10ppm	22		2	10	0.025	1125.00	12.17	12.32
50ppm	22		2	10	0.025	1126.00	36.67	36.73
100ppm	22		2	10	0.025	1128.00	72.52	73.16
200ppm	22		2	10	0.025	1117.00	150.90	153.90
BCR-1(1.a)	22		10	0.025	-0.237	6.82	6.57	6.47
BCR-1(1.b)	22		10	0.095	-0.112	15.98	16.19	16.20
BCR-1(2.a)	22		10	0.025	-0.038	11.51	10.44	10.38
BCR-1(2.b)	22		10	0.095	0.022	65.04	64.80	64.15
BCR-1(3.a)	22		10	0.025	-0.163	9.10	9.16	9.10
BCR-1(3.b)	22		10	0.095	-0.164	16.53	16.77	16.73
J1408-5.1(1.a)	22		10	0.025	-0.198	12.30	12.60	12.52
J1408-5.1(1.b)	22		10	0.095	0.129	15.98	76.57	76.41
J1408-5.1(2.a)	22		10	0.025	0.416	11.51	19.31	19.40
J1408-5.1(2.b)	22		10	0.095	-0.005	65.04	65.97	65.94
J1408-5.1(3.a)	22		10	0.025	-0.084	13.07	12.84	12.77
J1408-5.1(3.b)	22		10	0.095	0.1	73.69	73.51	73.88
G-2(1.a)	22		10	0.025	-0.019	8.01	6.84	6.88
G-2(1.b)	22		10	0.095	-0.147	7.57	7.52	7.48
G-2(2.a)	22		10	0.025	-0.281	5.15	5.05	5.00
G-2(2.b)	22		10	0.095	1.351	7.78	8.19	7.97
Blank A	22	2	10	0.1	2.18	5.38	5.17	5.14
Blank B	22	2	10	0.1	0.102	3.62	3.32	3.35
5ppm	22	2	10	0.1	0.914	39.69	39.80	39.69
10ppm	22	2	10	0.1	-0.036	67.10	68.00	67.69
50ppm	22	2	10	0.1	0.031	347.20	352.40	352.20
100ppm	22	2	10	0.1	0.245	685.60	698.80	697.60
200ppm	22	2	10	0.1	0.044	1200.60	1212.00	1209.60
G-2(1)	22	0.25	10	0.1	0.021	6.81	6.73	6.40
G-2(2)	22	0.25	10	0.15	0.131	6.51	6.77	6.49
034(1)	22	0.2502	10	0.1	0.456	47.31	48.18	47.85
034(2)	22	0.2502	10	0.15	0.203	36.35	36.05	35.96
107(1)	22	0.2506	10	0.1	0.578	30.92	22.12	21.53
107(2)	22	0.2506	10	0.15	1.019	50.60	51.03	50.74
101(1)	22	0.2506	10	0.1	0.443	6.98	6.83	6.84
101(2)	22	0.2506	10	0.15	0.285	7.04	7.04	6.93
076(1)	22	0.2498	10	0.1	0.888	9.71	9.51	9.48
076(2)	22	0.2498	10	0.15	0.558	13.35	12.43	12.41
069(1)	22	0.2505	10	0.1	-0.097	9.17	9.33	9.22
069(2)	22	0.2505	10	0.15	0.073	15.15	15.35	15.12
015(1)	22	0.2502	10	0.1	0.181	0.56	0.56	
015(2)	22	0.2502	10	0.15	0.286	0.63	0.15	
021(1)	22	0.2516	10	0.1	-0.018	8.01	8.28	8.34
021(2)	22	0.2516	10	0.15	-0.126	14.59	14.58	14.63
030(1)	22	0.2509	10	0.1	0.259	5.69	5.65	5.79
030(2)	22	0.2509	10	0.15	0.066	6.98	6.80	6.82
041(1)	22	0.2502	10	0.1	0.412	11.66	11.84	11.77
041(2)	22	0.2502	10	0.15	-0.004	9.30	9.05	8.87

Table B.2: Raw fluorometry table continued

Sample	CorrecConc	Net	Net-Blank	Corr-Fluor	Slope or Conc	Conc	r^2 or Avg	StDev
Blank	0	16.10	0.00	0				
10ppm	1053	101.36	85.26	2842	slope		r^2	
50ppm	4167	155.81	139.72	23287	5.42		0.982	
							Average	StDev
BCR-2(1)		27.18	11.08	1847	341.1	23.20	29.7	5.8
BCR-2(2)		31.10	15.00	2501	461.8	31.40		
BCR-2(3)		32.58	16.49	2748	507.3	34.50		

Continued on next page

Table B.2 – continued from previous page

Sample	CConc	Net	Net-Blank	Corr-Fluor	Slope or Conc	Conc	r^2 or Avg	StDev
Blank	0	7.25	0.00	0	slope		r^2	
10ppm	833	168.58	161.33	3433	4.91		0.999	
50ppm	4167	202.81	195.57	20586				
					V	conc in rock		
BCR-2(1)		27.22	19.97	2496	508.5	42.71		
BCR-2(2)		18.98	11.73	1467	298.8	25.10	Average	StDev
BCR-2(3)		17.73	10.48	1310	266.9	22.42	30.1	11.0
BlankB	0	6.01	0.00	0				
5ppm	417	140.45	134.44	1494	slope		r^2	
10ppm	833	140.80	134.79	2995	5.23		0.992	
50ppm	4167	172.74	166.73	18526				
100ppm	8333	210.37	204.36	45413				
							Average	Stdev
BJ1604(1)		251.02	245.01	27224	5202.8	353.79	275.1	72.7
BJ1604(2)		151.74	145.74	16193	3094.7	210.44		
BJ1604(3)		186.87	180.86	20096	3840.6	261.16		
Llang Gabbro(1)		19.96	13.96	1551	296.3	20.15	8.2	10.4
Llang Gabbro(2)		7.65	1.64	182	34.8	2.37		
Llang Gabbro(3)		7.45	1.44	160	30.6	2.08		
BJ1602(1)		18.54	12.53	1392	266.1	18.09	21.1	3.1
BJ1602(2)		22.78	16.77	1864	356.2	24.22		
BJ1602(3)		20.51	14.51	1612	308.0	20.95		
BCR-2(1)		22.93	16.92	1880	359.3	24.43	21.0	3.3
BCR-2(2)		20.34	14.33	1592	304.3	20.69		
BCR-2(3)		18.30	12.29	1366	261.0	17.75		
ACG(1)		11.17	5.16	573	109.6	7.45	6.2	1.3
ACG(2)		10.40	4.39	487	93.2	6.34		
ACG(3)		9.36	3.35	373	71.2	4.84		
Ruby Xenolith(1)		12.49	6.48	720	137.6	9.36	6.4	2.7
Ruby Xenolith(2)		9.89	3.88	431	82.4	5.60		
Ruby Xenolith(3)		8.91	2.90	322	61.6	4.19		
BJ1603(1)		61.14	55.14	6126	1170.8	79.61	30.6	42.4
BJ1603(2)		10.86	4.86	539	103.1	7.01		
BJ1603(3)		9.62	3.61	401	76.7	5.22		
J1408-5.1(1)		57.31	51.31	5701	1089.5	74.09	79.8	5.0
J1408-5.1(2)		63.94	57.93	6437	1230.2	83.65		
J1408-5.1(3)		62.50	56.49	6277	1199.6	81.57		
Ruby mtn Basalt(1)		44.21	38.21	4245	811.3	55.17	19.0	31.4
Ruby mtn Basalt(2)		7.31	1.31	145	27.7	1.89		
Ruby mtn Basalt(3)		5.92	-0.09	-10	-1.9	-0.13		
Llang 955LML1(1)		52.33	46.32	5147	983.6	66.89	38.1	26.0
Llang 955LML1(2)		27.64	21.63	2403	459.3	31.23		
Llang 955LML1(3)		17.28	11.27	1252	239.3	16.27		
BJ1601(1)		15.88	9.87	1097	209.6	14.25	7.5	5.9

Continued on next page

Table B.2 – continued from previous page

Sample	CConc	Net	Net-Blank	Corr-Fluor	Slope or Conc	Conc	r^2 or Avg	StDev
BJ1601(2)		8.17	2.17	241	46.0	3.13		
BJ1601(3)		9.65	3.64	404	77.3	5.26		
OMNG(1)		26.41	20.40	2267	433.2	29.46	29.8	0.8
OMNG(2)		26.20	20.19	2243	428.7	29.15		
OMNG(3)		27.24	21.23	2359	450.8	30.66		
Blank	0	27.46	0.00	0				
10ppm	833	338.03	310.56	6608	slope		r^2	
50 ppm	4167	375.94	348.47	36681	8.77		1.000	
							Average	StDev
BCR-2(1)		253.46	225.99	8370	954.4	70.63	57.2	22.4
BCR-2(2)		250.00	222.54	8242	939.8	69.55		
BCR-2(3)		127.80	100.34	3716	423.7	31.36		
BCR-2(1.2)		301.94	274.48	6099	695.5	51.47	27.5	21.3
BCR-2(2.2)		135.82	108.35	2408	274.6	20.32		
BCR-2(3.2)		85.02	57.55	1279	145.8	10.79		
Blank A	0	6.96	-0.56	-226				
Blank B	0	8.09	0.00	0				
5ppm	417	381.68	374.16	3939	slope		r^2	
10ppm	833	376.03	368.51	7370	6.08		0.954	
50ppm	4167	432.35	424.82	44718				
200ppm	16667	248.56	241.03	96413				
							Average	StDev
BJ1605(1)		17.56	10.04	1057	173.7	16.33	15.8	0.6
BJ1605(2)		17.30	9.77	1029	169.1	15.90		
BJ1605(3)		16.82	9.29	978	160.8	15.12		
BJ1606(1)		42.94	35.42	3728	612.7	57.59	51.9	6.4
BJ1606(2)		35.14	27.62	2907	477.8	44.91		
BJ1606(3)		40.28	32.76	3448	566.8	53.28		
96CR4(1)		39.12	31.60	3326	546.6	51.38	26.6	21.5
96CR4(2)		16.82	9.30	979	160.9	15.12		
96CR4(3)		15.70	8.17	860	141.4	13.29		
S. Lake(1)		9.56	2.04	214	35.2	3.31	5.6	2.2
S. Lake(2)		11.19	3.66	386	63.4	5.96		
S. Lake(3)		12.23	4.71	495	81.4	7.65		
CR56 Xenolith(1)		22.86	15.34	1615	265.4	24.94	23.7	3.0
CR56 Xenolith(2)		20.03	12.51	1316	216.4	20.34		
CR56 Xenolith(3)		23.46	15.94	1677	275.7	25.91		
Till 1253(1)		35.89	28.37	2986	490.8	46.13	38.4	6.8
Till 1253(2)		29.51	21.99	2314	380.4	35.76		
Till 1253(3)		27.98	20.46	2153	353.9	33.27		
BCR-2(1)		29.75	22.23	2340	384.5	36.15	37.3	1.6
BCR-2(2)		31.56	24.04	2530	415.9	39.09		
BCR-2(3)		30.02	22.50	2368	389.3	36.59		
CM Basalt(1)		42.02	34.50	3631	596.9	56.10	30.2	22.5
CM Basalt(2)		17.76	10.24	1078	177.1	16.65		

Continued on next page

Table B.2 – continued from previous page

Sample	CConc	Net	Net-Blank	Corr-Fluor	Slope or Conc	Conc	r^2 or Avg	StDev
CM Basalt(3)		18.46	10.93	1151	189.1	17.78		
CM 25(1)		63.89	56.36	5933	975.2	91.66	45.2	40.9
CM 25(2)		16.55	9.02	950	156.1	14.68		
CM 25(3)		25.60	18.08	1903	312.7	29.40		
Till 1236(1)		75.57	68.05	7163	1177.3	110.67	138.0	41.0
Till 1236(2)		80.22	72.69	7652	1257.6	118.22		
Till 1236(3)		121.34	113.82	11981	1969.1	185.09		
CR15(1)		12.09	4.57	481	79.1	7.43	38.0	51.6
CR15(2)		13.06	5.54	583	95.8	9.01		
CR15(3)		67.51	59.99	6314	1037.8	97.56		
CR56 Basalt(1)		20.08	12.55	1321	217.2	20.42	24.4	5.0
CR56 Basalt(2)		21.53	14.01	1474	242.3	22.78		
CR56 Basalt(3)		26.02	18.50	1947	320.0	30.08		
S. Tuya(1)		29.32	21.79	2294	377.0	35.44	17.3	16.0
S. Tuya(2)		14.43	6.91	727	119.5	11.23		
S. Tuya(3)		10.78	3.26	343	56.4	5.30		
CM Xeno-lith(1)		28.40	20.87	2197	361.1	33.95	37.6	5.8
CM Xeno-lith(2)		34.77	27.25	2868	471.4	44.31		
CM Xeno-lith(3)		28.83	21.31	2243	368.7	34.66		
Till 4(1)		50.61	43.08	4535	745.4	70.06	88.0	15.8
Till 4(2)		65.32	57.80	6084	999.9	93.99		
Till 4(3)		68.89	61.37	6460	1061.7	99.80		
Volc Creek(1)		19.06	11.54	1215	199.7	18.77	20.1	2.7
Volc Creek(2)		21.79	14.27	1502	246.9	23.21		
Volc Creek(3)		18.83	11.31	1190	195.7	18.39		
Till 1234(1)		69.97	62.45	6574	1080.4	101.56	112.1	18.7
Till 1234(2)		69.71	62.18	6546	1075.8	101.13		
Till 1234(3)		89.77	82.24	8657	1422.8	133.75		
J1408-5.1(1)		97.41	89.89	9462	1555.2	146.19	128.3	20.5
J1408-5.1(2)		72.62	65.10	6853	1126.3	105.87		
J1408-5.1(3)		89.17	81.65	8594	1412.6	132.78		
94BRE330 Xenolith(1)		35.90	28.38	2987	490.9	46.15	37.3	8.3
94BRE330 Xenolith(2)		25.73	18.20	1916	314.9	29.60		
94BRE330 Xenolith(3)		29.82	22.29	2347	385.7	36.26		

Continued on next page

Table B.2 – continued from previous page

Sample	CConc	Net	Net-Blank	Corr-Fluor	Slope or Conc	Conc	r^2 or Avg	StDev
S. Tuya Basalt(1)		16.02	8.49	894	147.0	13.81	15.1	2.7
S. Tuya Basalt(2)		15.72	8.20	863	141.9	13.34		
S. Tuya Basalt(3)		18.70	11.18	1177	193.4	18.18		
Blank	0	6.97	0.00	0				
B								
5ppm	417	302.89	295.92	3115				
10ppm	833	338.54	331.57	6631	slope		r^2	
50ppm	4167	292.83	285.86	30090	6.81		0.998	
100ppm	8333	310.29	303.32	60664				
200ppm	16667	284.43	277.46	110984				
							Average	StDev
Till 3072(1)		80.90	73.93	7782	1143.3	77.74	86.6	13.3
Till 3072(2)		103.87	96.90	10200	1498.6	101.90		
Till 3072(3)		83.25	76.27	8029	1179.6	80.21		
Till-4(1)		124.06	117.09	12325	1810.8	123.13	104.0	19.6
Till-4(2)		106.89	99.92	10518	1545.2	105.08		
Till-4(3)		86.77	79.80	8400	1234.1	83.92		
J1408-5.1(1)		82.51	75.54	7952	1168.2	79.44	82.6	19.1
J1408-5.1(2)		68.96	61.99	6525	958.6	65.19		
J1408-5.1(3)		104.99	98.02	10318	1515.9	103.08		
Till 3292(1)		89.46	82.49	8683	1275.7	86.74	65.6	20.7
Till 3292(2)		50.04	43.07	4534	666.1	45.29		
Till 3292(3)		68.59	61.62	6487	953.0	64.80		
Till 3095(1)		54.89	47.92	5044	741.1	50.40	51.4	0.9
Till 3095(2)		56.59	49.62	5223	767.3	52.18		
Till 3095(3)		56.08	49.11	5169	759.4	51.64		
Till 3079(1)		48.74	41.77	4397	646.0	43.93	46.8	9.0
Till 3079(2)		44.60	37.63	3961	581.9	39.57		
Till 3079(3)		60.98	54.01	5685	835.3	56.80		
BCR-2(1)		32.73	25.76	2712	398.4	27.09	29.5	2.9
BCR-2(2)		38.03	31.06	3269	480.3	32.66		
BCR-2(3)		34.33	27.36	2880	423.2	28.77		
BJ1601(1)		24.56	17.59	1851	272.0	18.49	13.4	5.7
BJ1601(2)		13.79	6.82	718	105.4	7.17		
BJ1601(3)		20.75	13.78	1450	213.0	14.49		
BJ1602(1)		31.59	24.62	2591	380.7	25.89	21.0	4.9
BJ1602(2)		22.30	15.33	1613	237.0	16.12		
BJ1602(3)		26.86	19.89	2094	307.6	20.92		
BJ1603(1)		19.33	12.36	1301	191.1	13.00	12.3	2.5
BJ1603(2)		15.97	9.00	948	139.2	9.47		
BJ1603(3)		20.61	13.64	1436	211.0	14.35		
BJ1604(1)		198.10	191.13	20118	2955.8	200.99	223.4	37.2
BJ1604(2)		260.24	253.26	26659	3916.7	266.34		
BJ1604(3)		199.97	193.00	20316	2984.8	202.96		

Continued on next page

Table B.2 – continued from previous page

Sample	CConc	Net	Net-Blank	Corr-Fluor	Slope or Conc	Conc	r^2 or Avg	StDev
	BB							
Blank	0	6.83	0.00					
B								
5ppm	1	11.68	4.85					
10ppm	2	22.36	15.53		slope		r^2	
50ppm	11	72.99	66.16		5.61		0.995	
100ppm	23	148.03	141.20					
200ppm	45	254.02	247.19					
							Average	StDev
BCR-2.1(1)		28.62	21.79	4	409.2	27.83	22.2	5.2
BCR-2.1(2)		20.58	13.75	2	258.2	17.56		
BCR-2.1(3)		23.35	16.52	3	310.2	21.09		
BCR-2.2(1)		34.11	27.27	5	512.2	34.83	33.0	1.8
BCR-2.2(2)		32.58	25.75	5	483.4	32.87		
BCR-2.2(3)		31.25	24.42	4	458.5	31.18		
BCR-2.3(1)		32.25	25.42	5	477.3	32.45	26.0	6.9
BCR-2.3(2)		27.85	21.02	4	394.8	26.84		
BCR-2.3(3)		21.55	14.71	3	276.3	18.79		
Till-4.1(1)		105.77	98.94	18	1857.8	126.33	130.3	3.4
Till-4.1(2)		110.15	103.32	18	1940.1	131.92		
Till-4.1(3)		110.66	103.83	19	1949.6	132.57		
Till-4.2(1)		88.19	81.36	15	1527.7	103.88	107.0	3.0
Till-4.2(2)		92.78	85.95	15	1613.9	109.74		
Till-4.2(3)		90.99	84.16	15	1580.3	107.46		
Till-4.3(1)		104.14	97.31	17	1827.2	124.25	125.8	9.5
Till-4.3(2)		98.57	91.74	16	1722.6	117.14		
Till-4.3(3)		113.30	106.47	19	1999.3	135.95		
LKSD-4.1(1)		822.94	816.11	146	15324.7	1042.08	1026.1	33.6
LKSD-4.1(2)		780.20	773.37	138	14522.2	987.51		
LKSD-4.1(3)		828.06	821.23	146	15421.0	1048.63		
LKSD-4.2(1)		729.53	722.70	129	13570.8	922.81	1039.4	107.6
LKSD-4.2(2)		837.47	830.64	148	15597.6	1060.64		
LKSD-4.2(3)		895.57	888.74	159	16688.7	1134.83		
LKSD-4.3(1)		734.21	727.38	130	13658.6	928.79	1127.0	171.8
LKSD-4.3(2)		962.54	955.71	170	17946.2	1220.34		
LKSD-4.3(3)		971.60	964.77	172	18116.4	1231.91		
G-2.1(1)		13.12	6.29	1	118.1	8.03	8.3	2.6
G-2.1(2)		11.46	4.63	1	87.0	5.91		
G-2.1(3)		15.45	8.62	2	161.9	11.01		

Continued on next page

Table B.2 – continued from previous page

Sample	CConc	Net	Net-Blank	Corr-Fluor	Slope or Conc	Conc	r^2 or Avg	StDev
G-2.2(1)		8.30	1.47	0	27.6	1.87	4.2	5.0
G-2.2(2)		7.38	0.54	0	10.2	0.69		
G-2.2(3)		14.64	7.81	1	146.6	9.97		
G-2.3(1)		8.42	1.59	0	29.8	2.03	2.8	4.0
G-2.3(2)		6.22	-0.61	0	-11.5	-0.78		
G-2.3(3)		12.34	5.51	1	103.5	7.04		
SY-4.1(1)		6.68	-0.15	0	-2.8	-0.19	0.5	0.6
SY-4.1(2)		7.52	0.69	0	13.0	0.88		
SY-4.1(3)		7.43	0.59	0	11.2	0.76		
SY-4.2(1)		10.76	3.93	1	73.8	5.02	5.4	1.0
SY-4.2(2)		10.50	3.67	1	68.9	4.68		
SY-4.2(3)		12.01	5.18	1	97.2	6.61		
SY-4.3(1)		18.70	11.86	2	222.8	15.15	18.2	3.3
SY-4.3(2)		20.75	13.92	2	261.3	17.77		
SY-4.3(3)		23.86	17.03	3	319.7	21.74		
BHVO-2.1(1)		22.24	15.41	3	289.3	19.68	11.4	7.2
BHVO-2.1(2)		13.12	6.29	1	118.1	8.03		
BHVO-2.1(3)		11.96	5.13	1	96.4	6.55		
BHVO-2.2(1)		10.04	3.21	1	60.3	4.10	3.0	1.9
BHVO-2.2(2)		10.01	3.18	1	59.7	4.06		
BHVO-2.2(3)		7.49	0.66	0	12.5	0.85		
BHVO-2.3(1)		9.13	2.29	0	43.1	2.93	4.3	1.3
BHVO-2.3(2)		11.12	4.29	1	80.6	5.48		
BHVO-2.3(3)		10.26	3.43	1	64.4	4.38		
Blank A	1420	2.93	4.68	0				
Blank B	1422	6.43	0.00	0	slope		r^2	
5ppm	1424	7.40	2.72	1	3.19		0.994	
10ppm	1426	12.26	7.58	2				
50ppm	1428	36.66	31.98	11				
100ppm	1429	72.80	68.12	23				
200ppm	1430	152.67	147.99	45				
			BB	V			Average	StDev
BCR-1(1.a)	7	2.18	0.68	274	24.1		29.0	6.9
BCR-1(1.b)	16	11.55	3.63	385	33.9			
BCR-1(2.a)	11	6.13	1.93	772	67.8		113.3	76.2
BCR-1(2.b)	65	59.96	18.82	2000	175.5			
BCR-1(3.a)	9	4.60	1.44	579	51.1		43.4	10.8

Continued on next page

Table B.2 – continued from previous page

Sample	CConc	Net	Net-Blank	Corr-Fluor	Slope or Conc	Conc	r^2 or Avg	StDev
BCR-1(3.b)	17	12.16	3.82	406	35.8			
J1408-5.1(1.a)	13	7.99	2.51	1006	88.4		119.7	44.3
J1408-5.1(1.b)	56	51.51	16.17	1718	151.0			
J1408-5.1(2.a)	16	11.64	3.66	1466	128.6		153.6	35.3
J1408-5.1(2.b)	66	60.97	19.14	2034	178.5			
J1408-5.1(3.a)	13	8.30	2.60	1044	91.9		147.2	78.1
J1408-5.1(3.b)	74	68.91	21.63	2299	202.4			
G-2(1.a)	7	2.58	0.81	325	28.5		18.6	13.9
G-2(1.b)	8	2.99	0.94	100	8.7			
G-2(2.a)	5	0.67	0.21	84	7.4		6.5	1.2
G-2(2.b)	7	1.95	0.61	65	5.7			
	BB							
Blank A	0	3.05	-0.14	0				
Blank B	0	3.33	0.14	0				
5ppm	1	38.81	35.62	1				
10ppm	2	67.63	64.44	2	slope		r^2	
50ppm	11	350.57	347.38	11	27.43		0.994	
100ppm	23	693.76	690.57	23				
200ppm	45	1207.36	1204.17	45				
				BB	V		Average	StDev
G-2(1)		6.63	3.44	0	12.7	1.11	0.9	0.3
G-2(2)		6.46	3.27	0	8.1	0.71		
034(1)		47.32	44.14	2	162.5	14.29	10.7	5.1
034(2)		35.92	32.73	1	80.7	7.10		
107(1)		24.28	21.09	1	77.7	6.82	8.5	2.3
107(2)		49.77	46.58	2	114.9	10.09		
101(1)		6.44	3.25	0	12.0	1.05	0.9	0.2
101(2)		6.72	3.53	0	8.7	0.76		
076(1)		8.68	5.49	0	20.2	1.78	1.9	0.1
076(2)		12.17	8.98	0	22.2	1.95		
069(1)		9.33	6.15	0	22.6	1.99	2.3	0.4
069(2)		15.13	11.95	0	29.5	2.59		
015(1)		0.38	-2.81	0	-10.3	-0.91	-0.8	0.2
015(2)		0.10	-3.08	0	-7.6	-0.67		
021(1)		8.23	5.04	0	18.6	1.62	2.1	0.6
021(2)		14.73	11.54	0	28.5	2.49		
030(1)		5.45	2.26	0	8.3	0.73	0.8	0.0
030(2)		6.80	3.61	0	8.9	0.78		
041(1)		11.34	8.16	0	30.0	2.64	2.0	1.0
041(2)		9.08	5.89	0	14.5	1.28		

Table B.3: Summary of N analyses of continental rocks, including tills, basalts, granites, gneisses, carbonates, and xenoliths. See Table B.5 for sample details. Shown are date analyzed, sample name, N concentration, the mean value for each sample on each day ($\bar{x}_d$), and overall mean and standard deviation ($\bar{x}_s \pm \sigma$). All concentrations are in ppm.

Date	Sample name	N (ppm)	$\bar{x}_d$	$\bar{x}_s \pm \sigma$
	Tills			Till-4
2016-07-05	Till 1253 (1)	46.1	38.4	111 ± 19
	Till 1253 (2)	35.8		Till1253
	Till 1253 (3)	33.3		38 ± 7
	Till 1236 (1)	110.7	138.0	Till 1236

Continued on next page

Table B.3 – continued from previous page

Date	Sample name	N (ppm)	$\bar{x}_d$	$\bar{x}_s \pm \sigma$
	Till 1236 (2)	118.2		138 ± 41
	Till 1236 (3)	185.1		Till 1234
	Till 4 (1)	70.1	88.0	112 ± 19
	Till 4 (2)	94.0		Till 3072
	Till 4 (3)	99.8		87 ± 13
	Till 1234 (1)	101.6	112.1	Till 3292
	Till 1234 (2)	101.1		66 ± 21
	Till 1234 (3)	133.7		Till 3095
2016-07-13	Till 3072(1)	77.7	86.6	51 ± 0.9
	Till 3072(2)	101.9		Till 3079
	Till 3072(3)	80.2		47 ± 9
	Till-4 (1)	123.1	104.0	
	Till-4(2)	105.1		All Tills
	Till-4(3)	83.9		Average
	Till 3292 (1)	86.7	65.6	81.2 ± 35.4
	Till 3292 (2)	45.3		
	Till 3292 (3)	64.8		
	Till 3095 (1)	50.4	51.4	
	Till 3095 (2)	52.2		
	Till 3095 (3)	51.6		
	Till 3079 (1)	43.9	46.8	
	Till 3079 (2)	39.6		
	Till 3079 (3)	56.8		
2016-07-20	Till-4.1 (1)	126.3	130.3	
	Till-4.1(2)	131.9		
	Till-4.1(3)	132.6		
	Till-4.2 (1)	103.9	107.0	
	Till-4.2(2)	109.7		
	Till-4.2(3)	107.5		
	Till-4.3(1)	124.3	125.8	
	Till-4.3(2)	117.1		
	Till-4.3(3)	135.9		
	Volcanics			
	Name	conc		BCR-2
2016-06-22	BCR-2 (1)	23.2	29.7	33 ± 14
	BCR-2 (2)	31.4		BJ1604
	BCR-2 (3)	34.5	Not included -¿	249 ± 59
2016-06-24	BCR-2 (1)	42.7	30.1	BJ1602
	BCR-2 (2)	25.1		21 ± 4
	BCR-2 (3)	22.4		BJ1603
2016-06-28	BJ1604 (1)	353.8	275.1	9.8 ± 3.9
	BJ1604 (2)	210.4		BJ1601
	BJ1604 (3)	261.2		10.5 ± 6
	BJ1602 (1)	18.1	21.1	Ruby mtn Basalt
	BJ1602 (2)	24.2		19 ± 31
	BJ1602 (3)	20.9		BJ1605
	BCR-2 (1)	24.4	21.0	15.8 ± 0.6
	BCR-2 (2)	20.7		BJ1606
	BCR-2 (3)	17.8		52 ± 6.5
Not included -¿	BJ1603 (1)	79.6	30.6	CR56 Basalt
	BJ1603 (2)	7.0		24 ± 5
	BJ1603 (3)	5.2		CM Basalt
	Ruby mtn Basalt (1)	55.2	19.0	30 ± 22
	Ruby mtn Basalt (2)	1.9		Volcano Creek
	Ruby mtn Basalt (3)	-0.1		20 ± 2.7
	BJ1601 (1)	14.3	7.5	South Tuya Basalt
	BJ1601 (2)	3.1		15 ± 2.7
	BJ1601 (3)	5.3		BHVO2
2016-06-29	BCR-2 (1)	70.6	57.2	6.3 ± 5.4
	BCR-2 (2)	69.5		
	BCR-2 (3)	31.4		All volcanics
	BCR-2 (1.2)	51.5	27.5	average
	BCR-2 (2.2)	20.3		21.4 ± 12.5
	BCR-2 (3.2)	10.8		
2016-07-05	BJ1605 (1)	16.3	15.8	
	BJ1605 (2)	15.9		
	BJ1605 (3)	15.1		
	BJ1606 (1)	57.6	51.9	
	BJ1606 (2)	44.9		

Continued on next page

Table B.3 – continued from previous page

Date	Sample name	N (ppm)	$\bar{x}_d$	$\bar{x}_s \pm \sigma$
	BJ1606 (3)	53.3		
	CR56 Basalt (1)	20.4	24.4	
	CR56 Basalt (2)	22.8		
	CR56 Basalt (3)	30.1		
	BCR-2 (1)	36.1	37.3	
	BCR-2 (2)	39.1		
	BCR-2 (3)	36.6		
	CM Basalt (1)	56.1	30.2	
	CM Basalt (2)	16.6		
	CM Basalt (3)	17.8		
	Volc Creek (1)	18.8	20.1	
	Volc Creek (2)	23.2		
	Volc Creek (3)	18.4		
	S. Tuya Basalt (1)	13.8	15.1	
	S. Tuya Basalt (2)	13.3		
	S. Tuya Basalt (3)	18.2		
2016-07-13	BCR-2 (1)	27.1	29.5	
	BCR-2 (2)	32.7		
	BCR-2 (3)	28.8		
	BJ1601 (1)	18.5	13.4	
	BJ1601 (2)	7.2		
	BJ1601 (3)	14.5		
	BJ1602 (1)	25.9	21.0	
	BJ1602 (2)	16.1		
	BJ1602 (3)	20.9		
	BJ1603 (1)	13.0	12.3	
	BJ1603 (2)	9.5		
	BJ1603 (3)	14.3		
	BJ1604 (1)	201.0	223.4	
	BJ1604 (2)	266.3		
	BJ1604 (3)	203.0		
2016-07-20	BCR-2.1 (1)	27.8	22.2	
	BCR-2.1 (2)	17.6		
	BCR-2.1 (3)	21.1		
	BCR-2.2 (1)	34.8	33.0	
	BCR-2.2 (2)	32.9		
	BCR-2.2 (3)	31.2		
	BCR-2.3 (1)	32.5	26.0	
	BCR-2.3 (2)	26.8		
	BCR-2.3 (3)	18.8		
	BHVO-2.1 (1)	19.7	11.4	
	BHVO-2.1 (2)	8.0		
	BHVO-2.1 (3)	6.6		
	BHVO-2.2 (1)	4.1	3.0	
	BHVO-2.2 (2)	4.1		
	BHVO-2.2 (3)	0.8		
	BHVO-2.3 (1)	2.9	4.3	
	BHVO-2.3 (2)	5.5		
	BHVO-2.3 (3)	4.4		
2016-08-02	BCR-1 (1.a)	24.1	29.0	
	BCR-1 (1.b)	33.9		
	BCR-1 (2.a)	67.8	67.8	
	BCR-1 (3.a)	51.1	43.4	
	BCR-1 (3.b)	35.8		
	Carbonates			
	Name	conc		
2016-06-28	J1408-5.1(1)	74.1	79.8	114 ± 40.9
	J1408-5.1(2)	83.7		
	J1408-5.1(3)	81.6		
2016-07-05	J1408-5.1(1)	146.2	128.3	
	J1408-5.1(2)	105.9		
	J1408-5.1(3)	132.8		
2016-07-13	J1408-5.1(1)	79.4	82.6	
	J1408-5.1(2)	65.2		
	J1408-5.1(3)	103.1		
2016-08-02	J1408-5.1(1.a)	88.4	122.7	
	J1408-5.1(1.b)	151.0		
	J1408-5.1(2.a)	128.6		
	J1408-5.1(2.b)	178.5	157.6	

Continued on next page

Table B.3 – continued from previous page

Date	Sample name	N (ppm)	$\bar{x}_d$	$\bar{x}_s \pm \sigma$
	J1408-5.1(3.a)	91.9		
	J1408-5.1(3.b)	202.4		
	Granitic			
	Name	conc		G-2
2016-06-28	Llang 955LML1 (1)	66.9	38.1	7.0 ± 7.1
	Llang 955LML1 (2)	31.2		Llang 955
	Llang 955LML1 (3)	16.3		38 ± 26
2016-07-05	96CR4 (1)	51.4	26.6	96CR4
	96CR4 (2)	15.1		26 ± 21
	96CR4 (3)	13.3		CR15
	CR15 (1)	7.4	38.0	38 ± 52
	CR15 (2)	9.0		SY-4
	CR15 (3)	97.6		9.1 ± 8
2016-07-20	G-2.1(1)	8.0	8.3	34.0
	G-2.1(2)	5.9		10.7 ± 5.1
	G-2.1(3)	11.0		107.0
	G-2.2(1)	1.9	4.2	8.5 ± 2.3
	G-2.2(2)	0.7		76.0
	G-2.2(3)	10.0		1.9 ± 0.12
	G-2.3(1)	2.0	4.5	41.0
				2.6
	G-2.3(3)	7.0		
			0.8	All Granite
	SY-4.1 (2)	0.9		15.8 ± 14.6
	SY-4.1 (3)	0.8		
	SY-4.2 (1)	5.0	5.4	
	SY-4.2 (2)	4.7		
	SY-4.2 (3)	6.6		
	SY-4.3 (1)	15.1	18.2	
	SY-4.3 (2)	17.8		
	SY-4.3 (3)	21.7		
2016-08-02	G-2 (1.a)	28.5	18.6	
	G-2 (1.b)	8.7		
	G-2 (2.a)	7.4	6.5	
	G-2 (2.b)	5.7		
2016-08-03	G-2 (1)	1.1	0.9	
	G-2 (2)	0.7		
	034 (1)	14.3	10.7	
	034 (2)	7.1		
	107 (1)	6.8	8.5	
	107 (2)	10.1		
	076 (1)	1.8	1.9	
	076 (2)	2.0		
	041 (1)	2.6	2.6	
	Mafic intrusive			
2016-06-28	Llang Gabbro (1)	20.2	8.2	
	Llang Gabbro (2)	2.4		
	Llang Gabbro (3)	2.1		
2016-08-03	069 (1)	2.0	2.3	
	069 (2)	2.6		
2016-08-03	Hornblendite			
	101 (1)	1.1	0.9	
	101 (2)	0.8		
	Olivine cumulate			
	021 (1)	1.6	2.1	
	021 (2)	2.5		
	030 (1)	0.7	0.8	
	030 (2)	0.8		
	Gneiss			
2016-06-28	OMNG (1)	29.5	29.8	29.8
	OMNG (2)	29.2		
	OMNG (3)	30.7		
	Xenoliths			
2016-06-28	Ruby Xenolith (1)	9.4	6.4	
	Ruby Xenolith (2)	5.6		
	Ruby Xenolith (3)	4.2		
	CM 25 (1)	91.7	45.2	
	CM 25 (2)	14.7		
	CM 25 (3)	29.4		

Continued on next page

Table B.3 – continued from previous page

Date	Sample name	N (ppm)	$\bar{x}_d$	$\bar{x}_s \pm \sigma$
2016-07-05	CR56 Xenolith (1)	24.9	23.7	
	CR56 Xenolith (2)	20.3		
	CR56 Xenolith (3)	25.9		
	CM 25 (1)	91.7	45.2	
	CM 25 (2)	14.7		
	CM 25 (3)	29.4		
	CM Xenolith (1)	33.9	37.6	
	CM Xenolith (2)	44.3		
	CM Xenolith (3)	34.7		
	94BRE330 Xenolith (1)	46.1	37.3	
	94BRE330 Xenolith (2)	29.6		
	94BRE330 Xenolith (3)	36.3		
	S. Tuya (1)	35.4	17.3	
	S. Tuya (2)	11.2		
	S. Tuya (3)	5.3		
	S. Lake (1)	3.3	5.6	
	S. Lake (2)	6.0		All Xenoliths
	S. Lake (3)	7.7		27.3 ± 16.6
	Lake sediments			
2016-07-20	LKSD-4.1(1)	1042.1		1064 ± 113
	LKSD-4.1(2)	987.5		
	LKSD-4.1(3)	1048.6		
	LKSD-4.2(1)	922.8		
	LKSD-4.2(2)	1060.6		
	LKSD-4.2(3)	1134.8		
	LKSD-4.3(1)	928.8		
	LKSD-4.3(2)	1220.3		
	LKSD-4.3(3)	1231.9		

Table B.4: Raw colourimetry data. Shown are standard solutions and rock standards. Average absorbance is average of readings 1-3, with corrected absorbance accounting for extra dilutions made during absorbance reading. Resulting N concentrations are given in ppm. To account for dilutions made during sample preparation (first run only), concentrations for LKSD shown below were multiplied by 166.7 and Till samples multiplied by 50 to calculate actual concentrations. The first set of analysis (D) were run on November 16, 2015 and the second set on January 29, 2016.

Sample	Reading 1	Reading 2	Reading 3	Average abs.	Corrected abs.	N (ppm)
Blank-A D	0.047	0.045	0.045	0.046		
Blank-B D	0.078	0.078	0.075	0.077		
5 ppm D	0.06	0.057	0.058	0.058		
10 ppm D	0.106	0.103	0.1	0.103		
5.1 D	0.43	0.432	0.431	0.431		66.1
SY4-A D	0.092	0.096	0.095	0.094		8.3
SY4-B D	0.096	0.096	0.098	0.097		8.7
SY4-C D	0.067	0.066	0.069	0.067		3.7
BCR2-A D	0.157	0.155	0.159	0.157		19.1
BCR2-B D	0.132	0.136	0.132	0.133		15
BCR2-C D	0.066	0.068	0.066	0.067		3.6
BHVO2-A D	0.067	0.063	0.065	0.065		3.3
BHVO2-B D	0.063	0.062	0.064	0.063		2.9
BHVO2-C D	0.074	0.068	0.069	0.07		4.2
G2-A D	0.051	0.052	0.049	0.051		0.8
G2-B D	0.056	0.056	0.054	0.055		1.6
G2-C D	0.062	0.058	0.062	0.061		2.5
BLST D	0.38	0.377	0.385	0.381		57.5
50 ppm D	0.351	0.361	0.352	0.355		
100 ppm D	0.638	0.633	0.642	0.638		
LKSD-A D	0.077	0.079	0.076	0.077		5.4
LKSD-B D	0.052	0.046	0.05	0.049		0.6
LKSD-C D	0.063	0.06	0.064	0.062		2.8
TILL-A D	0.054	0.06	0.054	0.056		1.7
TILL-B D	0.048	0.053	0.051	0.051		0.8

Continued on next page

Table B.4 – continued from previous page

Sample	Reading 1	Reading 2	Reading 3	Average abs.	Corrected abs.	
TILL-C D	0.059	0.059	0.062	0.06		2.4
200ppm D	1.218	1.193	1.195	1.202		
					Corrected abs	
Blank-A	0.012	0.009	0.01	0.01	0.01	
Blank-B	0.04	0.038	0.04	0.039	0.039	
5ppm	0.099	0.105	0.1	0.101	0.101	
10ppm	0.123	0.122	0.123	0.123	0.123	
5.1	0.538	0.534	0.536	0.536	0.536	60.7
SY-A	0.044	0.047	0.045	0.045	0.045	2
SY-B	0.041	0.039	0.04	0.04	0.04	1.4
SY-C	0.043	0.042	0.039	0.041	0.041	1.5
BCR-A	0.085	0.078	0.082	0.082	0.082	6.3
BCR-B	0.105	0.109	0.108	0.107	0.107	9.4
BCR-C	0.061	0.059	0.062	0.061	0.061	3.8
BHVO-A	0.065	0.06	0.065	0.063	0.063	4.2
BHVO-B	0.103	0.104	0.108	0.105	0.105	9.1
BHVO-C	0.033	0.036	0.033	0.034	0.034	0.6
G2-A	0.04	0.039	0.041	0.04	0.04	1.4
G2-B	0.025	0.024	0.021	0.023	0.023	-0.6
50ppm	0.379	0.377	0.375	0.377	0.377	
100ppm	0.888	0.885	0.907	0.893	0.893	
LKSD-A	0.061	0.062	0.063	0.062	8.455	1008.7
LKSD-B	0.053	0.054	0.053	0.053	7.273	867.3
LKSD-C	0.051	0.054	0.054	0.053	7.227	861.8
Till-A	0.047	0.049	0.045	0.047	1.923	226.8
Till-B	0.037	0.039	0.036	0.037	1.527	179.4
Till-C	0.035	0.027	0.035	0.032	1.323	154.9
200ppm	0.848	0.848	0.851	0.849	1.698	

Table B.5: Samples used in proof of concept application of fluorometry method. Rock types are Intrusive igneous (II), metamorphic (M), volcanic (V), carbonate (C), and tills (T). Samples were either collected by me (UVic), provided by Kelly Russell at the University of British Columbia (UBC), the BC Geological Survey (BCGS), or by Dante Canil and Jeff Larocque at UVic (UVic-LR). OMNG is the Omenica Gneiss and ACG is the Acasta Gneiss. SL stands for Strathcona lodge.

Sample	Rock type	Rock name	Location	Source	Lat.	Long.
OMNG	M	gneiss	Central BC	Uvic		
ACG	M	Gneiss	Northern Ontario	Uvic		
Ruby Mountain 95RM12 Xenolith	II	Xenolith	Ruby Mountain, BC	UBC	60.133	-123.550
BJ1603	V	Altered Tuff - Sicker Formation	Near SL, Van Island BC	Uvic	48.777	-123.374
J1408-5.1	C	C	Northwestern Namibia	Uvic		
Ruby Mountain 95RM12 Basalt	V	Basalt	Ruby Mountain, BC	UBC	60.133	-123.550
BJ1601	V	Altered Tuff - Sicker Formation	Near Duncan, BC	Uvic	48.777	-123.374
Chikoida Mountain 95CM25	II	Xenolith	Chikoida Mountain, BC	UBC	59.233	-133.046
Chikoida Mountain 95CM28	II	Xenolith	Chikoida Mountain, BC	UBC	59.233	-133.046
94BRE330	II/V	Xenolith /basalt		UBC		
Castle Rock CR15			Castle Rock, BC	UBC	52.533	-122.483
BJ1606	V	Basalt	Near SL, Van Island BC	Uvic	48.777	-123.374
Chikoida Mountain 95CM28	V	Basalt	Chikoida Mountain, BC	UBC	59.233	-133.046
BJ1605	V	Basalt	Ruckle Park, SSI, BC	Uvic	48.777	-123.374
S. Tuya 955T7	V	Basalt	S. Tuya, BC	UBC	59.033	-130.083
S. Tuya 955T8	II	Xenolith	S. Tuya, BC	UBC	59.033	-130.083
CR56	V	Basalt		UBC		
BJ1604	V	Basalt	Near SL, Van Island BC	Uvic	48.777	-123.374
Castle Rock 96CR4	II	Xenolith	Castle Rock, BC	UBC	52.533	-122.483
Llangorse Gabbro	II	Gabbro	Llangorse Mountain, BC	UBC	59.399	-132.805
Llangorse Mountain			Llangorse Mountain, BC	UBC	59.399	-132.805

Continued on next page

Table B.5 – continued from previous page

Sample	Rock type	Rock name	Location	Source	Lat.	Long.
Batholith 95LM21						
Surprise Lake Batholith	II	Xenolith	Surprise Lake, BC	UBC	50.142	-125.565
CR56	II	Xenolith		UBC		
BJ1602	V	Altered Tuff	Near SL, Van Island BC			
Volcano Creek	V	Basalt		UBC		
3292	T	T	Interior Plateau, BC	BCGS	52.642	-123.978
1253	T	T	Interior Plateau, BC	BCGS	52.509	-123.659
1234	T	T	Interior Plateau, BC	BCGS	53.684	-123.585
1236	T	T	Interior Plateau, BC	BCGS	53.785	-123.905
3072	T	T	Interior Plateau, BC	BCGS	53.000	-123.689
3079	T	T	Interior Plateau, BC	BCGS	53.052	-123.757
3095	T	T	Interior Plateau, BC	BCGS	53.161	-123.978
JL06-041	II	Granodiorite	WCC, Renfrew	UVic-LR	48.686	-124.383
JL06-034	II	Granite	IPS, Renfrew	UVic-LR		
JL06-076	II	Granodiorite	IPS, Renfrew	UVic-LR	48.632	-124.062
JL06-021	II	Ol. Cum.	WCC, Renfrew	UVic-LR	48.619	-124.486
JL06-101	II	Hornblendite	WCC, Renfrew	UVic-LR	48.638	-124.491
JL06-030	II	Ol. Cum.	WCC, Renfrew	UVic-LR	48.629	-124.296
JL06-107	II	Granite dyke	WCC, Renfrew	UVic-LR	48.622	-124.190
JL06-069	II	cumulate gabbro	WCC, Renfrew	UVic-LR	48.651	-124.749
JL06-015	II	Plag. Cum.	WCC, Renfrew	UVic-LR	48.619	-124.288

Appendix C

Snowball Earth geochemical supplemental data

Presented here are N, C, and trace element data from Chapter 4. All data are available as electronic files in the supplementary information to the publication (Johnson & Goldblatt, In review). Note that whole rock trace element (Tables C.1-C.4), laser ablation (Tables C.5-C.6), and N and C (Tables C.7-C.8) analyses are split into multiple tables due to formatting restrictions in this thesis. All samples are identified by a unique sample name, which is a stratigraphic height in a given section.

Table C.1: Whole rock trace element data in ppm. Sample names are shown as Section-Stratigraphic height, where height is distance above the base of the formation. Samples from section J1408 are abbreviated "08", those from J1409 "09", and those from J1413 "13". Samples with -A were run in duplicate, shown by -Dp. Several decarbonated samples (Dc) were also run.

Sample	Li	Be	B	Al	P	Sc	Ti	V	^{52}Cr	^{53}Cr	Mn	Fe	Co	Ni
J1408-5.1	6.6	0.51	25.0	11000	459	3.1	714	26.3	14.0	14	1120	7930	8	20
J1408-8.4	6.2	0.33	10.0	7560	478	2.2	443	11.4	7.0	6.8	1570	6060	7	18
J1408-9.1	3.8	0.23	6.4	4600	364	1.6	278	6.89	4.9	4.8	1610	5210	7	16
J1408-10.2c	16.0	0.5	33.0	14100	885	3.1	892	25.8	15.0	15	1120	10900	7	27
J1408-10.2a	6.9	0.29	15.0	7380	513	2.2	449	13.5	7.3	7.1	1000	5150	4	16
J1408-10.2d	1.5	0.13	5.2	2180	272	1.2	109	4.24	2.5	2.3	889	1760	2	7.2
J1408-10.2b	11.0	0.36	22.0	11100	774	3.2	676	19.4	11.0	11	1370	7490	7	25
J1408-12.4	20.0	0.45	23.0	12100	826	3.2	739	39.9	9.5	9.4	1020	8170	10	53
J1408-13.6	2.3	0.09	4.5	2020	478	0.74	115	12.1	4.3	4.1	638	2130	2	11
J1408-14.5	2.1	0.07	2.7	1640	318	0.68	88	5.75	2.5	2.3	438	1820	2	9.7
J1408-15.2	5.3	0.27	11.0	6740	648	2.2	384	13.5	6.0	5.9	542	4090	6	37
J1408-17.7	1.6	0.09	3.5	1760	375	0.6	98	3.56	2.2	2	300	2080	2	9.8
J1408-20.4	4.9	0.2	11.0	4380	610	1.6	289	10.7	6.4	6.3	319	4230	2	16
J1408-12.4-A	20.0	0.43	23.0	12100	807	3.3	731	40.1	9.3	9.2	1010	8300	10	53
J1408-12.4-Dp	20.0	0.46	23.0	12000	845	3.2	747	39.7	9.6	9.6	1030	8040	10	54
j1408-12.4-Dc	64.0	1.9	180.0	69300	10	7.2	5300	189	54.0	54	7	1890	3	57
J1413-9.0	18.0	0.96	63.0	28600	1060	6.4	1760	60.1	39.0	38	1010	23100	3	13
J1413-13.1	35.0	1.9	92.0	53000	804	12	3440	106	73.0	72	486	35300	7	34
J1413-18.7	53.0	2.6	110.0	73500	766	19	4440	171	100.0	99	413	41000	17	48
J1413-24.8	23.0	1.4	77.0	42700	1320	11	3050	86	61.0	60	1290	26200	13	22
J1413-29.3	28.0	1.6	84.0	47400	1120	12	3280	96.8	67.0	66	1680	22100	9	23
J1413-34.8	44.0	2.2	98.0	68100	984	17	4220	135	87.0	86	828	43800	10	36
J1413-40.8	51.0	2.7	110.0	76400	811	18	4490	149	93.0	92	432	50300	19	40

Continued on next page

Table C.1 – continued from previous page

Sample	Li	Be	B	Al	P	Sc	Ti	V	^{52}Cr	^{53}Cr	Mn	Fe	Co	Ni
J1413-45.5	51.0	2.5	110.0	73900	879	17	4510	146	91.0	89	681	51600	13	40
J1413-45.5-A	51.0	2.5	110.0	73800	870	17	4500	146	90.0	89	669	51400	13	40
J1413-45.5-Dp	51.0	2.5	110.0	74000	888	17	4530	145	91.0	90	693	51800	13	40
J1413-45.5-Dc	37.0	3.1	200.0	75000	13	19	4780	144	78.0	78	10	7460	1	2.9
J1409-0.1	4.8	0.45	11.0	6000	272	2.5	330	54.1	4.8	4.7	3990	12200	16	73
J1409-0.6	23.0	1	40.0	21000	575	6.8	1100	261	14.0	14	5260	26300	42	360
J1409-1.6b	20.0	0.88	33.0	19900	634	6.8	1150	74.3	16.0	16	5720	18800	18	150
J1409-1.6a	1.6	0.23	4.5	2440	239	2.1	135	7.78	3.9	3.9	5570	3830	13	62
J1409-2.6	5.5	0.36	15.0	9630	563	3.5	573	22.7	14.0	14	6490	7300	20	110
J1409-3.6	0.8	0.21	5.4	4360	358	1.9	309	17.3	7.0	6.8	6650	2980	22	80
J1409-4.6	1.4	0.17	3.7	2520	232	2	137	35.2	4.9	4.7	5900	1230	20	62
J1409-6.3	1.0	0.18	4.4	4190	474	2.3	263	22.3	7.4	7.4	5230	3360	19	53
J1409-7.1a	1.5	0.19	3.4	2460	272	2	157	20.2	3.9	3.7	6790	2220	20	48
J1409-7.1b	9.7	0.84	27.0	15500	426	6	850	58.9	17.0	17	4910	20900	15	64
J1409-7.8	18.0	1.2	47.0	23600	540	6.9	1410	65.2	17.0	17	3590	25100	18	92
J1409-1.6b-A	21.0	0.85	33.0	19700	626	6.7	1150	73.7	16.0	15	5740	18600	18	150
J1409-1.6b-Dp	20.0	0.91	32.0	20100	642	7	1140	75	16.0	16	5700	18900	17	150
J1409-1.6b-Dc	63.0	2.1	130.0	67300	6	12	4450	109	52.0	51	29	3390	2	130

Table C.2: WR trace element data continued

Sample	^{63}Cu	^{65}Cu	Zn	Ga	Ge	As	Rb	Sr	Y	Zr	Nb	Mo	Cd	Sn
J1408-5.1	17	18	20	7.1	1	20	19	700	13	51	2	0.12	0.14	0.53
J1408-8.4	7	7.5	20	10	0	0.24	13	700	9	33	1	0.27	0.09	0.29
J1408-9.1	3	2.9	15	6.8	0	0.16	7	600	7	21	1		0.07	0.19
J1408-10.2c	5	5.5	17	7.1	1	0.47	34	860	9	64	3		0.06	0.66
J1408-10.2a	4	4.3	11	5.1	0	0.44	16	1200	7	34	1		0.05	0.31
J1408-10.2d	2	2	5	3.4	0	0.28	4	1600	4	8.2	0	0.07	0.04	0.07
J1408-10.2b	7	8	17	10	1	0.95	23	1200	9	48	2	0.01	0.07	0.48
J1408-12.4	36	38	23	12	1	2.5	28	860	9	57	3	0.11	0.07	0.57
J1408-13.6	8	8.4	7	2.6	0	1.1	4	1000	4	9.3	0	0.35	0.06	0.07
J1408-14.5	6	6.6	5	2.7	0	1.2	3	850	3	8.6	0	0.04	0.05	0.06
J1408-15.2	15	16	16	5.3	0	1.2	12	1300	6	28	1		0.04	0.26
J1408-17.7	16	17	4	1.4	0	0.51	4	960	4	7.2	0	0.55	0.03	0.06
J1408-20.4	6	6.3	11	1.9	0	3.4	9	720	6	18	1	0.07	0.19	0.21
J1408-12.4-A	36	37	23	12	1	2.6	27	860	9	56	3	0.12	0.07	0.56
J1408-12.4-Dp	36	38	23	12	1	2.5	28	870	9	57	3	0.1	0.07	0.57
j1408-12.4-Dc	8	10	18	60	2	0.89	120	9.2	8	310	19	0.24	0.06	3.7
J1413-9.0	6	7.1	33	12	1	1	49	340	14	130	5	0.73	0.12	1.2
J1413-13.1	30	32	76	19	2	5	81	160	21	250	10	2.2	0.20	2.5
J1413-18.7	22	24	95	25	3	2.6	120	78	28	320	12	0.34	0.13	3.5
J1413-24.8	31	33	36	16	2	2.7	69	400	35	210	8	1	0.18	1.8
J1413-29.3	17	18	50	19	2	9.3	80	370	28	230	9	0.76	0.14	2.1
J1413-34.8	28	30	84	28	3	25	120	150	25	310	12	0.56	0.13	3.1
J1413-40.8	21	23	120	30	3	4.1	130	51	28	390	15	0.24	0.14	3.5
J1413-45.5	51	55	91	30	3	2.5	150	74	27	350	13	1.6	0.18	3.4
J1413-45.5-A	52	55	92	30	3	2.5	150	74	27	360	13	1.4	0.17	3.4
J1413-45.5-Dp	51	54	91	30	3	2.6	140	74	27	350	13	1.7	0.19	3.4
J1413-45.5-Dc	1	2.3	18	34	2	0.43	110	27	25	480	19		0.09	4.3
J1409-0.1	39	41	26	2.7	1	4.3	12	77	11	28	1	1.1	0.16	0.27
J1409-0.6	100	110	120	10	2	9.5	40	72	18	91	4	1.5	1.10	0.9
J1409-1.6b	170	180	44	12	1	10	36	74	18	88	4	1.7	0.21	0.83
J1409-1.6a	22	23	30	1.3	0	0.58	5	100	11	12	0	0.01	0.16	0.12
J1409-2.6	32	33	30	6.4	1	0.76	15	88	13	39	2	0.3	0.22	0.42
J1409-3.6	150	160	22	2.4	0	0.42	4	93	10	15	1	1.5	0.19	0.19
J1409-4.6	8	8.5	27	37	0	0.45	2	110	8	12	0	0.2	0.20	0.1
J1409-6.3	5	4.9	28	6.2	0	0.41	3	110	9	16	1	0.1	0.20	0.15
J1409-7.1a	10	11	30	38	0	0.6	2	130	8	12	0	0.04	0.22	0.11
J1409-7.1b	19	20	39	8.1	1	13	34	68	11	65	2	0.65	0.23	0.6
J1409-7.8	12	13	55	11	2	34	54	71	13	110	5	0.34	0.20	1.1
J1409-1.6b-A	170	180	44	12	1	10	37	74	18	88	4	1.5	0.20	0.84
J1409-1.6b-Dp	170	180	44	12	1	11	36	74	18	88	4	1.8	0.21	0.82
J1409-1.6b-Dc	1	2.5	30	37	2	0.93	120	3.5	11	260	15	0.31	0.05	2.9

Table C.3: WR trace element data continued

Sample	Sb	Cs	Ba	La	Ce	Pr	Nb	Sm	Eu	Gd	Tb	Dy	Ho	Er
J1408-5.1	0.1	1	190	9.6	18	2.7	11	2.5	0.67	2.2	0.36	2.2	0.58	1.1
J1408-8.4	0.1	0.8	320	7.6	14	2.2	9	2	0.47	1.7	0.28	1.6	0.43	0.81
J1408-9.1	0.04	0.5	220	6.2	11	1.8	7.7	1.6	0.37	1.4	0.23	1.3	0.36	0.66
J1408-10.2c	0.1	4	190	6.6	13	2.1	9.2	2.1	0.45	1.9	0.3	1.8	0.47	0.88
J1408-10.2a	0.07	2	150	5	9.8	1.5	6.6	1.5	0.31	1.3	0.21	1.2	0.32	0.6
J1408-10.2d	0.04	0.3	110	3.6	6.7	1.1	4.5	0.96	0.19	0.83	0.13	0.76	0.19	0.36
J1408-10.2b	0.09	2	290	6.9	14	2.1	9.1	2.1	0.42	1.8	0.3	1.7	0.45	0.84
J1408-12.4	0.5	3	390	8.4	16	2.5	11	2.3	0.54	2	0.31	1.8	0.47	0.87
J1408-13.6	0.04	0.3	76	1.7	2.8	0.61	2.8	0.64	0.14	0.6	0.1	0.59	0.16	0.3
J1408-14.5	0.04	0.3	85	1.8	3.4	0.62	2.8	0.62	0.15	0.58	0.09	0.56	0.15	0.28
J1408-15.2	0.04	0.9	170	4.7	9.6	1.6	7	1.6	0.32	1.3	0.21	1.2	0.3	0.55
J1408-17.7	0.04	0.4	40	1.7	3.1	0.67	3.1	0.71	0.15	0.63	0.1	0.6	0.16	0.3
J1408-20.4	0.1	1	42	3.4	5.7	1.3	5.8	1.4	0.28	1.2	0.19	1.1	0.28	0.53
J1408-12.4-A	0.5	3	380	8.4	16	2.5	11	2.3	0.55	2	0.31	1.8	0.46	0.87
J1408-12.4-Dp	0.5	3	390	8.3	16	2.5	11	2.3	0.53	2	0.31	1.8	0.47	0.87
j1408-12.4-Dc	0.3	8	2000	0.18	2.4	0.09	0.68	0.52	0.24	0.82	0.2	1.7	0.55	1.2
J1413-9.0	0.4	2	300	11	21	2.8	12	2.7	0.88	2.5	0.43	2.6	0.69	1.3
J1413-13.1	2	3	470	21	39	5.1	20	4.3	0.89	4	0.68	4.2	1.2	2.3
J1413-18.7	0.7	6	590	33	60	7.6	30	6.1	1.2	5.5	0.92	5.7	1.6	3
J1413-24.8	0.7	3	370	28	53	7.3	31	7	1.4	6.7	1.2	7.2	1.9	3.5
J1413-29.3	0.4	5	470	27	51	6.9	28	6.2	1.3	5.7	0.96	5.6	1.5	2.8
J1413-34.8	0.5	10	720	36	66	8.2	32	6.4	1.2	5.5	0.87	5.1	1.4	2.7
J1413-40.8	0.9	10	800	33	59	7.8	31	6.3	1.2	5.7	0.94	5.8	1.6	3.1
J1413-45.5	0.7	20	790	27	50	6.5	26	5.4	1.1	5.1	0.88	5.5	1.5	3
J1413-45.5-A	0.7	20	790	28	51	6.6	26	5.5	1.1	5.1	0.88	5.5	1.5	3
J1413-45.5-Dp	0.7	20	790	27	50	6.4	26	5.4	1.1	5.1	0.88	5.5	1.5	2.9
J1413-45.5-Dc	0.4	4	930	3.5	7.4	0.93	3.9	1.1	0.32	1.9	0.53	4.4	1.4	2.9
J1409-0.1	0.3	0.9	77	5.6	11	1.8	8.1	2	0.45	2	0.35	2.2	0.6	1.1
J1409-0.6	1	3	270	11	22	3.4	15	3.5	0.73	3.4	0.58	3.6	1	2
J1409-1.6b	0.4	2	360	13	25	3.9	17	3.8	0.79	3.5	0.59	3.6	0.98	1.9
J1409-1.6a	0.04	0.3	36	3.9	8.2	1.5	7.2	1.8	0.44	1.8	0.31	2	0.54	1
J1409-2.6	0.07	1	210	8.9	15	2.5	11	2.6	0.62	2.5	0.43	2.6	0.69	1.4
J1409-3.6	0.05	0.2	68	7	11	1.9	8.2	1.6	0.34	1.6	0.25	1.6	0.44	0.86
J1409-4.6	0.07	0.2	1400	3.9	6.7	1.2	5.4	1.1	0.3	1.1	0.18	1.2	0.35	0.7
J1409-6.3	0.05	0.1	200	3.6	6.4	1.1	5	1.1	0.29	1.2	0.19	1.3	0.35	0.71
J1409-7.1a	0.06	0.2	1400	5.4	9.3	1.5	6.2	1.2	0.31	1.2	0.2	1.2	0.36	0.74
J1409-7.1b	0.3	5	210	8.4	15	2.2	9	2.1	0.51	2.1	0.36	2.2	0.59	1.2
J1409-7.8	0.5	8	280	15	26	3.7	15	3.1	0.62	2.7	0.44	2.5	0.71	1.4
J1409-1.6b-A	0.4	3	360	13	25	3.9	17	3.9	0.79	3.5	0.59	3.6	1	2
J1409-1.6b-Dp	0.4	2	350	13	25	3.9	17	3.8	0.78	3.5	0.58	3.5	0.96	1.9
J1409-1.6b-Dc	0.3	8	1100	0.48	2.3	0.15	0.77	0.45	0.15	0.73	0.2	1.7	0.58	1.4

Table C.4: WR trace element data continued

Sample	Tm	Yb	Lu	Hf	Ta	W	Tl	^{206}Pb	^{207}Pb	^{208}Pb	Bi	Th	U
J1408-5.1	0.16	1	0.15	0.8	0.15	0.24	0.07	4.3	3.3	8.4	0.1	2	1.1
J1408-8.4	0.12	0.77	0.11	0.53	0.1	0.23	0.05	5.9	4.6	12	0.1	1.3	0.86
J1408-9.1	0.1	0.62	0.09	0.34	0.06	0.14	0.03	2.1	1.6	4.0	0.06	0.96	0.62
J1408-10.2c	0.13	0.81	0.12	1.1	0.21	0.4	0.18	1.2	0.75	2.0	0.1	3	1.6
J1408-10.2a	0.09	0.56	0.08	0.56	0.1	0.19	0.08	1.5	1.1	2.8	0.06	1.4	0.95
J1408-10.2d	0.06	0.37	0.05	0.13	0.03	0.05	0.02	1.1	0.76	2	0.02	0.43	0.75
J1408-10.2b	0.12	0.76	0.11	0.82	0.14	0.3	0.11	2.4	1.7	4.5	0.1	2.1	1.1
J1408-12.4	0.13	0.82	0.12	1.1	0.2	0.47	0.24	6.9	5.1	13	0.3	2.6	2.4
J1408-13.6	0.04	0.26	0.04	0.14	0.03	0.05	0.03	1.1	0.72	1.8	0.02	0.37	0.93
J1408-14.5	0.04	0.26	0.04	0.14	0.02	0.07	0.04	0.86	0.58	1.5	0.01	0.41	0.72
J1408-15.2	0.08	0.49	0.07	0.49	0.09	0.17	0.14	2.1	1.5	3.7	0.05	1.4	1.3
J1408-17.7	0.04	0.27	0.04	0.1	0.02	0.06	0.06	0.55	0.3	0.77	0.01	0.38	0.88
J1408-20.4	0.07	0.46	0.07	0.31	0.07	0.15	0.07	1.6	1.2	2.9	0.03	0.97	0.93
J1408-12.4-A	0.13	0.84	0.12	1.1	0.19	0.48	0.24	7.1	5.3	13	0.3	2.6	2.4
J1408-12.4-Dp	0.13	0.8	0.12	1	0.2	0.45	0.24	6.7	5.0	13	0.2	2.6	2.4
j1408-12.4-Dc	0.22	1.5	0.22	5.7	1.6	2.1	1.0	0.97	0.33	0.83	0.2	7.1	7.6
J1413-9.0	0.21	1.3	0.19	2.2	0.39	0.69	0.27	3.3	2.5	6.6	0.05	4.7	2.5
J1413-13.1	0.35	2.3	0.35	4.6	0.75	1.3	0.52	9.6	7.3	19	0.3	8.1	3.9
J1413-18.7	0.48	3.1	0.47	6.1	0.99	1.7	0.64	8.6	6.5	17	0.4	12	3.5
J1413-24.8	0.52	3.3	0.47	3.7	0.61	1.0	0.43	8.2	6.2	16	0.2	7.2	3.5

Continued on next page

Table C.4 – continued from previous page

Sample	Tm	Yb	Lu	Hf	Ta	W	Tl	^{206}Pb	^{207}Pb	^{208}Pb	Bi	Th	U
J1413-29.3	0.43	2.8	0.41	4.2	0.68	1.1	0.41	7.3	5.5	14	0.2	8.3	3
J1413-34.8	0.42	2.7	0.41	5.8	0.97	1.4	0.73	5.0	3.7	9.7	0.2	12	3.3
J1413-40.8	0.49	3.2	0.5	6.7	1.1	2.3	0.71	11	8.7	23	0.4	13	3.3
J1413-45.5	0.47	3.1	0.48	6.5	1.1	1.5	0.86	8.8	6.7	18	0.6	11	4.2
J1413-45.5-A	0.47	3.1	0.48	6.6	1.1	1.5	0.87	8.8	6.7	17	0.6	11	4.2
J1413-45.5-Dp	0.46	3.1	0.47	6.4	1.1	1.5	0.85	8.9	6.8	18	0.6	11	4.1
J1413-45.5-Dc	0.48	3.3	0.5	8.3	1.6	2.1	0.44	1.3	0.92	2.4	0.06	7.3	3.8
J1409-0.1	0.17	1.1	0.16	0.49	0.1	0.71	0.16	3.0	2.3	5.9	0.2	1	1.2
J1409-0.6	0.31	2.1	0.32	1.5	0.26	3.0	0.33	27	22	56	0.5	3.9	2.3
J1409-1.6b	0.3	1.9	0.29	1.6	0.29	0.95	0.31	6.0	4.8	12	0.4	4	1.6
J1409-1.6a	0.16	1	0.15	0.2	0.03	0.12	0.03	3.1	2.5	6.3	0.03	0.51	0.6
J1409-2.6	0.21	1.4	0.22	0.71	0.13	0.39	0.13	1.7	1.3	3.3	0.01	1.3	1.1
J1409-3.6	0.13	0.86	0.14	0.23	0.06	0.22	0.03	3.5	2.8	7.1	0.2	0.44	0.66
J1409-4.6	0.11	0.7	0.11	0.2	0.03	0.14	0.01	3.8	3.1	7.8	0.08	0.37	0.32
J1409-6.3	0.11	0.67	0.1	0.26	0.05	0.18	0.02	2.6	2.0	5.2	0.03	0.58	0.4
J1409-7.1a	0.11	0.76	0.12	0.2	0.03	0.13	0.02	2.7	2.1	5.3	0.03	0.5	0.48
J1409-7.1b	0.18	1.2	0.19	1.1	0.14	0.86	0.25	2.1	1.6	4.1	0.05	2.6	1.1
J1409-7.8	0.22	1.5	0.24	2	0.44	1.6	0.38	1.3	0.94	2.5	0.01	5	1.6
J1409-1.6b-A	0.3	1.9	0.29	1.6	0.29	0.96	0.32	6.0	4.8	12	0.4	4.1	1.6
J1409-1.6b-Dp	0.29	1.9	0.28	1.6	0.28	0.94	0.3	6.0	4.7	12	0.4	4	1.5
J1409-1.6b-Dc	0.27	2	0.33	4.7	1.2	2.8	0.94	0.51	0.29	0.78	0.2	4.1	3.5

Table C.5: Laser trace element data. Major elements (Na, Mg, Al, Si, P, K, Ca, Mn, and Fe) are given in wt. % X, all others in ppm. Sample names are shown as Section-Stratigraphic height-laser spot, where height is distance above the base of the formation and laser spot is defined as mineral-spot. As before, samples from section J1408 are abbreviated "08", those from J1409 "09", and those from J1413 "13". For example, sample 08-5.1 4-1 means sample was collected 5.1 m above the base of the formation, and laser analysis took place on spot 1 in thin section mineral 4. Type indicates primary mineralogy: clay (C), carbonate (B), or quartz (Q). Clay spots were mostly clay, with some fine carbonate. Carbonate spots were usually larger carbonate grains with only minor clay, and quartz grains were distinct quartz crystals. There was also one oxide (X) spot measured.

Sample	Type	Na	Mg	Al	Si	P	K	Ca	Sc	Ti	V	Cr	Mn
08-5.1 4-1	C	0.17	11.9	6.9	15.5	0.8	2.6	59.3	6.4	0.33	102	52	0.02
08-5.1 4-2	C	0.69	30.9	1.7	8.1	0.1	0.4	51.5	3.5	0.03	28	15	0.03
08-5.1 4-3	C	0.08	17.5	4.7	21.1	0.1	3.6	43.9	5.6	0.21	123	47	0.02
08-5.1 5-2	C	0.39	13.3	6.0	26.2	0.3	2.2	56.1	6.0	0.32	126	72	0.02
08-5.1 5-3	C	0.51	8.9	7.0	25.9	0.3	2.7	57.9	7.3	0.46	105	77	0.01
08-5.1 5-4	C	0.12	18.3	5.4	16.6	0.2	2	53.4	5.6	0.53	84	59	0.02
08-5.1 3-4	C	0.05	15.9	1.9	4.5	0.1	0.7	73.9	4.4	0.08	27	21	0.02
08-10.2 1-1	C	0.36	23.2	9.7	28.7	0.4	4	30.0	8.5	0.68	107	105	0.02
08-10.2 1-2	B	0.08	2.0	1.2	3.3	0.1	0.6	93.3	3.3	0.03	20	15	0.01
08-10.2 1-3	Q	0.04	0.3	0.0	99.0	0.0	0	0.0	5.4		1	6	
08-10.2 1-4	C	0.09	25.1	5.0	16.2	0.2	2.4	48.1	5.2	0.26	49	56	0.02
08-10.2 1-5	B	0.12	1.2	0.1	1.5	0.1	0.1	98.2	1.2		3	1	0.01
08-10.2 2-1	C	0.12	19.7	2.6	8.0	0.4	1.8	67.8	2.9	0.17	33	19	0.01
08-10.2 2-2	B	0.50	0.8	0.1	8.1	0.1	0.1	91.4	0.7	0.01	2	8	
08-10.2 2-3	C	0.83	0.2	15.6	63.8	0.1	15.9	2.8	2.3		2	3	
08-10.2 2-4	C	0.11	29.1	6.9	20.7	1.3	3.7	37.0	3.6	0.59	85	59	0.02
08-10.2 2-5	B	0.14	2.1	0.1	15.3	0.0	0	83.2	1.5	0.02	3	4	0.01
08-10.2 3-1	B	0.08	0.3	0.0	1.4	0.1	0	99.5	0.4		1	0	
08-10.2 3-2	B	0.07	1.1	0.6	2.5	0.1	0.5	96.2	2.2		6		0.01
08-10.2 4-1	Q	0.66	0.8	0.1	96.1	0.0	0	1.8	3.5		2		
08-10.2 4-2	B	0.10	2.0	0.2	3.8	0.0	0.2	94.6	4.0		2	5	0.01
08-10.2 4-3	B	0.14	0.5	0.0	5.4	0.1	0	95.0	4.6		1	3	0.01
08-10.2 4-4	C	0.28	30.1	1.3	7.4	0.1	0.6	55.4	4.3	0.08	34	19	0.02
08-10.2 4-5	C	0.08	1.4	27.4	47.5	0.1	1.6	21.5	4.1	0.09	78	57	
08-10.2 4-6	C	0.67	20.4	1.9	9.4	0.1	0.6	66.4	4.5	0.32	20	19	0.02
09-1.6 1-1	Q	0.04	0.2	0.0	99.1	0.0		0.0	3.4		1	1	
09-1.6 1-2	B	0.16	37.7	0.1	1.3	0.1	0	62.1	1.2		1	6	
09-1.6 1-3	C	0.11	36.2	1.2	3.7	0.1	0.5	57.6	6.1	0.02	11	10	0.11
09-1.6 2-1	B	0.06	40.9	0.0	1.4	0.1	0	58.9	0.5		0	1	0.07
09-1.6 2-2	B	0.21	44.4	0.1	1.4	0.0	0	55.5	0.3		0	2	

Continued on next page

Table C.5 – continued from previous page

Sample	Type	Na	Mg	Al	Si	P	K	Ca	Sc	Ti	V	Cr	Mn
09-1.6 2-3	C	0.48	35.6	2.6	19.8	0.1	2.2	38.9	5.7	0.17	22	42	0.1
09-1.6 3-1	Q	0.03	0.1	0.0	99.0	0.0	0	0.1	4.2		2		
09-1.6 3-2	B	0.10	41.7	0.0	1.8	0.1	0.1	57.5	3.8		0		0.13
09-1.6 3-3	C	0.46	42.8	0.0	1.9	0.1	0	55.6	4.9		12	4	0.11
09-1.6 4-1	Q?	0.15	9.2	0.1	77.4	0.0	0.1	12.6	5.1		0	3	0.02
09-1.6 4-2	C	0.34	36.7	1.8	11.4	0.2	1.3	47.2	5.7	0.06	32	23	0.09
09-1.6 4-3	C	0.13	29.8	4.1	20.8	0.1	1.8	42.1	8.8	0.16	41	22	0.09
09-1.6 4-4	X	0.54	10.0	1.8	43.7	0.3	1	13.0	4.2	2.41	245	19	0.03
09-1.6 5-1	C	0.11	26.8	7.7	28.3	0.1	3.2	32.4	14	0.53	75	46	0.06
09-1.6 5-2	C	0.12	24.0	4.5	34.5	0.3	2.8	32.1	11	0.43	97	54	0.08
09-1.6 5-3	C	0.34	14.4	12.4	50.0	0.0	2.1	18.4	8.2	0.10	119	19	0.06
09-1.6 6-1	B	0.06	39.0	0.6	12.3	0.1	0.1	47.9	4.9		8	3	0.07
09-1.6 6-2	B	0.50	38.3	0.8	5.0	0.0	0.4	54.3	8.6	0.03	15	7	0.11
13-24.8 2-1	Q	0.04	0.0	0.1	98.5	0.0	0	0.6	3.7	0.04	2	3	
13-24.8 2-2redo	Q	0.15	0.0	0.2	96.4	0.0	0.2	2.4	3.8		1	18	
13-24.8 2-3	Q	0.41	0.0	0.0	97.8	0.0	0	0.7	3.8	0.01	1	6	
13-24.8 2-4	C	2.46	7.3	12.8	42.2	0.1	3.3	17.0	19	1.23	136	128	
13-24.8 3-1	Q	0.44	0.0	0.1	98.3	0.1	0	0.4	5.8		2	6	
13-24.8 4-1	C	0.05	0.0	0.0	99.1	0.0	0	0.2	3.5	0.01	1	4	
13-24.8 6-1	Q	0.11	0.6	2.4	82.7		1	9.7	14	0.04	32	41	
13-24.8 6-2	C	0.75	22.9	2.2	6.1	0.1	1.7	49.7	5.1	0.07	24	12	0.01
13-24.8 6-3	C	0.09	17.1	2.4	11.0	0.1	0.1	43.5	9.6	0.04	91	30	0.01

Table C.6: LA data continued

Sample	Fe	Rb	Sr	Zr	Mo	Ba	La	Ce	Eu	Ho	Lu	U	Oxide sum
08-5.1 4-1	3.5	65	972	89.7	0.11	607	17.0	35	1.53	0.78	0.28	4.92	100.6
08-5.1 4-2	7.8	24	465	15.5	0.27	101	6.9	15	0.96	0.28	0.03	1.21	101.2
08-5.1 4-3	4.6	49	693	44.4	0.32	418	12.5	24	0.77	0.5	0.19	4.54	95.5
08-5.1 5-2	4.0	56	754	60.5	0.14	518	10.2	23	1.23	0.54	0.16	3.23	108.6
08-5.1 5-3	2.9	72	1040	248	0.19	583	15.4	32	1.79	1.16	0.45	9.97	106.1
08-5.1 5-4	5.2	52	678	68.1	0.23	492	9.8	20	1.02	0.48	0.21	4.3	101.3
08-5.1 3-4	4.3	23	1150	720	0.17	171	12.9	27	1.14	0.52	0.27	1.06	101.2
08-10.2 1-1	3.5	110	463	130	1.27	485	4.0	12	0.67	0.52	0.16	5.99	99.9
08-10.2 1-2	0.8	17	1530	6.1	0.22	82	16.5	35	0.86	0.61	0.23	1.01	101.3
08-10.2 1-3	0.0	0	0	0.2	0.16	1	0.1	0					99.5
08-10.2 1-4	3.7	68	747	41.8	0.34	288	6.8	19	0.61	0.42	0.14	2.33	100.7
08-10.2 1-5	0.2	0	4520	0.5		19	6.9	17	0.32	0.26	0.07	0.33	101.4
08-10.2 2-1	0.8	49	1400	53.6	6.16	156	6.2	16	0.59	0.38	0.16	3.64	101.1
08-10.2 2-2	0.4	3	1680	0.6	0.48	25	3.6	7	0.16	0.06	0.03	0.12	101.2
08-10.2 2-3	0.2	320	124	0.3	0.11	358	0.4	1	0.00	0.01	0.01	0.09	99.4
08-10.2 2-4	1.6	92	650	76.6	0.33	534	3.0	9	0.49	0.29	0.11	4.2	100.4
08-10.2 2-5	0.2	4	2420	2.1	0.07	105	5.5	10	0.33	0.17	0.07	0.6	101.1
08-10.2 3-1	0.1	0	1850	0.1		7	3.3	5	0.02	0.01	0.00	0.09	101.4
08-10.2 3-2	0.3	19	2560	3.1	5.59	108	5.3	10	0.53	0.52	0.21	0.75	101.4
08-10.2 4-1	0.1	0	31			8	0.0	1					99.5
08-10.2 4-2	0.4	3	1940	1.2		62	3.6	8	0.24	1.03	0.23	0.19	101.3
08-10.2 4-3	0.2	1	4480	2.7		13	11.5	30	1.92	1.57	0.49	0.18	101.3
08-10.2 4-4	6.1	15	972	18.9	0.11	90	6.3	19	0.98	0.36	0.05	1.03	101.2
08-10.2 4-5	0.4	45	316	12.9	0.06	153	3.6	6	0.08	0.1	0.01	0.32	100.0
08-10.2 4-6	1.5	16	1300	58.4	0.08	89	7.4	15	0.47	0.55	0.19	1.57	100.9
09-1.6 1-1	0.0	0	1	0	0.17	0	0.1	0			0.01		99.5
09-1.6 1-2	0.1	4	391	0.5	0.13	22	5.7	11	0.55	0.5	0.23	2.34	101.6
09-1.6 1-3	2.0	9	213	23.7	0.03	63	4.9	11	1.01	1	0.39	0.71	101.5
09-1.6 2-1	0.1	0	112	0.6	0.83	7	4.7	9	0.51	0.36	0.19	0.25	101.6
09-1.6 2-2	0.1	0	226	0.5	0.35	11	0.7	2	0.10	0.06	0.01	0.4	101.6
09-1.6 2-3	1.1	51	130	42.7		264	4.9	23	0.66	1.1	0.35	3.94	100.9
09-1.6 3-1	0.1	0	2	3.9		2	0.0	0			0.00	1.58	99.5
09-1.6 3-2	0.1	0	179	0.3		3	8.0	20	0.89	0.84	0.34	0.05	101.6
09-1.6 3-3	0.7	0	189	1.1		11	7.2	16	1.53	0.88	0.32	0.23	101.6
09-1.6 4-1	0.4	1	48	0.5	0.79	47	1.2	4	0.16	0.16	0.04		99.9
09-1.6 4-2	2.0	29	137	24.5		129	8.0	16	1.38	1.31	0.40	3.5	101.2
09-1.6 4-3	1.9	48	163	83.8	0.39	248	5.4	14	1.20	1.35	0.48	2.13	100.8
09-1.6 4-4	27.0	15	49	44.4	13.9	119	5.9	18	0.90	0.94	0.50	2.46	97.4
09-1.6 5-1	1.6	94	106	78.8	0.33	422	3.6	9	0.70	1	0.40	120	100.2
09-1.6 5-2	1.9	54	120	62.5		332	5.8	18	1.77	1.14	0.32	1.53	100.3

Continued on next page

Table C.6 – continued from previous page

Sample	Mn	Fe	Rb	Sr	Zr	Mo	Ba	La	Ce	Eu	Ho	Lu	U
09-1.6 5-3	2.4	65	69	44	0.89	264	1.9	6	0.52	0.62	0.22	0.89	100.1
09-1.6 6-1	1.2	3	137	2.4		29	4.0	8	0.49	0.65	0.17	0.39	101.3
09-1.6 6-2	2.0	10	202	7.1	1.39	95	4.9	13	1.09	1.25	0.30	0.5	101.4
13-24.8 2-1	0.1	1	9	0.3	0.36	6	0.2	1	0.02	0.01		0.37	99.4
13-24.8 2-2redo	0.1	10	3	0.6		3		2		0.01		0.07	99.5
13-24.8 2-3	0.4	1	17	0.3		3	0.1	1				0.15	99.5
13-24.8 2-4	13.5	110	104	127	3.29	495	28.4	75	1.27	1.03	0.44	6.25	98.7
13-24.8 3-1	0.1	2	1	0.2	0.19	2	0.1	0			0.01	0.09	99.5
13-24.8 4-1	0.0	1	1	0.1		3	0.5	0	0.01			0.02	99.5
13-24.8 6-1	3.2	33	59	13.9	2.03	108	9.8	8	1.18	0.08	0.29	1.18	99.6
13-24.8 6-2	17.3	25	210	47.3	2.46	79	52.5	92	2.26	0.65	0.23	4.87	100.9
13-24.8 6-3	26.4	10	161	85.3	4.20	33	47.7	101	2.66	1.24	0.54	6.94	100.7

Table C.7: Nitrogen and C stable isotope analyses, performed at the University of Washington Isolab. As before, samples from section J1408 are abbreviated "08", those from J1409 "09", and those from J1413 "13". MR is the McRae shale, a UW internal standard. Sample mass is decarbonated sample powder mass analyzed. N (mg) and C (mg) are mass of each element analyzed by the mass spec, obtained by peak area integration, while TN and TC (ppm) are concentration of each element in decarbonated powder. Isotope values are also given along with atomic C/N ratio. Insoluble is the fraction of sample left after decarbonation, thus whole rock N (WR N) and whole rock C (WR C) are concentrations corrected for dissolved fraction in ppm. N- and C- peak areas from mass spectrometer analysis are given, along with blank area and N-peak/blank ratio. As these ratios are mostly above 10, the contribution of the blank to sample signal is minimal. Ages are given, and are based on relative stratigraphic position.

Sample	Samp. mass (mg)	N (mg)	TN (ppm)	δ^{15}N	C (mg)	C (ppm)	δ^{13}C	at. C/N
13-13.1	61.407	0.0403	656	2.93	0.0351	572	-19.87	1.02
13-13.1	79.711	0.0533	669	2.72	0.0462	579	-19.6	1.01
13-29.3	55.052	0.0268	487	2.51	0.0753	1368	-16.74	3.28
13-29.3	79.981	0.0355	444	1.69	0.1084	1355	-16.6	3.56
13-29.3	108.979	0.0483	444	1.72	0.1479	1357	-16.56	3.57
08-5.1	56.254	0.0248	440	1.2	0.0182	323	-22.16	0.86
13-45.5	47.394	0.0212	447	1.2	0.0352	744	-17.71	1.94
09-7.8	52.502	0.0165	315	4.59	0.0056	107	-26.79	0.4
09-0.6	55.757	0.0156	279	3.46	0.0065	117	-18.37	0.49
13-34.8	86.18	0.0374	434	1.49	0.0577	670	-19.26	1.8
09-2.6	54.296	0.0129	237	2.8	0.0101	185	-24.67	0.91
13-24.8	59.155	0.0299	505	1.86	0.1078	1822	-16.26	4.2
09-6.3	81.483	0.0044	54	2.31	0.0318	390	-5.64	8.39
13-18.7	52.808	0.0290	549	2.24	0.0119	224	-22.22	0.48
09-1.6b	64.344	0.0161	250	4.25	0.0060	93	-21.47	0.43
09-0.1	57.559	0.0209	363	4.03	0.0221	384	-26.18	1.23
13-40.8	71.404	0.0326	456	1.99	0.0145	202	-22.59	0.52
09-1.6a	93.399	0.0067	72	3	0.0226	242	-15.56	3.93
13-9.0	64.816	0.0376	580	3.02	0.0441	680	-16.77	1.37
08-10.2c	77.462	0.0329	425	2.12	0.0148	191	-23.75	0.53
08-9.1	59.487	0.0142	239	2.03	0.0135	226	-23.25	1.1
08-10.2d	45.11	0.0156	345	2.57	0.0376	833	-26.01	2.81
08-15.2	60.112	0.0252	419	2.58	0.0670	1115	-27.1	3.1
08-8.4	75.27	0.0300	398	2.08	0.0200	266	-25.06	0.78
09-4.6	77.848	0.0043	55	3.77	0.0385	495	-18.6	10.4
09-7.1a	46.852	0.0059	126	4.4	0.0336	716	-17.75	6.62
08-14.5	28.031	0.0095	340	2.94	0.0250	892	-22.12	3.06
08-10.2b	61.417	0.0197	320	3.15	0.0157	255	-25.32	0.93
08-20.4	53.253	0.0235	441	2.29	0.0355	667	-22.93	1.76
08-17.7	36.791	0.0165	448	2.64	0.0397	1080	-22.36	2.81
09-7.1b	73.219	0.0175	239	5.82	0.0221	302	-21.38	1.47
08-13.6	43.725	0.0169	386	3.12	0.0377	861	-22.52	2.6
09-3.6	85.873	0.0061	72	3.33	0.0277	323	-8.52	5.27
08-10.2a	65.718	0.0250	381	2.61	0.0137	209	-23.76	0.64
08-12.4	70.497	0.0242	343	2.28	0.0098	139	-24.33	0.47
09-7.8	68.031	0.0226	332	5.16	0.0639	741	-17.23	1.93

Continued on next page

Table C.7 – continued from previous page

Sample	Samp. mass (mg)	N (mg)	TN (ppm)	δ^{15}N	C (mg)	C (ppm)	δ^{13}C	at. C/N
13-45.5	86.203	0.0387	449	1.54	0.0639	741	-17.23	1.93
08-12.4	67.648	0.0247	365	2.15	0.0106	157	-25.03	0.5
08-5.1	68.82	0.0319	463	1.51	0.0240	349	-22.47	0.88
13-18.7	78.293	0.0437	559	2.54	0.0166	212	-21.66	0.44
08-20.4	60.339	0.0271	449	2.33	0.0414	686	-23.36	1.78
13-40.8	62.29	0.0285	458	1.64	0.0116	186	-20.69	0.47
09-7.1b	59.021	0.0263	446	5.47	0.0331	560	-21.8	1.47
09-3.6	84.779	0.0062	73	3.43	0.0265	313	-9.91	4.97
08-10.2b	62.374	0.0196	315	3.01	0.0156	251	-25.88	0.93
13-9.0	72.507	0.0405	558	2.75	0.0477	658	-17	1.38
08-9.1	54.236	0.0134	247	2.73	0.0127	233	-22.89	1.1
08-10.2c	73.981	0.0282	381	1.67	0.0131	177	-23.96	0.54
09-6.3	81.869	0.0044	54	2.87	0.0304	372	-5.32	8.01
09-0.1	64.265	0.0239	372	4.21	0.0245	382	-25.48	1.2
08-8.4	73.726	0.0294	398	2.1	0.0204	276	-25.27	0.81
09-7.8	79.236	0.0266	335	5.36	0.0081	102	-25.03	0.35
08-12.4	81.945	0.0291	356	2.13	0.0133	163	-25.2	0.53
08-5.1	90.53	0.0415	459	1.55	0.0311	343	-22.4	0.87
09-7.1b	73.2	0.0327	447	5.61	0.0415	567	-22.1	1.48
13-9.0	102.525	0.0562	548	2.62	0.0672	656	-17.1	1.4
13-34.8	100.894	0.0409	405	1.69	0.0644	638	-18.52	1.84
13-18.7	98.71	0.0496	503	2.22	0.0189	192	-20.99	0.44
13-24.8	95.238	0.0443	465	2.01	0.1714	1799	-16.18	4.51
09-1.6b	96.55	0.0244	253	4.6	0.0087	90	-21.21	0.42
09-1.6a	107.918	0.0084	78	3.74	0.0257	238	-15.83	3.56
09-0.6	90.488	0.0229	253	3.58	0.0083	92	-21.05	0.42
MR	10.783	0.0119	1100	5.55	0.8245	76464	-37.77	81.09
MR	10.313	0.0117	1132	5.51	0.7876	76365	-37.72	78.69
MR	11.063	0.0124	1124	5.56	0.8428	76183	-37.67	79.08
MR	11.838	0.0136	1153	5.57	0.9037	76341	-37.7	77.25
MR	10.672	0.0122	1139	5.19	0.8179	76637	-37.76	78.49

Table C.8: N and C analyses continued

Sample	Insoluble	WR N	WR C	N-peak	C-peak	N-blank	Peak/blank	Age
13-13.1	0.566	371	324	144.93	26.30	3.77	38.48	646.71
13-13.1	0.566	379	328	197.74	34.95	2.79	70.87	646.71
13-29.3	0.472	230	646	96.48	56.43	3.77	25.62	645.85
13-29.3	0.472	210	640	130.83	81.57	3.34	39.2	645.85
13-29.3	0.472	210	641	177.83	111.42	3.30	53.84	645.85
08-5.1	0.105	46	34	89.01	13.62	3.77	23.63	640
13-45.5	0.659	295	490	76.14	26.41	3.77	20.22	645
09-7.8	0.219	69	23	59.38	4.21	3.77	15.77	633.9
09-0.6	0.201	56	24	56.00	4.87	3.77	14.87	634.9
13-34.8	0.595	258	398	134.35	43.25	3.77	35.67	645.57
09-2.6	0.122	29	22	46.33	7.54	3.77	12.3	634.6
13-24.8	0.445	225	811	107.52	80.74	3.77	28.55	646.18
09-6.3	0.067	4	26	15.91	23.84	3.77	4.22	634.3
13-18.7	0.668	367	150	104.25	8.88	3.77	27.68	646.42
09-1.6b	0.264	66	25	57.95	4.47	3.77	15.39	634.8
09-0.1	0.052	19	20	75.08	16.56	3.77	19.94	635
13-40.8	0.655	299	132	117.08	10.83	3.77	31.09	645.29
09-1.6a	0.102	7	25	24.14	16.96	3.77	6.41	634.7
13-9.0	0.312	181	212	135.28	33.03	3.77	35.92	647
08-10.2c	0.129	55	25	121.17	11.11	3.80	31.93	639.5
08-9.1	0.045	11	10	52.33	10.08	3.80	13.79	639.67
08-10.2d	0.044	15	37	57.32	28.14	3.80	15.1	639.17
08-15.2	0.061	26	68	92.74	50.22	3.80	24.44	638.33
08-8.4	0.084	33	22	110.32	14.99	3.80	29.07	639.83
09-4.6	0.043	2	21	15.89	28.84	3.80	4.19	634.4
09-7.1a	0.048	6	35	21.76	25.15	3.80	5.73	634.2
08-14.5	0.050	17	45	35.07	18.74	3.80	9.24	638.5
08-10.2b	0.049	16	12	72.33	11.74	3.80	19.06	639
08-20.4	0.045	20	30	86.40	26.60	3.80	22.77	638
08-17.7	0.019	8	20	60.71	29.76	3.80	16	638.17
09-7.1b	0.137	33	41	64.40	16.57	3.80	16.97	634.1

Continued on next page

Table C.8 – continued from previous page

Sample	Insoluble	WR N	WR C	N-peak	C-peak	N-blank	Peak/blank	Age (Ma)
08-13.6	0.060	23	52	62.08	28.21	3.80	16.36	638.67
09-3.6	0.085	6	27	22.60	20.79	3.80	5.96	634.5
08-10.2a	0.066	25	14	92.02	10.28	3.80	24.25	639.33
08-12.4	0.094	32	13	88.94	7.32	3.80	23.44	638.83
09-7.8	0.219	73	163	83.39	6.15	3.34	24.98	633.9
13-45.5	0.659	296	488	142.71	48.07	3.34	42.76	645
08-12.4	0.094	34	15	91.01	7.98	3.34	27.27	638.83
08-5.1	0.105	48	37	117.60	18.06	3.34	35.24	640
13-18.7	0.668	373	142	161.27	12.49	3.34	48.32	646.42
08-20.4	0.045	20	31	99.84	31.17	3.34	29.91	638
13-40.8	0.655	300	122	105.08	8.71	3.34	31.48	645.29
09-7.1b	0.137	61	76	97.06	24.89	3.34	29.08	634.1
09-3.6	0.085	6	26	22.96	19.96	3.34	6.88	634.5
08-10.2b	0.049	15	12	72.39	11.78	3.34	21.69	639
13-9.0	0.312	174	205	149.15	35.90	3.34	44.69	647
08-9.1	0.045	11	11	49.49	9.53	3.34	14.83	639.67
08-10.2c	0.129	49	23	103.82	9.87	3.34	31.11	639.5
09-6.3	0.067	4	25	16.33	22.90	3.34	4.89	634.3
09-0.1	0.052	19	20	88.24	18.46	3.34	26.44	635
08-8.4	0.084	33	23	108.03	15.34	3.30	32.7	639.83
09-7.8	0.219	73	22	97.75	6.07	3.30	29.59	633.9
08-12.4	0.094	34	15	107.20	10.04	3.30	32.45	638.83
08-5.1	0.105	48	36	152.80	23.43	3.30	46.26	640
09-7.1b	0.137	61	77	120.25	31.27	3.30	36.4	634.1
13-9.0	0.312	171	205	206.61	50.67	3.30	62.55	647
13-34.8	0.595	241	379	150.29	48.50	3.30	45.5	645.57
13-18.7	0.668	336	128	182.57	14.25	3.30	55.27	646.42
13-24.8	0.445	207	801	162.89	129.13	3.30	49.31	646.18
09-1.6b	0.264	67	24	90.41	6.59	2.79	32.4	634.8
09-1.6a	0.102	8	24	31.17	19.43	2.79	11.17	634.7
09-0.6	0.201	51	19	84.87	6.28	2.79	30.41	634.9
MR		1100	7.64×10^4	42.65	617.68	3.77	11.32	
MR		1132	7.64×10^4	42.95	590.01	3.80	11.32	
MR		1124	7.62×10^4	45.84	634.36	3.34	13.73	
MR		1153	7.63×10^4	50.21	681.03	3.30	15.2	
MR		1139	7.66×10^4	45.07	619.13	2.79	16.15	

Bibliography

Abbot, D. S., Voigt, A., & Koll, D. (2011). The Jormungand global climate state and implications for Neoproterozoic glaciations. *Journal of Geophysical Research: Atmospheres*, 116(D18).

Ader, M., Thomazo, C., Sansjofre, P., Busigny, V., Papineau, D., Laffont, R., Cartigny, P., & Halverson, G. P. (2016). Interpretation of the nitrogen isotopic composition of precambrian sedimentary rocks: Assumptions and perspectives. *Chemical Geology*, 429, 93–110.

Adler, J. F. & Williams, Q. (2005). A high-pressure X-ray diffraction study of iron nitrides: Implications for Earth's core. *Journal of Geophysical Research*, 110, 1–11.

Ahadnejad, V., Hirt, A. M., Valizadeh, M.-V., & Bokani, S. J. (2011). The ammonium content in the Malayer igneous and metamorphic rocks (Sanandaj-Sirjan Zone, Western Iran). *Geologica Carpathica*, 62(2), 171–180.

Algeo, T. J. & Tribovillard, N. (2009). Environmental analysis of paleoceanographic systems based on molybdenum–uranium covariation. *Chemical Geology*, 268(3), 211–225.

Arevalo, R., McDonough, W. F., & Luong, M. (2009). The K/U ratio of the silicate Earth: Insights into mantle composition, structure and thermal evolution. *Earth and Planetary Science Letters*, 278(3), 361–369.

Arevalo, R., McDonough, W. F., Stracke, A., Willbold, M., Ireland, T. J., & Walker, R. J. (2013). Simplified mantle architecture and distribution of radiogenic power. *Geochemistry, Geophysics, Geosystems*, 14(7), 2265–2285.

Barry, P. & Hilton, D. (2016). Release of subducted sedimentary nitrogen throughout Earth's mantle. *Geochemical Perspectives Letters*, 2, 148–159.

Barry, P., Hilton, D., Halldórsson, S., Hahm, D., & Marti, K. (2012). High precision nitrogen isotope measurements in oceanic basalts using a static triple collection noble gas mass spectrometer. *Geochemistry Geophysics Geosystems*, 13(1), 1–16.

Baur, W. & Wlotzka, F. (1969). *Handbook of Geochemistry*. Springer-Verlag.

Beaumont, V. & Robert, F. (1999). Nitrogen isotope ratios of kerogens in Precambrian cherts: a record of the evolution of atmosphere chemistry? *Precambrian Research*, 96(1), 63–82.

Bebout, G., Agard, P., Kobayashi, K., Moriguti, T., & Nakamura, E. (2013). Devolatilization history and trace element mobility in deeply subducted sedimentary rocks: Evidence from Western Alps HP/UHP suites. *Chemical Geology*, 342, 1–20.

Bebout, G., Cooper, D., Bradley, A. D., & Sadofsky, S. J. (1999a). Nitrogen-isotope record of fluid-rock interactions in the Skiddaw Auerole and granite, English Lake District. *American Mineralogist*, 84, 1495–1505.

Bebout, G. & Fogel, M. (1992). Nitrogen-isotope compositions of metasedimentary rocks in the Catalina Schist, California: implications for metamorphic devolatilization history. *Geochimica et Cosmochimica Acta*, 56(7), 2839–2849.

Bebout, G., Ryan, J., Leeman, W., & Bebout, A. (1999b). Fractionation of trace elements by subduction-zone metamorphism—effect of convergent-margin thermal evolution. *Earth and Planetary Science Letters*, 171(1), 63–81.

Bebout, G. E. (1997). Nitrogen isotope tracers of high-temperature fluid-rock interactions: Case study of the Catalina Schist, California. *Earth and planetary science letters*, 151(1), 77–90.

Berner, R. A. (1991). A model for atmospheric CO_2 over Phanerozoic time. *American Journal of Science*, 291, 339–376.

Berner, R. A. (1998). The carbon cycle and CO_2 over Phanerozoic time: the role of land plants. *Philosophical Transactions of the Royal Society of London. Series A, Mathematical and Physical Sciences*, 353(1365), 75–82.

Berner, R. A. (2006). Geological nitrogen cycle and atmospheric N_2 over phanerozoic time. *Geology*, 34(5), 413–415.

Bogard, D., Clark, R., Keith, J., & Reynolds, M. (1971). Noble gases and radionuclides in Lost City and other recently fallen meteorites. *Journal of Geophysical Research*, 76(17), 4076–4083.

Boyd, S. (2001). Nitrogen in future biosphere studies. *Chemical Geology*, 176(1), 1–30.

Boyd, S., Hall, A., & Pillinger, C. (1993). The measurement of δ^{15}N in crustal rocks by static vacuum mass spectrometry: Application to the origin of the ammonium in the Cornubian batholith, southwest England. *Geochimica et Cosmochimica Acta*, 57(6), 1339–1347.

Boyd, S. & Philippot, P. (1998). Precambrian ammonium biogeochemistry: a study of the Moine metasediments, Scotland. *Chemical Geology*, 144(3-4), 257–268.

Branner, J. C. (1897). Bacteria and the Decomposition of Rocks. *American Journal of Science*, 18, 438–442.

Bräuer, K. & Hahne, J. (2005). Methodical aspects of the ^{15}N-analysis of Precambrian and Paleozoic sediments rich in organic matter. *Chemical Geology*, 218, 361–368.

Bräuer, K., Kämpf, H., Niedermann, S., Strauch, G., & Weise, S. M. (2004). Evidence for a nitrogen flux directly derived from the European subcontinental mantle in the Western Eger Rift, central Europe. *Geochimica et cosmochimica acta*, 68(23), 4935–4947.

Breneman, A. (1889). The Fixation of Atmospheric Nitrogen. (Concluded from Issue 1). *Journal of the American Chemical Society*, 11(2), 31–48.

Bristow, L. A., Dalsgaard, T., Tiano, L., Mills, D. B., Bertagnolli, A. D., Wright, J. J., Hallam, S. J., Ulloa, O., Canfield, D. E., Revsbech, N. P., et al. (2016). Ammonium and nitrite oxidation at nanomolar oxygen concentrations in oxygen minimum zone waters. *Proceedings of the National Academy of Sciences*, 113(38), 10601–10606.

Brown, J., Colling, A., Park, D., Phillips, J., Rothery, D., & Wright, J. (1989). *Ocean chemistry and deep-sea sediments*, volume 5 of *Open University*. Butterworth-Heinemann.

Burgess, R., Cartigny, P., Harrison, D., Hobson, E., & Harris, J. (2009). Volatile composition of microinclusions in diamonds from the Panda kimberlite, Canada: implications for chemical and isotopic heterogeneity in the mantle. *Geochimica et Cosmochimica Acta*, 73(6), 1779–1794.

Busigny, V., Ader, M., & Cartigny, P. (2005a). Quantification and isotopic analysis of nitrogen in rocks at the ppm level using sealed tube combustion technique: A prelude to the study of altered oceanic crust. *Chemical geology*, 223(4), 249–258.

Busigny, V., Cartigny, P., & Philippot, P. (2011). Nitrogen isotopes in ophiolitic metagabbros: A re-evaluation of modern nitrogen fluxes in subduction zones and implication for the early earth atmosphere. *Geochimica et Cosmochimica Acta*, 75, 7502–7521.

Busigny, V., Cartigny, P., Philippot, P., Ader, M., & Javoy, M. (2003). Massive recycling of nitrogen and other fluid-mobile elements (K, Rb, Cs, H) in a cold slab environment: evidence from HP to UHP oceanic metasediments of the Schistes Lustrés nappe (western Alps, Europe). *Earth and Planetary Science Letters*, 215(1), 27–42.

Busigny, V., Laverne, C., & Bonifacie, M. (2005b). Nitrogen content and isotopic composition of oceanic crust at a superfast spreading ridge: A profile in altered basalts from ODP Site 1256, Leg 206. *Geochemistry, Geophysics, Geosystems*, 6(12), 1–16.

Busigny, V., Lebeau, O., Ader, M., Krapež, B., & Bekker, A. (2013). Nitrogen cycle in the late archean ferruginous ocean. *Chemical Geology*, 362, 115–130.

Byrne, B. & Goldblatt, C. (2014). Radiative forcings for 28 potential Archean greenhouse gases. *Climate of the Past*, 10, 1779–1801.

Campbell, A. J., Waddington, E. D., & Warren, S. G. (2011). Refugium for surface life on snowball earth in a nearly-enclosed sea? a first simple model for sea-glacier invasion. *Geophysical Research Letters*, 38(19).

Canfield, D. E. (2005). The early history of atmospheric oxygen: homage to Robert M. Garrels. *Annual Review of Earth and Planetary Sciences*, 33, 1–36.

Canfield, D. E., Glazer, A. N., & Falkowski, P. G. (2010). The evolution and future of Earth's nitrogen cycle. *Science*, 330(6001), 192–196.

Cartigny, P. (2005). Stable isotopes and the origin of diamond. *Elements*, 1(2), 79–84.

Cartigny, P., Boyd, S., Harris, J., & Javoy, M. (1997). Nitrogen isotopes in peridotitic diamonds from Fuxian, China: the mantle signature. *Terra Nova*, 9(4), 175–179.

Cartigny, P., Harris, J., & Javoy, M. (2001). Diamond genesis, mantle fractionations and mantle nitrogen content: a study of δ^{13}C–N concentrations in diamonds. *Earth and Planetary Science Letters*, 185(1), 85–98.

Catling, D. C. & Claire, M. W. (2005). How Earth's atmosphere evolved to an oxic state: a status report. *Earth and Planetary Science Letters*, 237(1), 1–20.

Chassefière, E., Wieler, R., Marty, B., & Leblanc, F. (2012). The evolution of Venus: Present state of knowledge and future exploration. *Planetary and Space Science*, 63, 15–23.

Chicarelli, M. I., Hayes, J., Popp, B. N., Eckardt, C. B., & Maxwell, J. R. (1993). Carbon and nitrogen isotopic compositions of alkyl porphyrins from the triassic serpiano oil shale. *Geochimica et cosmochimica acta*, 57(6), 1307–1311.

Clauer, N. & Kröner, A. (1979). Strontium and argon isotopic homogenization of pelitic sediments during low-grade regional metamorphism: the Pan-African upper Damara sequence of northern Namibia (South West Africa). *Earth and planetary science letters*, 43(1), 117–131.

Cooper, D. & Bradley, A. (1990). The ammonium content of granites in the English Lake District. *Geological Magazine*, 127(06), 579–586.

Corsetti, F. A., Olcott, A. N., & Bakermans, C. (2006). The biotic response to neoproterozoic snowball earth. *Palaeogeography, Palaeoclimatology, Palaeoecology*, 232(2), 114–130.

Crabb, J. & Anders, E. (1981). Noble gases in E-chondrites. *Geochimica et Cosmochimica Acta*, 45, 2443–2464.

Cremonese, L., Shields-Zhou, G., Struck, U., Ling, H.-F., Och, L., Chen, X., & Li, D. (2013). Marine biogeochemical cycling during the early Cambrian constrained by a nitrogen and organic carbon isotope study of the Xiaotan section, South China. *Precambrian Research*, 225, 148–165.

Crowe, S. A., Canfield, D. E., Mucci, A., Sundby, B., & Maranger, R. (2012). Anammox, denitrification and fixed-nitrogen removal in sediments from the lower st. lawrence estuary. *Biogeosciences*, 9(11), 4309–4321.

Cruz, M. D. R. (2011). NH_4-bearing micas in poly-metamorphic Alpujárride micas-chists and gneisses from the central zone of the Betic Cordillera (Spain): tectono-metamorphic and crystal-chemical constraints. *Mineralogy and Petrology*, 101(3-4), 225–244.

Dauphas, N. & Marty, B. (1999). Heavy nitrogen in carbonatites of the Kola Peninsula: A possible signature of the deep mantle. *Science*, 286(5449), 2488–2490.

Davies, T. & Gorsline, D. (1976). Oceanic sediments and sedimentary processes. *Chemical Oceanography*, 5(1), 80.

De Moor, J., Fischer, T., Sharp, Z., Hilton, D., Barry, P., Mangasini, F., & Ramirez, C. (2013). Gas chemistry and nitrogen isotope compositions of cold mantle gases from Rungwe Volcanic Province, southern Tanzania. *Chemical Geology*, 339, 30–42.

Delwiche, C. C. (1970). The nitrogen cycle. *Scientific American*, 223, 136–146.

Dixon, J. C., Campbell, S. W., & Durham, B. (2012). Geologic nitrogen and climate change in the geochemical budget of Kärkevagge, Swedish Lapland. *Geomorphology*, 167–168, 70–76.

Dobbin, L. (1935). Daniel Rutherford's Inaugural Dissertation. *Journal of Chemical Education*, 12(8), 370–375.

Drits, V. A., Lindgreen, H., & Salyn, A. L. (1997). Determination of the content and distribution of fixed ammonium in illite-smectite by x-ray diffraction: Application to north sea illite-smectite. *American Mineralogist*, 82(1), 79–87.

Duit, W., Jansen, J. B. H., van Breemen, A., & Bos, A. (1986). Ammonium micas in metamorphic rocks as exemplified by Dome de l'Agout (France). *American Journal of Science*, 286(9), 702–732.

Dymond, J., Suess, E., & Lyle, M. (1992). Barium in deep-sea sediment: A geochemical proxy for paleoproductivity. *Paleoceanography*, 7(2), 163–181.

Ekpo, B., Ibok, U., Essien, N., & Wehner, H. (2012). Geochemistry and organic petrography of cretaceous sediments of the calabar flank, southeastern, nigeria. *Marine and Petroleum Geology*, 35(1), 252–268.

Elkins, L., Fischer, T., Hilton, D., Sharp, Z., McKnight, S., & Walker, J. (2006). Tracing nitrogen in volcanic and geothermal volatiles from the Nicaraguan volcanic front. *Geochimica et Cosmochimica Acta*, 70(20), 5215–5235.

Erisman, J. W., Sutton, M. A., Galloway, J., Klimont, Z., & Winiwarter, W. (2008). How a century of ammonia synthesis changed the world. *Nature Geoscience*, 1(10), 636–639.

Evrard, V., Glud, R. N., & Cook, P. L. (2013). The kinetics of denitrification in permeable sediments. *Biogeochemistry*, 113, 563–572.

Exley, R., Boyd, S., Mattey, D., & Pillinger, C. (1987). Nitrogen isotope geochemistry of basaltic glasses: implications for mantle degassing and structure? *Earth and planetary science letters*, 81(2), 163–174.

Fennel, K., Follows, M., & Falkowski, P. G. (2005). The co-evolution of the nitrogen, carbon and oxygen cycles in the proterozoic ocean. *American Journal of Science*, 305(6-8), 526–545.

Fischer, T., Hilton, D., Zimmer, M., Shaw, A., Sharp, Z., & Walker, J. (2002). Subduction and recycling of nitrogen along the Central American margin. *Science*, 297(5584), 1154–1157.

Foley, S. F. & Jenner, G. A. (2004). Trace element partitioning in lamproitic magmas–the Gaussberg olivine leucitite. *Lithos*, 75, 19–38.

Franchi, I., Wright, I., & Pillinger, C. (1993). Constraints on the formation conditions of iron meteorites based on concentrations and isotopic compositions of nitrogen. *Geochimica et cosmochimica acta*, 57(13), 3105–3121.

Freudenthal, T., Wagner, T., Wenzhöfer, F., Zabel, M., & Wefer, G. (2001). Early diagenesis of organic matter from sediments of the eastern subtropical Atlantic: evidence from stable nitrogen and carbon isotopes. *Geochimica et Cosmochimica Acta*, 65(11), 1795–1808.

Frost, B. R. (1991). Introduction to oxygen fugacity and its petrologic importance. *Reviews in Mineralogy and Geochemistry*, 25(1), 1–9.

Frost, D. & McCammon, C. (2008). The redox state of Earth's mantle. *Annual Review of Earth and Planetary Sciences*, 36, 389–420.

Frost, D. J., Liebske, C., Langenhorst, F., McCammon, C. A., Trønnes, R. G., & Rubie, D. C. (2004). Experimental evidence for the existence of iron-rich metal in the earth's lower mantle. *Nature*, 428(6981), 409–412.

Fuchsman, C. A., Murray, J. W., & Konovalov, S. K. (2008). Concentration and natural stable isotope profiles of nitrogen species in the Black Sea. *Marine Chemistry*, 111(1), 90–105.

Fujimaki, H., Tatsumoto, M., & Aoki, K.-i. (1984). Partition coefficients of Hf, Zr, and REE between phenocrysts and groundmasses. *Journal of Geophysical Research: Solid Earth (1978–2012)*, 89(S02), B662–B672.

Galli, A., Le Bayon, B., Schmidt, M., Burg, J.-P., Caddick, M., & Reusser, E. (2011). Granulites and chrnockites of the Gruf Complex: Evidence for Permian ultra-high temperature metamorphism in the Central Alps. *Lithos*, 124, 17–45.

Ganeshram, R. S., Pedersen, T. F., Calvert, S. E., McNeill, G. W., & Fontugne, M. R. (2000). Glacial-interglacial variability in denitrification in the World's Oceans: Causes and consequences. *Paleoceanography*, 15(4), 361–376.

Garcia, H. E., Locarnini, R. A., Boyer, T. P., & Antonov, J. I. (2010). World ocean atlas 2009, volume 4: Nutrients (phosphate, nitrate, silicate).

Garvin, J., Buick, R., Anbar, A., Arnold, G., & Kaufman, A. (2009). Isotopic evidence for an aerobic nitrogen cycle in the latest Archean. *Science*, 323(5917), 1045–1048.

Gibson, E., Carr, L., Gilmour, I., & Pillinger, C. (1986). Earth's atmosphere during the archean as seen from carbon and nitrogen isotopic analysis of sediments. In *Lunar and Planetary Institute Science Conference Abstracts*, volume 17 (pp. 258–259).

Gibson, E. & Moore, C. (1971). The distribution of total nitrogen in iron meteorites. *Geochimica et Cosmochimica Acta*, 35, 877–890.

Gibson, E., Moore, C., & Lewis, C. (1971). Total nitrogen and carbon abundances in carbonaceous chondrites. *Geochimica et Cosmochimica Acta*, 35, 599–604.

Glasmacher, U., Zentilli, M., & Ryan, R. (2003). Nitrogen distribution in lower palaeozoic slates/phyllites of the meguma supergroup, nova scotia, canada: implications for au and zn–pb mineralisation and exploration. *Chemical geology*, 194(4), 297–329.

Godfrey, L. & Falkowski, P. (2009). The cycling and redox state of nitrogen in the Archaean ocean. *Nature Geoscience*, 2(10), 725–729.

Godfrey, L., Poulton, S., Bebout, G., & Fralick, P. (2013). Stability of the nitrogen cycle during development of sulfidic water in the redox-stratified late Paleoproterozoic Ocean. *Geology*, 41, 655–658.

Godfrey, L. V., Glass, J. B., et al. (2011). The geochemical record of the ancient nitrogen cycle, nitrogen isotopes, and metal cofactors. *Methods in enzymology*, 486, 483.

Goldblatt, C., Claire, M., Lenton, T., Matthews, A., Watson, A., & Zahnle, K. (2009). Nitrogen-enhanced greenhouse warming on early Earth. *Nature Geoscience*, 2(12), 891–896.

Goldblatt, C., Zahnle, K., Sleep, N., & Nisbet, E. (2010). The Eons of Chaos and Hades. *Solid Earth*, 1, 1–3.

Goldschmidt, V. M. (1937). The principles of distribution of chemical elements in minerals and rocks. the seventh Hugo Müller Lecture, delivered before the Chemical Society on March 17th, 1937. *Journal of the Chemical Society (Resumed)*, (pp. 655–673).

Govindaraju, K. (1994). Compilation of working values and sample description for 383 geostandards. *Geostandards Newsletter*, 18, 1–158.

Grady, M. M. & Pillinger, C. (1986). Carbon isotope relationships in winonaites and forsterite chondrites. *Geochimica et Cosmochimica Acta*, 50, 255–263.

Grady, M. M., Wright, I., Carr, L., & Pillinger, C. (1986). Compositional differences in enstatite chondrites based on carbon and nitrogen stable isotope measurements. *Geochimica et Cosmochimica Acta*, 50(12), 2799–2813.

Grady, M. M. & Wright, I. P. (2003). Elemental and isotopic abundances of carbon and nitrogen in meteorites. *Space Science Reviews*, 106(1), 231–248.

Greenfield, L. (1988). 3.2 Forms of Nitrogen in Beacon Sandstone Rocks Containing Endolithic Microbial Communities in Southern Victoria Land, Antarctica. *Polarforschung*, 58(2/3), 211–218.

Greenfield, L. (1991). Fixed ammonium in antarctic rocks and soils and a possible cause of underestimation. *Soil Biology and Biochemistry*, 23(4), 397–399.

Griffith, E. M. & Paytan, A. (2012). Barite in the ocean–occurrence, geochemistry and palaeoceanographic applications. *Sedimentology*, 59(6), 1817–1835.

Gruber, N. & Sarmiento, J. L. (1997). Global patterns of marine nitrogen fixation and denitrification. *Global Biogeochemical Cycles*, 11(2), 235–266.

Gu, Y. J. & Dziewonski, A. M. (2001). Variations in thickness of the upper mantle transition zone. In *Long-term observations in the oceans: Proceedings of the OHP/ION Joint Symposium, Japan, January* (pp. 21–27).

Haber, F. (1920). The Synthesis of Ammonia from its Elements. Nobel Lecture; available at www.nobelprize.org/nobel_prizes/chemistry/laureates/ 1918/haber-lecture.pdf.

Haendel, D., Mühle, K., Nitzsche, H.-M., Stiehl, G., & Wand, U. (1986). Isotopic variations of the fixed nitrogen in metamorphic rocks. *Geochimica et cosmochimica Acta*, 50(5), 749–758.

Halama, R., Bebout, G., John, T., & Scambelluri, M. (2012). Nitrogen recycling in subducted mantle rocks and implications for the global nitrogen cycle. *International Journal of Earth Sciences*, (pp. 1–19).

Halama, R., Bebout, G. E., John, T., & Schenk, V. (2010). Nitrogen recycling in subducted oceanic lithosphere: The record in high-and ultrahigh-pressure metabasaltic rocks. *Geochimica et Cosmochimica Acta*, 74(5), 1636–1652.

Halbout, J., Mayeda, T., & Clayton, R. N. (1986). Carbon isotopes and light element abundances in carbonaceous chondrites. *Earth and Planetary Science Letters*, 80, 1–18.

Hall, A. (1987). The ammonium content of Caledonian granites. *Journal of the Geological Society*, 144(4), 671–674.

Hall, A. (1988). The distribution of ammonium in granites from South-West England. *Journal of the Geological Society*, 145(1), 37–41.

Hall, A. (1993). Application of the indophenol blue method to the determination of ammonium in silicate rocks and minerals. *Applied geochemistry*, 8(1), 101–105.

Hall, A. (1999). Ammonium in granites and its petrogenetic significance. *Earth-Science Reviews*, 45(3), 145–165.

Hall, A., Bencini, A., & Poli, G. (1991). Magmatic and hydrothermal ammonium in granites of the Tuscan magmatic province, Italy. *Geochimica et Cosmochimica Acta*, 55(12), 3657–3664.

Hall, A., Pereira, M., & Bea, F. (1996). The abundance of ammonium in the granites of central spain, and the behaviour of the ammonium ion during anatexis and fractional crystallization. *Mineralogy and Petrology*, 56(1-2), 105–123.

Halliday, A. (2004). The Origin and Earliest History of Earth. *Treatise on Geochemistry*, 1, 509–558.

Halliday, A. N. (2013). The origins of volatiles in the terrestrial planets. *Geochimica et Cosmochimica Acta*, 105, 146–171.

Halverson, G. P., Hoffman, P. F., Schrag, D. P., Maloof, A. C., & Rice, A. H. N. (2005). Toward a Neoproterozoic composite carbon-isotope record. *Geological Society of America Bulletin*, 117(9-10), 1181–1207.

Hansen, E. & Stuk, M. (1993). Orthopyroxene-bearing, mafic migmatites at Cone Peak, California: evidence for the formation of migmatitic granulites by anatexis in an open system. *Journal of Metamorphic Geology*, 11, 291–307.

Hardy, R. W., Silver, W. S., et al. (1977a). A treatise on dinitrogen fixation. Section I and II, Inorganic and Physical Chemistry and Biochemistry. *A treatise on dinitrogen fixation. Section III, Biology.*

Hardy, R. W., Silver, W. S., et al. (1977b). A treatise on dinitrogen fixation. Section III, Biology. *A treatise on dinitrogen fixation. Section III, Biology.*

Harries, D., Hoppe, P., & Lagenhorst, F. (2015). Reactive ammonia in the solar protoplanetary disk and the origin of Earth's nitrogen. *Nature Geoscience*, 8, 97–101.

Hartmann, W. K. & Davis, D. R. (1975). Satellite-sized planetesimals and lunar origin. *Icarus*, 24(4), 504–515.

Hashizume, K. & Sugiura, N. (1995). Nitrogen isotopes in bulk ordinary chondrites. *Geochimica et cosmochimica acta*, 59(19), 4057–4069.

Hayes, J., Wedeking, K., & Kaplan, I. (1983). Precambrian organic geochemistry-preservation of the record.

Haynes, W., Bruno, T., & Lide, D., Eds. (2014). *CRC Handbook of Chemistry and Physics 95*. CRC Press.

Herzberg, C., Condie, K., & Korenaga, J. (2010). Thermal history of the earth and its petrological expression. *Earth and Planetary Science Letters*, 292(1), 79–88.

Hoering, T. (1955). Variations of nitrogen-15 abundance in naturally occurring substances. *Science*, 122(3182), 1233–1234.

Hoering, T. C. & Ford, H. T. (1960). The isotope effect in the fixation of nitrogen by Azotobacter. *Journal of the American Chemical Society*, 82(2), 376–378.

Hoffman, P. & Halverson, G. (2008). Otavi group of the Western Northern Platform, the Eastern Kaoko Zone and the Western Northern Margin Zone. In R. M. Miller (Ed.), *The Geology of Namibia, vol. 2* (pp. 13.69–13.136).: Geological Survey of Namibia.

Hoffman, P. F. (2011). Strange bedfellows: glacial diamictite and cap carbonate from the Marinoan (635 ma) glaciation in Namibia. *Sedimentology*, 58(1), 57–119.

Hoffman, P. F., Crockford, P. W., De Moor, A., Halverson, G. P., Hodgin, E. B., Holtzman, B. K., Jasechko, G. R., & Schrag, D. P. (2014). Cryogenian and early Ediacaran stratigraphy of Vrede Domes, Huab River, Kunene Region, Namibia. *Comminucations of the Geological Survey of Namibia*, (pp. 1–23).

Hoffman, P. F., Halverson, G. P., Domack, E. W., Husson, J. M., Higgins, J. A., & Schrag, D. P. (2007). Are basal Ediacaran (635 Ma) post-glacial "cap dolostones" diachronous? *Earth and Planetary Science Letters*, 258(1), 114–131.

Hoffman, P. F., Kaufman, A. J., Halverson, G. P., & Schrag, D. P. (1998). A Neoproterozoic snowball earth. *Science*, 281(5381), 1342–1346.

Hoffman, P. F. & Schrag, D. P. (2002). The snowball earth hypothesis: testing the limits of global change. *Terra nova*, 14(3), 129–155.

Hoffman, P. F., Tirrul, R., King, J., St-Onge, M., & Lucas, S. (1988). *Axial projections and modes of crustal thickening, eastern Wopmay orogen*, volume 218. Geological Society of America - Special paper.

Holland, H. D. (1984). *The chemical evolution of the atmosphere and oceans*. Princeton University Press.

Holloway, J. & Dahlgren, R. (2002). Nitrogen in rock: Occurrences and biogeochemical implications. *Global Biogeochemical Cycles*, 16(4), 65–1–65–17.

Holloway, J. M., Dahlgren, R. A., & Casey, W. H. (2001). Nitrogen release from rock and soil under simulated field conditions. *Chemical Geology*, 174(4), 403–414.

Holmes, R. M., Aminot, A., Kérouel, R., Hooker, B. A., & Peterson, B. J. (1999). A simple and precise method for measuring ammonium in marine and freshwater ecosystems. *Canadian Journal of Fisheries and Aquatic Sciences*, 56(10), 1801–1808.

Honma, H. (1996). High ammonium contents in the 3800 Ma isua supracrustal rocks, central west greenland. *Geochimica et cosmochimica acta*, 60(12), 2173–2178.

Honma, H. & Itihara, Y. (1981). Distribution of ammonium in minerals of metamorphic and granitic rocks. *Geochimica et Cosmochimica Acta*, 45(6), 983–988.

Hopp, J., Trieloff, M., Ott, U., Korochantseva, E. V., & Buykin, A. I. (2014). ^{39}Ar-^{40}Ar chronology of the enstatite chondrite parent bodies. *Meteoritics & Planetary Science*, 49(3), 358–372.

Imbus, S., Macko, S., Douglas Elmore, R., & Engel, M. (1992). Stable isotope (C, S, N) and molecular studies on the Precambrian Nonesuch Shale (Wisconsin-Michigan, USA): evidence for differential preservation rates, depositional environment and hydrothermal influence. *Chemical Geology: Isotope Geoscience section*, 101(3), 255–281.

Itihara, Y. & Honma, H. (1979). Ammonium in biotite from metamorphic and granitic rocks of Japan. *Geochimica et Cosmochimica Acta*, 43(4), 503–509.

Itihara, Y. & Suwa, K. (1985). Ammonium contents of biotites from precambrian rocks in finland: The significance of nh¡ sub¿ 4¡/sub¿¡ sup¿+¡/sup¿ as a possible chemical fossil. *Geochimica et Cosmochimica Acta*, 49(1), 145–151.

Itihara, Y., Suwa, K., & Hoshino, M. (1986). Organic matter in the Kavirondian sedimentary rocks of Archaean period in Kenya. *Geochemical Journal*, 20(4), 201–207.

Itihara, Y. & Tainosho, Y. (1989). Ammonium and insoluble nitrogen in precambrian rock from the Gawler Craton, Australia: Inference of life activity. *Journal of the Geological Society of Japan*, 95(6), 439–445.

Ivanova, M., Kononkova, N., Krot, A., Greenwood, R., Franchi, I. A., Verchovsky, A., Trieloff, M., Korochantseva, E., & Brandstätter, F. (2008). The Isheyevo meteorite: Mineralogy, petrology, bulk chemistry, oxygen, nitrogen, carbon isotopic compositions, and ^{40}Ar-^{39}Ar ages. *Meteoritics and Planetary Science*, 43(5), 915–940.

Jarrard, R. D. (2003). Subduction fluxes of water, carbon dioxide, chlorine, and potassium. *Geochemistry, Geophysics, Geosystems*, 4(5).

Javoy, M. (1998). The birth of the Earth's atmosphere: the behaviour and fate of its major elements. *Chemical geology*, 147(1-2), 11–25.

Javoy, M., Kaminski, E., Guyot, F., Andrault, D., Sanloup, C., Moreira, M., Labrosse, S., Jambon, A., Agrinier, P., Davaille, A., et al. (2010). The chemical composition of the earth: Enstatite chondrite models. *Earth and Planetary Science Letters*, 293(3), 259–268.

Jenkyns, H. C., Gröcke, D. R., & Hesselbo, S. P. (2001). Nitrogen isotope evidence for water mass denitrification during the early Toarcian (Jurassic) oceanic anoxic event. *Paleoceanography*, 16(6), 593–603.

Jia, Y. (2006). Nitrogen isotope fractionations during progressive metamorphism: A case study from the Paleozoic Cooma metasedimentary complex, southeastern Australia. *Geochimica et cosmochimica acta*, 70(20), 5201–5214.

Jia, Y. & Kerrich, R. (1999). Nitrogen isotope systematics of mesothermal lode gold deposits: Metamorphic, granitic, meteoric water, or mantle origin? *Geology*, 27(11), 1051–1054.

Jia, Y. & Kerrich, R. (2000). Giant quartz vein systems in accretionary orogenic belts: the evidence for a metamorphic fluid origin from δ^{15}N δ^{13}C studies. *Earth and Planetary Science Letters*, 184(1), 211–224.

Jia, Y. & Kerrich, R. (2004). A reinterpretation of the crustal N-isotope record: evidence for a ^{15}N-enriched Archean atmosphere? *Terra Nova*, 16(3), 102–108.

Jia, Y., Kerrich, R., Gupta, A., & Fyfe, W. (2003). ^{15}N–enriched Gondwana lamproites, eastern India: crustal N in the mantle source. *Earth and Planetary Science Letters*, 215(1), 43–56.

Johnson, B. W., Drage, N., Spence, J., Hanson, N., El-Sabaawi, R., & Goldblatt, C. (In review). Measurement of geologic N using mass spectrometry, colourimetry, and a newly adapted fluorometry technique. *Solid Earth*.

Johnson, B. W. & Goldblatt, C. (2015). The Nitrogen Budget of Earth. *Earth Science Reviews*.

Johnson, B. W. & Goldblatt, C. (In review). Marine primary productivity and oxygen production during Snowball Earth. *Nature Communications*.

Kadik, A., Kurovskaya, N., Ignat'ev, Y., Kononkova, N., Koltashev, V., & Plotnichenko, V. (2011). Influence of oxygen fugacity on the solubility of nitrogen, carbon, and hydrogen in FeO-Na_2O-SiO_2-Al_2O_3 melts in equilibrium with metallic iron at 1.5 GPa and 1400°C. *Geochemistry International*, 49(5), 429–438.

Kaid, N. A. & Cowan, N. B. (2015). The feeding zones of terrestrial planets and insights into Moon formation. *Icarus*, 252, 161–174.

Kanzaki, Y. & Murakami, T. (2013). Rate law of Fe (II) oxidation under low O_2 conditions. *Geochimica et Cosmochimica Acta*, 123, 338–350.

Kao, S. & Liu, K. (2000). Stable carbon and nitrogen isotope systematics in a human-disturbed watershed (lanyang-hsi) in taiwan and the estimation of biogenic particulate organic carbon and nitrogen fluxes. *Global Biogeochemical Cycles*, 14(1), 189–198.

Kavanagh, L. & Goldblatt, C. (2015). Using raindrops to constrain past atmospheric density. *Earth and Planetary Science Letters*, 413, 51–58.

Kelly, J. F. (2000). Stable isotopes of carbon and nitrogen in the study of avian and mammalian trophic ecology. *Canadian Journal of Zoology*, 78(1), 1–27.

Kerrich, R., Jia, Y., Manikyamba, C., & Naqvi, S. (2006). Secular variations of N-isotopes in terrestrial reservoirs and ore deposits. *Evolution of Early Earth's Atmosphere, Hydrosphere, And Biosphere: Constraints from Ore Deposits*, 198, 81–104.

Kerridge, J. (1985). Carbon, hydrogen and nitrogen in carbonaceous chondrites: Abundances and isotopic compositions in bulk samples. *Geochimica et Cosmochimica Acta*, 49, 1707–1714.

Khan, A. A. & Baur, W. H. (1972). Salt hydrates. vii. the crystal structures of sodium ammonium orthochromate dihydrate and magnesium diammonium bis (hydrogen orthophosphate) tetrahydrate and a discussion of the ammonium ion. *Acta Crystallographica Section B: Structural Crystallography and Crystal Chemistry*, 28(3), 683–693.

Kirschvink, J. L. (1992). Late proterozoic low-latitude global glaciation: the snowball earth. *The Proterozoic Biosphere*, (pp. 51–52).

Klingler, J., Mancinelli, R., & White, M. (1989). Biological nitrogen fixation under primordial martian partial pressures of dinitrogen. *Advances in Space Research*, 9(6), 173–176.

Klump, J., Hebbeln, D., & Wefer, G. (2000). The impact of sediment provenance on barium-based productivity estimates. *Marine Geology*, 169(3), 259–271.

Kolesov, G. M. (1995). Neutron activation analysis of environmental materials. *Analyst*, 120(5), 1457–1460.

Korenaga, J. (2010). Scaling of plate tectonic convection with pseudoplastic rheology. *Journal of Geophysical Research: Solid Earth (1978–2012)*, 115(B11).

Korenaga, J. (2011). Thermal evolution with a hydrating mantle and the initiation of plate tectonics in the early Earth. *Journal of Geophysical Research*, 116, 1–20.

Krooss, B. M., Friberg, L., Gensterblum, Y., Hollenstein, J., Prinz, D., & Littke, R. (2005). Investigation of the pyrolytic liberation of molecular nitrogen from palaeozoic sedimentary rocks. *International Journal of Earth Sciences*, 94(5-6), 1023–1038.

Kung, C. & Clayton, R. N. (1978). Nitrogen abundances and isotopic compositions in stony meteorites. *Earth and Planetary Science Letters*, 38, 421–435.

Le Hir, G., Ramstein, G., Donnadieu, Y., & Goddéris, Y. (2008). Scenario for the evolution of atmospheric pCO_2 during a snowball earth. *Geology*, 36(1), 47–50.

Lécuyer, C., Simon, L., & Guyot, F. (2000). Comparison of carbon, nitrogen and water budgets on Venus and the Earth. *Earth and Planetary Science Letters*, 181(1), 33–40.

Lee, C.-T. A., Luffi, P., & Chin, E. J. (2011). Building and destroying continental mantle. *Annual Review of Earth and Planetary Sciences*, 39, 59–90.

Li, L., Bebout, G., & Idleman, B. (2007). Nitrogen concentration and δ^{15}N of altered oceanic crust obtained on ODP Legs 129 and 185: Insights into alteration-related nitrogen enrichment and the nitrogen subduction budget. *Geochimica et Cosmochimica Acta*, 71, 2344–2360.

Li, L. & Bebout, G. E. (2005). Carbon and nitrogen geochemistry of sediments in the Central American convergent margin: Insights regarding subduction input fluxes, diagenesis, and paleoproductivity. *Journal of Geophysical Research: Solid Earth (1978–2012)*, 110(B11).

Li, L., Zheng, Y.-F., Cartigny, P., & Li, J. (2014). Anomalous nitrogen isotopes in ultrahigh-pressure metamorphic rocks from the Sulu orogenic belt: Effect of abiotic nitrogen reduction during fluid–rock interaction. *Earth and Planetary Science Letters*, 403, 67–78.

Li, Y., Huang, R., Wiedenbeck, M., & Keppler, H. (2015). Nitrogen distribution between aqueous fluids and silicate melts. *Earth and Planetary Science Letters*, 411, 218–228.

Li, Y. & Keppler, H. (2014). Nitrogen speciation in mantle and crustal fluids. *Geochimica et Cosmochimica Acta*, 129, 13–32.

Li, Y., Marty, B., Shcheka, S., Zimmermann, L., & Keppler, H. (2016). Nitrogen isotope fractionation during terrestrial core-mantle separation. *Geochemical Perspectives Letters*, 2(2), 138–147.

Li, Y., Wiedenbeck, M., Shcheka, S., & Keppler, H. (2013). Nitrogen solubility in upper mantle minerals. *Earth and Planetary Science Letters*, 377, 311–323.

Libourel, G., Marty, B., & Humbert, F. (2003). Nitrogen solubility in basaltic melt. Part I. Effect of oxygen fugacity. *Geochimica et Cosmochimica Acta*, 67(21), 4123–4135.

Limpert, E., Stahel, W. A., & Abbt, M. (2001). Log-normal distributions across the sciences: Keys and clues. *BioScience*, 51(5), 341–352.

Liss, P. & Slater, P. (1974). Flux of Gases across the Air-Sea Interface. *Nature*, 247, 181–184.

Liu, Y., Hu, Z., Gao, S., Günther, D., Xu, J., Gao, C., & Chen, H. (2008). In situ analysis of major and trace elements of anhydrous minerals by LA-ICP-MS without applying an internal standard. *Chemical Geology*, 257(1), 34–43.

Lyons, T. W., Anbar, A. D., Severmann, S., Scott, C., & Gill, B. C. (2009). Tracking euxinia in the ancient ocean: a multiproxy perspective and proterozoic case study. *Annual Review of Earth and Planetary Sciences*, 37, 507–534.

Marty, B. (1995). Nitrogen content of the mantle inferred from N_2–Ar correlation in oceanic basalts. *Nature*, 377(6547), 326–329.

Marty, B. (2012). The origins and concentrations of water, carbon, nitrogen and noble gases on Earth. *Earth and Planetary Science Letters*, 313, 56–66.

Marty, B. & Dauphas, N. (2003). The nitrogen record of crust–mantle interaction and mantle convection from Archean to present. *Earth and Planetary Science Letters*, 206(3), 397–410.

Marty, B., Hashizume, K., Chaussidon, M., & Wieler, R. (2003). Nitrogen isotopes on the Moon: Archives of the solar and planetary contributions to the inner solar system. *Space science reviews*, 106(1), 175–196.

Marty, B. & Humbert, F. (1997). Nitrogen and argon isotopes in oceanic basalts. *Earth and Planetary Science Letters*, 152(1), 101–112.

Marty, B. & Zimmermann, L. (1999). Volatiles (He, C, N, Ar) in mid-ocean ridge basalts: Assesment of shallow-level fractionation and characterization of source composition. *Geochimica et Cosmochimica Acta*, 63(21), 3619–3633.

Marty, B., Zimmermann, L., Pujol, M., Burgess, R., & Philippot, P. (2013). Nitrogen isotopic composition and density of the Archean atmosphere. *Science*, 342, 101–104.

Mason, B. (1979). Data of geochemistry sixth edition. *Geological Survey Professional Paper*, 440-B-1(Chapter B. Cosmochemistry).

Mathew, K. & Marti, K. (2001). Lunar nitrogen: indigenous signature and cosmic-ray production rate. *Earth and Planetary Science Letters*, 184, 659–669.

Mathew, K., Marty, B., Marti, K., & Zimmermann, L. (2003). Volatiles (nitrogen, noble gases) in recently discovered SNC meteorites, extinct radioactivities and evolution. *Earth and Planetary Science Letters*, 214, 27–42.

Mathew, K., Palma, R., Marti, K., & Lavielle, B. (2000). Isotopic signatures and origin of nitrogen in IIE and IVA iron meteorites. *Geochimica et Cosmochimica Acta*, 64(3), 545–557.

Matsumoto, T., Pinti, D., Matsuda, J., & Umino, S. (2002). Recycled noble gas and nitrogen in the subcontinental lithospheric mantle: Implications from N–He–Ar in fluid inclusions of SE Australian xenoliths. *Geochemical Journal of Japan*, 36(3), 209–218.

Mayne, K. (1957). Natural variations in the nitrogen isotope abundance ratio in igneous rocks. *Geochimica et Cosmochimica Acta*, 12(3), 185–189.

Mazor, E., Heymann, D., & Anders, E. (1970). Noble gases in carbonaceous chondrites. *Geochimica et Cosmochimica Acta*, 34(7), 781–824.

McInnes, A. S., Shepard, A. K., Raes, E. J., Waite, A. M., & Quigg, A. (2014). Simultaneous quantification of active carbon-and nitrogen-fixing communities and estimation of fixation rates using fluorescence in situ hybridization and flow cytometry. *Applied and environmental microbiology*, 80(21), 6750–6759.

Mikhail, S. & Howell, D. (2016). Outlooks in Earth and Planetary Materials: Chemistry and Mineralogy of Earth's Mantle: A petrological assessment of diamond as a recorder of the mantle nitrogen cycle. *American Mineralogist*, 101(4), 780–787.

Mikhail, S. & Sverjensky, D. A. (2014). Nitrogen speciation in upper mantle fluids and the origin of Earth's nitrogen-rich atmosphere. *Nature Geoscience*, 7, 816–819.

Mingram, B. & Bräuer, K. (2001). Ammonium concentration and nitrogen isotope composition in metasedimentary rocks from different tectonometamorphic units of the European Variscan belt. *Geochimica et Cosmochimica Acta*, 65(2), 273–287.

Mitchell, E. C., Fischer, T. P., Hilton, D. R., Hauri, E. H., Shaw, A. M., de Moor, J. M., Sharp, Z. D., & Kazahaya, K. (2010). Nitrogen sources and recycling at subduction zones: Insights from the Izu-Bonin-Mariana arc. *Geochemistry, Geophysics, Geosystems*, 11(2).

Mitchell, R. H. (1995). Melting experiments on a sanidine phlogopite lamproite at 4–7 GPa and their bearing on the sources of lamproitic magmas. *Journal of Petrology*, 36(5), 1455–1474.

Mohapatra, R., Harrison, D., Ott, U., Gilmour, J., & Trieloff, M. (2009). Noble gas and nitrogen isotopic components in Oceanic Island Basalts. *Chemical Geology*, 266(1), 29–37.

Mohapatra, R. & Murty, S. (2003). Precurors of Mars: Constraints from nitrogen and oxygen isotopic compositions of martioan meteorites. *Meteoritics and Planetary Science*, 38(2), 225–241.

Morford, S. L., Houlton, B. Z., & Dahlgren, R. A. (2011). Increased forest ecosystem carbon and nitrogen storage from nitrogen rich bedrock. *Nature*, 477(7362), 78–81.

Murphy, D., Collerson, K., & Kamber, B. (2002). Lamproites from Gaussberg, Antarctica: possible transition zone melts of Archaean subducted sediments. *Journal of Petrology*, 43(6), 981–1001.

Murty, S., Shukla, P., & Goel, P. (1983). Nitrogen in stone meteorites and terrestrial standards. *Geochemical Journal*, 17(4), 165–183.

Mysen, B. O. & Fogel, M. L. (2010). Nitrogen and hydrogen isotope compositions and solubility in silicate melts in equilibrium with reduced (N+ H)-bearing fluids at

high pressure and temperature: Effects of melt structure. *American Mineralogist*, 95(7), 987–999.

Mysen, B. O., Tomita, T., Ohtani, E., & Suzuki, A. (2014). Speciation of and D/H partitioning between fluids and melts in silicate-D-O-H-C-N systems determined in-situ at upper mantle temperatures, pressures, and redox conditions. *American Mineralogist*, 99(4), 578–588.

Mysen, B. O., Yamashita, S., & Chertkova, N. (2008). Solubility and solution mechanisms of NOH volatiles in silicate melts at high pressure and temperature-amine groups and hydrogen fugacity. *Am. Mineral*, 93, 1760–1770.

Nakagawa, T. & Tackley, P. J. (2012). Influence of magmatism on mantle cooling, surface heat flow and Urey ratio. *Earth and Planetary Science Letters*, 329, 1–10.

Narbonne, G. M. (2005). The ediacara biota: Neoproterozoic origin of animals and their ecosystems. *Annu. Rev. Earth Planet. Sci.*, 33, 421–442.

Niemi, N., Sahagian, D., Prooussevitch, A., & Carlson, W. (2005). : American Geophysical Union Fall Meeting.

Nishio, Y., Ishii, T., Gamo, T., & Sano, Y. (1999). Volatile element isotopic systematics of the Rodrigues Triple Junction Indian Ocean MORB: implications for mantle heterogeneity. *Earth and Planetary Science Letters*, 170(3), 241–253.

Nishizawa, M., Sano, Y., Ueno, Y., & Maruyama, S. (2007). Speciation and isotope ratios of nitrogen in fluid inclusions from seafloor hydrothermal deposits at 3.5 Ga. *Earth and Planetary Science Letters*, 254(3), 332–344.

Norris, T. L. & Schaeffer, O. A. (1982). Total nitrogen content of deep sea basalts. *Geochimica et Cosmochimica Acta*, 46(3), 371–379.

Och, L. M. & Shields-Zhou, G. A. (2012). The neoproterozoic oxygenation event: environmental perturbations and biogeochemical cycling. *Earth-Science Reviews*, 110(1), 26–57.

Oró, J. (1961). Comets and the formation of biochemical compounds on the primitive Earth. *Nature*, 190, 389–390.

Padhi, C. M., Korenaga, J., & Ozima, M. (2012). Thermal evolution of Earth with xenon degassing: a self-consistent approach. *Earth and Planetary Science Letters*, 341, 1–9.

Palme, H. & O'Neill, H. (2014). Cosmochemical Estimates of Mantle Composition. *Planets, Asteriods, Comets and The Solar System, Volume 2 of Treatise on Geochemistry (Second Edition). Edited by Andrew M. Davis. Elsevier, 2014., p. 149-211*, 1, 1–35.

Palot, M., Cartigny, P., Harris, J., Kaminsky, F., & Stachel, T. (2012). Evidence for deep mantle convection and primordial heterogeneity from nitrogen and carbon stable isotopes in diamond. *Earth and Planetary Science Letters*, 357, 179–193.

Palya, A. P., Buick, I. S., & Bebout, G. E. (2011). Storage and mobility of nitrogen in the continental crust: Evidence from partially melted metasedimentary rocks, Mt. Stafford, Australia. *Chemical Geology*, 281(3), 211–226.

Papineau, D., Mojzsis, S., Karhu, J., & Marty, B. (2005). Nitrogen isotopic composition of ammoniated phyllosilicates: case studies from Precambrian metamorphosed sedimentary rocks. *Chemical Geology*, 216(1), 37–58.

Papineau, D., Purohit, R., Goldberg, T., Pi, D., Shields, G. A., Bhu, H., Steele, A., & Fogel, M. L. (2009). High primary productivity and nitrogen cycling after the Paleoproterozoic phosphogenic event in the Aravalli Supergroup, India. *Precambrian Research*, 171(1), 37–56.

Partin, C., Bekker, A., Planavsky, N., Scott, C., Gill, B., Li, C., Podkovyrov, V., Maslov, A., Konhauser, K., Lalonde, S., Love, G., Poulton, S., & Lyons, T. W. (2013). Large-scale fluctuations in Precambrian atmospheric and oceanic oxygen levels from the record of U in shales. *Earth and Planetary Science Letters*, 369-370, 284–293.

Patterson, C. (1956). Age of meteorites and the earth. *Geochimica et Cosmochimica Acta*, 10(4), 230–237.

Patzer, A. & Schultz, L. (2002). Noble gases in enstatite chondrites ii: The trapped component. *Meteoritics & Planetary Science*, 37(4), 601–612.

Pearson, V., Sephton, M. A., Franchi, I., Gibson, J., & Gilmour, I. (2006). Carbon and nitrogen in carbonaceous chondrites: Elemental abundances and stable isotopic compositions. *Meteoritics and Planetary Science*, 41(12), 1899–1918.

Peel, K., Weiss, D., & Sigg, L. (2009). Zinc isotope composition of settling particles as a proxy for biogeochemical processes in lakes: Insights from the eutrophic Lake Greifen, Switzerland. *Limnology and Oceanography*, 54(5), 1699–1708.

Pepin, R. O. & Becker, R. H. (1982). Nitrogen isotopes in iron meteorites. *Meteoritics*, 17, 269.

Peters, K., Sweeney, R., & Kaplan, I. (1978). Correlation of carbon and nitrogen stable isotope ratios in sedimentary organic matter. *Limnololgy and Oceanography*, 23(4), 598–604.

Philippot, P., Busigny, V., Scambelluri, M., & Cartigny, P. (2007). Oxygen and nitrogen isotopes as tracers of fluid activities in serpentinites and metasediments during subduction. *Mineralogy and Petrology*, 91(1-2), 11–24.

Pinti, D. & Hashizume, K. (2011). Early life record from nitrogen isotopes. *Earliest Life on Earth: Habitats, Environments and Methods of Detection*, (pp. 183–205).

Pinti, D., Hashizume, K., & Matsuda, J. (2001). Nitrogen and argon signatures in 3.8 to 2.8 Ga metasediments: Clues on the chemical state of the Archean ocean and the deep biosphere. *Geochimica et Cosmochimica Acta*, 65(14), 2301–2315.

Pitcairn, I., Teagle, D., Kerrich, R., Craw, D., & Brewer, T. (2005). The behavior of nitrogen and nitrogen isotopes during metamorphism and mineralization: evidence from the Otago and Alpine Schists, New Zealand. *Earth and Planetary Science Letters*, 233(1), 229–246.

Plessen, B., Harlov, D. E., Henry, D., & Guidotti, C. V. (2010). Ammonium loss and nitrogen isotopic fractionation in biotite as a function of metamorphic grade in metapelites from western Maine, USA. *Geochimica et Cosmochimica Acta*, 74(16), 4759–4771.

Ponganis, K. & Marti, K. (2007). Nitrogen components in IAB/IIICD iron meteorites. *Meteoritics and Planetary Science*, 42(3), 331–346.

Pontes, F. V., Carneiro, M. C., Vaitsman, D. S., da Rocha, G. P., da Silva, L. I., Neto, A. A., & Monteiro, M. I. C. (2009). A simplified version of the total kjeldahl nitrogen method using an ammonia extraction ultrasound-assisted purge-and-trap system and ion chromatography for analyses of geological samples. *Analytica Chimica Acta*, 632(2), 284–288.

Power, J., Bond, J., Sandoval, F., & Willis, W. (1974). Nitrification in paleocene shale. *Science*, 183(4129), 1077–1079.

Prave, A. R., Condon, D. J., Hoffmann, K. H., Tapster, S., & Fallick, A. E. (2016). Duration and nature of the end-Cryogenian (Marinoan) glaciation. *Geology*, 44(8), 631–634.

Prombo, C. A. & Clayton, R. N. (1993). Nitrogen isotopic compositions of iron meteorites. *Geochimica et cosmochimica acta*, 57(15), 3749–3761.

Pujol, M., Marty, B., & Burgess, R. (2011). Chondritic-like xenon trapped in Archean rocks: A possible signature of the ancient atmosphere. *Earth and Planetary Science Letters*, 308(3), 298–306.

Quan, T., van de Schootbrugge, B., Field, M., Rosenthal, Y., & Falkowski, P. (2008). Nitrogen isotope and trace metal analyses from the Mingolsheim core (Germany): Evidence for redox variations across the Triassic-Jurassic boundary. *Global Biogeochemical Cycles*, 22(2), GB2014.

Quan, T. M., Adigwe, E. N., Riedinger, N., & Puckette, J. (2013a). Evaluating nitrogen isotopes as proxies for depositional environmental conditions in shales: Comparing Caney and Woodford Shales in the Arkoma Basin, Oklahoma. *Chemical Geology*, 360, 231–240.

Quan, T. M., Wright, J. D., & Falkowski, P. G. (2013b). Co-variation of nitrogen isotopes and redox states through glacial-interglacial cycles in the Black Sea. *Geochimica et Cosmochimica Acta*, 112, 305–320.

Rau, G., Arthur, M., & Dean, W. (1987). $^{15}N/^{14}N$ variations in Cretaceous Atlantic sedimentary sequences: implication for past changes in marine nitrogen biogeochemistry. *Earth and Planetary Science Letters*, 82(3), 269–279.

Rigby, D. & Batts, B. (1986). The isotopic composition of nitrogen in Australian coals and oil shales. *Chemical Geology: Isotope Geoscience section*, 58(3), 273–282.

Ringwood, A. & Anderson, D. L. (1977). Earth and venus: A comparative study. *Icarus*, 30(2), 243–253.

Robert, F. & Epstein, S. (1982). The concentration and isotopic composition of hydrogen, carbon and nitrogen in carbonaceous meteorites. *Geochimica et Cosmochimica Acta*, 46, 81–95.

Rollinson, H. R. (1993). *Using Geochecmical Data: Evaluation, Presentation, Interpretation*. Pearson.

Roskosz, M., Bouhifd, M., Jephcoat, A., Marty, B., & Mysen, B. (2013). Nitrogen solubility in molten metal and silicate at high pressure and temperature. *Geochimica et Cosmochimica Acta*, 121, 15–28.

Roskosz, M., Mysen, B. O., & Cody, G. D. (2006). Dual speciation of nitrogen in silicate melts at high pressure and temperature: an experimental study. *Geochimica et Cosmochimica Acta*, 70(11), 2902–2918.

Roulleau, E., Pinti, D., Stevenson, R., Takahata, N., Sano, Y., & Pitre, F. (2012). N, Ar and Pb isotopic co-variations in magmatic minerals: Discriminating fractionation processes from magmatic sources in Monteregian Hills, Québec, Canada. *Chemical Geology*.

Rudnick, R. & Gao, S. (2003). Composition of the Continental Crust. *Treatise on Geochemistry*, 3, 1–64.

Rudnick, R. & Gao, S. (2014). Composition of the Continental Crust. *Treatise on Geochemistry*, 4, 1–69.

Rutherford, D. (1772). *"Dissertatio Inauguralis de aere fixo, aut mephitico" (Inaugural dissertation on the air [called] fixed or mephitic)*. PhD thesis, University of Edinburgh.

Rysgaard, S., Risgaard-Petersen, N., Niels Peter, S., Kim, J., & Lars Peter, N. (1994). Oxygen regulation of nitrification and denitrification in sediments. *Limnology and Oceanography*, 39(7), 1643–1652.

Sadofsky, S. J. & Bebout, G. E. (2000). Ammonium partitioning and nitrogen-isotope fractionation among coexisting micas during high-temperature fluid-rock interac-

tions: Examples from the New England Appalachians. *Geochimica et Cosmochimica Acta*, 64(16), 2835–2849.

Sadofsky, S. J. & Bebout, G. E. (2003). Record of forearc devolatilization in low-T, high-P/T metasedimentary suites: Significance for models of convergent margin chemical cycling. *Geochemistry, Geophysics, Geosystems*, 4(4).

Sadofsky, S. J. & Bebout, G. E. (2004). Nitrogen geochemistry of subducting sediments: New results from the Izu-Bonin-Mariana margin and insights regarding global nitrogen subduction. *Geochemistry, Geophysics, Geosystems*, 5(3).

Sakai, H., Des Marais, D., Ueda, A., & Moore, J. (1984). Concentrations and isotope ratios of carbon, nitrogen and sulfur in ocean-floor basalts. *Geochimica et Cosmochimica Acta*, 48(12), 2433–2441.

Sander, R. (1999). Compilation of Henry‘s law constants for inorganic and organic species of potential importance in environmental chemistry. Max-Planck Institute of Chemistry, Air Chemistry Department Mainz, Germany.

Sandu, C., Lenardic, A., & McGovern, P. (2011). The effects of deep water cycling on planetary thermal evolution. *Journal of Geophysical Research*, 116, 1–15.

Sano, Y. & Pillinger, C. (1990). Nitrogen isotopes and N_2/Ar ratios in cherts: an attempt to measure time evolution of atmospheric δ^{15}N value. *Geochem. J*, 24, 315–325.

Sano, Y., Takahata, N., Nishio, Y., Fischer, T., & Williams, S. (2001). Volcanic flux of nitrogen from the Earth. *Chemical geology*, 171(3), 263–271.

Sano, Y., Takahata, N., Nishio, Y., & Marty, B. (1998). Nitrogen recycling in subduction zones. *Geophysical research letters*, 25(13), 2289–2292.

Scalan, R. S. (1955). *The isotopic composition, concentration, and chemical state of the nitrogen in igneous rocks*. PhD thesis, University of Arkansas.

Scholten, S. (1991). The distribution of nitrogen isotopes in sediments. *Geologica Ultraiectina*, 81, 101.

Schroeder, P. & McLain, A. (1998). Illite-smectites and the influence of burial diagenesis on the geochemical cycling of nitrogen. *Clay Minerals*, 33(4), 539–546.

Schulze, D. J., Coopersmith, H. G., Harte, B., & Pizzolato, L.-A. (2008). Mineral inclusions in diamonds from the Kelsey Lake Mine, Colorado, USA: Depleted Archean mantle beneath the Proterozoic Yavapai province. *Geochimica et Cosmochimica Acta*, 72(6), 1685–1695.

Scott, C., Lyons, T., Bekker, A., Shen, Y.-a., Poulton, S., Chu, X.-l., & Anbar, A. (2008). Tracing the stepwise oxygenation of the Proterozoic ocean. *Nature*, 452(7186), 456–459.

Sephton, M. A., Amor, K., Franchi, I. A., Wignall, P. B., Newton, R., & Zonneveld, J.-P. (2002). Carbon and nitrogen isotope disturbances and an end-Norian (Late Triassic) extinction event. *Geology*, 30(12), 1119–1122.

Sephton, M. A., Verchovsky, A., Bland, P., Gilmour, I., Grady, M. M., & Wright, I. (2003). Investigating the variations in carbon and nitrogen isotopes in carbonaceous chondrites. *Geochimica et Cosmochimica Acta*, 67(11), 2093–2108.

Shearer, C. & Papike, J. (1999). Magmatic evolution of the Moon. *American Mineralogist*, 84, 1469–1494.

Shukla, P., Kothari, B., & Goel, P. (1978). Simultaneous determination of nitrogen and lithium by thermal neutron activation analysis. *Analytica Chimica Acta*, 96(2), 259–269.

Sieczka, A. & Koda, E. (2016). Kinetic and equilibrium studies of sorption of ammonium in the soil-water environment in agricultural areas of central Poland. *Applied Sciences*, 6, 1–14.

Sigman, D., Karsh, K., & Casciotti, K. (2009). Ocean process tracers: nitrogen isotopes in the ocean. *Encyclopedia of ocean science,*.

Sleep, N. H. & Windley, B. F. (1982). Archean plate tectonics: constraints and inferences. *The Journal of Geology*, 90(4), 363–379.

Smart, K. A., Chacko, T., Stachel, T., Muehlenbachs, K., Stern, R. A., & Heaman, L. M. (2011). Diamond growth from oxidized carbon sources beneath the Northern Slave Craton, Canada: A δ^{13}C–N study of eclogite-hosted diamonds from the Jericho kimberlite. *Geochimica et Cosmochimica Acta*, 75(20), 6027–6047.

Smelov, A., Shatsky, V., Ragozin, A., Reutskii, V., & Molotkov, A. (2012). Diamondiferous archean rocks of the olondo greenstone belt (*western Aldan–Stanovoy shield*). *Russian Geology and Geophysics*, 53(10), 1012–1022.

Smith, E. M., Kopylova, M. G., & Peck, W. (2014). Implications of metallic iron for diamonds and nitrogen in the sublithospheric mantle. *Canadian Journal of Earth Sciences*, 51(5), 510–516.

Som, S. M., Buick, R., Hagadorn, J. W., Blake, T. S., Perreault, J. M., Harnmeijer, J. P., & Catling, D. C. (2016). Earth's air pressure 2.7 billion years ago constrained to less than half of modern levels. *Nature Geoscience*, 9, 448–451.

Som, S. M., Catling, D. C., Harnmeijer, J. P., Polivka, P. M., & Buick, R. (2012). Air density 2.7 billion years ago limited to less than twice modern levels by fossil raindrop imprints. *Nature*, 484(7394), 359–362.

Stachel, T. & Harris, J. W. (2009). Formation of diamond in the Earth's mantle. *Journal of Physics: Condensed Matter*, 21(36), 364206.

Stiehl, G. & Lehmann, M. (1980). Isotopenvariationen des stickstoffs humoser und bituminöser natürlicher organischer substanzen. *Geochimica et Cosmochimica Acta*, 44(11), 1737–1746.

Stüeken, E., Kipp, M. A., Koehler, M. C., & Buick, R. (2016). The evolution of earth's biogeochemical nitrogen cycle. *Earth-Science Reviews*, 160, 220–239.

Stüeken, E. E. (2013). A test of the nitrogen-limitation hypothesis for retarded eukaryote radiation: nitrogen isotopes across a Mesoproterozoic basinal profile. *Geochimica et Cosmochimica Acta*, 120, 121–139.

Sugiura, N. (1998). Ion probe measurements of carbon and nitrogen in iron meteorites. *Meteoritics and Planetary Science*, 33, 393–409.

Sugiura, N., Kiyota, K., & Hashizume, K. (1998). Nitrogen components in primitive ordinary chondrites. *Meteoritics and Planetary Science*, 33, 463–482.

Sugiura, N. & Zashu, S. (1995). Nitrogen isotopic composition of CK chondrites. *Meteoritics*, 30, 430–435.

Sullivan, P. J., Sposito, G., Strathouse, S., & Hansen, C. L. (1979). *Geologic nitrogen and the occurrence of high nitrate soils in the western San Joaquin Valley, California*. University of California, Division of Agriculture and Natural Resources.

Svensen, H., Bebout, G., Kronz, A., Li, L., Planke, S., Chevallier, L., & Jamtveit, B. (2008). Nitrogen geochemistry as a tracer of fluid flow in a hydrothermal vent complex in the karoo basin, south africa. *Geochimica et Cosmochimica Acta*, 72(20), 4929–4947.

Tainton, K. M. & McKenzie, D. (1994). The generation of kimberlites, lamproites, and their source rocks. *Journal of Petrology*, 35(3), 787–817.

Tappert, R., Stachel, T., Harris, J. W., Muehlenbachs, K., Ludwig, T., & Brey, G. P. (2005). Diamonds from jagersfontein (south africa): messengers from the sublithospheric mantle. *Contributions to Mineralogy and Petrology*, 150(5), 505–522.

Taylor, S. R. (1992). *Solar system evolution: a new perspective. An inquiry into the chemical composition, origin, and evolution of the solar system.* Cambridge University Press.

Taylor, S. R. & McLennan, S. M. (1985). *The continental crust: its composition and evolution*. Blackwell Scientific Pub., Palo Alto, CA.

Taylor, S. R. & McLennan, S. M. (1995). The geochemical evolution of the continental crust. *Reviews of Geophysics*, 33(2), 241–265.

Tesdal, J., Galbraith, E., & Kienast, M. (2013). Nitrogen isotopes in bulk marine sediment: linking seafloor observations with subseafloor records. *Biogeosciences*, 10(1), 101–118.

Thamdrup, B. (2012). New pathways and processes in the global nitrogen cycle. *Annual Review of Ecology, Evolution, and Systematics*, 43, 407–428.

Thomazo, C., Ader, M., & Philippot, P. (2011). Extreme ^{15}N-enrichments in 2.72-Gyr-old sediments: evidence for a turning point in the nitrogen cycle. *Geobiology*, 9(2), 107–120.

Thomazo, C., Pinti, D., Busigny, V., Ader, M., Hashizume, K., & Philippot, P. (2009). Biological activity and the Earth's surface evolution: Insights from carbon, sulfur,

nitrogen and iron stable isotopes in the rock record. *Comptes Rendus Palevol*, 8(7), 665–678.

Tolstikhin, I. & Marty, B. (1998). The evolution of terrestrial volatiles: a view from helium, neon, argon and nitrogen isotope modelling. *Chemical Geology*, 147(1-2), 27–52.

Tribovillard, N., Algeo, T. J., Lyons, T., & Riboulleau, A. (2006). Trace metals as paleoredox and paleoproductivity proxies: an update. *Chemical geology*, 232(1), 12–32.

Ueno, Y., Yoshioka, H., Maruyama, S., & Isozaki, Y. (2004). Carbon isotopes and petrography of kerogens in $\sim$ 3.5–Ga hydrothermal silica dikes in the North Pole area, Western Australia. *Geochimica et Cosmochimica Acta*, 68(3), 573–589.

Ussiri, D. & Lal, R. (2013). Global nitrogen cycle. *Soil Emission of Nitrous Oxide and its Mitigation*, (pp. 29–62).

van Zuilen, M. A., Mathew, K., Wopenka, B., Lepland, A., Marti, K., & Arrhenius, G. (2005). Nitrogen and argon isotopic signatures in graphite from the 3.8-ga-old isua supracrustal belt, southern west greenland. In *Lunar and Planetary Institute Science Conference Abstracts*, volume 69 (pp. 1241–1252).: Elsevier.

Veizer, J. & Mackenzie, F. (2003). Evolution of sedimentary rocks. *Treatise on geochemistry*, 7, 369–407.

Velinsky, D. J., Fogel, M. L., Todd, J. F., & Tebo, B. M. (1991). Isotopic fractionation of dissolved ammonium at the oxygen-hydrogen sulfide interface in anoxic waters. *Geophysical Research Letters*, 18(4), 649–652.

Visser, D. (1993). The metamorphic evolution of the Bamble sector, south Norway: A paragenetic and mineral chemical study of cordierite-orthoamphibole-bearing rocks with special reference to borosilicate-bearing mineral assemblages. *Geologica Ultraiectina*, 103, 1–159.

von der Handt, A. & Dalou, C. (2016). Quantitative EPMA of Nitrogen in Silicate Glasses. *Microscopy and Microanalysis*, 22(S3), 1810–1811.

von Zahn, U., Kumar, S., Niemann, H., & Prinn, R. (1983). *Venus*, volume 1. University of Arizona Press.

Wasson, J. & Kallemeyn, G. (1988). Compositions of chondrites. *Philosophical Transactions of the Royal Society of London. Series A, Mathematical and Physical Sciences*, 325(1587), 535–544.

Watanabe, Y., Naraoka, H., Wronkiewicz, D., Condie, K., & Ohmoto, H. (1997). Carbon, nitrogen, and sulfur geochemistry of Archean and Proterozoic shales from the Kaapvaal Craton, South Africa. *Geochimica et Cosmochimica Acta*, 61(16), 3441–3459.

Watenphul, A., Wunder, B., & Heinrich, W. (2009). High-pressure ammonium-bearing silicates: Implications for nitrogen and hydrogen storage in the Earth's mantle. *American Mineralogist*, 94(2-3), 283–292.

Watenphul, A., Wunder, B., Wirth, R., & Heinrich, W. (2010). Ammonium-bearing clinopyroxene: A potential nitrogen reservoir in the Earth's mantle. *Chemical Geology*, 270(1), 240–248.

Wedepohl, H. K. (1995). The composition of the continental crust. *Geochimica et Cosmochimica Acta*, 59(7), 1217–1232.

Weeks, M. E. (1933). The Discovery of the Elements. Chronology. *Journal of Chemical Education*, 10(4), 223–227.

Westerlund, K., Shirey, S., Richardson, S., Carlson, R., Gurney, J., & Harris, J. (2006). A subduction wedge origin for Paleoarchean peridotitic diamonds and harzburgites from the Panda kimberlite, Slave craton: evidence from Re–Os isotope systematics. *Contributions to Mineralogy and Petrology*, 152(3), 275–294.

Wheat, C. G., McManus, J., Mottl, M. J., & Giambalvo, E. (2003). Oceanic phosphorus imbalance: Magnitude of the mid-ocean ridge flank hydrothermal sink. *Geophysical research letters*, 30(17).

White, W. M. (2010). Oceanic island basalts and mantle plumes: the geochemical perspective. *Annual Review of Earth and Planetary Sciences*, 38, 133–160.

Whitman, W. B., Coleman, D. C., & Wiebe, W. J. (1998). Prokaryotes: the unseen majority. *Proceedings of the National Academy of Sciences*, 95(12), 6578–6583.

Whittaker, E. & Muntus, R. (1970). Ionic radii for use in geochemistry. *Geochimica et Cosmochimica Acta*, 34(9), 945–956.

Wiechert, U., Halliday, A., Lee, D.-C., Snyder, G., Taylor, L., & Rumble, D. (2001). Oxygen isotopes and the Moon-forming giant impact. *Science*, 294(5541), 345–348.

Williams, L., Wilcoxon, B., Ferrell, R., & Sassen, R. (1992). Diagenesis of ammonium during hydrocarbon maturation and migration, wilcox group, louisiana, usa. *Applied Geochemistry*, 7(2), 123–134.

Williams, L. B., Ferrell, R. E., Hutcheon, I., Bakel, A. J., Walsh, M. M., & Krouse, H. R. (1995). Nitrogen isotope geochemistry of organic matter and minerals during diagenesis and hydrocarbon migration. *Geochimica et Cosmochimica Acta*, 59(4), 765–779.

Williams, L. B. & Ferrell Jr, R. (1991). Ammonium substitution in illite during maturation of organic matter. *Clays and Clay Minerals*, 39(4), 400–408.

Winter, J. D. (2001). *An introduction to igneous and metamorphic petrology*, volume 697. Prentice Hall New Jersey.

Wlotzka, F. (1972). *Handbook of Geochemistry*, volume II. Springer-Verlag.

Workman, R. K. & Hart, S. R. (2005). Major and trace element composition of the depleted MORB mantle (DMM). *Earth and Planetary Science Letters*, 231(1), 53–72.

Yamaguchi, K. (2002). *Geochemistry of Archean–Paleoproterozoic black shales: The early evolution of the atmosphere, oceans, and biosphere*. PhD thesis, The Pennsylvania State University.

Yokochi, R. & Marty, B. (2006). Fast chemical and isotopic exchange of nitrogen during reaction with hot molybdenum. *Geochemistry, Geophysics, Geosystems*, 7(7), 1–6.

Yokochi, R., Marty, B., Chazot, G., & Burnard, P. (2009). Nitrogen in peridotite xenoliths: Lithophile behavior and magmatic isotope fractionation. *Geochimica et Cosmochimica Acta*, 73(16), 4843–4861.

Yui, T.-F., Kao, S.-J., & Wu, T.-W. (2009). Nitrogen and N-isotope variation during low-grade metamorphism of the Taiwan mountain belt. *Geochemical Journal*, 43(1), 15–27.

Zelenski, M., Taran, Y. A., Dubinina, E., Polyntseva, E., et al. (2012). Sources of volatiles for a subduction zone volcano: Mutnovsky volcano, Kamchatka. *Geochemistry International*, 50(6), 502–521.

Zerkle, A. L., Junium, C. K., Canfield, D. E., & House, C. H. (2008). Production of ^{15}N-depleted biomass during cyanobacterial N_2-fixation at high Fe concentrations. *Journal of Geophysical Research: Biogeosciences*, 113(G3).

Zhang, Y. & Yin, Q.-Z. (2012). Carbon and other light element contents in the Earth's core based on first-principles molecular dynamics. *Proceedings of the National Academy of Sciences*, 109(48), 19579–19583.

Zhang, Y. & Zindler, A. (1993). Distribution and evolution of carbon and nitrogen in Earth. *Earth and Planetary Science Letters*, 117(3), 331–345.